

**ECONOMIC COMMISSION FOR EUROPE**  
**Geneva**

**HEMISPHERIC TRANSPORT OF  
AIR POLLUTION  
2010**

**PART A: OZONE AND PARTICULATE MATTER**

**AIR POLLUTION STUDIES No. 17**

Edited by Frank Dentener, Terry Keating, and Hajime Akimoto

Prepared by the Task Force on Hemispheric Transport of Air Pollution  
acting within the framework of the  
Convention on Long-range Transboundary Air Pollution



**UNITED NATIONS**  
New York and Geneva, 2010

## NOTE

Symbols of United Nations documents are composed of capital letters combined with figures. Mention of such symbols indicates a reference to a United Nations document.

The designations employed and the presentation of the material in this publication do not imply the expression of any opinion whatsoever on the part of the Secretariat of the United Nations concerning the legal status of any country, territory, city or area, or of its authorities, or concerning the delimitation of its frontiers or boundaries.

In United Nations texts, the term “ton” refers to metric tons (1,000 kg or 2,204.6 lbs).

### *Acknowledgements*

*The task force co-chairs and the secretariat would like to acknowledge the assistance of EC/R, Inc., in preparing this publication. We would also like to acknowledge the invaluable contribution of the individual experts and the Convention's Programme Centres and Task Forces.*

ECE/EB.AIR/100

UNITED NATIONS PUBLICATION
<i>Sales No. 11.II.E.7</i>
<i>ISSN 1014-4625</i>
<i>ISBN 978-92-1-117043-6</i>

Copyright © United Nations, 2010  
All rights reserved

UNECE Information Service  
Palais des Nations  
CH-1211 Geneva 10  
Switzerland

Phone: +41 (0) 22 917 44 44  
Fax: +41 (0) 22 917 05 05  
E-mail: [info.ece@unece.org](mailto:info.ece@unece.org)  
Website: <http://www.unece.org>

# Contents

Tables.....	vii
Figures.....	ix
Chemical Symbols, Acronyms and Abbreviations .....	xv
Preface.....	xxv

## **Chapter 1 Conceptual Overview of Hemispheric or Intercontinental Transport of Ozone and Particulate Matter ..... 1**

1.1. Background and Introduction .....	1
1.2. Intercontinental or hemispheric transport of ozone and PM .....	2
1.2.1. Major ozone and PM sources .....	2
1.2.2. Major transport pathways.....	4
1.2.3. Chemistry and transformation processes.....	6
1.3. Key concepts for describing intercontinental transport processes.....	8
1.3.1. Global background and global baseline concentrations .....	8
1.3.2. Source Attribution and Source-Receptor Relationships.....	9
1.4. Major types of intercontinental transport processes .....	11
1.4.1. General circulation regimes .....	11
1.4.2. The mid-latitude cyclone airstreams.....	13
1.4.3. Deep convection.....	14
1.4.4. Diffuse or small scale atmospheric boundary layer venting.....	14
1.4.5. Slow, low altitude flow .....	15
1.4.6. Transport of polluted air masses into the atmospheric boundary layer of the receptor region.....	15
1.5. Impact of Present and Future Climate on Intercontinental Transport Processes.....	16
1.5.1. Present day climate variability and its impact on intercontinental transport processes.....	16
1.5.2. Climate Change and its effects on intercontinental transport processes.....	17
1.6. Chapter storylines.....	18
References .....	19

## **Chapter 2 Observational Evidence and Capabilities Related to Intercontinental Transport of Ozone and Particulate Matter ..... 25**

2.1. Introduction .....	25
2.2. Long-range Transport of Ozone and its Precursors.....	27
2.2.1. The View from Satellites .....	27
2.2.2. Direct Evidence for O <sub>3</sub> and Precursor Transport from In Situ and Lidar Measurements .....	28
2.2.3. Indirect evidence from long-term trends in baseline O <sub>3</sub> .....	32
2.2.4. Implications for Surface Ozone Air Quality in Receptor Regions .....	36
2.2.5. Summary, Remaining Uncertainties and Future Needs .....	38
2.3. Long-range Transport of Particulate Matter and its Precursors .....	39
2.3.1. Quantitative Estimates of Total Particulate Matter Transport from Satellites.....	39
2.3.2. In Situ and Lidar Observation of Particulate Matter Outflow from Continents .....	41
2.3.3. Observations of Particulate Matter in Continental Inflow .....	42
2.3.4. Trends in Surface site Observations of Particulate Matter.....	45
2.3.5. Implications for Surface Particulate Matter Air Quality in Receptor Regions.....	47
2.3.6. Summary, Remaining Uncertainties and Future Needs.....	48

2.4.	Observational Evidence for Attribution of Source Regions .....	49
2.4.1.	<i>Meteorologically-based source attribution studies</i> .....	50
2.4.2.	<i>Source attribution based on trace gas correlations and ratios</i> .....	52
2.4.3.	<i>Aerosol source attribution based on use of trace elements and isotopes</i> .....	53
2.4.4.	<i>Plume processing during long-range transport based on analysis of Lagrangian data and implications for global modelling of long-range pollutant transport</i> .....	56
2.5.	Research Needs .....	59
2.5.1.	<i>Surface Site Needs</i> .....	59
2.5.2.	<i>Vertical Profiling Needs</i> .....	60
2.5.3.	<i>Satellite Data Needs</i> .....	62
2.5.4.	<i>Intensive Campaign Needs</i> .....	63
2.5.5.	<i>Model evaluation against observations</i> .....	64
	References .....	65
<b>Chapter 3 Emission Inventories and Projections</b> .....		<b>77</b>
3.1.	Introduction .....	77
3.2.	Development of new emission datasets to study hemispheric transport of air pollution .....	78
3.2.1.	<i>EDGAR-HTAP emission inventory (2000-2005)</i> .....	78
3.2.2.	<i>Historical emission inventory in support of RCP scenarios (1850-2000)</i> .....	84
3.2.3.	<i>RCP scenarios (2000-2100)</i> .....	84
3.2.4.	<i>Incorporating local knowledge into global emission inventories: RAPIDC</i> .....	85
3.2.5.	<i>Uncertainties in emission estimates</i> .....	87
3.3.	Emissions from Natural Sources and Biomass Burning.....	91
3.3.1.	<i>Natural emissions</i> .....	91
3.3.2.	<i>Biomass burning</i> .....	92
3.4.	Anthropogenic Emissions, 1850-2050 .....	94
3.4.1.	<i>SO<sub>2</sub> emission trends</i> .....	96
3.4.2.	<i>NO<sub>x</sub> emission trends</i> .....	97
3.4.3.	<i>VOC emission trends</i> .....	97
3.4.4.	<i>BC emission trends</i> .....	97
3.4.5.	<i>CH<sub>4</sub> emission trends</i> .....	98
3.4.6.	<i>CO emission trends</i> .....	98
3.4.7.	<i>NH<sub>3</sub>emission trends</i> .....	98
3.4.8.	<i>OC emission trends</i> .....	98
3.5.	Evaluation of differences in emissions data: case study for Asia.....	108
3.5.1.	<i>Recent emission trends, 1980-2006</i> .....	108
3.5.2.	<i>Future scenarios to 2030</i> .....	111
3.6.	Integration among emissions, modelling, and observations.....	113
3.6.1.	<i>Constraining emissions with satellite observations</i> .....	114
3.6.2.	<i>Constraining emission inventories with observation data: Case studies in the United States</i> .....	119
	References .....	124
<b>Chapter 4 Global and Regional Modelling</b> .....		<b>135</b>
4.1.	Overview .....	135
4.1.1.	<i>Modelling approaches</i> .....	135
4.1.2.	<i>Model methods for quantifying source contributions to intercontinental transport</i> .....	136
4.1.3.	<i>Role of coordinated model studies</i> .....	137



4.2.	Quantifying intercontinental transport of ozone and precursors .....	138
4.2.1.	<i>Ozone in the troposphere</i> .....	138
4.2.2.	<i>Surface ozone</i> .....	139
4.2.3.	<i>Trends in surface ozone</i> .....	141
4.2.4.	<i>Source attribution</i> .....	142
4.2.5.	<i>Source-receptor relationships for surface ozone</i> .....	143
4.2.6.	<i>Policy-relevant metrics</i> .....	149
4.2.7.	<i>Interannual variability</i> .....	151
4.2.8.	<i>Influence of intercontinental transport through the depth of the troposphere</i> .....	152
4.2.9.	<i>Import/Export budgets from different regions</i> .....	154
4.2.10.	<i>Contribution to observed ozone trends</i> .....	155
4.2.11.	<i>Robustness of HTAP S/R Results</i> .....	156
4.3.	Quantifying intercontinental transport of aerosol .....	158
4.3.1.	<i>Aerosol budgets and transport</i> .....	158
4.3.2.	<i>AEROCOM-HTAP aerosol-specific experiments</i> .....	164
4.3.3.	<i>Seasonal variation of surface aerosol concentrations</i> .....	165
4.3.4.	<i>Source attribution</i> .....	165
4.3.5.	<i>Linearity of source-receptor relationships</i> .....	167
4.3.6.	<i>Model sulphur trend evaluation</i> .....	169
4.3.7.	<i>Interannual variability and impacts of resolution on S/R relationships</i> .....	169
4.4.	Hemispheric Transport Influences on deposition .....	170
4.4.1.	<i>Deposition of sulphur and reactive nitrogen, <math>N_r</math></i> .....	170
4.4.2.	<i>S/R relationships</i> .....	172
4.4.3.	<i>The Arctic</i> .....	172
4.4.4.	<i>Attribution to source categories</i> .....	173
4.5.	Uncertainty in model estimates of intercontinental transport .....	175
4.5.1.	<i>Uncertainty in model transport processes</i> .....	175
4.5.2.	<i>The influence of model resolution</i> .....	177
4.5.3.	<i>Uncertainty in model chemical mechanisms and natural emissions</i> .....	180
4.5.4.	<i>Summary of principal sources of model uncertainty and research needs</i> .....	181
4.6.	Future changes in S/R relationships .....	184
4.6.1.	<i>Changes with future emissions</i> .....	184
4.6.2.	<i>Changes with future climate</i> .....	187
	References .....	190

**Chapter 5 Impacts on Health, Ecosystems, and Climate .....199**

5.1.	Impacts of Long-range Transport on Human Health .....	200
5.1.1.	<i>Evidence for effects of ozone and PM on human health</i> .....	200
5.1.2.	<i>Quantified influences of long-range transport on human health</i> .....	207
5.1.3.	<i>Future changes in human health impacts due to LRT</i> .....	215
5.1.4.	<i>Major uncertainties and research needs</i> .....	215
5.2.	Impact of Long-range Transport on Ecosystems .....	216
5.2.1.	<i>Evidence for effects of ozone and PM on ecosystems</i> .....	216
5.2.2.	<i>Quantified influences of ICT pollution on ecosystems</i> .....	222
5.2.3.	<i>The potential vulnerability of ecosystems to long-range transport of <math>O_3</math></i> .....	227
5.2.4.	<i>Interactions with climate change</i> .....	230
5.2.5.	<i>Interactions with other pollutants</i> .....	233

5.3.	Impact of Long-range Transport on Climate .....	234
5.3.1.	<i>Effects of ozone and particulate matter on global average radiative forcing .....</i>	235
5.3.2.	<i>Radiative Forcing of Ozone and PM: Regional Extent and Effects of Varying Precursor Emissions .....</i>	239
5.3.3.	<i>Relevance of Regional Forcings for Regional and Global Climate .....</i>	247
5.3.4.	<i>Impacts of Long-Range Transport on Climate in the Arctic .....</i>	248
5.3.5.	<i>Future Changes in Forcings .....</i>	250
5.3.6.	<i>Future Research Needs .....</i>	250
	References .....	251
	<b>Chapter 6 Summary .....</b>	<b>265</b>
6.1.	Observational Evidence for Intercontinental Transport .....	265
6.2.	Modelling Analyses of Intercontinental Transport.....	266
6.2.1.	<i>Source Attribution.....</i>	266
6.2.2.	<i>Source-Receptor Sensitivity .....</i>	268
6.3.	The Impacts of Intercontinental Transport .....	270
6.4.	Future Scenarios .....	272
6.5.	Implications for International Policy .....	273
6.6.	Further research and analysis needs .....	273
	Key Challenges.....	274

## Appendix

Appendix A	Editors, Authors, & Reviewers .....	275
------------	-------------------------------------	-----

## Tables

<b>Chapter 1</b>	<b>Conceptual Overview of Hemispheric or Intercontinental Transport of Ozone and Particulate Matter</b>	
Table 1.1.	Approximate lifetimes of trace gases and PM in the atmospheric boundary layer and the free troposphere. ....	6
<b>Chapter 2</b>	<b>Observational Evidence and Capabilities Related to Intercontinental Transport of Ozone and Particulate Matter</b>	
Table 2.1.	Current nadir-viewing satellite remote sensing of tropospheric ozone and its precursors .....	28
<b>Chapter 3</b>	<b>Emission Inventories and Projections</b>	
Table 3.1.	EDGAR-HTAP categorisation of emission sources (as applied for the gridded maps) .....	79
Table 3.2.	Overview of the coverage of compounds and regions in the official emission datasets. ....	81
Table 3.3.	Some estimates of global annual emissions from natural sources.....	92
Table 3.4.	Summary of methods currently used to constrain emissions from modelling and observation .....	114
<b>Chapter 4</b>	<b>Global and Regional Modelling</b>	
Table 4.1.	Summary of model studies performed under the HTAP intercomparison .....	138
Table 4.2.	Annual and spatial mean surface O <sub>3</sub> response to 20% decreases in anthropogenic precursor emissions (NO <sub>x</sub> , CO, NMVOC, plus aerosols and their precursors). ....	144
Table 4.3.	Annual and seasonal mean estimates for the contribution to surface O <sub>3</sub> over the receptor region from anthropogenic O <sub>3</sub> precursor emissions in foreign source regions.....	146
Table 4.4.	Multi-model derived relative annual intercontinental responses (RAIRs) for surface concentration, deposition and column load of anthropogenic black carbon (BC), particulate organic matter (POM), sulphate (SO <sub>4</sub> ) and all sulphur species (SO <sub>2</sub> +SO <sub>4</sub> ).....	160
Table 4.5.	Multi-model (9 models) response of annual mean surface PM estimated as the sum of SO <sub>4</sub> and POM; column load of sulphate; and POM in receptor regions to 20% reductions of anthropogenic gas and aerosol emissions in the source regions.....	162
Table 4.6.	Surface concentrations in µg/m <sup>3</sup> in five receptor regions based on the median values of annual averages in 2001 from six global models.....	167
Table 4.7.	Fractional contribution to total N <sub>r</sub> deposition changes over each receptor region resulting from 20% anthropogenic NO <sub>x</sub> emission perturbations in each of the four source regions. ....	172
Table 4.8.	The influence of specific emissions sectors on daily average inorganic PM <sub>2.5</sub> concentrations over the U.S./N. America. ....	174
Table 4.9.	Relative annual intercontinental response under different future emission scenarios. ....	186

<b>Chapter 5</b>	<b>Impacts on Health, Ecosystems, and Climate</b>	
Table 5.1	Results from selected cohort and time series studies of PM and human mortality .....	205
Table 5.2.	Results from selected cohort and time series studies of ozone and human mortality .....	207
Table 5.3.	Annual avoided premature cardiopulmonary mortalities following 20% NO <sub>x</sub> , NMVOC, and CO emission reductions in each region, for the HTAP SR6 multi-model mean .....	209
Table 5.4.	Annual avoided premature cardiopulmonary and lung cancer mortalities due to 20% reductions in primary PM <sub>2.5</sub> and PM precursor emissions in each region.....	212
Table 5.5.	O <sub>3</sub> metrics used to derive dose-response relationships for ecosystem protection in air quality management. ....	219
Table 5.6.	Multi-model derived relative annual intercontinental response (RAIR) for aerosol optical depth for four HTAP regions, in SR6 simulations relative to SR1, by chemical component. ....	244
Table 5.7.	As Table 5.3.1, but for RAIR for TOA all-sky aerosol direct RF. ....	244
Table 5.8.	Global annual average TOA all-sky aerosol direct RF in response to the 20% reduction of anthropogenic emissions in 4 source regions, for the mean ± std. dev for SR1 and SR6 simulations of six HTAP models.....	245
Table 5.9.	Global annual average TOA all-sky aerosol direct RF efficiency relative to emissions from 4 source regions as derived from analysis of SR1 and SR6 runs of six HTAP models. ....	246

## Figures

<b>Chapter 1</b>	<b>Conceptual Overview of Hemispheric or Intercontinental Transport of Ozone and Particulate Matter</b>	
Figure 1.1.	Comparison of surface ozone mixing ratios at Mace Head.....	2
Figure 1.2.	Distribution of global anthropogenic-NO <sub>x</sub> emissions and biomass burning NO <sub>x</sub> from natural and anthropogenic fires.....	3
Figure 1.3.	Global distribution of human population and anthropogenic NO <sub>x</sub> emissions in the year 2005 .....	4
Figure 1.4.	Pathways of intercontinental pollution transport in the Northern Hemisphere .....	5
Figure 1.5.	General intercontinental transport processes.....	7
Figure 1.6.	Source attribution of the ozone found at a rural location in southern England .....	10
Figure 1.7.	Schematic diagram showing some of the main features of the atmosphere related to the transport of air pollutants.....	12
Figure 1.8.	Conceptual model of the airstreams within a mid-latitude cyclone; GOES-EAST infrared image.....	13
Figure 1.9.	A depiction of the links between domestic and foreign air pollution control policies, air quality, global climate change, and the role of HTAP.....	19
<b>Chapter 2</b>	<b>Observational Evidence and Capabilities Related to Intercontinental Transport of Ozone and Particulate Matter</b>	
Figure 2.1.	Summertime probability distribution functions of CO and O <sub>3</sub> measured between 2 and 10 km altitude by MOZAIC .....	27
Figure 2.2.	Example of long-range transport from Alaskan and Canadian wildfires to Europe observed by MOPITT over 15-23 July 2004. ....	29
Figure 2.3.	Example of tropospheric ozone columns determined by residual from OMI observations of total column O <sub>3</sub> , and MLS observations of stratospheric O <sub>3</sub> .....	29
Figure 2.4.	Time series of 30-min average CO, NO <sub>y</sub> and O <sub>3</sub> , and 1-hour average BC observations at the PICO-NARE Observatory (Azores, Portugal) during transport of boreal wildfire emissions to the site.....	30
Figure 2.5.	Ozone mixing ratio cross section in ppb measured at Observatoire de Haute Provence in July 2004; and vertical cross section of aerosol scattering ratio on the same days. ....	31
Figure 2.6.	O <sub>3</sub> and BC measured March-August 2006 at the Nepal Climate Observatory-Pyramid (NCO-P) at 5.1 km asl in the Khumbu valley of the Himalayas .....	32
Figure 2.7.	Springtime trends in O <sub>3</sub> concentrations measured in Europe; and in western North America and Japan. ....	34
Figure 2.8.	Average annual linear trends in O <sub>3</sub> concentrations in different seasons in Europe, North America and Japan. ....	35
Figure 2.9.	Monthly average O <sub>3</sub> mixing ratios in baseline air masses arriving at Mace Head, Ireland from 1987 – 2009 .....	37
Figure 2.10.	Correlation between the interpolated daily maximum 8-hr surface O <sub>3</sub> averages at Tuscan Butte with the O <sub>3</sub> mixing ratio measured by sondes 22 hours earlier at Trinidad Head.....	38
Figure 2.11.	A dust event that originated in the Sahara desert on 17 August 2007 and was transported to the Gulf of Mexico .....	40
Figure 2.12.	Evolution of dust plume characteristics for four case studies of dust transported from Africa to the Caribbean across the Atlantic in six days.....	41
Figure 2.13.	Estimates of annual pollution aerosol flux leaving Asia in the West Pacific and arriving in North America in the East Pacific for different latitude ranges.....	41
Figure 2.14.	Aerosol transport event observed at Cape Hedo, a sea level site at the northern tip of Okinawa Japan. ....	42
Figure 2.15.	Average sulphate levels measured at marine sites in the Northern and Southern hemispheres.....	43

Figure 2.16.	Concentrated trans-Pacific pollutant transport event observed at a mountaintop site near the west coast of North America.....	44
Figure 2.17.	Aerosol measurements marked by variation in CO concentrations..	45
Figure 2.18.	Annual mean nss-sulphate and nitrate concentrations on Bermuda during on-shore winds compared to eastern US SO <sub>2</sub> (Tg S/y) and NO <sub>x</sub> emissions (Tg N/yr).....	46
Figure 2.19.	Comparison of global mean AOD over ocean derived from different satellite input data and retrieval algorithms for an overlapping period since 2000..	48
Figure 2.20.	Contributions from three sources to surface PM <sub>2.5</sub> in three U.S. cities during an April 2001 episode of Asian dust transported to North America. ....	48
Figure 2.21.	Measured O <sub>3</sub> mixing ratios of 55-60 ppbv at Mt. Bachelor Observatory, Oregon on 1 May, 2006.....	51
Figure 2.22.	<sup>208</sup> Pb/ <sup>207</sup> Pb vs. <sup>206</sup> Pb/ <sup>207</sup> Pb in airborne particles at sites in California, in San Francisco Bay waters, and from a variety of Chinese sources. ....	55
Figure 2.23.	Ice-core records of atmospheric lead (Pb) pollution in central Greenland (altitude ~3000 m) and from Mt. Logan (altitude ~5500 m), Yukon Territory, Canada.....	56
Figure 2.24.	Trajectories 6 days backwards and forwards from the UK FAAM BAe146 flight track on 19 July 2004 showing links with upwind and downwind flights.....	57
Figure 2.25.	O <sub>3</sub> :CO correlations along Lagrangian plume match segment of a flight on 22 July 2004 by German DLR Falcon.....	58
Figure 2.26.	Network of surface-based remote observatories organized through the World Meteorological Organization's Global Atmospheric Watch (GAW) Program. ....	59
Figure 2.27.	Current locations in the Northern Hemisphere with frequent ozone and PM profiling of the troposphere by aerosol lidars, ozone lidars, and weekly ozonesondes .....	61
<b>Chapter 3</b>	<b>Emission Inventories and Projections</b>	
Figure 3.1.	Gridded maps of anthropogenic emission totals in 2005 for each compound in the EDGAR-HTAP emissions database .....	82
Figure 3.2.	Gridded maps of sector-specific anthropogenic emissions in 2005 in the EDGAR-HTAP emissions database .....	83
Figure 3.3.	Total global anthropogenic emissions of air pollutants and methane for the SRES scenarios .....	86
Figure 3.4.	Comparison between EDGARv3.2FT2000 and RAPIDC emission inventories for SO <sub>2</sub> for Botswana in the year 2000.....	87
Figure 3.5.	Comparison of the 2000 EDGAR-HTAP inventory to the emission inputs used in the SR1 run of the HTAP multi-model experiments representing 2001.....	90
Figure 3.6.	NO <sub>x</sub> emissions from biomass burning (forest fires, savannah burning, and grassland fires) by main world regions in the period 1970-2005.....	93
Figure 3.7.	Past, present and projected future trends of CO emissions from biomass burning (forest fires, savannah burning and agricultural residues in field burning) based on RCP scenarios.....	95
Figure 3.8.	Contribution of type of burning to global biomass burning (forest fires, savannah burning, and agricultural residues in field burning) emission based on AIM RCP 6.0 dataset.....	95
Figure 3.9.	Evolution of the spatial distribution of NO <sub>x</sub> (kg m <sup>-2</sup> sec <sup>-1</sup> ) emissions from forest fires in 2000, 2005, 2030, 2050 and 2100 based on AIM (RCP 6.0) datasets .....	96
Figure 3.10.	SO <sub>2</sub> emissions regional trends, future predictions, and sources. ....	100
Figure 3.11.	NO <sub>x</sub> emissions regional trends, future predictions, and sources. ....	101
Figure 3.12.	VOC emissions regional trends, future predictions, and sources. ....	102
Figure 3.13.	BC emissions regional trends, future predictions, and sources. ....	103
Figure 3.14.	CH <sub>4</sub> emissions regional trends, future predictions, and sources.....	104

Figure 3.15.	CO emissions regional trends, future predictions, and sources.....	105
Figure 3.16.	NH <sub>3</sub> emissions regional trends, future predictions, and sources. ....	106
Figure 3.17.	OC emissions regional trends, future predictions, and sources.....	107
Figure 3.18.	Time series of SO <sub>2</sub> , NO <sub>x</sub> , and BC emissions in Asia. ....	109
Figure 3.19.	Time series of SO <sub>2</sub> , NO <sub>x</sub> , and BC emissions in China. ....	110
Figure 3.20.	Schematic illustration of top-down approaches used to constrain emissions.....	113
Figure 3.21.	Tropospheric NO <sub>2</sub> columns for 2004-2005 determined from the SCIAMACHY satellite instrument; and Surface NO <sub>x</sub> emissions for 2004- 2005 .....	115
Figure 3.22.	Annual U.S. emissions from power plants and on-road vehicles from 1980- 2007, as estimated in six U.S. inventories.....	120
Figure 3.23.	Mixing ratios of VOC species from five measurement programs.....	122
Figure 3.24.	VOC emissions from on-road vehicles in the U.S. estimated by two emission inventories. ....	122
Figure 3.25.	Semi-log plot of temporal trends of observed ambient benzene-to-acetylene ratios from field study data compared to inventory ratios.....	123
 <b>Chapter 4 Global and Regional Modelling</b>		
Figure 4.1.	Schematic of the Eulerian forward modelling approach. ....	136
Figure 4.2.	Comparison of observed O <sub>3</sub> profiles from Goose Bay, Canada, Uccle, Belgium, and Yakutsk, Siberia with modelled profiles from the HTAP intercomparison. ....	139
Figure 4.3.	Comparison of monthly mean surface O <sub>3</sub> from models contributing to the HTAP intercomparison compared with observed O <sub>3</sub> from measurement networks over the northeastern U.S. (CASTNet), central Europe (EMEP) and Japan (EANET).....	140
Figure 4.4.	Comparison of maximum daily 8-hour averaged surface O <sub>3</sub> (MDA8 O <sub>3</sub> ) over different parts of the U.S. in spring 2001 from models contributing to the HTAP intercomparison with observations from the CASTNet network.....	140
Figure 4.5.	Comparison of surface O <sub>3</sub> trends from CAM-Chem and GISS-PUCCINI against observations at Zugspitze and Hohenpeissenberg, Germany and US Pacific Coast sites.....	141
Figure 4.6.	Source attribution for tropospheric O <sub>3</sub> over the globe and for annual mean surface O <sub>3</sub> over the four HTAP regions estimated by the report authors from source contributions in earlier published studies.....	143
Figure 4.7.	Model ensemble mean surface O <sub>3</sub> decrease in springtime (in ppbv) for the combined 20% emission reduction over each source region showing the spatial variation over each region and over the Arctic. ....	145
Figure 4.8.	Monthly mean surface O <sub>3</sub> decreases (in ppbv) over receptor regions for the combined 20% emission reductions (HTAP SR6 simulations) showing the seasonality of the responses and the variability between models.....	147
Figure 4.9.	Model ensemble surface O <sub>3</sub> decrease (ppb), annually and spatially averaged over the HTAP regions from 20% decreases in anthropogenic emissions of NO <sub>x</sub> , CO and NMVOC versus 20% decreases in anthropogenic CH <sub>4</sub> . ....	148
Figure 4.10.	The multi-model mean springtime response of daily maximum 8-hour surface O <sub>3</sub> over 9 regions of the U.S. to 20% anthropogenic emission reductions in all precursors from European, East Asian and South Asian sources.....	150
Figure 4.11.	Enhancement to afternoon background O <sub>3</sub> in surface air over the U.S. in summer due to anthropogenic precursor emissions from both Asia and Europe .....	151
Figure 4.12.	Change in surface maximum 8-hour O <sub>3</sub> (MDA8 O <sub>3</sub> ) in model grid cells containing major cities from HTAP intercomparison simulations with all anthropogenic emissions reduced by 20% (SR6 runs). ....	152

Figure 4.13.	The altitude profile of S/R relationships for O <sub>3</sub> (in ppbv) based on 20% emissions reductions used in the HTAP intercomparison, showing the seasonal and altitudinal evolution of these relationships.....	153
Figure 4.14.	Reductions in annual mean O <sub>3</sub> columns over each receptor region resulting from a 20% decrease in NO <sub>x</sub> emissions from each source region, and from all ‘foreign’ source regions.....	154
Figure 4.15.	Export fractions for NO <sub>y</sub> from each HTAP source region for each season for 15 models from the HTAP intercomparison .....	155
Figure 4.16.	Changes in annual mean surface O <sub>3</sub> over the HTAP receptor regions between 1960 and 2000 based on linearization of the results from six models that contributed to all SR simulations in the HTAP intercomparison. ....	156
Figure 4.17.	Seasonal mean percentage contribution from source regions to receptor regions in East Asia for spring and summer averaged over 6 years.....	157
Figure 4.18.	Sensitivity of surface O <sub>3</sub> abundance at Mt. Bachelor in the western U.S. to O <sub>3</sub> production in different regions of the world as inferred from the GEOS-Chem adjoint model.....	157
Figure 4.19.	Sensitivity of the calculated S/R relationship to the magnitude of NO <sub>x</sub> emission changes over Europe relative to current conditions. ....	158
Figure 4.20.	Relative annual intercontinental response of total sulphate deposition and sulphate aerosol column burden over each receptor region. ....	161
Figure 4.21.	Lifetime of sulphate originating from different regions showing the mean lifetime and lifetime in different models. ....	161
Figure 4.22.	Relative annual intercontinental response of surface PM concentration over the HTAP regions.....	162
Figure 4.23.	Model mean sulphur budget averaged over all four HTAP regions.....	163
Figure 4.24.	Sulphur export fraction out of source regions as computed by HTAP models, shown from all four HTAP regions as a function of dry removal within source regions.....	164
Figure 4.25.	Regional domains for anthropogenic and biomass burning sources in SR6 and SR6z, for biomass burning sources in SR6b, and for dust source regions in SR6d.....	164
Figure 4.26.	Emissions of anthropogenic sulphur and BC in anthropogenic source regions, POM in biomass burning regions, and dust in desert regions. ....	165
Figure 4.27.	Seasonal variations of surface concentrations of sulphate, BC, POM and dust for the five receptor regions from six models .....	166
Figure 4.28.	Sulphate wet deposition retrieved from the HTAP NILU database against three hindcast simulations.. ....	169
Figure 4.29.	Averaged annual import and export fluxes (Tg day <sup>-1</sup> ) from/into HTAP regions for total PM and their standard deviations from 10 year simulations.....	170
Figure 4.30.	Total ensemble-mean deposition of oxidized sulphur and the effects of 20% emission reductions in the four HTAP regions .....	171
Figure 4.31.	Total ensemble-mean deposition of N <sub>r</sub> from the HTAP intercomparison and the effects of 20% emission reductions in the four HTAP regions. ....	171
Figure 4.32.	Sensitivity of surface CO, SO <sub>4</sub> , BC and O <sub>3</sub> over the Arctic to emissions from the principal HTAP source regions. ....	172
Figure 4.33.	Accumulated deposition of BC on snow from an ensemble of 13 models contributing to the HTAP intercomparison. ....	173
Figure 4.34.	Normalized sensitivities of the surface PM <sub>2.5</sub> concentrations in April with respect to stack SO <sub>x</sub> emissions, NO <sub>x</sub> surface emissions, SO <sub>4</sub> <sup>2-</sup> initial conditions, and NH <sub>4</sub> <sup>+</sup> initial conditions.. ....	173
Figure 4.35.	Attribution of aircraft, shipping and traffic sectors on column and surface ozone .....	175
Figure 4.36.	Ratio of CO abundance in the lowest 3 km of the atmosphere to the abundance in the lowest 500 m for North American sources over North America and for South Asian sources over North America .....	176



Figure 4.37.	Comparison of CO vertical distributions in the high-resolution (WRF-Chem) and global-scale (MOZART) models with aircraft observations of a pollution lofting event over East Asia. ....	178
Figure 4.38.	Calculated eastward flux of CO through a wall at 25-40°N along 140°E at altitudes between 4-8.5 km calculated with WRF-Chem and MOZART models. ....	178
Figure 4.39.	Impacts of model resolution on the calculated O <sub>3</sub> response over East Asia in March 2001 to a 20% reduction in anthropogenic emissions of O <sub>3</sub> precursors in Europe. ....	179
Figure 4.40.	Seasonal variations in the effect of 20% emission changes in E. Asia on monthly mean surface O <sub>3</sub> in major cities in the U.S. and the effect of N. America emission changes on cities in East Asia from studies with the CMAQ model at 36-km resolution. ....	180
Figure 4.41.	Uncertainties associated with modelling intercontinental transport and its impacts on source/receptor relationships and source attribution as summarised in this chapter. ....	182
Figure 4.42.	Mean surface O <sub>3</sub> changes over the four HTAP receptor regions following the four RCP scenarios from 2000 to 2050, based on linearization of the six models that contributed results to all SR simulations in the HTAP intercomparison. ....	185
Figure 4.43.	Regional annual mean surface O <sub>3</sub> changes between 2000 and 2030 following the most polluted RCP 8.5 emission scenario for three models contributing to the HTAP Future Emission runs. ....	185
Figure 4.44.	Contribution to annual mean surface O <sub>3</sub> changes for RCP 8.5 and RCP 2.6 scenarios from changes in CH <sub>4</sub> concentration, emission changes over the receptor region and emission changes from outside the receptor region ....	186
Figure 4.45.	Difference in annual-average surface O <sub>3</sub> concentrations between the 2090s and 2000s decade for GISS-PUCCINI-ModelE, STOC-HadAM3 and UM-CAM. ....	189
Figure 4.46.	Impact of 20% reductions of the O <sub>3</sub> precursor emissions (NO <sub>x</sub> , NMVOCs, and CO) in the NA source region on annual-mean surface O <sub>3</sub> over the receptor regions for the 2000s and 2090s decades. ....	190
 <b>Chapter 5 Impacts on Health, Ecosystems, and Climate</b>		
Figure 5.1.	Ozone air quality standards in ppb for different nations, as well as international guidelines and estimates of preindustrial background and present-day baseline ....	199
Figure 5.2.	Current 24-hr. and annual mean PM <sub>2.5</sub> standards for selected countries, and U.S. allowable 24-hr emissions increment for Class I areas under the Prevention of Significant Deterioration rule ....	200
Figure 5.3.	Estimates of the effect on all natural mortality per 10 µg m <sup>-3</sup> increase in PM reported in several recent meta-analyses and multicity studies. ....	203
Figure 5.4.	Relative risk of mortality from all-natural causes and ischemic heart disease per 10 µg m <sup>-3</sup> PM <sub>2.5</sub> from current US and European cohort studies ....	204
Figure 5.5.	Annual avoided premature cardiopulmonary mortalities per 1,000 km <sup>2</sup> and per million people resulting from 20% NO <sub>x</sub> , NMVOC, and CO emission reduction in the region shown and a 20% global methane mixing ratio reduction. ....	209
Figure 5.6.	Annual avoided premature nonaccidental mortalities in each region from 20% NO <sub>x</sub> , NMVOC, and CO emission reductions in the same region. ....	210
Figure 5.7.	Annual avoided premature mortalities from 10% anthropogenic NO <sub>x</sub> reductions in each of nine world regions, at steady state and using a low-concentration threshold of 25 ppb. ....	211
Figure 5.8.	Annual adult premature mortalities in each receptor region associated with inter-continental transport of fine aerosols (PM <sub>2.5</sub> ) and non-dust aerosols from the nine other source regions. ....	214

Figure 5.9.	Influence potential ratios of inter-continental transport of fine (PM <sub>2.5</sub> ) sulphate aerosols. ....	215
Figure 5.10.	Relative contribution of each HTAP region to crop damage in each of 4 regions for run SR6 using Mx and AOT40 indices. ....	224
Figure 5.11.	Time development of soil acidification damage according to a modelling study for Asia using best available data for soil and deposition parameters .....	226
Figure 5.12.	The WWF G200 regions, showing total N deposition rates for the year 2000 .....	227
Figure 5.13.	Average wheat crop production losses due to O <sub>3</sub> estimated for the year 2000 using European and North American concentration based exposure-response relationships. ....	228
Figure 5.14.	Global assessment of the key biodiversity areas at high risk from O <sub>3</sub> impacts; projected percent decrease in gross primary productivity due to O <sub>3</sub> within the Global 200 priority conservation areas.....	231
Figure 5.15.	Change in land carbon at the end of the year following the HTAP 20% NO <sub>x</sub> emission reductions. ....	232
Figure 5.16.	Simulated change in diffuse fraction contribution to land carbon accumulation between 1950 and 1980 .....	233
Figure 5.17.	IPCC AR4 summary of averages and ranges of global mean radiative forcing in units of Watts per square meter between 1750 and 2005 for major forcing agents, including CO <sub>2</sub> , CH <sub>4</sub> , N <sub>2</sub> O, ozone, land use, aerosols, and solar irradiance. ....	236
Figure 5.18.	Schematic diagram showing the major radiative forcing mechanisms related to aerosols.....	237
Figure 5.19.	Annual total-sky instantaneous RF (mWm <sup>-2</sup> ) due to short-term changes in O <sub>3</sub> from a 10% reduction in surface anthropogenic NO <sub>x</sub> emissions from each of nine world regions .....	240
Figure 5.20.	Change in annual average RF per unit change in NO <sub>x</sub> emissions for 10% regional NO <sub>x</sub> reductions in Figure 5.3.3.....	240
Figure 5.21.	Radiative forcing from 1750 to 2000 .....	241
Figure 5.22.	Change in global surface temperature for the years following a 1 Tg emission reduction in the first year. The normalisation is per Tg N, C and CO for NO <sub>x</sub> , VOC and CO. ....	242
Figure 5.23.	The annual average all-sky aerosol direct RF (Wm <sup>-2</sup> ) at the top of atmosphere and at the surface resulting from 20% reductions of anthropogenic emissions over North America, Europe, East Asia, and South Asia.....	243
Figure 5.24.	Global annual mean all-sky SW DRF at top-of-atmosphere, at surface, and in the atmosphere by BC emissions from different regions. ....	246
Figure 5.25.	Forcing mechanisms in the Arctic environment resulting from the poleward transport of mid-latitude gas and particulate phase pollutants. The season of maximum forcing at the surface (F <sub>s</sub> ) is indicated for each forcing agent .....	248
Figure 5.26.	Estimates of the contribution of particular species to preindustrial to present-day Arctic surface temperature trends.....	249

# Chemical Symbols, Acronyms and Abbreviations

## Chemical Abbreviations

C – carbon  
CH<sub>4</sub> – methane  
CO – carbon monoxide  
CO<sub>2</sub> – carbon dioxide  
F-gases – fluorine-containing halogenated substances that are potent greenhouse gases:  
hydrofluorocarbons (HFCs), perfluorocarbons (PFCs), and sulfur hexafluoride (SF<sub>6</sub>)  
HCHO – formaldehyde  
Hg – mercury  
H<sub>2</sub>SO<sub>4</sub> – sulphuric acid  
HNO<sub>3</sub> – nitric acid  
HO<sub>x</sub> – hydrogen oxide radicals  
Mn – manganese  
N – nitrogen  
NH<sub>3</sub> – ammonia  
N<sub>2</sub>O – nitrous oxide  
N<sub>2</sub>O<sub>5</sub> – dinitrogen pentoxide  
NO – nitric oxide  
NO<sub>2</sub> – nitrogen dioxide  
NO<sub>3</sub> – nitrate  
NO<sub>x</sub> – nitrogen oxides  
NO<sub>y</sub> – total inorganic oxidized nitrogen  
Nr – total reactive nitrogen (including NO<sub>y</sub> and NH<sub>x</sub>)  
nss-SO<sub>4</sub> – non-seasalt sulphate  
OH – hydroxyl radical  
O<sub>3</sub> – ozone  
P – phosphorus  
Pb – lead  
Rn – radon  
Si – silicon  
SO<sub>2</sub> – sulphur dioxide  
SO<sub>4</sub> – sulphate  
SO<sub>x</sub> – sulphur oxides  
Sr – strontium  
δ<sup>34</sup>S – a stable isotope of sulphur

## Acronyms and Abbreviations

AAOD – Absorption Aerosol Optical Depth  
ABC – Atmospheric Brown Cloud  
ABL – Atmospheric Boundary Layer  
AC&C – Atmospheric Chemistry and Climate Initiative  
ACCENT – Atmospheric Composition Change the European Network of Excellence  
ACE – Aerosol Characterization Experiments  
ACE-Asia – Asian Pacific Regional Aerosol Characterization Experiment  
ACS – American Cancer Society  
ACT – Advanced Combustion Technology  
AEROCE – Atmosphere/Ocean Chemistry Experiment

AEROCOM – Aerosol Comparisons between Observations and Models (a global aerosol model intercomparison project)  
 AERONET – NASA Aerosol Robotic Network  
 AERONOX – a soil emissions model  
 AF – North Africa  
 AFstY – accumulated stomatal ozone flux  
 AHSMOG – Adventist Health Study on the Health Effects of Smog  
 AIM – Asian Pacific Integrated Model  
 AIRS – Atmospheric Infrared Sounder  
 ALTO – Airborne Lidar for Tropospheric Ozone  
 AMS – Aerosol Mass Spectrometer  
 AOD – Aerosol Optical Depth  
 AOTxx – Accumulated Ozone Concentration over a Threshold over a Growing Season, where xx is the threshold concentration in ppb  
 APHENA – Air Pollution and Health: A European and North American Approach  
 APINA – Air Pollution Information Network for Africa  
 AQ – Air Quality  
 AQS – Air Quality Standards  
 Aqua – A NASA Polar-Orbiting Satellite  
 AR – Arctic  
 AS – Asia  
 ASea – Adjacent Marine Regions  
 ASIA – Asia excluding the Middle East  
 ASL – above sea level  
 ATLID – Atmospheric Lidar, instrument planned for Earth Clouds, Aerosols, and Radiation Explorer satellite mission  
 ATS – American Thoracic Society  
 ATSR – Along Track Scanning Radiometer  
 Aura – a NASA polar orbiting satellite  
 AVHRR – Advance Very High Resolution Radiometer  
 BC – Black Carbon  
 C3 – the photosynthetic mechanism used by most plants  
 C4 – an alternative photosynthetic pathway  
 CALIOP – Cloud-Aerosol Lidar with Orthogonal Polarisation  
 CALIPSO – Cloud-Aerosol Lidar and Infrared Pathfinder Satellite Observations  
 CAM – Community Atmosphere Model  
 CAMCHEM – Community Atmosphere Model with Chemistry  
 CAPMoN – Canadian Air and Precipitation Monitoring Network  
 CAPTEX – Cross-Appalachian Tracer Experiment  
 CARIBIC – Civil Aircraft for Regular Investigation of the Atmosphere Based on an Instrument  
 CASTNET – Clean Air Status and Trends Network  
 CCB – Cold Conveyor Belt  
 CCC – Chemical Coordinating Centre  
 CCN – Cloud Condensation Nuclei  
 CCSP – U.S. Climate Change Science Program  
 CDNC – Cloud Droplet Number Concentration  
 CEIP – Centre on Emission Inventories and Projections  
 CEMs – Continuous Emission Monitoring Systems  
 CERE – Centre d’Enseignement et de Recherche en Environnement Atmosphérique  
 CESY – China Energy Statistics Yearbook  
 CHASER – Chemical Atmospheric General Circulation Model for Study of Atmospheric Environment and Radiative Forcing

CHN – China  
 CHN-NCP – North China Plain  
 CHN-NE – NE China  
 CHN-SE – SE China  
 CHN-YRB – Yangtze River Basin  
 CIESIN – Center for International Earth Science Information Network  
 CIFEX – Cloud Indirect Forcing Experiment  
 CIRES – Cooperative Institute for Research in Environmental Science  
 CLE – Current Legislation Scenario  
 CLRTAP – Convention on Long Range Transboundary Air Pollution  
 CMAQ – Community Multiscale Air Quality Model  
 CMAQ DDM – Community Multiscale Air Quality Model with Direct Decoupled Method  
 CMDL – Climate Modeling and Diagnostics Laboratory  
 CMIP5 – Climate Model Intercomparison Program #5  
 CNR – The National Research Council, Italy  
 CNRS – Centre National de la Recherche Scientifique, France  
 CONUS – Continental United States  
 CORINAIR – Coordination of Information on the Environment – Air  
 COSAM – Comparison of Large Scale Atmospheric Sulphate Aerosol Models  
 CRF – Concentration-Response Function  
 CTM – Chemical Transport Model  
 CUNY – The City University of New York  
 DA – Dry Airstream  
 DJF – December, January, February  
 DLR – Deutsches Zentrum fuer Luft  
 DMS – Dimethylsulfide  
 DU – Dobson Units  
 EA – East Asia  
 EANET – Acid Deposition Monitoring Network in East Asia  
 EARLINET – European Aerosol Research Lidar Network  
 EC – Elemental Carbon  
 ECB – East Siberia  
 ECHAM5-HAMMOZ – an atmospheric model (ECHAM), with aerosol (HAM) and  
 tropospheric chemistry (MOZ) modules  
 ECMWF – European Centre for Medium Range Weather Forecasting  
 EDGAR – Emissions Database for Global Atmospheric Research  
 EDGAR-HYDE – An extension of the EDGAR data set back to 1890  
 EEA – European Environment Agency  
 EMEP – Cooperative Programme for Monitoring and Evaluation of the Long-range  
 Transmission of Air Pollutants in Europe  
 ENSO – El Niño Southern Oscillation  
 ENVISAT – European Space Agency Environmental Satellite  
 EOTC – European Open Top Chamber  
 ES – Event Simulations  
 ETEX – European Tracer Experiment  
 EU – European Union  
 FC – Future Climate  
 FE – Future Emissions  
 FLEXPART – a Lagrangian particle dispersion model  
 FO3 – Calculated Stomatal Flux into the Plant  
 FRSGC – Frontier Research System for Global Change, Japan  
 Fs – Maximum Forcing at the Surface  
 FSU – Former Soviet Union  
 FT – Free Troposphere  
 GACP – Global Aerosol Climatology Project

GAINS – Greenhouse gas and Air pollution Interactions and Synergies  
 GAM – Generalized Additive Model  
 GASP – Aerosol/Smoke Product from the GOES EAST satellite  
 GAW – Global Atmospheric Watch Programme (within WMO)  
 GCAM – Global Change Assessment Model  
 GCM – General Circulation Model  
 GEMAQ – Global Environmental Multiscale Air Quality Model  
 GEMS – Global and Regional Earth-system (Atmosphere) Monitoring using Satellite and In-situ Data  
 GEO – Geostationary Orbit  
 GEOS-CHEM – A global 3-D atmospheric composition model driven by data from the Goddard Earth Observing System  
 GFDL – Geophysical Fluid Dynamics Laboratory, NOAA, U.S.  
 GFED – Global Fire Emissions Database  
 GHG – Greenhouse Gases  
 GICC – Gestion et Impacts du Changement Climatique  
 GISS – Goddard Institute for Space Studies, NASA, U.S.  
 GISS-PUCCINI – GISS model for Physical Understanding of Composition-Climate Interactions and Impacts  
 GMI – Global Modeling Initiative  
 GOCART – Goddard Global Ozone Chemistry Aerosol Radiation Transport  
 GOES-EAST – Geostationary Operational Environmental Satellite, Eastern Continental United States  
 GOME – Global Ozone Monitoring Experiment  
 GPP – Gross Primary Productivity  
 GPWv3 – Gridded Population of the World, Version 3  
 GRACE – Gravity Recovery and Climate Experiment  
 GRAPE – Global Retrieval of ATSR Cloud Parameters and Evaluation  
 GWEM – Global Wildland Fire Emission Model  
 GWP – Global Warming Potential  
 GWP100 – Global Warming Potential Over 100 Years  
 HadAM3 – U.K. Meteorological Office Hadley Centre Earth Systems Climate Model  
 HadGEM – U.K. Meteorological Office Hadley Centre Global Environmental Model  
 HEI – Health Effects Institute  
 hPa – hectopascal  
 HPO – Mt. Happo, Japan  
 HTAP – Hemispheric Transport of Air Pollution  
 i – Index  
 IAGOS – Integration of routine Aircraft measurements into a Global Observing System  
 IASI – Infrared Atmospheric Sounding Interferometer  
 ICARTT – International Consortium for Atmospheric Research on Transport and Transformation  
 ICP – International Cooperative Programme  
 ICT – Intercontinental Transport  
 IDC+ – Other South East Asia  
 IEA – International Energy Agency  
 IGAC – International Global Atmospheric Chemistry  
 IGAC Lagrangian 2K4 – First Inter-Continental Pseudo-Lagrangian Experiment  
 IIASA – International Institute for Applied Systems Analysis  
 IMAGE – Integrated Model to Assess the Global Environment  
 IMPACT – Integrated Massively Parallel Atmospheric Chemical Transport Model  
 IMPROVE – Interagency Monitoring of Protected Visual Environments  
 IN – Indian Subcontinent  
 INCA – Interaction of Chemistry and Aerosol Model  
 INDOEX – Indian Ocean Experiment

INTEX – Intercontinental Chemical Transport Experiment  
 IPCC – Intergovernmental Panel on Climate Change  
 IPCC AR4 – Intergovernmental Panel on Climate Change Fourth Assessment Report  
 IPCC AR5 – Intergovernmental Panel on Climate Change Fifth Assessment Report  
 IPCC SRES – IPCC Special Report on Emission Scenarios, 2000  
 IPs – Influence Potentials  
 ITCT – Intercontinental Transport and Chemical Transformation Experiment  
 ITCT-2K2 – Intercontinental Transport and Chemical Transformation 2002 Experiment  
 ITOP – Intercontinental Transport of Ozone and Precursors  
 ITZ – Intertropical Convergence Zone  
 JGCRI – Joint Global Change Research Institute  
 JGSEE – The Joint Graduate School of Energy and Environment  
 JJA – June, July, August  
 JOSIE – Juelich Ozone Sonde Intercomparison Experiment  
 JPN – Japan  
 JPN-E+W – Korea and Mainland Japan  
 JRC – Joint Research Centre  
 K – Kelvin  
 km – kilometers  
 KOR – Korea  
 L – Low  
 LAM – Latin America and Caribbean  
 LATMOS-IPSL – Laboratoire Atmospheres, Milieux et Observations Spatiales-Pierre  
     Simon Laplace Institute  
 LDMz – Laboratoire de Meteorologie Dynamique Zoom model  
 LEO – Low Earth Orbit  
 LLGE – Laboratoire de Glaciologie et Géophysique de l'Environnement  
 LLGHGs – Long-lived Greenhouse Gases  
 LLNL – Lawrence Livermore National Lab, U.S.  
 LMD-IPSL – Laboratoire de Météorologie Dynamique-Pierre Simon Laplace Institute  
 LPDM – Lagrangian Particle Dispersion Models  
 LRT – Long-range Transboundary  
 LRTAP – Long-range Transboundary Air Pollution  
 LS – Lower Stratosphere  
 LWC – Liquid Water Content  
 m – meters  
 M12 – Daylight (12 hours) Growing Season Average  
 M7 – Daylight (7 hours) Growing Season Average  
 MACC – Monitoring Atmospheric Composition and Climate  
 MAF – Middle East plus Africa  
 MAM – March, April, May  
 MARM – Ministry of the Environment, Rural and Marine Media of Spain  
 MBO – Mt. Bachelor Observatory  
 MDA8 O3 – Maximum Daily 8-h Average Ozone  
 ME – Middle East  
 ME00 – 3 Model-mean for 2000s Climate  
 ME90 – 3 Model-mean for 2090s Climate  
 MED – Median  
 MEGAN – Model of Emissions of Gases and Aerosols from Nature  
 MESSAGE – Model for Energy Supply Strategy Alternatives and their General  
     Environmental Impact  
 MetOP – a European polar-orbiting meteorological satellite  
 MFR – Maximum Feasible Reduction scenario  
 mg – milligrams

MILAGRO – Megacity Initiative: Local and Global Research Observations  
 MISR – Multiangle Imaging Spectro-Radiometer  
 MLS – Microwave Limb Sounder  
 MMO1 – Multi-model Mean and Ranges with 2001 Climate  
 MOCAGE – Model of Large Scale Atmospheric Chemistry, Meteo-France  
 MODIS – Moderate Resolution Imaging Spectroradiometer  
 MOPITT – Measurements of Pollution in the Troposphere  
 MOZAIC – Measurement of Ozone on Airbus In-service Aircraft  
 MOZART – Model of Ozone and Related Tracers  
 MOZGN – MOZART modified by GFDL and NCAR  
 MSC-E – Meteorological Synthesizing Centre-East  
 MSC-W – Meteorological Synthesizing Centre-West  
 Mx – Combination of M7 and M12  
 NA – North America  
 NAAQS – National Ambient Air Quality Standards  
 NAO – North Atlantic Oscillation  
 NAPAP – National Acid Precipitation Assessment Program, U.S.  
 NARE – North Atlantic Regional Experiment  
 NASA – National Aeronautics and Space Administration, U.S.  
 NASA DC-8 – a NASA fixed wing aircraft  
 NATAIR – Natural and biogenic emissions and assessment of impacts on air quality  
 nc – non-crustal  
 NCAR – National Center for Atmospheric Research, U.S.  
 NCLAN – National Crop Loss Assessment Network  
 NCO-P – Nepal Climate Observatory Pyramid  
 NE – Eurasian Boreal  
 NEAQS – New England Air Quality Study  
 NEGTA – National Expert Group on Transboundary Air Pollution  
 NEI – National Emissions Inventory  
 NEI99 – National Emissions Inventory 1999  
 ng/m<sup>3</sup> – nanograms per cubic meter  
 NH – Northern Hemisphere  
 NIES – National Institute for Environmental Studies (Japan)  
 NILU – Norwegian Institute for Air Research  
 NL – Netherlands  
 NLCS – Netherlands Study on Diet and Cancer  
 NMHCs – Non-Methane Hydrocarbons  
 NMVOCs – Non-Methane Volatile Organic Compounds  
 NOAA – National Oceanic and Atmospheric Administration, U.S.  
 NOAA WP-3D – a NOAA fixed wing aircraft  
 NRC – National Research Council  
 NW – North American Boreal  
 OC – Organic Carbon  
 OECD – Organization for Economic Co-operation and Development  
 OECD90 – Organization for Economic Co-operation Member States as of 1990  
 OHP – Observatoire de Haute Provence  
 OMI – Ozone Monitoring Instrument  
 PAN – Peroxyacetyl Nitrate  
 PAPA – Public Health and Air Pollution in Asia  
 PATMOS-x – AVHRR Pathfinder Atmospheres Extended project  
 PBL – Planetary Boundary Layer  
 PCFA – Post Cold Front Airstream  
 PFC – Policy Failed Case  
 PgC – petagram carbon



PHOBEA – Photochemical Ozone Budget of the Eastern North Pacific Atmosphere Campaign

PHOENICS – Particles of Human Origin Extinguishing Natural Solar Radiation in Climate Systems

PHOTOCOMP – IPCC Photochemical Model Intercomparison

PICO-NARE Observatory – North Atlantic Regional Experiment Observatory at Mt. Pico, Azores

PJ – Polar Jet

PM – Particulate Matter

PM<sub>2.5</sub> – Particulate Matter with a Diameter of 2.5 Micrometers or Less

PM<sub>10</sub> – Particulate Matter with a Diameter of 10 Micrometers or Less

POD<sub>y</sub> – Phytotoxic O<sub>3</sub> Dose above a Stomatal Flux Threshold Over a Growing Season

POET – Precursors of Ozone and their Effects in the Troposphere (an EU project)

POLARCAT – Polar study using Aircraft, Remote Sensing, Surface Measurements and Models, of Climate Chemistry, Aerosols and Transport

POM – Polycyclic/Particulate Organic Matter

POPs – Persistent Organic Pollutant

ppbv – Parts per Billion by Volume

pptv – Parts per Trillion by Volume

PSC – Policy Succeed Case

PSD Class I – Class I Areas under the Prevention of Significant Deterioration Rule

PV – Potential Vorticity

pvu – Potential Vorticity Unit

QRT – Quartile

RAIR – Relative Annual Intercontinental Response

RAPIDC – Regional Air Pollution in Developing Countries

RCP – Representative Concentration Pathway

REAS – Regional Emissions Inventory in Asia

REF – Reference Scenario

RETRO – Re-analysis of the tropospheric chemical composition project

RF – Radiative Forcing

RMT – Other Northern Hemispheric Mid-Latitude Regions

ROSE – Rural Oxidants in the Southern Environment study

RoTAP – Review of Transboundary Air Pollution

ROW – Rest of World

S/R – Source-Receptor

SA – Source Attribution

SA – South Asia

SAEFL – Swiss Agency for Environment, Forest, and Landscape

SCAB – South Coast Air Basin

SCAQS – Southern California Air Quality Study

SCIAMACHY – Scanning Imaging Absorption Spectrometer for Atmospheric Chartography/Chemistry

SCS – Six Cities Study

SE – Africa-Asia

SeaWiFS – Sea-viewing Wide Field of View Sensor

SEI – Stockholm Environmental Institute

SJ – Subtropical Jet

SLC – Salt Lake City

SLCFs – Short-Lived Climate Forcers

SOA – Secondary Organic Aerosol

SON – September, October, November

SOS – Southern Oxidant Study

SP2 – Single Particle Soot Photometer

SPARC – Stratospheric Processes and Their Role in Climate (part of WMO)

SPRINTARS – Spectral Radiation-Transport Model for Aerosol Species  
 SRES – IPCC Special Report on Emissions Scenarios  
 SRx – TF HTAP Source-Receptor Experiment x  
 SST – Sea Surface Temperatures  
 STILT – Stochastic Time-Inverted Lagrangian Transport model  
 STOCHEM – A global three dimensional Lagrangian transport chemical model  
 STR – Stratosphere  
 SUM06 – the sum of all hourly ozone concentrations greater than 0.06 parts per million  
 SW – Low-Latitude Regions of North America  
 SW DRF – Short-Wave Direct Radiative Forcing  
 TEMIS – Tropospheric Emission Monitoring Internet Service  
 TEOM – Tapered Element Oscillating Microbalance  
 TES – Tropospheric Emission Spectrometer  
 TexAQS – Texas Air Quality Study  
 TF HTAP – Task Force on Hemispheric Transport of Air Pollutants  
 Tg – Teragrams  
 TM5 – a 3-dimensional atmospheric chemistry-transport zoom model  
 TOA – Top of the Atmosphere  
 TOMS – Total Ozone Mapping Spectrometer  
 TP – TF HTAP Tracer Process Studies  
 TRACE-A – Transport and Chemical Evolution over the Atlantic  
 TRACE-P – Transport and Chemical Evolution over the Pacific  
 TRANSCOM – Atmospheric Tracer Transport Model Intercomparison Project  
 TROICA-8 – The eighth Trans-Siberian Railway Observations Into the Chemistry of the  
 Atmosphere expedition  
 ΔTs – Global Mean Equilibrium Surface Temperature Response  
 TSP – Total Suspended Particles  
 U.S. EPA – United States Environmental Protection Agency  
 UAVs – Un-manned Aerial Vehicles  
 UCAR – University Corporation for Atmospheric Research, U.S.  
 UCI – University of California at Irvine  
 UJF – Université Joseph Fourier  
 U.K. – United Kingdom  
 UK COMEAP – Committee on the Medical Effects of Air Pollutants, United Kingdom  
 UK FAAM BAe146 – U.K.'s Facility for Airborne Atmospheric Measurements fixed wing  
 aircraft  
 ULAQ – an atmospheric chemistry-climate model from the University of L'Aquila, Italy  
 UM-CAM – a global chemistry-climate model built by the University of Cambridge upon the  
 U.K. Met Office's Unified Model  
 UNECE – United Nations Economic Commission for Europe  
 UNFCCC – United Nations Framework Convention on Climate Change  
 UPMC – University of Pierre et Marie Curie  
 UPS – Unités Propres de Service (part of CNRS)  
 USDA ARS – U.S. Department of Agriculture Agricultural Research Service  
 U.S. – United States of America  
 UT – Upper Troposphere  
 UTC – Coordinated Universal Time  
 UV – Ultraviolet  
 UVSQ – University of Versailles Saint Quentin  
 VOCs – Volatile Organic Compounds  
 W/m<sup>2</sup> – Watts per Square Meter  
 W126 – Weighted Accumulation Over a Growing Season  
 WCB – Warm Conveyor Belt  
 WDCGG – World Data Centre for Greenhouse Gases  
 WHI – Women's Health Initiative observational study

WHO – World Health Organization  
WMO – World Meteorological Organization  
WRF-Chem – Weather Research Forecast model with Chemistry  
WWF G200 eco-regions – World Wildlife Federation Global 200 eco-regions  
Zoom-CiTTy – a high-resolution parcel model with chemistry  
 $\lambda$  – Climate Sensitivity  
 $\mu\text{g}/\text{m}^3$  – Micrograms per cubic meter  
 $\mu\text{m}$  – Micrometre



## Preface

In December 2004, in recognition of an increasing body of scientific evidence suggesting the potential importance of intercontinental flows of air pollutants, the Convention on Long-range Transboundary Air Pollution (LRTAP Convention) created the Task Force on Hemispheric Transport of Air Pollution (TF HTAP). Under the leadership of the European Union and the United States, the TF HTAP was charged with improving the understanding of the intercontinental transport of air pollutants across the Northern Hemisphere for consideration by the Convention. Parties to the Convention were encouraged to designate experts to participate, and the task force chairs were encouraged to invite relevant experts to participate from countries outside the Convention.

Since its first meeting in June 2005, the TF HTAP has organized a series of projects and collaborative experiments designed to advance the state-of-science related to the intercontinental transport of ozone (O<sub>3</sub>), particulate matter (PM), mercury (Hg), and persistent organic pollutants (POPs). It has also held a series of 15 meetings or workshops convened in a variety of locations in North America, Europe, and Asia, which have been attended by more than 700 individual experts from more than 38 countries. The TF HTAP leveraged its resources by coordinating its meetings with those of other task forces and centres under the convention as well as international organisations and initiatives such as the World Meteorological Organization, the United Nations Environment Programme's Chemicals Programme and Regional Centres, the International Geosphere-Biosphere Program-World Climate Research Program's Atmospheric Chemistry and Climate (AC&C) Initiative, and the Global Atmospheric Pollution Forum.

In 2007, drawing upon some of the preliminary results of the work program, the TF HTAP developed a first assessment of the intercontinental transport of ozone and particulate matter to inform the LRTAP Convention's review of the 1999 Gothenburg Protocol (UNECE Air Pollution Series No. 16).

The current 2010 assessment consists of 5 volumes. The first three volumes are technical assessments of the state-of-science with respect to intercontinental transport of ozone and particulate matter (Part A, this volume), mercury (Part B), and persistent organic pollutants (Part C). The fourth volume (Part D) is a synthesis of the main findings and recommendations of Parts A, B, and C organized around a series of policy-relevant questions that were identified at the TF HTAP's first meeting and, with some minor revision along the way, have guided the TF HTAP's work. The fifth volume of the assessment is the TF HTAP Chairs' report to the LRTAP Convention, which serves as an Executive Summary.

The objective of *HTAP 2010* is not limited to informing the LRTAP Convention but, in a wider context, to provide data and information to national governments and international organizations on issues of long-range and intercontinental transport of air pollution and to serve as a basis for future cooperative research and policy action.

*HTAP 2010* was made possible by the commitment and voluntary contributions of a large network of experts in academia, government agencies and international organizations. We would like to express our most sincere gratitude to all the contributing experts and in particular to the Editors and Chapter Lead Authors of the assessment, who undertook a coordinating role and guided the assessment to its finalisation.

We would also like to thank the other task forces and centres under the LRTAP Convention as well as the staff of the Convention secretariat and EC/R Inc., who supported our work and the production of the report.

André Zuber and Terry Keating  
Co-chairs of the Task Force on Hemispheric Transport of Air Pollution



# Chapter 1

## Conceptual Overview of Hemispheric or Intercontinental Transport of Ozone and Particulate Matter

**Lead Authors: Owen Cooper and Dick Derwent**

**Authors: Bill Collins, Ruth Doherty, David Stevenson, Andreas Stohl, Peter Hess**

### 1.1. Background and Introduction

When the Executive Body to the Convention on Long-range Transboundary Air Pollution took the decision to establish the Task Force on Hemispheric Transport of Air Pollution (TF HTAP) in December 2004, it was on the basis of a growing understanding of the issues surrounding the hemispheric and intercontinental transport of air pollutants. It was recognised that whilst current regional emissions on their own created pollution levels that exceeded internationally-agreed air quality objectives, hemispheric transport could exacerbate local and regional air quality problems. Two particular pollutants of concern, and the focus of this report, are ozone and particulate matter (PM), known for their detrimental impacts on human health (these impacts and others are described in Chapter 5). There was well-documented evidence for the intercontinental transport of ozone and PM but, at that time, the significance of this intercontinental influence on the design of air pollution control policies was not well understood. The European Union, in drawing up its Thematic Strategy on Clean Air for Europe during 2004, became aware of the significance of intercontinental transport and the importance of sources of pollution beyond its borders and sphere of influence, in meeting its air quality goals.

During its first meeting in 2005 the Task Force on Hemispheric Transport of Air Pollution (TF HTAP) produced some policy-relevant science questions to guide the development of its activities, beginning with the most basic question: How does the intercontinental or hemispheric transport of air pollutants affect air pollution concentration or deposition levels in the Northern Hemisphere? Observations at surface sites along the United States west coast give an indication of the ozone levels in baseline air masses (those air masses unaffected by local sources of pollution) undergoing intercontinental transport across the North Pacific Ocean. During springtime when the influence of intercontinental pollution transport is strong, ozone mixing ratios in recent years have averaged 38-45 parts per billion by volume (ppbv) [Parrish *et al.*, 2009], roughly 50-60% of the current U.S. ozone air quality standard (Chapter 5), and 75-90% of the World Health Organization (WHO) ozone standard (Chapter 5). Meanwhile springtime baseline ozone at the west coast of Europe has averaged 45-48 ppbv [Parrish *et al.*, 2009], which is 75-80% of the European ozone standard (Chapter 5), and 88-94% of the WHO standard. Baseline ozone levels above the surface layer are even greater, averaging 85% of the U.S. ozone air quality standard at 3-8 kilometres (km) above western North America during springtime [Cooper, 2010]. Tropospheric ozone has experienced widespread increases over the past few decades (Chapter 2) and the recent increasing trends in baseline ozone observed at inflow sites in North America and Europe (Figure 1.1) will necessarily have acted to offset some of the improvements in air quality expected from regional and local pollution controls. Intercontinental ozone transport is therefore a significant issue for policy-makers, based on current observations. If baseline ozone levels continue to rise, then these issues will become more pressing as the ozone pollution from local and regional sources decreases due to emissions controls.

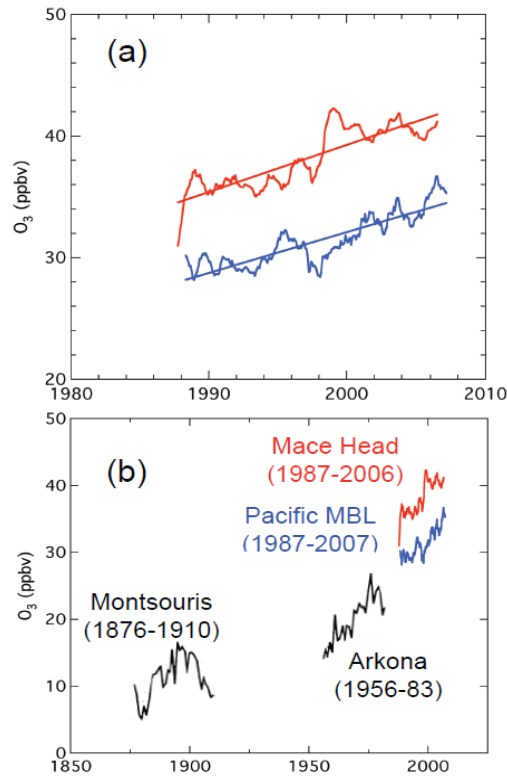


**Figure 1.1.** Comparison of surface ozone mixing ratios at Mace Head (red) on the west coast of Ireland, and a composite of data from several sites along the west coast of the U.S. (blue). b) An additional comparison to earlier measurements at two surface sites in western Europe. [Reprinted from Figure 12 in Parrish, D., et al., (2009), Increasing ozone in marine boundary layer inflow at the west coasts of North America and Europe, *Atmospheric Chemistry and Physics*, 9:1303-1323.]

## 1.2. Intercontinental or hemispheric transport of ozone and PM

On the intercontinental or hemispheric scale, the quantity of pollution emitted in one location and the fraction that ultimately reaches a particular downwind location is dependent on three factors: 1) the quantity of the pollutant emitted or produced at the source, 2) the meteorological conditions that transport the pollution from one continent to another, and 3) the physical and chemical transformation processes that modify the quantity and composition of the pollution during transport that lasts from days to weeks. These topics are introduced below.

### 1.2.1. Major ozone and PM sources

Near the Earth's surface (the troposphere) the trace gas ozone has a variety of sources including downward transport from the stratosphere, photochemical production from natural ozone precursor sources such as lightning or wild fires, and photochemical production from ozone precursors emitted by human activities such as fossil fuel combustion or crop burning. Air pollutants (e.g. CO, NO<sub>x</sub>) that are directly emitted from a source into the atmosphere are referred to as primary pollutants. In contrast, ozone is a secondary pollutant, meaning that it is produced from chemical reactions involving precursor gases, accounting for approximately 90% of the ozone in the troposphere (10% is directly transported from the stratosphere) [Stevenson *et al.*, 2006]. PM is a complex mixture of extremely small particles and liquid droplets with a broad compositional range, and may have primary and/or secondary sources.

The magnitude and impact of hemispheric and intercontinental scale transport of ozone and PM is initially determined by the global distribution of emissions, and their spatial relation to the major



meteorological transport pathways. Emissions that affect ozone and PM concentrations in the atmosphere are sulphur dioxide (SO<sub>2</sub>), nitrogen oxides (NO<sub>x</sub>), non-methane volatile organic compounds (NMVOC), ammonia (NH<sub>3</sub>), methane (CH<sub>4</sub>), organic carbon (OC), black carbon (BC) and carbon monoxide (CO); these emissions are discussed in detail in Chapter 3. Modelling studies indicate that man-made, or anthropogenic, emissions of pollutants have a major influence on the quantity of trace gases and PM found in the atmosphere. These studies estimate that in the troposphere (the lowest layer of the atmosphere) the burden of PM in the form of particulate sulphate and black carbon particles has increased by factors of 3 and 6, respectively, since preindustrial times. Meanwhile, the tropospheric burden of ozone has increased by 30-50% [Horowitz, 2006; Lamarque *et al.*, 2005].

Figure 1.2 provides an example of present day anthropogenic emissions with NO<sub>x</sub> (= NO + NO<sub>2</sub>), an important precursor of ozone, as well as some PM (e.g. nitrate particles). Global emissions of anthropogenic NO<sub>x</sub> from fossil fuel combustion (excluding shipping and aviation) for the year 2005 are shown, along with biomass burning emissions [van der Werf *et al.*, 2006]. Biomass burning emissions can have a large inter-annual variability [Duncan *et al.*, 2003; van der Werf *et al.*, 2006], while anthropogenic NO<sub>x</sub> emissions tend to shift gradually over time, in response to changing economic conditions and pollution control measures. For example, satellite measurements of column NO<sub>2</sub> indicate that NO<sub>x</sub> emissions increased during 1996-2005 in China (up to 29% per year) and other locations in Asia, while emissions decreased in Europe and the U.S. [van der A *et al.*, 2008]. The most recent bottom-up inventories indicate South and East Asia NO<sub>x</sub> emissions increased 44% during 2001-2006, with an increase of 55% within China [Zhang *et al.*, 2009a], while NO<sub>x</sub> emissions decreased by 30% across Europe (1990-2005) [Royal Society, 2008], and by 37% across the U.S. (1985-2008) [U.S. EPA, 2009].

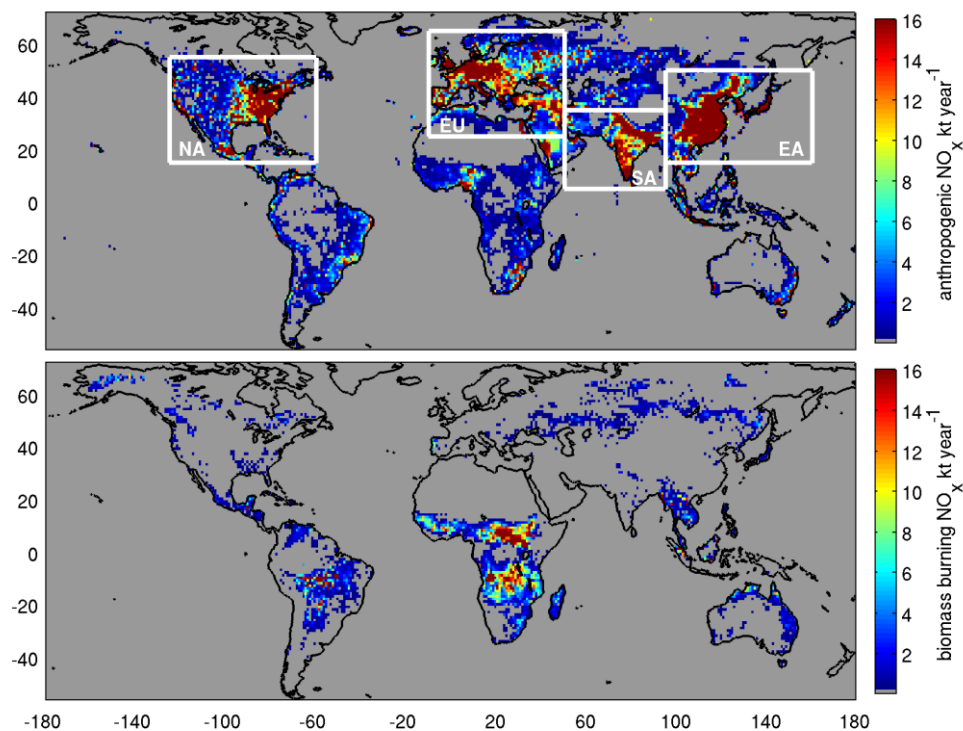


**Figure 1.2.** Distribution of global anthropogenic-NO<sub>x</sub> emissions (top), and biomass burning NO<sub>x</sub> from natural and anthropogenic fires (bottom) during the year 2005. Data are in units of kilo-tons NO<sub>x</sub> per 1x1 degree grid cell per year. Anthropogenic NO<sub>x</sub> emissions are from the latest EDGAR-HTAP inventory (as described in Section 3.2.1), while biomass burning emissions are from the Global Fire Emissions Database version 2 (GFEDv2) [van der Werf *et al.*, 2006]. White boxes encompass the four main TF HTAP source-receptor regions, North America (NA), Europe (EU), South Asia (SA) and East Asia (EA).

This report focuses on four broad emissions regions in the northern hemisphere, North America (NA), Europe (EU), South Asia (SA) and East Asia (EA), all outlined in Figure 1.2. The

largest emissions of anthropogenic NO<sub>x</sub> in the Northern Hemisphere are located in the eastern United States and southeastern Canada (within NA), western and central Europe (EU), and South Asia (SA) and East Asia (EA). Global emissions of anthropogenic NO<sub>x</sub> are roughly seven times those of biomass burning NO<sub>x</sub> emissions [Schultz and Rast, 2007]. By far, the majority of global biomass burning occurs in the tropics and is mainly caused by human activity, with natural wildfires being more prevalent in temperate and boreal forests [Crutzen and Andreae, 1990]. Estimates of natural sources of NO<sub>x</sub> from lightning and soil vary widely but together are approximately one third of anthropogenic emissions [Schultz and Rast, 2007; Schumann and Huntrieser, 2007].

The anthropogenic NO<sub>x</sub> emissions shown in Figure 1.2 are representative of the spatial distribution of human activity across the globe, but are by no means proportional to the number of people in the various regions as shown by Figure 1.3. While the Northern Hemisphere contains the great majority of people (88%), 90% of anthropogenic NO<sub>x</sub> emissions, and roughly 50% of biomass burning NO<sub>x</sub> emissions, per capita emissions vary widely across nations. Broadly speaking, North America has the highest per capita anthropogenic NO<sub>x</sub> emissions while South Asia has the lowest (Figure 1.3).

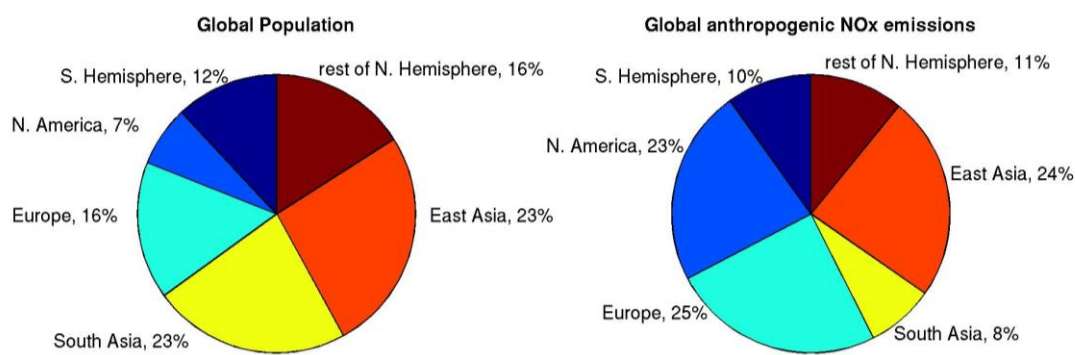


**Figure 1.3.** Global distribution of human population and anthropogenic NO<sub>x</sub> emissions in the year 2005. Population data from Center for International Earth Science Information Network (<http://sedac.ciesin.columbia.edu/gpw/>), emissions data from the latest HTAP inventory as described in Section 3.2.1. The regions designated by North America, Europe, South Asia and East Asia are shown in Figure 1.2.

### 1.2.2. Major transport pathways

This section briefly introduces the major pathways of intercontinental transport, summarized in Figure 1.4 [Stohl and Eckhardt, 2004]. The processes that govern this transport are described in Section 1.4, while observations of pollution within these pathways are reviewed in Chapter 2. The models that simulate intercontinental transport processes are reviewed in Chapter 4.

The mid-latitudes cover most of the major emissions regions within North America, Europe and East Asia. Transport in this region is dominated by the westerly winds that transport emissions from East Asia across the North Pacific Ocean to North America, from North America across the North Atlantic Ocean to Europe, and from Europe into the Arctic and central Asia. Pollutants that are lofted into the mid- and upper troposphere travel further and faster than pollutants that remain in the lower troposphere due to the stronger winds at altitude, especially in the vicinity of the jet stream. The westerly winds are stronger in winter than summer and therefore pollutants are transported at greater speeds and over greater distances during the winter months.

Transport of pollutants emitted in the tropics is dominated by the tropical easterlies or trade winds at the surface. Of the four major emissions regions in the northern hemisphere, only South Asia is dominated by the easterlies in winter, although emissions from Europe can still travel south to northern Africa, and some emissions from North America and East Asia can also reach the tropics. In summertime the easterlies extend their influence northward allowing more emissions

from NA, EU and EA to influence the tropics. Also during this season the North American and Asian summer monsoons develop driving surface emissions northward, while at the same time producing widespread thunderstorms which rapidly loft pollutants from the surface to the upper troposphere. In the upper troposphere, stronger winds can transport the pollutants further than had they remained close to the surface.

The location of the emissions regions with respect to the dominant atmospheric transport pathways has a strong influence on the frequency and strength of intercontinental pollution transport events. For example, the emissions regions along the east coasts of Asia and North America are at the origins of the North Atlantic and North Pacific mid-latitude cyclone storm tracks, which can loft the emissions into the mid- and upper troposphere and transport them to downwind continents in a matter of days. In contrast, Europe is at the end of the North Atlantic storm track and its emissions stay closer to the surface, especially in winter.

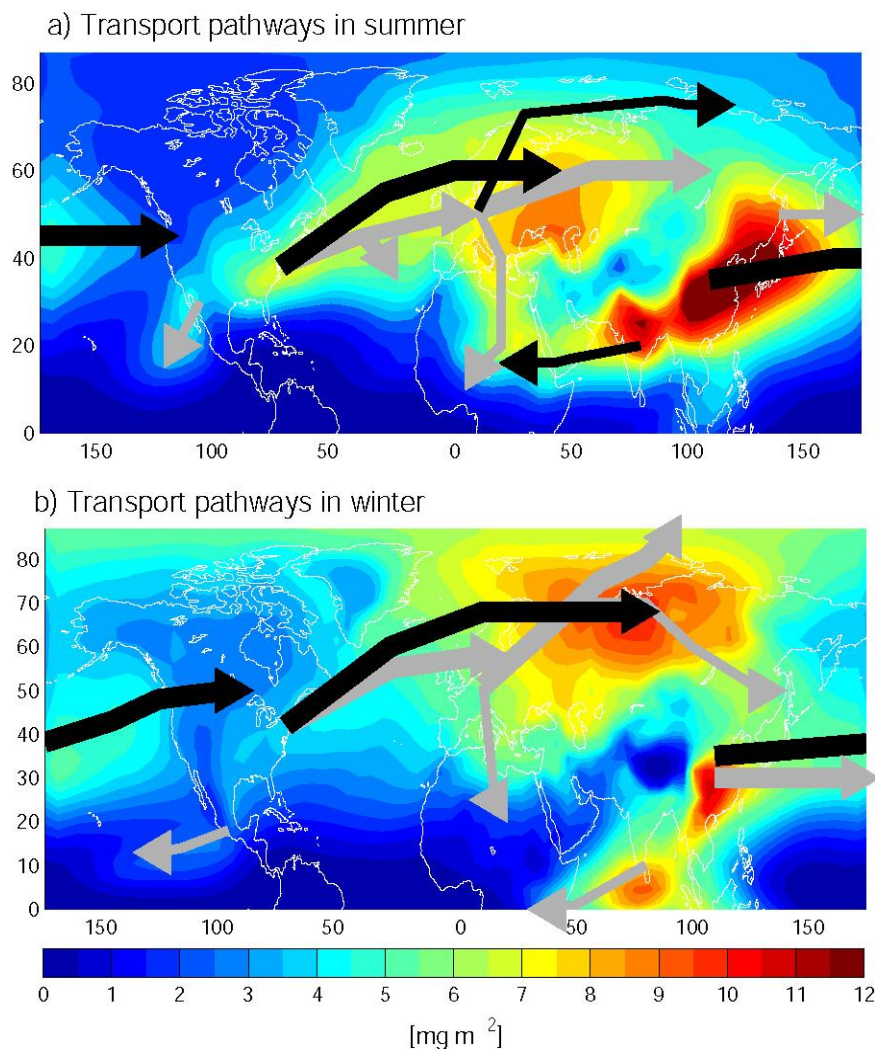


**Figure 1.4.** Pathways of intercontinental pollution transport in the Northern Hemisphere. Shading indicates the location of the total column of a passive anthropogenic CO tracer released over the Northern Hemisphere continents after 8-10 days of transport, and averaged over 15 years. Shown are transport pathways in summer (June, July, August; upper panel), and winter (December, January, February; lower panel). Gray arrows show transport in the lower troposphere (< 3 km) and black arrows show transport in the mid- and upper troposphere (> 3 km). [Image reproduced from Chapter 1, Figure 2, page 6, of Stohl, A. and S. Eckhardt [2004], *Intercontinental Transport of Air Pollution: An Introduction*, in *Intercontinental Transport of Air Pollution*, edited by A. Stohl, with kind permission of Springer Science and Business Media B.V.]

### 1.2.3. Chemistry and transformation processes

Intercontinental pollution transport occurs on timescales of days to weeks, longer than the atmospheric lifetimes of some pollutants (Table 1.1), and ample time for the trace gases and PM emitted or produced at the source to undergo removal or chemical transformation. By the time the polluted air mass arrives at a downwind continent it is likely to have very different chemical properties than it did at the source. The chemical transformation processes that occur during intercontinental transport are numerous and complex. A few of the most important chemical transformation processes experienced by polluted air masses during transport are depicted in Figure 1.5 and described below, using transport from Asia to North America as an example. The descriptions of these processes are supported by studies conducted across many of the world's oceans, and are generally applicable to most intercontinental transport routes.

**Table 1.1.** Approximate lifetimes of trace gases and PM in the atmospheric boundary layer and the free troposphere. Lifetimes are highly variable depending on altitude, time of day, season, and proximity to emissions regions.

Trace gas or PM	Approximate lifetime in the atmospheric boundary layer	Approximate lifetime in the free troposphere
NO <sub>2</sub>	hours	days
SO <sub>2</sub>	days	days to weeks
CO	weeks to months	weeks to months
VOCs	hours to months	hours to months
CH <sub>4</sub>	8-9 years	8-9 years
NH <sub>3</sub>	days	days
PM	hours to days	days to weeks
ozone	hours to days	weeks to months

Pollution transported from Asia to North America originates in the atmospheric boundary layer (ABL) of eastern Asia where primary air pollutants such as NO<sub>x</sub>, SO<sub>2</sub>, CO, NMVOC and PM are directly emitted from combustion and industrial sources. During daytime, sunlight initializes photochemical reactions that allow NO<sub>x</sub> and NMVOC to react and form the secondary pollutant, ozone. Ozone becomes a source of the OH radical, a powerful oxidant that reacts with and transforms many pollutants in the atmosphere. Sometimes referred to as the cleaning agent of the atmosphere, OH is also the dominant species that removes CH<sub>4</sub> and CO from the atmosphere, and it plays an important role in the oxidation of SO<sub>2</sub> to H<sub>2</sub>SO<sub>4</sub>, (sulphuric acid) which is a source of particulate sulphate. Other gases that can react to form PM known as secondary aerosols are NO<sub>x</sub>, NH<sub>3</sub>, and NMVOC. While these and many other chemical transformation processes occur within the continental ABL, trace gases and PM are also removed from the atmosphere via wet and dry deposition. Dry deposition occurs when the gases or PM come into contact with Earth's surface and are taken up or adsorbed onto surfaces. Dry deposition rates depend on the surface type (e.g. vegetation, water, ice) and the rate at which constituents are transported to the ground. Wet deposition occurs when precipitation transports water soluble trace gases (such as sulphuric or nitric acid) and PM to the Earth's surface.



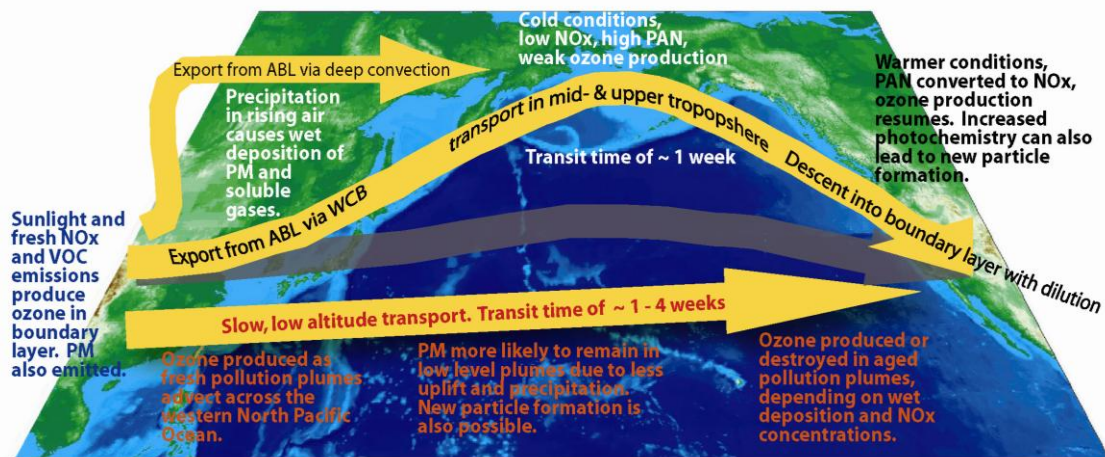


**Figure 1.5.** General intercontinental transport processes. Blue text on the left applies to continental boundary layer processes, red text applies to low level transport and black/white text applies to high altitude transport.

When weather systems export polluted air masses from the Asian continental ABL across the North Pacific Ocean towards North America, the subsequent removal and chemical transformation depends on whether the air mass is exported to the lower troposphere, generally less than 3 km in altitude, or to the mid- and upper troposphere. Polluted air masses exported to the mid- and upper troposphere experience strong uplift via deep convection or warm conveyor belts (WCBs) (these meteorological processes are described in Section 1.4), rising 3 to 15 km above the Earth's surface (Figure 1.5). As these air masses rise and cool, water vapour from the ABL condenses into clouds. The ensuing precipitation removes most of the water soluble trace gases and PM via wet deposition. By the time the polluted air mass reaches the mid- or upper troposphere, most of the  $\text{NO}_x$  has been converted to other species such as peroxyacetyl nitrate (PAN) or nitric acid and there is relatively little left for continued ozone production [Li *et al.*, 2004; Miyazaki *et al.*, 2005; Stohl *et al.*, 2002b]. Much of the reactive nitrogen is in the form of PAN, an important reservoir of  $\text{NO}_x$  [Singh *et al.*, 1992; Zhang *et al.*, 2008]. The clear, cold and dry conditions of the upper troposphere also lead to significantly different chemistry than at the surface, with, for example, a much longer  $\text{NO}_x$  lifetime.

Eventually, these aged, polluted air masses descend towards the surface. The air warms as it descends, allowing thermal decomposition of PAN that releases  $\text{NO}_x$ . This new supply of  $\text{NO}_x$  causes the resumption of ozone production [Hudman *et al.*, 2004; Zhang *et al.*, 2008], however the descending air mass can encounter higher concentrations of water vapour in the lower troposphere which destroys some of the newly formed ozone [Real *et al.*, 2007]. Increased ozone concentrations can also lead to the oxidation of any remaining  $\text{SO}_2$  in the air mass, with the resulting sulphuric acid nucleating new particles that condense to form particulate mass [Brock *et al.*, 2004; Dunlea *et al.*, 2009]. A common location for polluted air masses to descend is the eastern North Pacific Ocean [Cooper *et al.*, 2004; Hudman *et al.*, 2004; Zhang *et al.*, 2008]. Portions of these warming and photochemically active air masses can eventually descend into the North America ABL and contribute to the local pollution burden. However the dilution that occurs during transport is so extensive that the Asian pollution is difficult to detect in the North American ABL, especially where local sources of pollution are strong [Zhang *et al.*, 2009a].

Different chemical transformation processes occur in air masses that remain in the lower troposphere. The lower troposphere contains more water vapour than the mid- and upper troposphere, which leads to net ozone destruction when  $\text{NO}_x$  concentrations are low. However, if  $\text{NO}_x$  concentrations are maintained above a critical threshold, ozone production will occur [Logan *et al.*, 1981; Reeves *et al.*, 2002]. Over the oceans, the lowest few hundred meters of the lower troposphere is occupied by the marine boundary layer, which is usually stable, moist and isolated from the air above. Ozone production in the marine boundary layer typically occurs within the first few days of pollution export from the continent, at least during the warm season. During winter net ozone

destruction appears to be more typical [Parrish *et al.*, 1998]. Transport of air masses in the lower troposphere, above the marine boundary layer, can result in NO<sub>x</sub> being released as PAN leading to enhanced ozone concentrations such as over the Azores in the middle of the North Atlantic Ocean at 3 km [Owen *et al.*, 2006; Val Martin *et al.*, 2008]. However, in the lower troposphere, nitric acid is formed preferentially to PAN and, in the presence of clouds will dissolve into cloud droplets leading to reductions in available NO<sub>x</sub>. In this case, although substantial ozone may have been produced over the continental source region, ozone destruction, due to high water vapour concentrations will prevail downwind. If ozone and water vapour concentrations remain high, the resulting OH can destroy pollutants such as CO [Real *et al.*, 2008].

Regarding PM, lower tropospheric transport tends to experience less precipitation than air masses that are lofted to the mid- and upper troposphere. As a result, wet deposition is less and PM concentrations are much greater in the lower troposphere than in the mid- and upper troposphere [Heald *et al.*, 2006; van Donkelaar *et al.*, 2008]. Furthermore, greater precipitation in winter appears to explain why lower concentrations of PM are transported to the surface of western North America in winter compared to summer [Jaffe *et al.*, 2005].

**FINDING: The quantity of ozone or PM transported from one continent to another is determined by the initial quantity of these pollutants either emitted or produced in the source continent, the altitude to which the pollutants are exported, the transport speed, and the deposition and chemical transformation that occurs during transport.**

### 1.3. Key concepts for describing intercontinental transport processes

#### 1.3.1. Global background and global baseline concentrations

Global, or hemispheric, background and baseline concentrations are terms that are often used interchangeably. To bring order and consistency to the discussion of hemispheric or intercontinental pollution transport, these terms are defined here for the purposes of this assessment report. The term baseline concentration will refer to observations of pollutants, while the term global or hemispheric background concentration will refer to modelled concentrations of pollutants.

A baseline concentration is an observation made at a site when it is not influenced by recent, locally emitted or produced pollution. These baseline sites are typically situated in locations with minimal and infrequent impact from local sources of anthropogenic pollution. Observations may be made continuously and subsequently sorted, or air samples taken only when meteorological conditions are such that the recorded concentrations are free from the local contamination. Time series of baseline concentrations provide the range and frequency of pollutant concentrations transported to the site from upwind locations. However the requirement that only recently emitted or produced local pollution be excluded means that baseline concentrations may contain traces of local pollutants that were emitted many days earlier and became well-mixed with other air masses. There is no strict definition of “recently” emitted or produced local sources of anthropogenic pollution.

The global or hemispheric background concentration of a pollutant is a model construct that estimates the atmospheric concentration of a pollutant due to natural sources only. It is a straightforward modelling exercise to quantify the global background concentrations of any pollutant resulting only from natural sources by using a variety of source-apportionment, labelling and source-receptor techniques. The relatively long-lived air quality pollutants like ozone, CO, and PM, or the greenhouse gases, are pervasive in the northern hemisphere. Because their lifetimes are longer than the time taken to advect around a latitude circle, it is unlikely that a location can be found that only observes naturally occurring concentrations of these pollutants. Therefore, global or hemispheric background concentrations of long-lived pollutants cannot be observed. The global or hemispheric background concentrations of these species can only be determined by models and these concentrations will always be less than baseline observations which contain natural and anthropogenic contributions. In contrast, for short-lived air quality species like SO<sub>2</sub> or NO<sub>2</sub> it is possible to find some locations in the northern hemisphere unaffected by anthropogenic emissions allowing the direct observation of global or hemispheric background concentrations. However such locations are

relatively few and models are still required to estimate the global or hemispheric background concentrations for most places in the northern hemisphere.

In addition to global or hemispheric background concentrations, the terms urban background and rural or regional background are also widely used in the literature. Urban background concentrations are those observed in urban areas away from the direct influence of heavily-trafficked roads and chimney stacks. Rural or regional background concentrations are those observed at locations where there is little influence from urban sources of pollution. Note that while urban, rural and regional background concentrations are based on observations, global and hemispheric background values are model constructs.

In light of the definitions above, care must be taken when considering common expressions such as, ‘the observed growing hemispheric background ozone concentrations’. There is little supporting evidence for an increase in natural (not influenced by human activities) sources of ozone and its precursors such as lightning, wild fires and stratosphere-troposphere exchange. In this case, the usage of ‘background’ is inappropriate and ‘observed growing hemispheric ozone levels’ would be a more appropriate reference to the growing influence of human activities on tropospheric ozone for which there is more supporting evidence.

**FINDING: Baseline concentrations refer to observations made at a site when it is not influenced by recent, locally emitted or produced anthropogenic pollution. The term global or hemispheric background concentration is a model construct that estimates the atmospheric concentration of a pollutant due to natural sources only.**

### *1.3.2. Source Attribution and Source-Receptor Relationships*

Policy-makers have come to recognise only relatively recently the importance of hemispheric transport of air pollution to the achievement of air quality guidelines, standards and targets. Source attribution and source-receptor relationships are important concepts in this context. They are used to define how much individual source regions contribute to ground-level pollution in absolute and relative terms and how much hemispheric pollution transport contributes to the frequency and severity of pollution episodes.

Source attribution or source apportionment is the process by which a concentration or deposition is split into a number of components (or fractions) that represent a source contribution. In principle, the sum of all components should add up to the observed or modelled concentration (or unity). For the simple case of an inert tracer or for the components of an exactly linear chemical system, different source attribution approaches will give a similar impression of the importance of different sources [Seibert and Frank, 2004]. However, source attribution under one emission scenario may be different from the source attribution after emissions have changed. For example, the source attributions for ozone and PM measured in a highly polluted location are distinctly different for the pre-industrial and present-day atmospheres [Horowitz, 2006; Lelieveld and Dentener, 2000].

Most source attribution studies for ozone have employed the “tagging” or “labelling” methods where pollutants from specific source regions are “tagged” or “labelled” and explicitly tracked in the model using extra model variables. In this way, each molecule or particle, whether “tagged” or not is given the same local, instantaneous removal rate. These tagging techniques have led to some important findings regarding tropospheric chemistry. Using ozone as an example:

- 1) An ozone “tagging” analysis on the global scale found that production of ozone in the middle, upper and continental lower troposphere all make significant contributions (10 - 50 %) to ozone concentrations throughout the troposphere [Wang *et al.*, 1998];
- 2) Transport from polluted continental source regions generally accounts for more than 40% of the ozone in remote locations [Sudo and Akimoto, 2007];
- 3) Over Europe, North American and Asian sources of ozone contribute substantially to the annual ozone budget, accounting for approximately 11 and 8 %, respectively, while European

sources contribute only 9 %. These contributions show marked seasonalities because of the interactions between the chemical and transport processes [Auvray and Bey, 2005].

4) “Labelled” ozone in a global model coupled to a regional model provided a source attribution of the ozone measured at a rural location in southern England during January 2006 (see Figure 1.6). Averaged over the 12-month study period, two-thirds of the ozone found at this site was advected by large-scale intercontinental processes and one-third from production on the regional scale within Europe. Of the ozone brought by intercontinental transport, the largest contribution came from North America and the western North Atlantic, with smaller contributions from the stratosphere, Asia and the Pacific [Derwent, 2008].

5) A global chemical transport model provided ozone source attributions for 8 locations in North America during March 2001. At most locations intercontinental transport contributes about 10 – 20 ppbv, with significant location-location and day-by-day variability [Fiore *et al.*, 2003].

Whilst these source attributions for ozone go a long way towards answering the policy questions addressing ozone and its hemispheric scale transport, they have some drawbacks and limitations. There are technical issues surrounding the “tagging” and “labelling” schemes that mean that it is difficult to separate the contributions to ozone from natural and anthropogenic sources of VOCs and NO<sub>x</sub> and from surface and elevated sources such as lightning and aircraft. Also, such source attributions are highly model- and location-specific.

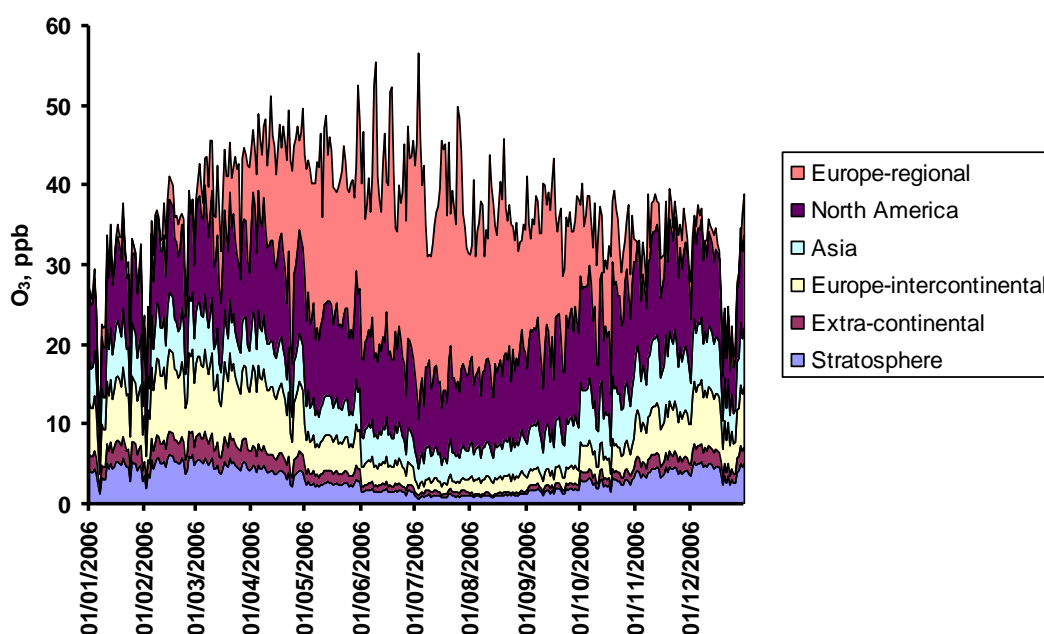


**Figure 1.6.** Source attribution of the ozone found at a rural location in southern England during 2006 [Derwent, 2008]. Europe-regional refers to the ozone advected directly over the local- and regional-scales to the location. North America to that formed over that continent and over the North Atlantic and east Pacific; Asia to that formed over that continent and over the western Pacific; Europe-intercontinental to that advected around latitude circles and back into Europe; Extra-continental refers to that from interhemispheric transport. [Reprinted from Figure 1 in Derwent, R. G. (2008), *New Directions: Prospects for regional ozone in north-west Europe*, *Atmospheric Environment*, 42:1958-1960, with permission from Elsevier.]

The term “source-receptor” relationship describes the sensitivity of concentrations or depositions at a “receptor” location to a change in emissions from a “source” location [Seibert and Frank, 2004]. It is a key concept which is used in this document to assess the impact of emissions from an upwind continent or region on a downwind receptor location [Derwent *et al.*, 2004; Fiore *et al.*, 2002; Wild and Akimoto, 2001]. Source-receptor relationships are different in concept to source



attributions [Venkatram and Karamchandani, 1986] and imply a response at a particular receptor location to a change in the emission from a particular source. However, the two terms are linked by the fact that multiplying the source-receptor relationship by the emissions flux yields the source attribution for the simple case of an inert tracer or for the components of an exactly linear system. For ozone, with its non-linear relationship between NO<sub>x</sub> and VOC precursor emissions, this multiplication does not yield the same perceptions about the importance of intercontinental sources and intercontinental transport.

Calculations of source-receptor relationships can be classified into source-oriented and receptor-oriented approaches. The source-oriented approach is the most commonly-used approach, where emissions from a particular source region are perturbed and these perturbations are propagated forward in time throughout the model domain. In the receptor-oriented approach, the perturbation in the receptor region from a change in emissions is traced back in time through the model domain.

**FINDING: Source attribution and source-receptor relationships are widely applied analytical techniques used to define how much individual source regions contribute to ground-level pollution in absolute and relative terms, and how much hemispheric pollution transport contributes to the frequency and severity of pollution episodes.**

## 1.4. Major types of intercontinental transport processes

### 1.4.1. General circulation regimes

The great majority of intercontinental pollutant transport occurs within the troposphere which extends from the surface to about 8 km in cold polar regions, and up to 16-18 km in tropical regions (Figure 1.7). The general tropospheric circulation can be roughly divided into three regimes: the subtropics and tropics, the mid-latitudes (30°-60°) and the polar regions. Of these three regions transport processes are best understood in the mid-latitudes.

Transport in the mid-latitudes is generally from west to east, heavily influenced by mid-latitude cyclones which also impart a strong north-south component to the transport (see discussion below and Figure 1.8). During the summer months, however, deep convective processes play an important role over land. At mid-latitudes, wind speeds generally increase with height, causing pollutants at higher altitudes to be transported rapidly. This is especially true in the vicinity of the polar and subtropical jet streams, which vary in location and intensity from day to day. Thus, processes that loft pollutants into the mid- to upper troposphere are most conducive to long-range intercontinental transport. Winds are generally stronger in winter than in summer, causing intercontinental transport to be more rapid during winter months. Meridional (south-north) winds are generally weaker than zonal (west-east) winds, thus pollutants tend to be transported zonally (i.e. along latitude circles).

The tropics and subtropics are dominated by the Hadley cell with rising motion within deep convective cumulus towers in the deep tropics (often within the Intertropical Convergence Zone), which is balanced by subsident motion in the subtropics. The meridional winds associated with the Hadley cell are poleward throughout much of the free troposphere, but with a return equator-ward flow confined near the surface (Figure 1.7). In the tropics and subtropics, intercontinental transport is generally from east to west, guided by the trade winds throughout the lower and mid-troposphere (Figure 1.7).

A number of studies have shown impediments to transport (i.e., transport barriers) between the extra-tropics and the tropics [Bowman and Carrie, 2002; Bowman and Erukhimova, 2004; Hess, 2005; Pierrehumbert and Yang, 1993]. These barriers imply that air within the mid-latitudes tends to recirculate within the mid-latitude region, and air within the tropics and subtropics tends to recirculate within the tropics and subtropics. Thus, baseline concentrations at mid-latitude sites are most immediately affected by mid-latitude emissions, with a much smaller contribution from tropical sources. Equator-ward transport between the extra-tropics and tropics occurs primarily in shallow flow near the Earth's surface associated with the equator-ward branch of the Hadley circulation, and often occurs behind cold fronts [Bowman and Carrie, 2002; Bowman and Erukhimova, 2004]. The poleward return-

flow occurs in a more diffuse circulation in the upper troposphere associated with the upper branch of the Hadley cell (Figure 1.7). Species concentrations, even for long-lived constituents can be significantly different between the northern and southern hemispheres. Large interhemispheric differences have been observed in the concentrations of many of the long-lived species, suggesting that the transport between the northern and southern hemispheres is slow. The timescale for transport between the hemispheres is on the order of a year [Jacob *et al.*, 1987; Patra *et al.*, 2009; Prather *et al.*, 1987].

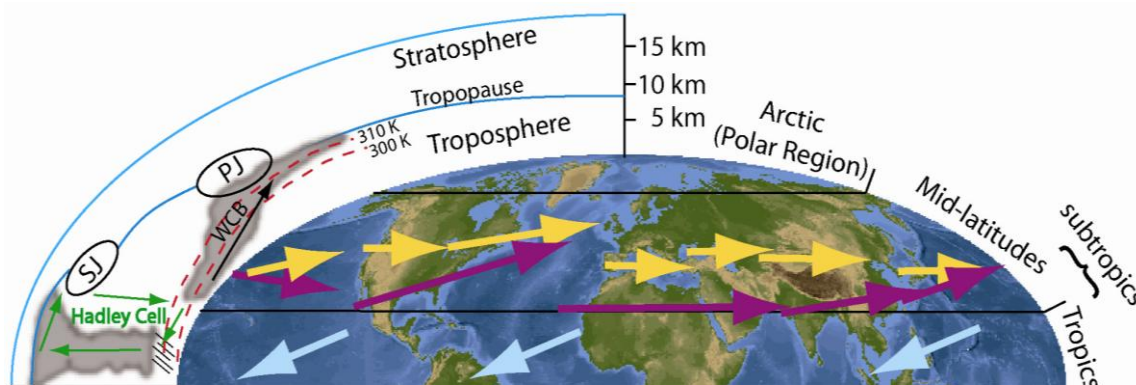


**Figure 1.7.** Schematic diagram showing some of the main features of the atmosphere related to the transport of air pollutants. The vertical cross section shows the average location of the tropopause (the boundary between the troposphere and stratosphere) and the polar (PJ) and subtropical (SJ) jet streams during winter. Vertical transport during winter is dominated by deep convective clouds in the tropics (the upward branch of the Hadley cell) and WCBs in the mid-latitudes, as described in Section 1.3.2. The average location of the jet stream is shown across the entire Northern Hemisphere for winter (magenta arrows) and summer (yellow arrows); locations of the tropical easterlies are also shown (light blue arrows). Also shown are the winter locations of the 300 K and 310 K potential temperature surfaces (red).

In the northern hemisphere polar region, the cold and stable lower troposphere forms a dome over the Arctic, largely isolating the region from low latitude pollution that is emitted into warm air masses that ascend into the mid- and upper troposphere above the Arctic. Pollutant transport into the Arctic lower troposphere occurs preferentially from Europe when the outer regions of the Arctic dome pass over northern Europe, take up fresh emissions and then retreat back into the Arctic [Law and Stohl, 2007].

The temperature gradients that maintain the Arctic dome are aligned according to the potential temperature structure of the atmosphere which guides global atmospheric transport. The potential temperature is a measure of an air mass's temperature, adjusted for the temperature changes that are caused by variations in atmospheric pressure as the air mass is transported vertically. In general, the potential temperature of the atmosphere increases with altitude and an air mass with a typical (for the mid- to upper troposphere) potential temperature of 310 kelvin (K) lies stably above an air mass with a potential temperature of 305 K. These two air masses will not mix unless energy is added to the lower layer or removed from the upper layer so that the two air masses achieve equal potential temperature. As a result, atmospheric transport is constrained by surfaces of constant potential temperature and will follow these surfaces in the absence of heating or strong mixing.

Potential temperature surfaces are generally oriented upward and poleward in the mid-latitudes (Figure 1.7). Therefore, poleward moving air tends to ascend, while equator-ward moving air tends to sink. Mid-latitude meridional stirring occurs along constant potential temperature surfaces on timescales up to 10 days [Bowman and Carrie, 2002; Bowman and Erukhimova, 2004]. Transport along potential temperature surfaces that intersect the surface of the Earth occurs primarily through the action of mid-latitude cyclones [Hess, 2005]. However, above the 310 K potential temperature surface most of the air parcels have been vertically transported through deep convective cloud which is the typical situation in the mid and upper troposphere of the tropics and subtropics [Hess, 2005]. Once a polluted air mass reaches such a high potential temperature, it cannot return to the surface until it has cooled. Because radiative cooling is a relatively slow process, the potential temperature

structure of the atmosphere limits the rate at which polluted air from warm regions of the Earth's surface can be transported to the mid- and upper troposphere and then back down to cool regions of the Earth's surface.

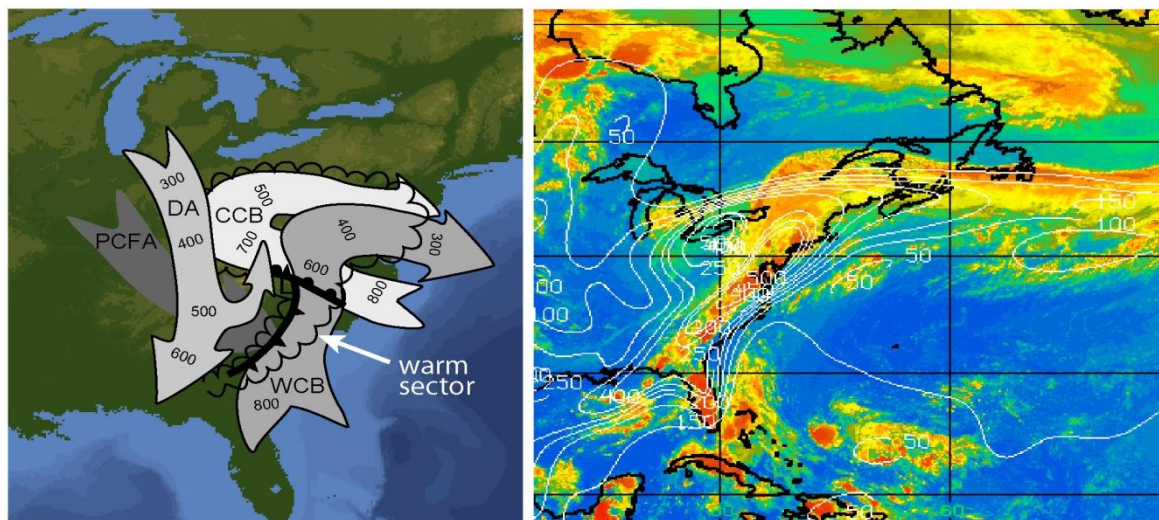


**Figure 1.8.** (Left) Conceptual model of the airstreams within a mid-latitude cyclone: WCB, cold conveyor belt (CCB), dry airstream (DA), and the post-cold-front airstream (PCFA). The relationships of the airstreams to the centre of the surface low (L) and the warm and cold fronts are shown, as is the edge of the cloud shield formed by the WCB and CCB (scalloped lines). The numbers on the WCB and CCB indicate the pressure (hPa) at the top of these airstreams, while numbers on the DA indicate the pressure at the bottom of the airstream. [Reprinted from Figure 2 in Cooper, O.R., et al., (2002), Trace gas composition of mid-latitude cyclones over the western North Atlantic Ocean: A conceptual model, *Journal of Geophysical Research*, 107(D7): doi:10.1029/2001JD000901.] (Right) GOES-EAST infrared image on July 27, 2004, with yellows and reds indicating cold, high altitude cloud tops, and blues indicating the Earth's surface. The cloud band along the U.S. east coast is a weak summertime WCB advecting polluted air over the western North Atlantic Ocean, indicated by the white contours which depict an anthropogenic carbon monoxide tracer ( $\text{mg m}^{-2}$ ). This polluted air mass was transported to Europe in the upper troposphere over the next four days [Methven et al., 2006].

#### 1.4.2. The mid-latitude cyclone airstreams

Mid-latitude cyclones tracking from west to east are important mechanisms for the export of trace gases and PM from the east coasts of Asia and North America throughout the year, even in summer when these weather systems are weaker [Cooper et al., 2002; Kiley and Fuelberg, 2006; Merrill and Moody, 1996; Stohl et al., 2002a]. The cyclones are typically composed of four airstreams (Figure 1.8) that influence trace gas mixing ratios and relationships in the troposphere [Bethan et al., 1998; Cooper et al., 2002; Stohl and Trickl, 1999]. Three of these airstreams, the WCB, cold conveyor belt, and dry airstream produce the distinctive comma cloud of a mature mid-latitude cyclone [Bader et al., 1995; Browning and Monk, 1982; Browning and Roberts, 1994; Carlson, 1998]. The WCB is located on the eastern side of the cyclone, ahead of the surface cold front. The air originates at low altitudes in the warm sector of the cyclone and travels poleward, and over many hours ascends into the mid- and upper troposphere, above the cold conveyor belt. The dry airstream, which is associated with stratospheric intrusions, originates at high altitudes in the upper troposphere and lowermost stratosphere on the poleward side of the cyclone and descends into the mid- and lower troposphere on the polar side of the cold front. The post cold front airstream is the cold, dry, and stable air mass in the lower and mid-troposphere that flows behind the cyclone cold front and beneath the dry airstream [Cooper et al., 2002].

The WCB is the most important airstream for rapid intercontinental pollutant transport because of its ability to loft polluted ABL air from the cyclone warm sector to the upper troposphere

in the vicinity of the jet stream. Following the mid-latitude cyclone storm tracks, the jet stream then rapidly transports the pollutants downwind. Transport times from the moment North American ABL air is lifted within the WCB until it reaches the European free troposphere are typically 3-4 days [Eckhardt *et al.*, 2004; Stohl *et al.*, 2002a], and in some cases less than 2 days [Stohl *et al.*, 2003]. Several additional days are required for the North American emissions to reach the European surface with the greatest influence over the Mediterranean due to trapping and anticyclonic descent of the emissions through the Azores' high [Stohl *et al.*, 2002a]. The greater distance associated with trans-Pacific transport results in slightly longer transport times, and in some instances requires two WCBs to transport emissions from Asia to North America [Cooper *et al.*, 2004]. However, WCB transport does not necessarily end at the next downwind continent. These polluted airstreams can remain aloft for days and circle the globe as distinct polluted air masses [Stohl *et al.*, 2007].

Mid-latitude cyclones can also export pollutants from Asia and North America at low altitudes as discussed in Section 1.3.5, either when the warm sector of the storm pushes offshore and the WCB is too weak to loft the pollutants, or when the cold stable air in the post cold front airstream quickly advects fresher emissions offshore.

#### *1.4.3. Deep convection*

Deep convection is an important mechanism for vertically transporting air pollutants out of the ABL and into the middle and upper troposphere [Dickerson *et al.*, 1987; Lelieveld and Crutzen, 1994], where the stronger winds can rapidly transport the pollutants across intercontinental distances. Convection is triggered when the atmospheric temperature profile is unstable, such as occurs during daytime when the land is warm, or when cooler air masses are advected over a warm ocean surface. When convection is sufficiently deep, condensation of water vapour in convective cells releases latent heat and leads to cloud formation.

Convective systems encompass small-scale fair weather cumuli, active thunderstorms (cumulonimbus clouds), deep convective clouds with no precipitation, and mesoscale convective systems [Cotton *et al.*, 1995]. The corresponding lifetime of these systems increases with their size from minutes to about half a day. Another weather system shaped by organized deep convection is the tropical cyclone (including tropical depressions, tropical storms, hurricanes and typhoons), whose lifetime is on the order of a week. Furthermore, in summertime over land, even the WCBs of mid-latitude cyclones are characterized by embedded deep convection, and the distinction between deep convection and WCB ascent becomes somewhat arbitrary [Kiley and Fuelberg, 2006]. A particular form of convection, pyro-convection, occurs over large forest fires and can inject large quantities of PM and trace gases into the upper troposphere and also deep into the stratosphere [Fromm *et al.*, 2000; Fromm *et al.*, 2005; Jost *et al.*, 2004].

Globally, the mass flux out of the ABL due to deep convection is comparable to the mass flux caused by the large-scale ascent in mid-latitude cyclones [Cotton *et al.*, 1995]. In addition, the ascent in deep convective cells takes only minutes, whereas the ascent in cyclones takes from hours up to two days. For trace gases with a rather short lifetime in the lower troposphere, such as SO<sub>2</sub>, this has the consequence that relatively large quantities can reach the mid- or upper troposphere in convective cells [Dickerson *et al.*, 2007], while much lower quantities would reach these altitudes in the slower vertical transport within WCBs.

#### *1.4.4. Diffuse or small scale atmospheric boundary layer venting*

Export of pollution from the ABL to the free troposphere can occur whenever an air parcel is transferred above the boundary-layer height. Over land, the height of the ABL has a distinct diurnal cycle with a daytime maximum, a nighttime minimum and the formation of a residual layer during the transition from day to night [Stull, 1988]. This residual layer is decoupled from the surface and experiences higher wind speeds than the air in the ABL, particularly when a nocturnal low-level jet is present [Angevine *et al.*, 1996]. The residual-layer air can (partly) remain in the free troposphere the next day if the ABL is less deep than on the previous day, or if other vertical transport processes lift it to higher altitudes.

Topography has a large influence on vertical pollution transport, as it generates variability in the ABL height, and the formation and breaking of orographic gravity waves above the ABL, which can cause mixing between different air masses. In particular, the mountain-valley wind systems encountered in mountainous regions can trigger vertical lofting. For example, in the Alps under fair weather conditions in summer, three times the valley volume can be lofted into the free troposphere per day [Furger *et al.*, 2000; Henne *et al.*, 2004], while CO mixing ratios over 2200 ppbv at 2500-3500 m were observed above Beijing due to vertical forcing of surface emissions up the nearby mountain slopes [Chen *et al.*, 2009]. Once pollutants are vented from the ABL they are subject to the long-range transport processes discussed above. On the other hand, during stable conditions (particularly in winter), pollutants can also accumulate in the valley atmosphere, preventing them from being transported over long distances, as occurs in Mexico City [De Foy *et al.*, 2008]. Mountain ranges also influence the large-scale flow, sometimes preventing transport over and across the mountain range.

#### *1.4.5. Slow, low altitude flow*

Air masses can also be transported over long distances without being lifted, albeit at slower speeds than in the mid- and upper troposphere. Often, this involves the formation of a residual layer, following the collapse of a daytime ABL. Or, pollutants can be emitted into a strongly stable ABL, confining transport to the lowermost troposphere with little vertical motion. Because dry deposition and the potential for cloud formation are limited under such conditions, PM and trace gases can be transported over long distances, even though transport speeds are lower than in the upper troposphere. Arctic Haze [Barrie, 1986], which can cover large parts of the Arctic in winter and spring, is often the result of such low-level long-range transport [Klonecki *et al.*, 2003; Stohl, 2006]. The phenomenon has also been observed downwind of North America, where layers with extremely high concentrations of oxidized nitrogen were found far downwind over the North Atlantic Ocean [Neuman *et al.*, 2006]. These layers can even reach the Azores [Owen *et al.*, 2006; Val Martin *et al.*, 2008] and Europe [Guerova *et al.*, 2006; Li *et al.*, 2002; Real *et al.*, 2008]. Similar transport pathways have been identified across the Pacific [Holzer *et al.*, 2005; Liang *et al.*, 2004]. The large-scale haze layers over the Indian Ocean generated by the winter monsoon outflow from southern Asia also have limited vertical extent until the flow reaches the intertropical convergence zone (ITZ) [Ramanathan *et al.*, 2001].

#### *1.4.6. Transport of polluted air masses into the atmospheric boundary layer of the receptor region*

The discussion so far has focused on the export of pollutants from the ABL of the source region, followed by long range transport, but the descent of polluted air masses to the surface of the receptor region is an equally important process. Rapid intercontinental transport (< 2 weeks) from Asia to North America and from North America to Europe occurs primarily in the free troposphere, and the main pathway to the surface of the receptor region is slow descent through anticyclones at the ends of the Pacific and Atlantic storm tracks [Cooper *et al.*, 2004; Hudman *et al.*, 2004; Stohl *et al.*, 2002a]. The descent of polluted air masses into the ABL of the receptor region appears to dominate over slow marine boundary layer or lower tropospheric transport across the oceans. These descending air masses warm as they approach the surface, forming a stable subsidence inversion. Transport past the subsidence inversion and into the ABL requires small scale processes that are parameterized in global or hemispheric scale transport models due to their coarse resolution.

Focusing on the North Pacific Ocean, the large majority of air that travels from the surface of Asia to the surface of the North American west coast transits the Pacific above an altitude of 2.2 km. Only in summer does low altitude transport account for a large share of Asian air reaching North America (50%) [Holzer and Hall, 2007]. Modelling of ozone in Asian air masses reaching North America shows that while ozone production can increase in the lower troposphere due to PAN decomposition, much of this air descends to the surface over the eastern Pacific and is advected westwards, without directly impacting North America. The major influence of Asian ozone on the North American surface is due to air subsiding from the mid- and upper troposphere [Zhang *et al.*, 2008]. However, during descent from the free troposphere to the surface of western North America



these air masses can be diluted by a factor of three, explaining why Asian pollution plumes are difficult to detect at the surface [Zhang *et al.*, 2009b].

Similar processes have been documented for North American pollution plumes transported eastward to Europe. The fastest moving plumes associated with the transport within the jet stream enter the northern European region in the mid- and upper troposphere. Slower moving plumes become entrained by the Azores High and descend to the European surface in the vicinity of the Alps and the Mediterranean region further south [Stohl *et al.*, 2002a]. North American pollution plumes have been observed at high altitude measurement sites in the Alps, but the imported pollution becomes indistinguishable from local pollution at low altitude European sites [Huntrieser *et al.*, 2005].

**FINDINGS: Intercontinental pollution transport is guided by the general circulation of the atmosphere and to a first approximation, constrained by the potential temperature structure of the atmosphere. Large-scale, rapid intercontinental transport frequently occurs in the warm conveyor belt of mid-latitude cyclones. Deep convection in tropical and mid-latitude regions is also a major mechanism for exporting pollution from the ABL to the mid- and upper troposphere where it can be rapidly transported towards a downwind continent. Intercontinental transport also occurs in the lower troposphere, but at slower speeds. The most intense pollution plumes are found in the mid- and upper troposphere but to be relevant to air quality in a downwind continent, the pollution must descend to the surface. As the plumes descend they are diluted and can be difficult to distinguish from local pollution, especially in receptor regions with relatively high emissions.**

**RECOMMENDATION: While great progress has been made in forecasting and intercepting intercontinental pollution plumes in the free troposphere, to date there has been little focus on measuring the composition of these plumes as they descend into the boundary layer of the receptor continent. Focused aircraft campaigns should be directed at sampling intercontinental pollution plumes as they descend from the free troposphere to the surface of a receptor continent. These measurements would reveal the impact of plumes on surface air quality and would be used to verify model simulations of these key downward transport processes.**

## **1.5. Impact of Present and Future Climate on Intercontinental Transport Processes**

### *1.5.1. Present day climate variability and its impact on intercontinental transport processes*

The description of intercontinental transport (ICT) processes so far has focused on the roles of emissions, typical transport pathways and chemical transformation. However, all three of these components can be affected by inter-annual to decadal climate variations. Much of the variability in intercontinental transport pathways, especially across the oceans is associated with oscillating sea-level pressure patterns. The most important of these oscillations are: 1) the North Atlantic Oscillation (NAO), in which the positive phase coincides with low pressure over Iceland and stronger than average westerly winds; there is little evidence for variability on preferred time scales and links to sea surface temperature are not well established [Hurrell *et al.*, 2003]; and 2) El Niño Southern Oscillation (ENSO), in which sea level pressure oscillates between the eastern Pacific and the western Pacific–Indian Ocean region, and is coupled to sea surface temperature variations in the equatorial Pacific. The El Niño phase recurs about every five years and is associated with warm sea surface temperatures in the eastern equatorial Pacific Ocean and dry, high pressure conditions over the western Pacific–Indian Ocean region.

In the northern mid-latitudes, source-receptor relationships are modulated by the NAO, with increased transport of North American emissions to northwest Europe, and increased transport of European emissions to the Arctic during the positive phase of the NAO. Positive values of Arctic Oscillation and NAO are associated with increased transport of U.S. emissions to Europe [Hess and Lamarque, 2007; Li *et al.*, 2002], and increased transport of European emissions to the Arctic and northern North America respectively, in winter [Duncan and Bey, 2004; Eckhardt *et al.*, 2003].

ENSO is the dominant mode of climate variability in the tropics and sub-tropics and affects climate in a number of world regions [Ropelewski and Halpert, 1987]. During El Niño winters

enhanced convection and stronger eastward transport of East Asian emissions in the subtropical eastern Pacific has been simulated [Liu *et al.*, 2005]. Dry conditions associated with the intense 1997/8 El Niño event led to increased biomass burning and widespread trace gas and PM emissions over Indonesia and the maritime continent [Duncan *et al.*, 2003; Ziemke and Chandra, 2003]. The anomalies in emissions, transport patterns and cloud cover altered tropospheric chemistry in this region, affecting concentrations of ozone and in some cases OH [Doherty *et al.*, 2006; Duncan *et al.*, 2003; Hess and Mahowald, 2009; Voulgarakis *et al.*, 2010]. Increases in stratosphere-troposphere exchange following El Niño events have also been simulated [Zeng and Pyle, 2005], which may lead to increases in ozone transported in mid-latitude airstreams.

Decreasing trends in mid-latitude cyclones over the past decades have been identified in the observational record and from meteorological reanalyses [Leibensperger *et al.*, 2008]. It has been suggested that decreasing mid-latitude cyclone frequency over the 1980–2006 period may have offset by half the ozone air quality gains in the northeastern U.S. from reductions in anthropogenic emissions [Leibensperger *et al.*, 2008]. This decrease in mid-latitude cyclone frequency has been associated with an increase at high-latitudes or a poleward shift of the storm track [McCabe *et al.*, 2001] and a positive trend in the Northern Annular Mode or Arctic Oscillation, and NAO [Harnik and Chang, 2003] during the 1970s through the 1990s. The poleward movement of the storm track is consistent with the widening of the tropical belt and the Hadley cell as estimated from multiple observational datasets over the past 2-3 decades [Seidel *et al.*, 2008].

### 1.5.2. Climate Change and its effects on intercontinental transport processes

Changes in climate will affect meteorological transport processes as well as the chemical environment and lifetime of the transported pollutants and hence the concentrations of pollutants arriving at downwind continents. Projections of changes in regional climate are generally less robust than those on larger hemispheric scales [Giorgi *et al.*, 2001].

Specific meteorological processes (e.g. mid-latitude airstreams, deep convection, subsidence; see Section 1.4) affect export of pollution from a source region and its import into the receptor region. These processes exhibit natural variability, but, in addition, if emission locations change, and/or climate changes, the intersection of pollution source regions and meteorology may also change, and this, in turn, may change export and import processes and magnitudes.

Warmer temperatures and higher water vapour concentrations in the future will affect background ozone as well as source-receptor relationships. Warmer temperatures affect ozone concentrations through: a) decreasing the lifetime of peroxyacetyl nitrate (PAN) and b) increasing biogenic emissions of isoprene [Jacob and Winner, 2009]. Increased water vapour in highly polluted areas has competing effects on ozone production [Jacob and Winner, 2009]. A number of coupled climate-chemistry model studies show increased water vapour in high emission source regions leading overall to increased local production of ozone [Hauglustaine *et al.*, 2005; Murazaki and Hess, 2006]. Once exported from a source region, the extent of long-range transport depends upon the lifetime of the pollutant and its precursors. For ozone, this is determined by chemical loss and dry deposition. For NO<sub>x</sub>, as discussed above, its reservoir PAN is strongly temperature-sensitive. Changes in wet deposition of the nitric acid reservoir may also be important for the NO<sub>x</sub> lifetime. The global mean lifetime of tropospheric ozone decreases as a result of increased water vapour in a warmer climate [Stevenson *et al.*, 2006]. For the case of PM, the lifetimes are heavily dependent on the wet deposition processes (i.e. the lifetimes decrease as wet deposition rates increase). Changes in cloud properties, precipitation patterns, and the quantity of precipitation resulting from climate change will impact the transport distances of PM.

A number of consistent changes in transport patterns under climate change scenarios have emerged from model, theoretical, and observational studies. An increasing trend in the positive phase of the NAO in climate change scenarios [Miller *et al.*, 2006], consistent with a preferential northerly location of future mid-latitude storm tracks in general circulation model simulations has been reported [Yin, 2005]. This is likely to lead to less frequent large-scale venting of the boundary layer and increased ozone pollution episodes in the major mid-latitude emission source regions [Leibensperger

*et al.*, 2008]. Mass balance analyses suggest that convective mass fluxes in the tropics will decrease in the future [Held and Soden, 2006], but future changes in convection height which is uncertain may also be important for the lofting of pollutants. Changes in export from source regions together with changes in transport patterns will determine future source-receptor relationships. The extent to which future changes in transport patterns affect pollution episodes and source-receptor relationships remains uncertain (see section 4.6.2).

**FINDING: Climate variations on inter-annual to decadal time scales can modify intercontinental transport pathways, emissions and chemical transformation processes. In addition, a warmer future climate is expected to modify intercontinental transport pathways, emissions and chemical transformation processes.**

## 1.6. Chapter storylines

This section provides the storylines of Chapters 2-6, which cover the observational evidence for intercontinental transport of air pollution (ICT), global emissions of trace gases and PM, model simulations of ICT, and the impacts of ICT on human health, ecosystems and the radiative forcing of climate. While this scientific assessment report does not establish policy for air pollution controls, it does demonstrate how ICT can affect compliance with air quality standards, a primary concern for policymakers. Figure 1.9 depicts the linkages between policy, air pollutants, ICT, climate change and air quality standard violations. The following narrative of the figure highlights the key process and indicates the chapters (2-5) that address them.

National and local air pollution control policies regulate the emissions (3) of trace gases and PM relevant for air quality, climate change, or both. Atmospheric chemistry and meteorology remove and transform a portion of the primary emissions, producing secondary pollutants (1, 2, and 4). Domestic emission and production of air quality species, with a contribution from foreign sources, may lead to exceedances of domestic air quality standards (2, 4, and 5). This figure focuses on air quality standard exceedances rather than average air quality conditions, because from a practical standpoint, exceedances are typically the motivation for changing national and local policies aimed at controlling emissions. Achievement of this goal may partly depend upon foreign policies.

In addition to present influences of policy and emissions on compliance with air quality standards, global climate change will affect future scenarios. While some PM has a negative impact on radiative forcing (i.e. cooling), the net effect of the emission of climate species (see Figure 1.9) is positive radiative forcing which warms the climate (5). A warmer climate can then influence emissions of climate sensitive trace gases and PM, and alter transport pathways and chemical lifetime and processing (4), with implications for human and ecosystem impacts (5). These climate change effects may influence local, national and foreign air pollution control policies.



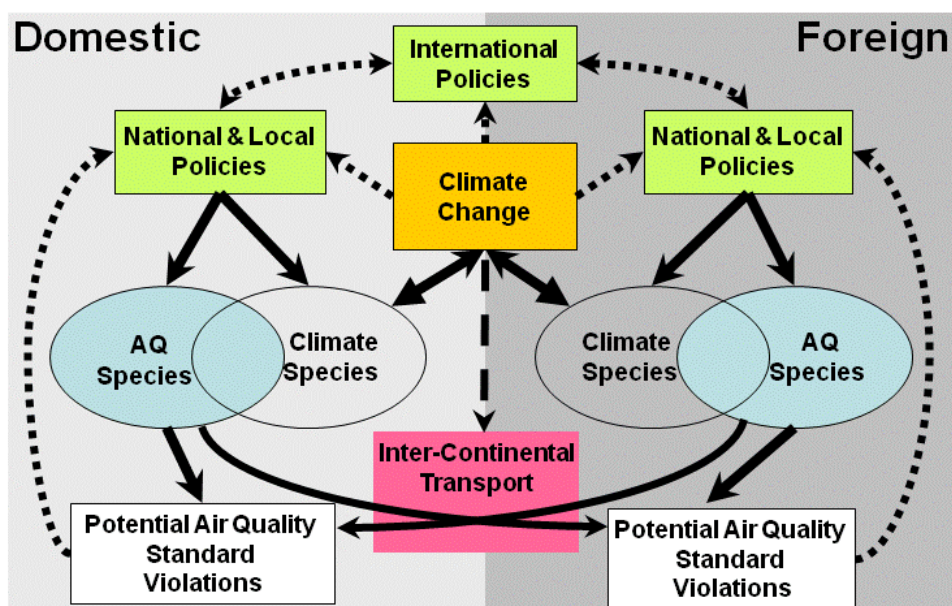


**Figure 1.9.** A depiction of the links between domestic and foreign air pollution control policies, air quality, global climate change, and the role of the intercontinental transport of air pollution. The arrows indicate causal influences (solid single-headed arrows), effects of climate change on climate/AQ species and their feedback on climate (double-headed arrows), a potential climate change influence on hemispheric transport processes (dashed arrow), and influences on policy (dotted arrows). AQ Species (e.g. ozone, PM, CO, NO<sub>x</sub>, SO<sub>2</sub>) and Climate Species (e.g. CO<sub>2</sub>, CH<sub>4</sub>, ozone, PM, N<sub>2</sub>O) are the ambient concentrations of trace gases and PM, both emitted directly and produced within the atmosphere. Therefore these ovals contain the influence of anthropogenic and natural emissions, as well as meteorological and chemistry processes. Ozone and PM are found at the intersection of the AQ and Climate Species ovals. HTAP indicates the hemispheric transport of air pollution and includes meteorological processes and chemical transformation processes. The foreign pollution transported to a domestic location may have sources in many different nations.

## References

- Angevine, W. M., et al. (1996), Local meteorological features affecting chemical measurements at a north Atlantic coastal site, *Journal of Geophysical Research*, 101(22): 28935-28946.
- Auvray, M., and I. Bey (2005), Long-range transport to Europe: Seasonal variations and implications for the European ozone budget, *Journal of Geophysical Research*, 110(D11303).
- Bader, M. J., et al. (Eds.) (1995), *Images in weather forecasting: A practical guide for interpreting satellite and radar imagery*, 499 pp., University Press, Cambridge
- Barrie, L. A. (1986), Arctic air pollution: An overview of current knowledge, *Atmospheric Environment*, 20(4): 643-663.
- Bethan, S., et al. (1998), Chemical air mass differences near fronts, *Geophysical Research Letters*, 103(D11): 13413-13434.
- Bowman, K. P., and G. D. Carrie (2002), The Mean-Meridional Transport Circulation of the Troposphere in an Idealized GCM, *Journal of the Atmospheric Sciences*, 59(9): 1502-1514.
- Bowman, K. P., and T. Erukhimova (2004), Comparison of Global-Scale Lagrangian Transport Properties of the NCEP Reanalysis and CCM3, *Journal of Climate*, 17(5): 1135-1146.
- Brock, C. A., et al. (2004), Particle characteristics following cloud-modified transport from Asia to North America, *Journal of Geophysical Research*, 109(D23S26).
- Browning, K. A., and G. A. Monk (1982), A simple model for the synoptic analysis of cold fronts, *Quarterly Journal of the Royal Meteorological Society*, 108(456): 435-452.
- Browning, K. A., and N. M. Roberts (1994), Structure of a frontal cyclone, *Quarterly Journal of the Royal Meteorological Society*, 120(520): 23.

- Carlson, T. N. (1998), *Midlatitude Weather Systems*, 507 pp., American Meteorological Society, Boston.
- Chen, Y., et al. (2009), Aircraft study of mountain chimney effect of Beijing, China, *Journal of Geophysical Research*, *114*(D08306).
- Cooper, O. R., et al. (2002), Trace gas composition of mid-latitude cyclones over the western North Atlantic Ocean: A conceptual model, *Journal of Geophysical Research*, *107*(D7): 4056-4068.
- Cooper, O. R., et al. (2004), A case study of trans-Pacific warm conveyor belt transport: The influence of merging airstreams on trace gas import to North America, *Journal of Geophysical Research*, *109*(D23S08).
- Cooper, O. R., et al. (2010), Increasing springtime ozone mixing ratios in the free troposphere over western North America, *Nature* *463*: 344-348.
- Cotton, W. R., et al. (1995), Cloud venting -- A review and some new global annual estimates, *Earth-Science Reviews*, *39*(3-4): 38.
- Crutzen, P. J., and M. O. Andreae (1990), Biomass burning in the tropics: Impact on atmospheric chemistry and biogeochemical cycles, *Science*, *250*: 1669-1678.
- De Foy, B., et al. (2008), Basin-scale wind transport during the milagro field campaign and comparison to climatology using cluster analysis, *Atmospheric Chemistry and Physics*, *8*(5): 1209-1224.
- Derwent, R. G., et al. (2004), Intercontinental transport and the origins of the ozone observed at surface sites in Europe, *Atmospheric Environment*, *38*(13): 1891-1901.
- Derwent, R. G. (2008), New Directions: Prospects for regional ozone in north-west Europe, *Atmospheric Environment*, *42*: 1958-1960.
- Dickerson, R. R., et al. (1987), Thunderstorms: An Important Mechanism in the Transport of Air Pollutants, *Science*, *235*(4787): 460-465.
- Dickerson, R. R., et al. (2007), Aircraft observations of dust and pollutants over northeast China: Insight into the meteorological mechanisms of transport, *Journal of Geophysical Research*, *112*(D24S90).
- Doherty, R., et al. (2006), Tropospheric O<sub>3</sub> and El Nino-Southern Oscillation: influence of atmospheric dynamics, biomass burning emissions, and future climate change, *Journal of Geophysical Research*, *111*(D19304).
- Duncan, B. N., et al. (2003), Interannual and seasonal variability of biomass burning emissions constrained by satellite observations, *Journal of Geophysical Research*, *108*(D2): 4100-4121.
- Duncan, B. N., and I. Bey (2004), A modeling study of export pathways of pollution from Europe: Seasonal and interannual variations (1987-1997), *Journal of Geophysical Research*, *109*(D08301).
- Dunlea, E. J., et al. (2009), Evolution of Asian aerosols during transpacific transport in INTEX-B f, *Atmospheric Chemistry and Physics*, *9*: 7257-7287.
- Eckhardt, S., et al. (2003), The North Atlantic Oscillation controls air pollution transport to the Arctic, *Atmospheric Chemistry and Physics*, *3*: 1769-1778.
- Eckhardt, S., et al. (2004), A 15-Year Climatology of Warm Conveyor Belts, *Journal of Climate*, *17*(1): 218-237.
- Fiore, A. M., et al. (2002), Background ozone over the United States in summer: origin, trend, and contribution to pollution episodes, *Journal of Geophysical Research*, *107*(D15): 4275-4299.
- Fiore, A. M., et al. (2003), Variability in surface ozone background over the United States: Implications for Air Quality Policy, *Journal of Geophysical Research - Atmospheres*, *108*(D24): 4787-4798.
- Fromm, M., et al. (2000), Observations of boreal forest fire smoke in the stratosphere by POAM III, SAGE II, and lidar in 1998, *Geophysical Research Letters*, *27*(9): 1407-1410.
- Fromm, M., et al. (2005), Pyro-cumulonimbus injection of smoke to the stratosphere: Observations and impact of a super blowup in northwestern Canada on 3-4 August 1998, *Journal of Geophysical Research*, *110*(D08205).
- Furger, M., et al. (2000), The VOTALP Mesolcina Valley Campaign 1996 - concept, background and some highlights, *Atmospheric Environment*, *34*(9): 1395-1412.
- Giorgi, F., et al. (2001), Regional Climate Information - Evaluation and Projections, in *Climate Change 2001: The scientific basis: Contribution of Working Group 1 to the Third Assessment Report of the Intergovernmental Panel on Climate Change*, edited by J. T. Houghton, et al., 583-638 pp., Cambridge University Press, Cambridge.
- Guerova, G., et al. (2006), Impact of transatlantic transport episodes on summertime ozone in Europe, *Atmospheric Chemistry and Physics*, *6*: 2057-2072.

- Harnik, N., and E. K. M. Chang (2003), Storm track variations as seen in radiosonde observations and reanalysis data, *Journal of Climate*, 16(3): 480-495.
- Hauglustaine, D. A., et al. (2005), Future tropospheric ozone simulated with a climate-chemistry-biosphere model, *Geophysical Research Letters*, 32: L24807.
- Heald, C. L., et al. (2006), Concentrations and sources of organic carbon aerosols in the free troposphere over North America, *Journal of Geophysical Research*, 111(D23S47).
- Held, I. M., and B. J. Soden (2006), Robust responses of the hydrological cycle to global warming, *Journal of Climate*, 19(21): 5686-5699.
- Henne, S., et al. (2004), Quantification of topographic venting of boundary layer air to the free troposphere, *Atmospheric Chemistry and Physics*, 4(2): 497-509.
- Hess, P., and N. Mahowald (2009), Interannual variability in hindcasts of atmospheric chemistry: the role of meteorology, *Atmospheric Chemistry and Physics*, 9: 5261-5280.
- Hess, P. G. (2005), A comparison of two paradigms: The relative global roles of moist convective versus nonconvective transport, *Journal of Geophysical Research* 110(D20): D20302.
- Hess, P. G., and J.-F. Lamarque (2007), Ozone source attribution and its modulation by the Arctic oscillation during the spring months, *Journal of Geophysical Research*, 112(D11303).
- Holzer, M., et al. (2005), Seasonality and weather-driven variability of transpacific transport, *Journal of Geophysical Research* 110(D23103).
- Holzer, M., and T. M. Hall (2007), Low-level transpacific transport, *Journal of Geophysical Research*, 112(D09103).
- Horowitz, L. W. (2006), Past, present, and future concentrations of tropospheric ozone aerosols: Methodology, ozone evaluation, and sensitivity to aerosol wet removal, *Journal of Geophysical Research*, 111(D22211).
- Hudman, R. C., et al. (2004), Ozone production in transpacific Asian pollution plumes and implications for ozone air quality in California, *Journal of Geophysical Research*, 109(D23S10).
- Huntrieser, H., et al. (2005), Intercontinental air pollution transport from North America to Europe: Experimental evidence from airborne measurements and surface observations, *Journal of Geophysical Research*, 110(D01305).
- Hurrell, J. W., et al. (Eds.) (2003), *The North Atlantic Oscillation: Climate Significance and Environmental Impact*, 279 pp., American Geophysical Union, Washington, DC. Geophysical Monograph 134
- Jacob, D. J., et al. (1987), Atmospheric distribution of <sup>85</sup>Kr simulated with a general circulation model, *Journal of Geophysical Research*, 92(D6): 6614-6626.
- Jacob, D. J., and D. A. Winner (2009), Effect of climate change on air quality, *Atmospheric Environment*, 43(1): 51-63.
- Jaffe, D., et al. (2005), Seasonal cycle and composition of background fine particles along the west coast of the US *Atmospheric Environment*, 39(2): 297-306.
- Jost, H.-J., et al. (2004), In-situ observation of midlatitude forest fire plumes deep in the stratosphere, *Geophysical Research Letters*, 31(L11101).
- Kiley, C. M., and H. E. Fuelberg (2006), An examination of summertime cyclone transport processes during Intercontinental Chemical Transport Experiment (INTEX-A), *Journal of Geophysical Research*, 111(D24S06).
- Klonecki, A., et al. (2003), Seasonal changes in the transport of pollutants into the Arctic troposphere - model study, *Journal of Geophysical Research*, 108(D48367).
- Lamarque, J.-F., et al. (2005), Tropospheric ozone evolution between 1890 and 1990, *Journal of Geophysical Research*, 110(D08304).
- Law, K. S., and A. Stohl (2007), Arctic air pollution: Origins and impacts, *Science*, 315(5818): 1537-1540.
- Leibensperger, E. M., et al. (2008), Sensitivity of U.S. air quality to midlatitude cyclone frequency and implications of 1980-2006 climate change, *Atmospheric Chemistry and Physics*, 8(23): 7075-7086.
- Lelieveld, J., and P. J. Crutzen (1994), Role of deep cloud convection in the ozone budget of the troposphere, *Science*, 264(5166): 1759-1761.
- Lelieveld, J., and F. J. Dentener (2000), What Controls tropospheric ozone?, *Journal of Geophysical Research*, 105(D3): 3531-3551.

- Li, Q., et al. (2002), Transatlantic transport of pollution and its effects on surface ozone in Europe and North America, *Journal of Geophysical Research*, 107(D134166).
- Li, Q., et al. (2004), Export of NO<sub>y</sub> from the North American boundary layer: Reconciling aircraft observations and global model budgets, *Journal of Geophysical Research*, 109(D02313).
- Liang, Q., et al. (2004), Long-range transport of Asian pollution to the northeast Pacific: Seasonal variations and transport pathways of carbon monoxide, *Journal of Geophysical Research*, 109(D23S07).
- Liu, J., et al. (2005), Analysis of seasonal and interannual variability in transpacific transport, *Journal of Geophysical Research*, 110(D04302).
- Logan, J. A., et al. (1981), Tropospheric chemistry: A global perspective, *Journal of Geophysical Research*, 86(C8): 7210-7254.
- McCabe, G. J., et al. (2001), Trends in Northern Hemisphere surface cyclone frequency and intensity, *Journal of Climate*, 14(12): 2763-2768.
- Merrill, J. T., and J. L. Moody (1996), Synoptic meteorology and transport during the North Atlantic Regional Experiment (NARE) intensive: Overview, *Journal of Geophysical Research*, 101(D22): 28903-28921.
- Methven, J., et al. (2006), Establishing Lagrangian connections between observations within air masses crossing the Atlantic during the International Consortium for Atmospheric Research on Transport and Transformation, *Journal of Geophysical Research*, 111(D23S62).
- Miller, R. L., et al. (2006), Forced annular variations in the 20th century intergovernmental panel on climate change Fourth Assessment Report models, *Journal of Geophysical Research*, 111(D18101).
- Miyazaki, K., et al. (2005), Roles of transport in the seasonal variation of the total ozone amount, *Journal of Geophysical Research*, 110(D18309).
- Murazaki, K., and P. Hess (2006), How does climate change contribute to surface ozone change over the United States?, *Journal of Geophysical Research*, 111(D05301).
- Neuman, J. A., et al. (2006), Reactive nitrogen transport and photochemistry in urban plumes over the North Atlantic Ocean, *Journal of Geophysical Research*, 111(D23S54).
- Owen, R. C., et al. (2006), An analysis of the mechanisms of North American pollutant transport to the Central North Atlantic lower free troposphere, *Journal of Geophysical Research*, 111: D23S58.
- Parrish, D., et al. (1998), Relationships between ozone and carbon monoxide at surface sites in the North Atlantic region, *Journal of Geophysical Research - Atmospheres*, 103(D11): 13357-13376.
- Parrish, D., et al. (2009), Increasing ozone in marine boundary layer inflow at the west coasts of North America and Europe, *Atmospheric Chemistry and Physics*, 9: 1303-1323.
- Patra, P. K., et al. (2009), Transport mechanisms for synoptic, seasonal and interannual SF<sub>6</sub> variations and "age" of air in troposphere, *Atmospheric Chemistry and Physics*, 9: 1209-1225.
- Pierrehumbert, R. T., and H. Yang (1993), Global chaotic mixing on isentropic surfaces, *Journal of Atmospheric Science*, 50(15): 2462-2480.
- Prather, M. J., et al. (1987), Chemistry of the global troposphere: Fluorocarbons as tracers of air motion, *Journal of Geophysical Research*, 92(D6): 6579-6613.
- Ramanathan, V., et al. (2001), Indian Ocean Experiment: An integrated analysis of the climate forcing and effects of the great Indo-Asian haze, *Journal of Geophysical Research*, 106(D22): 28371-28398.
- Real, E., et al. (2007), Processes influencing ozone levels in Alaskan forest fire plumes during long-range transport over the North Atlantic, *Journal of Geophysical Research*, 112: D10S41.
- Real, E., et al. (2008), Lagrangian analysis of low altitude anthropogenic plume processing across the North Atlantic, *Atmospheric Chemistry and Physics*, 8: 7737-7754.
- Reeves, C. E., et al. (2002), Potential for photochemical ozone formation in the troposphere over the North Atlantic as derived from aircraft observations during ACSOE, *Journal of Geophysical Research*, 107(D23): 4707-4720.
- Ropelewski, C. F., and M. S. Halpert (1987), Global and regional scale precipitation patterns associated with El-Niño Southern Oscillation, *Monthly Weather Review*, 115: 1606-1626.
- Royal Society (2008), Ground-level ozone in the 21st century: future trends, impacts and policy implications, 148 pp, The Royal Society, London.
- Schultz, M., and S. Rast (2007), Emission data sets and methodologies for estimating emissions, 77 pp, REanalysis of the TROpospheric chemical composition over the past 40 years (RETRO). *Work Package 1, Deliverable D1-6*. [http://retro.enes.org/reports/D1-6\\_final.pdf](http://retro.enes.org/reports/D1-6_final.pdf)

- Schumann, U., and H. Huntrieser (2007), The global lightning-induced nitrogen oxides source, *Atmospheric Chemistry and Physics*, 7: 3823-3907.
- Seibert, P., and A. Frank (2004), Source-receptor matrix calculation with a Lagrangian particle dispersion model in backward mode, *Atmospheric Chemistry and Physics*, 4: 51-63.
- Seidel, D. J., et al. (2008), Widening of the tropical belt in a changing climate, *Nature Geoscience*, 1: 21-24.
- Singh, H. B., et al. (1992), Relationship of peroxyacetyl nitrate to active and total odd nitrogen at northern high-latitudes: Influence of reservoir species on NO<sub>x</sub> and O<sub>3</sub>, *Journal of Geophysical Research*, 97(D15): 16523-16530.
- Stevenson, D. S., et al. (2006), Multimodel ensemble simulations of present-day and near-future tropospheric ozone, *Journal of Geophysical Research*, 111(D08301).
- Stohl, A., and T. Trickl (1999), A textbook example of long-range transport: Simultaneous observations of ozone maxima of stratospheric and North America origin in the free troposphere over Europe, *Journal of Geophysical Research*, 104(D23): 30445-30462.
- Stohl, A., et al. (2002a), On the pathways and timescales of intercontinental air pollution transport, *Journal of Geophysical Research*, 107(D23): 4684-4700.
- Stohl, A., et al. (2002b), Export of NO<sub>y</sub> from the North American boundary layer during 1996 and 1997 North Atlantic Regional Experiments, *Journal of Geophysical Research*, 107(D11): 4131-4145.
- Stohl, A., et al. (2003), A backward modeling study of intercontinental pollution transport using aircraft measurements, *Journal of Geophysical Research*, 108(D12): 4370-4387.
- Stohl, A., and S. Eckhardt (2004), Intercontinental Transport of Air Pollution: An Introduction, in *Intercontinental Transport of Air Pollution*, edited by A. Stohl, Springer, Berlin.
- Stohl, A. (2006), Characteristics of atmospheric transport into the Arctic troposphere, *Journal of Geophysical Research*, 111(D11306).
- Stohl, A., et al. (2007), Aircraft measurements over Europe of an air pollution plume from Southeast Asia – aerosol and chemical characterization, *Atmospheric Chemistry and Physics*, 7(3): 913-937.
- Stull, R. B. (1988), *An Introduction to Boundary Layer Meteorology*, Kluwer Academic Publishers, Dordrecht, Holland.
- Sudo, K., and H. Akimoto (2007), Global source attribution of tropospheric ozone: Long-range transport from various source regions, *Journal of Geophysical Research*, 112(D12302).
- U.S. EPA (2009), National Emissions Inventory (NEI) Air Pollutant Emissions Trends Data, U.S. Environmental Protection Agency, <http://www.epa.gov/ttnchie1/trends/>
- Val Martin, M., et al. (2008), Large-scale impacts of anthropogenic pollution and boreal wildfires on the nitrogen oxides over the central North Atlantic region, *Journal of Geophysical Research*, 113(D17308).
- van der A, R. J., et al. (2008), Trends, seasonal variability and dominant NO<sub>x</sub> source derived from a ten year record of NO<sub>2</sub> measured from space, *Journal of Geophysical Research*, 113: D04302.
- van der Werf, G. R., et al. (2006), Interannual variability in global biomass burning emissions from 1997 to 2004, *Atmospheric Chemistry and Physics*, 6: 3423-3441.
- van Donkelaar, A., et al. (2008), Analysis of aircraft and satellite measurements from the Intercontinental Chemical Transport Experiment (INTEX-B) to quantify long-range transport of East Asian sulfur to Canada, *Atmospheric Chemistry and Physics*, 8: 2999-3014.
- Venkatram, A., and P. Karamchandani (1986), Source-receptor relationships. A look at acid deposition modeling, *Environmental Science & Technology*, 20(11): 1084-1091.
- Voulgarakis, A., et al. (2010), Interannual variability of tropospheric composition: The influence of changes in emissions, meteorology and clouds, *Atmospheric Chemistry & Physics*, 10: 2491-2506.
- Wang, Y. H., et al. (1998), Global simulation of tropospheric O<sub>3</sub>-NO<sub>x</sub>-hydrocarbon chemistry 3. Origin of tropospheric ozone and effects of nonmethane hydrocarbons, *Journal of Geophysical Research*, 103(D9): 10757-10767.
- Wild, O., and H. Akimoto (2001), Intercontinental transport of ozone and its precursors in a three dimensional globe CTM, *Journal of Geophysical Research* 106(D21): 27729-27744.
- Yin, J. H. (2005), A consistent poleward shift of the storm tracks in simulations of the 21st century climate., *Geophysical Research Letters*, 32(L18701).
- Zeng, G., and J. A. Pyle (2005), Influence of El Nino Southern Oscillation on stratosphere/troposphere exchange and the global tropospheric ozone budget, *Geophysical Research Letters*, 32(L01814).

- Zhang, L., et al. (2008), Transpacific transport of ozone pollution and the effect of recent Asian emission increases on air quality in North America: An integrated analysis using satellite, aircraft, ozonesonde, and surface observations, *Atmospheric Chemistry and Physics*, 8(20): 6117-6136.
- Zhang, L., et al. (2009a), Intercontinental source attribution of ozone pollution at western U.S. sites using an adjoint method, *Geophysical Research Letters*, 36(L11810).
- Zhang, Q., et al. (2009b), Asian emissions in 2006 for the NASA INTEX-B mission, *Atmospheric Chemistry and Physics*, 9: 5161-5153.
- Ziemke, J. R., and S. Chandra (2003), La Nina and El Nino - induced variabilities of ozone in the tropical lower atmosphere during 1970-2001, *Geophysical Research Letters*, 30(3): 1142-1145.

## Chapter 2

# Observational Evidence and Capabilities Related to Intercontinental Transport of Ozone and Particulate Matter

**Lead Authors: Kathy Law, David Parrish**

**Co-authors: Steve Arnold, Elton Chan, Gao Chen, Owen Cooper, Dick Derwent, David Edwards, Dan Jaffe, Dorothy Koch, Paolo Laj, Randall Martin, John Methven, Paul Monks, Stuart Penkett, Joe Prospero, Patricia Quinn, Lorraine Remer, Johannes Staehelin, Rich Scheffe, Akinori Takami, Hiroshi Tanimoto, Valerie Thouret, Solene Turquety, Christian Zdanowicz, Jerry Ziemke**

### 2.1. Introduction

For several decades it has been possible to measure particulate matter, ozone (O<sub>3</sub>) and their important precursors at even the lowest concentrations found in the most remote regions of the Northern Hemisphere. Even the earliest measurements found that long-range transport exerts a strong influence on these observed concentrations. For example, dust of Asian origin was observed throughout the North Pacific region [Duce *et al.*, 1980; Prospero, 1979] and studies at the west coast of North America in 1985 identified the influence of Asian emissions on the sulphur budget [Andreae *et al.*, 1988] and on the concentrations of O<sub>3</sub>, hydrocarbons, and peroxyacetyl nitrate (PAN) [Parrish *et al.*, 1992]. It has also been clear since at least the 1980s that increasing anthropogenic emissions of NO<sub>x</sub> since preindustrial times have led to pronounced ozone concentration increases throughout the Northern Hemisphere [e.g., Crutzen, 1988].

This chapter aims to document observational evidence for the long-range transport of pollutants between continents. The focus is on the transport of O<sub>3</sub> and particulate matter (PM) from major emission regions of the Northern Hemisphere and their impact on observed concentrations in downwind receptor regions. This includes trans-Pacific and trans-Atlantic transport as well as transport out of Europe and transport to the Arctic. O<sub>3</sub> and a certain fraction of PM such as sulphate are secondary pollutants produced from precursor emissions such as carbon monoxide (CO), NO<sub>x</sub>, and sulphur dioxide (SO<sub>2</sub>) (see Chapter 1). They are produced close to source regions, especially in the case of PM, before being transported downwind. During transport pollutant concentrations will change due to photochemical production from transported precursors, photochemical and physical loss processes (dry, wet deposition, microphysics) and mixing with air of different composition. Thus, there is no point-to-point relationship between source and receptor. Air masses arriving at a downwind location will be the result of complex air mass histories, and will include components related to emissions from various source regions.

The signature of long-range pollutant transport in downwind measurements depends on the lifetime of the particular pollutant and the extent to which a pollutant plume mixes with other air masses. For PM and other pollutants with short lifetimes, on the order of a few days, long-range transport between continents is observed in the form of discrete plumes with pollutant concentrations significantly greater than those usually encountered. Often such a plume can be directly attributed to a particular upwind source. In favourable cases particular plumes can be tracked in satellite data over periods of several days.

For O<sub>3</sub> and CO, pollutants with lifetimes of weeks to months in the free troposphere, mixing of air masses with different histories plays a dominant role in defining the spectrum of concentrations found in any region of the troposphere. Photochemical production can also be important for O<sub>3</sub>. Mixing can significantly modify discrete plume signatures. Figure 2.1 shows the concentration distributions of CO and O<sub>3</sub> derived from 176 separate ascents and descents of MOZAIC aircraft into two North American west coast cities during the summers of 2003-2006. These distributions exemplify the plume signatures that result after trans-Pacific transport. At each city the CO distribution is well defined as a log-normal distribution of mixing ratios, with only a very few ( $\approx 1 - 2$  % of the total data) higher concentration plumes distinguishable from this general distribution, and only at Portland, Oregon (U.S.). Similarly, the O<sub>3</sub> distributions exhibit very few plumes (<1 % of the

data) with concentrations greater than 100 parts per billion by volume (ppbv), which generally reflect air masses with a stratospheric origin. Thus, the entire troposphere can be envisioned as completely filled with plumes of continuously varying concentrations in the process of intermixing and dispersing. The broad distribution of concentrations represents the plumes responsible for transporting the large majority of O<sub>3</sub> and CO between continents, and the discrete, more concentrated plumes contribute only minimally. Impacts from a particular emission region will therefore be reflected in the average and associated variability of observed concentrations at a particular downwind location, and not as a series of discrete events. The fact that air arrives over a downwind continent as a continuous distribution of air masses with different emission histories from both anthropogenic and natural sources makes it difficult to quantify the contribution directly attributable to a particular emission region from observations alone.

Abundant evidence of episodes of long-range transport of elevated concentrations of both O<sub>3</sub> and PM is available as exemplified in this chapter, but determination of the impact of observed transport on downwind regional air quality presents further challenges, i.e. how does import of pollutants from a particular source region change concentrations in the boundary layer of the receptor region. It is clear there are preferential regions for pollutant import over receptor regions (see Chapter 1), but import of pollutants in the free troposphere does not mean that these air masses then descend into the boundary layer. Robust, quantitative determination of the pollution import into a region would require a dense network of vertically resolved measurements, which presently does not exist.

Various definitions have been employed in attempts to quantify the contribution of long-range transport to the observed concentrations and temporal changes in concentrations of pollutants observed in downwind measurements (see Chapter 1). The term “background” is often used to describe concentrations at “clean, remote” sites that have not been influenced by anthropogenic pollution. However, for relatively long-lived pollutants such as O<sub>3</sub>, all sites in the northern hemisphere are influenced by anthropogenic emissions, so that the use of this term is ambiguous. The term “baseline” is used here to describe concentrations in air masses without the contribution from local anthropogenic emissions. Diagnosis of baseline concentrations is not straightforward because of the complex air mass histories described above. Analysis of decadal changes in mean O<sub>3</sub> concentrations at representative receptor region sites can provide indications of the impact of changing anthropogenic emissions. However, it must be recognized that changes in the observed concentrations can be confounded by changes in natural sources and changes in transport patterns. Furthermore, different changes of anthropogenic emissions in different source regions can complicate the picture. Thus, observing concentration changes and attributing them to changes in upwind emissions is complex.

In this Chapter, we first consider the direct observational evidence for long-range transport of O<sub>3</sub> (Section 2.2) and PM (Section 2.3) from satellite, aircraft, and ground-based data. Long-term changes (trends) in the amount of O<sub>3</sub> or PM at appropriate measurement locations are also discussed. Section 2.4 summarizes results arising from the use of meteorologically-based and data-based techniques (e.g. constituent ratios) to quantify the sources contributing to measurements collected at particular locations. Results and subsequent analysis from field experiments specifically designed to quantify the processing occurring during long-range transport are also discussed. A summary of future research needs is given in Section 2.5. In this chapter the term “aerosols” is often used interchangeably with “particulate matter (PM)” as is customary in the field of atmospheric chemistry, even though “aerosols” technically refers to the suspension of PM in air.

**FINDING: The signature of long-range pollutant transport in measurements made downwind of sources depends on the lifetime of the particular pollutant. Discrete plumes of enhanced concentrations characterize pollutants with short lifetimes and no photochemical sources, while continuous distributions of concentrations represent transport of pollutants with longer lifetimes. In the latter case, the entire troposphere can be envisioned as completely filled with plumes of continuously varying concentrations in the process of intermixing and dispersing.**

**RECOMMENDATION: For longer-lived species such as O<sub>3</sub> and CO a broad distribution of concentrations represents plumes responsible for transporting the large majority of these species between continents. This broad distribution of baseline concentrations of such species**



requires fuller characterization by measurement programs to allow comparison with global model calculations, and for input as boundary conditions into regional air quality models.

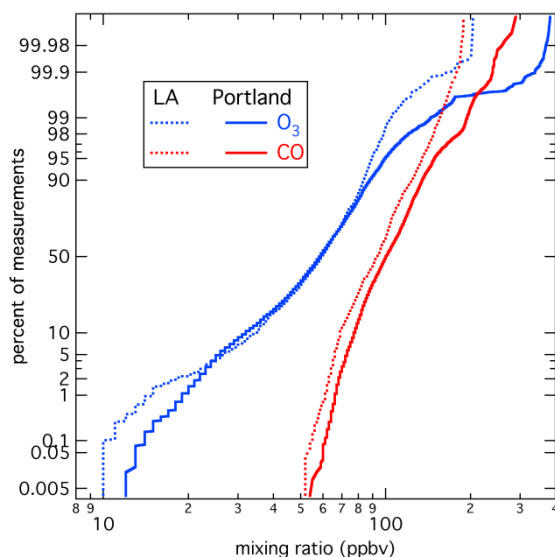


**Figure 2.1.** Summertime probability distribution functions of CO (red lines) and O<sub>3</sub> (blue lines) measured between 2 and 10 km altitude by MOZAIC (<http://mozaic.aero.obs-mip.fr>) aircraft on descents into and ascents out off Portland, Oregon (solid lines) and Los Angeles, California (dotted lines) on the U.S. west coast.

## 2.2. Long-range Transport of Ozone and its Precursors

### 2.2.1. The View from Satellites

The major advances in satellite remote sensing over the last decade now provide a global perspective of intercontinental pollution transport and the impact of that transport upon downwind receptor regions. Table 2.1 summarizes satellite remote sensing capabilities of tropospheric O<sub>3</sub> and its precursors. Only downward (nadir) viewing instruments are included here. All fly in near-polar, sun-synchronous, low Earth orbits. Observations at low and mid-latitudes are at a constant local time; sampling frequency increases at high latitudes. These instruments employ passive techniques, observing either solar backscatter (SCIAMACHY, OMI, GOME-2) or thermal emission (MOPITT, TES, AIRS, IASI). Retrievals of NO<sub>2</sub> and formaldehyde (HCHO) are tropospheric columns, while the retrievals of CO and O<sub>3</sub> often have some vertical profile information (typically 0.5-2 Degrees of Freedom for Signal). Other observations include nitric acid (HNO<sub>3</sub>) [Wespes *et al.*, 2009] and glyoxal [Wittrock *et al.*, 2006]. Two recent workshops assessed air quality applications from space [Edwards, 2006; EU, 2006], and two recent reviews describe capabilities for satellite remote sensing of air quality [Fishman *et al.*, 2008; Martin, 2008].

Satellite observations of CO provide the most compelling remote-sensing evidence for long-range transport of trace gases. Animations of satellite observations for successive days reveal clear visualization of transport from continental source regions across oceans. Published examples of long-range transport of CO within the Northern Hemisphere include transport both from Asia to North America [Heald *et al.*, 2003; Zhang *et al.*, 2008] and from North America to Europe [Guerova *et al.*, 2006; Pfister *et al.*, 2006]. Figure 2.2 shows a multi-day average of a CO plume from intense wildfires in Alaska and Canada. The plume can be traced across North America and the Atlantic Ocean to Europe. Aircraft measurements as part of the ICARTT aircraft campaign that sampled this plume corroborate the long-range transport. Inverse modelling using the MOZART chemical transport model showed that the fires emitted about as much CO as did human-related activities in the continental U.S, during the same time period, about 30 teragrams (Tg) CO for June-August, 2004. Modelling and measurements show that emissions from the 2004 North American wildfires caused ground-level concentrations of O<sub>3</sub> to increase by 25 per cent or more in parts of the northern

continental U.S. and the central North Atlantic and by 10 per cent as far away as Europe [Pfister et al., 2006; Val Martin et al., 2006, see also discussion in Section 2.4]. Satellite observations of NO<sub>2</sub> also provide evidence of long-range transport from North America to Europe [Guerova et al., 2006; Martin et al., 2006].

Satellite observations of tropospheric O<sub>3</sub> columns have matured considerably over the last decade to reveal mid-latitude features with increasing confidence [Creilson et al., 2003; Liu et al., 2010; Schoeberl et al., 2007; Worden, 2007; Ziemke et al., 2006]. Figure 2.3 presents examples for a summer and an autumn month (northern hemisphere). The O<sub>3</sub> columns shown are dominated by free-tropospheric concentrations, and elevated topography reduces local O<sub>3</sub> columns (i.e. western North America, Himalayas). Nonetheless, significant O<sub>3</sub> enhancements are apparent in regions of large precursor emission, for example, the eastern U.S. [see also Creilson et al., 2003] and East Asia in July. A broad enhanced region in the northern mid-latitudes is associated with export of O<sub>3</sub> and its precursors from adjacent continental regions [Ziemke et al., 2006]. The enhancement over the Middle East reflects a combination of lightning, pollution sources, and dynamics, as inferred from GEOS-Chem simulations [Liu et al., 2009]. Lightning, biomass burning, and stratospheric O<sub>3</sub> contribute to the O<sub>3</sub> column enhancements in the southern tropics in October, as indicated by GEOS-Chem simulations [Savauge et al., 2007].

**Table 2.1.** Current nadir-viewing satellite remote sensing of tropospheric ozone and its precursors

Instrument	Platform	Meas. Period	Typical Nadir Res. (km)	Equator Crossing Time <sup>a</sup>	Global coverage (days) <sup>b</sup>	Spectral Range (μm)	NO <sub>2</sub>	HCHO	CO	O <sub>3</sub>
MOPITT	Terra	2000-	22x22	10:30	3.5	2.3, 4.7			X	
AIRS	Aqua	2002-	14x14	1:30	1	3.7-16			X	
SCIA-MACHY	Envisat	2002-	60x30	10:00	6	0.23-2.3	X	X	X	X
OMI	Aura	2004-	24x13	1:45	1	0.27-0.50	X	X		X
TES	Aura	2004-	8x5	1:45	n/a	3.3-15.4			X	X
GOME-2	MetOp	2006-	80x40	9:30	1	0.24-0.79	X	X		X
IASI	MetOp	2006-	12x12	9:30	0.5	3.6-15.5			X	X

<sup>a</sup>Crossing time occurs at both AM and PM.

<sup>b</sup>Value given for clear-sky conditions. Clouds impede the retrieval.

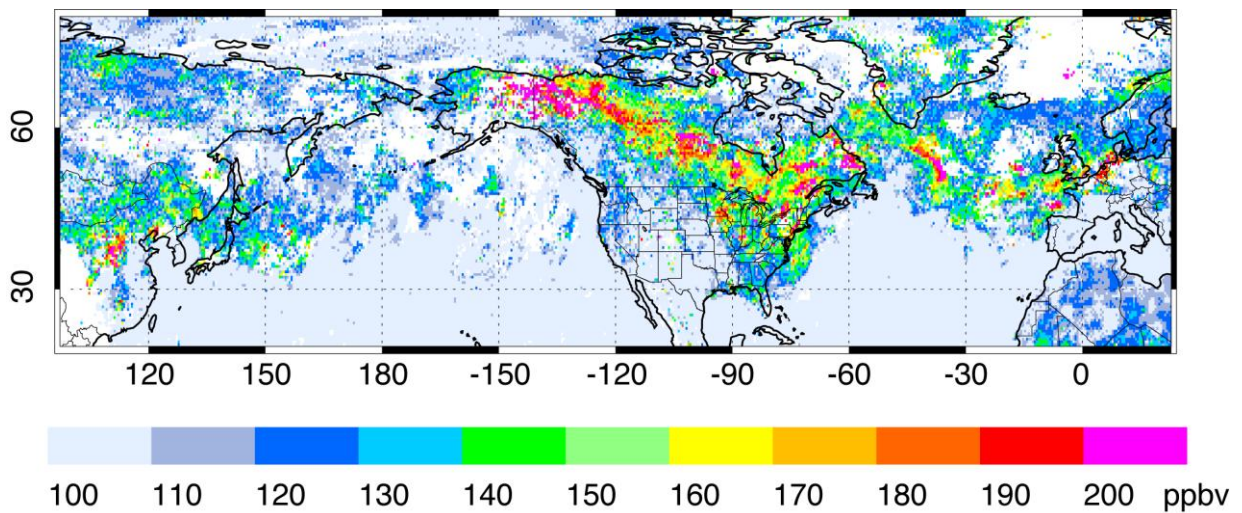
<sup>c</sup>MOPITT: Measurements Of Pollution In The Troposphere; AIRS: Atmospheric Infrared Sounder; SCIAMACHY: SCanning Imaging Absorption SpectroMeter for Atmospheric CHartography; OMI: Ozone Monitoring Instrument; TES: Tropospheric Emission Spectrometer; GOME: Global Ozone Monitoring Experiment; IASI: Infrared Atmospheric Sounding Interferometer

### 2.2.2. Direct Evidence for O<sub>3</sub> and Precursor Transport from In Situ and Lidar Measurements

Because of the complexity of its sources, correlations of in-situ observations of O<sub>3</sub> with other tracers is the most certain and direct means to identify episodic long-range transport of O<sub>3</sub> of anthropogenic origin. Tracers such as CO, NO<sub>x</sub>, non-methane hydrocarbons, mercury (Hg) and aerosols have all been used to help identify sources of O<sub>3</sub> in polluted airmasses. The quantitative relationship between O<sub>3</sub> and a tracer is often expressed as an enhancement ratio, which is the ratio of the increase of O<sub>3</sub> to that of the tracer during the transport episode (see Section 2.4.2). Numerous studies have identified long-range transport of anthropogenically generated O<sub>3</sub> across the Pacific and/or Atlantic Oceans. In some cases, intercontinental transport of O<sub>3</sub> has been shown to significantly impact the surface concentrations and even contribute to exceedances of local ambient air quality standards (see Section 2.2.4).

#### **Trans-Atlantic transport**

Many studies have documented long-range transport of O<sub>3</sub> and its precursors across the North Atlantic [Honrath et al., 2004; Huntrieser et al., 2005; Stohl and Trickl, 1999; Stohl et al., 2003; Trickl et al., 2003; Val Martin et al., 2006]. Sources include both boreal fire plumes as well as urban and industrial pollution. The transport occurs mostly in the free troposphere and has been detected by aircraft and lidar



### Carbon Monoxide Mixing Ratio (ppbv) at 700 hectopascals

**Figure 2.2.** Example of long-range transport from Alaskan and Canadian wildfires to Europe observed by MOPITT over 15-23 July 2004. Plumes of anthropogenic pollution can also be seen leaving Asia and crossing the Pacific Ocean. [Reprinted with permission from Figure 2.6 in *Global Sources of Local Pollution: an Assessment of Long-Range Transport of Key Air Pollutants to and from the United States*, [2010], by the National Academy of Sciences, Courtesy of the National Academies Press, Washington, D.C.]

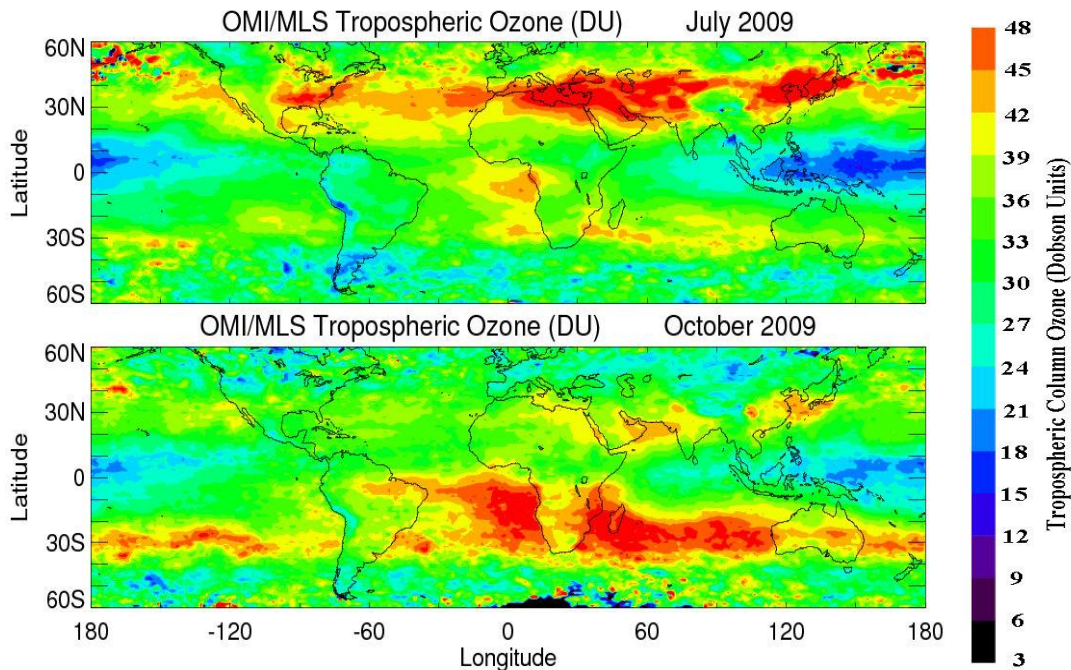


**Figure 2.3.** Example of tropospheric ozone columns determined by residual from OMI observations of total column  $O_3$ , and MLS observations of stratospheric  $O_3$  [Ziemke *et al.*, 2006]. Values reflect a complex interplay of long-range transport, in situ chemical production, loss processes, and stratospheric sources.

and at surface sites in the Alps. At Mace Head, a low elevation site on the west coast of Ireland, Derwent et al. [1997] found 5 probable cases of North American influence but the concentrations were quite low. The only major North American export event to show a strong direct impact on low altitude European sites involved smoke plumes from the widespread forest fires in Canada [Forster et al., 2001].

The International Global Atmospheric Chemistry (IGAC)-sponsored ITCT Lagrangian 2K4 experiment, which was part of the ICARTT, ITOP and INTEX-A field campaigns in summer 2004, provided the opportunity to observe (and model) in situ formation of O<sub>3</sub> during transport from emission regions in North America. In total 4 aircraft were used, along with surface and ozonesonde observations [Fehsenfeld et al., 2006]. Measurements of CO, black carbon (BC), NO<sub>x</sub>, total reactive nitrogen (NO<sub>y</sub>) and O<sub>3</sub> were also made at the PICO-NARE Observatory (38.5°N, 28.4°W) at 2.2 kilometres above sea level (km asl) in the Azores. This site is well situated to observe long-range transport since the Azores are frequently impacted by airflow from middle and high latitudes [Honrath et al., 2004; Owen et al., 2006; Val Martin et al., 2006; Val Martin et al., 2008]. Indeed, North American emissions emitted 6 to 15 days earlier, frequently impacted the PICO-NARE station during summer 2004 [Val Martin et al., 2006]. Figure 2.4 shows an example that included the highest concentration of CO yet recorded at the station.

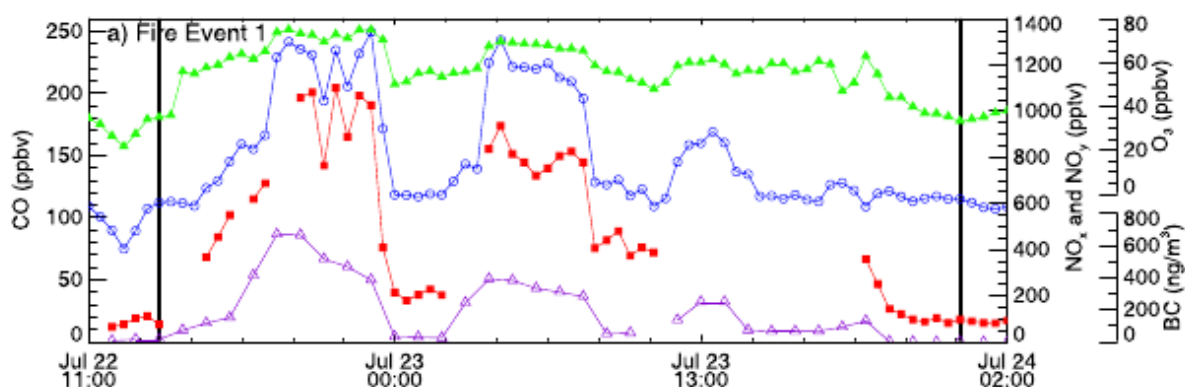


**Figure 2.4.** Time series of 30-min average CO, NO<sub>y</sub> and O<sub>3</sub>, and 1-hour average BC observations at the PICO-NARE Observatory (Azores, Portugal) during transport of boreal wildfire emissions to the site. CO is plotted with open blue circles, NO<sub>y</sub> with red squares, BC with open purple triangles and O<sub>3</sub> with green triangles. Vertical solid lines bound the transport event. [Adapted from Figure 3 in Val Martin, M., et al. (2006), Significant enhancements of nitrogen oxides, black carbon, and ozone in the North Atlantic lower free troposphere resulting from North American boreal wildfires, *Journal of Geophysical Research*, 111(D23S60).]

In summer 2004 two ground-based ozone lidars at Observatoire de Haute Provence (OHP) in south France (43.9°N, 5.7°E, 0.7 km asl) measured vertical profiles of O<sub>3</sub> and aerosol scattering ratio from the boundary layer to the tropopause (Figure 2.5). The largest variability in the columns was due to local pollution within the boundary layer and stratosphere-troposphere exchange. Several O<sub>3</sub> rich layers within the free troposphere also had aerosol enhancements and were related to long-range transport of biomass burning emissions from North America [Real et al., 2007]. These polluted layers were thin (< 1 km) and remained coherent as they were transported over the Atlantic Ocean. The layers observed above OHP exhibited O<sub>3</sub> mixing ratios 50% greater than values in adjacent air and increased the tropospheric column O<sub>3</sub> by 5 to 10% [Ravetta et al., 2007]. In 2004 aircraft as part of the MOZAIC program also measured fire plumes originating from Alaska in the free troposphere over the eastern U.S., the North Atlantic and Western Europe [http://mozaic.aero.obs-mip.fr, Elguindi et al., 2010]. Note that while CO was strongly enhanced in the MOZAIC vertical profiles, O<sub>3</sub> was not. Detailed analyses of such cases and in particular Lagrangian cases where the same air masses were sampled several times have shown significant O<sub>3</sub> production in certain plumes (e.g. forest fire plumes) whilst in other cases mixing and photochemical destruction dominated. Further examples are discussed in Section 2.4.



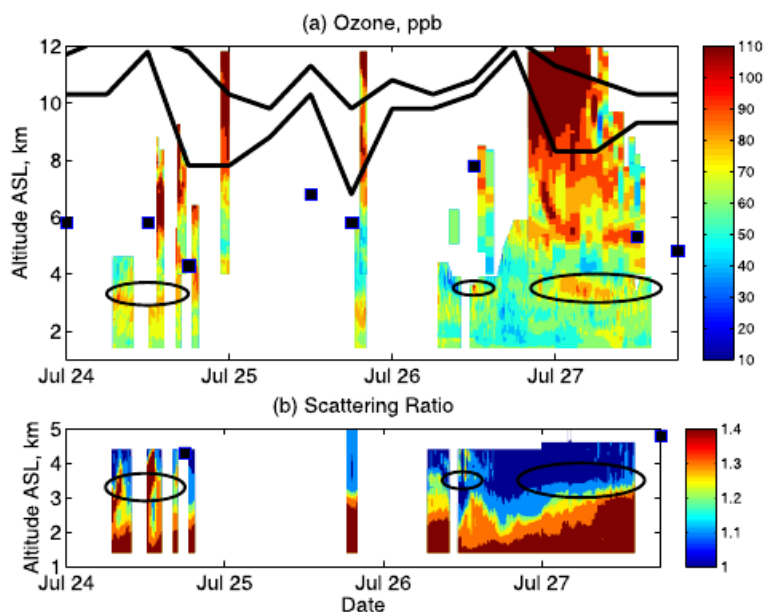


**Figure 2.5.** (a) Ozone mixing ratio cross section in ppb measured at Observatoire de Haute Provence in July 2004. Tick marks correspond to 0000 UT. This figure combines vertical profiles measured by 2 ozone lidars. ECMWF analyses have been used to compute potential vorticity (PV) profiles in order to estimate the height of the tropopause (PV = 1 pvu for the lower thick black line, PV = 2 pvu for the upper one) and spot stratospheric intrusions (large squares). (b) Vertical cross section of aerosol scattering ratio (a quantity proportional to the aerosol concentration) derived from the 316-nm wavelength ALTO lidar on the same days. Ozone rich layers related to long-range transport are circled in black. [Adapted from Ravetta, F., et al. (2007), Long-range transport and tropospheric ozone variability in the western Mediterranean region during the Intercontinental Transport of Ozone and Precursors (ITOP-2004) campaign, *Journal of Geophysical Research*, 112(D10S46).]

### **Trans-Pacific transport**

The greater transport distance and increased complexity of transport patterns make it more difficult to detect long-range transport across the Pacific Ocean. Our understanding of trans-Pacific transport of O<sub>3</sub> and other pollutants has been improved by recent studies, e.g. the NASA led INTEX-A and B campaigns, which measured from aircraft over North America and the eastern North Pacific [Singh *et al.*, 2006; Singh *et al.*, 2009] and from the Mt. Bachelor Observatory (MBO) at 2.7 km asl in central Oregon [Jaffe *et al.*, 2005a; Weiss-Penzias *et al.*, 2007]. During INTEX-A, which took place in the summer of 2004, several plumes of Asian origin were encountered as far downwind as over eastern North America [e.g., Liang *et al.*, 2007]. Fischer *et al.* [2009] report on PAN decomposition and O<sub>3</sub> production during subsidence based upon observations from the Mt Bachelor Observatory. This work indicates that transport of PAN and its subsequent decomposition to NO<sub>x</sub> has a significant impact on the O<sub>3</sub> concentrations in air arriving at North America. Reidmiller *et al.* [2009] report on interannual variability in long-range transport using satellite data and observations from Mt. Bachelor, combined with the GEOS-CHEM model. They conclude that variations in transport and biomass burning emissions largely drive the year-to-year variations in CO seen in the eastern Pacific atmosphere. Weiss-Penzias *et al.* [2007] identified ten separate episodic pollution transport events from Asian industrial sources arriving at Mt. Bachelor. In these events the Hg/CO enhancement ratio appears to be a unique tracer of Asian pollution plumes, being 3-4 times higher in Asian plumes compared to U.S. or biomass burning plumes.

In the past few years efforts have been made to measure pollutant concentrations in air masses above East Asia, especially within China where emissions are rapidly increasing. These studies [Ding *et al.*, 2009] have revealed pollutant concentrations that are much greater than those encountered over Europe or North America [e.g. Hudman *et al.*, 2007; 2008]. High pollutant levels detected above the boundary layer over China include a plume at 2.6 km above northeast China with O<sub>3</sub> and CO as high as 140 ppbv and 1185 ppbv, respectively [Ding *et al.*, 2009] and a layer of pollution at 2.5-3.5 km

above Beijing, lofted by upslope mountain flow, with 90 ppbv of O<sub>3</sub> and 2200 ppbv of CO. Ding et al. [2008] examined O<sub>3</sub> from the MOZAIC campaign and found higher concentrations in the lower troposphere than other large Northern Hemispheric cities. These strong Asian pollution plumes contain far more CO than has been detected in Asian plumes transported to above western North America [maximum CO of ~300 ppbv, Nowak et al., 2004], indicating the degree of dilution that occurs during transport.

### ***Transport across South Asia, Europe and East Asia***

The impact of European pollution on Asia has been demonstrated from ground-based observations at Mondy in East Siberia [Pochanart et al., 2003]. During the TROICA-8 expedition [Turnbull et al., 2009]  $\Delta^{14}\text{CO}_2$  was measured together with CO, sulphur hexafluoride and perchloroethylene along the Trans-Siberian railway between Moscow (Russia, 55°44' N, 37°33' E) and Khabarovsk (Russia, 48°33' N, 135°06' E) in March-April 2004. They observed an increase of  $\Delta^{14}\text{CO}_2$  (a measure of the fossil fuel contribution to measured carbon dioxide concentration) and a decrease of CO from West to East, which they interpreted to reflect emission and transport of anthropogenic species from Europe to Asia. More recently, the Nepal Climate Observatory-Pyramid (NCO-P) at 5.1 km asl was established in the Khumbu valley in the Himalayas [Bonasoni et al., 2008]. Figure 2.6 shows O<sub>3</sub> and BC measured at the observatory. Pollutant transport with high O<sub>3</sub> (63±9 ppbv) to the site is common in the pre-monsoon period. According to back-trajectory analysis, they concluded that it was probably related to continental outflow from Eurasia with an upper troposphere/lower stratosphere influence. O<sub>3</sub> enhancements occurred both with and without enhancements in other tracers. In mid-June O<sub>3</sub> and BC were transported to the site from anthropogenic sources to the east near the India-Pakistan border.

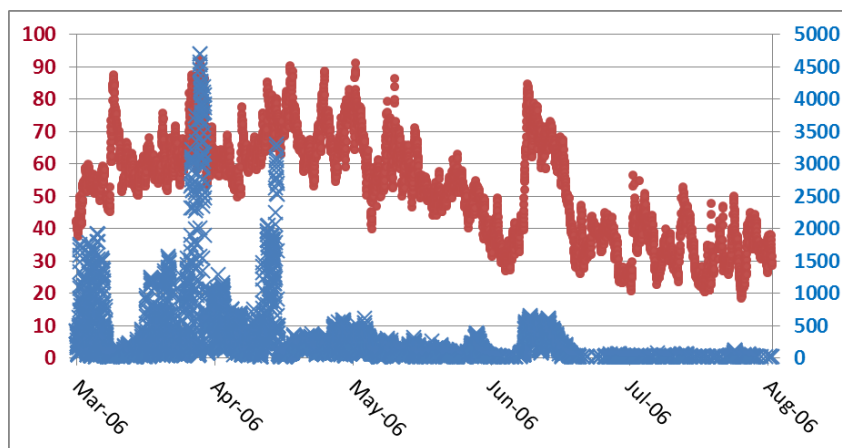


**Figure 2.6.** O<sub>3</sub> and BC measured March-August 2006 at the Nepal Climate Observatory-Pyramid (NCO-P) at 5.1 km asl in the Khumbu valley of the Himalayas. [Adapted from Figures 6 and 8 from Bonasoni, P., et al. (2008), The ABC-Pyramid Atmospheric Observatory in Himalaya for aerosol, ozone and halocarbon measurements, *Science of the Total Environment*, 391: 252-261, with permission from Elsevier.] O<sub>3</sub> is shown in red circles on left axis (ppbv) and BC in blue crosses on right axis (nanograms per cubic meter). The first high O<sub>3</sub> event in early March was attributed to UT/LS transport due to meteorological conditions and an absence of other pollutant tracers. The high O<sub>3</sub> event in mid-June, which also showed a BC enhancement, was attributed to anthropogenic pollution arriving from the east.

### ***2.2.3. Indirect evidence from long-term trends in baseline O<sub>3</sub>***

During the latter half of the 20<sup>th</sup> century baseline concentrations of O<sub>3</sub> increased markedly at northern mid-latitudes. This increase has been documented by a variety of observational studies, and is generally attributed to increasing anthropogenic emissions of the precursors that fuel photochemical O<sub>3</sub> production. These increased emissions accompanied the growth and development of the economies of the industrialized nations [e.g., Horowitz, 2006; Lamarque et al., 2005]. This observed increase in O<sub>3</sub> concentrations is one of the most important manifestations of the hemispheric transport of air pollution. Uncertainty remains regarding the magnitude of the increase from pre-industrial to present

day since pre-industrial O<sub>3</sub> concentrations are poorly known, few measurements were made before the late 1970s, and different data sets for the same region do not always give consistent results. Since global models cannot reproduce the very low O<sub>3</sub> levels suggested by the measurements of that time [e.g. *Mickley et al.*, 2001], the quantitative assignment of the cause of the increase is also uncertain. This section reviews the strongest observational evidence for these temporal trends. The primary focus is on the O<sub>3</sub> concentrations in onshore flow at the west coasts of Europe and North America with some comparisons to trends observed in Asian outflow. Without a west coast, it is more difficult to establish long-term trends for baseline O<sub>3</sub> entering Asia, especially from the more limited observational record in this region. The O<sub>3</sub> concentrations in onshore flow most clearly show the influence of long-range transport, since they represent baseline O<sub>3</sub> concentrations.

Figures 2.7 and 2.8 summarize the results from several data sets that provide the strongest evidence for increasing baseline O<sub>3</sub> concentrations at northern mid-latitudes since the mid-20<sup>th</sup> century. Figure 2.7 shows results from spring. In this season intercontinental flow is most important, observational data are most abundant, and influences from regional photochemical O<sub>3</sub> production are relatively small. Figure 2.8 compares springtime trends with those in other seasons. These data represent the longest, highest quality measurement records available from sites that are likely to represent baseline O<sub>3</sub> changes. The studies vary in the time period covered, and in the degree to which regional influences may obscure baseline trends. Given this variability, a simple statistical approach is chosen. Linear and quadratic polynomial least-squares fits are made to seasonally averaged data from each site. Baseline data are examined where available (i.e. only at Mace Head and Pacific marine boundary layer). The polynomial fit is included in Figure 2.7 only if the quadratic term is significant. At least up to the year 2000 the linear trends have remained remarkably constant over many of the individual data records. One can argue that there has been a levelling off or even decrease at the European stations, particularly at the three central European sites (Hohenpeissenberg, Jungfraujoch and Zugspitze) where the quadratic term is statistically significant, and negative. For these three sites the average trends in Figure 2.8 are derived from the linear-least squares fits made to the portion of the data record before 2000. For all sites the slope of the linear trend derived from this statistical approach is the best estimate of the average annual change in the measured O<sub>3</sub> for the season and period selected. In all cases 95% confidence limits are calculated for the slope. Unfortunately, very few data sets have been selected for baseline conditions, but all the sites are located where trends in baseline O<sub>3</sub> are expected to dominate the trends in average O<sub>3</sub>. Consistency in the derived trends over large regions supports the assumption that the derived trends represent the baseline O<sub>3</sub> trend.

Beginning in the 19<sup>th</sup> century a long record of apparently reliable O<sub>3</sub> measurements in ambient air was collected in Europe. Measurements performed at the Montsouris Observatory close to Paris from 1876 to 1912 using a solution chemistry method show low O<sub>3</sub> concentrations (10-15 ppbv) in the planetary boundary layer (PBL) [*Volz and Kley*, 1988]. Similar measurements were conducted from 1956-1983 at Arkona, a coastal site on the Baltic Sea [*Feister and Warmbt*, 1987], and the series was continued at the nearby Zingst site (Figures 2.7 and 2.8). The earliest springtime measurements at Arkona show O<sub>3</sub> concentrations around 15 ppbv followed by an increase (amounting to about 20 ppbv) to the present Zingst concentrations. However, it remains difficult to judge whether SO<sub>2</sub>, an interference of the chemical method, produced a negative bias in these earlier measurements, although data affected by SO<sub>2</sub> transport from the capital of Paris were removed by using local wind measurements at the Montsouris Observatory [*Volz and Kley*, 1988]. Solution chemistry measurements performed at Arosa, an alpine valley site at 1.8 km asl in the Swiss Alps in the 1950s also showed low annual mean values of around 20 ppbv [*Staehelin et al.*, 1994], and O<sub>3</sub> was also measured in Arosa during some clear nights in the 1930s (using long-path ultraviolet measurements). These 1930s measurements yielded similar values to the 1950s solution chemistry measurements, which supports their reliability (note that the large increase in anthropogenic O<sub>3</sub> precursor emissions took place in the decades after World War II).

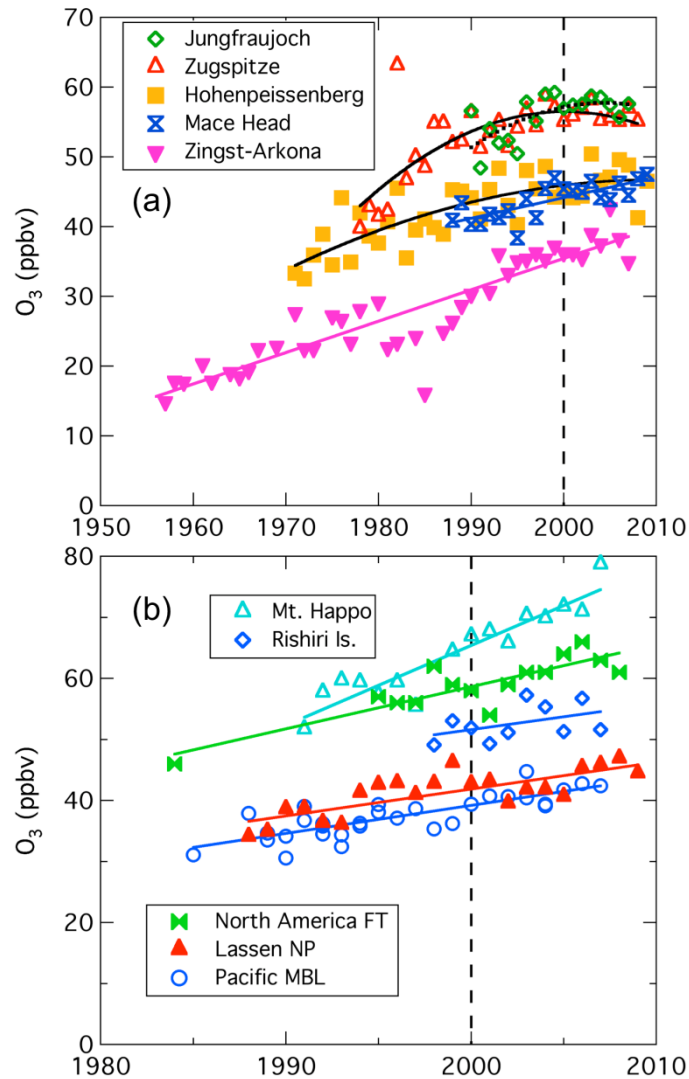


**Figure 2.7.** Springtime trends in  $O_3$  concentrations measured in (a) Europe and (b) western North America and Japan. The lines (in colour) indicate the linear regressions to the data, and the curves (in black) indicate quadratic polynomial fits to the three central European sites over the time span of the lines. Arkona and Zingst are two sites located close to the Baltic Sea. Mace Head is located at the west coast of Ireland. Hohenpiessenberg (1.0 km asl) and Zugspitze (3.0 km asl) are in southern Germany, and Jungfrauoch (3.6 km asl) is in Switzerland. The North American data are from several sea level Pacific coastal sites and Lassen National Park (1.8 km asl) near the west coast, and from the free troposphere over the western part of the continent. The Japanese data are from Mt. Happo (1.9 km asl) on the Japanese mainland and Rishiri, a northern (45N) sea level island site.

Overall, a consistent trend of increasing  $O_3$  has been observed at European surface sites through the second half of the 20<sup>th</sup> century, beginning with the early measurements summarized above, and continuing with modern measurement methods. Figure 2.7a shows that long, continuous European surface  $O_3$  records from the rural Hohenpeissenberg (Stefan Gilge, Hohenpeissenberg Meteorological Observatory, German Meteorological Service, Hohenpeissenberg, Germany, personal communication, 2010) and the mountaintop Zugspitze (Hans-Eckhart Scheel Karlsruhe Institute of Technology, IMK-IFU, personal communication, 2010) sites in southern Germany, as well as the shorter records for the marine Mace Head [Derwent *et al.*, 2007] and the mountaintop Jungfrauoch sites [Bronnimann *et al.*, 2002], all approximately parallel the Arkona-Zingst springtime record, at least until 2000. A similar trend is also seen in continuous surface  $O_3$  measurements at another alpine high altitude site: Sonnblick (Austria, 3.1 km asl). The data from the Figure 2.8 demonstrate that  $O_3$  has increased during all seasons with some indication of greater increases in spring and winter, and



smaller increases in summer and particularly autumn. Trends determined from springtime data sets from Arosa in the 1930s, 1950s and around 1990 [Stahelin *et al.*, 1994] and summertime data from Jungfraujoch in the 1930s [Crutzen, 1988], which define the end points of the trends for those two sites in Figure 2.8, are consistent with the trends extracted from the continuous data sets.

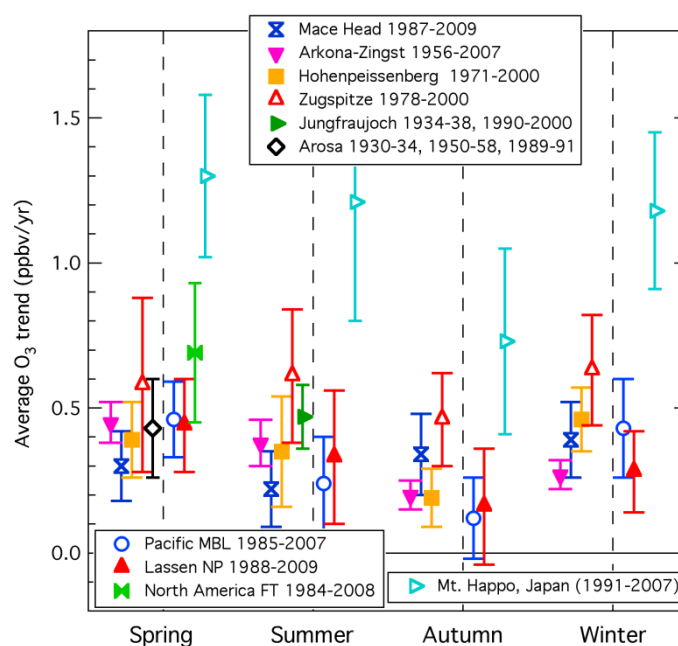


**Figure 2.8.** Average annual linear trends in O<sub>3</sub> concentrations in different seasons in Europe (left of dashed lines), North America and Japan (right of dashed lines). The slopes of linear regressions of seasonally averaged data (e.g., the lines in Figure 2.7) provide the trends. The sites, symbols and period of the linear trend determination are the same as in Figure 2.7, except for the three central European sites, where the linear fits end in 2000.

Trends derived from the more limited North American measurements (Figures 2.7 and 2.8) are consistent with each other and similar to the European trends although they continue after 2000. No long-term record is available from a single North American marine boundary layer site that is suitable for characterizing baseline O<sub>3</sub> concentrations arriving at North America. However, Parrish *et al.* [2009] combined baseline data from several North American marine sites to derive seasonal baseline trends (included in Figures 2.7 and 2.8) that are approximately the same as those from Mace Head. Similarly, trends at a long-term, rural site near the west coast of North America that can be considered to represent trends in O<sub>3</sub> in onshore flow (Lassen National Park) parallel the marine boundary layer trends. A recent study that combined all available free troposphere data for springtime over western North America [Cooper, 2010] derived a trend in approximate accord with the trends derived from the surface measurements, and the trends were stronger in air with strong influence from the South and East Asian boundary layer. Although shorter than the European records, the three North American trends indicate increasing baseline O<sub>3</sub> in air entering North America from at least the mid-1980s to the present.

At inland North American sites consistent baseline O<sub>3</sub> concentration trends are difficult to discern. Jaffe and Ray [2007] report that average O<sub>3</sub> concentrations generally increased from 1987–2004 at rural sites in the western US, but the rate of increase varied from 0 to 0.5 ppbv/yr across 9 sites. Oltmans *et al.* [2006] find no generally increasing trends in average O<sub>3</sub> concentrations over North America. It may well be that at interior North American locations, the increase in baseline O<sub>3</sub> concentrations is obscured by decreasing regional and local O<sub>3</sub> production due to decreasing emissions of O<sub>3</sub> precursors within North America. Indeed, the US Environmental Protection Agency (<http://www.epa.gov/airtrends/ozone.html#oznat>) notes that maximum O<sub>3</sub> concentrations are decreasing throughout the country in response to reduced precursor emissions.

Long-term, continuous O<sub>3</sub> measurements are limited in Asia, but those that exist generally indicate increasing O<sub>3</sub> concentrations. In Japan, continuous measurements at Mt. Happo Observatory (1.9 km asl) show a springtime O<sub>3</sub> increase of  $1.30 \pm 0.28$  ppbv/yr from 1991 to 2007 [Tanimoto, 2009] and positive trends in all seasons that are the most rapid increases found in any of the data sets investigated here (see Figure 2.7b and 2.8). Six Pacific Rim island sites [Tanimoto *et al.*, 2009], e.g. Rishiri Island included in Figure 2.7, together give on average an increasing springtime trend of  $0.62 \pm 0.36$  ppbv/yr, but trends from individual stations are not statistically significant due to their short time span. West of Japan, Beijing experienced annual average O<sub>3</sub> increases in the PBL of 5-8 ppbv between 1995 and 2005, as measured by MOZAIC aircraft profiles [Ding *et al.*, 2008].

Increasing export of O<sub>3</sub> from Asia is expected from observed increases in regional O<sub>3</sub> concentrations. In the region of Taipei, Taiwan (25° N), yearly surface O<sub>3</sub> averaged across several sites increased during 1994-2003 at the rate of 0.96 ppbv/yr [Chou *et al.*, 2006]. In southern China, average yearly O<sub>3</sub> increased by about 50% between the late 1980s and 1990s at an urban monitoring site in Hong Kong (22° N) [Chan *et al.*, 2003]. A coastal site southeast of Hong Kong shows an O<sub>3</sub> rate of increase of 0.58 ppbv year<sup>-1</sup> for yearly data during 1994-2007 [Wang *et al.*, 2009]. In East Asia, generally all sites show that O<sub>3</sub> has increased over the past 20 years as would be expected from the strong increases in regional O<sub>3</sub> precursor emissions (e.g. see Figs. 3.9 and 3.10). The rate of increase is on the order of 1 ppbv/yr, somewhat stronger than the rate of increase in Europe and North America.

Ozonesondes provide some of the longest-term records of the evolution of baseline O<sub>3</sub> over Europe, as well as North America and Japan, but their usefulness appears limited. The three long-term European records (based on Brewer Mast sensors at Hohenpeissenberg, Germany; Payerne, Switzerland; and Uccle, Belgium) provide the longest continuous records of O<sub>3</sub> in the free troposphere. They show strongly increasing concentrations from 1970 to 1990, but the three records show large deviations [see Logan *et al.*, 1999]. The O<sub>3</sub> evolution derived from the ozonesonde measurements of Hohenpeissenberg and Payerne do not agree well with the nearby mountain surface series of Jungfraujoch and Zugspitze in the early part of the 1990s [Ordóñez, 2006]. The O<sub>3</sub> changes obtained from regular aircraft measurements of MOZAIC data since 1994 [Thouret *et al.*, 2006; Zbinden *et al.*, 2006] are more consistent with the surface O<sub>3</sub> measurements of Jungfraujoch and Zugspitze than those of the ozonesonde records from Hohenpeissenberg and Payerne. A recent comparison of O<sub>3</sub> changes in the upper troposphere derived from climatologies of the regular aircraft measurements from the project GASP (1975-1979) and MOZAIC (1994-2001) programs showed unexplained differences with the changes derived from the ozonesonde measurements [Schnadt Poberaj *et al.*, 2009]. The air sampled by ozonesondes, high alpine surface stations and regular aircraft (MOZAIC) are not identical, so some differences in measured O<sub>3</sub> concentrations are expected (e.g. high mountain sites can be affected by local wind systems, which remain to be analyzed in more detail). Nevertheless, it appears that the baseline O<sub>3</sub> evolution over Europe until around 2000 is probably more reliably described by high mountain sites and MOZAIC data than by the European ozonesondes. The records from the surface sites, aircraft and sondes show nearly consistent variability since 2000 compared to earlier times, which might point to some data quality problems in the earlier sonde data (Jennifer Logan, Department of Earth and Planetary Sciences, Harvard University, Cambridge, Massachusetts, USA, personal communication, 2009).

In summary, various studies have found significant positive temporal trends in the O<sub>3</sub> concentrations at northern temperate latitudes. However, there remains significant uncertainty regarding the magnitude and exact cause of these increases.

#### 2.2.4. Implications for Surface Ozone Air Quality in Receptor Regions

Even though the O<sub>3</sub> surface concentrations on the downwind sides of the Atlantic and Pacific oceanic basins are the lowest found in the northern mid-latitudes, these concentrations still raise air quality concerns in regions receiving marine air inflow. These concerns arise both from human health and crop and ecosystem damage perspectives.

The concentrations of O<sub>3</sub> in air masses arriving at the Atlantic coastal fringes of Europe have been steadily rising over the past several decades (see Section 2.2.3), and have now reached levels

that exceed internationally accepted air quality guidelines and targets set for the protection of human health [50 ppb, maximum 8-hour level, WHO, 2006] and vegetation [40 ppb, accumulated time above 40 ppb, Fuhrer *et al.*, 1997]. Figure 2.9 presents the average monthly level of O<sub>3</sub> observed in baseline air masses arriving at Mace Head, Ireland taken from Simmonds *et al.* [2004] and extended up to July 2008. Monthly averages now exceed 40 ppb during much of the growing season in all years and approach or exceed 50 ppb in some spring months.

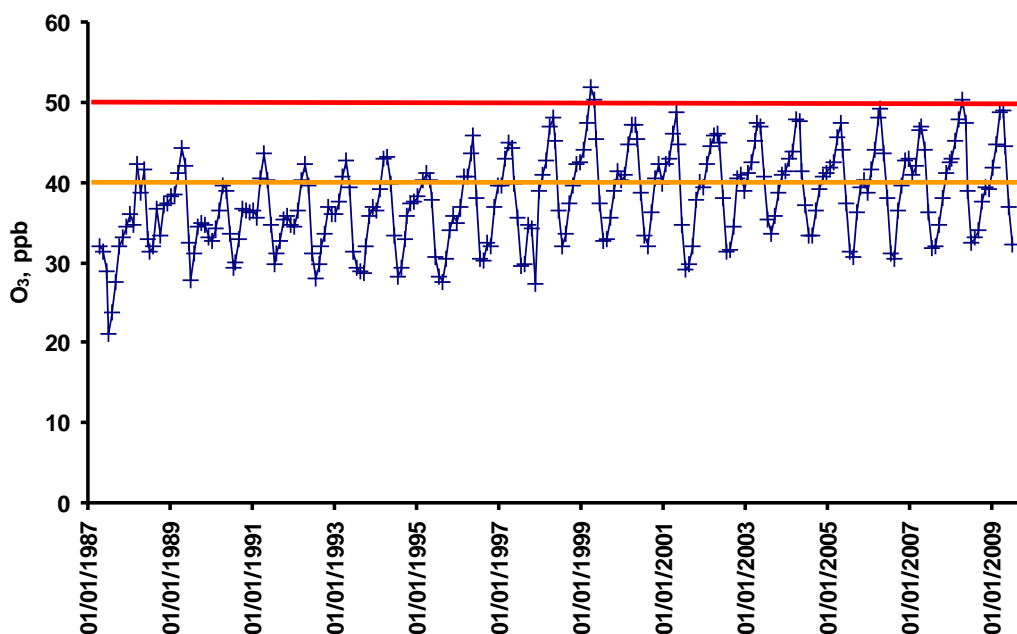


**Figure 2.9.** Monthly average O<sub>3</sub> mixing ratios in baseline air masses arriving at Mace Head, Ireland from 1987 – 2009, showing the 40 ppb and 50 ppb thresholds set for the protection of vegetation (orange line) and human health (red line), respectively.

As these baseline air masses travel further into the continent of Europe from the coastal fringes, surface uptake and photochemical destruction will necessarily erode the levels in Figure 2.9, whilst descent of ozone-rich air from above and photochemical production may supplement them. Figure 1.6 shows a model calculation of how a baseline air mass would further evolve during transport to southern England as a function of season; the sum of all contributions except Europe-regional represents the baseline O<sub>3</sub> contribution at this further downwind site. Under these conditions, intercontinental transport will still represent a substantial fraction of any subsequent exceedance of air quality standards set in Europe for the protection of human health and vegetation.

The O<sub>3</sub> concentrations in air flowing into Japan have significant air quality impacts. Tanimoto [2009] reported the increase in the number of air quality standard exceedances for surface O<sub>3</sub> in spring at Mt. Happo (HPO), a rural mountain site in Japan (36.7°N, 137.8°E, 1.85 km asl) that is largely influenced by long-range transport from the Eurasian continent. From 1999 to 2006 the number of days that O<sub>3</sub> exceeded 84 ppbv increased from 10 to 15 to about 30, approximately doubling over the course of 8 years. In 2006 HPO experienced O<sub>3</sub> levels exceeding 120 ppbv for the first time. This increase in the frequency of high-ozone episodes, which exceed the air quality standard thresholds, is likely due to significantly increased O<sub>3</sub> transport from the upwind regions. Trends in the tropospheric NO<sub>2</sub> columns over east-central China in spring indicate that region possibly contributes to the large O<sub>3</sub> increase at HPO.

The impact of the long-range transport of O<sub>3</sub> is also substantial in western North America on the eastern side of the Pacific Ocean. Air with low O<sub>3</sub> concentrations flows ashore within the marine boundary layer, but a strong vertical gradient is present above the boundary layer at the North American west coast. Ozonesondes launched from Trinidad Head, California, a coastal NOAA observatory (<http://www.esrl.noaa.gov/gmd/obop/thd/>), find that summertime O<sub>3</sub> mixing ratios

average only  $23 \pm 7$  ppbv ( $\pm$  one standard deviation) at 100 m, but are more than twice as high ( $53 \pm 16$  ppbv) at 2 km [Oltmans *et al.*, 2008]. As the onshore marine airflow encounters the complex topography that characterizes much of the North American west coast, ozone-rich air from above the marine boundary layer may be transported to the surface.

Some experimental analysis does indicate that transported baseline  $O_3$  makes a major contribution to surface  $O_3$  at some western North American sites, even during periods when the U.S. National Ambient Air Quality Standard (NAAQS) is exceeded. Jaffe *et al.* [2004] discuss an  $O_3$  exceedance that occurred in the Seattle, Washington area due to long-range transport of fire emissions from Siberia. In addition, summertime surface  $O_3$  in California's Central Valley directly inland from the Trinidad Head ozone sonde launch site often exceeds the NAAQS as indicated in Figure 2.10 [Parrish *et al.*, 2010]. The mean maximum 8-hr average  $O_3$  on exceedance days (i.e. those days when 8-hr average  $O_3$  exceeds 75 ppbv) is 20 ppbv higher than on non-exceedance days. The transported baseline  $O_3$ , as measured 22 hours earlier by the Trinidad Head sondes, is also higher (by 11 ppbv) on exceedance days, which indicates that about half of the average excess  $O_3$  on exceedance days is due to a larger baseline contribution. The remaining difference is presumably due to greater local and regional photochemical  $O_3$  production. The average transported baseline  $O_3$  on the exceedance days (59 ppbv) accounts for a very substantial fraction of the 75 ppbv standard.

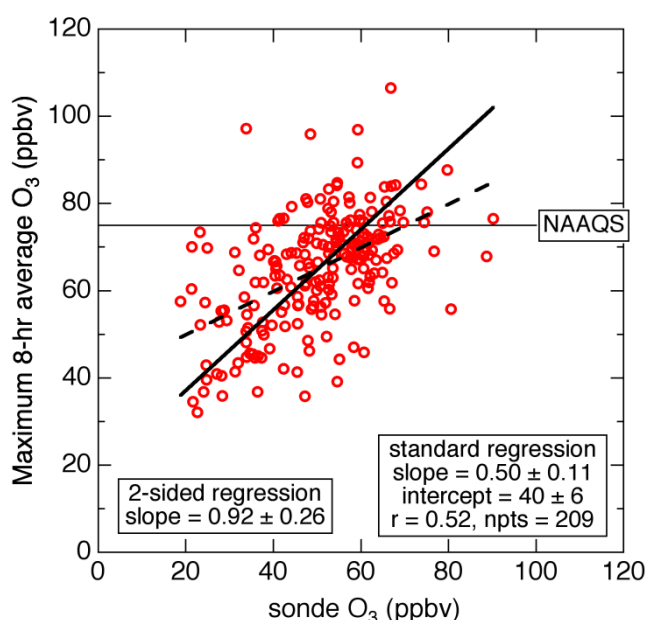


**Figure 2.10.** Correlation between the interpolated daily maximum 8-hr surface  $O_3$  averages at Tuscan Butte (a California surface site 200 km inland from the Pacific coast) with the  $O_3$  mixing ratio measured by sondes 22 hours earlier at Trinidad Head. The sonde mixing ratios are averaged over altitudes from 1.0 to 2.5 km. The solid line shows the bi-variate linear, least-squares regression to the data, and the dashed line shows the standard regression.

### 2.2.5. Summary, Remaining Uncertainties and Future Needs

**FINDING:** Satellites clearly observe long-range transport of CO. Source gases with shorter lifetimes such as  $NO_2$ , are transformed more quickly in the atmosphere, making detection of transport difficult far from emission regions. Distinct signatures of long-range transport of  $O_3$ , which has both natural and anthropogenic sources, are difficult to detect by satellite, although significant  $O_3$  enhancements are apparent over and downwind of regions with large precursor emissions. Present satellite retrievals are limited to tropospheric columns with little vertical profile information.

**RECOMMENDATION:** Further work is needed on quantitative satellite-based estimates of long-range transport of  $O_3$ , its inter-annual variability and its relation to changes in baseline  $O_3$  concentrations.

**FINDING:** Measurements suggest that during the latter half of the 20th century, concentrations of O<sub>3</sub> at northern mid-latitudes increased by a factor of 2 or more. It is likely that much of this increase is due to increases in anthropogenic emissions of O<sub>3</sub> precursors. Within the limits of the measurement records, the increase has been comparable throughout all longitudes, and has occurred in all seasons. More recently, faster increases appear to have taken place downwind of eastern Asia, and the increase within the boundary layer of central Europe and North America has slowed.

**RECOMMENDATION:** The measurements documenting changes in surface and free tropospheric O<sub>3</sub> over the last several decades need to be systematically and collectively reviewed using consistent methods of analysis. Further, appropriate, systematic comparison with global models, which currently have problems accurately reproducing observed trends [e.g., *Lamarque et al.*, 2010], is required as an on-going activity.

**FINDING:** Measurements show that onshore marine airflow above the marine boundary layer can carry O<sub>3</sub> concentrations that approach urban air quality standards, and that air can mix to the surface and contribute substantially to air quality standard violations. This is particularly noticeable in low emission regions. The impact depends upon vertical mixing of air into the PBL, which is enhanced by complex topography.

**RECOMMENDATION:** Conduct focused research efforts that couple measurements with models to better quantify the process of air exchange between boundary layer and free troposphere in order to fully understand how free tropospheric O<sub>3</sub> enhanced by long-range pollution transport is mixed to surface.

### 2.3. Long-range Transport of Particulate Matter and its Precursors

Observations of haze layers in the Arctic during spring [*Shaw*, 1975], later attributed to transport from Eurasia [*Shaw*, 1995], and acid deposition in Canadian and Scandinavian lakes [*Likens and Bormann*, 1974] were the first recorded indications of the large-scale spatial transport of aerosol pollution. In the mid-1990s it became clear that long-range transport of PM could affect a downwind continent and significantly increase baseline concentrations [*Keating et al.*, 2005]. Since that time, a number of studies focused on regional PM levels strongly suggest that trans-boundary contributions dominate the observed concentrations in many areas. Development of new observing tools, improvements to the existing emission models and inventories, and a better understanding of chemical transformations and removal processes now provide better constraints on fundamental processes that drive the global distributions of the key aerosol species. Comprehensive studies that combine analysis of satellite-derived and ground-based observations with modelled back trajectories offer evidence that trends in emissions on one continent can affect PM trends thousands of kilometres downwind [*Karnieli et al.*, 2009].

Satellite images depict the transport of aerosols over thousands of kilometres for specific events and in time-averaged statistics. Transport mainly occurs in the free troposphere along the major pathways of long-range transport of gas pollutants. Direct evidence for transport at high altitude can be derived from lidar networks or high altitude ground-based stations [*Matthias et al.*, 2004]. It is believed that direct aerosol injection into elevated layers is not very efficient from anthropogenic sources in urban/industrial settings in contrast to forest fire plumes, which are convectively lofted above the ABL by the thermal energy of the fires [*Park et al.*, 2004].

#### 2.3.1. Quantitative Estimates of Total Particulate Matter Transport from Satellites

Satellites provide a unique view of the transport of aerosols across ocean basins capturing specific events and aiding interpretation of in situ measurements. Time-averaged images of satellite-retrieved aerosol optical depth (AOD), a measure of total column PM loading, reveal the major pathways of aerosol transport from Asia across the Pacific Ocean to North America, and from Africa west across the Atlantic Ocean. At first such satellite imagery was only two dimensional, but recent analysis of CALIPSO (Cloud-Aerosol Lidar and Infrared Pathfinder Satellite Observations) observations is allowing depictions of three-dimensional aerosol transport [*Ben-Ami et al.*, 2009], e.g. Figure 2.11 [*Liu et al.*, 2008]. Altitude information is especially important for calculations of mass



flux and to determine what fraction of the PM seen from satellite are in the ABL, thereby affecting local air quality. Within the past few years, satellites have begun to provide quantitative information on intercontinental aerosol transport. The Multiangle Imaging SpectroRadiometer (MISR) is able to characterize AOD, size and degree of nonsphericity. Figure 2.12 shows results from a study [Kalashnikova and Kahn, 2008] where particle loading, size and nonsphericity all decreased during transport across the Atlantic.

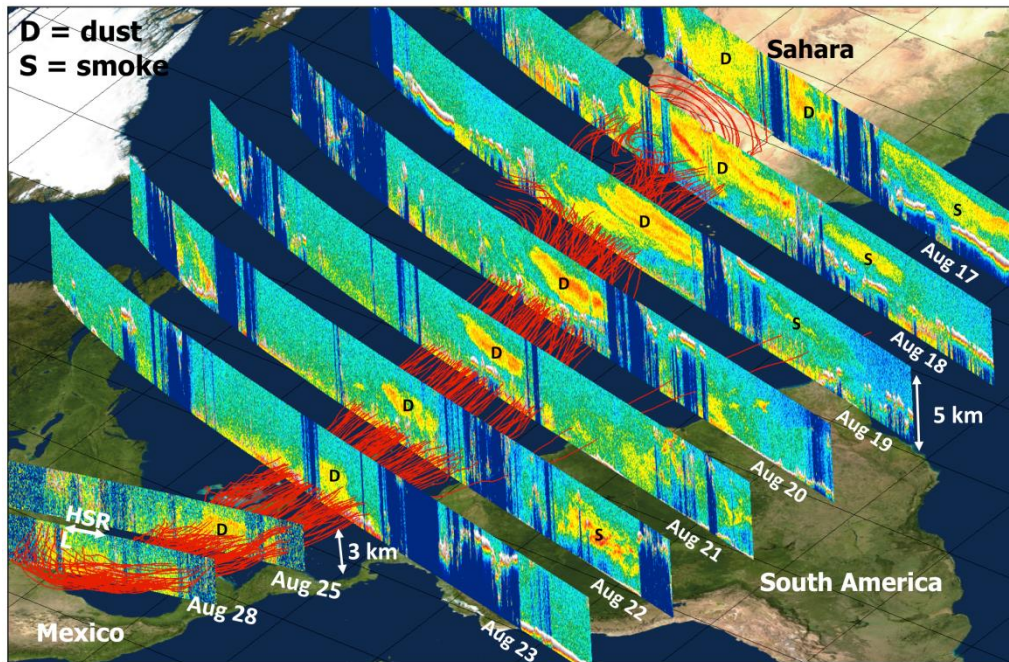


**Figure 2.11.** A dust event that originated in the Sahara desert on 17 August 2007 and was transported to the Gulf of Mexico. Red lines represent back trajectories indicating the transport track of the dust event. Vertical images are 532 nm attenuated backscatter coefficients measured by CALIPSO when passing over the dust transport track. The letter “D” designates the dust layer, and “S” represents smoke layers from biomass burning in Africa (17–19 August) and South America (22 August). Graphic courtesy of Kurt Severance at NASA Langley Research Center.

Following Kaufman et al. [2005], who applied a quantitative method to determine the net transport of dust from Africa to the Amazon basin, Yu et al. [2008] have used MODerate resolution Imaging Spectroradiometer (MODIS) aerosol products to determine the transport of “pollution” PM across the Pacific Basin. They isolated the pollution portion of the aerosol optical thickness measured by MODIS and translated the optical thickness to total column mass using a relationship derived from field experiments. Analyzed wind fields then allowed a quantitative calculation of the amount of pollution PM mass leaving the Asian continent and the amount arriving at North America (Figure 2.13). MODIS observed about 18 Tg/yr leaving Asia within the latitude range of 30 to 60°N and 4.4 Tg/yr arriving in North America. This compares well with results from the Goddard Global Ozone Chemistry Aerosol Radiation Transport (GOCART) and Global Modelling Initiative (GMI) chemical transport models where the model PM was defined as the sum of the BC, organic material and sulphate. The MODIS data show a seasonal cycle with a transport maximum in spring, but transport is observed in all seasons. Uncertainty analysis showed that the estimation of the aerosol transport altitude contributes the largest uncertainty to the satellite-based estimate.

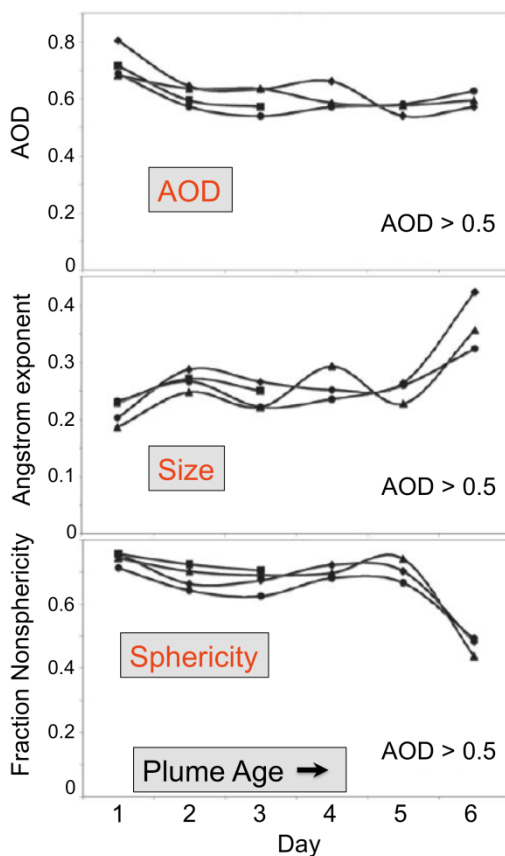


**Figure 2.12.** Evolution of dust plume characteristics for four case studies of dust transported from Africa to the Caribbean across the Atlantic in six days. Top: AOD, a total column measure of PM loading, decreases due to dry deposition. Center: Angstrom Exponent, an inverse measure of particle size. Particles on Day 6 are smaller than on Day 1 due to gravitational settling of the larger particles. Bottom: Particle sphericity showing less nonspherical fraction at the end of the transport due to increase in the hygroscopicity of particles and/or the removal of dust. [Reprinted from Figure 11 in Kalashnikova, O. V., and R. A. Kahn (2008), Mineral dust plume evolution over the Atlantic from MISR and MODIS aerosol retrievals, *Journal of Geophysical Research*, 113(D24204).]

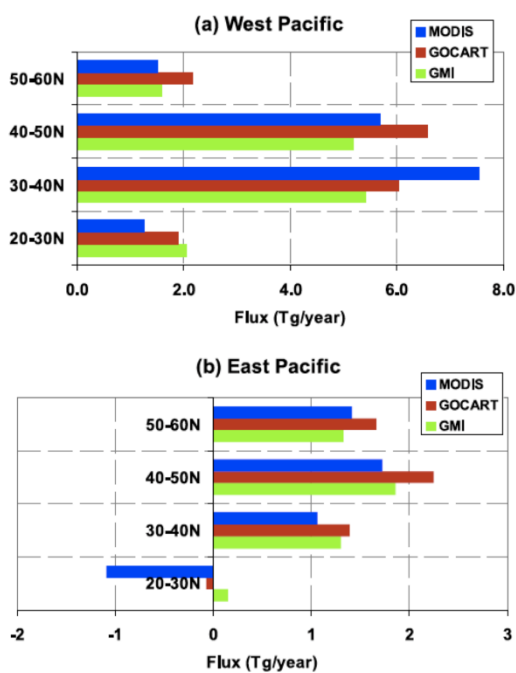


**Figure 2.13.** Estimates of annual pollution aerosol flux leaving Asia in the West Pacific (a) and arriving in North America in the East Pacific (b) for different latitude ranges. The blue bars are derived from MODIS aerosol products, and the red and green bars are derived from model calculations. [Reprinted from Figure 7 in Yu, H., et al. (2008), A satellite-based assessment of transpacific transport of pollution aerosol, *Journal of Geophysical Research*, 113(D14S12).]

### 2.3.2. In Situ and Lidar Observation of Particulate Matter Outflow from Continents

The outflow of PM and its precursors from mainland Asia and North America has been studied from downwind island sites. Bermuda, a site of long-term measurements from the AEROCE (Atmospheric/Ocean Chemistry Experiment) campaign [Prospero, 2001], has provided much information on the outflow of  $O_3$ , PM and their precursors from North America. In Asia, dust and

anthropogenic PM transported from the mainland have been observed in Japan. Figure 2.14 illustrates one event with two peaks evident due to anthropogenic PM. The elemental carbon/organic carbon (EC/OC) ratio remained at 0.2 during the whole episode, which indicates anthropogenic PM was present even when dust dominated [Takami *et al.*, 2006]. Episodes of enhanced SO<sub>2</sub> concentrations measured at the summit of Mt. Fuji, Japan (3.8 km asl) provide another example of Asian outflow. Enhanced CO and radon (<sup>222</sup>Rn) concentrations always accompanied the enhanced SO<sub>2</sub> concentrations, and backward trajectories for such events indicate an Asian continental origin [Igarashi *et al.*, 2006].

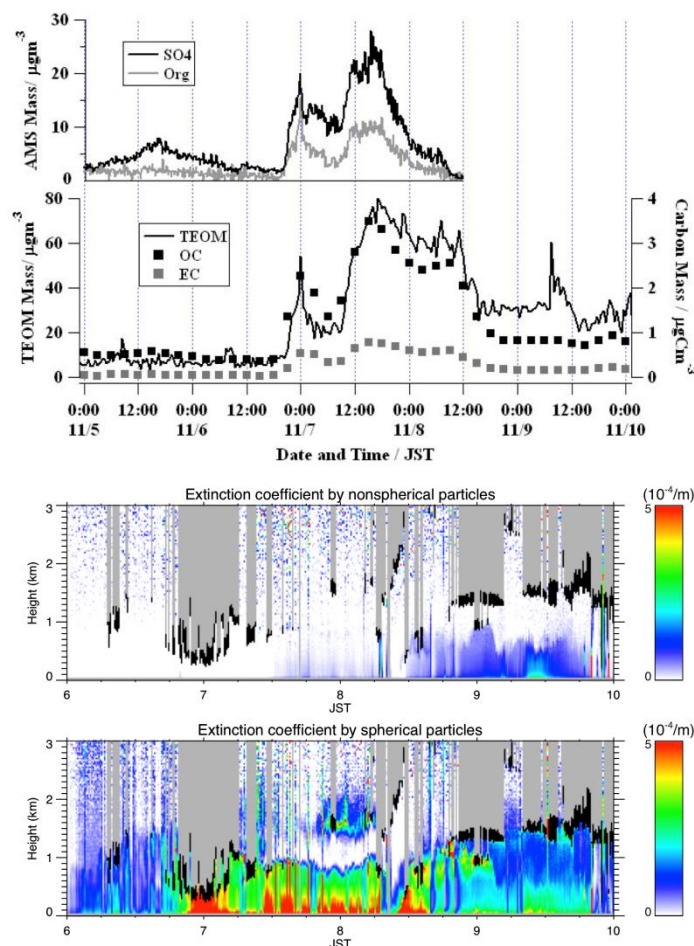


**Figure 2.14.** Aerosol transport event observed at Cape Hedo, a sea level site at the northern tip of Okinawa Japan. From top: (a) sulphate and organic components; (b) organic carbon, elemental carbon and PM<sub>2.5</sub>; and vertical distributions of (c) dust (non-spherical particles) and (d) deliquesced anthropogenic aerosol (spherical particles). [Reprinted from Takami, A., *et al.* (2006), Transport of anthropogenic and dust aerosol observed at Cape Hedo, Okinawa, *Journal of Aerosol Research*, 21(4): 341-347. Copyright 2006 Japan Association of Aerosol Science and Technology.]

### 2.3.3. Observations of Particulate Matter in Continental Inflow

Measurements on the eastern sides of the North Atlantic and North Pacific Oceans record the arrival of pollution PM from North America and Asia, respectively. At Mace Head, Ireland, anthropogenic sulphate has accounted for 85-90% of the total non-sea salt sulphate (nss) sulphate during marine inflow conditions, indicating that the aerosol arrived from across the ocean [Savoie *et al.*, 2002]. The nss sulphate values at Mace Head are several times greater than found at similar latitudes in the Southern Hemisphere, providing further evidence for an anthropogenic source (Figure 2.15) [Barrie *et al.*, 2001]. The ICARTT campaigns provided information on pollution transport across the North Atlantic Ocean. Putaud *et al.* [2004] and Van Dingenen *et al.* [2004] provided an extended review of physical and chemical properties of PM in Europe. It is shown that the regional background in Europe is



$7.0 \pm 4.1$  micrograms per cubic meter ( $\mu\text{g}/\text{m}^3$ ) for  $\text{PM}_{10}$  and  $4.8 \pm 2.4$   $\mu\text{g}/\text{m}^3$  for  $\text{PM}_{2.5}$  and that this background is not only due to natural sources but also to long-range transport of anthropogenic PM.

Because forest fire emissions can be injected into the upper troposphere, forest fire aerosols are efficiently transported over long-distances. Aerosol layers transported from North America to Europe have been captured by lidars over Western and Central Europe [Forster *et al.*, 2001; Wandinger *et al.*, 2004] and by surface measurement of BC concentrations. Analyses from EARLINET (European Aerosol Research Lidar Network) have shown that aerosol plumes from the anthropogenic sources in the North American boundary layer are generally not similarly intense [EARLINET, 2003]. Other examples of long-range transport of fire plumes include smoke originating from the Ural region travelling both northwest towards Scandinavia and eastward, across Canada, Scandinavia and eastern Europe before returning to Russia in a little more than 2 weeks [Damoah *et al.*, 2004].

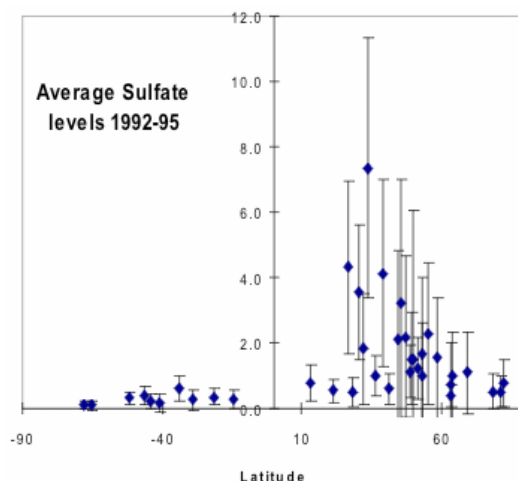


**Figure 2.15.** Average sulphate levels measured at marine sites in the Northern and Southern hemispheres [Barrie *et al.*, 2001].

Measurements also demonstrate that Asian industrial sources account for at least some of the baseline PM concentrations that are observed at the west coast of North America [Wilkening *et al.*, 2000]. Figure 2.16 illustrates an episode of elevated sub-micron aerosol scattering that corresponds to approximately  $20 \mu\text{g}/\text{m}^3$  of  $\text{PM}_{10}$ . The observed  $\text{Hg}^0/\text{CO}$  ratio in this episode indicates that the detected aerosol was associated with Asian industrial sources, not mineral dust or biomass burning [Jaffe *et al.*, 2005b; Weiss-Penzias *et al.*, 2007]. Using surface aerosol measurements from the Interagency Monitoring for Protected Visual Environments (IMPROVE) measurement sites together with a global chemical transport model, Heald *et al.* [2006] estimate the mean Asian sulphate enhancement in the northwestern U.S. in spring is  $0.16 \pm 0.08 \mu\text{g}/\text{m}^3$ . This is much smaller than the annual average ambient air quality standard of  $15 \mu\text{g}/\text{m}^3$  for  $\text{PM}_{2.5}$ , but is higher than the estimated natural concentration of  $0.09 \mu\text{g}/\text{m}^3$  presently used as the objective for regulating visibility in U.S. wilderness areas. Interestingly, no such Asian enhancements are observed for nitrate or for organic carbon (OC) aerosol. A significant sulphate contribution from Asian emissions is supported by the recent study of van Donkelaar *et al.* [2008] as part of the INTEX-B campaign, which found that 56% of the measured sulphate between 500–900 hectopascals over British Columbia is due to East Asian sources, and that there has been a 72–85% increase in the relative contribution of East Asian sulphate to the total burden in spring off the northwest coast of the U.S. since 1985. The ITCT-2K2 campaign observed additional evidence of trans-Pacific transport of anthropogenic Asian aerosols. Figure 2.17 illustrates PM measurements made during an aircraft profile through layered plumes marked by variations in CO concentrations. Transport modelling identified Asia as the emission source region. Another ITCT-2K2 flight observed particle size distributions and sulphate mass concentrations consistent with nearly pure sulphuric acid particle formation in the central North Pacific Ocean. The transport of gas-phase precursors from Asia and formation of particles in the mid-Pacific avoids the scavenging in cyclonic systems that remove PM from the atmosphere. Such mid-oceanic PM production suggests a larger potential for particle pollution to arrive during intercontinental transport events [Brock *et al.*, 2004].

BC, defined as the light-absorbing fraction of carbonaceous aerosols, has complex climatic implications involving atmospheric heating and snow and ice surface warming. BC is difficult to sense remotely due to its small contribution to PM mass and aerosol optical depth. However its absorbing properties allow detection in the aerosol index product from Total Ozone Mapping Spectrometer (TOMS) [Torres *et al.*, 2002] or more recently OMI [Torres *et al.*, 2007]. Since these products are most sensitive to high-altitude absorbing aerosols, they are most useful for detecting biomass burning aerosols, but they are also somewhat sensitive to dust outflow. To some extent long-range transport of black carbon can also be detected using the absorption aerosol optical depth (AAOD) products from AERONET (AERosol ROBotic NETwork) [Dubovik *et al.*, 2002], with the caveat that this product is sensitive to absorbing dust as well as black carbon. Atlantic and Pacific outflow regions have relatively large AAOD (0.005 to 0.01), and high latitude sites such as Bonanza Creek Alaska and Tomsk, Russia have substantial AAOD (0.01 to 0.02) similar to levels characteristic of Europe.

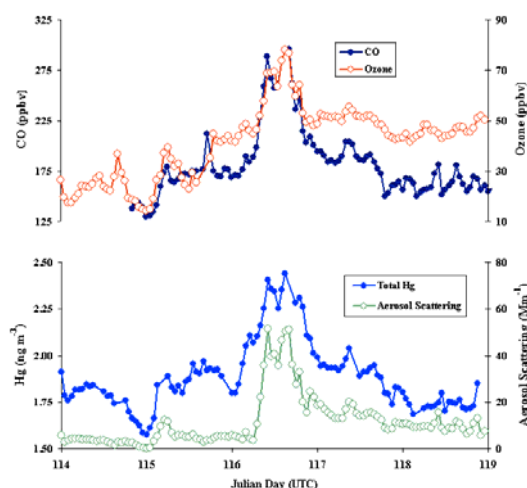


**Figure 2.16.** Concentrated trans-Pacific pollutant transport event observed at a mountaintop site near the west coast of North America. Observations of O<sub>3</sub>, aerosols, Hg and CO in a plume transported from Asia to the Mt. Bachelor Observatory in Oregon near the west coast of the U.S, in April 2004. The O<sub>3</sub> vs. CO linear correlation gives an R<sup>2</sup> value of 0.8 and a slope of 0.22. [Reprinted from Figure 4 in Jaffe, D. A., et al. (2005b), Export of atmospheric mercury from Asia, *Atmospheric Environment*, 39(17): 3029-3038, with permission from Elsevier.]

Better understanding of BC long-range transport requires improved quantification of the vertical distribution of BC. With the development of the SP2 instrument, high quality BC measurements with high vertical resolution are becoming available from aircraft campaigns [e.g. Schwarz *et al.*, 2006]. Aircraft campaigns near Houston and Costa Rica [Schwarz *et al.*, 2006; Schwarz *et al.*, 2008] indicate that BC concentrations decrease with altitude by about two orders of magnitude between the boundary layer and the upper free troposphere, which implies efficient scavenging of BC during vertical transport in these regions. On the other hand, aircraft SP2 measurements indicate substantial BC pollution in the Arctic, with increasing concentrations within the lower troposphere [Koch *et al.*, 2009, Figures 9 and 10]. This view is broadly consistent with the AERONET and OMI perspective of relatively clean BC conditions in the remote lower latitudes of the northern hemisphere but substantial pollution at higher latitudes. The substantial pollution occurs in spite of decreasing BC trends in recent decades in North American surface measurements [Sharma *et al.*, 2006] and snow [Hegg *et al.*, 2009], but with snow concentrations in Eurasia 2-3 times those in North American snow. As future campaigns measure BC in the free troposphere, understanding of long-range BC transport should greatly improve.

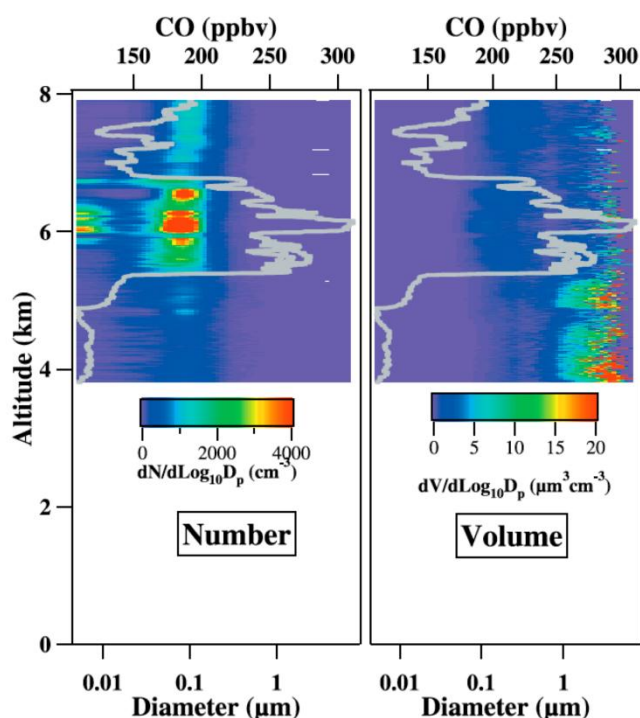


**Figure 2.17.** Aerosol measurements marked by variation in CO concentrations. Vertical distributions of CO with aerosol particle number size distribution (left) and particle volume size distribution (right) in a plume of emissions transported from Asia. The measurements were made near the west coast of North America on 5 May 2002. [Adapted from Figure 2 in Brock, C. A., et al. (2004), Particle characteristics following cloud-modified transport from Asia to North America, *Journal of Geophysical Research*, 109(D23S26), doi:10.1029/2003JD004198.]

### 2.3.4. Trends in Surface site Observations of Particulate Matter

As discussed in previous sections, satellite remote sensing observations can clearly identify the intercontinental transport of PM. Complementary in-situ surface measurements have revealed that the long-range transport events could have significant impact on surface PM loading in receptor regions. Furthermore, the analysis of the long-term trend observed in the receptor regions provides an effective measure of the “integrated effect” of the transport processes in larger spatial and temporal scales, e.g., the long-range transport influence on the receptor regional-scale PM loading and baseline concentrations. In this section, we discuss the long-term trends observed in receptor regions, by both in-situ and remote sensing measurements, under the influence of the transport from the East Asian, North American, and European sources. In addition, comparisons are made between the observed long-term trend and the emission trends in the source regions.

Analyses of measurements of nitrate and anthropogenic nss sulphate concentrations on island sites in the Pacific and the Atlantic provide temporal trends, which show the effect of the long-range transport of these pollutants from the East Asian, European, and North American source regions. The trend in nss sulphate pollution is estimated by computing the “natural” nss-SO<sub>4</sub><sup>-</sup> based on the methanesulfonic acid concentrations and subtracting from the total nss sulphate. On Midway Island anthropogenic sulphate concentrations approximately doubled from 1981 to the mid-1990s [Prospero *et al.*, 2003], a trend that closely matches the increase in SO<sub>2</sub> emissions from China over that period [Streets *et al.*, 2000]. Nitrate concentrations yield a similar trend over the same time period. The measurements made in Bermuda show coherent patterns in the annual mean concentrations of nss sulphate and nitrate (Figure 2.18). The nss sulphate decreased steadily from the start of the measurements until the mid-1990s, then stabilized and finally increased slightly through the remainder of the period. The emissions of SO<sub>2</sub> from U.S. sources decreased substantially over this time period by an amount that roughly corresponds to the nss sulphate trend observed at Bermuda, yet

the timing of the decreases are markedly different; the U.S. SO<sub>2</sub> emissions decreased sharply between 1994 and 1995 when more stringent controls were mandated. In contrast, there is no substantial change in nitrate over this period, in agreement with the trend in NO<sub>x</sub> emissions, which shows only a very slight increase over the period. The substantial differences between the aerosol record and the emissions record demonstrate the challenges in attempting to monitor long-term trends at distant receptor sites.

Aerosol sulphate and nitrate measurements have also been made continuously on Barbados since 1989. This record suggests that nitrate remained unchanged and that nss-SO<sub>4</sub><sup>-</sup> decreased by about 20%. Approximately half of the nitrate and nss sulphate at Barbados is attributable to anthropogenic sources [Savoie *et al.*, 2002], predominately from European sources [Hamelin *et al.*, 1989]. If one assumes that the change in nss sulphate concentration is due to the transport of pollutants and if one considers that about half of the nss sulphate is natural (from DMS), then the actual decrease in sulphate pollution is roughly 40%, a change that is consistent with the sharp drop in European SO<sub>2</sub> emissions over this time period [EMEP, 2004]. However the absence of a discernable change in Barbados nitrate concentrations is puzzling in light of the substantial reduction of European emissions of NO<sub>x</sub>, roughly 25% [EMEP, 2004].

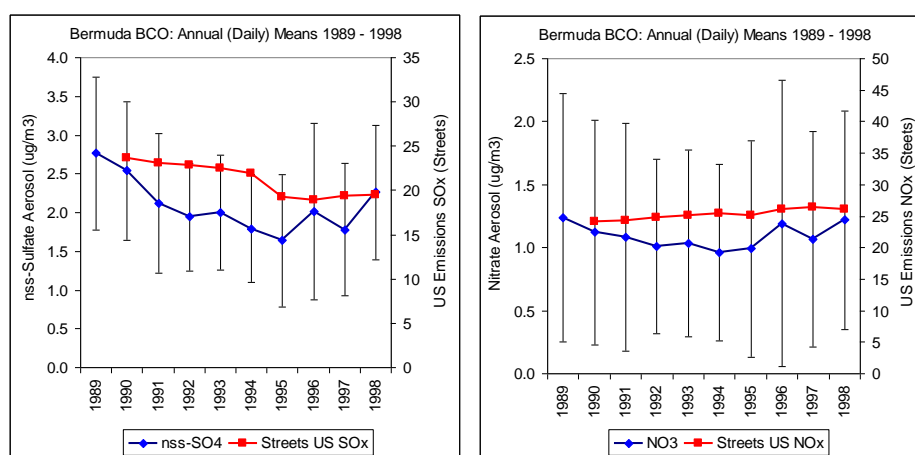


**Figure 2.18.** Annual mean nss-sulphate and nitrate concentrations on Bermuda during on-shore winds compared to eastern US SO<sub>2</sub> (Tg S/y) and NO<sub>x</sub> emissions (Tg N/yr). Bars indicate the standard deviations of the monthly means from which the annual means are derived. [Based on data discussed in part in Savoie *et al.*, 2002]

The phenomenon of Arctic Haze occurs each winter and early spring due to rapid, meridional transport of anthropogenic PM from the northern mid-latitudes to the Arctic. The result is a dramatic increase in aerosol mass concentration. The haze is composed of a varying mixture of sulphate, organics, ammonium, nitrate, dust, and BC [e.g., Li and Barrie, 1993; Quinn *et al.*, 2002]. It is also rich in distinct heavy metals, allowing for the identification of particular industrial sources [e.g., Rahn and McCaffrey, 1980]. Long term trends in the aerosol chemical composition and optical properties of Arctic Haze have been monitored at stations within the Arctic including Barrow, Alaska (71.3°N, 156.8°W); Alert, Canada (82.5°N, 62.3W); and Station Nord, Greenland (81.4°N, 16.6°W).

The longest record of sulphate concentrations in the Arctic (1980 to present at Alert) reveals no change in sulphate concentration during the 1980s [Sirois and Barrie, 1999] followed by a decline beginning in 1991. A similar decline through the 1990s was observed in sulphate concentrations at Station Nord [Heidam *et al.*, 2004] and in light scattering and absorption at Barrow [Bodhaine and Dutton, 1993]. A combined modelling and measurement analysis of sulphate concentrations at Station Nord was able to account for scatter in measured concentrations due to changing meteorology [Heidam *et al.*, 2004]. With the meteorological variability removed, it was possible to attribute the decrease in concentration to a reduction in emissions. The model that was used estimates that more than 70% of the sulphur measured at Station Nord is emitted from the region making up the former Soviet Union. This result is supported by a 50% decrease in Russian sulphur emissions reported to

EMEP during the 1990s [Vestreng, 2003]. It is not clear from this analysis how reductions from Europe and North America influenced the sulphate concentrations at Station Nord.

The decreasing trend in sulphate at Alert detected through the 1990s has continued into the present century [Quinn *et al.*, 2007]. In contrast to sulphate, nitrate concentrations have increased during the Arctic Haze season at Alert over the period from 1981 to 2003. This increase may be a result of increasing vehicle usage in regions of the former Soviet Union. Quinn *et al.* [2009] compared ratios of tracer species measured at Barrow during the Arctic Haze season from 1976-1977 and 1997-2008 to assess trends in Arctic Haze aerosol over this 30-year period and changes in source regions. The tracer species considered in the analysis included nss sulphate (derived from fossil fuel combustion), non-crustal (nc) vanadium (V) (derived from the combustion of heavy residual oil), and nc manganese (Mn) (derived from iron, steel, and ferro-alloy manufacturing, coal and oil combustion, and mining). Based on these two data sets, concentrations of nss sulphate and nc V have decreased at Barrow by about 60% over this 30 year period. Consistency in the ratios of nss sulphate to nc V and nc Mn to nc V between the two data sets indicates that, while emissions have decreased in source regions, the source regions themselves have remained the same over this time period.

Satellites have been used to estimate temporal changes of aerosols through measurements of the AOD, which is a good indication of aerosol loading. Satellite AOD measurements provide the most comprehensive view of the atmospheric aerosols on global and regional scales. The available satellite AOD data products span nearly 2 decades. Mishchenko *et al.* [2007] analyzed the temporal variation in the globally averaged GACP (Global Aerosol Climatology Project) AOD data, which were derived from Advanced Very High Resolution Radiometer (AVHRR) radiance measurements. The GACP AOD showed a small increase, i.e., 0.03 or ~3% over 14 years, but a statistically significant decrease from 1991 to 2005. More recently, Thomas *et al.* [2010] found an increase in global AOD of 0.024/decade between 1995 and 2001. This study was based on the Global Retrieval of ATSR Cloud Parameters and Evaluation (GRAPE) dataset, which was derived from ATSR-2 (Along Track Scanning Radiometer-2) observations. These authors attributed the global GRAPE increase to regional increases over the North Pacific, Tropical Pacific, and Tropical Indian oceans. It was also noted that there were significant differences between the GACP and GRAPE AOD data, approaching 0.5, and both datasets showed significantly larger shorter-term variations (uncorrelated) than the derived long-term trend. Li *et al.* [2009] presented a more extensive comparison of the satellite AOD data, including MISR, MODIS, and GACP (Figure 2.19). This comparison also showed a considerable difference between the AOD datasets in terms of absolute magnitude as well as short-term and long-term temporal variations. Again, the shorter-term variations are much larger than the long-term changes. These authors concluded that most of the current satellite observation-based AOD are inadequate for analysis of long-term changes without significant improvement in calibration/validation, cloud screening, characterization of aerosol microphysical and optical properties, and surface reflectance.

### *2.3.5. Implications for Surface Particulate Matter Air Quality in Receptor Regions*

Particles transported over long distances can have a negative impact on urban air quality, although observed events are generally limited to dust transport. Figure 2.20 illustrates a particularly pronounced event. The dust was transported initially in the free troposphere, and then brought to the surface through a combination of processes, which differed from region to region. Subsequent mixing with local pollutants led to PM<sub>2.5</sub> concentrations exceeding the new U.S. daily standard of 35 µg/m<sup>3</sup>. During this specific case, the dust passed above the Pacific Northwest (i.e. Seattle, Washington) and had greater impact at the surface in the Rocky Mountains and eastern United States. Even in events when the percent increase in concentration is small, it may be sufficient to cause local exceedances of air quality standards.

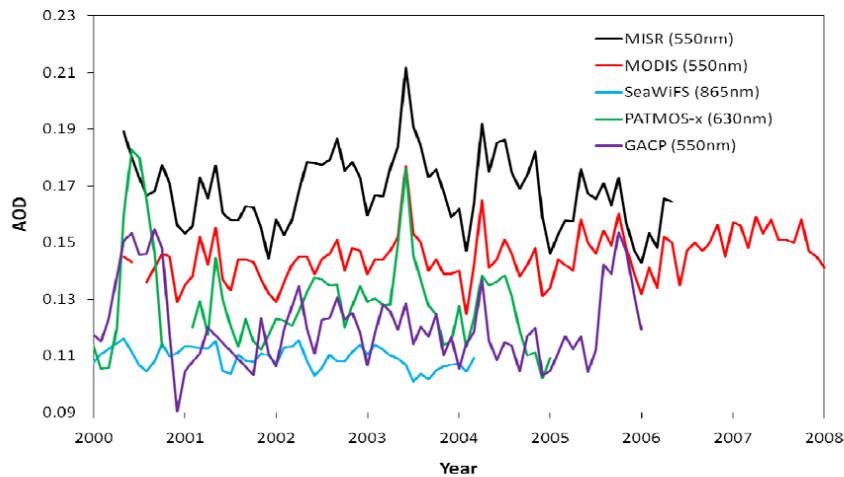


**Figure 2.19.** Comparison of global mean AOD over ocean derived from different satellite input data and retrieval algorithms for an overlapping period since 2000. Different retrieval algorithms assume different aerosol models. [Reprinted from Figure 1 in Li, Z., et al. (2009), Uncertainties in satellite remote sensing of aerosols and impact on monitoring its long-term trend: A review and perspective, *Annales Geophysicae*, 27: 2755-2770.]

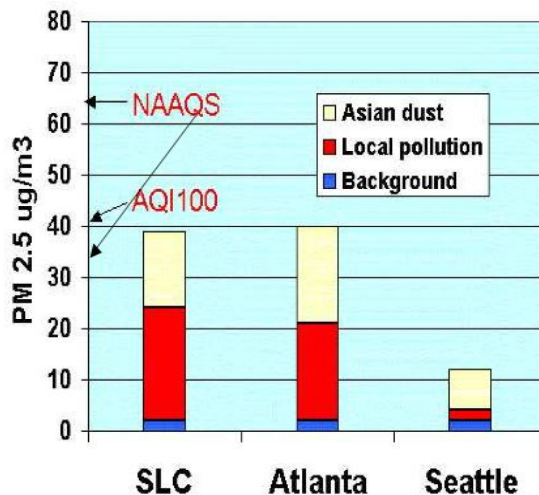


**Figure 2.20.** Contributions from three sources to surface PM<sub>2.5</sub> in three U.S. cities (Salt Lake City, Utah; Atlanta, Georgia and Seattle, Washington) during an April 2001 episode of Asian dust transported to North America. [Adapted from Jaffe, D., et al. [2003], The 2001 Asian Dust Events: Transport and Impact on Surface Aerosol Concentrations in the U.S., *EOS: Transactions of the American Geophysical Union*, 84(46): 501-507.]

Until recently, satellite observational tools were unable to provide robust source apportionments. The added capability of CALIPSO may significantly improve quantitative estimates of PM flux and the impact of transported particles on air quality at ground level over broad regions. However, even the enhanced observational capabilities are insufficient to provide robust quantitative air quality assessments alone. To provide an answer, improved observational capabilities will need to be combined with modelling in a synergistic approach.

### 2.3.6 Summary, Remaining Uncertainties and Future Needs

**FINDING:** In situ measurements have established the importance of intercontinental transport of PM from dust, forest fires, and anthropogenic sources. In some case studies of in situ measurements have illuminated secondary aerosol formation far from the sources of transported precursors.



**FINDING:** Ground-based lidar networks and mountain top measurement sites in Europe, North America and Asia provide large continuous data sets that characterize the frequency and intensity of aerosol transport events and the meteorological conditions responsible for them. They also provide important information on aerosol particle properties. Operational procedures for dust outbreak monitoring in near real time are implemented at several mountain sites in Europe.

**RECOMMENDATION:** Discussion is required regarding the optimum observation strategy for in situ and surface remote measurements for further characterizing intercontinental transport of aerosols. A particular focus should be on measurements to quantify the sources and properties of the organic and black carbon components of transported PM, which are currently poorly understood. The mechanisms for the transport and removal of PM also need to be addressed.

**FINDING:** Over the last few years, satellites have begun to provide quantitative information on intercontinental aerosol transport, including estimates of the amount of dust and pollution transported, the altitude of transport and, in some cases, aerosol particle properties.

**FINDING:** Observed trends of PM (e.g. SO<sub>4</sub>) in downwind locations are closely related to the emission trends in the source regions with the impact of long-range transport more evident in remote regions less affected by local sources such as the Arctic. Satellite measurements are currently not precise and accurate enough for monitoring the long-term changes.

**RECOMMENDATION:** Analysis of available datasets should be supported to better quantify aerosol particle properties and the PM fluxes (pollution, dust, biomass-burning emissions) between continents in the Northern Hemisphere and to/from regions to the north (Arctic) and south (e.g. Africa). Surface in situ and remote measurements as well as satellite observations can provide important contributions.

**FINDING:** Long-range transport of aerosols can have air quality and climatic implications, at northern latitudes especially in the outflow from the Asian continent and in the Arctic region. Observational studies alone have not well quantified either the impact on local air quality or the climatic implications.

**RECOMMENDATION:** To inform air quality control decisions, better methodologies are required to extract the long-range transport contribution from measured overall PM concentrations. Characterizing long-range transport of black carbon is particularly important for understanding climatic implications.

#### **2.4. Observational Evidence for Attribution of Source Regions**

Enhancements in trace gas and aerosol concentrations associated with long-range transport of pollution from sources upstream may persist for several days in the free troposphere, where residence times are enhanced. During transport, atmospheric mixing acts to dilute these enhancements, as air masses of different histories are mixed together creating a spectrum of chemical signatures downstream from the source region. This provides a challenge in attributing source regions of long-range transport events using observations from research aircraft and surface stations, since discrete chemical signatures associated with source regions may be completely masked by mixing. Nevertheless, observed relationships among chemical tracers can be used to detect the influence of upstream source regions on the composition of a given region of the atmosphere. Knowledge of source relationships between tracers and their atmospheric processing, and observations of tracers of different atmospheric lifetimes, can be used to yield estimates of the influence of remote upstream sources on atmospheric composition. Moreover, methods for combining in situ or satellite tracer observations with backward modelling techniques provide powerful constraints on the pathways of long-range pollution transport, our understanding of chemical processing during individual transport events and attribution of contributions from different source regions and types. Improvements in the quality of analyzed wind fields from meteorological services has also enabled more robust attribution of contributing source regions to a given receptor region downstream.

### 2.4.1. Meteorologically-based source attribution studies

On the intercontinental or hemispheric scale, meteorology-based analyses for accurately determining the emission source regions of gases or PM at a particular receptor require the use of transport models. These modelling techniques currently fall into two categories: 1) backward simulations with Lagrangian particle dispersion models (LPDM); and 2) adjoints to chemical transport models (CTM). These methods are designed for exploring emission regions (both known and unknown) and transport pathways backwards in time from an in situ trace gas or PM measurements. They are also complementary to the more traditional approach of using a model to emit tracers from known emission sources and seeing if they advect forwards in time to the receptor location.

LPDM backward simulations initialized from a receptor (measurement) location is the now the most commonly used method of meteorological-based source attribution studies. Simpler back trajectories are still used but they are limited in the quantitative information they can provide on the contribution from a source region, and do not perform as well in regions of strong shear or convection. LPDMs calculate the transport pathways of air masses (often referred to as “particles” because they are assumed to be infinitesimally small) following the winds resolved in atmospheric analyses or forecasts. The models also include a stochastic step to represent the effects of unresolved turbulence and convection [Stohl *et al.*, 2002]. The parameterised “random walk” shuffles particles, each weighted with the same tracer mass, so that their sum within a volume represents the effects of advection and diffusive mixing on passive tracer concentration [Legras *et al.*, 2003]. At present, LPDMs have not yet been developed to include chemical or aerosol processing or detailed descriptions of deposition processes where non-linearities in chemical transformation may be important.

For tracers, such as CO where a linear loss can be included, LPDM simulations lead to a relatively accurate representation of transport which takes into account the shear, turbulence and convection encountered by a volume of air as it travels from source to receptor. The dynamics of the atmosphere also conspire to allow accurate simulation of tracer structures formed by advection on scales an order of magnitude finer than the resolution of the wind field [Methven and Hoskins, 1999] allowing simulations at high resolution (< 0.5 degrees). LPDM backward simulations have become known as retroplumes [Stohl *et al.*, 2003] which can be calculated in various forms and resolutions by models such as FLEXPART [Stohl *et al.*, 2005], STILT [Gerbig *et al.*, 2003; Lin *et al.*, 2003] or HYSPLIT ([http://www.arl.noaa.gov/HYSPLIT\\_info.php](http://www.arl.noaa.gov/HYSPLIT_info.php)). The method involves releasing a multitude (often tens of thousands) of trajectory particles in the receptor volume and tracking their location for several days backwards in time using high resolution (1° x 1° or finer) global wind fields. The sum of the residence time of all particles in the boundary layer establishes the “footprint” of the retroplume and indicates the surface emission region influencing the measured trace gas or PM. Multiplying the footprint residence time by co-located surface emission rates estimates the contribution of that source region to the trace gas quantity measured at the receptor. One of the first examples of the use of the retroplume technique for source attribution of a long-range transport event, demonstrated that aircraft-based measurements of enhanced CO and NO<sub>y</sub> in the free troposphere above Europe during November, 2001, originated in the boundary layer of North America and travelled to Europe via a warm conveyor belt [Stohl *et al.*, 2003]. Approximately half of the CO in the plume came from various anthropogenic sources in the eastern U.S., with the main contribution coming from the New York region. The technique has also been used to show how elevated O<sub>3</sub> and CO above the California coast originated in a broad region of south and east Asia with subsequent transport to California via two successive warm conveyor belts [Cooper *et al.*, 2004]. Retroplumes have also shown how Asian pollution can be rapidly transported eastwards in the upper troposphere to Europe in as little as 6 days [Stohl *et al.*, 2007b]. Application to aircraft and surface measurements in the Arctic has recently revealed the pathways of biomass burning emissions from Europe [Stohl *et al.*, 2007a] and central Asia [Warneke *et al.*, 2007] to Spitzbergen and northern Alaska, respectively. A recent development in this technique is to calculate retroplume climatologies for thousands of in situ measurements at a given location over many years. The purpose is to identify the typical transport patterns and source regions associated with a subset of measurements such as enhanced or depleted trace gas or PM events [Cooper, 2010; Hirdman *et al.*, 2010].



Meteorologically-based source attribution studies can also be conducted with CTM adjoints. While adjoint capabilities have been around slightly longer than the retroplume technique, they have not been as widely applied to intercontinental- or hemispheric-scale studies, although they are gaining in popularity. The adjoint works in the same spatial and temporal resolution as the CTM to which it is attached and provides similar output to retroplumes, identifying the source region of an air mass at a particular receptor as well as its transport pathway. On the hemispheric scale, adjoint studies have a coarser horizontal resolution than the retroplume studies (roughly  $2^\circ \times 2.5^\circ$  vs.  $1^\circ \times 1^\circ$ ). The advantage of adjoints over retroplumes is that they can be used to not only determine the source region of a trace gas or PM measurement, but can also identify the chemical and physical mechanisms that modify the trace gas or PM during transport, provided these mechanisms are handled by the CTM.

Application of adjoints to pollution plume studies began with the development of the adjoint to the HANK CTM which demonstrated that the techniques could identify plume transport from Asia to Mauna Loa Observatory, Hawaii [Vukicevic and Hess, 2000]. Adjoints have been recently applied to explore processes that influence intercontinental transport to North America. Henze et al. [2009] used the GEOS-Chem adjoint to determine the source regions of inorganic  $\text{PM}_{2.5}$  precursor emissions for monitoring sites throughout the U.S. and found that intercontinental influences are small, though transboundary influences within North America are significant, with strong influence from  $\text{SO}_x$  emissions in Mexico. Zhang et al. [2009] determined that Mount Bachelor Observatory in the northwestern U.S. experiences distinct Asian  $\text{O}_3$  pollution episodes, with most of the  $\text{O}_3$  production occurring over East Asia, adding to a diffuse background production distributed over the extra-tropical northern hemisphere (Figure 2.21). The adjoint also showed that transpacific pollution plumes transported in the free troposphere are diluted by a factor of 3 when entrained into the boundary layer, explaining why these plumes are undetectable in U.S. surface air.

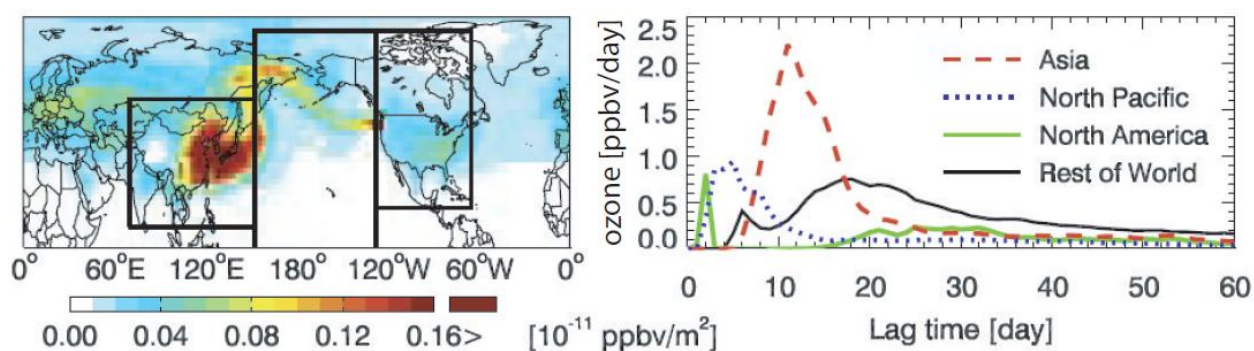


**Figure 2.21.** Measured  $\text{O}_3$  mixing ratios of 55-60 ppbv at Mt. Bachelor Observatory, Oregon on 1 May, 2006, were determined as having a 50% contribution from Asian sources based on the global GEOS-CHEM model. The model adjoint showed that much of the  $\text{O}_3$  production over the past 60 days occurred within Asia (left panel shows where  $\text{O}_3$  production occurred) roughly 10 days earlier (right panel shows when  $\text{O}_3$  production occurred in 4 different regions over the previous 60 days), although production also occurred as the Asian pollution plume crossed the North Pacific Ocean and descended into the mid-troposphere over North America. [Reprinted from Figure 2a in Zhang, L., et al. (2009), Intercontinental source attribution of ozone pollution at western U.S. sites using an adjoint method, *Geophysical Research Letters*, 36(L11810).]

**FINDING: High resolution particle dispersion models provide powerful techniques for the identification of pollutant source regions.**

**FINDING: Recent developments in adjoint modelling techniques provide useful insights into the sources and the chemical transformation processes that influence trace gases and aerosols during long-range transport.**

**RECOMMENDATION: There is a need for further application of particle dispersion models to the analysis of long-time series of ozone and PM, with the goal of determining the impact of source regions on long-term trends and inter-annual variability.**

**RECOMMENDATION: Development of LPDMs to include full treatments of chemical and aerosol processing and wet/dry deposition as a complement to Eulerian models is needed.**

*2.4.2. Source attribution based on trace gas correlations and ratios*

Relationships among atmospheric chemical tracers are powerful observation-based tools for assessing source contributions and probing chemical and physical processing in air masses undergoing long-range transport. For example, the ratio  $\Delta\text{O}_3:\Delta\text{CO}$ , used as an estimate of the excess in  $\text{O}_3$  and CO above background in different plumes, has been used to identify long-range transport events and estimate photochemical  $\text{O}_3$  enhancement in polluted air masses downstream of the continents [Bertschi *et al.*, 2004; Parrish *et al.*, 1993].  $\Delta\text{NO}_y:\Delta\text{CO}$  has been used as a measure of export efficiencies of anthropogenic emissions from continental regions [Li *et al.*, 2004; Stohl *et al.*, 2002; Val Martin *et al.*, 2006] and correlations between  $\text{O}_3$  and PAN in aged air can be used to infer photochemical influence from sources upstream [Parrish *et al.*, 1992]. These trace gas relationships can also be useful in distinguishing plumes from different sources (e.g. boreal forest fires versus anthropogenic pollution), however, care has to be taken when using  $\Delta\text{O}_3:\Delta\text{CO}$  to infer  $\text{O}_3$  production. Secondary production of CO from non-methane volatile organic compound oxidation and  $\text{O}_3$  deposition or photochemical  $\text{O}_3$  loss during transport may modify observed slopes [Chin *et al.*, 1994], and photochemical destruction of CO may increase the  $\Delta\text{O}_3:\Delta\text{CO}$  slope [Real *et al.*, 2010]. Tracer variability within an air mass and sharp tracer gradients at its edges may also complicate the use of ratios, where observations are non-representative of the plume average or are affected by background air at the point of sampling. Since plumes do not remain isolated, in reality their chemical signatures are influenced by the history of different backgrounds and source signatures with which they have mixed during transport. Price *et al.* [2004] showed  $\Delta\text{O}_3:\Delta\text{CO}$  slopes in plumes transported in the upper troposphere were likely influenced by mixing with higher ozone concentrations. In addition, the choice of criteria used to define  $\Delta\text{O}_3:\Delta\text{CO}$  above background can result in differences in slope values [Pfister *et al.*, 2006] and inference of plume source and photochemical activity. On a larger scale, correlations between satellite observations of tropospheric  $\text{O}_3$  and CO over the Pacific have been used to identify and track events of trans-Pacific photochemical  $\text{O}_3$  transport [Zhang *et al.*, 2008].

The increasingly routine observation of a range of non-methane hydrocarbons (NMHC) during airborne missions and at free tropospheric surface sites is proving valuable for identifying and examining long-range transport events in the troposphere. Many simple alkane and alkene species have atmospheric lifetimes useful for probing processing on timescales for intercontinental transport (2-5 days). The robust source relationships among different NMHCs, their range of typical atmospheric lifetimes, and their common chief sink (the OH radical) have been used to infer photochemical ageing and OH concentrations from NMHC ratio observations during long-range transport events [Parrish *et al.*, 1992; Price *et al.*, 2004]. Atmospheric mixing destroys the idealised evolution of tracer ratios expected through only photochemical processing of an air mass, which can inhibit their use in source attribution or inference of plume processing. Nevertheless, results from the ICARTT pseudo-Lagrangian experiment (see 2.4.4) showed that on spatial and temporal scales of intercontinental transport, well-defined NMHC ‘fingerprints’ can be retained in air masses over several days in the free troposphere. These NMHC fingerprints allowed successful pseudo-Lagrangian links to be identified. In addition, they provided a powerful independent validation of atmospheric transport model derived links among observation platforms. Lewis *et al.* [2007] demonstrated distinct NMHC signatures of large enhancements in acetylene relative to acetaldehyde and acetone in biomass burning plumes intercepted near the Azores compared with North American anthropogenic plumes, enabling robust separation of these two source types. The use of NMHC ratios in conjunction with  $\Delta\text{O}_3$  estimates can also be used to investigate relationships between  $\text{O}_3$  photochemical production and plume age [Helmig *et al.*, 2008]. Using statistical inference techniques applied to observed NMHC ratios in the ICARTT pseudo-Lagrangian air masses, Arnold *et al.* [2007] estimated mean OH concentration, dilution rates and background air mass NMHC composition, characteristic of air masses of anthropogenic and biomass burning origin in the summertime North Atlantic troposphere using robust relationships among NMHCs with a wide range of lifetimes, such that their OH oxidation during the 1-3 days between export from North America and aircraft interception produced an

appreciable change in NMHC ratios. Combination of NMHC ratios with Lagrangian particle dispersion model simulations has also allowed quantification of the different contribution of photochemistry, emissions and mixing [Honrath *et al.*, 2008; Parrish *et al.*, 2007].

Nevertheless, recent studies have indicated that other oxidants such as halogens (chlorine, bromine radicals) or nitrate may play an important role in the formation (or destruction) of tropospheric O<sub>3</sub>. For example, chemical measurements in coastal regions of the Gulf of Mexico during the summer 2006 TexAQS study for the first time confirmed that nitryl chloride is a key atmospheric species that couples the nitrogen and halogen chemistries of the marine boundary layer [Osthoff *et al.*, 2008]. The use of inert tracers (e.g. perfluorocarbons), which have no chemical sinks, has also been used recently as part of the DLR POLARCAT-GRACE campaign to follow air masses over a few days providing important constraints on atmospheric mixing among different air masses (Hans Schlager, Deutsches Zentrum fuer Luft - und Raumfahrt (DLR) Institut fuer Physik der Atmosphaere, Wessling, Germany, personal communication, 2010).

**FINDING: Increasingly routine observations of concentrations of ozone and aerosol precursors as well as reservoir species such as PAN, onboard research aircraft and at observatory sites have allowed fingerprinting of different sources and quantification of timescales for plume processing by photochemistry and mixing, and coupled with atmospheric transport models these observations can now allow the detailed source history of a given air mass to be untangled.**

**RECOMMENDATION: Development of in situ techniques for measuring trace gas and aerosol species at higher temporal resolution, and with improved detection limits (e.g. <1pptv for NMHCs), would improve the detection of LRT events. Improved knowledge about NMHC emissions to better constrain estimates of chemical processing based on NMHC ratios is also required.**

**RECOMMENDATION: Assess the role of oxidants other than OH in pollutant processing, such as halogens and nitrate and the role of heterogeneous processes in polluted and non-polluted regions.**

**RECOMMENDATION: Further development of techniques based on the release and re-sampling of inert tracers to allow quantification of mixing processes during long-range transport.**

#### *2.4.3. Aerosol source attribution based on use of trace elements and isotopes*

Although there now exist instrumental capabilities to measure the physical and chemical properties of pollutant aerosols in great detail, there are still relatively few reliable “tracers” that are uniquely source-specific; largely because aerosol source signatures (nature or anthropogenic) are rarely unique and because there is a large degree of atmospheric mixing during hemispheric-scale transport. In the case of natural particulate matter such as mineral dust, a combination of mineralogical and geochemical/isotopic properties can be used to identify the source regions(s). Over the past decade, a vast number of studies have documented the global dispersion of desert dust from East Asian deserts, in particular from northwestern China and southern Mongolia. Dust from these regions has been tracked as far as Alaska, the Yukon, Greenland and the European Alps [Bory *et al.*, 2003; Grousset *et al.*, 2003; Yasunari and Yamazaki, 2009; Zdanowicz *et al.*, 2006]. Many of these studies make use of source-specific mineralogical abundances, elemental ratios, or the stable isotope ratios of strontium (Sr), eodymium (Nd) and lead (Pb) in the clay-size fraction of dust aerosols to identify their source(s). This has been facilitated by concerted efforts to map the compositional characteristics of different dust sources in eastern Asia [e.g. Yang *et al.*, 2009; Zheng *et al.*, 2009]. Trace element abundances and ratios also allow for trends in atmospheric mineral dust loading to be investigated in ice cores. Kaspari *et al.* [2009] recently developed a proxy record of dust aerosols from a Mt Everest ice core. The record suggests that Asian dust outbreaks have become more frequent since the 1800s, but provides no conclusive evidence of an anthropogenic impact on these trends. However, these trends are at odds with results from another core from the western Tibetan Plateau [Yang *et al.*, 2006]. Meanwhile, a record from Mt Wrangell in Alaska suggests a recent increase in the trans-Pacific transport of Asian dust in the springtime [Yasunari *et al.*, 2007].

For short-lived anthropogenic aerosols (e.g., trace metals, sulphate, and BC) the challenge of identifying distant sources is greater. This is because the compositional properties of these aerosols (e.g., elemental or isotopic abundances) are either not sufficiently characterized, or too variable, or both, to be unequivocally attributed to specific sources or source regions. Typically, compositional properties of pollutant aerosols are used to apportion total concentrations among various source types (e.g., fuel combustion vs. industrial refining) using some type of factor analysis, rather than to identify specific regional point sources [e.g. *Viana et al.*, 2008] although there are exceptions.

Lead (Pb) isotope ratios have proven particularly useful to trace back long-range airborne metal pollution to various source regions, because the stable Pb isotope composition of fumes from fuel combustion, or from some industrial processes, can carry a source-specific signature inherited from the ore from which the Pb was extracted [*Komarek et al.*, 2008]. However, some pollution sources, such as base metal smelters, may have time-varying emission signatures [e.g. *Simonetti et al.*, 2004]. More commonly, the Pb isotope ratios of aerosols are compared with the air mass signature of various possible source regions, and the relative contributions of these regions are estimated using a mass balance model such as the U.S. EPA's IsoSource [e.g. *Sturges et al.*, 1993]. The essential requirement for this method is that the source signatures be well characterized. Fortunately, research efforts in recent decades have allowed the Pb isotope signatures of regional airsheds in both hemispheres to be defined [*Bollhofer and Rosman*, 2000; 2001; 2002]. Lead isotope measurements in aerosols and in snow and ice from Greenland, Arctic Canada and alpine regions have provided evidence of changing levels and sources of atmospheric Pb to the remote atmosphere over past decades and centuries [e.g. *Mercier*, 2000; *Sherrell et al.*, 2000; *Shotyk et al.*, 2005; *Veysseyre et al.*, 2001]. These records show declining trace metal pollution after the 1980s in the North Atlantic sector and in western Europe, but a Pb isotope record from corals in the western Pacific testifies to a growing export of atmospheric Pb from China, which may have contributed up to 64 % of the Pb increase in the last two decades of the 20<sup>th</sup> century. This is in agreement with Pb isotope data from China [*Mukai et al.*, 2001] and Pb deposition trends recorded in snow on the opposite side of the North Pacific [*Osterberg et al.*, 2008]. A time series of aerosol Pb isotope data at a pair of sites on the west coast of California demonstrates how Pb isotope analysis has been used to resolve trans-Pacific versus local Pb sources [*Ewing et al.*, 2010]. While the trans-Pacific Pb generally co-occurs with peaks in sample mass and silicon (Si) content due to trans-Pacific dust events, high Pb concentrations relative to sample mass and Si content are taken as evidence that the trans-Pacific Pb is primarily anthropogenic in origin (see Figure 2.22).

The source identification of anthropogenic sulphate aerosols is more challenging because there are also multiple natural sources that contribute to the observed sulphate burden in the atmosphere. However, advances in the stable isotope characterization of sulphur ( $\delta^{34}\text{S}$ ) in aerosols and precipitation now allow for the relative contributions of these source types to be estimated. As with Pb isotopes, the method requires that the  $\delta^{34}\text{S}$  of possible reservoirs and sources (e.g., industrial  $\text{SO}_2$  gases, marine biogenic sulphate) be determined with sufficient precision to discriminate among these sources. Also, sulphur isotope ratios in the atmosphere can be modified during heterogeneous phase reactions, in particular oxidation pathways, and the effects of these reactions must be quantified [*Leung et al.*, 2001]. In pioneering studies, *Nriagu et al.* [1991] and *Norman et al.* [1999] used sulphur isotope measurements to estimate the relative contributions of natural (primarily marine) and non-marine, primarily anthropogenic sources (including smelter emissions) to sulphate aerosols collected at Alert, Arctic Canada. Since then, several other studies have applied the method to characterize the sources of atmospheric sulphate in Europe [*Novak et al.*, 2001], North America [*Wadleigh et al.*, 2001], China [*Mukai et al.*, 2001] and over the Atlantic Ocean [*Patris et al.*, 2000; *Wadleigh*, 2004]. Measurements of  $\delta^{34}\text{S}$  have also been applied to Greenland ice cores in order to document the changing burden of anthropogenic sulphate in the polar atmosphere since pre-industrial times [*Patris et al.*, 2002]. As coal combustion remains one of the dominant man-made sources of  $\text{SO}_2$  in the atmosphere, and as China emerges as the dominant emitter [*Lu et al.*, 2010; *Osterberg et al.*, 2008], efforts are now being directed at refining the sulphur isotope characterization of Chinese coal sources.

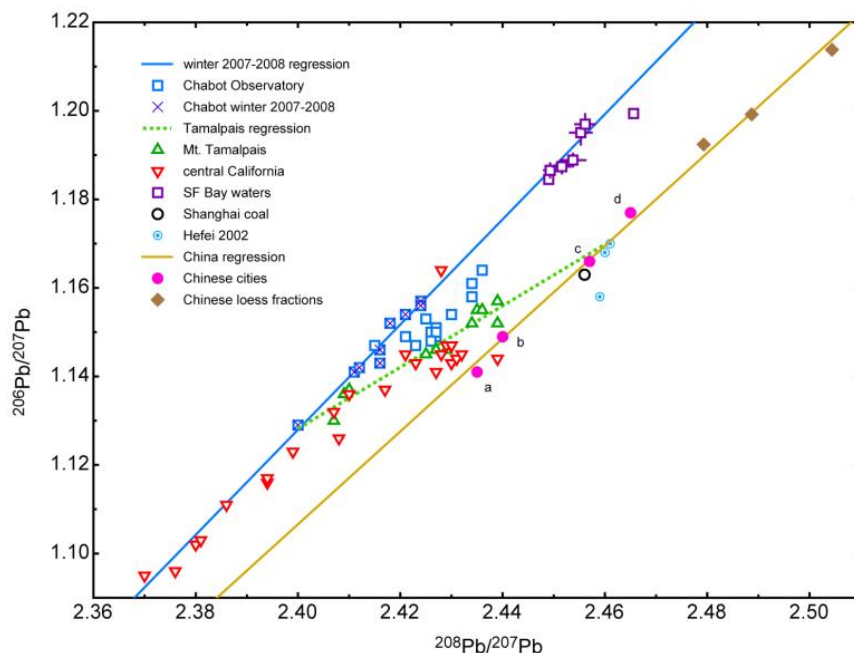


**Figure 2.22.**  $^{208}\text{Pb}/^{207}\text{Pb}$  vs.  $^{206}\text{Pb}/^{207}\text{Pb}$  in airborne particles at sites in California (Chabot Observatory, Mt. Tamalpais and central California surface sites), in San Francisco Bay waters, and from a variety of Chinese sources. Linear regression lines are shown in blue for wintertime Chabot samples, light brown for Chinese cities and loess, and dotted green for Mt. Tamalpais. [Reprinted from Figure 1 in Ewing, S. A., et al. (2010), Pb Isotopes as an Indicator of the Asian Contribution to Particulate Air Pollution in Urban California, *Environmental Science & Technology*, 44(23): 8911-8916. Copyright 2010 American Chemical Society.]

Similarly, new analytical developments, in particular the measurement of carbon isotope ratios in organic aerosols, are now allowing for BC in air or deposited in snow to be apportioned among source types such as biomass burning, biofuel combustion, fossil fuel combustion, etc. [Hegg *et al.*, 2009]. The microcrystalline structure and trace element composition of soot may also reveal the type of emission process and help distinguish between, for example, BC emitted by industrial plants from that emitted by diesel engines [VanderWal *et al.*, 2010]. But the objective of fingerprinting specific regional sources of BC in long-range aerosols remains largely elusive.

With or without diagnostic tracers, attribution of aerosols to specific source regions can also be attempted by comparing observed temporal trends at receptor sites with emission trends from potential source regions. Ice cores from polar and alpine regions, which contain records of atmospheric aerosol deposition extending back over decades to millennia, have proven useful in this respect. While these records cannot, as yet, be directly interpreted in terms of aerosol loadings, the deposition histories developed from ice cores provide solid evidence of the intercontinental transport of anthropogenic aerosols from specific continental regions. In particular, the sources of atmospheric sulphate and/or nitrate aerosols have been investigated in Greenland [Bigler *et al.*, 2002], the Norwegian and Canadian Arctic [Goto-Azuma and Koerner, 2001; Kekonen *et al.*, 2002; Moore *et al.*, 2006], the European Alps [Preunkert *et al.*, 2001; Preunkert *et al.*, 2003] and western North America [Yalcin and Wake, 2001]. As well, the provenance of atmospheric Pb in the Arctic atmosphere has been investigated using cores from Greenland and the Canadian North [McConnell *et al.*, 2002; Osterberg *et al.*, 2008; Shotyk *et al.*, 2005] (Figure 2.23). More recently, McConnell *et al.* [2007] developed a detailed record of BC deposition from central Greenland, which points to a predominance of North American sources prior to the mid-20<sup>th</sup> century, and the growing influence of east Asian sources since 1951.

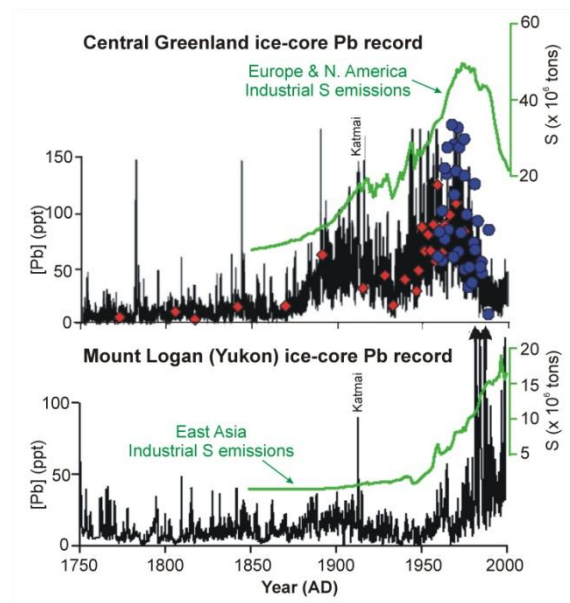


**Figure 2.23.** Ice-core records of atmospheric lead (Pb) pollution in central Greenland (altitude ~3000 m) and Mt. Logan (altitude ~5500 m), Yukon Territory, Canada. Black lines are high-resolution measurements of Pb from Greenland [reprinted from Figure 1a in McConnell, J. R., et al. (2002), A 250-year high-resolution record of Pb flux and crustal enrichment in central Greenland, *Geophysical Research Letters*, 29(23): 2130-2133] and Mt. Logan [reprinted from Figure 3a in Osterberg, E., et al. (2008), Ice core record of rising lead pollution in the North Pacific atmosphere, *Geophysical Research Letters*, 35(L05810)]. Coloured symbols in upper panel are spot measurements from earlier studies. Also shown are reported industrial sulphur gas emissions from North America and Europe and from East Asia [from Osterberg et al., 2008].

**FINDING: Measurements of trace elements and isotopic ratios can provide useful fingerprints for different source types and emission regions influencing aerosol composition.**

**FINDING: Analysis of long-term aerosol and trace element records provides information about inter-annual variability in source attribution at a particular downwind measurement site as well as insights into how emissions may have changed in the past.**

**RECOMMENDATION: Further development is needed of isotope and geochemical fingerprinting techniques for the identification of different source types and, in the case of stable isotopes information about chemical processes occurring during transport. Proxy records of aerosol deposition (e.g. from ice cores) also provide useful tests for models over multi-decadal timescales.**

#### 2.4.4. Plume processing during long-range transport based on analysis of Lagrangian data and implications for global modelling of long-range pollutant transport

An ideal framework for assessing the processes influencing the evolution of pollutant concentrations during long-range transport away from source regions is to sample the same air mass several times at successively greater downwind distances. Such a Lagrangian approach assumes that an air mass can be tracked with sufficient accuracy during transport. Since this is, in reality, difficult to achieve, such attempts are often called pseudo-Lagrangian experiments. They were first attempted over rather short spatial (few hundred kilometres) and temporal scales (1-2 days) as part of, for example, the first and second Aerosol Characterization Experiments (ACE) [e.g. Raes et al., 2000] or downwind of biomass burning regions over the southern Atlantic during TRACE-A [Mauzerall et al., 1998].

Since the mid-2000s, as noted in Section 2.4.1, the ability to accurately forecast tracer (e.g., CO) distributions several days downwind from source regions has improved. This led to the planning and execution of the first inter-continental pseudo-Lagrangian experiment (IGAC Lagrangian 2K4), which took place as part of the ICARTT field campaign, to investigate long-range transport of



pollutants between North America and Europe. It was the first time that dedicated flights were planned to sample the same air masses on inter-continental scales with multiple aircraft based in North America, the Azores and Europe [Fehsenfeld *et al.*, 2006].

Several Lagrangian matches were identified post-campaign covering a variety of different meteorological situations [Methven *et al.*, 2006]. One case is shown for illustration in Figure 2.24 when anthropogenic pollution was transported across the North Atlantic. Continuous, but slow, entrainment from the polluted low level outflow helped to maintain elevated pollutant levels (e.g., sulphate aerosol) in the marine boundary layer below. In another case of pollution outflow, Real *et al.* [2008] used a photochemical model initialized with upwind data, and compared to downwind data allowing a detailed evaluation of the processes influencing O<sub>3</sub> levels during long-range transport. Initially O<sub>3</sub> and oxidized nitrogen concentrations were very high but hypothesized washout of HNO<sub>3</sub> combined with O<sub>3</sub> destruction was needed to explain the lower concentrations observed off the west coast of Ireland. Nevertheless, observed O<sub>3</sub> concentrations were still higher than average concentrations observed during summer at Mace Head, Ireland. This case also highlighted that high O<sub>3</sub> and water concentrations, observed close to the source regions, can lead to significant CO destruction making the use of CO as a tracer less than ideal in this case. In another case of long-range transport of an Alaskan forest fire plume, the trade-off between photochemical O<sub>3</sub> production from PAN decomposition and destruction due to increasing water vapour during descent into Europe were both found to be important as well as mixing with upper tropospheric air masses [Real *et al.*, 2007]. In both cases, it was difficult to determine an actual import of pollutants into the European PBL although in the latter case, the biomass burning plume was also observed in the lower troposphere in the south of France [Ravetta *et al.*, 2007, see Section 2.2.1].

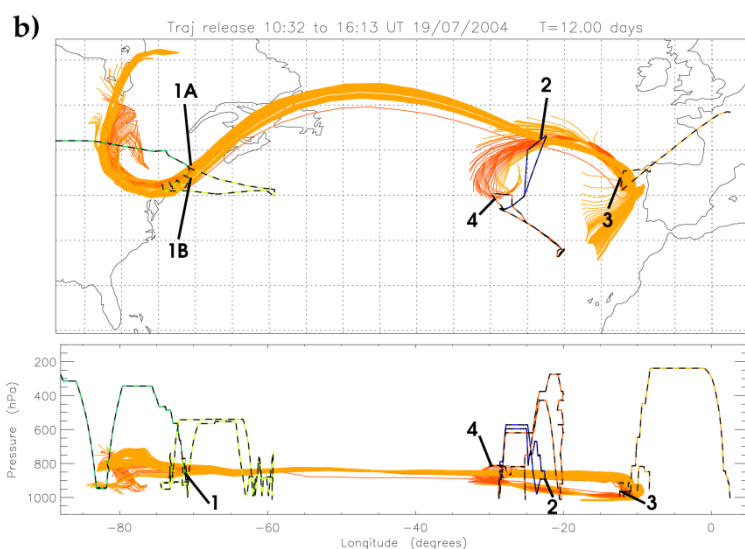


**Figure 2.24.** Trajectories 6 days backwards and forwards from the UK FAAM BAe146 flight track on 19 July 2004 (blue) showing links with upwind and downwind flights. Matching flights were: NASA DC8 15 July (dark green), NOAA WP-3D 15 July (light green), DLR Falcon 22 July (orange) and FAAM BAe146 25 July (red), numbered in time order. [Adapted from Figure 2b in Methven, J., *et al.* (2006), Establishing Lagrangian connections between observations within air masses crossing the Atlantic during the International Consortium for Atmospheric Research on Transport and Transformation, *Journal of Geophysical Research*, 111(D23S62)] (case 1).

Analysis of the ICARTT forest fire case led to the application of parcel dispersion modelling techniques previously employed in the stratosphere to determine tropospheric mixing rates [Pisso *et al.*, 2009]. These approaches, based on the FLEXPART model and including a stochastic representation of mixing, were used to demonstrate the need for high spatial resolution calculations to reproduce observed plumes, many thousand kms downwind from source regions. Pisso *et al.* [2009] also estimated that global models need to be run with at least 40 km horizontal and 500 meter vertical

resolution in order to simulate long-range transport of pollutant plumes. Rastigejev et al. [2010] also showed that numerical diffusion, inherent in global Eulerian models, is dominating plume dilution even at increasing grid resolution. They suggest that adaptive gridding or embedded Lagrangian treatments of pollutant plumes are needed. Inclusion of photochemistry in the calculations of Pisso et al. [2009], representing resolutions of a few km, showed the importance of multiple air mass origins in governing measured concentrations of O<sub>3</sub> and CO along downwind flights [Real et al., 2010]. An example is shown in Figure 2.25. Runs of the model reproduced observed correlation patterns and demonstrated the importance of chemical destruction as well as production in producing observed trace gas correlations. Results from a global model (MOCAGE) were unable to reproduce these correlations because the plume was too smeared out. Real et al. [2010] also estimated errors associated with resolution on net O<sub>3</sub> production showing that significant errors (up to 20-50%) can occur at plume edges compared to low resolution simulations which smear out gradients. Wild and Prather [2001] also quantified the impact of horizontal resolution on photochemical O<sub>3</sub> production, finding errors ranging from 27% at 5.5 degrees to 5% at 1.1 degrees. However, as already suggested errors might become non-linear below 1 degree.

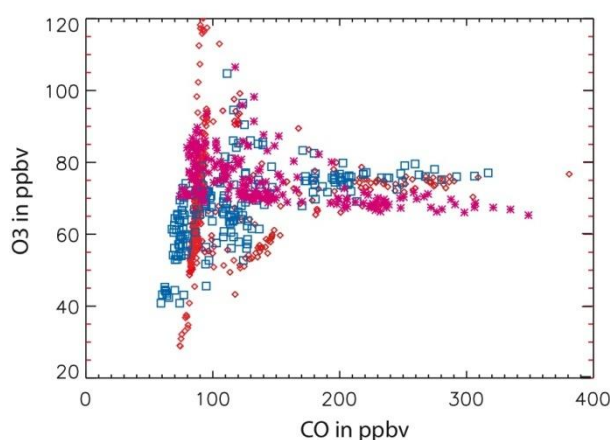


**Figure 2.25.** O<sub>3</sub>:CO correlations along Lagrangian plume match segment of a flight on 22 July 2004 by German DLR Falcon – measurements are shown as red diamonds; simulated results using a high resolution parcel model (Zoom-CiTTy) with chemistry are shown as blue rectangles; model runs without chemistry are shown as pink stars. [Adapted from Figure 10 in Real, E., et al. (2010), Toward a novel high-resolution modeling approach for the study of chemical evolution of pollutant plumes during long-range transport, *Journal of Geophysical Research* 115(D12302).]

**FINDING: Pseudo-Lagrangian experiments provide unique and very useful constraints on the processing of long-range transport plumes by allowing the observation of air mass evolution in a flow-relative framework. Subsequent data analysis revealed detailed information regarding the photochemical evolution of anthropogenic and biomass burning plumes during long-range transport.**

**RECOMMENDATION: Lagrangian experiments should be used to rigorously assess the performance of global models, and the impact of resolution on long-range transport simulations requires further investigation. The comparison of model NMHC ratios with those observed would also provide constraints on models' abilities to represent the source contributions to long-range transport plumes, retain plume structure and representation of their dilution to the background.**

**FINDING: Developments in high-resolution Lagrangian modelling have allowed estimates of the resolutions needed to capture long-range transport of pollutant plumes in global models, which are currently too diffusive leading to the artificial dilution of pollutant plumes. The resolution issue is important for modelling pollutant events as well as modelling background pollutant levels where errors can occur if modelled lifetimes are incorrect.**



**RECOMMENDATION: Improved horizontal and vertical resolution in global models together with the further development of plume in-grid techniques for pollutant plume transport is needed.**

**RECOMMENDATION: A better understanding of air mass entrainment from the free troposphere into the planetary boundary layer is required through dedicated field experiments, to improve estimates of the impacts of long-range ozone transport on regional air quality in receptor regions.**

## 2.5. Research Needs

### 2.5.1. Surface Site Needs

A comprehensive ground-based global monitoring system is required for many purposes, including data provision for comparison with global models of chemistry and transport, and detection of trends in emissions of primary pollutants and their secondary products produced by atmospheric processing. The only truly global network for fulfilling this requirement is contained in the World Meteorological Organization (WMO) Global Atmospheric Watch (GAW) program which organizes the measurements of a large range of chemical species at sites distributed globally ([http://www.wmo.int/pages/prog/arep/gaw/gaw\\_home\\_en.html](http://www.wmo.int/pages/prog/arep/gaw/gaw_home_en.html)). The data are stored at the World Data Centre for Greenhouse Gases (WDCGG). Figure 2.26 shows the locations of the sites for measurement of reactive and greenhouse gases. This global network is complemented by national and transnational networks that cover regions e.g. EMEP in Europe, the Clean Air Status and Trends Network (CASTNET) in the US, and the Canadian Air and Precipitation Monitoring Network (CAPMoN). For the detection of episodes of long-range intercontinental transport of gaseous pollutants however, only a few sites are capable of producing useful information. For aerosols it is a different matter and many sites in remote locations reveal transport events. As discussed in Section 2.2.2, mountaintop sites are particularly useful for detecting long-range transport events arriving on the western coasts of North America and Europe and even Europe to Asia transport.



**Figure 2.26.** Network of surface-based remote observatories organized through the World Meteorological Organization's Global Atmospheric Watch (GAW) Program.

The WMO GAW program measures gaseous species, including CO, O<sub>3</sub>, selected volatile organic compounds (VOCs), NO<sub>x</sub> and NO<sub>y</sub> compounds, and SO<sub>2</sub>. A new global network for measuring VOCs has just been created within the GAW program and a network for global measurements of NO<sub>x</sub> and NO<sub>y</sub> compounds is planned. Unfortunately, no global network exists for SO<sub>2</sub> although this species, and all the others mentioned, are measured by EMEP and CASTNET.

These regional networks were set up to follow trends in emissions of primary pollutants and to establish the regional background of secondary pollutants which can be strongly influenced by long-range transport from region to region. While some networks exist in southeast Asia, such as in Taiwan and Japan, there is a need to further develop long-term measurement networks in this important emission region, and especially in China and other parts of southeast Asia.

**RECOMMENDATION: Continue current ground-based networks into the future with additions made to the range of constituents measured and additional sites in optimal locations for characterization of long-range transport and long-term changes in pollutant concentrations. Such networks require continued maintenance with proper attention paid to calibration and data quality issues.**

### 2.5.2. Vertical Profiling Needs

Instrumented surface sites provide continuous in-situ measurements of trace gases and aerosols that are valuable for identifying annual trends as well as seasonal and diurnal variability. However, with the exception of a few high mountain top sites, they are only representative of the lowest few hundred meters of the atmosphere and need to be supplemented with vertical profiling through the full troposphere to allow, in particular better quantification of the export and import of pollutants to and from emission regions. This requires frequent vertical profiling at key locations on the upwind and downwind edges of the continents and especially in regions susceptible to pollution import (see Chapter 1) where long-range transport of pollutants may lead to exceedence of pollution thresholds for air quality and crops. The three methods currently used for the vertical profiling of O<sub>3</sub> and PM are described below.

#### *Ozonesondes*

These balloon-borne instruments are routinely launched year-round at approximately 35 sites in the northern hemisphere, typically one to three times per week, providing measurements at 100 m resolution through the troposphere. However very few sites are ideally located for determining the baseline O<sub>3</sub> impacting a continent (Figure 2.27). While ozonesonde datasets have provided information about long-term changes in O<sub>3</sub> concentrations [e.g. *Oltmans et al.*, 2006], difficulties arise associated with changes in techniques over time and calibration, which make interpretation of these records problematic [*Schnadt Poberaj et al.*, 2009; *Smit et al.*, 2007]. A recent study reported increasing free tropospheric O<sub>3</sub> over western North America during springtime, 1995-2008, using large data sets composed primarily of MOZAIC data (see below). This study found that weekly ozonesonde profiles at a particular location were not frequent enough to detect increasing O<sub>3</sub> trends in the free troposphere [*Cooper*, 2010]. Detection of the trend would require ozonesonde profiles on a daily basis. It can be noted that the annual cost of operating a hypothetical northern hemisphere ozonesonde network of 60 sites with daily profiles is on the order of 20 million US\$.

#### *Ozone and aerosol lidars*

Lidars are ground-based lasers that measure O<sub>3</sub> mixing ratios and PM loadings with vertical resolution better than 1 km through much of the troposphere, with some having the capability to reach the tropopause. These instruments cannot however measure through clouds. Figure 2.27 shows the locations of most of the tropospheric ozone and aerosol lidars in the northern hemisphere. There are very few O<sub>3</sub> lidars, all in North America, Europe and New Zealand, while the number of aerosol lidars is at least 70 with a large proportion in East Asia. As noted in Sections 2.2 and 2.3, ground-based lidars contribute very valuable information about long-range transport of O<sub>3</sub> and PM.

#### *Commercial aircraft*

Since 1994 the European MOZAIC program (<http://mozaic.aero.obs-mip.fr>) has measured O<sub>3</sub>, water vapour, CO and NO<sub>y</sub> from up to five commercial Airbus aircraft. To date the program has measured over 60,000 vertical profiles, mostly in Europe, the eastern U.S. and Japan. The most frequently sampled cities are shown in Figure 2.27. The data have been used for a wide variety of studies and, as shown in the recent study by Cooper et al. [2010], can be used for the analysis of O<sub>3</sub> trends in the free troposphere. Some limitations of the program are that measurements in the

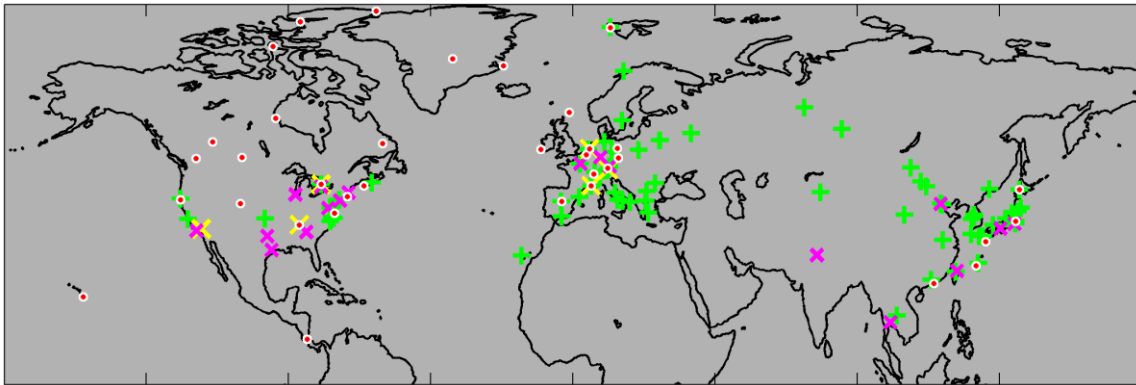


**Figure 2.27.** Current locations in the Northern Hemisphere with frequent ozone and PM profiling of the troposphere by: aerosol lidars (green +) [Bosenberg and Hoff, 2008], ozone lidars (yellow x) and weekly ozonesondes (white/red dots) (www.woudc.org). Also shown are the cities frequently sampled by MOZAIC/IAGOS commercial aircraft (magenta x) during 1995-2010.

lowermost troposphere are contaminated by local airport effects, data are collected from a finite number of cities, flight routes are often biased to certain times of day, and scientists have no control over where profiles occur. The MOZAIC program is being replaced by the new IAGOS program (<http://www.iagos.org/>) from mid-2010 with an increased number of measurements of trace gases ( $O_3$ , CO,  $CO_2$ ,  $NO_y$ ,  $NO_x$ , and water), PM and cloud particles. The goal is an initial fleet of 10-20 long-range commercial aircraft operated by a range of international carriers providing cost-effective profiling (approximately \$500 per profile) around the world. The data will be available in near real time to weather services and Earth observation service centres. In addition, the CARIBIC (Civil Aircraft for Regular Investigation of the Atmosphere Based on an Instrument Container) [Brenninkmeijer *et al.*, 2007] program that began in 1997 has joined IAGOS. The latest phase of CARIBIC uses one commercial A340 Airbus conducting approximately 40 flights per year between Frankfurt and destinations around the world. While the CARIBIC aircraft flies less frequently than its MOZAIC counterparts, it makes a wider range of measurements, which includes  $O_3$  and PM (particle number, size distribution and composition).

Routine monitoring from dedicated aircraft could also augment future vertical profiling of  $O_3$  and PM. For example, the NOAA Earth System Research Laboratory contracts privately owned aircraft to make routine vertical measurements of carbon cycle gases from sixteen locations across North America. A similar program could be created to measure  $O_3$  and PM. The recent development of Un-manned Aerial Vehicles (UAVs) that can carry significant payloads (up to 900 kg), fly up to 30 hours and reach altitudes near 20km (see e.g., <http://uas.noaa.gov/> and <http://www.nasa.gov/centers/dryden/aircraft/GlobalHawk/>), could eventually provide the ideal monitoring for quantifying long-range transport of  $O_3$  and PM in the northern hemisphere. Such aircraft could be flown several times per week on routine survey missions along the western coast of a receptor region. However, the cost of such a program would be large, and the use of UAVs in the capacity of routine air quality monitoring has not yet been fully developed.

**FINDING: Lidars, ozonesondes and commercial aircraft provide frequent profiling of  $O_3$  and PM at many locations across the northern hemisphere. However, very few of the profiling locations are ideally situated to quantify baseline  $O_3$  and PM flowing into the continents.**

**RECOMMENDATION: Additional profile measurements are much needed to provide information on the vertical distribution of pollutant layers Commercial aircraft measurements should be expanded, especially within the continents (North America, Asia, Europe), and with additional measurements of trace gases and aerosols. Additional ground-based lidars should be sited to yield the best quantification of baseline  $O_3$  and PM impacting downwind continents.**

**RECOMMENDATION: Development is needed of the capability to use unmanned aerial vehicles for measuring pollutant profiles in regions of pollutant import over receptor regions.**

**RECOMMENDATION: Maintenance of the long-term record from ozonesondes is required.**

**RECOMMENDATION: Added emphasis should be placed upon measurements designed to quantify the import of pollutants into the planetary boundary layer of receptor continents.**

### 2.5.3. Satellite Data Needs

Satellite remote sensing provides a valuable data source to assess the impacts of long-range transport and derive pollutant emissions. Efforts in a few key areas offer high potential to further enhance this capability. One such area is data access where excellent examples exist of publicly available satellite data, often in near real-time. Making all scientific satellite data available for free in an easily accessible and timely manner would increase the value of the measurements to the wider scientific community (e.g. through tools like Giovanni (<http://disc.sci.gsfc.nasa.gov/giovanni>), and TEMIS ([www.temis.nl](http://www.temis.nl))). This should include regular updates from data providers following product improvements together with documentation detailing, in particular, the quality of the data and methodology for its scientific use.

Further quantification of error estimates and improvement in satellite retrievals are also needed. Great progress has been made in developing retrieval algorithms that yield quantitative results that can be compared with models and other measurements in a consistent manner. Nonetheless, continued effort is needed to achieve a clear understanding of the accuracy and precision of these measurements. In addition to an assessment and quantification of the main error sources in the retrieval processes under different characteristic conditions (background, urban pollution, biomass burning, etc.) and measurement scenarios (dependent on meteorology, surface type, time of day etc.) systematic comparisons against independent measurements are necessary. A challenge is that surface and aircraft measurements available for retrieval evaluation are often at different spatial and temporal scales than the satellite measurements, and have different inherent measurements sensitivities to the atmospheric quantity of interest, which can lead to ambiguous comparisons. Therefore, although the development of systematic vertical profiling (Section 2.5.2) would clearly help, dedicated validation activities are needed that span a satellite pixel (typically ~15km for recent instruments such as IASI/METOP), and include profile information, for a range of pollutants, seasons and atmospheric conditions. This evaluation effort must persist over the entire mission duration to establish confidence in trend detection in the presence of possible instrumentation drifts over time.

Continued investment in retrieval development could contribute to significant advances in assessment of long-range transport. For example, nascent tropospheric HNO<sub>3</sub> retrievals [Wespes *et al.*, 2009] could provide insight into O<sub>3</sub> sources. Emerging developments in retrievals of ammonia [Beer, 2008; Clarisse *et al.*, 2009] and SO<sub>2</sub> [Lee *et al.*, 2009] offer a constraint on PM sources. The development of multispectral retrieval techniques and better instrumental spectral resolution have the potential to improve vertical profile information and allow discrimination of the lowermost troposphere from the free troposphere for species such as CO [Deeter *et al.*, 2009] and O<sub>3</sub> [Liu *et al.*, 2010; Worden *et al.*, 2007]. In addition to these passive observations, innovative approaches using active remote sensing (the CALIOP lidar in space onboard CALIPSO since 2006 and the future ATLID onboard the EarthCare mission) provide valuable complementary information on the altitude and shape of the transported plumes.

Finally, most current satellite missions able to make measurements of processes relevant for long-range transport are maturing and could soon end. For example, with the exception of GOME-2 and IASI-METOP, the instruments in Table 2.1 are all operating beyond their planned lifetimes. Planning for the next generation of satellites is beginning, but progress is slow due to limited resources, and the current wealth of data is unlikely to be maintained over the next few years as the current instruments expire. Proposals for future missions are recognizing the complementary nature of measurements of trace gases and PM from both low Earth orbit (LEO), which provides global coverage, and geostationary orbit (GEO), which allows for continental-scale measurements at relatively high spatiotemporal resolution. Indeed, a tantalizing possibility for the future would be the international implementation of a constellation of LEO and GEO platforms providing detailed coverage of most of

the globe. This would permit comprehensive investigation of pollution events, transport and atmospheric composition processes at different altitudes and across spatial and temporal scales.

**FINDING: Current satellite datasets for trace gases and aerosols provide critical spatial and temporal information for improved understanding of transport pathways and emission strengths.**

**FINDING: Many current satellites measuring atmospheric composition are reaching the end of their missions so future capabilities may be reduced.**

**RECOMMENDATION: Continued efforts are required to improve retrieval accuracy, to improve vertical resolution, and to develop modelling tools to interpret the observations.**

**RECOMMENDATION: The development and launch of geostationary satellites measuring trace gas and aerosols is needed provide much improved temporal coverage over key emission regions of the northern hemisphere.**

**RECOMMENDATION: High priority should be given to developing future low Earth orbit missions, accelerating the implementation timetable, and fostering international cooperation on shared use of available data and coordinated future mission planning.**

#### *2.5.4. Intensive Campaign Needs*

Intensive field campaigns provide abundant opportunities to advance our understanding of the hemispheric transport of air pollution. Each campaign generally deploys a wide array of newly developed, state-of-the-art instruments in a coordinated manner on several mobile (aircraft, ship) platforms and at surface sites. These instruments include in-situ and remote-sensing measurements. Strategies to answer open research questions guide the planning of such studies, so the results invariably advance our understanding on multiple fronts.

Issues relevant to long-range pollutant transport that can be addressed by intensive campaigns using instrumented aircraft are manifold. Emission sources can be characterized and their emissions quantified for primary pollutants, greenhouse gases, and precursors of O<sub>3</sub> and PM. The chemical transformation of emitted species can be followed through the formation of secondary species (both gas-phase and aerosol), and on to the ultimate destruction and deposition processes. Atmospheric transport mechanisms can be identified and their relative importance determined. This includes not only transport of pollutants away from emission regions but also their long-range transport to receptor regions and import into the boundary from the free troposphere. This latter aspect has yet to be investigated in detail in many regions.

In addition to addressing specific issues, intensive field campaigns provide extensive and detailed data sets that serve as benchmarks for testing chemical-transport model simulations. In particular, Lagrangian experiments making multiple samplings of the same air mass during long-range transport between continents can provide important information on chemical and aerosol processing as well as deposition processes and mixing rates in the troposphere.

Although far less expensive than a single satellite instrument, an intensive campaign does challenge the resources that are typically available for field measurements at a national level. Hence, the larger campaigns are beyond the capabilities of a single agency or even nation, and therefore must be planned wisely and coordinated at an international level.

**FINDING: Intensive field campaigns provide one of our most important means of advancing our understanding of atmospheric chemistry and transport in general, and the long-range transport of pollutants in particular. Lagrangian experiments are particularly useful in this regard.**

**RECOMMENDATION: Intensive field campaigns should be conducted frequently focusing on key issues where large uncertainties remain in our understanding of long-range transport of pollutants between continents such as the import of pollutants into the boundary layer over downwind receptor regions. Given the extensive resources required, it is essential to carefully**

**plan such experiments, ideally within international frameworks that can mobilize a large scientific community to address a particular issue.**

**RECOMMENDATION: Continued development of high quality, accurate measurements of trace gases and aerosols, in conjunction with quality control assessments, for use in intensive field campaigns is needed. The development of methods based on, for example, the release of inert tracers and fingerprinting techniques (using in-situ measurements of isotopes, VOCs), would allow significant advances in our ability to follow pollution plumes, and in source identification and verification of emission inventories.**

#### *2.5.5. Model evaluation against observations*

The results presented in this chapter have focused on observational evidence for long-range transport of pollutants. Data analyses using multiple parcel models or trace gas correlations/ratios were also presented as a means of identifying source regions. Global CTMs are the tools used to estimate the impact of different emission regions on downwind regions (see Chapter 4). Here we comment on their usefulness for this purpose and the methodologies employed for evaluating their performance in terms of ability to simulate pollutant long-range transport. Comparison with observations is generally used as a means of evaluating model performance. Previous studies analyzing multi-model ensembles [e.g. *Dentener et al.*, 2005; *Fiore et al.*, 2009] largely focused on comparison with surface data. For example, *Fiore et al.* [2009] attempted to assess model skill by comparing with surface O<sub>3</sub> observations binned over different sub-regions. While certain biases were evident, it was difficult to attribute causes, in part due the large differences in, for example modelled VOC emissions, which varied by a factor of 10 across models. Other studies have compared models with monthly mean ozonesonde data [e.g., *Stevenson et al.*, 2006]. Such comparisons do not test model ability to simulate observed variability including particular episodes. Accurately reproducing such data and attributing sources remains a challenge for current global models. Additional development and application of computationally efficient algorithms (such as adjoint approaches) are valuable to calculate model sensitivities to multiple parameters, such as long-range transport or emission sources.

Detailed comparison of specific global models with data collected as part of intensive field campaigns does allow advances in our understanding of processes influencing the model results and discrepancies with the data. For example, *Hudman et al.* [2008] used INTEX-NA data to conclude that EPA CO emissions are too high by 60%. Modelling associated with analysis of Lagrangian data also provides important information about the processes governing pollutant concentrations during particular long-range transport events (see Section 2.4.4). Results showed that plume signatures are diluted too rapidly in current global models due to too coarse resolution [*Pisso et al.*, 2009; *Real et al.*, 2010] and diffusive advection schemes [*Rastigejev et al.*, 2010] confirming the need to run global Eulerian models at higher resolution or to include in-grid plume treatments.

Many datasets exist which can be further exploited to improve model capabilities in terms of long-range pollutant transport. In particular, this includes satellite data and vertical profile data from, for example, the MOZAIC program. The ability of models to reproduce the full spectrum of measured concentrations (e.g. Figure 2.1), measured long-term trends (e.g. Figures 2.7 and 2.8), and the relationships among measured species needs to be assessed. The continued development of a dedicated data portal to house or link to relevant datasets would be beneficial in this regard.

**FINDING: Current datasets (surface, lidar, ship, aircraft, sonde and satellite) provide information about monthly, seasonal and inter-annual variability of certain trace gases and aerosol species, which can be used to assess model performance.**

**FINDING: Multi-species analysis of field campaign data often provides new insights into chemical and aerosol processing leading to improvements in their representation in CTMs.**

**RECOMMENDATION: Increased use of vertical profile data is needed, especially data collected at high temporal resolution (daily) and satellite data for the evaluation of global model performance and for quantifying the impact of emissions from one region on downwind regions.**

**RECOMMENDATION: Combined use of campaign and routine monitoring data to assess and improve model treatment of pollutant import into the lower troposphere over downwind receptor regions is needed.**

## References

- Andreae, M. O., et al. (1988), Vertical distribution of dimethylsulfide, sulfur dioxide, aerosol ions, and radon over the Northeast Pacific Ocean, *Journal of Atmospheric Chemistry*, 6(1): 149-173.
- Arnold, S. R., et al. (2007), Statistical inference of OH concentrations and air mass dilution rates from successive observations of nonmethane hydrocarbons in single air masses, *Journal of Geophysical Research*, 112(D10S40).
- Barrie, L. A., et al. (2001), A comparison of large scale atmospheric sulphate aerosol models (COSAM): overview and highlights, *Tellus Series B - Chemical and Physical Meteorology*, 53(5): 615-645.
- Beer, R., et al. (2008), First satellite observations of lower tropospheric ammonia and methanol, *Geophysical Research Letters*, 35(L09801).
- Ben-Ami, Y., et al. (2009), Patterns of North African dust transport over the Atlantic: winter vs. summer, based on Calipso first year data, *Atmospheric Chemistry and Physics*, 9: 7867-7875.
- Bertschi, I. T., et al. (2004), PHOBEA/ITCT 2002 airborne observations of transpacific transport of ozone, CO, volatile organic compounds, and aerosols to the northeast Pacific: Impacts of Asian anthropogenic and Siberian boreal fire emissions, *Journal of Geophysical Research*, 109(D23S12).
- Bigler, M., et al. (2002), Sulphate record from a northeast Greenland ice core over the last 1200 years based on continuous flow analysis, *Annals of Glaciology*, 35: 250-256.
- Bodhaine, B. A., and E. G. Dutton (1993), A long-term decrease in Arctic haze at Barrow, Alaska, *Geophysical Research Letters*, 20(10): 947-950.
- Bollhofer, A., and K. Rosman, Jr. (2000), Isotopic source signatures for atmospheric lead: The Northern Hemisphere, *Geochimica et Cosmochimica Acta*, 64: 3251-3262.
- Bollhofer, A., and K. Rosman, Jr. (2001), Isotopic source signatures for atmospheric lead: The Southern Hemisphere, *Geochimica et Cosmochimica Acta*, 65: 1727-1740.
- Bollhofer, A., and K. Rosman, Jr. (2002), The temporal stability in lead isotopic signatures at selected sites in the Southern and Northern Hemispheres, *Geochimica et Cosmochimica Acta*, 66: 1375-1386.
- Bonasoni, P., et al. (2008), The ABC-Pyramid Atmospheric Observatory in Himalaya for aerosol, ozone and halocarbon measurements, *Science of the Total Environment*, 391: 252-261.
- Bory, A. J. M., et al. (2003), Two distinct seasonal Asian source regions for mineral dust deposited in Greenland (NorthGRIP), *Geophysical Research Letters*, 30(4): 1167-1170.
- Bosenberg, J., and R. Hoff (2008), Plan for the implementation of the GAW Aerosol Lidar Observation Network GALION, 52 pp, World Meteorological Organization, Hamburg, Germany. *WMO TD No. 1443*
- Brenninkmeijer, C. A. M., et al. (2007), Civil aircraft for the regular investigation of the atmosphere based on an instrumented container: The new CARIBIC system, *Atmospheric Chemistry and Physics*, 7: 5277-5339.
- Brock, C. A., et al. (2004), Particle characteristics following cloud-modified transport from Asia to North America, *Journal of Geophysical Research*, 109(D23S26).
- Bronnimann, S., et al. (2002), Trends in near surface ozone concentrations in Switzerland, *Atmospheric Environment*, 36: 2841-2853.
- Chan, C. Y., et al. (2003), Urban and background ozone trend in 1984-1999 at subtropical Hong Kong, South China, *Ozone: Science & Engineering*, 25(6): 513-522.

- Chin, M., et al. (1994), Relationship of ozone and carbon monoxide over North America, *Journal of Geophysical Research*, 99(D7): 14565-14574.
- Chou, C. C.-K., et al. (2006), The trend of surface ozone in Taipei, Taiwan, and its causes: Implications for ozone control strategies, *Atmospheric Environment*, 40(21): 3898-3908.
- Clarisse, L., et al. (2009), Global ammonia distribution derived from infrared satellite observations, *Nature Geoscience*, 2(7): 479-483.
- Cooper, O. R., et al. (2004), A case study of trans-Pacific warm conveyor belt transport: The influence of merging airstreams on trace gas import to North America, *Journal of Geophysical Research*, 109(D23S08).
- Cooper, O. R., et al. (2010), Increasing springtime ozone mixing ratios in the free troposphere over western North America, *Nature* 463: 344-348.
- Creilson, J. K., et al. (2003), Intercontinental transport of tropospheric ozone: a study of its seasonal variability across the North Atlantic utilizing tropospheric ozone residuals and its relationship to the North Atlantic Oscillation, *Atmospheric Chemistry and Physics*, 3: 2053-2066.
- Crutzen, P. J. (1988), Tropospheric ozone: an overview, in *Tropospheric Ozone Regional and Global Scale Interactions*, edited by I. S. A. Isaksen, 3-33 pp., D. Reidel, Dordrecht.
- Damoah, R., et al. (2004), Around the world in 17 days - hemispheric-scale transport of forest fire smoke from Russia in May 2003, *Atmospheric Chemistry and Physics*, 4: 1311-1321.
- Deeter, M. N., et al. (2009), CO retrievals based on MOPITT near-infrared observations, *Journal of Geophysical Research*, 114(D04303).
- Dentener, F., et al. (2005), The impact of air pollutant and methane emission controls on tropospheric ozone and radiative forcing: CTM calculations for the period 1990-2030, *Atmospheric Chemistry and Physics*, 7(5): 1731-1755.
- Derwent, R. G., et al. (1997), Observation and interpretation of the seasonal cycles in the surface concentrations of ozone and carbon monoxide at Mace Head, Ireland, from 1990 to 1994, *Atmospheric Environment*, 32(2): 145-157.
- Derwent, R. G., et al. (2007), Trends over a 20-year period from 1987 to 2007 in surface ozone at the atmospheric research station, Mace Head, Ireland, *Atmospheric Environment*, 41(39): 9091-9098.
- Ding, A., et al. (2009), Transport of north China air pollution by midlatitude cyclones: Case study of aircraft measurements in summer 2007, *Journal of Geophysical Research*, 114(D08304).
- Ding, A. J., et al. (2008), Tropospheric ozone climatology over Beijing: Analysis of aircraft data from the MOZAIC program, *Atmospheric Chemistry and Physics*, 8: 1-13.
- Dubovik, O., et al. (2002), Variability of absorption and optical properties of key aerosol types observed in worldwide locations, *Journal of Atmospheric Science*, 59: 590-608.
- Duce, R. A., et al. (1980), Long-range atmospheric transport of soil dust from Asia to the Tropical North Pacific: Temporal variability, *Science*, 209: 1522-1524.
- EARLINET (2003), EARLINET: A European Aerosol Research Lidar Network to establish an Aerosol Climatology, Final Report for the Period February 2000 to February 2003, Max Planck Institut für Meteorologie, Hamburg, Germany.
- Edwards, D. P. (2006), Air quality remote sensing from space, *Eos, Transactions of the American Geophysical Union*, 87(33).
- Elguindi, N., et al. (2010), Current status of the ability of the GEMS/MACC models to reproduce the tropospheric CO vertical distribution as measured by MOZAIC, *Atmospheric Chemistry and Physics Discussions*, 3: 391-449.
- EMEP (2004), EMEP Assessment, Part I: European Perspective, edited by G. Lovblad, et al., 180 pp., European Monitoring and Evaluation Programme, Oslo, Norway.



- EU (2006), Remote Sensing of Air Pollution, edited by A. Borowiak and F. Dentener, 64 pp., Institute for Environment and Sustainability 2006, European Commission, Ispra, Italy. EUR 22330 EN.
- Ewing, S. A., et al. (2010), Pb Isotopes as an Indicator of the Asian Contribution to Particulate Air Pollution in Urban California, *Environmental Science & Technology*, 44(23): 8911-8916.
- Fehsenfeld, F. C., et al. (2006), International Consortium for Atmospheric Research on Transport and Transformation (ICARTT): North America to Europe—Overview of the 2004 summer field study, *Journal of Geophysical Research*, 111(D23S01).
- Feister, W., and W. Warmbt (1987), Long-term measurements of surface ozone in the German Democratic Republic, *Journal of Atmospheric Chemistry*, 5: 1-21.
- Fiore, A. M., et al. (2009), Multimodel estimates of intercontinental source-receptor relationships for ozone pollution, *Journal of Geophysical Research*, 114(D04301).
- Fischer, E. V., et al. (2009), Meteorological Controls on Observed Peroxyacetyl Nitrate (PAN) at Mount Bachelor during the spring of 2008, *Journal of Geophysical Research*, 115(D03302).
- Fishman, J., et al. (2008), Remote sensing of tropospheric pollution from space, *Bulletin of the American Meteorological Society*, 89(6): 805-821.
- Forster, C., et al. (2001), Transport of boreal forest fire emissions from Canada to Europe, *Journal of Geophysical Research*, 106(D19): 22887-22906.
- Fuhrer, J., et al. (1997), Critical levels for ozone effects on vegetation in Europe *Environmental Pollution*, 97(1-2): 91-106.
- Gerbig, C., et al. (2003), Toward constraining regional-scale fluxes of CO<sub>2</sub> with atmospheric observations over a continent: 2. Analysis of COBRA data using a receptor-oriented framework, *Journal of Geophysical Research*, 108(D244757).
- Goto-Azuma, K., and R. Koerner (2001), Ice-core studies of anthropogenic sulfate and nitrate trends in the Arctic, *Journal of Geophysical Research*, 106(D5): 4959-4969.
- Grousset, F. E., et al. (2003), Case study of a Chinese dust plume reaching the French Alps, *Geophysical Research Letters*, 30(6).
- Guerova, G., et al. (2006), Impact of transatlantic transport episodes on summertime ozone in Europe, *Atmospheric Chemistry and Physics*, 6: 2057-2072.
- Hamelin, B., et al. (1989), Lead isotopes in trade wind aerosols at Barbados: The influence of European emissions over the North Atlantic, *Journal of Geophysical Research*, 94(C11): 16243-16250.
- Heald, C. L., et al. (2003), Asian outflow and trans-Pacific transport of carbon monoxide and ozone pollution: An integrated satellite, aircraft, and model perspective, *Journal of Geophysical Research*, 108(D244804).
- Heald, C. L., et al. (2006), Transpacific transport of Asian anthropogenic aerosols and its impact on surface air quality in the United States, *Journal of Geophysical Research*, 111(D14310).
- Hegg, D. A., et al. (2009), Source attribution of Black Carbon in Arctic snow, *Environmental Science & Technology*, 43: 4016-4021.
- Heidam, N. Z., et al. (2004), Arctic atmospheric contaminants in NE Greenland: levels, variations, origins, transport, transformations and trends 1990-2001, *Science of The Total Environment*, 331(1-3): 5-28.
- Helmig, D., et al. (2008), Nonmethane hydrocarbons at Pico Mountain, Azores: 1. Oxidation chemistry in the North Atlantic region, *Journal of Geophysical Research*, 113(D20S91).
- Henze, D. K., et al. (2009), Inverse modeling and mapping US air quality influences of inorganic PM<sub>2.5</sub> precursor emissions using the adjoint of GEOS-Chem, *Atmospheric Chemistry and Physics*, 9: 5877-5903.
- Hirdman, D., et al. (2010), Source identification of short-lived air pollutants in the Arctic using statistical analysis of measurement data and particle dispersion model output, *Atmospheric Chemistry and Physics*, 10: 669-693.

- Honrath, R. E., et al. (2004), Regional and hemispheric impacts of anthropogenic and biomass burning emissions on summertime CO and O<sub>3</sub> in the North Atlantic lower free troposphere, *Journal of Geophysical Research*, 109(D24310).
- Honrath, R. E., et al. (2008), Nonmethane hydrocarbons at Pico Mountain, Azores: 2. Event-specific analysis of the impacts of mixing and photochemistry on hydrocarbon ratios, *Journal of Geophysical Research*, 113(D20S92).
- Horowitz, L. W. (2006), Past, present, and future concentrations of tropospheric ozone aerosols: Methodology, ozone evaluation, and sensitivity to aerosol wet removal, *Journal of Geophysical Research*, 111(D22211).
- Hudman, R. C., et al. (2007), Surface and lightning sources of nitrogen oxides over the United States: Magnitudes, chemical evolution, and outflow, *Journal of Geophysical Research*, 112(D12S05).
- Hudman, R. C., et al. (2008), Biogenic versus anthropogenic sources of CO in the United States, *Geophysical Research Letters*, 35(L04801).
- Huntrieser, H., et al. (2005), Intercontinental air pollution transport from North America to Europe: Experimental evidence from airborne measurements and surface observations, *Journal of Geophysical Research*, 110(D01305).
- Igarashi, Y., et al. (2006), Seasonal variations in SO<sub>2</sub> plume transport over Japan: Observations at the summit of Mt. Fuji from winter to summer, *Atmospheric Environment*, 40(36): 7018-7033.
- Jaffe, D., et al. (2003), The 2001 Asian Dust Events: Transport and Impact on Surface Aerosol Concentrations in the U.S., *Eos, Transactions American Geophysical Union*, 84(46): 501-507.
- Jaffe, D., et al. (2005a), Seasonal cycle and composition of background fine particles along the west coast of the US *Atmospheric Environment*, 39(2): 297-306.
- Jaffe, D., and J. Ray (2007), Increase in surface ozone at rural sites in the western US, *Atmospheric Environment*, 41(26): 5452-5463.
- Jaffe, D. A., et al. (2004), Long-range transport of Siberian biomass burning emissions and impact on surface ozone in western North America, *Geophysical Research Letters*, 31(L16106).
- Jaffe, D. A., et al. (2005b), Export of atmospheric mercury from Asia, *Atmospheric Environment*, 39(17): 3029-3038.
- Kalashnikova, O. V., and R. A. Kahn (2008), Mineral dust plume evolution over the Atlantic from MISR and MODIS aerosol retrievals, *Journal of Geophysical Research*, 113(D24204).
- Karnieli, A., et al. (2009), Temporal trend in anthropogenic sulfur aerosol transport from central and eastern Europe to Israel, *Journal of Geophysical Research*, 114(D00D19).
- Kaspari, S., et al. (2009), A high-resolution record of atmospheric dust composition and variability since A.D. 1650 from a Mount Everest ice core, *Journal of Climate*, 22(14).
- Kaufman, Y. J., et al. (2005), Dust transport and deposition observed from the Terra-Moderate Resolution Imaging Spectroradiometer (MODIS) spacecraft over the Atlantic Ocean, *Journal of Geophysical Research*, 110(D10S12).
- Keating, T., et al. (2005), Air quality impacts of intercontinental transport, *EM / Air and Waste Management Association*(October): 28-30.
- Kekonen, T., et al. (2002), An 800 year record of nitrate from the Lomonosovfonna ice core, Svalbard, *Annals of Glaciology*, 35: 261-265.
- Koch, D., et al. (2009), Evaluation of black carbon estimations in global aerosol models, *Atmospheric Chemistry and Physics*, 9: 9001-9026.
- Komarek, M., et al. (2008), Lead isotopes in environmental sciences: A review, *Environment International*, 34: 562-577.
- Lamarque, J.-F., et al. (2005), Tropospheric ozone evolution between 1890 and 1990, *Journal of Geophysical Research*, 110(D08304).

- Lamarque, J. F., et al. (2010), Historical (1850-2000) gridded anthropogenic and biomass burning emissions of reactive gases and aerosols: Methodology and application, *Atmospheric Chemistry and Physics*, 10: 7017-7039.
- Lee, C., et al. (2009), Retrieval of vertical columns of sulfur dioxide from SCIAMACHY and OMI: Air mass factor algorithm development and validation, *Journal of Geophysical Research*, 114(D22303).
- Legras, B., et al. (2003), Vertical diffusivity in the lower stratosphere from Lagrangian back-trajectory reconstructions of ozone profiles, *Journal of Geophysical Research*, 108(D18): 4562-4570.
- Leung, F.-Y., et al. (2001), Sulfur isotopic fractionation in the gas-phase oxidation of sulfur dioxide initiated by hydroxyl radicals, *Journal of Physical Chemistry*, 105: 8073-8076.
- Lewis, A. C., et al. (2007), Chemical composition observed over the mid-Atlantic and the detection of pollution signatures far from source regions, *Journal of Geophysical Research*, 112(D10S39).
- Li, Q., et al. (2004), Export of NO<sub>y</sub> from the North American boundary layer: Reconciling aircraft observations and global model budgets, *Journal of Geophysical Research*, 109(D02313).
- Li, S.-M., and L. A. Barrie (1993), Biogenic Sulfur Aerosol in the Arctic Troposphere: 1. Contributions to Total Sulfate, *Journal of Geophysical Research*, 98(D11): 20613-20622.
- Li, Z., et al. (2009), Uncertainties in satellite remote sensing of aerosols and impact on monitoring its long-term trend: A review and perspective, *Annales Geophysicae*, 27: 2755-2770.
- Liang, Q., et al. (2007), Summertime influence of Asian pollution in the free troposphere over North America, *Journal of Geophysical Research*, 112(D12S11).
- Likens, G. E., and F. H. Bormann (1974), Acid rain: a serious regional environmental problem, *Science*, 184(4142): 1176-1179.
- Lin, J. C., et al. (2003), A near-field tool for simulating the upstream influence of atmospheric observations: The Stochastic Time-Inverted Lagrangian Transport (STILT) model, *Journal of Geophysical Research*, 108(D16).
- Liu, J. J., et al. (2009), Analysis of the summertime buildup of tropospheric ozone abundances over the Middle East and North Africa as observed by the Tropospheric Emission Spectrometer instrument, *Journal of Geophysical Research*, 114(D05304).
- Liu, X.-H., et al. (2010), Ozone profile retrievals from the Ozone Monitoring Instrument, *Atmospheric Chemistry and Physics*, 10: 2521-2537.
- Liu, Z., et al. (2008), CALIPSO lidar observations of the optical properties of Saharan dust: A case study of long-range transport, *Journal of Geophysical Research*, 113(D7): D07207.
- Logan, J. A., et al. (1999), Trends in the vertical distribution of ozone: A comparison of two analyses of Ozone Sonde data, *Journal of Geophysical Research*, 104(D21): 26373-26399.
- Lu, Z., et al. (2010), Sulfur dioxide emissions in China and sulfur trends in East Asia since 2000, *Atmospheric Chemistry and Physics Discussions*, 10: 8657-8715.
- Martin, R. V., et al. (2006), Evaluation of space-based constraints on global nitrogen oxide emissions with regional aircraft measurements over and downwind of eastern North America, *Journal of Geophysical Research*, 111(D15308).
- Martin, R. V. (2008), Satellite remote sensing of surface air quality, *Atmospheric Environment*, 42(34): 7823-7843.
- Matthias, V., et al. (2004), The vertical aerosol distribution over Europe: Statistical analysis of Raman lidar data from 10 EARLINET stations, *Journal of Geophysical Research*, 109(D18201).
- Mauzerall, D. L., et al. (1998), Photochemistry in biomass burning plumes and implications for tropospheric ozone over the tropical South Atlantic, *Journal of Geophysical Research*, 103(D7): 8401-8423.
- McConnell, J., et al. (2007), 20th-century industrial black carbon emissions altered Arctic climate forcing, *Science*, 317: 1381-1384.

- McConnell, J. R., et al. (2002), A 250-year high-resolution record of Pb flux and crustal enrichment in central Greenland, *Geophysical Research Letters*, 29(23): 2130-2133.
- Mercier, G. (2000), Lead isotope composition and elemental abundances in atmospheric aerosols collected at Alert station (Canadian Arctic) in 1994-1995: Sources and trajectories, 55 pp, Universite du Quebec a Montreal.
- Methven, J., and B. Hoskins (1999), The Advection of High-Resolution Tracers by Low-Resolution Winds, *Journal of the Atmospheric Sciences*, 56(18): 3262-3285.
- Methven, J., et al. (2006), Establishing Lagrangian connections between observations within air masses crossing the Atlantic during the International Consortium for Atmospheric Research on Transport and Transformation, *Journal of Geophysical Research*, 111(D23S62).
- Mickley, L. J., et al. (2001), Uncertainty in preindustrial abundance of tropospheric ozone: Implications for radiative forcing calculations, *Journal of Geophysical Research*, 106(D4): 3389-3399.
- Mishchenko, M. I., et al. (2007), Long-Term Satellite Record Reveals Likely Recent Aerosol Trend, *Science*, 315(5818): 1543-.
- Moore, J., et al. (2006), Sulfate source inventories from a Svalbard ice core record spanning the Industrial Revolution, *Journal of Geophysical Research*, 111(D15307).
- Mukai, H., et al. (2001), Regional characteristics of sulfur and lead isotope ratios in the atmosphere at several Chinese urban sites, *Environmental Science & Technology*, 35: 1064-1071.
- Norman, A. L., et al. (1999), Sources of aerosol sulphate at Alert: Apportionment using stable isotopes, *Journal of Geophysical Research*, 104: 11619-11631.
- Novak, M., et al. (2001), Temporal trends in the isotope signature of air-borne sulfur in Central Europe, *Environmental Science & Technology*, 35: 255-260.
- Nowak, J., et al. (2004), Gas-phase chemical characteristics of Asian emission plumes observed during ITCT 2K2 over the eastern North Pacific Ocean, *Journal of Geophysical Research*, 109(D23S19).
- NRC (2010), Global sources of local pollution: an Assessment of long-range transport of key air pollutants to and from the United States, 234 pp, National Research Council, The National Academies, Washington, DC.
- Nriagu, J. O., et al. (1991), Origin of sulfur in Canadian arctic haze from isotope measurements, *Nature*, 349: 142-145.
- Oltmans, S. J., et al. (2006), Long-term changes in tropospheric ozone, *Atmospheric Environment*, 40(17): 3156-3173.
- Oltmans, S. J., et al. (2008), Background ozone levels of air entering the west coast of the US and assessment of longer-term changes, *Atmospheric Environment*, 42(24): 6020-6038.
- Ordóñez, C. (2006), Trend analysis of ozone and evaluation of nitrogen dioxide satellite data in the troposphere over Europe, Swiss Federal Institute of Technology, Zurich.
- Osterberg, E., et al. (2008), Ice core record of rising lead pollution in the North Pacific atmosphere, *Geophysical Research Letters*, 35(L05810).
- Osthoff, H. D., et al. (2008), High levels of nitryl chloride in the polluted subtropical marine boundary layer, *Nature Geoscience*, 1(5): 324-328.
- Owen, R. C., et al. (2006), An analysis of the mechanisms of North American pollutant transport to the Central North Atlantic lower free troposphere, *Journal of Geophysical Research*, 111: D23S58.
- Park, R. J., et al. (2004), Natural and transboundary pollution influences on sulfate-nitrate ammonium aerosols in the United States: Implications for policy, *Journal of Geophysical Research*, 109(D15204).
- Parrish, D., et al. (2009), Increasing ozone in marine boundary layer inflow at the west coasts of North America and Europe, *Atmospheric Chemistry and Physics*, 9: 1303-1323.

- Parrish, D. D., et al. (1992), Indication of photochemical histories of Pacific air masses from measurements of atmospheric trace species at Point Arena, California, *Geophysical Research Letters*, 19(14): 15883-15901.
- Parrish, D. D., et al. (1993), Export of North America ozone pollution to the North Atlantic Ocean, *Science*, 259(5100): 1436-1439.
- Parrish, D. D., et al. (2007), Effects of mixing on evolution of hydrocarbon ratios in the troposphere, *Journal of Geophysical Research*, 112(D10S34).
- Parrish, D. D., et al. (2010), Impact of transported background ozone inflow on summertime air quality in a California ozone exceedance area, *Atmospheric Chemistry and Physics*, 10: 10093-10109.
- Patris, N., et al. (2000), Isotopic composition of sulfur in size-resolved marine aerosols above the Atlantic Ocean, *Journal of Geophysical Research*, 105: 14449-14457.
- Patris, N., et al. (2002), First sulfur isotope measurements in central Greenland ice cores along the preindustrial and industrial periods, *Journal of Geophysical Research*, 107(D11): 4115-4125.
- Pfister, G. G., et al. (2006), Ozone production from the 2004 North American boreal fires, *Journal of Geophysical Research*, 111(D24S07).
- Pisso, I., et al. (2009), Estimation of mixing in the troposphere from Lagrangian trace gas reconstructions during long-range pollution plume transport, *Journal of Geophysical Research*, 114(D1): 9301-9311.
- Pochanart, P., et al. (2003), Regional background ozone and carbon monoxide variations in remote Siberia/East Asia, *Journal of Geophysical Research*, 108(D1): 4028-4045.
- Prather, M., et al. (2001), Atmospheric chemistry and greenhouse gases, in *Climate change 2001: The scientific basis: Contribution of Working Group I to the Third Assessment Report of the Intergovernmental Panel on Climate Change*, edited by J. T. Houghton, et al., 49 pp., Cambridge University Press, New York.
- Preunkert, S., et al. (2001), Sulfate trends in a Col du Dome (French Alps) ice core: A record of anthropogenic sulfate levels in the European midtroposphere over the twentieth century, *Journal of Geophysical Research*, 106: 31991-32004.
- Preunkert, S., et al. (2003), A seasonally resolved alpine ice core record of nitrate: Comparison with anthropogenic inventories and estimation of preindustrial emissions of NO in Europe, *Journal of Geophysical Research*, 108(D21): 4681-4690.
- Price, H. U., et al. (2004), Photochemistry, ozone production, and dilution during long-range transport episodes from Eurasia to the northwest United States, *Journal of Geophysical Research*, 109(D23S13).
- Prospero, J. M. (1979), Mineral and sea-salt aerosol concentrations in various ocean regions, *Journal of Geophysical Research*, 84(C2): 725-731.
- Prospero, J. M. (2001), The Atmosphere-Ocean Chemistry Experiment (AEROCE): Background and major accomplishments, *IGACTivities Newsletter*, 24.
- Prospero, J. M., et al. (2003), Long-term record of NSS-sulfate and nitrate in aerosols on Midway Island, 1981-2000: Evidence of increased (now decreasing?) anthropogenic emissions from Asia, *Journal of Geophysical Research*, 108(D14019).
- Putaud, J.-P., and F. Raes (2004), A European aerosol phenomenology - 2: Chemical characteristics of particulate matter at kerbside, urban, rural and background sites in Europe, *Atmospheric Environment*, 38: 2579-2595.
- Quinn, P. K., et al. (2002), A 3-year record of simultaneously measured aerosol chemical and optical properties at Barrow, Alaska, *Journal of Geophysical Research*, 107(D11): 4130-4145.
- Quinn, P. K., et al. (2007), Arctic haze: Current trends and knowledge gaps, *Tellus*, 59B: 99-114.
- Quinn, P. K., et al. (2009), Decadal trends in aerosol chemical composition at Barrow, Alaska: 1976-2008, *Atmospheric Chemistry and Physics*, 9(22): 8883-8888.

- Raes, F., et al. (2000), The 2nd Aerosol Characterization Experiment (ACE-2): General overview and main results, *Tellus Series B-Chemical and Physical Meteorology*, 52(2): 111-125.
- Rahn, K. A., and R. J. McCaffrey (1980), On the origin and transport of the winter Arctic Aerosol, *Annals of the New York Academy of Sciences*, 338(1): 486-503.
- Rastigejev, Y., et al. (2010), Resolving intercontinental pollution plumes in global models of atmospheric transport, *Journal of Geophysical Research*, 115(D02302).
- Ravetta, F., et al. (2007), Long-range transport and tropospheric ozone variability in the western Mediterranean region during the Intercontinental Transport of Ozone and Precursors (ITOP-2004) campaign, *Journal of Geophysical Research*, 112(D10S46).
- Real, E., et al. (2007), Processes influencing ozone levels in Alaskan forest fire plumes during long-range transport over the North Atlantic, *Journal of Geophysical Research*, 112: D10S41.
- Real, E., et al. (2008), Lagrangian analysis of low altitude anthropogenic plume processing across the North Atlantic, *Atmospheric Chemistry and Physics*, 8: 7737-7754.
- Real, E., et al. (2010), Toward a novel high-resolution modeling approach for the study of chemical evolution of pollutant plumes during long-range transport, *Journal of Geophysical Research* 115(D12): D12302.
- Reidmiller, D. R., et al. (2009), Interannual variability of long-range transport as seen at the Mt. Bachelor observatory, *Atmospheric Chemistry and Physics*, 9(2): 557-572.
- Sauvage, B., et al. (2007), Quantification of the factors controlling tropical tropospheric ozone and the South Atlantic maximum, *Journal of Geophysical Research*, 112(D09309).
- Savoie, D. L., et al. (2002), Marine biogenic and anthropogenic contributions to non-sea-salt sulfate in the marine boundary layer over the North Atlantic Ocean, *Journal of Geophysical Research*, 107(D18): 4356-4376.
- Schnadt Poberaj, C., et al. (2009), Long-term changes in UT/LS ozone between the late 1970s and the 1990s deduced from the GASP and MOZAIC aircraft programs and from ozonesondes, *Atmospheric Chemistry and Physics*, 9: 5343-5369.
- Schoeberl, M. R., et al. (2007), A trajectory-based estimate of the tropospheric ozone column using the residual method, *Journal of Geophysical Research*, 112(D24S49).
- Schwarz, J. P., et al. (2006), Single-particle measurements of midaltitude black carbon and lightscattering aerosols from the boundary layer to the lower stratosphere, *Journal of Geophysical Research*, 111(D16207).
- Schwarz, J. P., et al. (2008), Coatings and their enhancement of black carbon light absorption in the tropical atmosphere, *Journal of Geophysical Research*, 113(D03203).
- Sharma, S., et al. (2006), Variations and sources of the equivalent black carbon in the high Arctic revealed by long-term observations at Alert and Barrow: 1989-2003, *Journal of Geophysical Research*, 111(D14208).
- Shaw, G. E. (1975), The vertical distribution of atmospheric aerosols at Barrow, Alaska, *Tellus*, 27: 39-49.
- Shaw, G. E. (1995), The Arctic haze phenomenon, *Bulletin of the American Meteorological Society*, 76: 2403-2413.
- Sherrell, R. M., et al. (2000), Temporal variability of Cd, Pb, and Pb isotope deposition in central Greenland snow, *Geochemistry Geophysics Geosystems*, 1(5): 1002-1023.
- Shotyk, W., et al. (2005), Predominance of industrial Pb in recent snow (1994-2004) and ice (1842-1996) from Devon Island, Arctic Canada, *Geophysical Research Letters*, 32(L21814).
- Simmonds, P. G., et al. (2004), Significant growth in surface ozone at Mace Head, Ireland, 1987-2003, *Atmospheric Environment*, 38(28): 4769-4778.
- Simonetti, A., et al. (2004), Pb isotopic investigation of aircraft-sampled emissions from the Horne smelter (Rouyn, Quebec): Implications for atmospheric pollution in northeastern North America, *Geochimica et Cosmochimica Acta*, 68(16): 3285-3294.

- Singh, H. B., et al. (2006), Overview of the summer 2004 Intercontinental Chemical Transport Experiment - North America (INTEX-A), *Journal of Geophysical Research*, 111(D24S01).
- Singh, H. B., et al. (2009), Chemistry and transport of pollution over the Gulf of Mexico and the Pacific: Spring 2006 INTEX-B campaign overview and first results, *Atmospheric Chemistry and Physics*, 9: 2301-2318.
- Sirois, A., and L. A. Barrie (1999), Arctic lower tropospheric aerosol trends and composition at Alert, Canada: 1980-1995, *Journal of Geophysical Research*, 104(D9): 11599-11618.
- Smit, H. G. J., et al. (2007), Assessment of the performance of ECC-ozonesondes under quasi-flight conditions in the environmental simulation chamber: Insights from the Juelich Ozone Sonde Intercomparison Experiment (JOSIE), *Journal of Geophysical Research*, 112(D19306).
- Staehelin, J., et al. (1994), Surface ozone trends at Arosa (Switzerland), *Atmospheric Environment*, 28: 75-87.
- Stevenson, D. S., et al. (2006), Multimodel ensemble simulations of present-day and near-future tropospheric ozone, *Journal of Geophysical Research*, 111(D08301).
- Stohl, A., and T. Trickl (1999), A textbook example of long-range transport: Simultaneous observations of ozone maxima of stratospheric and North America origin in the free troposphere over Europe, *Journal of Geophysical Research*, 104(D23): 30445-30462.
- Stohl, A., et al. (2002), On the pathways and timescales of intercontinental air pollution transport, *Journal of Geophysical Research*, 107(D23): 4684-4700.
- Stohl, A., et al. (2003), A backward modeling study of intercontinental pollution transport using aircraft measurements, *Journal of Geophysical Research*, 108(D12): 4370-4387.
- Stohl, A., et al. (2005), Technical note: The Lagrangian particle dispersion model FLEXPART version 6.2, *Atmospheric Chemistry and Physics*, 5: 2461-2474.
- Stohl, A., et al. (2007a), Arctic smoke – record high air pollution levels in the European Arctic due to agricultural fires in Eastern Europe in spring 2006, *Atmospheric Chemistry and Physics*, 7: 511-534.
- Stohl, A., et al. (2007b), Aircraft measurements over Europe of an air pollution plume from Southeast Asia – aerosol and chemical characterization, *Atmospheric Chemistry and Physics*, 7(3): 913-937.
- Streets, D. G., et al. (2000), Sulfur dioxide emissions in Asia in the period 1985 -1997, *Atmospheric Environment*, 34(26): 4413-4424.
- Sturges, W. T., et al. (1993), Stable lead isotope ratios in Alaskan arctic aerosols, *Atmospheric Environment*, 27(17-18): 2865-2871.
- Takami, A., et al. (2006), Transport of anthropogenic and dust aerosol observed at Cape Hedo, Okinara, *Journal of Aerosol Research*, 21(4): 341-347.
- Tanimoto, H. (2009), Increase in springtime tropospheric ozone at a mountainous site in Japan for the period 1998-2006, *Atmospheric Environment*, 43: 1358-1363.
- Tanimoto, H., et al. (2009), Asian anthropogenic emissions and decadal trends in springtime tropospheric ozone over Japan: 1998-2007, *Geophysical Research Letters*, 36(L23802).
- Thomas, G. E., et al. (2010), Validation of the GRAPE single view aerosol retrieval for ATSR-2 and insights into the long term global AOD trend over the ocean, *Atmospheric Chemistry and Physics*, 10(10): 4849-4866.
- Thouret, V., et al. (2006), Tropopause referenced ozone climatology and inter-annual variability (1994-2003) from the MOZAIC programme, *Atmospheric Chemistry and Physics*, 6(4): 1033-1051.
- Torres, O., et al. (2002), A long-term record of aerosol optical depth from TOMS observations and comparison to AERONET measurements, *Journal of Atmospheric Science*, 59(3): 398-413.
- Torres, O., et al. (2007), Aerosols and surface UV products from Ozone Monitoring Instrument observations: An overview, *Journal of Geophysical Research*, 112(D24S47).

- Trickl, T., et al. (2003), Intercontinental transport and its influence on the ozone concentrations over central Europe: Three case studies, *Journal of Geophysical Research*, 108(D12): 8530-8552.
- Turnbull, J. C., et al. (2009), Spatial distribution of  $^{14}\text{CO}_2$  across Eurasia: Measurements from the TROICA-8 expedition, *Atmospheric Chemistry and Physics*, 9: 175-187.
- Val Martin, M., et al. (2006), Significant enhancements of nitrogen oxides, black carbon, and ozone in the North Atlantic lower free troposphere resulting from North American boreal wildfires, *Journal of Geophysical Research*, 111(D23S60).
- Val Martin, M., et al. (2008), Large-scale impacts of anthropogenic pollution and boreal wildfires on the nitrogen oxides over the central North Atlantic region, *Journal of Geophysical Research*, 113(D17308).
- Van Dingenen, R., and F. Raes (2004), A European aerosol phenomenology - 1: Physical characteristics of particulate matter at kerbside, urban, rural and background sites in Europe, *Atmospheric Environment*, 38: 2561-2577.
- van Donkelaar, A., et al. (2008), Analysis of aircraft and satellite measurements from the Intercontinental Chemical Transport Experiment (INTEX-B) to quantify long-range transport of East Asian sulfur to Canada, *Atmospheric Chemistry and Physics*, 8: 2999-3014.
- VanderWal, R., et al. (2010), Fingerprinting soot (towards source identification): Physical structure and chemical composition, *Aerosol Science*, 41: 108-117.
- Vestreng, V. (2003), Review and revision. Emission data reported to CLRTAP, 134 pp, Norwegian Meteorological Institute, Oslo. *MSC-W Technical Report 1/03*.  
[http://emep.int/publ/reports/2003/mscw\\_note\\_1\\_2003.pdf](http://emep.int/publ/reports/2003/mscw_note_1_2003.pdf)
- Veysseyre, A. M., et al. (2001), Tracing the origin of pollution in French Alpine snow and aerosols using lead isotopic ratios, *Environmental Science & Technology*, 35(22): 4463-4469.
- Viana, M. T., et al. (2008), Source apportionment of particulate matter in Europe: A review of methods and results, *Journal of Aerosol Science*, 39: 827-849.
- Volz, A., and D. Kley (1988), Evaluation of the Montsouris series of ozone measurements made in the 19th century, *Nature*, 332(6161): 240-242.
- Vukicevic, T., and P. Hess (2000), Analysis of tropospheric transport in the Pacific Basin using the adjoint technique, *Journal of Geophysical Research*, 105(D6): 7213-7230.
- Wadleigh, M. A., et al. (2001), Areal distribution of sulphur and oxygen isotopes in sulphate of rain over eastern North America, *Journal of Geophysical Research*, 106(D18): 20883-20895.
- Wadleigh, M. A. (2004), Sulphur isotopic composition of aerosols over the western North Atlantic Ocean, *Canadian Journal of Fisheries and Aquatic Sciences*, 61(5): 817-825.
- Wandinger, U., et al. (2004), Air mass modification over Europe: EARLINET aerosol observations from Wales to Belarus, *Journal of Geophysical Research*, 109(D24205).
- Wang, T., et al. (2009), Increasing surface ozone concentrations in the background atmosphere of Southern China, 1994-2007, *Atmospheric Chemistry and Physics*, 9: 6217-6227.
- Warneke, C., et al. (2007), Determination of urban volatile organic compound emission ratios and comparison with an emissions database, *Journal of Geophysical Research*, 112(D10S47).
- Weiss-Penzias, P., et al. (2007), Quantifying Asian and biomass burning sources of mercury using the Hg/CO ratio in pollution plumes observed at the Mount Bachelor observatory, *Atmospheric Environment*, 41(21): 4366-4379.
- Wespes, C., et al. (2009), Global distributions of nitric acid from IASI/MetOP measurements, *Atmospheric Chemistry and Physics*, 9: 7949-7962.
- WHO (2006), Air quality guidelines: Global update 2005: Particulate matter, ozone, nitrogen dioxide, and sulfur dioxide, 22 pp, World Health Organization, Geneva. *WHO/SDE/PHE/OEH/06.02*.  
[http://whqlibdoc.who.int/hq/2006/WHO\\_SDE\\_PHE\\_OEH\\_06.02\\_eng.pdf](http://whqlibdoc.who.int/hq/2006/WHO_SDE_PHE_OEH_06.02_eng.pdf)
- Wilkening, K. E., et al. (2000), Trans-Pacific air pollution, *Science*, 290: 65-67.



- Wittrock, F., et al. (2006), Simultaneous global observations of glyoxal and formaldehyde from space, *Geophysical Research Letters*, 33(L16804).
- Worden, H. M., et al. (2007), Comparison of Tropospheric Emission Spectrometer (TES) ozone profiles to ozonesondes: Methods and initial results, *Journal of Geophysical Research*, 112(D03309).
- Worden, J. R., et al. (2007), Improved tropospheric ozone profile retrievals using OMI and TES radiances, *Geophysical Research Letters*, 34(L01809).
- Yalcin, K., and C. Wake (2001), Anthropogenic signals recorded in an ice core from Eclipse Icefield, Yukon Territory, Canada, *Geophysical Research Letters*, 28: 4487-4490.
- Yang, J., et al. (2009), Isotopic evidences for provenance of East Asian dust, *Atmospheric Environment*, 43: 4481-4490.
- Yang, M., et al. (2006), Microparticle content records of the Dundee ice core and dust storms in northwestern China, *Journal of Asian Earth Sciences*, 27: 223-229.
- Yasunari, T. J., et al. (2007), Intra-annual variations in atmospheric dust and tritium in the North Pacific region detected from an ice core from Mount Wrangell, Alaska, *Journal of Geophysical Research*, 112(D10208).
- Yasunari, T. J., and K. Yamazaki (2009), Impacts of Asian dust storm associated with the stratosphere-to-troposphere transport in the spring of 2001 and 2002 on dust and tritium variations in Mount Wrangell ice core, Alaska, *Atmospheric Environment*, 43: 2582-2590.
- Yu, H., et al. (2008), A satellite-based assessment of transpacific transport of pollution aerosol, *Journal of Geophysical Research*, 113(D14S12).
- Zbinden, R. B., et al. (2006), Mid-latitude tropospheric ozone columns from the MOZAIC program: Climatology and interannual variability, *Atmospheric Chemistry and Physics*, 6: 863-881.
- Zdanowicz, C., et al. (2006), Asian dustfall in the St. Elias Mountains, Yukon, Canada, *Geochimica et Cosmochimica Acta*, 70: 3493-3507.
- Zhang, L., et al. (2008), Transpacific transport of ozone pollution and the effect of recent Asian emission increases on air quality in North America: An integrated analysis using satellite, aircraft, ozonesonde, and surface observations, *Atmospheric Chemistry and Physics*, 8(20): 6117-6136.
- Zhang, L., et al. (2009), Intercontinental source attribution of ozone pollution at western U.S. sites using an adjoint method, *Geophysical Research Letters*, 36(L11810).
- Zheng, S., et al. (2009), Mineralogical characteristics of soil dust from source regions in northern China, *Particuology*, 7: 507-512.
- Ziemke, J. R., et al. (2006), Tropospheric ozone determined from Aura OMI and MLS: Evaluation of measurements and comparison with the global modeling initiative's chemical transport model, *Journal of Geophysical Research*, 111(D19303).



## Chapter 3

### Emission Inventories and Projections

**Lead Authors:** David Streets and John van Aardenne

**Contributing Authors:** Bill Battye, Savitri Garivait, Doug Grano, Alex Guenther, Zbigniew Klimont, Jean-Francois Lamarque, Zifeng Lu, Greet Maenhout, Toshimasa Ohara, David Parrish, Steven Smith, and Harry Vallack

#### 3. 1. Introduction

Gridded global, regional, and national emission estimates exist for many of the pollutants that are important for assessing the hemispheric transport of air pollution (SO<sub>2</sub>, NO<sub>x</sub>, NMVOC, NH<sub>3</sub>, CH<sub>4</sub>, OC, BC, PM, and CO). Some of these are publicly available, whereas others are used by individual research groups or government agencies to study specific aspects of emissions or atmospheric processes. Most inventories are developed by combining emission factors, in units of mass of emissions per unit of activity, with activity levels or proxies thereof. The quality of emission inventories varies widely, however, and is difficult to assess objectively. For developed countries, the inventories for some pollutants from some sectors are viewed to be of high quality, as they have been crosschecked by field studies and laboratory tests and through air quality modelling. Examples of high-quality inventories would be the SO<sub>2</sub> emissions from power generation in North America and Europe. For other pollutants and sectors, the quality of inventories may be considerably lower. For developing and newly industrializing countries, the quality of emission inventories is generally poor, due to a lack of actual emissions measurements and intensive ambient observations, incompleteness of the activity data, and absence of test-based emission factors. A shorter history of inventory development in these regions also means a lack of expertise and institutional capacity to perform such tasks. Many developing and newly industrializing countries lie within the Northern Hemisphere, and they provide challenges to the compilation of a complete and reliable inventory of all species.

Major uncertainties in emission inventories are associated with inadequate knowledge of open biomass burning (forest and grassland fires, agriculture waste burning), biofuel use (for heating and cooking), artisanal industry, residential combustion of coal, and agricultural production systems. These inadequacies propagate into higher uncertainties in emissions for the pollutants that are mainly associated with these activities, such as CO, PM, OC, BC, CH<sub>4</sub>, NH<sub>3</sub>, and individual NMVOC species. The factors that lead to unreliable emission estimates are discussed in section 3.2.5. In many remote regions of the world it is difficult to develop complete statistical data for all types of human activity; as a result, some sources may be missing or undercounted, and there is therefore a tendency to underestimate emissions. Also, there are some source types that are relevant for the intercontinental transport of air pollution but less relevant for local air quality management, including marine (though ship emissions are becoming of major importance in some European and North American cities) and aviation emissions, natural emissions (including various methane sources, soil and lightning NO<sub>x</sub>, volcanoes, and windblown mineral dust), agricultural emissions, and biomass burning in remote areas. These source types may need greater attention from the Task Force on Hemispheric Transport of Air Pollutants (TF HTAP) than they have received thus far from national governments. In recent years, some new tools have become available to address the uncertainties in emission inventories, including direct (forward) and inverse modelling of air quality observations (from ground-based monitors, aircraft, or satellites) and laboratory tests of combustion and similar processes. These new techniques may not only improve the accuracy of emission inventories, but they also offer the possibility of providing the basis for more rapid updates of emissions than can presently be obtained using statistics-based methods. Bringing together the scientific communities in these areas is a valuable function of the TF HTAP.

The emissions chapter of the *HTAP Interim Assessment Report* [Klimont and Streets, 2007] presented an overview of gridded global emission datasets that are relevant for studies of hemispheric transport of air pollutants, available methodologies for construction of emission inventories and scenarios, and sources of uncertainty in emission datasets. The main recommendations of the interim

assessment report with respect to the TF HTAP's efforts to assess and improve emission inventories were to: (i) incorporate emission inventories with local knowledge into global emission inventories; (ii) identify those emission estimates and uncertainties that are most important for understanding the intercontinental transport of air pollution, as part of an iterative process among the model, measurement, and inventory communities; (iii) account for other efforts to develop future emission projections and to identify the magnitudes and distributions (e.g., spatial/temporal) of expected future emissions; and (iv) improve emission inventories and development of projections for Asia.

This chapter seeks to address each of these recommendations. Section 3.2 describes the development of new global and regional emission inventories and projections that are now available for studying long-range transport of air pollution. The results of these efforts are presented in sections 3.3 and 3.4, which describe the magnitudes and trends of natural and anthropogenic emission sources that drive intercontinental transport. Section 3.5 presents a detailed discussion of several emission inventories for Asia, which has the largest and fastest growing anthropogenic emissions. Section 3.6 presents existing studies and ongoing research efforts designed to provide top-down constraints on emission estimates by a process of iteration among emission inventories, observations, and modelling.

## **3.2. Development of new emission datasets to study hemispheric transport of air pollution**

Atmospheric models use emission inventories of different origins and quality, depending on the purpose of the modelling activity and available resources. Many emission inventories exist that cover past, present and future anthropogenic emissions of various air pollutants [see, for example, Table 1 in *Monks et al.*, 2009]. Two important global emission inventories that are not discussed in this chapter are POET (<http://www.aero.jussieu.fr/projet/ACCENT/POET.php>) and RETRO ([http://retro.enes.org/data\\_emissions.shtml](http://retro.enes.org/data_emissions.shtml)). Some inventories provide global coverage with relatively coarse spatial resolution, while others deal with particular regions and specific compounds at finer spatial resolution. Some inventories do not focus on total releases to the atmosphere—omitting some source categories or technology types, such as aircraft or shipping—and the discrepancies can differ by pollutant. Most inventory activities have been established in developed countries, while reliable information is still lacking for the developing world, particularly for very fast changing economies, e.g., China and India [*Monks et al.*, 2009]. In rapidly growing megacities, it is possible to assemble emission inventories using local statistics, knowledge of large emitting sources, and local air quality monitoring networks, as demonstrated for Delhi by Mohan et al. [2007], but at regional scale these methods become impractical. Inventories are constantly being refined, building upon the existing data with new information. For example, more recently developed regional datasets are being integrated into global datasets and satellite observations are now being used to help estimate emissions.

This section describes several new global datasets that have been developed based on existing and recently improved datasets and are now available for studying hemispheric and global scale transport: EDGAR-HTAP, the RCP historical inventory, and the RCP future scenarios. Emphasis in this section is on the EDGAR-HTAP inventory, which was specifically developed to meet the needs of the HTAP hemispheric transport assessment. This section also describes efforts to improve emission estimates in regions of the world where the global inventories may be most uncertain. The section ends with a discussion of the overall uncertainty associated with currently available emission inventories.

### *3.2.1. EDGAR-HTAP emission inventory (2000-2005)*

Currently available global emission inventories differ in the compounds included, regions and emission sources covered, and spatial and temporal resolution. Atmospheric modellers, therefore, often compile their own emission inputs, drawing upon different pieces of the available inventories that are related to their specific project. This is the case with most of the HTAP multi-model experiments described in the *HTAP Interim Assessment Report* and in Chapter 4 of this report, where atmospheric modelling groups were asked to provide their own best estimates for emissions for a given year. Although the variability introduced by the different emission estimates captures some of the real uncertainty in the magnitude of the emissions, the variability makes it difficult to compare modelling results.

In the *HTAP Interim Assessment Report*, the TF HTAP recommended further efforts for harmonization of emission inventories. The recommendations included reaching out to other organizations and research projects to facilitate the incorporation of other emission inventories with local knowledge into global emission inventories, especially in regions where emission factors and activity data are poorly known. The European Commission's Joint Research Centre initiated a project to implement this recommendation. The result of this project is the EDGAR-HTAP inventory, the development of which is described below.

The goal of the EDGAR-HTAP project is to compile a global emissions dataset for 2000 to 2005 using, to the extent possible, official or scientific inventories at the national or regional scale that are likely to be accepted by policy makers in each region of the world. The resulting inventory is a compilation as opposed to a consistent inventory calculated using activity data and emission factors. In order to provide a complete global picture of emissions, this compilation of different official inventories needed to be represented in a harmonized way, and gap-filled with global emission data of EDGARv4.1, as recently made public at <http://edgar.jrc.ec.europa.eu> [EC/JRC/PBL, 2010]. The Intergovernmental Panel on Climate Change (IPCC) code—defined by the IPCC Guidelines (1996) and conforming with the United Nations Framework Convention on Climate Change (UNFCCC) Common Reporting Format, CRF—is used as the key for harmonizing the sectoral data. A corresponding EDGAR-HTAP coding system is developed to allow aggregation at different levels of detail. It should be mentioned that different levels of detail are presented for the different countries in order to avoid subtraction of country-specific emission data. Moreover, the database system allows the user to calculate for given activity datasets the implied emission factor and so to compare the level of emission and abatement measures across regions. To provide the modelling community with consistent gridding of these emissions, the resulting emissions by country and sector are allocated to a  $0.1^\circ \times 0.1^\circ$  grid using the EDGARv4.1 database. The highest aggregation level, as represented in Table 3.1, is used for presenting the gridded maps for each year and each significant compound of that aggregated sector. The combination of policy and scientific inventories makes this inventory different from the work by Lamarque et al. [2010], as described in section 3.2.2.

**Table 3.1.** EDGAR-HTAP categorisation of emission sources (as applied for the gridded maps)

<b>Source emission category at highest level of aggregation</b>	<b>IPCC sectors</b>
htap_1_aircraft	1.A.3.a
htap_2_ships	1.A.3.d
htap_3_energy_combustion_&_fuel_production/distribution	1.A.1.a, 1.A.1.b, 1.A.1.c, 1.A.2, 1.B.1, 1.B.2
htap_4_industry_processes	2.A, 2.B, 2.C, 2.D, 2.G
htap_5_ground_transport	1.A.3.b, 1.A.3.c, 1.A.3.e
htap_6_residential	1.A.4, 1.A.5
htap_7_solvents	3.A, 3.B, 3.C, 3.D
htap_8_agriculture	4.A, 4.B, 4.C, 4.D (not 4E)
htap_9_agricultural_waste_burning	4.F, 4.G
htap_10_waste	6.A, 6.B, 6.C, 6.D

Pollutants included in the EDGAR-HTAP inventory are carbon monoxide (CO), nitrogen oxides (NO<sub>x</sub>), sulphur dioxide (SO<sub>2</sub>), non-methane volatile organic compounds (NMVOC), methane (CH<sub>4</sub>), ammonia (NH<sub>3</sub>), black carbon (BC), as well as particulate matter in coarse + fine (PM<sub>10</sub>) and fine (PM<sub>2.5</sub>) fractions. The EDGAR-HTAP inventory has been compiled using the following inventories in descending priority order:

- 1. Inventories submitted by Parties to the UNFCCC.** So-called Annex I countries (industrialized countries and economies in transition) report annual emissions of greenhouse gases (CO<sub>2</sub>, CH<sub>4</sub>, N<sub>2</sub>O, F-gases) and indirect greenhouse gases pollutants (CO, NMVOC, NO<sub>x</sub>

and SO<sub>2</sub>). These data have to follow specific guidelines in reporting and inventory construction and are subject to review by external inventory expert teams. For the EDGAR-HTAP inventory, UNFCCC emissions data were downloaded from the UNFCCC data portal ([http://unfccc.int/ghg\\_data](http://unfccc.int/ghg_data)) in the CRF format. Non-Annex I parties submit emission inventory data to the UNFCCC periodically under different reporting requirements than Annex I parties. These data vary in quality and detail, especially regarding air pollutants, and do not provide complete time-series. For this reason, non-Annex I data were not used in the EDGAR-HTAP inventory. UNFCCC emissions follow IPCC source classifications.






- 2. Inventories submitted by Parties to the LRTAP convention.** Countries that are parties to the LRTAP Convention provide annual emission inventory data for CO, NH<sub>3</sub>, NMVOC, NO<sub>x</sub>, SO<sub>x</sub>, particulate matter, heavy metals and persistent organic pollutants. These inventories are reported to the European Monitoring and Evaluation Programme's (EMEP) Centre on Emission Inventories and Projections (CEIP). Emissions as reported by Parties have been kindly provided by CEIP (Robert Wankmueller, personal communication, 2009). These data have been summed to IPCC source categories using the conversion table from the Nomenclature for Reporting to CRF.

The UNFCCC and EMEP datasets have been combined for each country and source category, giving priority to the (internationally reviewed) UNFCCC data. Data gaps in time series are filled using interpolation or extrapolation from the last/first year available. Where a complete time series of a compound is missing (BC and OC), EDGARv4.1 is used for gap-filling. International aviation and international navigation are excluded from this combined official inventory dataset and are taken from EDGARv4.1 bunker data. For the United States, the U.S. EPA National Emission Inventory (NEI) data for the years 2002 and 2005 have been included in the EDGAR-HTAP, replacing the UNFCCC data described above [U.S. EPA, 2009].

- 3. Asian countries.** For countries in Asia (except China and Japan) the REAS inventory [Ohara *et al.*, 2007] has been included by country and detailed sector for CH<sub>4</sub>, CO, NO<sub>x</sub>, SO<sub>2</sub>, NH<sub>3</sub>, OC and BC emissions (J. Kurokawa, personal communication, 2009). Emissions have been allocated to IPCC source categories. For those sectors where REAS emissions were reported to be zero, gaps were filled using inter/extrapolation to complete time series or EDGARv4.1 data to complete missing compounds (i.e., NMVOC, PM<sub>10</sub> and PM<sub>2.5</sub>). REAS data for agriculture were available only for the year 2000 and for this sector data from EDGARv4.1 have been used. Emissions in Japan have been taken from the official inventory submitted to the UNFCCC, completed with REAS data for NH<sub>3</sub>, OC and BC. For China, emissions were provided by IIASA (Z. Klimont, personal communication, 2009) taken from the GAINS-China dataset. Data were available for the years 2000 and 2005 and the years in between have been interpolated and allocated to the IPCC source categories. No gap-filling with EDGARv4.1 was necessary for China.

**Other countries, missing sectors, international shipping and international aviation.** Emissions from non-Annex I countries and countries outside Asia are taken from the EDGARv4.1 dataset (<http://edgar.jrc.ec.europa.eu/overview.php>). When inventories described under steps 1-3 did not provide emissions for a specific compound or sector, data were included from EDGARv4.1. This concerns mainly emissions of BC and OC for Annex I countries (to gap-fill EMEP data) and agricultural emissions, and NMVOC, PM<sub>10</sub> and PM<sub>2.5</sub> emissions for Asian (except China and Japan) countries (to gap-fill REAS data). Emissions from international shipping and from international aviation are taken from EDGARv4.1. For the international shipping and aviation, the EDGARv4.1 data were calculated using IEA/OECD [2007] fuel consumption and methodology; emission factors were taken from Dalsøren *et al.* [2009; 2007] and Eyring *et al.* [2005] for shipping and Eyring *et al.* [2004] for aviation. An overview of the coverage of species by each official dataset and the geo-coverage of the various emission datasets is presented in Table 3.2.

**Table 3.2.** Overview of the coverage of compounds and regions in the official emission datasets.

Order of priority	1. UNFCCC	2. EMEP	3. REAS	4. GAINS	5. EDGARv4.1
CO	X	X	X	X	X
NOx	X	X	X	X	X
SO2	X	X	X	X	X
NMVOC	X	X		X	X
NH3		X	X	X	X
CH4	X		X	X	X
PM2.5		X		X	X
PM10		X		X	X
OC			X	X	X
BC			X	X	X
geocoverage					

The resulting emissions by country and IPCC source category are allocated to a  $0.1^\circ \times 0.1^\circ$  grid, as defined in the EDGARv4.1 database. The  $0.1^\circ \times 0.1^\circ$  grid follows a reference country and sea grid definition based on GPWv3 [CIESIN, 2005]. Allocation of emissions is based on geographical data such as location of energy and manufacturing facilities, road networks, shipping routes, human and animal population density and agricultural land use. The resulting emissions estimates are presented in the context of historical trends and future scenarios in section 3.4. All grid maps for all years and all compounds at sectoral level are made available on the HTAP wiki site (<http://htap.icg.fz-juelich.de/data/>), together with other related documentation tables.

Figures 3.1 and 3.2 summarize the major spatial features of the EDGAR-HTAP inventory. Figure 3.1 presents total emissions in the year 2005 of the ten major species included in the EDGAR-HTAP inventory ( $\text{NO}_x$ ,  $\text{SO}_2$ ,  $\text{CH}_4$ ,  $\text{NH}_3$ , NMVOC, CO,  $\text{PM}_{10}$ ,  $\text{PM}_{2.5}$ , BC and OC). Note that the emissions do not include biogenic emissions from land use change and forestry or savannah burning. Figure 3.2 presents a second series of maps for each of these species showing some of the key contributing source types. These source types have been chosen so that a perspective on the global distributions of all major source types can be obtained. Source types included in Figure 3.2 are: international and domestic aviation, shipping in international and inland waterways, waste disposal, agriculture, industrial solvent use, agricultural waste burning, energy combustion and fuel production, industrial process emissions, residential, and ground transportation by road and rail.



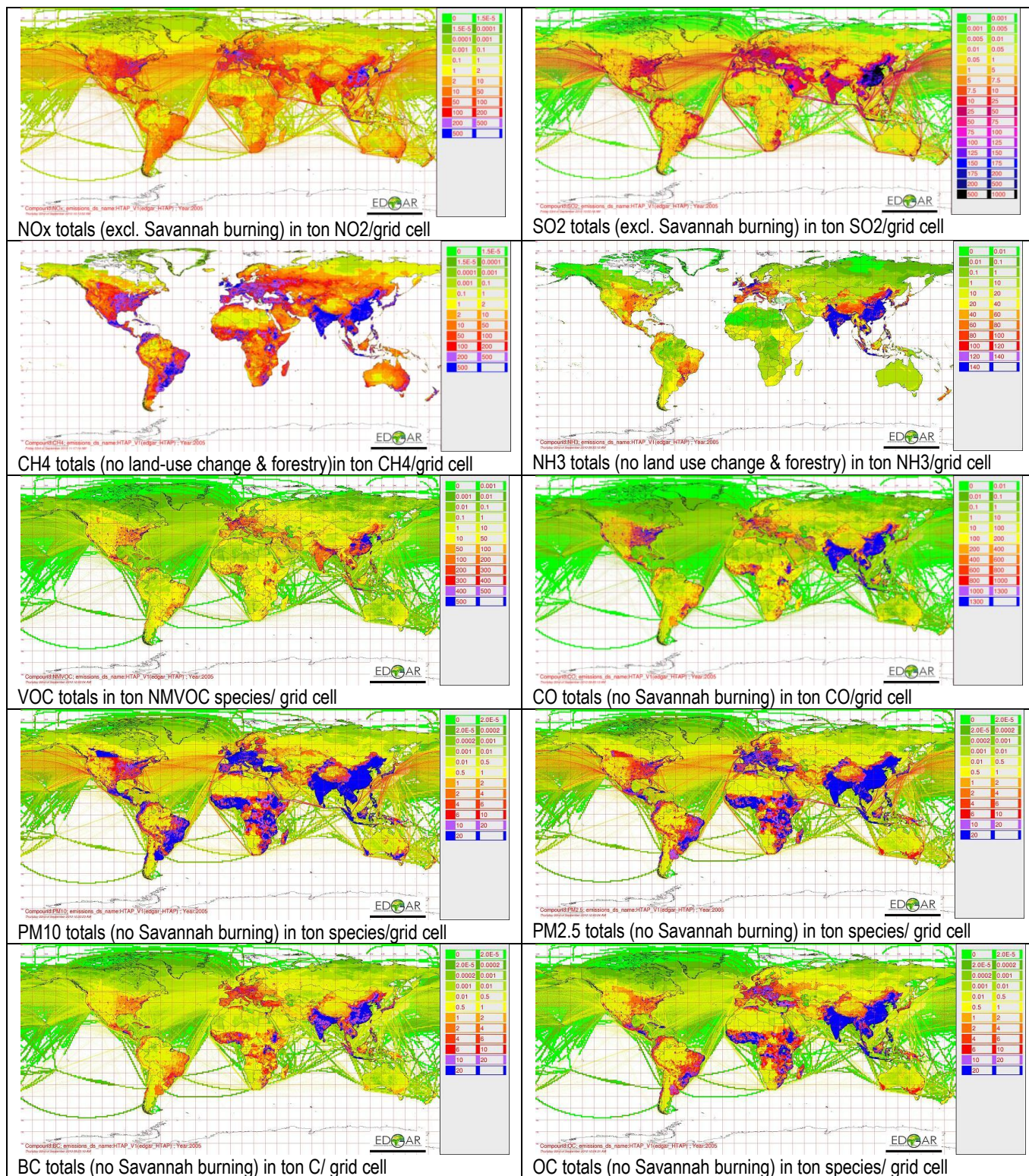


**Figure 3.1.** Gridded maps of anthropogenic emission totals in 2005 for each compound in the EDGAR-HTAP emissions database on a 0.1° × 0.1° grid (in tons of species/grid cell). (Please note: biomass is included but neither biogenic emissions from land use change and forestry nor savannah burning). [Graphic courtesy of European Commission Joint Research Centre.]



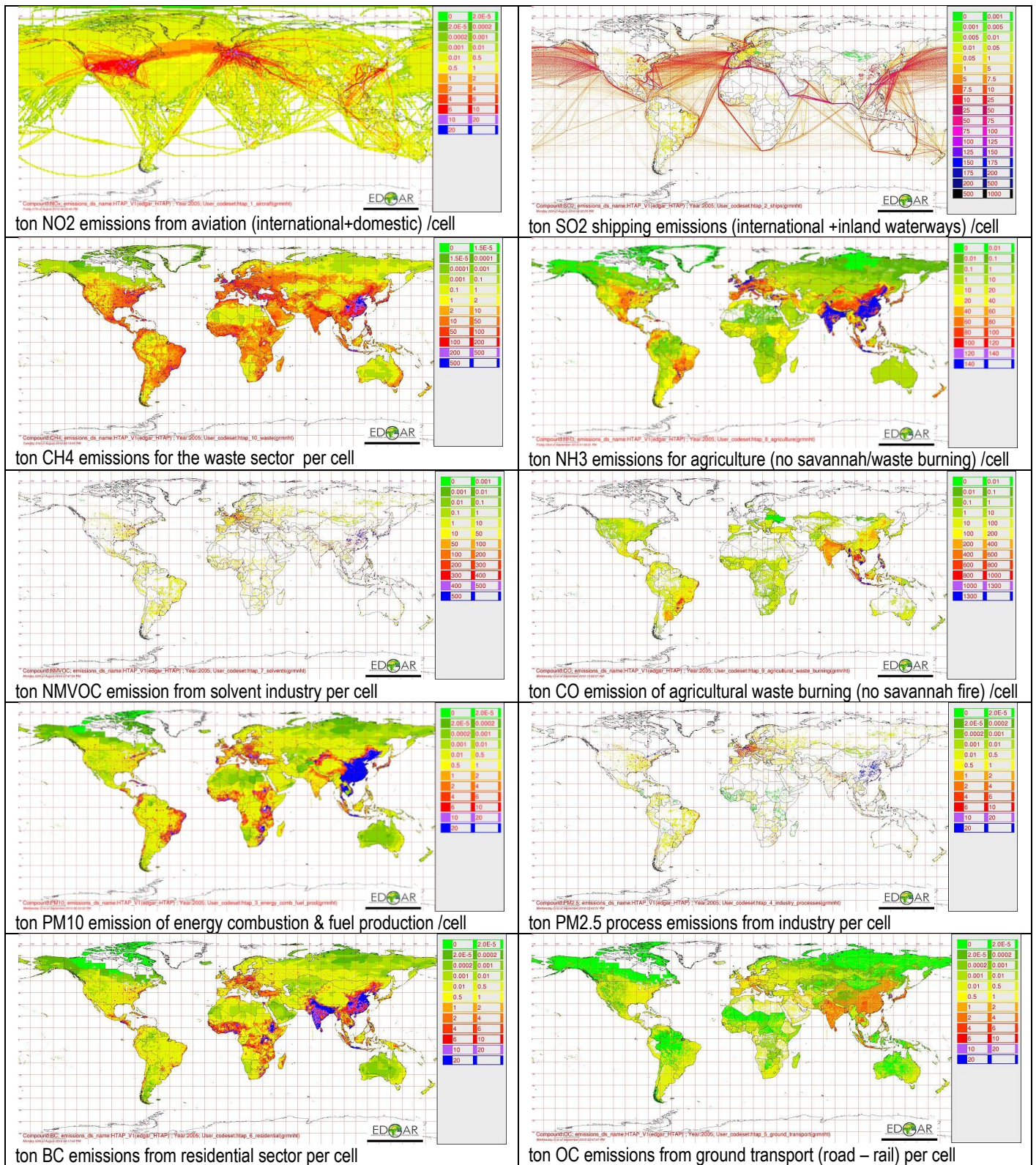


**Figure 3. 2.** Gridded maps of sector-specific anthropogenic emissions in 2005 in the EDGAR-HTAP emissions database on a  $0.1^\circ \times 0.1^\circ$  grid (in tons of species/grid cell). [Graphic courtesy of European Commission Joint Research Centre.]

### 3.2.2. Historical emission inventory in support of RCP scenarios (1850-2000)

Just ahead of the EDGAR-HTAP project, a new global, gridded emission dataset was developed covering the historical period (1850-2000) in decadal increments at a resolution of  $0.5^\circ \times 0.5^\circ$  [Lamarque *et al.*, 2010]. The primary purpose of this inventory, which we will refer to as the Historical RCP Inventory, is to provide consistent gridded emissions of reactive gases and aerosols for use in chemical transport model simulations (for the simulation of tropospheric ozone and aerosols) needed by climate models for the Climate Model Intercomparison Program #5 (CMIP5) in support of the IPCC Fifth Assessment Report (AR5). Similar to the EDGAR-HTAP project, a set of existing regional and global inventories, covering 40 regions and 12 sectors, were combined to capture a best estimate for the year 2000. The historical reconstruction of each emitted species, for each region and sector, is then forced to agree with the year-2000 estimate, ensuring continuity between past and 2000 emissions. The past-to-present emission estimates are then linked to the scenario-specific future trends of emissions (see section 3.2.3 below) to provide a unified trend from 1850 to 2100. The resulting historical trends are described further in section 3.4.

### 3.2.3. RCP scenarios (2000-2100)

In addition to the historical emission inventories, a set of future emission scenarios, known as Representative Concentration Pathways (RCPs), has been developed to contribute to IPCC AR5. The development of the RCPs was the start of a new process for development of scenarios and improving interaction among integrated assessment, climate modelling, and impacts, adaptation, and vulnerability communities contributing to the IPCC. The RCPs are a set of emissions, concentrations, and land-cover change projections designed to present a set of pathways selected to span the range of total climate forcing seen in the research literature. The four RCPs cover a range of total radiative forcing in 2100 from 2.6 to 8.5  $\text{W/m}^2$ . Note that the RCP scenarios cannot be taken together as a consistent set. They were developed by different modelling teams and use different underlying assumptions. The RCP 8.5 scenario, for example, should not be interpreted as a reference (no climate policy case) for any of the other scenarios. New socioeconomic and emissions scenarios will be developed in a follow-up stage to be used with climate model simulations performed using the RCP scenarios. A full description of the new scenarios approach can be found in Moss *et al.* [2010].

The RCP scenarios are labelled with their putative 2100 value for total anthropogenic radiative forcing, including greenhouse gases, aerosols, and tropospheric aerosols. The lowest forcing scenario is the RCP 3-PD (“peak and decline”) scenario (also called RCP 2.6) developed by the IMAGE modelling team of the Netherlands Environmental Assessment Agency [van Vuuren *et al.*, 2007]. This emission pathway is representative for scenarios in the literature leading to very low greenhouse-gas concentration levels. Radiative forcing in this scenario first reaches a value around 3.1  $\text{W/m}^2$  by mid-century, returning to 2.6  $\text{W/m}^2$  by 2100. In order to reach such radiative forcing levels, greenhouse-gas emissions—and, indirectly, emissions of air pollutants—are reduced substantially over time.

The highest forcing scenario is the RCP 8.5 developed by the MESSAGE modelling team and the IIASA Integrated Assessment Framework at the International Institute for Applied Systems Analysis (IIASA), Austria. The RCP 8.5 is characterized by increasing greenhouse-gas emissions over time and is representative of scenarios in the literature leading to high greenhouse-gas concentration levels. The underlying scenario drivers and resulting development pathways are based on the A2r scenario, as detailed in [Riahi *et al.*, 2007].

The two intermediate radiative forcing scenarios are the RCP 4.5 and RCP 6.0 scenarios. These were implemented by the respective teams as climate policy scenarios in order to reach the specified radiative forcing targets. The climate characteristics (e.g., total radiative forcing) of the two pathways can be considered generally representative of a broader set of scenarios that reach these forcing levels [Moss *et al.*, 2010]. These could, potentially, include scenarios without explicit climate policy. The RCP 4.5 scenario was developed by the GCAM (formerly MiniCAM) modelling team at the Joint Global Change Research Institute (JGCRI), Pacific Northwest National Laboratory. It is a stabilization scenario where total radiative forcing is stabilized before 2100 by employment of a range

of technologies and strategies for reducing greenhouse-gas emissions. The scenario drivers and technology options are detailed in Clarke et al. [2007], non-CO<sub>2</sub> and pollution control assumptions in Smith and Wigley [2006], and additional detail on the simulation of land use and terrestrial carbon emissions given by Wise et al. [2009]. The RCP 6.0 scenario is developed by the AIM modelling team at the National Institute for Environmental Studies (NIES), Japan. It is a stabilization scenario where total radiative forcing is stabilized after 2100 without overshoot by employment of a range of technologies and strategies for reducing greenhouse-gas emissions. The details of the scenario are described in Fujino et al. [2006] and Hijioka et al. [2008].

Air pollutant emissions in the RCP scenarios were calibrated to the consensus year 2000 inventory described in Lamarque et al. [2010]. All scenarios include central assumptions for pollution controls that tend to increase in stringency over time as incomes increase, particularly in developing countries. If used for air pollution analysis, it is also important to note that three of the RCP scenarios were implemented as climate policy scenarios. This means that pollutant and greenhouse-gas emissions are generally lower in the RCP scenarios than in the corresponding reference scenarios without a climate policy. Climate policies were assumed to be implemented in all global regions in these scenarios, which implies that indirect effects on pollutant emissions occur in all regions as well.

The amount of departure from the associated reference scenario depends largely on the magnitude of the policy mitigation effort. In the RCP 6.0 scenario pollutant emissions are modestly lower for most of the century, with larger and earlier differences in the RCP 4.5 scenario. The RCP 3-PD (2.6) scenario requires the largest and earliest changes in the energy system, resulting in SO<sub>2</sub> emission reductions of approximately 50% from the reference case by 2050. The emissions implications of climate policy also depend on the gas. The largest impact of a climate policy is on SO<sub>2</sub>, with lesser impacts on NO<sub>x</sub> emissions.

Figure 3.3 shows the RCP scenario emissions as compared to the so-called SRES scenarios that were used in previous IPCC assessments, as well as a set of scenarios from the literature. These four graphs are presented to give a broad indication of potential future trends in emissions of four key species, as well as the extent of divergence of different estimates. Detailed presentation of emission projections can be found in section 3.4. Due, at least in part, to the effects of the assumed greenhouse-gas limits in these scenarios, the RCP scenarios generally do not cover the full range in the literature for pollutant emissions. Part of the difference, however, could also be due to the fact that the RCP scenarios are from a newer generation of models. The SRES scenarios, for example, did not include pollution control measures other than for SO<sub>2</sub> [Smith and Wigley, 2006] and newer scenarios for these emissions are generally lower. SO<sub>2</sub> emissions in the RCP scenarios are lower in the near-term than earlier scenarios in the literature, which is due, in part, to lower baseline emissions and more aggressive sulphur controls in recent years than was assumed in many previous long-term scenarios.

#### *3.2.4. Incorporating local knowledge into global emission inventories: RAPIDC*

The aim of the Regional Air Pollution in Developing Countries (RAPIDC) programme, coordinated by the Stockholm Environment Institute (SEI), is to facilitate the development of agreements and protocols for preventing and controlling air pollution. A major component of the RAPIDC programme has been to develop emission inventory preparation capacity within South Asia and southern Africa. It is anticipated that this process will also provide local information that improves larger-scale inventories such as EDGAR.

Essential to the RAPIDC work has been close cooperation with two relevant regional air pollution networks, the *Malé Declaration on Control and Prevention of Air Pollution and its Likely Transboundary Effects for South Asia* and the *Air Pollution Information Network for Africa* (APINA). At an early stage in the RAPIDC programme, in collaboration with network members in the regions, SEI produced emission inventory preparation manuals tailored to the needs of the two regions. Network members and governments were closely involved in the manuals' development to ensure local intellectual ownership. It was agreed that the manuals should focus on anthropogenic emissions of the main regional air pollutants (SO<sub>2</sub>, NO<sub>x</sub>, CO, NMVOC, NH<sub>3</sub>, PM<sub>10</sub> and PM<sub>2.5</sub>). The Malé Declaration and APINA emission inventory manuals (and associated Excel workbooks) were then



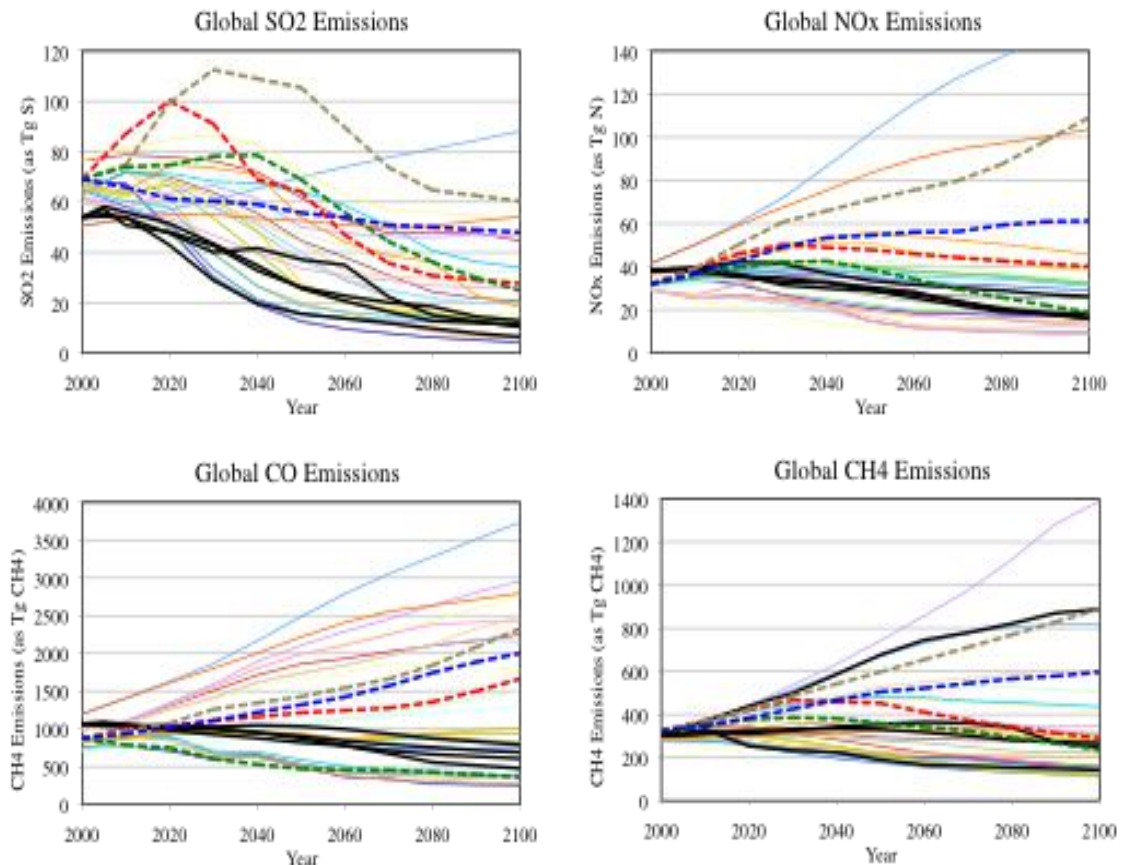


**Figure 3.3.** Total global anthropogenic emissions of air pollutants and methane for the SRES scenarios [IPCC, 2000, thick dotted colored lines], a selection of post-SRES scenarios from the literature [thin lines from van Vuuren *et al.*, 2008] and the RCP scenarios (www.iiasa.ac.at/web-apps/tnt/RcpDb/; thick black lines).

used for capacity building and the compilation of national inventories by trained participants from each country. These manuals have also been adapted to produce the more generic approach of the Global Atmospheric Pollution Forum Emission Manual (<http://sei-international.org/gap-the-global-air-pollution-forum-emission-manual>) which has been used for capacity building in other parts of Asia and which was the basis for the further development of the Atmospheric Brown Cloud (ABC) emission inventory preparation manual. Within RAPIDC, comprehensive national air pollutant emission inventories have been compiled for four of the Malé Declaration countries (Bangladesh, Bhutan, Nepal and Sri Lanka) and for the seven APINA countries (Botswana, Malawi, Mozambique, South Africa, Tanzania, Zambia and Zimbabwe).

Comparisons between the EDGARv3.2FT2000 (the version prior to EDGARv4) and RAPIDC inventories have been made and the discrepancies used to pinpoint errors in the RAPIDC inventories (Figure 3.4). In some cases, however, the discrepancies are likely due to a lack of relevant data in the EDGAR inventory. For example, for SO<sub>2</sub> emissions in Botswana the most obvious difference is found for industrial processes, where a value of 94 kilotonnes was reported in the RAPIDC/APINA inventory (emitted from the Selebi Phikwe copper smelter) compared to a value of zero in EDGARv3.2FT2000. The RAPIDC inventory also reports substantially higher SO<sub>2</sub> emissions from fuel combustion in both the power and industry sectors. For the power sector, this may be due to an assumption within the EDGAR inventory of coal sulphur content somewhat lower than the 1.36% used in the RAPIDC inventory. However, for industrial fuel combustion, the reason for the discrepancy is likely to be differences in fuel consumption data used. EDGARv3.2FT2000 relies on the energy balances reported by the International Energy Agency (IEA), which appear to be incomplete as they do not include the 210 kilotonnes coal burnt in the non-ferrous metals sector (i.e.,

the copper smelters) nor the fuel consumed in Botswana's non-metallic minerals sector. Thus the root cause of the difference here would appear to be deficiencies in the IEA database used in EDGAR. This illustrates how local knowledge, gained through the RAPIDC process, can capture significant emissions that may be missed in global inventory initiatives such as EDGAR. An on-going process of detailed comparisons among the RAPIDC, EDGAR, and other inventories will hopefully lead to improvements in all of them.

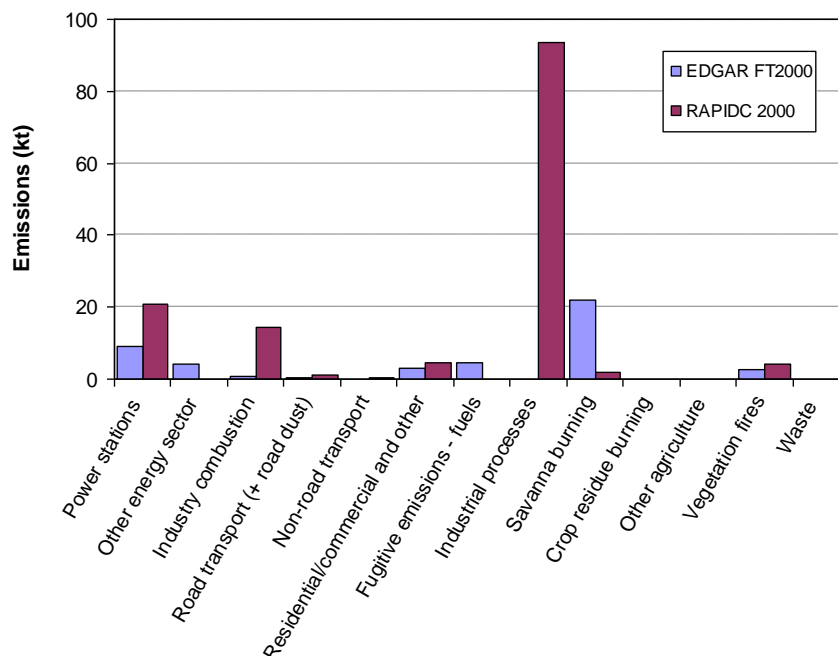


**Figure 3.4.** Comparison between EDGARv3.2FT2000 and RAPIDC emission inventories for SO<sub>2</sub> for Botswana in the year 2000.

### 3.2.5. Uncertainties in emission estimates

An uncertainty estimate is one of the quality indicators of an emission inventory and can be used to prioritise efforts to improve the inventory. Verification has been defined as:

the collection of activities and procedures conducted during the planning and development, or after the completion of an inventory that can be used to establish its reliability for the intended application of the inventory [IPCC, 2006].

Verification methods include comparisons of different inventories, comparisons of results of alternative methods, and using emissions in models to compare with atmospheric measurements. These methods are complementary. Statistical approaches to estimate uncertainties in emission inventory levels and trends have been developed at large scale by the IPCC [2006] and in more specific applications [e.g., Frey and Zheng, 2002]. Two approaches are typically used: simple error propagation and Monte Carlo simulations. The main challenges in estimating inventory uncertainties are, however, uncertainty in the input data and developing methods to quantify systematic errors. For most inventory applications the random component of an uncertainty estimate will be small compared to the systematic component. The IPCC [2006] lists the following sources of uncertainties to consider: lack of completeness, inventory model (estimation equation), lack of data, lack of representativeness of data, statistical random sampling error, measurement error, misreporting or misclassification, and missing data. Systematic expert judgments can be used to complement other sources of information on uncertainties. The usual metric for expressing uncertainty estimates is two standard deviations as a percentage of the mean.

In recent years there have been a number of new analytical tools applied to the elucidation of emissions emanating from sources in the northern hemisphere. Techniques include improved direct (forward) modelling and inverse modelling, making use of improved ground-station monitoring

networks, and aircraft observations during large-scale field campaigns. Also, a new generation of satellites has provided trends based on column data that have been compared with emission trends. More often than not, the observation-based methods have suggested that emission estimates obtained from inventories, particularly for developing and newly industrializing countries, are too low. These important new tools and methods are described in section 3.6.

Uncertainties in inventories will vary by region, source, pollutant, and inventory year. Uncertainty estimates for all world regions are not available. Generally it is expected that regions with the longest experience in compiling inventories and with well-developed statistical systems (e.g., Western Europe, North America and Japan) compile inventories with lower uncertainties than other regions. Formal quantification of uncertainties in emission inventories of non-greenhouse gas species has been performed in a few cases, e.g., Rypdal [2002] and the examples shown below.

The primary reasons for differences in uncertainties among sources are (i) activity statistics are missing or weak; (ii) emission factors and technologies are known better for some sources than for others; and (iii) emissions depend on natural and variable factors such as temperature and precipitation. Usually, emissions related to the household sector, agriculture, and waste disposal are more uncertain than for transportation and large stationary sources. Natural sources and semi-natural sources (e.g., forest fires) are more uncertain than anthropogenic sources. The factors leading to uncertainty are many and varied. To mention just a few examples, emissions may be strongly dependent on process conditions (e.g., burning vs. smouldering), on the level of abatement (e.g., new catalyst vs. broken catalyst), and on such unpredictable things as equipment vapour leakage. Data quality is strongly influenced by the extent of data available. For example, the speciation of NMVOC may be based on very few individual measurements that are extrapolated with dubious reliability to seemingly related emission sources that have not been measured. Laboratory and field testing of sources is an expensive proposition, so often the speciation of NMVOC emissions in China or India is based on measurements taken in Europe or North America, whether or not the sources can be considered equivalent. Note that some emissions are more easily constrained (e.g., SO<sub>2</sub> due to fuel S content, CO<sub>2</sub> due to carbon content, and even Hg due to fuel/ore content) than others (e.g., CO emissions that depend on excess oxygen availability during combustion or the temperature-dependent emissions of semi-volatile PM).

Uncertainties for individual pollutants differ also with the level of experience of compiling an inventory, and these uncertainties typically can be reduced over time. SO<sub>2</sub> inventories have a long history in Europe and North America and are considered relatively reliable in those regions. For other world regions, inadequate information about the sulphur content of fuels and sulphur removal efficiencies may add to the uncertainty. NO<sub>x</sub> inventories are generally regarded as less certain than SO<sub>2</sub> inventories, while NMVOC and CO inventories carry high uncertainties. Due to the short experience in compiling PM, BC, and OC inventories and the lack of data on the distribution of technology types in key regions, these are even more uncertain. In addition, PM emissions are very dependent on the abatement equipment installed and whether it is working as designed; the difference between a collection efficiency of 99% and 99.9% is a factor of 10 in the emissions. BC and OC inventories have uncertainty ranges from -25 % to a factor of two (higher for open burning) [Bond *et al.*, 2004]. Typical reported ranges of uncertainty estimates for Europe are: SO<sub>2</sub>: ±5%, NO<sub>x</sub>: ±14%, NMVOC: 10-39% and CO: ±32% [EMEP, 2006]. The TRACE-P inventory [Streets *et al.*, 2003] estimated uncertainties in Asian emissions that ranged from ±16% for SO<sub>2</sub> and ±37% for NO<sub>x</sub> to more than a factor of four for BC and OC. Within Asia, there was wide variation among countries and regions, with emission uncertainties in Japan being similar to those in Europe, and emissions in South Asia having high uncertainty. This topic is addressed further in our special review of Asian emission inventories in section 3.5.

A lower bound estimate of the uncertainty in the emission data used in the HTAP multi-model experiments discussed in the *HTAP Interim Assessment Report* and in Chapter 4 of this report can be obtained by comparing the emissions used in the modelling to the estimates from different inventories. Figure 3.5 shows the EDGAR-HTAP 2000 emissions compared to the total emissions and anthropogenic emissions used in the SR1 experiments for 2001. The comparisons are provided for the

global total and each of the HTAP source regions. For the SR1 inputs, the means of the total and anthropogenic emissions are shown along with the maximum and minimum values for the ensemble. While the “anthropogenic” mean is calculated using data from all model runs, the “total” mean is calculated only from model runs that included both anthropogenic and natural emissions. Some of the differences are due to emissions associated with land-use changes and savannah burning, which are not included in the EDGAR-HTAP 2000 data.

**FINDING: Present-day emissions of most species important for intercontinental transport are relatively well understood by sector and world region. The spatial distribution of present-day emissions (gridded fields) is also reasonably well known.**

**RECOMMENDATION: Present-day emissions of some species are still unreliable in some parts of the world (e.g., black carbon and NMVOC emissions from developing countries, ammonia emissions, natural emissions), and additional resources are needed to measure the emission factors of key sources and to conduct surveys of activity levels. In particular, natural sources such as soil emissions, windblown dust, volcanoes, and remote biomass burning rarely fall within the purview of national governments and may need greater attention from the TF HTAP.**

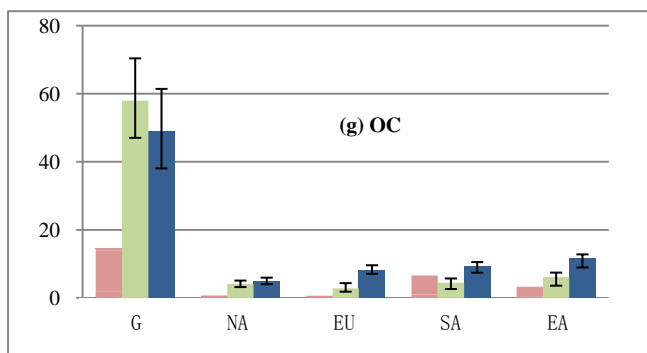
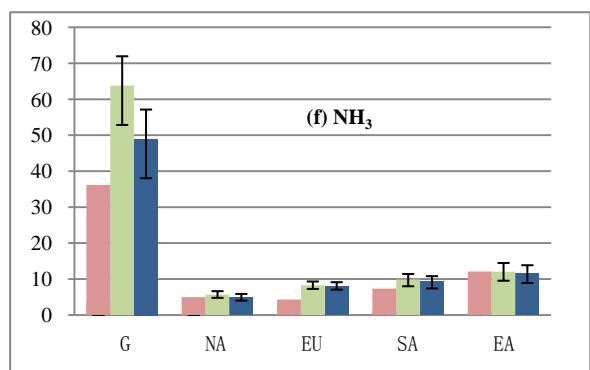
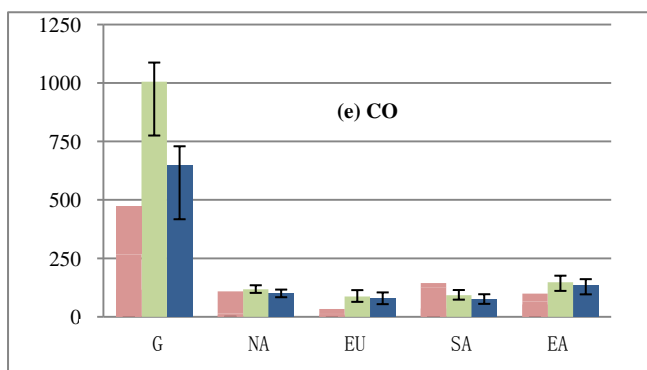
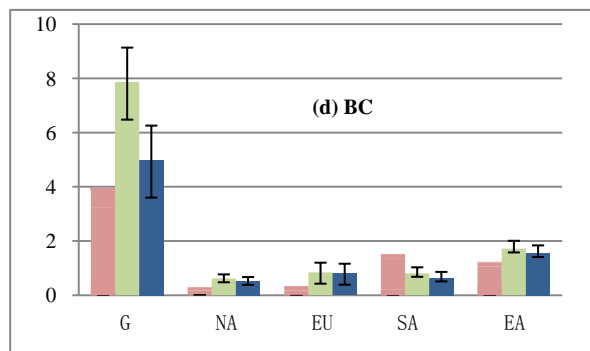
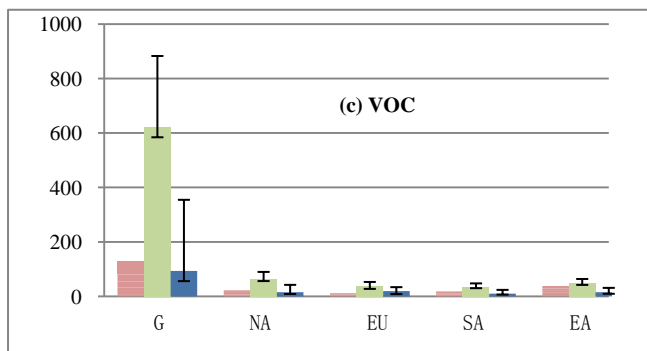
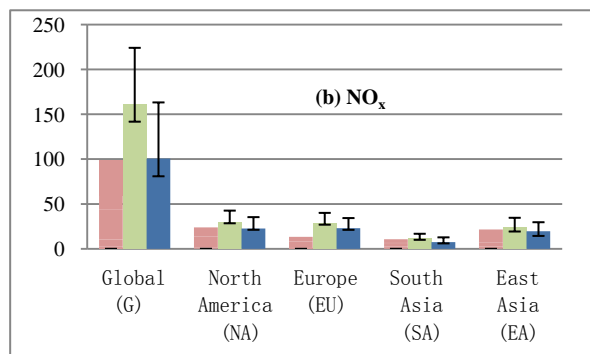
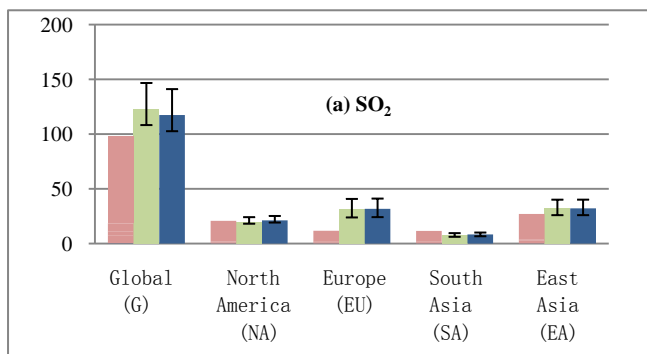
**FINDING: Long-term emission trend datasets (century-scale) are becoming available and present a new opportunity to characterize intercontinental pollution flows in the past and future. Uncertainties are higher the further away we get from present-day conditions. Gridded emission distributions for the past and future are rudimentary.**

**RECOMMENDATION: Harmonization of past, present, and future emissions over time and space needs additional work. New spatially distributed proxy datasets are needed to more accurately distribute past and future emissions over the Earth’s surface.**

**FINDING: The reliability of emission data varies considerably by species, sector, and world region. This adds uncertainty to our ability to reliably model intercontinental transport among different world regions; it means that some source/receptor relationships are inherently better known than others because of inadequacies in our ability to quantify some of the source terms.**

**RECOMMENDATION: Greater emphasis needs to be placed on quantification of emission uncertainties. In addition, bringing together scientific communities working on emission inventories, satellite retrievals, laboratory tests, ground-based monitoring, and aircraft field campaigns could be a valuable function of the TF HTAP that would constrain emission estimates and narrow uncertainties. Making use of the local knowledge that goes into national or regional emission inventories can be helpful in improving global inventories.**





■ 2000 EDGAR-HTAP  
■ 2001 SR1 Total Emissions  
■ 2001 SR1 Anthropogenic Emissions  
 Emissions in Tg/yr

**Figure 3. 5.** Comparison of the 2000 EDGAR-HTAP inventory to the emission inputs used in the SR1 run of the HTAP multi-model experiments representing 2001. The comparison is presented for the global total and each of the four HTAP source regions. For the SR1 inputs, the means of the total and anthropogenic emissions are shown along with the maximum and minimum values for the ensemble. The EDGAR-HTAP 2000 data does not include any land use change emissions.

### 3.3. Emissions from Natural Sources and Biomass Burning

Though air quality is a measure of the anthropogenic perturbation of the “natural” atmospheric state, it has to be considered in the wider context of the interactions with natural emissions and biomass burning [Monks *et al.*, 2009]. The term “natural” in this context should not be equated with “free of human influence,” in light of the significant impacts of all kinds of human activities on vast areas of the global land surface [Haberl, 2007]. Natural emissions and biomass burning are significant contributors to the emission load of the atmosphere. Natural emissions include CH<sub>4</sub> from termites, mineral dust from deserts, NO<sub>x</sub> emissions from lightning, sea salt, dimethyl sulphide from oceans, SO<sub>2</sub> from volcanic activities and VOC emissions from vegetation. Biomass burning results from both natural and anthropogenic fires. The uncertainties associated with natural and biomass burning emissions are substantial.

#### 3.3.1 Natural emissions

Natural sources of atmospheric gases and particles include living and dead organisms, soil, lightning, oceans, and volcanoes. Natural emissions occur in the absence of people, but human activities can substantially alter these emissions. Methods have been developed for estimating global emissions of trace gases and particles from all major natural sources, including, for example, plant foliage VOC [Guenther *et al.*, 2006], mineral dust [Mahowald *et al.*, 2006], volcanic SO<sub>2</sub> [Andres and Kasgnoc, 1998], lightning NO<sub>x</sub> [Price *et al.*, 1997], soil NO<sub>x</sub> [Lee *et al.*, 1997], wetlands methane [Fung *et al.*, 1991], and wildfires [van der Werf *et al.*, 2003]. The resolutions of these models range from hourly and 1 km × 1 km for plant foliage VOC to monthly and 1° × 1° for wetlands methane. The uncertainties associated with natural emissions are substantial and are highly dependent on the spatial and temporal scales considered. For example, annual global isoprene emissions are known to within a factor of two, but the uncertainty associated with isoprene emission at a particular hour and location can exceed a factor of five [Guenther *et al.*, 2006]. In addition, uncertainties vary greatly for the various compounds emitted from vegetation foliage and wildfires. For example, the uncertainties associated with emissions of sesquiterpenes from foliage and NH<sub>3</sub> from wildfires are much higher than those associated with isoprene from foliage and CO<sub>2</sub> from fires.

A high resolution (1 km × 1 km) biogenic VOC and NO<sub>x</sub> emission model (MEGAN) and driving variables are available at <http://cdp.ucar.edu>. A high resolution (10 km × 10 km) inventory of NO<sub>x</sub>, SO<sub>2</sub>, NH<sub>3</sub>, PM, NMVOC, CH<sub>4</sub>, CO and dimethyl sulphide emissions from natural sources in Europe was completed in 2007 [NATAIR, <http://natair.ier.uni-stuttgart.de>, see Friedrich, 2009, and references therein]. Emission sources included as “natural” comprise vegetation (especially forests and forest and agricultural soils), primary biological aerosol particles, wild animals, humans, anoxic soil processes in wetlands, macro- and micro-seepages from geothermal and non-geothermal sources, wind-blown dust and Saharan dust, volcanoes, and lightning. Emissions from pets, biomass burning, and forest fires are also dealt with, even though they are often considered to be anthropogenic activities. The methodology developed to estimate emissions from these sources will be used to update the EMEP/CORINAIR Guidebook.

Uncertainty assessments of natural emission sources have focused on comparisons of available input databases, e.g., Guenther *et al.* [2006], Ito and Penner [2004] and Hoelzemann *et al.* [2004]. The uncertainties associated with emission factors and emission algorithms are more difficult to quantify for natural sources. Comparisons of different emission estimates for any of these sources tend to agree within about a factor of two on annual global scales. However, the models are generally based on at least some of the same emission factor data and so are not independent estimates. Global satellite observations are beginning to provide a valuable tool for assessing emissions of, among many others: foliar isoprene [Shim *et al.*, 2005], wildfires [Pfister *et al.*, 2005], lightning [Boersma *et al.*, 2005], methane [Frankenberg *et al.*, 2005], and mineral dust [Mahowald *et al.*, 2003]. These observations are valuable both for providing some confidence in natural emission estimates and for indicating regions and seasonalities of major discrepancies.

As estimates of present-day natural emissions have improved, research efforts have focused more on how these emissions will respond to climate and landcover change. Natural emissions of

mineral dust, wetland methane, foliar VOC, and wildfires are all very sensitive to changes in landcover (e.g., vegetation type and density) and soil moisture [e.g., *Flannigan et al.*, 2005; *Guenther et al.*, 2006; *Mahowald et al.*, 2006]. Foliar VOC emissions are also sensitive to ambient temperature and solar radiation. Emissions can vary by a factor of two or more on time scales of years to decades. An improved understanding of the processes controlling these variations is required for accurate predictions of future natural emissions.

Table 3.3 presents a summary of some recent estimates of the relative magnitudes of emissions from the major natural emission sources. Biomass burning is included in this table and also expanded on in section 3.3.10. Each one of these species/source categories is the subject of ongoing scientific research, and we present selected results to give an idea of the relative magnitudes of natural source contributions. This table is not exhaustive in either species or sources.

**Table 3.3.** Some estimates of global annual emissions from natural sources

	Biogenic	Desert/Soil Dust	Soil	Geogenic	Biomass burning/wildfires
NMVOC	500 to 750 Tg (isoprene)				78 Tg
NO <sub>x</sub>			7 Tg N (microbial production of NO)	5 Tg N (lightning) 12.2 Tg N (lightning)	8 Tg N
CH <sub>4</sub>	200-400 Tg (wetlands, bogs, swamps, and tundra) 10-200 Tg (termites)			40-60 Tg	50-100 Tg (tropical)
PM <sub>2.5</sub>		671 Tg			
PM <sub>10</sub>		4483 Tg			
SO <sub>2</sub>				13.4 Tg (volcanic)	3.8 Tg

#### Notes

Biogenic VOC: 500-750 Tg isoprene from Guenther et al. [2006].

Biomass burning and soil NO<sub>x</sub>: from Lee [1997]. Biomass inventory includes deforestation, savannah burning, agricultural waste burning, and biofuel combustion, yielding an estimate of 8 Tg N yr<sup>-1</sup>. This estimate includes sources beyond the tropics. Further refinement of the AERONOX soils emission model resulted in an estimate of 7 Tg N yr<sup>-1</sup>. Biomass burning emissions of NMVOC and SO<sub>2</sub> from Lamarque et al. [2010].

Dust: PM<sub>2.5</sub> and PM<sub>10</sub> data from Mahowald et al. [2006], based on modelling and satellite observations of aerosol optical depth.

Lightning NO<sub>x</sub>:

\*5 Tg N (± 3 Tg) [from *Schumann and Huntrieser*, 2007].

\*5 Tg N from Lee [1997].

\* 12.2 Tg N from Price [1997].

Biogenic CH<sub>4</sub> from Fung et al. [1991]:

\*Wetlands, bogs, swamps, and tundra: 200-400 Tg CH<sub>4</sub>.

\*Termites: 10-200 Tg CH<sub>4</sub>.

\*Tropical biomass burning: 50-100 Tg CH<sub>4</sub>.

Geogenic CH<sub>4</sub> from Etiope and Klusman [2010].

Volcanic: 13.4 Tg SO<sub>2</sub> [from *Andres and Kasgnoc*, 1998].

### 3.3.2. Biomass burning

In the last few decades biomass burning has been recognized as an important source of atmospheric trace gases and particulate matter, which may exert a significant influence on atmospheric chemistry, particularly in the tropics, and in the longer term on climate [*Hao and Liu*, 1994; *Schultz et al.*, 2008; *Seiler and Crutzen*, 1980]. Types of vegetation cover subjected to fires

include forestland, wooded land, grassland, and agricultural land. Recent studies aimed at investigating the spatial and temporal distributions of vegetation burning using satellite data to identify burn area have started to evaluate the interannual variability of wildfire emissions on global and regional scales, [e.g., *Duncan et al.*, 2003; *Schultz et al.*, 2008; *van der Werf et al.*, 2004; *van der Werf et al.*, 2006]. The results showed that wildfires have a large interannual variability [*Duncan et al.*, 2003], and therefore the resulting emissions are very variable in time and space. Globally, biomass burning contributes at present about 50% of the total direct CO and BC emissions [*Pétron et al.*, 2004] and about 15% of surface NO<sub>x</sub> emissions [*IPCC*, 2001].

An illustration of the interannual variability of biomass burning NO<sub>x</sub> emissions is shown in Figure 3.6, which is obtained by combining the RETRO biomass burning dataset [*Schultz et al.*, 2008] with the GFED dataset [*van der Werf et al.*, 2003]. The types of biomass burning considered included forest fires, savannah burning and grassland fires by main regions in the period 1970-2005.

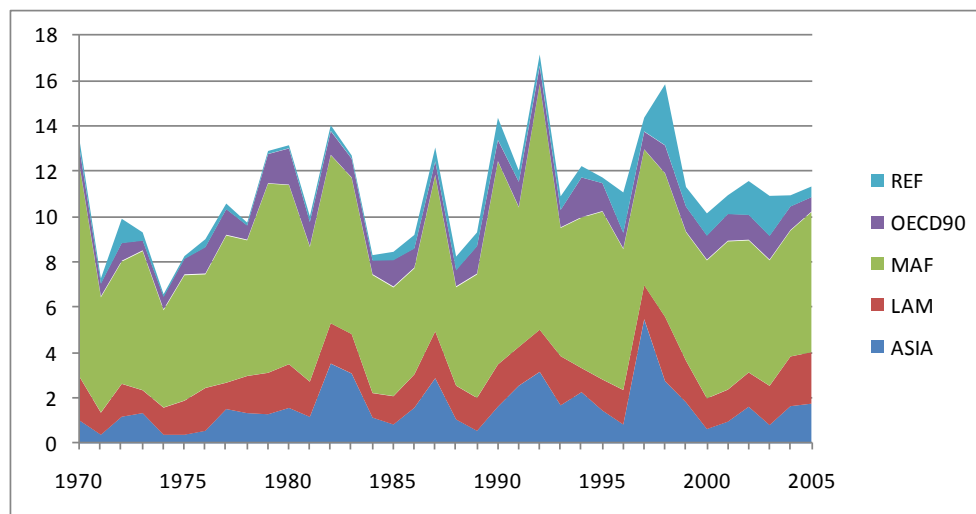


**Figure 3.6.** NO<sub>x</sub> emissions from biomass burning (forest fires, savannah burning, and grassland fires) by main world regions in the period 1970-2005. For the definition of world regions, REF = Central and Eastern Europe + Russia; OECD90 = OECD member states as of 1990; MAF = Middle East + Africa; LAM = Latin America and Caribbean; ASIA =Asia excluding the Middle East. See IPCC publications for countries included in each world region.

From Figure 3.6 it is clear that the Middle East and Africa region, MAF, constitutes the major contributor to global biomass burning NO<sub>x</sub> emissions. The extensive savannah burning in this region contributes about 50% of global emissions from biomass burning. The contribution from MAF is rather constant over the period 1970-2005. The region displaying a high inter-annual variability is ASIA, mainly due to cropland burning, although the absolute value of the contribution is smaller than that of MAF, with a peak in 1997-1998 that coincided with the important forest fires in Indonesia. In this regard, Chang and Song [2010], based on a comparison of new high spatial resolution global burned area products, L3JRC (1 km resolution) with MDC45A1 (500 m resolution) over the domain of tropical Asia running from India to Indonesia, indicated that these satellite datasets led to better classifications of vegetation cover type and more representative burned areas, which are still nevertheless subject to high uncertainties, when compared, for example, to GFED products.

According to Ito and Penner [2004] and detailed by Schultz et al. [2008], there are three main types of uncertainty that limit the potential accuracy of any global long-term biomass burning emission dataset. First, for burned areas, data on accurate long-term monitoring of fire scars have become available only recently, generally for periods after 1995, and thoroughly performed in only a few regions. Although these satellite fire products have provided key information on the spatial and temporal patterns of fire occurrence, their quantitative use is still limited because of remote sensor limitations, satellite orbital drift, cloud and smoke presence, and especially limited statistics of ground calibrations, and because retrieval procedures may vary for different ecosystems and observing conditions [e.g., *Giglio and Kendall*, 2004]. It should be noted that fires in the mid-latitude regions

are well monitored with sophisticated networks, while those in the tropics are still scattered and scarce, due to limited resources at the local level for records and accessibility. This was revealed when tropical Asia experienced some of the most severe wildland fire events under extreme climatic conditions [Chang and Song, 2010; Streets et al., 2003]. Second, regarding the fuel consumption, fire severity and hence the amount of fuel actually combusted in a fire, depends on the fuel characteristics (load and density, moisture, vegetation type, organic content and moisture of the soil) and the rate of spreading, which is determined largely by wind speed, fraction of fuel consumed by the fire, fuel bulk density, topography, etc. These factors are highly variable even within a single fire and they are poorly documented on larger scales. A few studies have tried taking these factors into account on a case-by-case basis, but very few data are able to support general parameterizations for global-scale modelling of fire emissions. Finally, for emission factors, the amounts of individual chemically active trace species and aerosols released from a fire depend on the fuel type and fire characteristics, and are often poorly determined. In practice, the emission factors compiled by Andreae and Merlet [2001] have become a reference dataset used by many modellers. Results from different studies nevertheless stress that more complete combustion, as in flaming fires, would lead to a larger fraction of highly oxidized species (e.g., CO<sub>2</sub>, NO<sub>x</sub>), while smouldering fires release more material in reduced form (e.g., CO, NH<sub>3</sub> and NMVOC species), which indicates that emission factors may vary with season, and that fire characteristics can be very different from one fire to another even within the same geographical location.

Given the high uncertainty of biomass burning emissions and the variability in time and space, recent studies [Chang and Song, 2010; Lamarque et al., 2010; Mieville et al., 2010; Schultz et al., 2008] have investigated past and present trends of emissions from biomass burning in order to improve inputs to global and regional climate and atmospheric chemistry models, e.g., those related to the RCP scenarios for supporting IPCC AR5. A compilation of these studies for the past and present trends in combination with future projections can provide information on the capacity of emission models to represent the contribution of biomass burning to global emissions. Figure 3.7 illustrates the trends of CO emissions from global biomass burning according to several different models and scenarios. The result of a comparison of RCP scenario projections shows that AIM seems to better capture the global biomass burning trends, but is also the only model to indicate an increase of CO from this emission source, ranging from a contribution of 45% to global direct emission of CO in 2000 to more than 70% in 2100.

An analysis of the AIM dataset of future projections vs. vegetation type is shown in Figure 3.8, which indicates that the future increase results from intensification of savannah burning, especially in MAF, and in forest fires in ASIA and LAM. Figure 3.9 displays the evolution of the spatial distribution of forest fires based on AIM (RCP 6.0) outputs.

### **3.4. Anthropogenic Emissions, 1850-2050**

This section presents an overview of important past, present, and future anthropogenic emission trends for those compounds relevant for hemispheric transport of air pollution, using emission datasets described in section 3.2. Historic and future projected emissions covering the period 1850-2050 are illustrated in line graphs for eight pollutants in Figures 3.10 – 3.17 for each of the four HTAP source regions (see Figure 1.2 in chapter A1) and globally. Projected emissions represent four RCP future scenarios (2.6, 4.0, 6.0, and 8.5) out to 2050 (see section 3.2.3). These historic and future emission datasets include agricultural waste burning, land use change, and savannah burning.

In addition, Figures 3.10 – 3.17 include bar charts that show emissions from key source categories for each of the four HTAP regions and globally for the year 2000 from the EDGAR-HTAP and RCP inventories, for 2030 from the RCP 8.5 scenario, and for 2050 from the RCP 2.6 scenario. In the bar charts for the RCP scenarios, the following source categories are considered: energy, industrial and waste; air transport and shipping; land transport; solvents; residential; agriculture (including waste burning); savannah burning; and land-use change. The EDGAR-HTAP inventory includes emissions from biomass burning (including agricultural waste burning), but does not include emissions from savannah burning or land use change (deforestation fires and biogenic emissions).

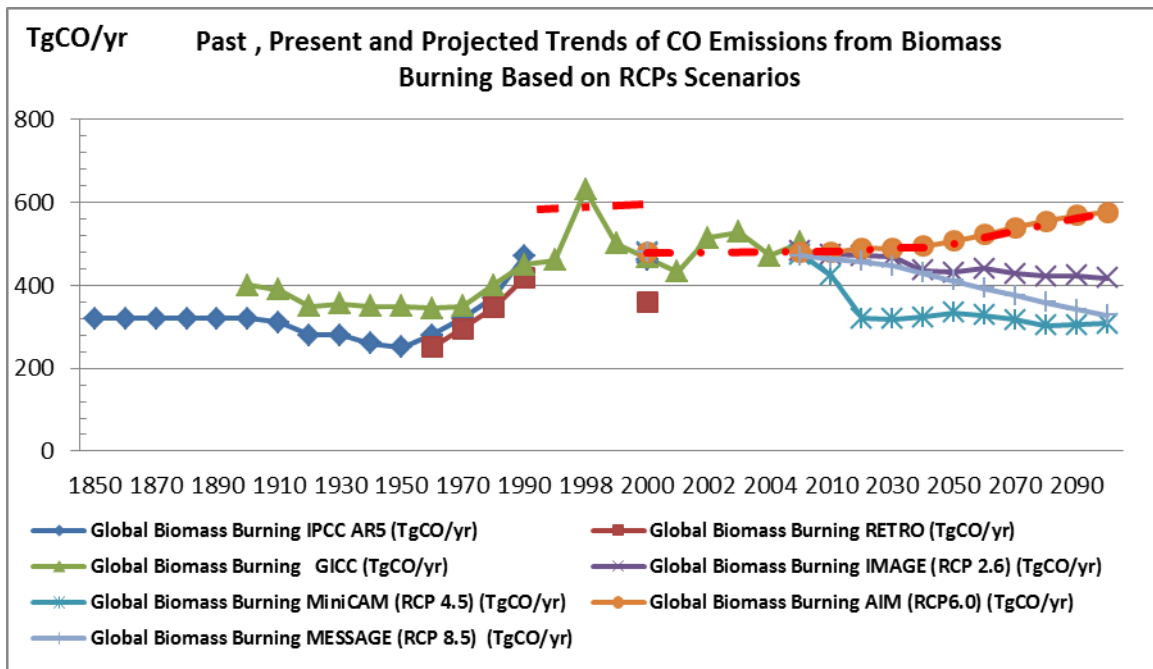


**Figure 3.7.** Past, present and projected future trends of CO emissions from biomass burning (forest fires, savannah burning and agricultural residues in field burning) based on RCP scenarios. Past trends are compiled from Lamarque et al. [2010] for IPCC AR5, Mieville et al. [2010] for GICC, and Schultz et al. [2008] for RETRO. Future projections are retrieved from the RCP database ([www.iiasa.ac.at/web-apps/tnt/RcpDb/](http://www.iiasa.ac.at/web-apps/tnt/RcpDb/)). The red dashed line represents the moving average trend line of future projections of global biomass burning emissions resulting from AIM (RCP 6.0) underlying the capture of past trends by this emission model.

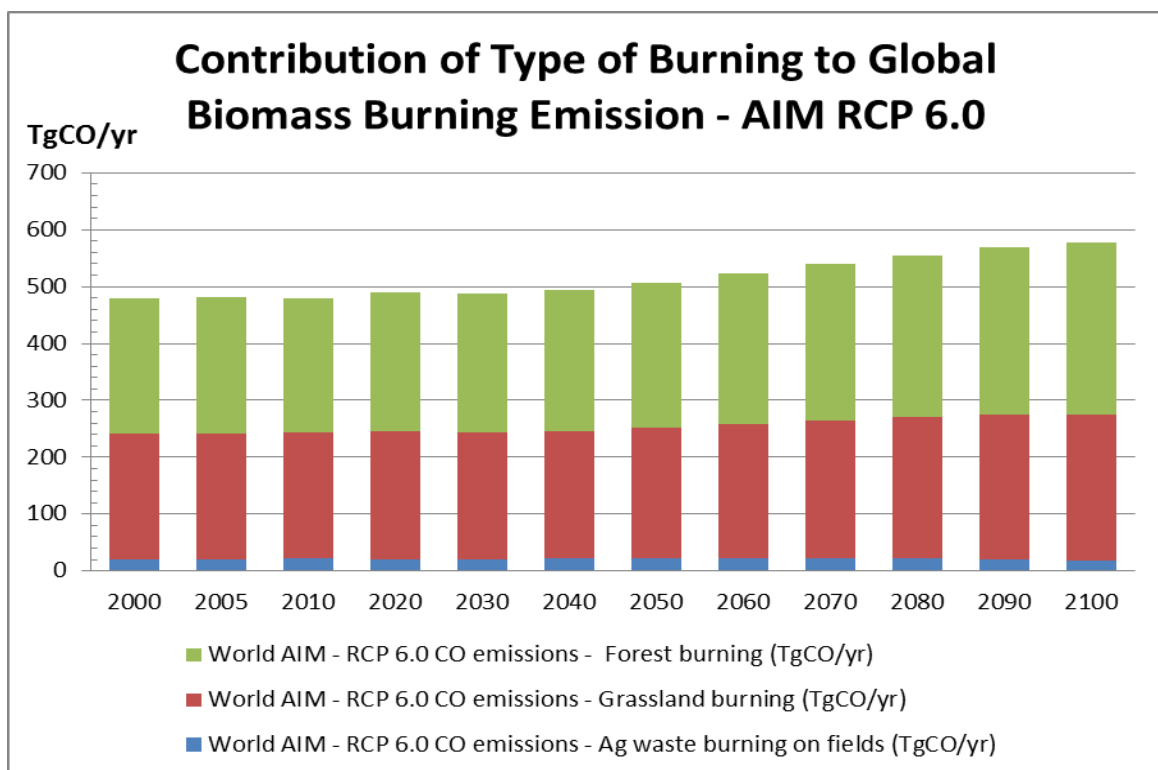


**Figure 3.8.** Contribution of type of burning to global biomass burning (forest fires, savannah burning, and agricultural residues in field burning) emission based on AIM RCP 6.0 dataset ([www.iiasa.ac.at/web-apps/tnt/RcpDb/](http://www.iiasa.ac.at/web-apps/tnt/RcpDb/)).

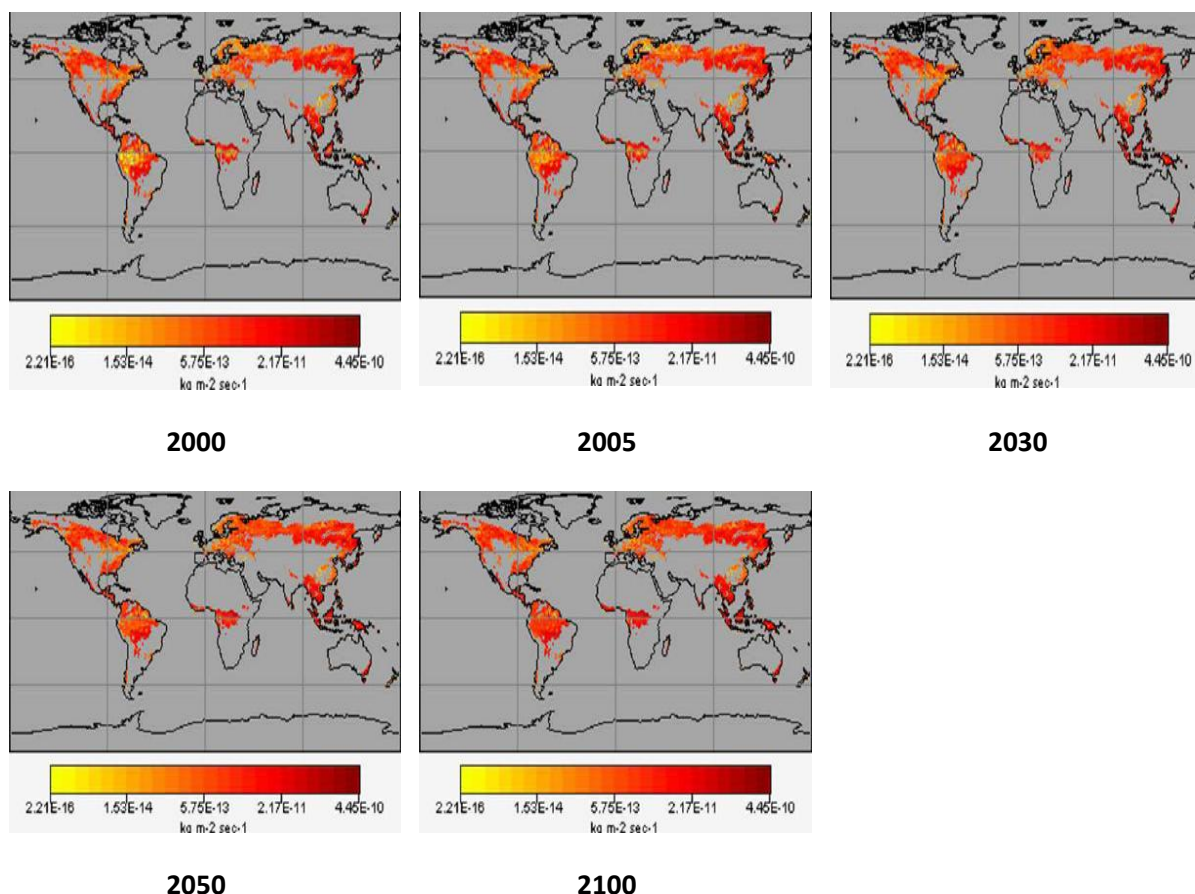


**Figure 3.9.** Evolution of the spatial distribution of  $\text{NO}_x$  ( $\text{kg m}^{-2} \text{sec}^{-1}$ ) emissions from forest fires in 2000, 2005, 2030, 2050 and 2100 based on AIM (RCP 6.0) datasets ([www.iiasa.ac.at/web-apps/tnt/RcpDb/](http://www.iiasa.ac.at/web-apps/tnt/RcpDb/)).

It is not possible in the space available to go into a detailed assessment of the driving forces for the future trends and their relationship to events that have occurred in the distant and recent past. One general characteristic of the recent trends is the dramatic decreases, often discontinuities, in emissions in Europe and North America between 1980 and 2000, as a result (in part) of environmental pressure/legislation, coupled with the economic turndown, especially in Eastern Europe. Major interventions such as these are not expected in the future and cannot therefore be incorporated into future scenario descriptions. Trends are in some sense fatalistic in the way they extrapolate current situations. Climate-related scenarios such as the RCPs cannot consider the potential for such discontinuities, which may be the consequence of and political response to the environmental pressures that are actually described in the scenario.

### 3.4.1. $\text{SO}_2$ emission trends

Global  $\text{SO}_2$  emissions steadily increased from 1850 to 1950, as shown in Figure 3.10. Following 1950 there was a rapid rise in emissions which peaked about 1980. From 1980-2000, global emissions dropped about 20%, due to emission reductions in Europe and, to a lesser extent, reductions in North America. Emissions were dominated by Europe and North America until 2000 when East Asian emissions became roughly equal to emissions from Europe or North America. Global  $\text{SO}_2$  emissions steadily decline after 2005 and by 2050 are 30, 50 or 70% less than year 2000 levels, depending on RCP scenario. Emissions in Europe and North America steadily decline by 60-90% from year 2000 levels by 2050. Depending on the RCP scenario, East Asia emissions peak in 2005, 2010, 2020 or 2040 and then sharply decline. The energy, industrial and waste sectors dominate global  $\text{SO}_2$  emissions (accounting for 70-75%) in all three periods (2000, 2030 and 2050). By 2050, global emissions in the energy, industrial and waste sectors decline over 70%. A steep decline in



emissions from the energy, industrial and waste sectors is projected for Europe and North America beginning 2000-2030. In Asia, however, emissions from the energy, industrial and waste sectors rise from 2000 to 2030 and then fall. In East Asia, a very steep decline (80%) is projected for the energy, industrial and waste sectors in the 2030-2050 period. Emissions from air transport and shipping are reduced over 90% by 2050 in all regions. Residential emissions are sharply decreased in East Asia, Europe and North America (about 90%), but are projected to increase in South Asia.

#### *3.4.2. NO<sub>x</sub> emission trends*

Global NO<sub>x</sub> emissions steadily increased from 1850 to 1940, as shown in Figure 3.11. After 1940 there was a rapid rise in emissions until 1990. After peaking in 2005 or 2010, global NO<sub>x</sub> emissions decline about 25% by 2050 compared to year 2000, except in RCP 8.5, in which emissions peak in 2020 and decline only about 10% by 2050. The majority of global emissions were from Europe and North America until 2000. Emissions from Europe and North America are shown to have peaked in 1990 and 2005, respectively. By 2050, emissions in Europe and North America are projected to decline from 2000 levels by 30-50% and by 50-70%, respectively. East Asia emissions peak in 2010, 2020, or 2040, depending on RCP scenario and then decline. Emissions from South Asia begin to decline in the 2040-2050 timeframe. Global NO<sub>x</sub> emissions are dominated by three categories in 2000-2030: energy, industrial and waste, air transport and shipping, and land transport (collectively 70-75% of total global emissions). Global emissions increase from 2000-2030 primarily due to increases in the energy, industrial and waste category especially from Asia, despite reductions in Europe and North America in the same category. Global emissions decline from 2030 to 2050 almost entirely due to a steep decline in land transportation emissions; other source groups are expected to have only small changes.

#### *3.4.3. VOC emission trends*

Global VOC emissions gradually increased from 1850 to 1940, as shown in Figure 3.12. Following 1940, there was a more rapid rise in global emissions, which initially peaked in 1990, slightly declined in 2000 and then increased. Depending on RCP scenario, global VOC emissions peak in 2010, 2030 or 2040 then decline. Overall, the global VOC emissions trend was mostly flat from 1980 to 2050. Emissions from Europe and especially North America gradually decline from 1980 levels through 2050. Large emissions from East Asia peak in 2010, 2020, 2030, or 2040, depending on RCP scenario. Emissions in South Asia continue to rise through 2050. Global VOC emissions are distributed fairly evenly over several source categories in the RCT scenarios shown in Figure 3.12. Of the eight categories, only air transport and shipping and agriculture are small. Global emissions show a small overall decline by 2050 due to reductions in the land transportation, land use and residential categories. One source category generally dominates emissions in a few regions; for example, energy, industry and waste in Europe and residential in South Asia. Other regions have significant emissions from several source categories.

#### *3.4.4. BC emission trends*

Global BC emissions gradually increased from 1850 to the early 2000s, although there was little change between 1910 and 1950, as shown in Figure 3.13. Between 1970 and 1980 there was a more rapid rise in global emissions, due largely to an emissions increase in East Asia. By 2050, global emissions are projected to decline from year 2000 levels by about 10% to 35%, depending on RCP scenario. Emissions in North America peaked in 1920, declined until 1960, were fairly constant through the early 2000s and then declined. Emissions in Europe peaked in 1910, were fairly constant from 1910-1980, and then gradually declined. Emissions in East Asia sharply increased from 1950 to 1990 and became larger than emissions from any other region for the period 2000 to 2040. Emissions in South Asia show a steady increase through at least 2020 and by 2050 are roughly equal to emissions from East Asia. Global BC emissions are projected to decline by 2050. This decrease is primarily due to decreases in emissions in the energy, industry and waste category, which account for 30% of the reductions shown from 2000 to 2050. There are also decreases in land transport emissions in Europe and North America and residential emissions in East Asia.

### 3.4.5. CH<sub>4</sub> emission trends

Global CH<sub>4</sub> emissions gradually increased from 1850 to 1950, as shown in Figure 3.14. Following 1950, there was a more rapid rise in global emissions, which initially peaked in 1990, slightly declined in 2000 and then increased. The future emissions projections vary greatly depending on RCP scenario. In the RCP 8.5 scenario, global CH<sub>4</sub> emissions rise rapidly from 2000 through 2050, increasing 125%. In RCP 4.5 and 6.0, global emissions show a modest increase of about 15% from 2000 levels. In RCP 2.6, global emissions peak in 2010 then decline by almost 40% from 2000 levels in 2050. All regions show a similar trend as in the global case: a gradual historic increase peaking in 1990, large projected increases in RCP 8.5 and significant decreases in RCP 2.6. In RCP 4.5 and 6.0 scenarios, changes are smaller but can be increases or decreases, depending on region. Emissions from East and South Asia show the steepest rise in emissions in RCP 8.5. Between 2010 and 2020 there is a large decline in emissions globally due to decreases in East Asia and North America in RCP 2.6. Global CH<sub>4</sub> emissions are dominated by two categories: agriculture and energy, industry and waste. Global emissions from these two categories account for over 80% of total global emissions throughout 2000-2050 and were of similar magnitude in year 2000. Global emissions increase nearly 70% from 2000 to 2030 then sharply decline from 2030 to 2050 to nearly 40% less than year 2000 emissions. These global emission changes primarily reflect changes in emissions from the energy, industry and waste sector. All regions show a similar pattern of overall increases in emissions in 2030 and decreases from 2030-2050 due to changes in agriculture and especially energy, industry and waste.

### 3.4.6. CO emission trends

Global CO emissions gradually increased from 1850 to 1940, as shown in Figure 3.15. Following 1940, there was a more rapid rise in global emissions which peaked in 1990. Depending on RCP scenario, global emissions peak in 1990, 2005, or 2020 then decline. From 2000-2050, the global CO emissions trend shows modest decreases of 15-20% in all scenarios, except RCP 6.0 which showed less than a 5% reduction. The largest emitting region shifts from North America to East Asia from about 1990 to 2020. Depending on RCP scenario, the largest emitting region is either East Asia or South Asia from 2030-2050. Global CO emissions are significant in several source categories. Of the eight categories shown, only air transport and shipping, agriculture, and solvents are small. Global emissions show about a 25% decline by 2050 due primarily to reductions in the land transportation category with smaller decreases in land use and energy, industry, and waste. Emission trends in savannah burning and residential are flat.

### 3.4.7. NH<sub>3</sub> emission trends

Global NH<sub>3</sub> emissions gradually increased from 1850 to 1940, as shown in Figure 3.16. Following 1940, there was a more rapid rise in global emissions, which initially peaked in 1990, slightly declined in 2000 and then gradually increased through 2050. By 2050, global emissions are projected to increase from year 2000 levels by about 15-45%, depending on RCP scenario. Emissions are projected to increase by 2050 in all regions, although the amount of increase varies considerably by region and RCP scenario, ranging from a less than 5% decrease in Europe in RCP 4.5 to an over 100% increase in South Asia in RCP 2.6. The larger emitting regions in the 21<sup>st</sup> century are East Asia, Europe, and South Asia. Global NH<sub>3</sub> emissions are dominated by agriculture. Agriculture accounts for about 75-85% of total global emissions throughout 2000-2050. Global emissions increase over 30% from 2000 to 2030 due to a 45% increase in emissions from agriculture, then increase more gradually from 2030 to 2050 to about 40% above year 2000 global emissions.

### 3.4.8. OC emission trends

Global OC emissions gradually increased from 1850 to the early 2000s, as shown in Figure 3.17. After 2005 or 2020, global emissions are projected to decline in 2050 from year 2000 levels by about 20%, except in RCP 6.0 which shows a slight increase. Emissions in Europe peaked in 1940 then gradually declined through 2000. Emissions in North America peaked in 1870-1920 and were nearly constant 1960-2000. By 2050, emissions in Europe and North America are projected to decline

from year 2000 levels by 30-70% and 15-45%, respectively. From about 1980 to 2030, the largest emissions region is East Asia. Emissions in South Asia steadily increase and by 2040 are roughly equal to emissions from East Asia. Global OC emissions are projected to decline by 2050. This decrease is primarily due to decreases in emissions in the energy, industry and waste category, which account for 30% of the reductions shown from 2000 to 2050. There are also decreases in land transport emissions in Europe and North America and residential emissions in East Asia.

**FINDING:** A long-term dataset of major anthropogenic emissions from 1850-2100 at  $0.1^\circ \times 0.1^\circ$  spatial resolution is now available for use in chemical transport models to probe the changing nature of intercontinental transport over time. Historical and recent emissions are built on Lamarque et al. [2010] and EDGAR-HTAP. Future emissions use the IPCC AR5 Representative Concentration Pathway (RCP) scenarios, which embody an integrated view of the future drivers of emissions (socioeconomics, regulation, technology, and climate policy).

**RECOMMENDATION:** Comparison of the EDGAR-HTAP emissions dataset used in this HTAP Assessment with other global and regional studies of past, present, and future emissions is needed to provide confidence in the estimates.

**FINDING:** Emission estimates for natural sources of emissions are not so well developed as for anthropogenic emissions. Emission “events” (forest fires, dust storms, volcanic eruptions, etc.) rely on remote sensing and other techniques that are only available for the recent past (last decade or two). Long-term trends in natural source emissions are not well understood.

**RECOMMENDATION:** New techniques need to be developed to simulate episodic emissions of natural species for the past and future. Long-term average trends in such emissions (century-scale) also require additional work.

**FINDING:** Even though a basic understanding of the direct emissions from natural sources has been achieved in recent years, aided by satellite observations of global ecosystems, they are usually treated as stable inputs, unaffected by events taking place around them.

**RECOMMENDATION:** A more holistic view of natural emissions in the context of changing environments and climate modification needs to be developed. We can no longer treat natural emissions as unchanging over time. Environmental changes that affect natural emissions need greater emphasis. These include, for example, land-use changes that affect CH<sub>4</sub> emissions, precipitation changes that affect biomass burning and mineral dust releases, and temperature changes that affect biogenic NMVOC releases, soil NO<sub>x</sub>, lightning NO<sub>x</sub>, etc.

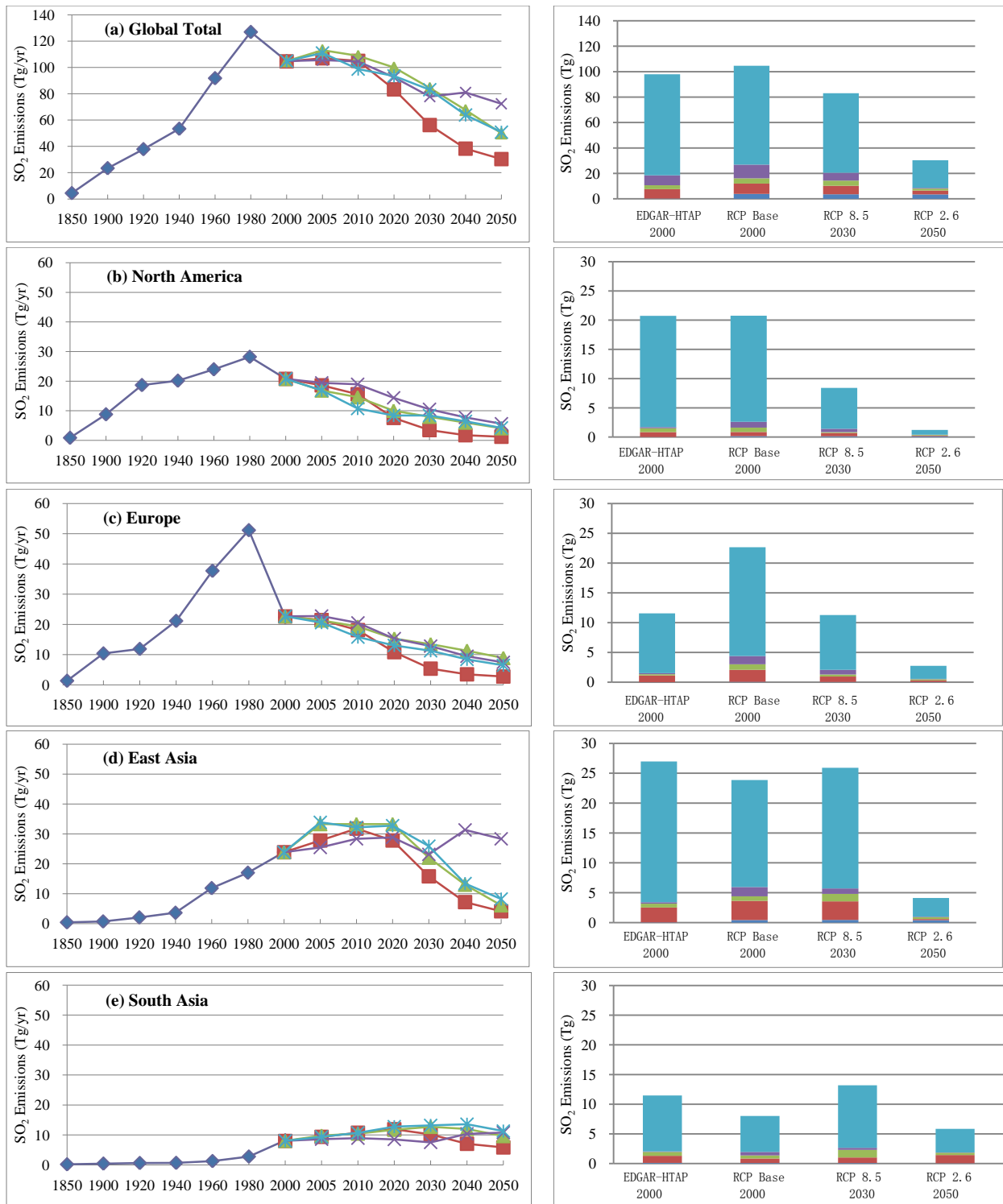


**Figure 3.10.** SO<sub>2</sub> emissions regional trends, future predictions, and sources. Emission trends from 1850-2050 and four RCP scenarios from 2000-2050 are shown for the global total and for the four source regions from the HTAP multi-model experiments [left column]. For each region, sources of SO<sub>2</sub> are shown for the 2000 EDGAR-HTAP inventory, the 2000 RCP base case, the 2030 RCP 8.5 scenario, and the 2050 RCP 2.6 scenario [right column].

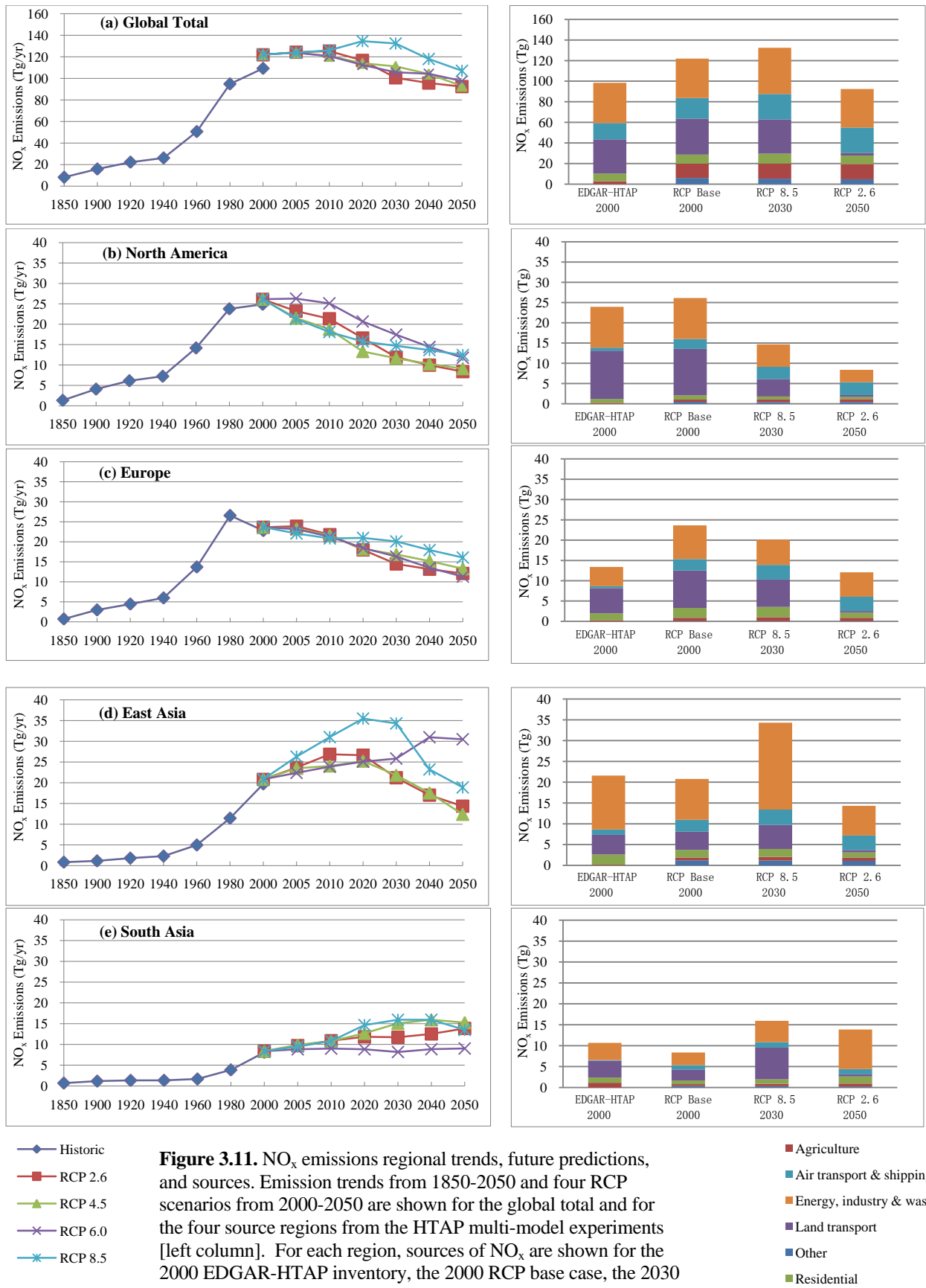


**Figure 3.11.** NO<sub>x</sub> emissions regional trends, future predictions, and sources. Emission trends from 1850-2050 and four RCP scenarios from 2000-2050 are shown for the global total and for the four source regions from the HTAP multi-model experiments [left column]. For each region, sources of NO<sub>x</sub> are shown for the 2000 EDGAR-HTAP inventory, the 2000 RCP base case, the 2030 RCP 8.5 scenario, and the 2050 RCP 2.6 scenario [right column].

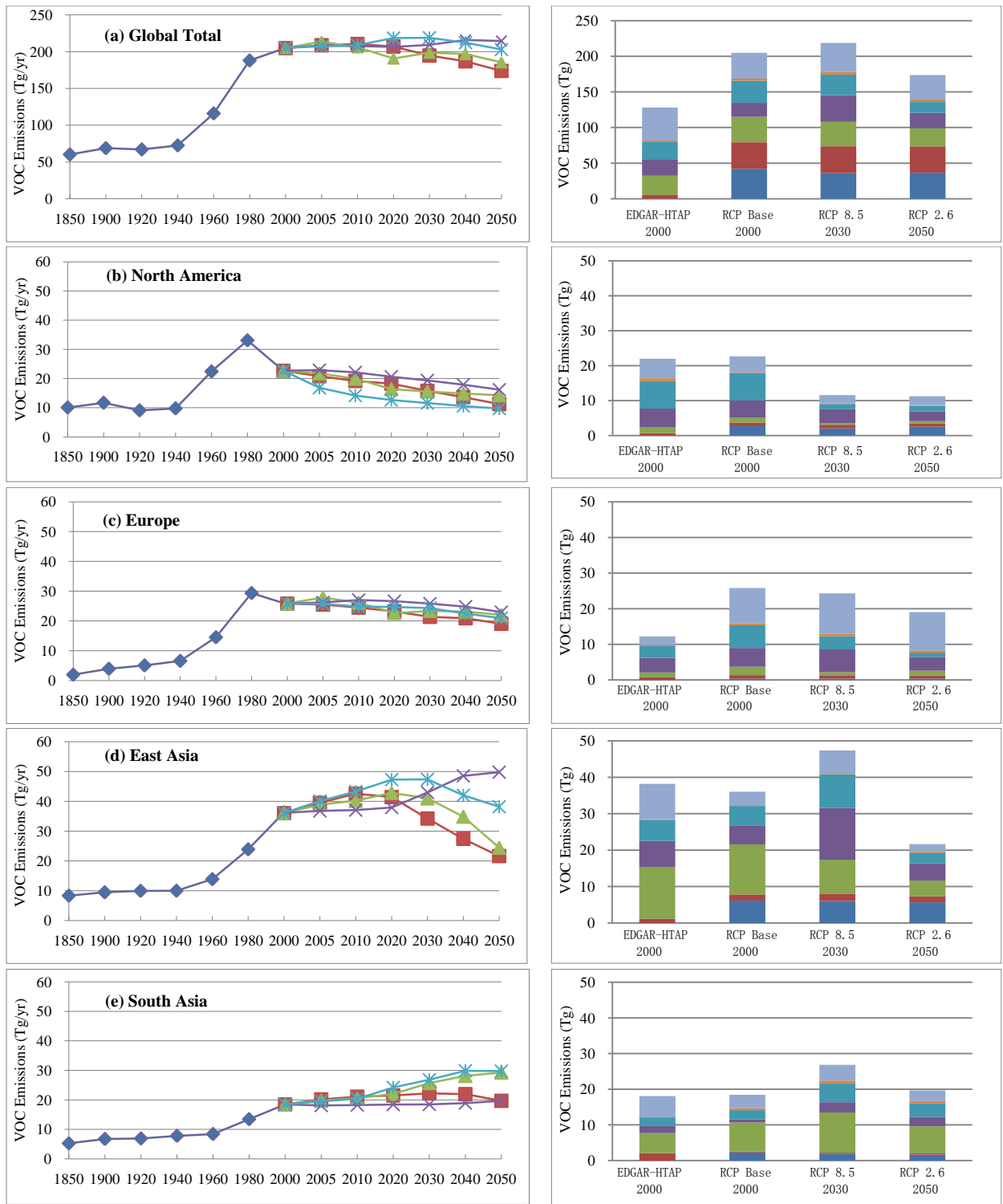


**Figure 3.12.** VOC emissions regional trends, future predictions, and sources. Emission trends from 1850-2050 and four RCP scenarios from 2000-2050 are shown for the global total and for the four source regions from the HTAP multi-model experiments [left column]. For each region, sources of VOC are shown for the 2000 EDGAR-HTAP inventory, the 2000 RCP base case, the 2030 RCP 8.5 scenario, and the 2050 RCP 2.6 scenario [right column].

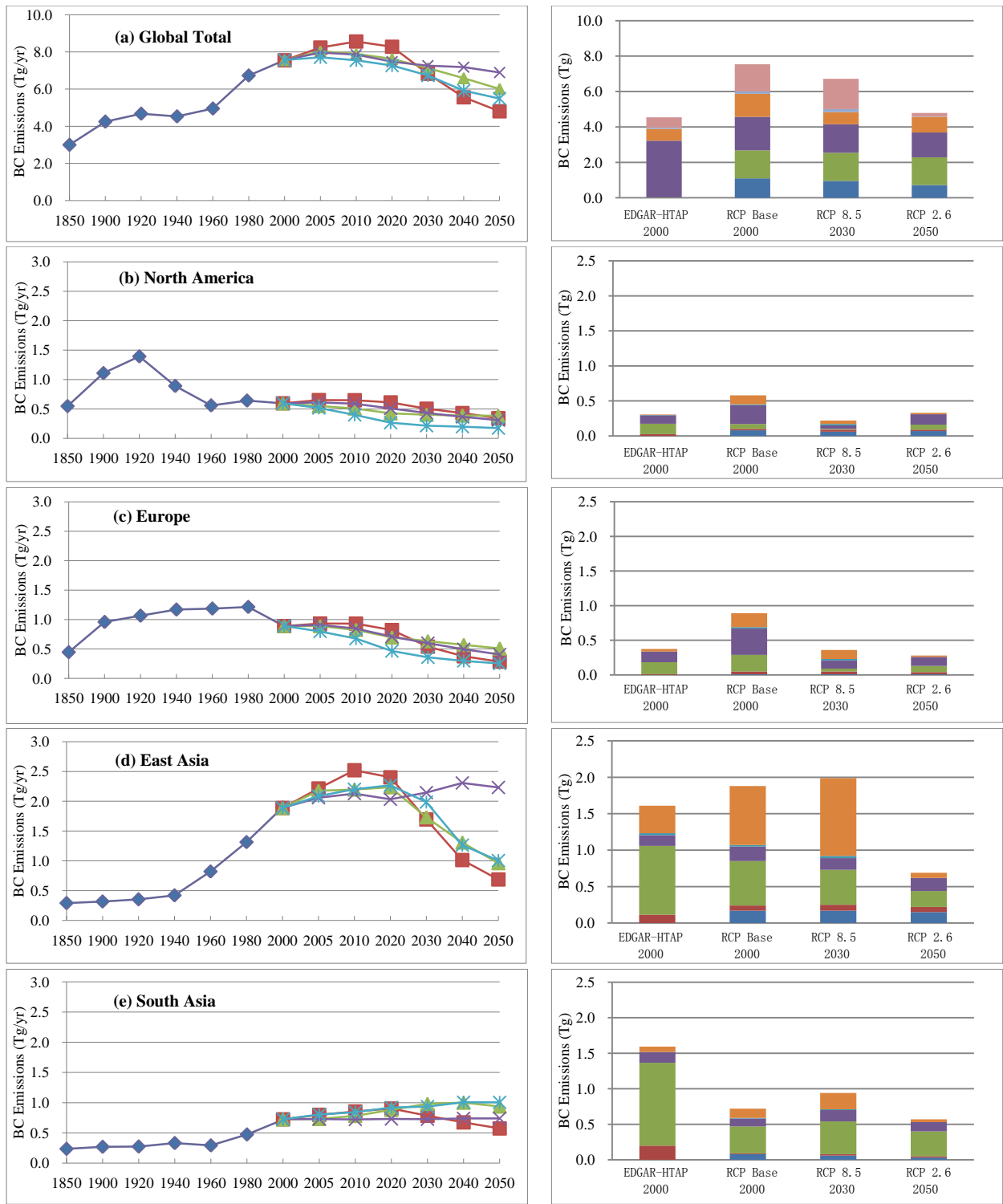


**Figure 3.13.** BC emissions regional trends, future predictions, and sources Emission trends from 1850-2050 and four RCP scenarios from 2000-2050 are shown for the global total and for the four source regions from the HTAP multi-model experiments [left column]. For each region, sources of BC are shown for the 2000 EDGAR-HTAP inventory, the 2000 RCP base case, the 2030 RCP 8.5 scenario, and the 2050 RCP 2.6 scenario [right column].

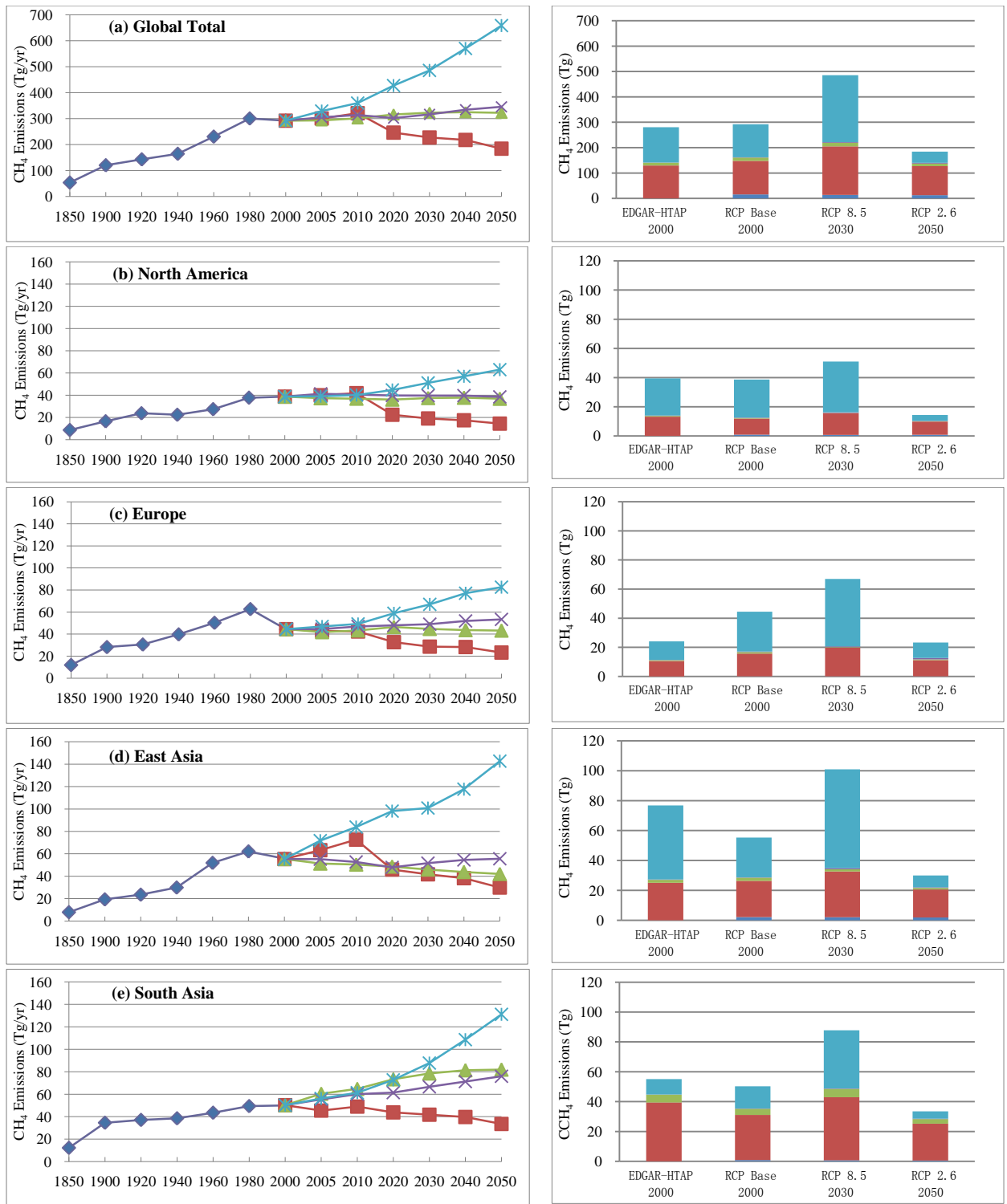


**Figure 3.14.** CH<sub>4</sub> emissions regional trends, future predictions, and sources. Emission trends from 1850-2050 and four RCP scenarios from 2000-2050 are shown for the global total and for the four source regions from the HTAP multi-model experiments [left column]. For each region, sources of CH<sub>4</sub> are shown for the 2000 EDGAR-HTAP inventory, the 2000 RCP base case, the 2030 RCP 8.5 scenario, and the 2050 RCP 2.6 scenario [right column].



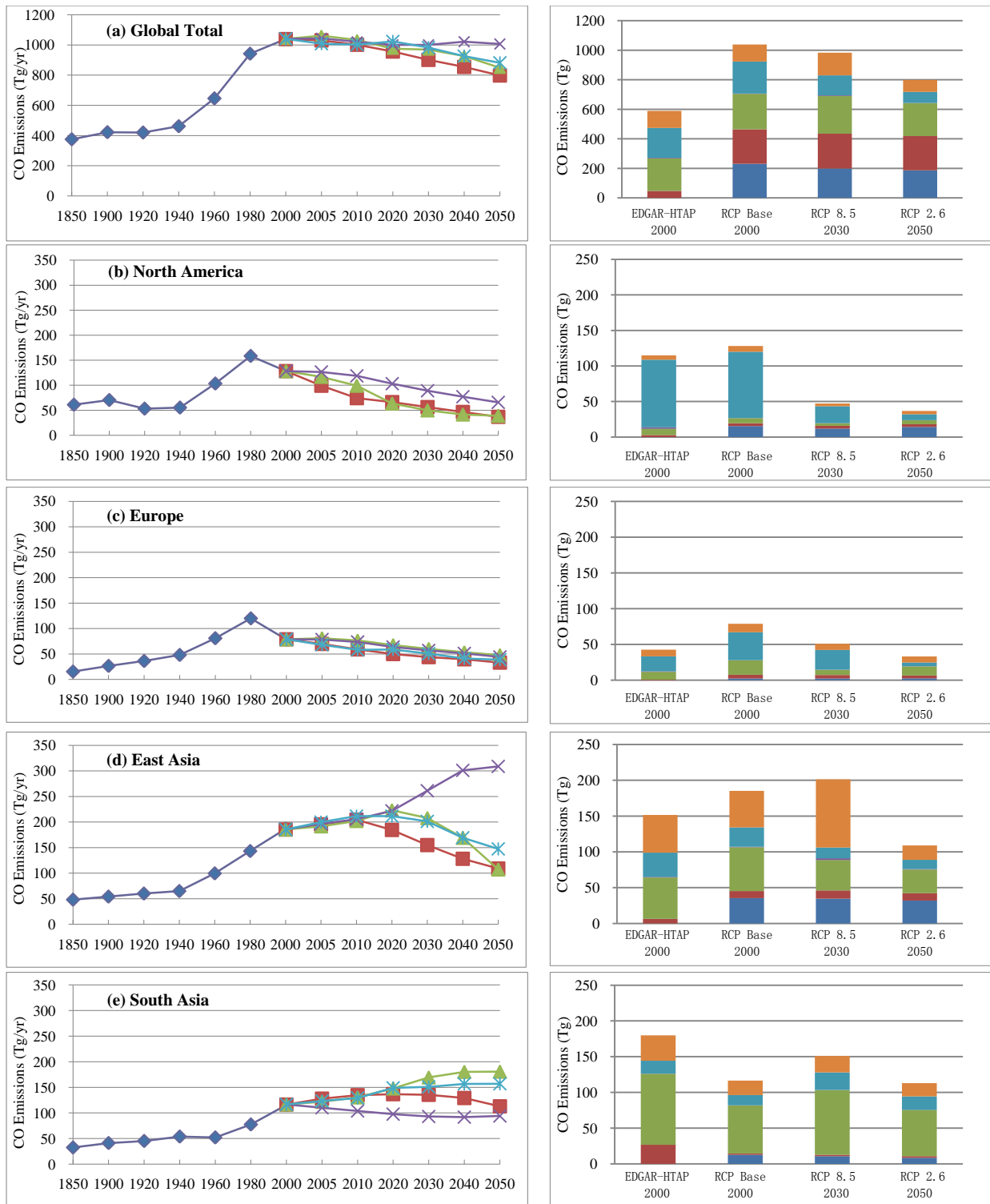


**Figure 3.15.** CO emissions regional trends, future predictions, and sources. Emission trends from 1850-2050 and four RCP scenarios from 2000-2050 are shown for the global total and for the four source regions from the HTAP multi-model experiments [left column]. For each region, sources of CO are shown for the 2000 EDGAR-HTAP inventory, the 2000 RCP base case, the 2030 RCP 8.5 scenario, and the 2050 RCP 2.6 scenario [right column].

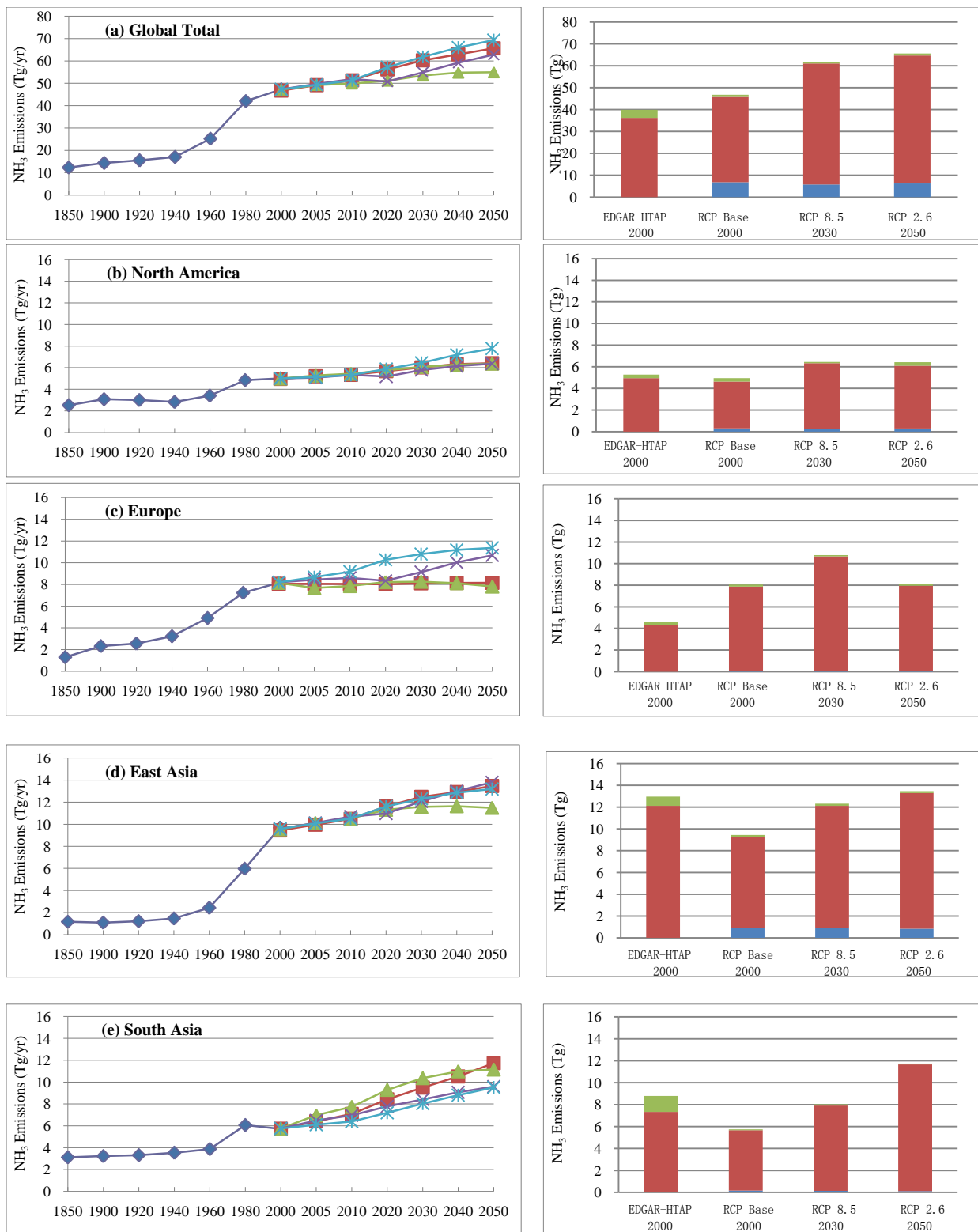


**Figure 3.16.** NH<sub>3</sub> emissions regional trends, future predictions, and sources. Emission trends from 1850-2050 and four RCP scenarios from 2000-2050 are shown for the global total and for the four source regions from the HTAP multi-model experiments [left column]. For each region, sources of NH<sub>3</sub> are shown for the 2000 EDGAR-HTAP inventory, the 2000 RCP base case, the 2030 RCP 8.5 scenario, and the 2050 RCP 2.6 scenario [right column].

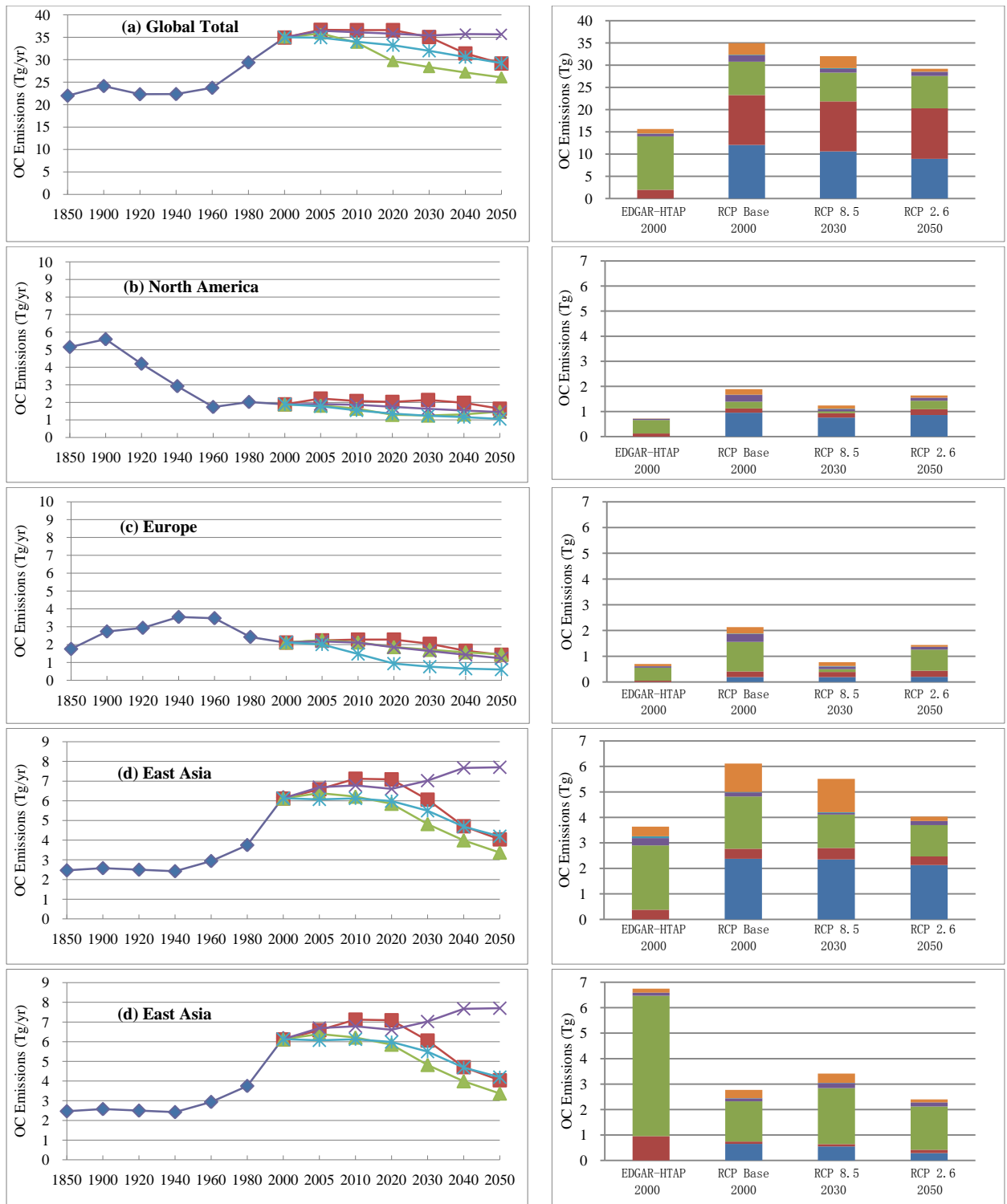


**Figure 3.17.** OC emissions regional trends, future predictions, and sources. Emission trends from 1850-2050 and four RCP scenarios from 2000-2050 are shown for the global total and for the four source regions from the HTAP multi-model experiments [left column]. For each region, sources of OC are shown for the 2000 EDGAR-HTAP inventory, the 2000 RCP base case, the 2030 RCP 8.5 scenario, and the 2050 RCP 2.6 scenario [right column].

### 3.5. Evaluation of differences in emissions data: case study for Asia

Anthropogenic emissions in Asia are larger than those in Europe and North America combined and are expected to continue to increase in the future [Akimoto, 2003]. In fact, recent tropospheric satellite observations have demonstrated that NO<sub>x</sub> emissions in China have accelerated dramatically since 2000 [Irie *et al.*, 2009; Richter *et al.*, 2005; van der A *et al.*, 2006; Zhang *et al.*, 2007]. In light of this situation, the development, improvement, and verification of Asian emission inventories for the past, present, and future are very important for the understanding and management of the regional and global atmospheric environment. In the last few years a number of authors reassessed their emission inventories and future projections for Asia. Different regional emission inventories for air pollutants in Asia are compared in this section. Figures 3.18 and 3.19 compare emissions for Asia and China from 1980 to 2030, according to the emission inventories for SO<sub>2</sub>, NO<sub>x</sub>, and BC that are most widely used today: GAINS [Klimont *et al.*, 2009], REAS [Ohara *et al.*, 2007], INTEX-B [Zhang *et al.*, 2009a] and others. The older IPCC SRES and newer RCP scenario values for Asia are also considered.

#### 3.5.1. Recent emission trends, 1980-2006

##### *Sulphur dioxide*

Historical estimates of SO<sub>2</sub> emissions in Asia show a similar pattern in all studies, although the absolute values vary greatly. According to the REAS inventory, total emissions of SO<sub>2</sub> in Asia increased from 1980 to 1996, but subsequently decreased till 1999, reflecting a decrease in fuel consumption due to the Asian economic crisis; after 2000 SO<sub>2</sub> emissions increased at a phenomenal rate. They increased by 2.2 times in the period 1980–2003, and, notably, by 3.2 times in India and 2.5 times in China [Ohara *et al.*, 2007]. For SO<sub>2</sub> emissions in 2000 in Asia, the GAINS value (34.9 Mt) was almost the same as the INTEX-B value (35.5 Mt) but lower than REAS (41.2 Mt). However, for 2006 the GAINS value (48.1 Mt) for 2005 is similar to the INTEX-B value (47.0 Mt) for 2006. For SO<sub>2</sub> emissions in 2000 (in 2001 for INTEX-B) for China, the GAINS value (23.2 Mt) was almost the same as the INTEX-B value (22.9 Mt) but higher than the SEPA estimate (20.0 Mt) [State Environmental Protection Administration of China, Beijing, 2003] and lower than REAS (27.6 Mt). Similarly, for 2005 (in 2006 for INTEX-B), the relative order in emissions is similar to that for 2000 and the maximum difference is almost 30%: GAINS (34.6 Mt), INTEX-B (31.0 Mt), SEPA (25.9 Mt). The main reason is the differences in the fuel consumption values used in each inventory [Ohara *et al.*, 2007] and the differences in the impacts of emission control [see Klimont *et al.*, 2009; Zhang *et al.*, 2009a]. The overall trends of Chinese SO<sub>2</sub> emissions for the period 1990 to 2006 are similar among REAS, GAINS, SEPA and Streets *et al.* [2001; 2003] and also similar to INTEX-B. Before 2000, the REAS variation corresponded to that of Streets *et al.* [2001; 2003]. The variation in SEPA [2003] was similar to that in REAS during 1986–1994 but about 7 Mt yr<sup>-1</sup> lower. In contrast, there were large differences between SEPA and REAS in the decreasing trend of SO<sub>2</sub> emissions during 1995 and 2000, reflecting the differences in coal consumption in each inventory [Akimoto *et al.*, 2006].

##### *Nitrogen oxides*

For the Asian total NO<sub>x</sub> emissions for 2000 and 2005, the values of REAS, GAINS, and INTEX-B (for 2001 and 2006, respectively) are within a 10% variance (25.1–26.1 Mt for 2000, 32.9–36.8 Mt for 2005). For Chinese NO<sub>x</sub> emissions for 2000, the values of REAS (11.2 Mt), GAINS (11.7 Mt), and Tian *et al.* (2005; 11.9 Mt) were almost the same, whereas the INTEX-B value for 2001 (13.4 Mt) was higher than the values of other inventories. In a more recent year, the REAS value (19.2 Mt for 2005) was almost the same as the INTEX-B value (20.8 Mt for 2006), whereas the GAINS value (16.9 Mt for 2005) was almost 10% lower than the REAS value. Total emissions of NO<sub>x</sub> in Asia showed a monotonic increase between 1980 and 2006 with no dips, in contrast to the pattern of SO<sub>2</sub> emissions. According to the REAS inventory, the emissions increased by a factor of 3.5 from 1980–2005, with values of 10.7 Mt in 1980 and 35.0 Mt in 2005. In particular, Chinese NO<sub>x</sub> emissions increased dramatically by 5.0 times from 1980 to 2005, with the higher growth after 2000

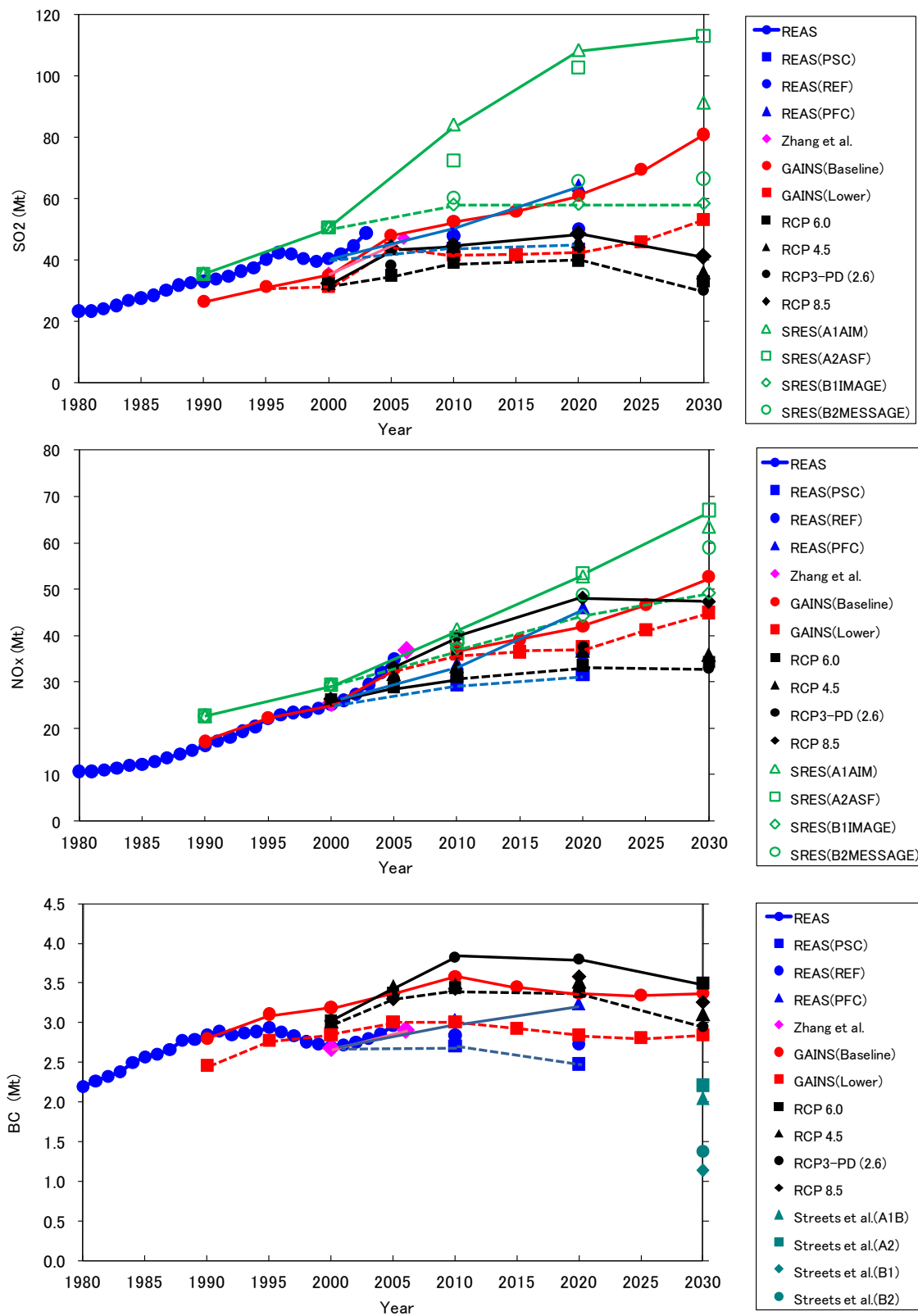


**Figure 3.18.** Time series of SO<sub>2</sub>, NO<sub>x</sub>, and BC emissions in Asia.

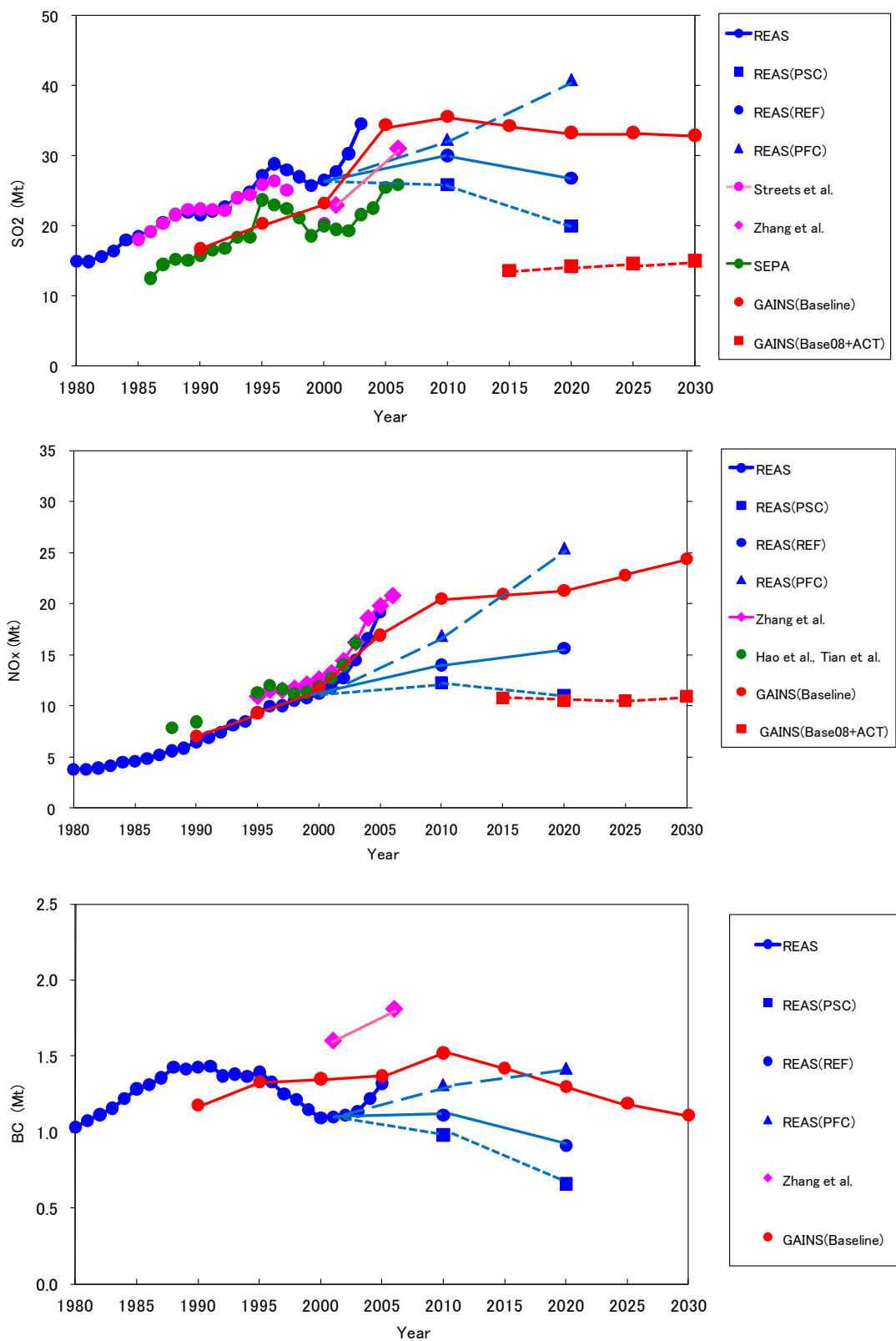


**Figure 3.19.** Time series of SO<sub>2</sub>, NO<sub>x</sub>, and BC emissions in China.

(by 1.7 times over only 5 years [Ohara *et al.*, 2007]). These trends in China's NO<sub>x</sub> emissions in REAS were consistent with those in other inventories, including GAINS, INTEX-B, and Chinese researchers' results [Hao *et al.*, 2002; Tian *et al.*, 2005]. Zhang *et al.* [2007] compared a 10-year regional trend of NO<sub>x</sub> emissions in China from 1995 to 2004 with the NO<sub>2</sub> column trends observed from GOME and SCIAMACHY. The results showed that China's NO<sub>x</sub> emissions increased by 70% during 1995-2004. NO<sub>x</sub> emissions and satellite-based NO<sub>2</sub> columns show agreement in temporal evolution. However, the growth rate from the emission inventory is lower than that from the satellite observations, especially in wintertime. The reasons for the discrepancy cannot yet be identified.

### **Black Carbon**

The Asian emission inventory for BC demonstrates that the emissions from China and India were dominant, as they were for SO<sub>2</sub> and NO<sub>x</sub> emissions. Residential consumption of biofuel and coal was the dominant contributor to BC emissions. For the Asian total BC emissions in 2000, the GAINS value (3.19 Mt) was higher than INTEX-B (2.68 Mt) and REAS (2.70 Mt). This feature is similar to that for 2005 (or 2006): (GAINS (3.36 Mt), INTEX-B (2.91 Mt), and REAS (2.96 Mt)). The estimates of Asian emissions for 1996 in the global carbonaceous particle inventories [Bond *et al.*, 2004; Streets *et al.*, 2004] were 2.65 Mt (central value), which corresponds to 2.88 Mt for 1996 in REAS. In contrast, the value of China's BC emissions is much different between inventories: emissions estimated for 2000 by REAS (1.09 Mt) were lower than those of GAINS (1.35 Mt) and much lower than those of INTEX-B (1.60 Mt) for 2001. On the other hand, China's BC emissions in 2005 (or 2006) of REAS (1.32 Mt) were quite similar to those of GAINS (1.37 Mt) but lower than those of INTEX-B (1.81 Mt) for 2006. The Indian BC emissions for 2000 as estimated by REAS (0.80 Mt) were the same as those of Dickerson *et al.* [2002], which were based on the INDOEX (Indian Ocean Experiment) observations, and were almost same as those of GAINS (0.84 Mt), but higher than those of TRACE-P (0.52 Mt). For Indian emissions in about 1995, the GAINS value (0.77 Mt) and the REAS value (0.79 Mt) are close to the 0.83 Mt (central value; range 0.31–1.94 Mt) estimated by Parashar *et al.* [2005], but higher than the values of 0.31 Mt by Reddy and Venkataraman [2002] and 0.48 Mt (central value; range 0.31–1.04 Mt) by Bond *et al.* [2004]. For Indian BC emissions in 2005 (or 2006), the value of GAINS (1.03 Mt) was higher than that of REAS (0.79 Mt) and much higher than that of INTEX-B (0.34 Mt) for 2006. It should be noted that the estimated BC emissions are highly variable because of the high uncertainties in residential fuel consumption (especially biofuels) and their emission factors [Bond *et al.*, 2004]; uncertainties are typically much higher than for SO<sub>2</sub> and NO<sub>x</sub>. Total BC emissions in Asia increased by 1.04 times and 1.20 times in REAS and GAINS, respectively, over the period 1990–2005. After 2000 the increases from 2000 to 2005 (for INTEX-B, from 2001 to 2006) are 1.05 times (GAINS), 1.09 times (INTEX-B), and 1.10 times (REAS). These increases are caused by the increases of emissions in China and India. The GAINS results show that the increase in BC emissions from 1990 to 2005 in India was highest (1.47 times), but that in China was comparatively small (1.16 times).

#### **3.5.2. Future scenarios to 2030**

Projected emissions depend strongly on the underlying assumptions of the emission scenarios. In this section, we compare forecasts of future emissions in various scenarios for Asian countries: GAINS [Klimont *et al.*, 2009], REAS [Ohara *et al.*, 2007], SRES [IPCC, 2000], RCP (see section 3.2.3), and Streets *et al.* [2004]. Recently, IIASA [Klimont *et al.*, 2009] developed mid-term (to 2030) scenarios of air pollutant emissions in Asia with the GAINS model. They presented a set of Asian emission projections for SO<sub>2</sub>, NO<sub>x</sub>, BC, and OC during the period 1990–2030. For the future evolution of emission factors, they developed two projections simulating varying levels of the implementation of air pollution legislation. These define upper (baseline) and lower (very optimistic assumptions about implementation of legislation) bounds for the presented GAINS projections. The projections based on the four representative SRES scenarios [IPCC, 2000] were used in the evaluation. For A1, the results of the AIM model were selected, for A2 the ASF model, for B1 the IMAGE model, and for B2 the MESSAGE model. Ohara *et al.* [2007] developed three REAS emission scenarios for 2010 and 2020 in China: Policy Failed Case (PFC), Reference (REF), and



Policy Succeed Case (PSC), which resemble the storylines presented by SRES A2, B2, and B1, respectively.

### ***Sulphur dioxide***

The future emission trends in Asia and China are compared for several inventories. The projected trends, of course, depend strongly on the emission scenarios provided by each researcher and reveal marked differences among projections. The decline of emissions in 2000 is not visible in SRES scenarios since they were developed before the data for the year 2000 were available. For this reason there are large differences among the four SRES scenarios, largely corresponding to different assumptions about coal consumption in China. The SRES B1 and B2 projections show moderate growth, because less coal increase is assumed, while the SRES A1 and A2 scenarios reproduce the observed stronger growth after 2000. After 2005 all of the scenarios show that growth in SO<sub>2</sub> emissions will slow down. Generally, all the projections of the SRES scenarios tend to estimate the upper values in the projection range of SO<sub>2</sub> emissions, since the SRES scenarios tend to underestimate the impact of control technologies. In contrast, all projections of the RCP scenarios show very similar results, indicating lower growth and lower absolute emission levels throughout the projection period and the common peak of emissions in 2020. The growth rates for the REAS PFC, REF, and PSC scenarios are similar to those of the SRES A2, B2, and B1, respectively. The GAINS scenarios show a very similar range to REAS, between 40 and 60 Mt in 2020. While the upper value in GAINS (GAINS baseline) is similar to the REAS PFC, the lower bound in GAINS (GAINS optimistic case) is almost same as the REAS PSC. As for the future emission trends in China, the projection of the GAINS baseline gives an upper estimate of the projection range, though the projected growth of the REAS PFC scenario is highest for the period 2010-2020. The GAINS ACT case (“Baseline08 + ACT” in the <http://gains.iiasa.ac.at/index.php/gains-asia>; ACT means “Advanced Combustion Technology”) projects a minimum value in the range for the period 2015-2030.

### ***Nitrogen oxides***

The projected trends reveal differences among projections, compared with the small differences among estimates for the years before 2006. Although all scenarios demonstrate a steady growth, there is a larger difference in the projections. Generally, all the projections of the SRES scenarios forecast a rapid growth of NO<sub>x</sub> emissions. In contrast, the three projections of the RCP scenarios, excluding RCP 8.5, show very similar results, indicating lower growth and lower absolute emission levels, and their values are almost the same in 2030. The GAINS baseline increases rapidly from 2000 to 2010, but then the impact of tighter legislation in the transportation sector leads to a slowdown in emissions [Klimont *et al.*, 2009]. The lower range of the GAINS forecasts shows the effect of the alternative energy scenario, where higher efficiency improvements and lower coal use is assumed [Klimont *et al.*, 2009]. The SRES B1 scenario and the GAINS baseline follow very similar trajectories throughout the period. Their growth and emission levels are similar to those for RCP 8.5 and REAS PFC scenarios. The lowest growth rates and lowest emission levels are estimated in the REAS PSC scenario; these estimates for the period 2000-2020 are similar to those of the three projections of the RCP scenarios (excluding RCP 8.5). In these cases the projected growth is moderate, which may be driven by lower fuel consumption and optimistic assumptions about the penetration and performance of control technologies. We also compared the future emission trends in China according to several inventories. The projection of the GAINS baseline gives an upper estimate of the projection range, though the projected growth of the REAS PFC scenario is highest for the period 2010-2020. The GAINS ACT scenario projects a minimum value in the range and gives estimates in 2020 similar to the REAS PSC scenario. It should be noted from Figure 3.19 that the dramatic growth for the period 2000-2006 in NO<sub>x</sub> emissions has overshoot all of the projections for 2010. This means that every scenario failed to project the rapid growth in Chinese NO<sub>x</sub> emissions in the period 2000-2010. Actually, the trends of column NO<sub>2</sub> data from the GOME and OMI satellites indicate more rapid growth in Chinese NO<sub>x</sub> emissions than is indicated by the emission inventories for the period 1996–2008 [Fishman *et al.*, 2008; Irie *et al.*, 2009; Zhang *et al.*, 2007].

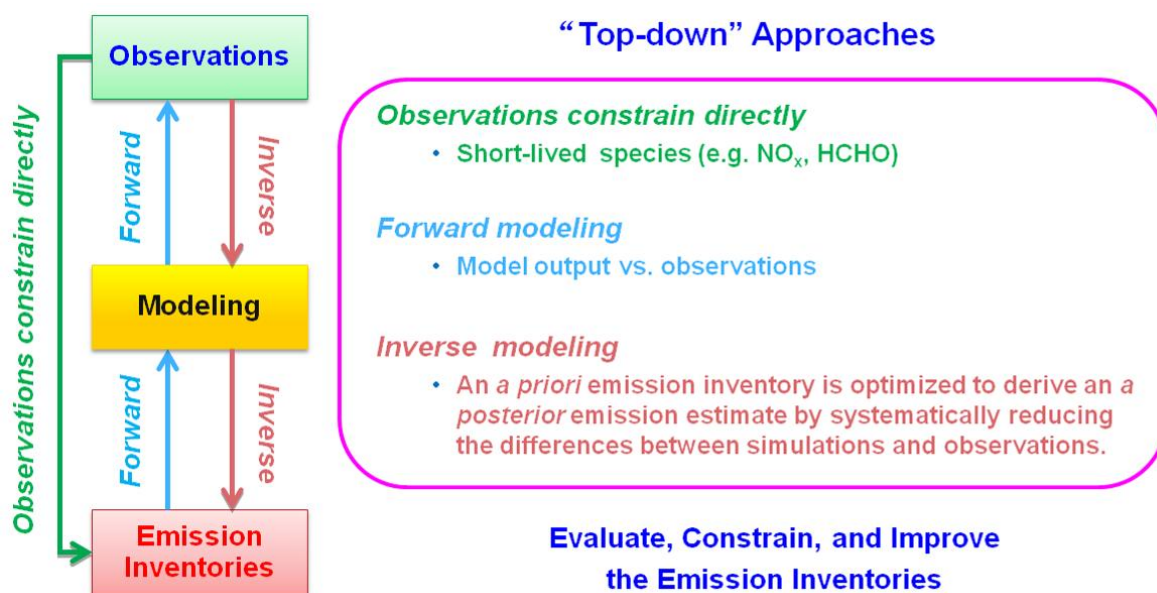


Figure 3.20. Schematic illustration of top-down approaches used to constrain emissions

### Black Carbon

The time series of BC emissions shows a steady decline after 2010 for all scenarios, excluding the REAS PFC scenario. All other cases vary in extent of the drop in emissions. The projections based on the SRES scenario [Streets *et al.*, 2004] show a strong decline because the SRES scenario assumes the elimination of residential coal in China by 2030 and the significant reduction of biofuel use in Asia [Klimont *et al.*, 2009]. In the GAINS baseline, biofuel use in the residential sector in India and most other countries remains fairly constant over time, while in China it declines by nearly 20% compared to the year 2000 [Klimont *et al.*, 2009]. At the same time, residential use of coal continues to grow [Klimont *et al.*, 2009]. The relative growth shows a similar trend for REAS, GAINS and all RCP scenarios for the period 2000-2020. The projections based on the four RCP scenarios follow a very similar trajectory throughout the period, and their values are very close to those of the GAINS baseline.

**FINDING:** Emission estimates are not always similar among inventories compiled by different research groups, and sometimes the differences are large. This is especially true for developing world regions where reliable statistical data may be lacking and key source types have not been tested in the field.

**RECOMMENDATION:** It may not be possible to completely harmonize all emission inventories, but it will be helpful to explore the underlying reasons for differences and to be prepared to adopt new information as it becomes available, especially new emission test data.

**FINDING:** Local knowledge of sources, technologies, and activity levels can provide valuable insight into the reasons for discrepancies in emission estimates.

**RECOMMENDATION:** The reliability of global emission inventories, such as EDGAR-HTAP and GAINS, and continental-scale emission inventories, such as REAS and TRACE-P for Asia, can benefit from incorporation of knowledge from local studies that have heavy user-community or country-level involvement, such as RAPIDC. The support of in-country training and capacity building is encouraged.

### 3.6. Integration among emissions, modelling, and observations

Emission inventories developed by the so-called “bottom-up” approach contain a wide range of uncertainties, which may be associated with activity data from statistics, activity-specific emission factors, and temporal and spatial allocation factors. In the past decade, a number of new techniques

have been applied to address these uncertainties and to evaluate, constrain, and improve the emission inventories. As illustrated in Figure 3.20, these techniques include direct (forward) and inverse modelling of air quality observations, etc. For short-lived species (e.g., NO<sub>2</sub>, HCHO), their emissions sometimes can be constrained directly by observations. Generally, the observations are from ground-based monitoring networks, aircraft and balloon-based measurements, and satellite retrievals. Since ground-based and airborne measurements of air pollutants are temporally and spatially limited, the repeating global coverage of satellite instruments provides a valuable new source of observations [see, e.g., *Martin, 2008; Palmer, 2008*]. Among all the techniques, inverse modelling is a growing field of interest in providing emission constraints. In this “top-down” approach, an a priori emission inventory used in a chemical transport model (CTM) is optimized to derive an a posteriori emission estimate by systematically reducing the differences between model simulations and atmospheric observations. So far, the inverse modelling of trace-gas emissions has not been limited to chemically inert species (e.g., CO<sub>2</sub>) [*Ciais et al., 1995; Enting and Mansbridge, 1989*] or long-lived species (e.g., CH<sub>4</sub>) [*Butler et al., 2004; Houweling et al., 1999*], but extended to relatively reactive species such as NO<sub>x</sub>, CO, HCHO, etc. Table 3.4 summarizes a selection of satellite data that provide direct or indirect constraints on the emissions of the six major species (i.e., NO<sub>x</sub>, CO, SO<sub>2</sub>, CH<sub>4</sub>, NMVOC, and PM) reviewed in this section. For a review of satellite missions the reader is referred to Chapter 2. The following text presents an overview of the application of observations (especially for satellite observations) and modelling to emission inventory improvement for these species, which are so closely tied to hemispheric transport.

**Table 3.4.** Summary of methods currently used to constrain emissions from modelling and observation

	NO <sub>x</sub>	CO	SO <sub>2</sub>	CH <sub>4</sub>	NMVOC	PM
Observations constrain directly	√		√		√	
Forward modelling	√	√	√			√
Inverse modelling	√	√		√	√	√
Satellite data						
TOMS			√			
MOPITT		√				
GOME	√		√		√	
SCIAMACHY	√	√	√	√	√	√
OMI	√		√		√	
GOME-2	√		√		√	
TES		√				
MODIS			√			√
MISR			√			√

### 3.6.1. Constraining emissions with satellite observations

#### *Nitrogen oxides*

Due to the large increase in the NO/NO<sub>2</sub> ratio with altitude and the short lifetime of NO<sub>x</sub> in the lower mixed layer, especially in summer, tropospheric NO<sub>2</sub> columns retrieved from satellites are closely correlated with land surface NO<sub>x</sub> emissions [*Kim et al., 2006; Leue et al., 2001; Martin et al., 2003; Richter et al., 2005; Toenges-Schuller et al., 2006; Zhang et al., 2007*]. As an example shown in the left panel of Figure 3.21, high tropospheric NO<sub>2</sub> columns retrieved from the SCIAMACHY instrument identify the major NO<sub>x</sub> emission sources over eastern North America, northern Europe,

and East Asia. In recent years, trends analysis on the observed NO<sub>2</sub> columns has been used to infer trends of NO<sub>x</sub> emissions, and it is expected that, to a first approximation, changes in NO<sub>2</sub> columns and NO<sub>x</sub> emissions are closely related, e.g., [Richter et al., 2005]. Using a linear regression method, Richter et al. [2005] studied the trends of tropospheric NO<sub>2</sub> columns retrieved from GOME and SCIAMACHY over the years 1996-2004. They found that NO<sub>2</sub> concentrations decreased in Europe and the central east coast of the U.S. but increased dramatically in Asia, particularly in the east central region of China. These findings were further confirmed by Irie et al. [2005] and van der A et al. [2006; 2008]. Besides interannual changes, satellite measurements were reported to be able to monitor the NO<sub>2</sub> seasonal [van der A et al., 2006; van der A et al., 2008], monthly [Zhang et al., 2007], weekly [Beirle et al., 2003], and even day-to-day variations [Blond et al., 2007; Wang et al., 2007a]. Also, they can monitor the regional and local NO<sub>x</sub> emission changes. For example, Kim et al. [2006] found that the NO<sub>2</sub> columns derived from SCIAMACHY could detect the NO<sub>x</sub> emission reduction of power plants implementing NO<sub>x</sub> controls in the eastern U.S.; Zhang et al. [2009b] identified the construction of large new power plants in Inner Mongolia, China, from three OMI NO<sub>2</sub> retrievals; Wang et al. [2007a] reported a 40% reduction of NO<sub>x</sub> emissions in Beijing, China, due to traffic restrictions imposed during the Sino-African Summit by using OMI observations; and the short-term emission control measures implemented during the 2008 Beijing Olympic and Paralympic Games were studied and found to be effective, through combined analysis of observation and models [Mijling et al., 2009; Wang et al., 2009; Witte et al., 2009].

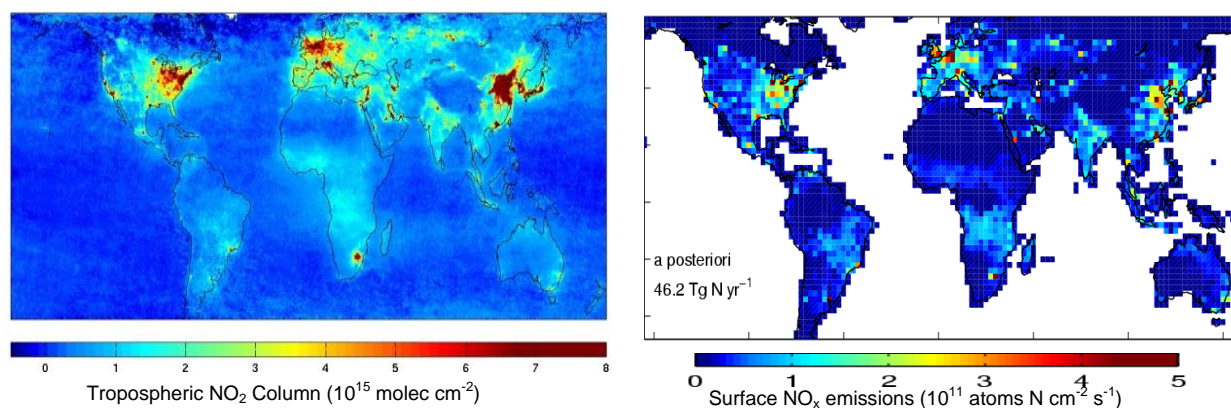


**Figure 3.21.** (Left) Tropospheric NO<sub>2</sub> columns for 2004-2005 determined from the SCIAMACHY satellite instrument. (Right) Surface NO<sub>x</sub> emissions for 2004-2005 determined through inverse modelling of the SCIAMACHY observations using a chemical transport model (GEOS-Chem). Aircraft measurements as part of the ICARTT aircraft campaign support the SCIAMACHY inventory. [Reprinted from Figures 4 and 7 in Martin, R. V., et al. (2006), Evaluation of space-based constraints on global nitrogen oxide emissions with regional aircraft measurements over and downwind of eastern North America, *Journal of Geophysical Research*, 111(D15308).]

The assumption that the changes in NO<sub>2</sub> columns are directly proportional to changes in NO<sub>x</sub> emissions may not always be true. Hence, it is better to use forward and inverse modelling that can explicitly account for the transport and chemical processing of NO<sub>x</sub>. Column concentrations can, of course, also be modelled. Kim et al. [2009] carried out simulations with the WRF-Chem model for the western U.S. and compared the simulation results with SCIAMACHY and OMI NO<sub>2</sub> retrievals. They found that the NO<sub>x</sub> emissions contained in the U.S. EPA NEI99 inventory over large urban areas along the west coast appeared to be overestimated. For East Asia, the modelled NO<sub>2</sub> columns of forward modelling with different bottom-up inventories (e.g., TRACE-P, EDGAR, REAS, CORP) underestimated the satellite retrievals during the past decade, implying the underestimation of NO<sub>x</sub> emissions in East Asia [Han et al., 2009; He et al., 2007; Ma et al., 2006; Shi et al., 2008; Uno et al., 2007]. Compared with these forward modelling studies, “top-down” inverse modelling techniques quantify the discrepancies between observations and model predictions. Wang et al. [2004] evaluated China’s TRACE-P NO<sub>x</sub> and CO emissions [Streets et al., 2003], using ground-station and aircraft

observations during the TRACE-P field campaign and suggested the need for a 47% and 43% increase of China's NO<sub>x</sub> and CO emissions, respectively. Leue et al. [2001] first quantified the global NO<sub>x</sub> budget from GOME NO<sub>2</sub> retrievals with a fixed global NO<sub>x</sub> lifetime. Using the local GEOS-Chem relationship between NO<sub>2</sub> columns and NO<sub>x</sub> emissions, Martin et al. [2003] improved this approach, and found that significant regional differences existed between *a priori* and *a posteriori* inventories. Following the work of Martin et al. [2003], Jaeglé et al. [2004; 2005] partitioned GOME top-down NO<sub>x</sub> sources among fuel combustion, biomass burning, and soil emissions by exploiting the spatial-temporal distribution of remotely sensed fires and *a priori* information on the location of regions dominated by fuel combustion. An example of “top-down” global emissions of surface NO<sub>x</sub> is shown in the right panel of Figure 3.21, which is determined through inverse modelling of the SCIAMACHY observations (left panel of Figure 3.21) using the GEOS-Chem model [Martin et al., 2006].

To take into account the non-linear relationship between NO<sub>x</sub> emissions and NO<sub>2</sub> columns caused by chemical feedbacks, four-dimensional variational data assimilation and Kalman filter methods have been applied to inverse techniques [Kurokawa et al., 2009; Müller and Stavrakou, 2005; Napelenok et al., 2008; Stavrakou et al., 2008; Zhao and Wang, 2009]. Also, featuring higher spatial resolution, the current generation of satellite instruments makes it possible to resolve regional and local NO<sub>x</sub> emissions [Kim et al., 2006; Konovalov et al., 2006; Kurokawa et al., 2009; Martin et al., 2006; Napelenok et al., 2008; Quelo et al., 2005; Wang et al., 2007b; Zhao and Wang, 2009]. Recently, the difference of NO<sub>2</sub> columns at the overpass times of the different satellites was utilized to infer information about NO<sub>x</sub> emissions. Boersma et al. [2008] compared the NO<sub>2</sub> retrievals from OMI (13:30 local overpass time) and SCIAMACHY (10:00 local overpass time) to infer the diurnal variation of NO<sub>x</sub> emissions globally. Lin et al. [2010] constrained the Chinese anthropogenic NO<sub>x</sub> emissions from four sectors (industry, power plants, mobile, and residential) by using the different passing time of GOME-2 and OMI (10:00 vs. 13:30 local time). Basically, the *a posteriori* emissions obtained from inverse modelling schemes improve the agreement between the modelled and measured data and significantly reduce the uncertainty in the *a priori* inventory [Konovalov et al., 2006; Martin et al., 2003]. It also should be noticed that the “top-down” inverse emission estimates are sensitive to the choice of model and retrieval, which is concluded by van Noije et al. [2006] from a systematic inter-comparison of three different NO<sub>2</sub> retrievals with 17 global CTMs.

The additional knowledge obtained from remote sensing and modelling communities helps inventory compilers to locate problem areas in the emission estimates and to re-examine the emission inventory. For example, based on the NO<sub>2</sub> column trends from Richter et al. [2005] and Irie et al. [2005], Akimoto et al. [2006] concluded that the Chinese energy consumption data provided by the International Energy Agency (IEA) and the China Energy Statistics Yearbook (CESY) for the years 1996-2002 are underestimated. They recommended that IEA and country-total CESY statistics should not be used in Chinese emission inventory studies for this period. Zhang et al. [2007] used a dynamic bottom-up methodology to estimate NO<sub>x</sub> emissions in China from 1995 to 2004 and to reconcile the trends with the NO<sub>2</sub> column trends observed from GOME and SCIAMACHY. They used a similar methodology to develop a new inventory of air pollutant emissions in Asia for the NASA INTEX-B mission, which was reported to be in good agreement with observations [Zhang et al., 2009a, and references therein].

### **Carbon monoxide**

Compared to NO<sub>x</sub>, the longer lifetime of CO (a few weeks to a few months, depending on location and season) makes it more difficult to distinguish the different sources and the relative contributions of local and transported pollution from space [Clerbaux et al., 2008]. Hence, CO observations are usually used in conjunction with CTMs to evaluate important CO sources such as fossil-fuel combustion, biofuel combustion, and open biomass burning [e.g., Arellano et al., 2004; Heald et al., 2004; Pétron et al., 2004; Pfister et al., 2005]. Before the early 2000s, only surface and airborne measurements were used in CO inverse modelling studies [Bergamaschi et al., 2000; Kasibhatla et al., 2002; Palmer et al., 2003b; Pétron et al., 2002; Wang et al., 2004]. Almost all these simulations suggested that anthropogenic CO emissions contained in bottom-up inventories were significantly underestimated throughout the Northern Hemisphere, particularly in Asia. Bergamaschi et

al. [2000] first applied inverse modelling techniques to CO by using the NOAA/CMDL dataset at 31 globally distributed sites. Their estimation of the *a posteriori* CO source strength in the Northern Hemisphere was ~800 Tg/yr, considerably higher than the inventory-based estimates of 300-550 Tg/yr [IPCC, 1996; Olivier *et al.*, 1996] and suggesting a considerable unrecognized source at high latitudes.

The work of Kasibhatla *et al.* [2002] suggested that the source of CO from fossil-fuel and biofuel combustion in Asia during 1994 was 110-140 Tg/yr, higher than their *a priori* inventory. An even higher CO flux from Asia was reported by Pétron *et al.* [2002]. For China, Palmer *et al.* [2003b] used the TRACE-P aircraft observations and the GEOS-Chem model to derive a 54% increase in anthropogenic emissions relative to the *a priori*, which was comparable to the results of Wang *et al.* [2004]. The new space-based measurements of tropospheric CO (e.g., MOPITT, SCIAMACHY, and TES) provide improved estimates of CO sources due to the high spatial coverage of the dataset. Arellano *et al.* [2004] first used remote sensing CO measurements (MOPITT) to quantify regional CO sources, finding CO emissions in East Asia were about a factor of 1.8-2 higher than bottom-up estimates. Heald *et al.* [2004] quantified the Asian CO sources to be 361 Tg/yr by using the observations from both the MOPITT satellite and the TRACE-P aircraft. Pétron *et al.* [2004] presented the time-dependent inversion of CO global surface fluxes based on the MOPITT CO retrievals. Recent improvements to CO inversions include developing adjoint models with/without a four-dimensional variational data assimilation system [Kopacz *et al.*, 2009; Müller and Stavrou, 2005; Tanimoto *et al.*, 2008; Yumimoto and Uno, 2006], grid-based [Stavrou and Müller, 2006], and multi-instrument inversions [Jones *et al.*, 2009; Turquety *et al.*, 2008].

In addition to inverse modelling, observations were also used in conjunction with forward modelling analysis to evaluate emission estimates. Using the TRACE-P CO emission inventory as an example, numerous studies were performed to compare the results of various models with aircraft, ground-based and satellite observations during the TRACE-P mission [Allen *et al.*, 2004; Carmichael *et al.*, 2003; Heald *et al.*, 2003; Kiley *et al.*, 2003; Suntharalingam *et al.*, 2004; Tan *et al.*, 2004]. Although the temporal and spatial variations of observed CO were well captured by the models, the model predictions were persistently lower than the observations [Allen *et al.*, 2004; Heald *et al.*, 2003; Kiley *et al.*, 2003]. Carmichael *et al.* [2003] suggested that this under-prediction may be related to an underestimation of emissions from the residential sector, while Tan *et al.* [2004] attributed it to the overestimation of the combustion efficiency of coal-burning facilities. Also, Tan *et al.* [2004] suggested that anthropogenic Chinese CO emissions should be ~50% higher than the TRACE-P data, and, by making this adjustment, the model calculations were in better agreement with observations [Suntharalingam *et al.*, 2004; Tan *et al.*, 2004].

The findings from these top-down constraints were able to be used to improve our understanding of emissions and guide us in identifying inadequacies in the bottom-up approach. Revisiting China's CO emission inventory after the TRACE-P mission is the first success story for integrating both the bottom-up and top-down approaches [Streets *et al.*, 2006]. Motivated by the forward and inverse modelling results, Streets *et al.* [2006] re-examined the source characteristics and concluded that emissions from cement kilns, brick kilns, and the iron and steel industry were underestimated. The updated anthropogenic CO emissions from China in 2001 are 36% higher than the TRACE-P estimates, and the modelled results based on this updated inventory were reported to be in good agreement with observations [Kopacz *et al.*, 2009; Streets *et al.*, 2006; Tanimoto *et al.*, 2008; Yumimoto and Uno, 2006; Zhang *et al.*, 2009a].

### ***Sulphur dioxide***

In the last few years remote sensing techniques have been applied to monitor and quantify SO<sub>2</sub> emissions from both natural and anthropogenic sources. The early instruments such as TOMS provided a long-term record of SO<sub>2</sub> emissions from volcanic eruptions [Krueger *et al.*, 1995] and exceptional SO<sub>2</sub> pollution events [Carn *et al.*, 2004]. Due to the low sensitivity at lower altitudes, anthropogenic SO<sub>2</sub> is much more difficult to detect from space than volcanic SO<sub>2</sub> [Khokhar *et al.*, 2008]. The sensitivity improvement of the current generation of instruments (e.g., GOME-2, SCIAMACHY, and OMI) makes it possible to identify the sources of strong anthropogenic SO<sub>2</sub> emissions such as smelters and coal-fired power plants [Carn *et al.*, 2007; Khokhar *et al.*, 2008;



*Krotkov et al.*, 2008; *Li et al.*, 2010]. At present, the retrieval of SO<sub>2</sub> columns still contains large uncertainties, which are related to cloud cover, SO<sub>2</sub> profile and aerosols, as well as interference by the absorption signals of ozone. However the quality of SO<sub>2</sub> column data is improving [i.e., *Lee et al.*, 2009] and has promise for informing anthropogenic emission inventories in some regions. Additionally, satellite AOD trends are also able to constrain SO<sub>2</sub> emissions. For example, van Donkelaar et al. [2008] analysed AOD data from MISR and MODIS for 2000-2006 with the GEOS-Chem model, which, if associated entirely with sulphate aerosol, would be consistent with an annual growth in Chinese sulphur emissions of 6.2% and 9.6%, respectively.

### ***Methane***

For CH<sub>4</sub>, the inverse modelling technique was first applied to emission estimates by using surface observations [*Bergamaschi et al.*, 2005; *Bousquet et al.*, 2006; *Chen and Prinn*, 2006; *Hein et al.*, 1997; *Houweling et al.*, 1999; *Mikaloff Fletcher et al.*, 2004]. Since the network of surface measurements is very sparse, the observations only contain statistically significant information about emissions on continental scales at best [*Houweling et al.*, 1999]. In contrast, space-borne instruments can provide important constraints on the spatial and temporal emission distributions of CH<sub>4</sub>, particularly in tropical regions where surface CH<sub>4</sub> is poorly monitored [*Meirink et al.*, 2006]. Using the SCIAMACHY instrument, Frankenberg et al. [2005] retrieved the global CH<sub>4</sub> distribution and observed unexpectedly high CH<sub>4</sub> concentrations over tropical rainforests. Their subsequent source inversion studies indicated the underestimation of bottom-up CH<sub>4</sub> emissions in these regions [*Frankenberg et al.*, 2006]. However, the inverse estimates based on the SCIAMACHY retrievals are also significantly higher than those based on global surface measurements [*Bergamaschi et al.*, 2007; *Meirink et al.*, 2008], and this implied a potential systematic error for satellite retrievals. Later, Frankenberg et al. [2008a; 2008b] reported a major revision of SCIAMACHY retrievals based on an update of spectroscopic parameters of water vapour and CH<sub>4</sub>. Based on the revised retrievals, inversions yielded a more consistent picture than with inversions using ground-based stations only [*Bergamaschi et al.*, 2009; *Frankenberg et al.*, 2008a]. Recently, the revised SCIAMACHY retrievals have been used in conjunction with gravity anomaly measurements from the GRACE satellite to infer the contributions of wetlands and rice paddies to CH<sub>4</sub> emissions [*Bloom et al.*, 2010].

### ***Non-Methane Volatile Organic Compounds***

Due to the short lifetime of reactive NMVOC and the high yield of formaldehyde (HCHO) during NMVOC oxidation, HCHO measurements from space can provide important constraints for the spatial distribution of NMVOC emissions [*Barkley et al.*, 2008; *Fu et al.*, 2007; *Millet et al.*, 2006; *Millet et al.*, 2008; *Palmer et al.*, 2003b; *Palmer et al.*, 2006]. In North America, the HCHO enhancement from isoprene emissions far exceeds that from the other NMVOC emissions during the growing seasons [*Lee et al.*, 1998; *Sumner et al.*, 2001]. Hence, HCHO column data from space can be used as an effective proxy for isoprene emissions [*Millet et al.*, 2006]. Palmer et al. [2003a] first developed an approach for deriving isoprene emissions using GOME HCHO retrievals over North America. Following their work, Abbot et al. [2003] and Palmer et al. [2006] found that the general seasonal and interannual variability of GOME-retrieved HCHO data is consistent with knowledge of isoprene emissions. Shim et al. [2005] extended the above studies to the global scale, deriving the *a posteriori* estimate of the annual global isoprene emissions to be about 50% larger than the *a priori* estimate. Millet et al. [2008] developed updated relationships between HCHO columns and isoprene emissions from GEOS-Chem and used them to infer top-down constraints on isoprene emissions in North America from OMI data. From the comparison of the OMI-derived emissions and bottom-up isoprene emission inventory MEGAN, they also optimized the MEGAN emission factors for broadleaf trees (the main isoprene source). Compared with North America, isoprene emissions in East and South Asia are less dominant because of the complex overlap of anthropogenic, biogenic, and biomass burning emissions. Fu et al. [2007] used a 6-year record of GOME HCHO columns to improve emission estimates of NMVOC (including isoprene, alkenes, HCHO and xylenes) in this region. They found that wintertime GOME observations can diagnose anthropogenic reactive NMVOC emissions from China, leading to an estimate 25% higher than the TRACE-P inventory. Besides HCHO, glyoxal (CHOCHO) can also be measured from satellite instruments such as



SCIAMACHY, OMI, and GOME-2. Synergistically, HCHO and CHOCHO satellite columns in a two-compound inverse modelling framework have been applied to constrain the continental sources of CHOCHO [Stavrakou *et al.*, 2009].

### ***Particulate matter***

Observations and model simulations can also be used to evaluate PM sources. Dubovik *et al.* [2008] retrieved global aerosol source emissions from MODIS AOD data by inverting the GOCART aerosol transport model. The global secondary organic aerosol (SOA) formation from irreversible uptake of dicarbonyls (glyoxal and methylglyoxal) was quantified [Fu *et al.*, 2008], implying the possibility of using satellite observations of NMVOC to estimate the SOA budget in the future. In Asia, forward and inverse modelling studies concluded that the TRACE-P estimates of BC are qualitatively correct at the national level, but the spatial distributions are questionable [Carmichael *et al.*, 2003; Clarke *et al.*, 2004; Hakami *et al.*, 2005; Uno *et al.*, 2003; Zhang *et al.*, 2009a]. In the continental United States, top-down inverse estimates of BC emissions [Hu *et al.*, 2009] are in good agreement with bottom-up inventories [Bond *et al.*, 2004; U.S. EPA, 2009]. Inverse modelling for ammonia emissions [i.e., Gilliland *et al.*, 2006; Henze *et al.*, 2009] has been particularly valuable due to the large uncertainty in that source.

### ***3.6.2. Constraining emission inventories with observation data: Case studies in the United States***

This section has two goals: first, to describe temporal trends and NMVOC speciation of some emissions from U.S. sources as estimated from ambient measurements; and second, to compare those estimates with the trends included in emission inventories. These estimates will address on-road vehicles and electric power plants. The U.S. EPA finds that these two sources were responsible for the majority of anthropogenic CO, NO<sub>x</sub> and SO<sub>2</sub> and a large fraction of the NMVOC emitted in the country over the past 25 years.

#### ***Temporal trends and evaluation of U.S. power-plant emissions***

Power-plant emission inventories for the U.S. are believed to be very accurate, and many detailed hourly emission data are available, because generally these emissions are measured by Continuous Emission Monitoring Systems (CEMS), which are required by the U.S. EPA's Acid Rain Program and the NO<sub>x</sub> Budget Trading Program. The U.S. EPA regularly reports estimated emissions and their trends over the previous decades, generally in annual National Air Quality and Emissions Trends Reports (<http://www.epa.gov/ttn/chief/trends/index.html>). Comparisons of a recent historical sample of these Trends Reports [U.S. EPA, 1995; 2000; 2003] with an earlier inventory developed for NAPAP [Saeger *et al.*, 1989] and the most recent emission Trends Tables ("1970 – 2006 Average Annual Emissions, All Criteria Pollutants", posted July 2007) are shown in Figure 3.22, for NO<sub>x</sub> and SO<sub>2</sub> from fuel combustion in electric utilities. It is clear that there has been little variation in the emission estimates for any given year, with only the NO<sub>x</sub> emissions in the 1995 Trends Report significantly different (as much as 19% higher) than the later estimates.

According to the inventories in Figure 3.22, over the last 26 years U.S. NO<sub>x</sub> and SO<sub>2</sub> emissions from electric utility power plants have decreased by factors of 2.0 and 1.8, respectively. The substantial reductions of power-plant SO<sub>2</sub> emissions during the 1990's and of power-plant NO<sub>x</sub> emissions in the past decade are a direct result of pollutant-specific cap-and-trade control strategies mandated by the EPA's Acid Rain Program and the NO<sub>x</sub> Budget Trading Program. The power-plant emissions measured by CEMS have been checked against aircraft flux determinations based on ambient measurements in the downwind emission plumes, and the two sets of observations generally agree with standard deviations of less than ±14% [Peischl *et al.*, 2010]. A larger-scale confirmation of the recent power-plant NO<sub>x</sub> emission reductions is demonstrated by satellite observations over the Ohio River Valley, a region in the central U.S. with a high density of coal-fired power plants that dominate the NO<sub>x</sub> emissions [Kim *et al.*, 2006]. Satellite NO<sub>2</sub> vertical columns over the Ohio River Valley declined by 40% between 1999 and 2005, a trend consistent with CEMS-reported declines in power-plant NO<sub>x</sub> emissions. The consistency of the CEMS-based inventory over the years, and the

correspondence of the CEMS data with aircraft flux and satellite determinations, indicate that these inventories of U.S. power-plant emissions are accurate.

### Temporal trends and evaluation of U.S. on-road vehicle emissions

Making accurate estimates of on-road vehicle emissions is much more difficult than the analogous task for power plants. Bottom-up, on-road emission models integrate the product of emission factors (e.g., g/km driven) for a diverse, constantly evolving vehicle fleet and highly variable activity factors. The different emission models that have been used over the years have yielded results that differ widely in some important respects. Figure 3.22 shows estimated on-road emissions of NO<sub>x</sub> and CO from the five references discussed in the previous section plus one additional Trends Report [U.S. EPA, 1990] and compares those estimates to emissions inferred from ambient measurements [Parrish, 2006]. For NO<sub>x</sub> the emission inventories differ significantly in the temporal trends of the emissions. The most recent evaluation suggests decreasing NO<sub>x</sub> emissions throughout the 25 years, while the earlier calculations suggest increasing NO<sub>x</sub> emissions through the decade of the 1990's. The emissions inferred from ambient data support the earlier trend estimates. All the emission models and the inferred emissions agree that CO emissions have decreased continually by 3 to 5%/year. However, there is significant disagreement regarding the magnitude of the CO emissions. The most recent inventory is approximately a factor of two larger than emissions inferred from ambient measurements.

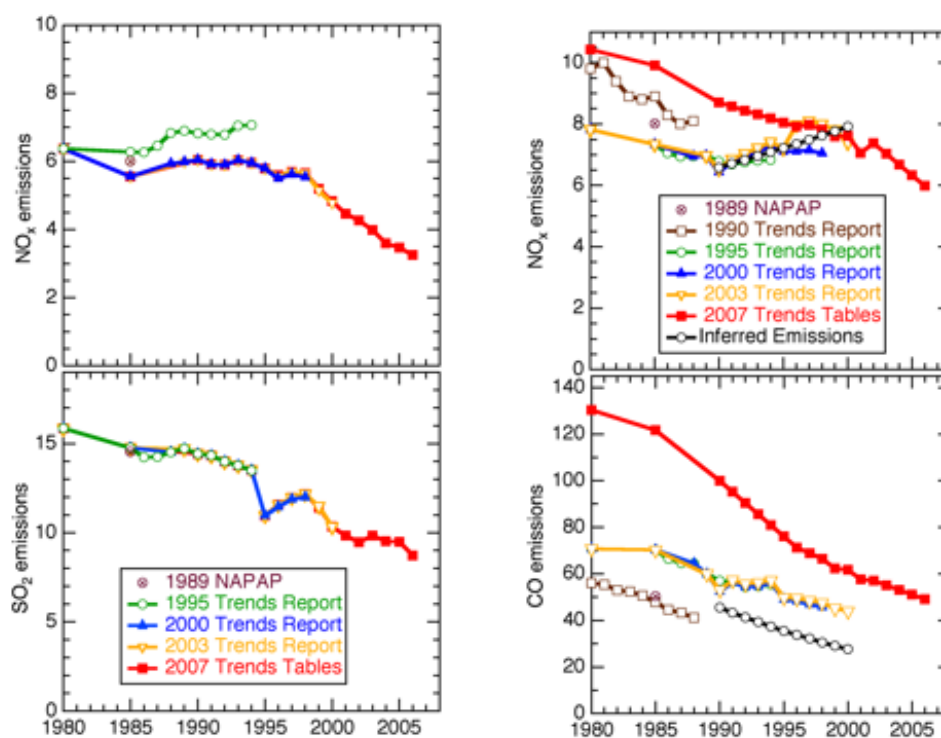


**Figure 3.22.** Annual U.S. emissions from (a) power plants and (b) on-road vehicles from 1980-2007, as estimated in six U.S. inventories and inferred from ambient observations. Units are million metric tons/year. The dates in the annotation indicate the year of publication of the inventory report.

Other investigators have inferred fuel-based emission factors (grams of pollutant per kg of gasoline or diesel burned) from roadside observations, which can be compared to the emission factors used in emission models. For example, multi-year monitoring programs in several U.S. cities suggest that the average CO and NO<sub>x</sub> fuel-based emission factors for gasoline vehicles declined by an average of 7 to 9 %/yr since the mid-1990's [Ban-Weiss *et al.*, 2008; Bishop and Stedman, 2008; Harley *et al.*, 2005]. These declines are thought to be the result of continual improvements to the emission control systems on U.S. gasoline-powered vehicles. In contrast, NO<sub>x</sub> emission factors inferred from roadside

observations of diesel-powered vehicles, which produce relatively little CO, appear to have decreased only slightly over the past decade [Ban-Weiss *et al.*, 2008].

The study by Kim *et al.* [2006] also examined the northeastern U.S. urban corridor stretching from Washington, DC, in the south to Boston in the north. This region, dominated by mobile source NO<sub>x</sub> emissions, saw only a slight decrease in satellite-retrieved NO<sub>2</sub> vertical columns between 1997 and 2005. This finding suggests that, overall, mobile source NO<sub>x</sub> emissions have not changed much over this time period. In addition to year-to-year variability of on-road emissions, clear differences between weekday and weekend U.S. urban NO<sub>x</sub> emissions resulting primarily from motor vehicle use patterns have been documented by in-situ [Harley *et al.*, 2005] and satellite methods [Beirle *et al.*, 2003]. Because of differential control of gasoline and diesel vehicle emissions, the weekly cycle in U.S. on-road NO<sub>x</sub> emissions is predicted to have changed over the past decade [Harley *et al.*, 2005].

The important lesson from these evaluations is that without the support of direct measurements (as CEMS provides for power-plant sources), it is not possible to develop bottom-up inventories that are accurate enough for some of the scientific uses to which they are applied. However, bottom-up inventories are indispensable components of photochemical models, and the foundation upon which our knowledge of pollutants in the atmosphere is based. A continuing process of inventory development is clearly required: testing of emission inventories through top-down evaluations; inventory improvement; evaluation of the top-down tests; and then repeating this process until the top-down tests of the inventories indicate sufficient accuracy for the intended use of the inventory.

### ***Temporal trends and speciation of on-road vehicle VOC emissions***

The speciation of ambient hydrocarbon concentrations in several cities across the globe (Figure 3.23) reveals a large degree of similarity. This similarity spans cities in North America and Asia, has remained generally constant over the past two decades in the U.S., and persists over wide ranges of absolute concentrations. A two-part hypothesis most likely explains this similarity. First, gasoline-fuelled vehicle exhaust and the associated evaporative gasoline emissions dominate the ambient hydrocarbon concentrations in all of these urban areas. Second, there is no large difference in the hydrocarbon composition of gasoline and exhaust emissions among these urban areas.

Comparison of datasets collected in U.S. cities over the past three decades indicates that a substantial decrease (something like an order of magnitude) in hydrocarbon emissions has occurred even while total distance travelled by on-road vehicles has nearly tripled. This change is at least partially responsible for the decrease in concentrations between the two U.S. studies in Figure 3.23. The ambient concentration data suggest that the emission decrease has been larger than indicated by U.S. emission inventories, while the global EDGAR inventory does not capture any significant decrease (Figure 3.24). Evidently, U.S. strategies aimed toward controlling hydrocarbon emissions, based upon automobile catalytic converters, minimization of gasoline evaporation and other vehicle emission control strategies, have been very successful—indeed, more successful than indicated by emission inventories. Unless the emission inventory uncertainties, particularly in the global inventory, can be substantially reduced, retrospective analyses of anthropogenic influences on tropospheric composition will be uncertain to an important degree.

Evaluation of ambient VOC measurements can also provide detailed, critical tests of VOC speciation in inventories. Benzene and acetylene are examined here. Both of these hydrocarbons are in the top ten in terms of ambient concentrations in U.S. cities, and they react slowly in the atmosphere. Fortin *et al.* [2005] argued that these species are primarily emitted by on-road vehicles, and they showed that the benzene-to-acetylene ratio is remarkably invariant throughout the U.S. in any given year and exhibits long-term trends in response to VOC emission control measures (Figure 3.25). Before 1994, the ratio increased slowly due to the preferential removal of acetylene by automotive catalytic converters. In 1994, in response to the 1990 U.S. Clean Air Act Amendments, specific benzene control measures were introduced, which reduced the benzene-to-acetylene ratio dramatically in the following decade.

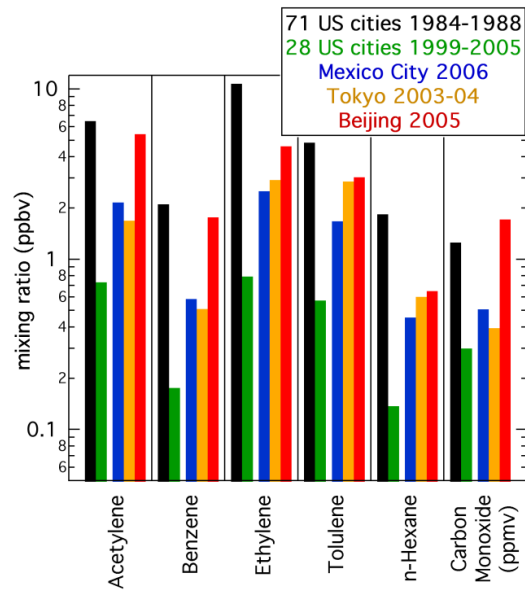


**Figure 3.23.** Mixing ratios of VOC species from five measurement programs. The median VOC concentrations in U.S. cities in 1984-88 are taken from Table 2 of Seila et al. [1989], and the mean concentrations in U.S. cities in 1999-2005 are the means of the city mean mixing ratios from Table 2 of Baker et al. [2008]. Seila et al. [1989] did not report CO measurements; the CO concentration for the U.S. cities in 1984-88 is estimated from the median acetylene mixing ratio and the CO-to-acetylene ratio reported by those same authors for a tunnel study conducted in New York City in 1982 [Lonneman et al., 1986].

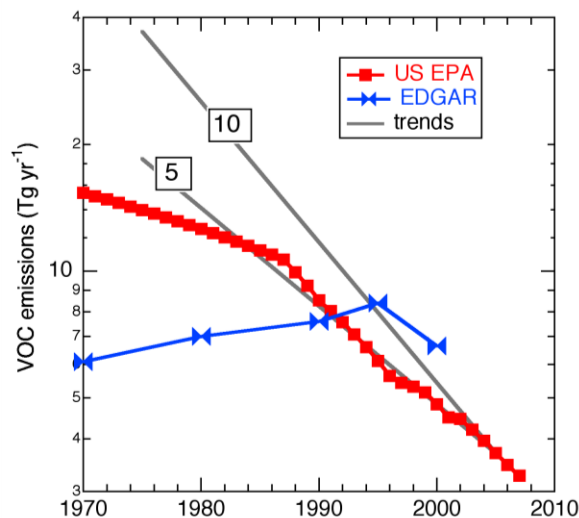


**Figure 3.24.** VOC emissions from on-road vehicles in the U.S. estimated by two emission inventories. The 2008 U.S. EPA emissions are from the latest (August, 2008) emission tables posted on the website of the EPA Technology Transfer Network: Clearinghouse for Inventories & Emission Factors (<http://www.epa.gov/ttn/chief/trends/index.html>). The EDGAR emissions are from EDGAR 3.2 FT2000 [van Aardenne et al., 2005] for 2000, EDGAR 3.2 [Olivier and Berdowski, 2001] for 1990 and 1995 and EDGAR-HYDE 1.3 [van Aardenne et al., 2001] for 1970, 1980 and 1990. The fossil-fuel consumption emissions of EDGAR-HYDE 1.3 were multiplied by 0.864 to bring them into agreement with the 1990 on-road emissions of EDGAR 3.2. The grey lines indicate exponential trends necessary to account for a factor of 5 or 10 decrease in emissions between 1975 and 2005.

The measured ambient ratios and their trend can be compared to the VOC speciation in emission inventories. Figure 3.25 shows benzene-to-acetylene emission ratios extracted from three recent U.S. national emission inventories, both for on-road vehicles and inventory totals. The NEI 1996 and 1999 numbers were obtained by applying the SPECIATE software (EPA Clearinghouse for Inventories and Emissions Factors: <http://www.epa.gov/ttn/chief/emch/speciation/index.html>) to the respective NEI. The 1996 number agrees to within 10% with the 1996 National Toxic Air Pollutant inventory for benzene (<http://www.epa.gov/ttn/atw/nata/>).

The comparison between the ambient and inventory ratios in Figure 3.25 is quite poor. The inventory ratios for total emissions are a factor of 3 to 4 higher than the ambient values; those for on-road emissions are also significantly higher than observed. Further, the temporal trends are not clearly in agreement. Although the recent trend in the inventory appears to parallel the ambient trend, it is for the wrong reasons. The ambient ratio is believed to have decreased due to reduced benzene emissions, but the inventory benzene emissions have remained approximately constant while the acetylene emissions have increased, particularly in the on-road emissions. In conclusion, the VOC speciation in the U.S. NEI as tested by these two example species appears to be in error by a factor of three to four, and the temporal trend in the inventory emissions is not consistent with the observations. There is a critical need for a re-evaluation of the VOC speciation throughout the U.S. national emission inventory, and by implication similarly derived inventories worldwide. Correctly interpreted, reliable ambient concentration measurements must be one of the important guides for this re-evaluation.

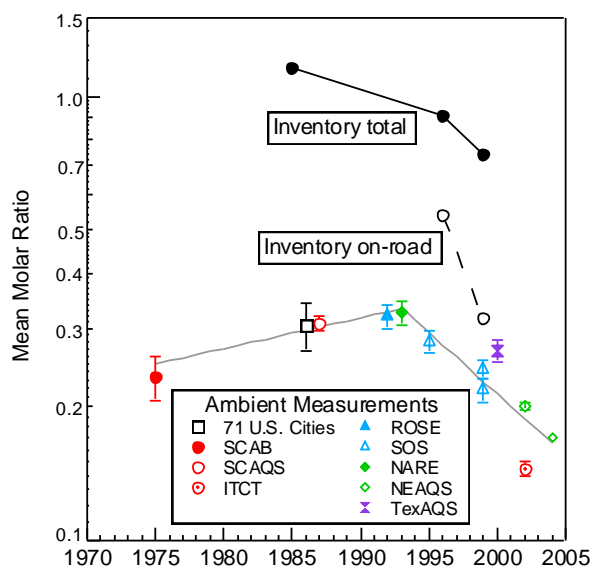


**Figure 3.25.** Semi-log plot of temporal trends of observed ambient benzene-to-acetylene ratios from field study data compared to inventory ratios. The colours of the symbols indicate geographic location: U.S. Urban (black), California (red), southeast U.S. (blue), northeast U.S. (green), and Texas (purple). The error bars indicate the 95% confidence limit of the mean. The grey lines indicate estimated ambient trends before and after 1993. The inventory ratios are from three national U.S. inventories. [Adapted from Figure 2 in Fortin, T. J., et al. (2005), Temporal changes in U.S. benzene emissions inferred from atmospheric measurements, *Environmental Science & Technology*, 39: 1403-1408. Copyright 2005 American Chemical Society.]

**FINDING:** The integrated study of emissions, forward and inverse modelling, and satellite and ground observations can usefully bound source magnitudes and lead to improved emission inventories.

**RECOMMENDATION:** Previous studies demonstrate a clear need for the development of an integrated framework of emissions, models, and observations that can be readily applied to

**different intercontinental transport situations and can quickly adapt to new technical capabilities as they arise (new satellite retrievals, new network data releases, etc.).**

**FINDING:** Emission events (dust storms, volcanic eruptions, forest fires, etc.) are detectable in many of the observational datasets (aircraft campaigns, ground-station monitoring, satellite retrievals, etc.). It may be possible to quantify the magnitudes of such emission events for some species, by coordinated application of these measurement tools.

**RECOMMENDATION:** Emphasis should be placed on identifying unique signatures of episodic emission releases in the observational record and their subsequent transport (e.g., tracking dust storms) in order to improve source quantification and modelling of long-range processing and deposition.

**FINDING:** Emission inventories only provide information about primary releases of pollutants; they do not directly estimate secondary species such as ozone and secondary organic aerosol.

**RECOMMENDATION:** Careful study of the large-scale relationships between primary precursor emissions (e.g., emission ratios, speciation profiles) and observed secondary species (from satellites, campaigns, networks) can advance our understanding of the mechanisms of formation of the secondary species and our ability to select effective mitigation options for the primary species.

## References

- Abbot, D. S., et al. (2003), Seasonal and interannual variability of North American isoprene emissions as determined by formaldehyde column measurements from space, *Geophysical Research Letters*, 30(17): 1886-1889.
- Akimoto, H. (2003), Global air quality and pollution, *Science*, 302: 3.
- Akimoto, H., et al. (2006), Verification of energy consumption in China during 1996-2003 by using satellite observational data, *Atmospheric Environment*, 40(40): 7663-7667.
- Allen, D., et al. (2004), Evaluation of pollutant outflow and CO sources during TRACE-P using model-calculated, aircraft-based, and measurements of pollution in the troposphere (MOPITT)-derived CO concentrations, *Journal of Geophysical Research*, 109: D15S03.
- Andreae, M. O., and P. Merlet (2001), Emission of trace gases and aerosols from biomass burning, *Global Biogeochemical Cycles*, 15(4): 955-966.
- Andres, R. J., and A. D. Kasgnoc (1998), A time-averaged inventory of subaerial volcanic sulfur emissions, *Journal of Geophysical Research*, 103(D19): 25251-25261.
- Arellano, A. F., et al. (2004), Top-down estimates of global CO sources using MOPITT measurements, *Geophysical Research Letters*, 31(L01104).
- Baker, A. K., et al. (2008), Measurements of nonmethane hydrocarbons in 28 United States cities, *Atmospheric Environment*, 42: 170-182.
- Ban-Weiss, G. A., et al. (2008), Carbonyl and nitrogen dioxide emissions from gasoline- and diesel-powered motor vehicles, *Environmental Science & Technology*, 42(11): 3944-3950.
- Barkley, M. P., et al. (2008), Net ecosystem fluxes of isoprene over tropical South America inferred from Global Ozone Monitoring Experiment (GOME) observations of HCHO columns, *Journal of Geophysical Research*, 113(D20304).
- Beirle, S., et al. (2003), Weekly cycle of NO<sub>2</sub> by GOME measurements: a signature of anthropogenic sources, *Atmospheric Chemistry and Physics*, 3: 2225-2232.
- Bergamaschi, P., et al. (2000), Inverse modeling of the global CO cycle; 1. Inversion of CO mixing ratios, *Journal of Geophysical Research*, 105(D2): 19.

- Bergamaschi, P., et al. (2005), Inverse modeling of national and European CH<sub>4</sub> emissions using the atmospheric zoom model TM<sub>5</sub>, *Atmospheric Chemistry and Physics*, 5: 2431-2460.
- Bergamaschi, P., et al. (2007), Satellite cartography of atmospheric methane from SCIAMACHY onboard ENVISAT: 2. Evaluation based on inverse model simulations, *Journal of Geophysical Research*, 112(D02304).
- Bergamaschi, P., et al. (2009), Inverse modeling of global and regional CH<sub>4</sub> emissions using SCIAMACHY satellite retrievals, *Journal of Geophysical Research*, 114(D22301).
- Bishop, G. A., and D. H. Stedman (2008), A decade of on-road emissions measurements, *Environmental Science & Technology*, 42(5): 1651-1656.
- Blond, N., et al. (2007), Intercomparison of SCIAMACHY nitrogen dioxide observations, in situ measurements and air quality modeling results over Western Europe, *Journal of Geophysical Research*, 112(D10311).
- Bloom, A. A., et al. (2010), Large-scale controls of methanogenesis inferred from methane and gravity spaceborne data, *Science*, 327: 322-325.
- Boersma, K. F., et al. (2005), Estimates of lightning NO<sub>x</sub> production from GOME satellite observations, *Atmospheric Chemistry and Physics*, 5(9): 2311-2331.
- Boersma, K. F., et al. (2008), Intercomparison of SCIAMACHY and OMI tropospheric NO<sub>2</sub> columns: observing the diurnal evolution of chemistry and emissions from space, *Journal of Geophysical Research*, 113(D16S26).
- Bond, T. C., et al. (2004), A technology-based global inventory of black and organic carbon emissions from combustion, *Journal of Geophysical Research*, 109(D12403).
- Bousquet, P., et al. (2006), Contribution of anthropogenic and natural sources to atmospheric methane variability, *Nature*, 443: 439-443.
- Butler, T. M., et al. (2004), Mass balance inverse modeling of methane in the 1990s using a Chemistry Transport Model, *Atmospheric Chemistry and Physics*, 4: 2561-2580.
- Carmichael, G. R., et al. (2003), Evaluating regional emission estimates using the TRACE-P observations, *Journal of Geophysical Research*, 108(D21): 8810-8826.
- Carn, S. A., et al. (2004), Fire at Iraqi sulfur plant emits SO<sub>2</sub> clouds detected by Earth Probe TOMS, *Geophysical Research Letters*, 31(L19105).
- Carn, S. A., et al. (2007), Sulfur dioxide emissions from Peruvian copper smelters detected by the Ozone Monitoring Instrument, *Geophysical Research Letters*, 34(L09801).
- Chang, D., and Y. Song (2010), Estimates of biomass burning emissions in tropical Asia based on satellite-derived data, *Atmospheric Chemistry and Physics*, 10: 2335-2351.
- Chen, Y., and R. G. Prinn (2006), Estimation of anthropogenic methane emissions between 1996 and 2001 using a three-dimensional global chemical transport model, *Journal of Geophysical Research*, 111(D10307).
- Ciais, P., et al. (1995), Partitioning of ocean and land uptake of CO<sub>2</sub> as inferred by δ<sup>13</sup>C measurements from NOAA Climate Monitoring and Diagnostics Laboratory Global Air Sampling Network, *Journal of Geophysical Research*, 100: 5051-5070.
- CIESIN (2005), Gridded population of the world, version 3 (GPWv3), Center for International Earth Science Information Network (CIESIN), USA.
- Clarke, A. D., et al. (2004), Size distributions and mixtures of dust and black carbon aerosol in Asian outflow: Physiochemistry and optical properties, *Journal of Geophysical Research*, 109(D15S09).
- Clarke, L., et al. (2007), Scenarios of Greenhouse Gas Emissions and Atmospheric Concentrations, 154 pp, Office of Biological & Environmental Research, U.S. Department of Energy, Washington, DC.
- Clerbaux, C., et al. (2008), Carbon monoxide pollution from cities and urban areas observed by the Terra/MOPITT mission, *Geophysical Research Letters*, 35(L03817).



- Dalsøren, S. B., et al. (2009), Update on emissions and environmental impacts from the international fleet of ships: The contribution from major ship types and ports, *Atmospheric Chemistry and Physics*, 9(6): 2171-2194.
- Dalsøren, S. B., et al. (2007), Environmental impacts of the expected increase in sea transportation, with a particular focus on oil and gas scenarios for Norway and Northwest Russia, *Journal of Geophysical Research*, 112(D02310).
- Dickerson, R. R., et al. (2002), Analysis of black carbon and carbon monoxide observed over the Indian Ocean: implications for emissions and photochemistry, *Journal of Geophysical Research*, 107(D19): 8017-8027.
- Dubovik, O., et al. (2008), Retrieving global aerosol sources from satellites using inverse modeling, *Atmospheric Chemistry and Physics*, 8: 209-250.
- Duncan, B. N., et al. (2003), Interannual and seasonal variability of biomass burning emissions constrained by satellite observations, *Journal of Geophysical Research*, 108(D2): 4100-4121.
- EC/JRC/PBL (2010), Emission Database for Global Atmospheric Research (EDGAR), release version 4.1, European Commission, Joint Research Centre, Netherlands Environmental Assessment Agency, <http://edgar.jrc.ec.europa.eu>
- EMEP (2006), Transboundary acidification, eutrophication and ground level ozone in Europe since 1990 to 2004, 93 pp, European Monitoring and Evaluation Programme. [http://www.emep.int/publ/reports/2006/status\\_report\\_1\\_2006\\_ch.pdf](http://www.emep.int/publ/reports/2006/status_report_1_2006_ch.pdf)
- Enting, I. G., and J. V. Mansbridge (1989), Seasonal sources and sinks of atmospheric CO<sub>2</sub>, Direct inversion of filter data, *Tellus, Series B - Chemical and Physical Meteorology*, 41B: 111-126.
- Etiopie, G., and R. W. Klusman (2010), Microseepage in drylands: Flux and implications in the global atmospheric source/sink budget of methane, *Global and Planetary Change*, 72(4): 265-274.
- Eyers, C. J., et al. (2004), AERO2k global aviation emissions inventories for 2002 and 2025, Technical Report, 144 pp, European Commission, Farnborough, UK. *qinetiq/04/01113*
- Eyring, V., et al. (2005), Emissions from international shipping: 1. The last 50 years, *Journal of Geophysical Research*, 110(D17305).
- Fishman, J., et al. (2008), Remote sensing of tropospheric pollution from space, *Bulletin of the American Meteorological Society*, 89(6): 805-821.
- Flannigan, M. D., et al. (2005), Future area burned in Canada, *Climate Change*, 72(1-2): 1-16.
- Fortin, T. J., et al. (2005), Temporal changes in U.S. benzene emissions inferred from atmospheric measurements, *Environmental Science & Technology*, 39: 1403-1408.
- Frankenberg, C., et al. (2005), Assessing methane emissions from global space-borne observations, *Science*, 308(5724): 1010 - 1014.
- Frankenberg, C., et al. (2006), Satellite cartography of atmospheric methane from SCIAMACHY on board ENVISAT: Analysis of the years 2003 and 2004, *Journal of Geophysical Research*, 111(D07303).
- Frankenberg, C., et al. (2008a), Tropical methane emissions: A revised view from SCIAMACHY on board ENVISAT, *Geophysical Research Letters*, 35(L15811).
- Frankenberg, C., et al. (2008b), Pressure broadening in the 2ν<sub>3</sub> band of methane and its implication on atmospheric retrievals, *Atmospheric Chemistry and Physics*, 8: 5061-5075.
- Frey, H. C., and J. Zheng (2002), Quantification of variability and uncertainty in utility NO<sub>x</sub> emission inventories, *Journal of the Air and Waste Management Association*, 52(9): 1083-1095.
- Friedrich, R. (2009), Natural and biogenic emissions of environmentally relevant atmospheric trace constituents in Europe, *Atmospheric Environment*, 43: 1377-1379.
- Fu, T.-M., et al. (2007), Space-based formaldehyde measurements as constraints on volatile organic compound emissions in east and south Asia, *Journal of Geophysical Research*, 112(D06312).

- Fu, T. M., et al. (2008), Global budgets of atmospheric glyoxal and methylglyoxal, and implications for formation of secondary organic aerosols, *Journal of Geophysical Research*, 113(D15303).
- Fujino, J., et al. (2006), Multi-gas mitigation analysis on stabilization scenarios using AIM global model, *The Energy Journal, Multi-Greenhouse Gas Mitigation and Climate Policy*(Special Issue #3): 343-354.
- Fung, I., et al. (1991), Three-dimensional model synthesis of the global methane cycle, *Journal of Geophysical Research*, 96(D7): 13033-13065.
- Giglio, L., and J. D. Kendall (2004), Commentary on "Improving the seasonal cycle and interannual variations of biomass burning aerosol sources" by Generoso et al., *Atmospheric Chemistry and Physics*, 4: 585-587.
- Gilliland, A. B., et al. (2006), Seasonal NH<sub>3</sub> emissions for the continental United States: Inverse model estimation and evaluation, *Atmospheric Environment*, 40: 4986-4998.
- Guenther, A., et al. (2006), Estimates of global terrestrial isoprene emissions using MEGAN (Model of Emissions of Gases and Aerosols from Nature), *Atmospheric Chemistry and Physics*, 6: 3181-3210.
- Haberl, H., et al. (2007), Quantifying and mapping the human appropriation of net primary production in Earth's terrestrial ecosystems, *Proceedings of the National Academy of Science, USA*, 104: 12942-12947.
- Hakami, A., et al. (2005), Adjoint inverse modeling of black carbon during the Asian Pacific Regional Aerosol Characterization Experiment, *Journal of Geophysical Research*, 110(D14301).
- Han, K. M., et al. (2009), Investigation of NO<sub>x</sub> emissions and NO<sub>x</sub>-related chemistry in East Asia using CMAQ-predicted and GOME-derived NO<sub>2</sub> columns, *Atmospheric Chemistry and Physics*, 9: 1017-1036.
- Hao, J., et al. (2002), Emission inventories of NO<sub>x</sub> from commercial energy consumption in China, 1995-1998, *Environmental Science & Technology*, 36: 552-560.
- Hao, W. M., and M. H. Liu (1994), Spatial and temporal distribution of tropical biomass burning, *Global Biogeochemical Cycles*, 8: 495-503.
- Harley, R. A., et al. (2005), Changes in motor vehicle emissions on diurnal to decadal time scales and effects on atmospheric composition, *Environmental Science & Technology*, 39: 5356-5362.
- He, Y., et al. (2007), Variations of the increasing trend of tropospheric NO<sub>2</sub> over central east China during the past decade, *Atmospheric Environment*, 41: 4865-4876.
- Heald, C. L., et al. (2003), Asian outflow and trans-Pacific transport of carbon monoxide and ozone pollution: An integrated satellite, aircraft, and model perspective, *Journal of Geophysical Research*, 108(D244804).
- Heald, C. L., et al. (2004), Comparative inverse analysis of satellite (MOPITT) and aircraft (TRACE-P) observations to estimate Asian sources of carbon monoxide, *Journal of Geophysical Research*, 109(D23306).
- Hein, R., et al. (1997), An inverse modeling approach to investigate the global atmospheric methane cycle, *Global Biogeochemical Cycles*, 11(1): 43-76.
- Henze, D. K., et al. (2009), Inverse modeling and mapping US air quality influences of inorganic PM<sub>2.5</sub> precursor emissions using the adjoint of GEOS-Chem, *Atmospheric Chemistry and Physics*, 9: 5877-5903.
- Hijioka, Y., et al. (2008), Global GHG emissions scenarios under GHG concentration stabilization targets, *Journal of Global Environmental Engineering*, 13: 97-108.
- Hoelzemann, J. J., et al. (2004), Global Wildland Fire Emission Model (GWEM): Evaluating the use of global area burnt satellite data, *Journal of Geophysical Research*, 109(D14S04).
- Houweling, S., et al. (1999), Inverse modeling of methane sources and sinks using the adjoint of a global transport model, *Journal of Geophysical Research*, 104: 26137-26160.

- Hu, Y., et al. (2009), Top-down analysis of the elemental carbon emissions inventory in the United States by inverse modeling using Community Multiscale Air Quality model with decoupled direct method (CMAQ-DDM), *Journal of Geophysical Research*, 114(D24302).
- IEA/OECD (2007), Energy balances of OECD and Non-OECD Countries, <http://data.iaea.org>
- IPCC (1996), Climate Change 1995: The Science of Climate Change - A Contribution of Working Group I to the Second Assessment Report, edited by J. T. Houghton, et al., Cambridge University Press, Cambridge.
- IPCC (2000), Emissions Scenarios, edited by N. Nakicenovic and R. Swart, 570 pp., Cambridge University Press, Cambridge.
- IPCC (2001), Climate Change, Synthesis Report. A Contribution of Working Groups I, II, and III to the Third Assessment Report of the Intergovernmental Panel on Climate Change, edited by R. T. Watson and C. W. Team, 398 pp., Cambridge University Press, Cambridge, United Kingdom and New York, NY, USA.
- IPCC (2006), 2006 IPCC Guidelines for National Greenhouse Gas Inventories, edited by S. Eggleston, et al., Institute for Global Environmental Strategies (IGES) on behalf of the Intergovernmental Panel on Climate Change, Hayama, Japan.
- Irie, H., et al. (2005), Evaluation of long-term tropospheric NO<sub>2</sub> data obtained by GOME over East Asia in 1996-2002, *Geophysical Research Letters*, 32(L11810).
- Irie, H., et al. (2009), Characterization of OMI tropospheric NO<sub>2</sub> measurements in East Asia based on a robust validation comparison, *Scientific Online Letters of the Atmosphere*, 5: 117-120.
- Ito, A., and J. E. Penner (2004), Global estimate of biomass burning emissions based on satellite imagery for the year 2000, *Journal of Geophysical Research*, 109(D14S05).
- Jaeglé, L., et al. (2004), Satellite mapping of rain-induced nitric oxide emissions from soils, *Journal of Geophysical Research*, 109(D21310).
- Jaeglé, L., et al. (2005), Global partitioning of NO<sub>x</sub> sources using satellite observations: Relative roles of fossil fuel combustion, biomass burning and soil emissions, *Faraday Discussions*, 130: 407-423.
- Jones, D. B. A., et al. (2009), The zonal structure of tropical O<sub>3</sub> and CO as observed by the Tropospheric Emission Spectrometer in November 2004 - Part 1: Inverse modeling of CO emissions, *Atmospheric Chemistry and Physics*, 9: 3547-3562.
- Kasibhatla, P., et al. (2002), Top-down estimate of a large source of atmospheric carbon monoxide associated with fuel combustion in Asia, *Geophysical Research Letters*, 29(19): 1900-1903.
- Khokhar, M. F., et al. (2008), Temporal trends of anthropogenic SO<sub>2</sub> emitted by non-ferrous metal smelters in Peru and Russia estimated from satellite observations, *Atmospheric Chemistry and Physics Discussions*, 8: 17393-17422.
- Kiley, C. M., et al. (2003), An intercomparison and evaluation of aircraft-derived and simulated CO from seven chemical transport models during the TRACE-P experiment, *Journal of Geophysical Research*, 108(D21): 8819-8846.
- Kim, S.-W., et al. (2006), Satellite-observed U.S. power plant NO<sub>x</sub> emission reductions and their impact on air quality, *Geophysical Research Letters*, 33(L22842).
- Kim, S. W., et al. (2009), NO<sub>2</sub> columns in the western United States observed from space and simulated by a regional chemistry model and their implications for NO<sub>x</sub> emissions, *Journal of Geophysical Research*, 114(D11301).
- Klimont, Z., and D. G. Streets (2007), Emissions inventories and projections for assessing hemispheric or intercontinental transport, United Nations, Geneva.
- Klimont, Z., et al. (2009), Projections of SO<sub>2</sub>, NO<sub>x</sub> and carbonaceous aerosols emissions in Asia, *Tellus B*, 61(4): 602-617.
- Konovalov, I. B., et al. (2006), Inverse modelling of the spatial distribution of NO<sub>x</sub> emissions on a continental scale using satellite data, *Atmospheric Chemistry and Physics*, 6: 1747-1770.

- Kopacz, M., et al. (2009), Comparison of adjoint and analytical Bayesian inversion methods for constraining Asian sources of carbon monoxide using satellite (MOPITT) measurements of CO columns, *Journal of Geophysical Research*, 114(D04305).
- Krotkov, N. A., et al. (2008), Validation of SO<sub>2</sub> retrievals from the Ozone Monitoring Instrument over NE China, *Journal of Geophysical Research*, 113(D16S40).
- Krueger, A. J., et al. (1995), Volcanic sulfur dioxide measurements from the total ozone mapping spectrometer instruments, *Journal of Geophysical Research*, 100(D7): 14057-14076.
- Kurokawa, J., et al. (2009), Adjoint inverse modeling of NO<sub>x</sub> emissions over eastern China using satellite observations of NO<sub>2</sub> vertical column densities, *Atmospheric Environment*, 43(11): 1878-1887.
- Lamarque, J. F., et al. (2010), Historical (1850-2000) gridded anthropogenic and biomass burning emissions of reactive gases and aerosols: Methodology and application, *Atmospheric Chemistry and Physics*, 10: 7017-7039.
- Lee, C., et al. (2009), Retrieval of vertical columns of sulfur dioxide from SCIAMACHY and OMI: Air mass factor algorithm development and validation, *Journal of Geophysical Research*, 114(D22303).
- Lee, D. S., et al. (1997), Estimations of global NO<sub>x</sub> emissions and their uncertainties, *Atmospheric Environment*, 31(12): 1735-1749.
- Lee, Y. N., et al. (1998), Atmospheric chemistry and distribution of formaldehyde and several multioxygenated carbonyl compounds during the 1995 Nashville/Middle Tennessee Ozone Study, *Journal of Geophysical Research*, 103(D17): 22449-22462.
- Leue, C., et al. (2001), Quantitative analysis of NO<sub>x</sub> emissions from GOME satellite image sequences, *Journal of Geophysical Research*, 106(D6): 5493-5506.
- Li, C., et al. (2010), Recent large reduction in sulfur dioxide emissions from Chinese power plants observed by the Ozone Monitoring Instrument, *Geophysical Research Letters*, 37(L08807).
- Lin, J. T., et al. (2010), Constraint of anthropogenic NO<sub>x</sub> emissions in China from different sectors: A new methodology using multiple satellite retrievals, *Atmospheric Chemistry and Physics*, 10: 63-78.
- Lonneman, W. A., et al. (1986), Non-methane organic composition in the Lincoln Tunnel, *Environmental Science & Technology*, 20: 790-796.
- Ma, J., et al. (2006), Comparison of model-simulated tropospheric NO<sub>2</sub> over China with GOME-satellite data, *Atmospheric Environment*, 40(4): 593-604.
- Mahowald, N., et al. (2003), Interannual variability in atmospheric mineral aerosols from a 22-year model simulation and observational data, *Journal of Geophysical Research*, 108(D12): 4352-4371.
- Mahowald, N. M., et al. (2006), Change in atmospheric mineral aerosols in response to climate: Last glacial period, preindustrial, modern, and doubled carbon dioxide climates, *Journal of Geophysical Research*, 111(D10202).
- Martin, R. V., et al. (2003), Global inventory of nitrogen oxide emissions constrained by space-based observations of NO<sub>2</sub> columns, *Journal of Geophysical Research*, 108(D17): 4537-4548.
- Martin, R. V., et al. (2006), Evaluation of space-based constraints on global nitrogen oxide emissions with regional aircraft measurements over and downwind of eastern North America, *Journal of Geophysical Research*, 111(D15308).
- Martin, R. V. (2008), Satellite remote sensing of surface air quality, *Atmospheric Environment*, 42(34): 7823-7843.
- Meirink, J. F., et al. (2006), Sensitivity analysis of methane emissions derived from SCIAMACHY observations through inverse modelling, *Atmospheric Chemistry and Physics*, 6: 1275-1292.
- Meirink, J. F., et al. (2008), Four-dimensional variational data assimilation for inverse modeling of atmospheric methane emissions: Analysis of SCIAMACHY observations, *Journal of Geophysical Research*, 113(D17301).

- Mieville, A., et al. (2010), Emissions of gases and particles from biomass burning during the 20th century using satellite data and an historical reconstruction, *Atmospheric Environment*, 44(11): 1469-1477.
- Mijling, B., et al. (2009), Reduction of NO<sub>2</sub> detected from space during the 2008 Beijing Olympic Games, *Geophysical Research Letters*, 36(L13801).
- Mikaloff Fletcher, S. E., et al. (2004), CH<sub>4</sub> sources estimated from atmospheric observations of CH<sub>4</sub> and its <sup>13</sup>C/<sup>14</sup>C isotopic ratios: 1. Inverse modeling of source processes, *Global Biogeochemical Cycles*, 18(GB4004).
- Millet, D. B., et al. (2006), Formaldehyde distribution over North America: Implications for satellite retrievals of formaldehyde columns and isoprene emission, *Journal of Geophysical Research*, 111(D24S02).
- Millet, D. B., et al. (2008), Spatial distribution of isoprene emissions from North America derived from formaldehyde column measurements by the OMI satellite sensor, *Journal of Geophysical Research*, 113(D02307).
- Mohan, M., et al. (2007), Preparation and validation of gridded emission inventory of criteria air pollutants and identification of emission hotspots for megacity Delhi, *Environmental Monitoring and Assessment*, 130: 323-339.
- Monks, P. S., et al. (2009), Atmospheric composition change - global and regional air quality, *Atmospheric Environment*, 43(33): 5268-5350.
- Moss, R. H., et al. (2010), Representative concentration pathways: A new approach to scenario development for the IPCC Fifth Assessment Report, *Nature*, 463: 747-756.
- Müller, J.-F., and T. Stavrou (2005), Inversion of CO and NO<sub>x</sub> emissions using the adjoint of the IMAGES model, *Atmospheric Chemistry and Physics*, 5: 1157-1186.
- Napelenok, S. L., et al. (2008), A method for evaluating spatially resolved NO<sub>x</sub> emissions using Kalman filter inversion, direct sensitivities, and space-based NO<sub>2</sub> observations, *Atmospheric Chemistry and Physics*, 8: 5603-5614.
- Ohara, T., et al. (2007), An Asian emission inventory of anthropogenic emission sources for the period 1980-2020, *Atmospheric Chemistry and Physics*, 7(16): 4419-4444.
- Olivier, J. G. J., et al. (1996), Description of EDGAR Version 2.0, National Institute of Public Health and Environment, Bilthoven, The Netherlands.
- Olivier, J. G. J., and M. Berdowski (2001), Global emissions sources and sinks, in *The Climate System*, edited by J. Berdowski, et al., 33-78 pp., A. A. Balkema, Brookfield, Vt.
- Palmer, P. I., et al. (2003a), Mapping isoprene emissions over North America using formaldehyde column observations from space, *Journal of Geophysical Research*, 108(D6): 4180-4192.
- Palmer, P. I., et al. (2003b), Inverting for emissions of carbon monoxide from Asia using aircraft observations over the western Pacific, *Journal of Geophysical Research*, 108(D21): 8828-8839.
- Palmer, P. I., et al. (2006), Quantifying the seasonal and interannual variability of North American isoprene emissions using satellite observations of the formaldehyde column, *Journal of Geophysical Research*, 111(D12315).
- Palmer, P. I. (2008), Quantifying sources and sinks of trace gases using space-borne measurements: Current and future science, *Philosophical Transactions of the Royal Society*, 366: 4509-4528.
- Parashar, D. C., et al. (2005), Carbonaceous aerosol emissions from India, *Atmospheric Environment*, 39(40): 7861-7871.
- Parrish, D. D. (2006), Critical evaluation of US on-road vehicle emission inventories, *Atmospheric Environment*, 40(13): 2288-2300.
- Peischl, J., et al. (2010), A top-down analysis of emissions from selected Texas power plants during TexAQ5 2000 and 2006, *Journal of Geophysical Research*, 115(D16303).

- Pétron, G., et al. (2002), Inverse modeling of carbon monoxide surface emissions using Climate Monitoring and Diagnostics Laboratory network observations, *Journal of Geophysical Research*, 107(D24): 4761-4784.
- Pétron, G., et al. (2004), Monthly CO surface sources inventory based on the 2000-2001 MOPITT satellite data, *Geophysical Research Letters*, 31(L21107).
- Pfister, G., et al. (2005), Quantifying CO emissions from the 2004 Alaskan wildfires using MOPITT CO data, *Geophysical Research Letters*, 32(L11809).
- Price, C., et al. (1997), NO<sub>x</sub> from lightning: 1. Global distribution based on lightning physics, *Journal of Geophysical Research*, 102(D5): 5929-5942.
- Quelo, D., et al. (2005), Inverse modeling of NO<sub>x</sub> emissions at regional scale over northern France: Preliminary investigation of the second-order sensitivity, *Journal of Geophysical Research*, 110(D24310).
- Reddy, M. S., and C. Venkataraman (2002), A 0.25° x 0.25° inventory of aerosol and sulfur dioxide emissions from India: II. Biomass combustion, *Atmospheric Environment*, 36: 699-712.
- Riahi, K., et al. (2007), Scenarios of long-term socio-economic and environmental development under climate stabilization, *Technological Forecasting and Social Change*, 74(7): 887-935.
- Richter, A., et al. (2005), Increase in tropospheric nitrogen dioxide over China observed from space, *Nature*, 437(7055): 129-132.
- Rypdal, K. (2002), Uncertainties in the Norwegian emission inventories of acidifying pollutants and volatile organic compounds, *Environmental Science & Policy*, 5: 233-246.
- Saeger, M., et al. (1989), The 1985 NAPAP emissions inventory (version 2): Development of the annual data and modelers' tape, U.S. Environmental Protection Agency, Washington, DC. EPA-600/7-89-012a
- Schultz, M. G., et al. (2008), Global wildland fire emissions from 1960 to 2000, *Global Biogeochemical Cycles*, 22(GB2002).
- Schumann, U., and H. Huntrieser (2007), The global lightning-induced nitrogen oxides source, *Atmospheric Chemistry and Physics*, 7: 3823-3907.
- Seila, R. L., et al. (1989), Project Summary: Determination of C<sub>2</sub> to C<sub>12</sub> ambient air hydrocarbons in 39 U.S. cities, from 1984 through 1986, U.S. Environmental Protection Agency, Washington, DC. EPA/600/S3-89/058
- Seiler, W., and J. P. Crutzen (1980), Estimates of the gross and net fluxes of carbon between the biosphere and the atmosphere from biomass burning, *Climate Change*, 2: 207-247.
- SEPA (2003), Report on the state of the environment in China, State Environmental Protection Administration of China, Beijing.
- Shi, C., et al. (2008), Tropospheric NO<sub>2</sub> columns over East Central China: Comparisons between SCIAMACHY measurements and nested CMAQ simulations, *Atmospheric Environment*, 42: 7165-7173.
- Shim, C., et al. (2005), Constraining global isoprene emissions from Global Ozone Monitoring Experiment (GOME) formaldehyde column measurements, *Journal of Geophysical Research*, 110(D24301).
- Smith, S. J., and T. M. L. Wigley (2006), Multi-gas forcing stabilization with the MiniCAM, *Energy Journal*(Special Issue #3): 373-391.
- Stavrakou, T., and J.-F. Müller (2006), Grid-based versus big region approach for inverting CO emissions using Measurement of Pollution in the Troposphere (MOPITT) data, *Journal of Geophysical Research*, 111(D15304).
- Stavrakou, T., et al. (2008), Assessing the distribution and growth rates of NO<sub>x</sub> emission sources by inverting a 10-year record of NO<sub>2</sub> satellite columns, *Geophysical Research Letters*, 35(L10801).
- Stavrakou, T., et al. (2009), The continental source of glyoxal estimated by the synergistic use of spaceborne measurements and inverse modeling, *Atmospheric Chemistry and Physics*, 9: 8431-8446.

- Streets, D. G., et al. (2001), Trends in emissions of acidifying species in Asia, 1985-1997, *Water Air and Soil Pollution*, 130: 187-192.
- Streets, D. G., et al. (2003), An inventory of gaseous and primary aerosol emissions in Asia in the year 2000, *Journal of Geophysical Research*, 108(D21): 8809-8831.
- Streets, D. G., et al. (2004), On the future of carbonaceous aerosol emissions, *Journal of Geophysical Research*, 109(D24212).
- Streets, D. G., et al. (2006), Revisiting China's CO emissions after the Transport and Chemical Evolution over the Pacific (TRACE-P) mission: Synthesis of inventories, atmospheric modeling, and observations, *Journal of Geophysical Research*, 111(D14306).
- Sumner, A. L., et al. (2001), A study of formaldehyde chemistry above a forest canopy, *Journal of Geophysical Research*, 106(D20): 24387-24405.
- Suntharalingam, P., et al. (2004), Improved quantification of Chinese carbon fluxes using CO<sub>2</sub>/CO correlations in Asian outflow, *Journal of Geophysical Research*, 109(D18S18).
- Tan, Q., et al. (2004), An evaluation of TRACE-P emission inventories from China using a regional model and chemical measurements, *Journal of Geophysical Research*, 109(D22305).
- Tanimoto, H., et al. (2008), Diagnosing recent CO emissions and ozone evolution in East Asia using coordinated surface observations, adjoint inverse modeling, and MOPITT satellite data, *Atmospheric Chemistry and Physics*, 8: 3867-3880.
- Tian, B., et al. (2005), Diurnal cycle of summertime deep convection over North America: A satellite perspective, *Journal of Geophysical Research*, 110(D08108).
- Toenges-Schuller, N., et al. (2006), Global distribution pattern of anthropogenic nitrogen oxide emissions: Correlation analysis of satellite measurements and model calculations, *Journal of Geophysical Research*, 111: D05312.
- Turquety, S., et al. (2008), CO emission and export from Asia: An analysis combining complementary satellite measurements (MOPITT, SCIAMACHY and ACE-FTS) with global modeling, *Atmospheric Chemistry and Physics*, 8: 5187-5204.
- U.S. EPA (1990), National Air Pollution and Emissions Trends Report, 1988, 158 pp, United States Environmental Protection Agency, Research Triangle Park, NC. *EPA-450/4-90-002*
- U.S. EPA (1995), National Air Pollutant and Emission Trends Report, 1900-1994, United States Environmental Protection Agency, Research Triangle Park, NC. *EPA-454/R-95-011*
- U.S. EPA (2000), National Air Pollutant Emission Trends Report, 1900-1998, 238 pp, United States Environmental Protection Agency, Research Triangle Park, NC. *EPA-454/R-00-002*
- U.S. EPA (2003), National Air Quality and Emissions Trends Report, 2003 Special Studies Edition, 70 pp, Office of Air Quality Planning and Standards, U.S. Environmental Protection Agency, Research Triangle Park, NC. *EPA-454/R-03-005*
- U.S. EPA (2009), National Emissions Inventory (NEI) Air Pollutant Emissions Trends Data, U.S. Environmental Protection Agency, <http://www.epa.gov/ttnchie1/trends/>
- Uno, I., et al. (2003), Analysis of surface black carbon distributions during ACE-Asia using a regional-scale aerosol model, *Journal of Geophysical Research*, 108(D23): 8636-8646.
- Uno, I., et al. (2007), Systematic analysis of interannual and seasonal variations of model-simulated tropospheric NO<sub>2</sub> in Asia and comparison with GOME-satellite data, *Atmospheric Chemistry and Physics*, 7: 1671-1681.
- van Aardenne, J. A., et al. (2001), A 1° × 1° resolution data set of historical anthropogenic trace gas emissions for the period 1890-1990, *Global Biogeochemical Cycles*, 15(4): 909-928.
- van Aardenne, J. A., et al. (2005), The EDGAR 3.2 Fast Track 2000 dataset (32FT2000), Emission Database for Global Atmospheric Research (EDGAR) Consortium, [http://www.mnp.nl/edgar/Images/Description\\_of\\_EDGAR\\_32FT2000\(v8\)\\_tcm32-22222.pdf](http://www.mnp.nl/edgar/Images/Description_of_EDGAR_32FT2000(v8)_tcm32-22222.pdf)



- van der A, R. J., et al. (2006), Detection of the trend and seasonal variation in tropospheric NO<sub>2</sub> over China, *Journal of Geophysical Research*, 111: D12317.
- van der A, R. J., et al. (2008), Trends, seasonal variability and dominant NO<sub>x</sub> source derived from a ten year record of NO<sub>2</sub> measured from space, *Journal of Geophysical Research*, 113: D04302.
- van der Werf, G., et al. (2004), Continental scale partitioning of fire emissions during the 1997 to 2001 El Nino/La Nina period, *Science* 303: 73-76.
- van der Werf, G. R., et al. (2003), Carbon emissions from fires in tropical and subtropical ecosystems, *Global Change Biology*, 9(4): 547-562.
- van der Werf, G. R., et al. (2006), Interannual variability in global biomass burning emissions from 1997 to 2004, *Atmospheric Chemistry and Physics*, 6: 3423-3441.
- van Donkelaar, A., et al. (2008), Analysis of aircraft and satellite measurements from the Intercontinental Chemical Transport Experiment (INTEX-B) to quantify long-range transport of East Asian sulfur to Canada, *Atmospheric Chemistry and Physics*, 8: 2999-3014.
- van Noije, T. P. C., and et al. (2006), Multi-model ensemble simulations of tropospheric NO<sub>2</sub> compared with GOME retrievals for the year 2000, *Atmospheric Chemistry and Physics*, 6: 2943-2979.
- van Vuuren, D., et al. (2007), Stabilizing greenhouse gas concentrations at low levels: An assessment of reduction strategies and costs, *Climatic Change*, 81(2): 119-159.
- van Vuuren, D., et al. (2008), Temperature increase of 21st century mitigation scenarios, *Proceedings of the National Academy of Sciences of the U.S.A.*, 105(40): 15258-15262.
- Wang, Y., et al. (2004), Asian emissions of CO and NO<sub>x</sub>: Constraints from aircraft and Chinese station data, *Journal of Geophysical Research*, 109(D24304).
- Wang, Y., et al. (2007a), Traffic restrictions associated with the Sino-African summit: Reductions of NO<sub>x</sub> detected from space, *Geophysical Research Letters*, 34(L08814).
- Wang, Y., et al. (2007b), Seasonal variability of NO<sub>x</sub> emissions over east China constrained by satellite observations: Implications for combustion and microbial sources, *Journal of Geophysical Research*, 112(D06301).
- Wang, Y., et al. (2009), Ozone air quality during the 2008 Beijing Olympics: Effectiveness of emission restrictions, *Atmospheric Chemistry and Physics*, 9: 5237-5251.
- Wise, M. A., et al. (2009), Implications of limiting CO<sub>2</sub> concentrations on land use and energy, *Science*, 324: 1183-1186.
- Witte, J. C., et al. (2009), Satellite observations of changes in air quality during the 2008 Beijing Olympic and Paralympics, *Geophysical Research Letters*, 36(L17803).
- Yumimoto, K., and I. Uno (2006), Adjoint inverse modeling of CO emissions over Eastern Asia using four-dimensional variational data assimilation, *Atmospheric Environment*, 40: 6836-6845.
- Zhang, Q., et al. (2007), NO<sub>x</sub> emission trends for China, 1995-2004: The view from the ground and the view from space, *Journal of Geophysical Research*, 112(D22306).
- Zhang, Q., et al. (2009a), Asian emissions in 2006 for the NASA INTEX-B mission, *Atmospheric Chemistry and Physics*, 9: 5161-5153.
- Zhang, Q., et al. (2009b), Satellite observations of recent power plant construction in Inner Mongolia, China, *Geophysical Research Letters*, 36: L15809.
- Zhao, C., and Y. Wang (2009), Assimilated inversion of NO<sub>x</sub> emission over east Asia using OMI NO<sub>2</sub> column measurements, *Geophysical Research Letters*, 36(L06805).



## Chapter 4

### Global and Regional Modelling

**Lead Authors:** Greg Carmichael, Oliver Wild

**Co-authors:** Arlene Fiore, Tracey Holloway, Meiyun Lin, Ruth Doherty, Jan Eiof Jonson, Joshua Fu, Sunling Gong, Mian Chin, Denise Mauzerall, Yuxuan Wang, Bill Collins, Michael Schulz, David Reidmiller, Junfeng Liu, Yang Zhang, Yun Fat Lam

#### 4.1. Overview

Effective implementation of policy to decrease ambient pollutant levels requires knowledge of the contribution of pollutant sources (e.g., from natural sources versus those due to human activities, or from local versus regional versus intercontinental sources) to the observed pollutant distributions. While observational methods provide clear evidence for intercontinental transport, and can help fingerprint specific source contributions (see Chapter 2), these measurements are generally not in operational networks, and are often not regionally representative. Thus at present, observation-based approaches alone cannot provide the information on source attribution (S/A) and source/receptor (S/R) relationships needed to make better informed policy decisions about hemispheric pollution. Numerical models incorporate our current understanding of the physical and chemical processes which control atmospheric composition, and are designed to predict the relationships between emissions and the resulting pollution distributions in the atmosphere. These models allow us to explore the importance of different processes and to attribute observed enhancements in pollutant concentrations to particular sources. In this chapter we discuss methods for quantifying intercontinental transport using numerical models, and summarize recent estimates of the magnitude and uncertainty in these effects, both from the published literature and from the model intercomparison organized under the Task Force (hereafter referred to as the HTAP intercomparison). The capabilities and limitations of current models are analyzed, along with the sensitivity of S/R relationships to future changes in emissions and climate. Further activities needed to improve the modelling capabilities and the estimates of hemispheric transport of pollutants are identified.

##### 4.1.1. Modelling approaches

Chemical transport models (CTMs) provide a representation of the chemical, transport and removal mechanisms that control the distributions of constituents in the atmosphere, as introduced in Chapter A1, based around a given set of emissions. They reflect our current understanding of these processes, which is informed by theoretical, laboratory and field experiments that focus on particular components of the system. A number of different types of models are useful for exploring intercontinental transport, and we outline here the different approaches that may be taken, summarizing their strengths, requirements and limitations. These range from point-based dispersion models, representing the transport and evolution of a single plume of pollutants from a source region, to regional or global-scale grid-based models that represent large-scale atmospheric composition.

Atmospheric dispersion models are commonly used to quantify ground-level pollutant concentrations and deposition <50 km downwind of point, line and area sources. These models have been evaluated at larger scales (~1000 km) with observations from field studies, e.g., CAPTEX (Cross-Appalachian Tracer Experiment) and ETEX (European Tracer Experiment), to build confidence in their use in scientific, regulatory and policy applications [Galmarini *et al.*, 2004; Klug *et al.*, 1992]. Lagrangian particle dispersion models are now the most commonly used tools for meteorological based source attribution studies. These models initiate backward trajectories from a receptor location and calculate the transport pathways of air masses (often referred to as particles because they are assumed to be infinitesimally small) following the winds resolved in atmospheric analyses or forecasts. The models also include a stochastic step to represent the effects of unresolved turbulence and convection [Stohl *et al.*, 2002]. The parameterised “random walk” shuffles particles, each weighted with the same tracer mass, so that their sum within a volume represents the effects of advection and diffusive mixing on passive tracer concentration [Legras *et al.*, 2003]. The models

(described in more detail in Chapter 2) have not yet been developed to include chemical or aerosol processing or detailed descriptions of deposition processes where non-linearities in chemical transformation may be important.

Eulerian (gridded) CTMs are the most commonly used tools for studying intercontinental transport. CTMs divide the atmosphere into discrete grid-boxes in which transport and chemical processes are calculated. A schematic of the Eulerian modelling approach is shown in Figure 4.1. Typical resolutions are tens of vertical levels between the Earth's surface and the tropopause and a few degrees horizontally in global models to tens of kilometres or less in regional models. Common modes of operation are “off-line”, where a CTM ingests large volumes of meteorological data from a driving numerical weather prediction model or global atmospheric circulation (i.e., climate) model and “free-running”, where tracers are included directly in a global atmospheric circulation model which is often driven by observed sea surface temperatures (SSTs) for present-day simulations. In most studies to date that have estimated intercontinental S/R relationships, there is no coupling from the atmospheric chemistry back to the meteorology which determines the transport and dispersion of air pollution. CTMs require pollutant emission inventories and schemes to represent processes relevant to intercontinental transport such as advection, turbulent mixing, convection, chemical production and loss, wet scavenging and dry deposition. Many of these processes operate on scales smaller than resolved explicitly by the models, and so are heavily parameterized, increasing uncertainty in the capabilities of current CTMs to represent quantitatively intercontinental transport.

New developments in modelling intercontinental transport at finer scales include nested-grid, global-to-regional modelling, which allows for inclusion of a regional window over a source or receptor continent with a higher spatial resolution embedded in a global domain. Higher resolution nested-grid models can resolve better the localized regions of intense upward advection and convection responsible for lifting chemicals from the near-surface environment, a mechanism poorly represented in coarser-resolution global simulations [Chen *et al.*, 2009b; Wang *et al.*, 2004].

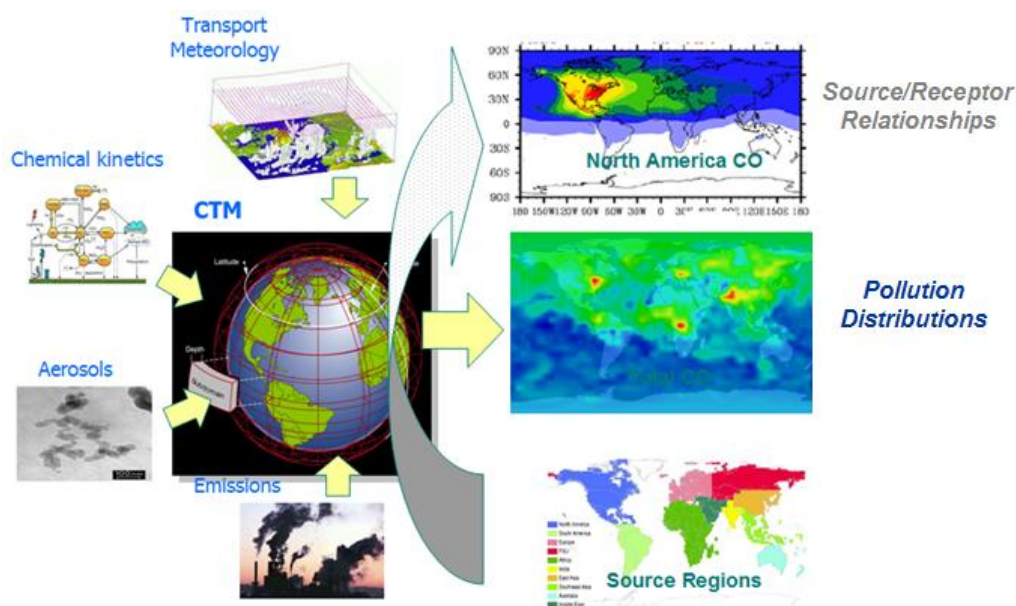


**Figure 4.1.** Schematic of the Eulerian forward modelling approach. The model represents various processes that impact pollutant transport, chemistry and removal of pollutants. These models can be applied in S/R and source attribution studies, where emissions from specific source regions are followed through the atmosphere.

#### 4.1.2. Model methods for quantifying source contributions to intercontinental transport

From scientific and policy perspectives it is useful to estimate the contribution of specific emission sources to air pollution levels. The distinction between source attribution (S/A), the contribution of a particular source to the absolute concentrations observed at a given location, and

source-receptor (S/R) relationship, the relative extent to which concentrations at a specific location change when a particular source is perturbed in an arbitrary manner, is made in Chapter 1, Section 1.3. Both approaches rely heavily on models for quantification, as independent verification from observations is difficult (see Chapter 2). The use of models for these source contribution applications is illustrated in Figure 4.1. For inert tracers, the approaches give similar results as the contribution of all sources at a particular receptor is additive [Seibert and Frank, 2004], and this is a good approximation for most aerosol species [Liu et al., 2009]. However, for many reactive species such as ozone (O<sub>3</sub>), which have a non-linear dependence on precursor concentrations, the contribution of a given source change at a downwind receptor location is dependent on the magnitude of all other sources, not the specified source alone. Over intercontinental distances additional O<sub>3</sub> precursor emissions typically lead to successively smaller increases in O<sub>3</sub> over receptor regions, reflecting the reduced efficiency of O<sub>3</sub> formation [Liu et al., 1987].

Two different approaches have been used to quantify the contribution of a specific source region to the pollution amounts at a receptor area (see section 1.3.2). The *emission sensitivity approach* requires two simulations: 1) a standard ‘control’ run that includes all emission sources and is designed so that predicted pollution levels can be directly compared with observations and 2) an additional simulation where emissions from a specific source region or category are perturbed. The contribution from that particular source is then determined by the difference between the predicted distributions from the two runs [Chin et al., 2007; Fiore et al., 2009; Jacob et al., 1999; Park et al., 2004; Wild and Akimoto, 2001; Wild et al., 2004a]. When relatively small emission changes are applied, this approach provides the sensitivity of receptor region responses around current conditions.

The second approach is the *tagged tracer method*, in which the distribution of idealized pollutant tracers is calculated, each of which is emitted or produced only inside a particular designated source region. The concentration of each pollutant tracer tagged by its source region then represents the contribution of that source region. Many independent source regions or categories can be tagged within a single model simulation, but this may require special model design. This method has been used in studies addressing a wide variety of issues using both global and regional chemistry transport models [Auvray and Bey, 2005; Bian et al., 2007; Fiore et al., 2002; Li et al., 2002; Li et al., 2008; Sudo and Akimoto, 2007; Wang et al., 1998]. The method provides a good estimate of source contributions for directly-emitted primary pollutants, and has been shown to work well for most aerosol species [Liu et al., 2009]. However, it is problematic for catalytically-produced secondary pollutants such as O<sub>3</sub> where rapid chemical interconversion precludes a simple representation of the source term. Application of this approach for O<sub>3</sub> has either involved complex tagging of key precursors along with simplified assumptions about production [e.g., Horowitz et al., 1998], or a simpler tagging of O<sub>3</sub> produced over particular regions [e.g., Sudo and Akimoto, 2007]. Although this latter approach is far simpler, it is domain-based rather than source-based, and therefore does not reflect the contribution of precursor emissions from a given source region. Due to the nature of the advection algorithms used in models, neither of these tagging approaches is entirely conservative, so typically the sum of the fractional contribution from all source regions does not equal unity.

The techniques discussed above are *forward* approaches to source contribution calculation. In these methods the impacts of emissions from a specific region are estimated for every grid cell within the modelling domain (e.g., globally). An alternative and complimentary approach is to focus on pollution levels at a particular receptor, and calculate only the contributions from those sources that contribute to pollution levels at this receptor. This receptor (or *backward*) approach can be thought of as running the models in reverse, and can be efficiently done using adjoint models [Carmichael et al., 2008], or for inert tracers using reverse particle models such as the FLEXPART model [Stohl et al., 1998]. The adjoint approach has been used in regional receptor-based source-contribution studies [Hakami et al., 2006], and in global O<sub>3</sub> and aerosol applications [Henze et al., 2009; Zhang et al., 2009].

#### 4.1.3. Role of coordinated model studies

The majority of studies summarized in this chapter have applied global or regional Eulerian models to explore the emission, transport and removal of O<sub>3</sub>, aerosols and their precursors. Many studies have focused on intercontinental transport from one or more source regions [e.g., Berntsen et

*al.*, 1996; *Bey et al.*, 2001], but there is little consistency between studies in terms of the techniques used, the spatial extent of source and receptor regions, or in the metrics applied to quantify transport downwind. Given the large variation in approaches and objectives of these studies it is hard to draw consistent conclusions from them or to identify and quantify key weaknesses in our current understanding. To address this, five sets of coordinated model studies were performed as part of the HTAP intercomparison, adopting a coherent, standardized framework in the modelling approach, definition of regions, choice of meteorological year, and diagnostics to provide consistent estimates of the effects of intercontinental transport. The diversity of model results produced with this approach allows a more direct, quantitative assessment of some of the current uncertainty in our understanding of emissions, transport, and chemical or microphysical processes. These additional experiments are summarized in Table 4.1. The major intercomparison study (SR) focused on quantifying current source-receptor relationships for O<sub>3</sub> and aerosols and characterizing model uncertainty, while subsequent studies addressed specific aspects including the contribution of transport processes to this uncertainty (TP), ability to reproduce observed transport events (ES) and the likely effects of future changes in emissions (FE) and climate (FC).

**Table 4.1.** Summary of model studies performed under the HTAP intercomparison

Model Study	Brief Description	No. of Participants
<b>SR:</b> Source-receptor studies	Sensitivity study with 20% changes to anthropogenic emissions over four major source regions in 2001 to quantify source-receptor relationships	32
<b>TP:</b> Tracer process studies	Repeat of SR with specified emissions and standardized tracers to explore differences in model transport and mixing processes	25
<b>ES:</b> Event Simulations	Explore model ability to reproduce specific intercontinental transport events observed during the ICARTT campaign in 2004	7
<b>FE:</b> Future emissions studies	Repeat of SR under different scenarios for future emissions in 2030 (RCP8.5) and 2050 (RCP2.6) conditions	4
<b>FC:</b> Future climate studies	Repeat of SR under different climate conditions corresponding to present-day and 2100 SRES-A2 climates	3

One advantage of this multi-model approach is that differences between models highlight the uncertainties associated with representation of key atmospheric processes. When combined with observational data, this allows identification of model weaknesses and a clearer assessment of model reliability. Additionally, ensemble mean results are often found to compare better with observations than those of any one model [e.g., *Vautard et al.*, 2006]. In this chapter we draw on valuable conclusions from previous model intercomparisons, in particular ACCENT/PHOTOCOMP [*Dentener et al.*, 2006], AEROCOM [*Textor et al.*, 2006], TRANSCOM [*Law et al.*, 2008], and RETRO [*Schultz et al.*, 2007] which provide additional insight into the strengths and weaknesses of current models.

## 4.2. Quantifying intercontinental transport of ozone and precursors

In this section we evaluate the capabilities of current models to describe tropospheric O<sub>3</sub> and its trends. We summarize model estimates of the tropospheric budgets of O<sub>3</sub> and precursors, evaluate model strengths and weaknesses by comparison with observations, and quantify S/R relationships for intercontinental transport.

### 4.2.1. Ozone in the troposphere

Recent evaluation of tropospheric composition from 25 models run for year 2000 as part of the ACCENT/PHOTOCOMP model intercomparison [*Stevenson et al.*, 2006] using a common set of emissions indicates that the tropospheric O<sub>3</sub> burden, below the 150 parts per billion by volume (ppbv) O<sub>3</sub> level, is 340±40 Tg. The O<sub>3</sub> burden for year 2001 derived from 13 models contributing to the HTAP intercomparison, using differing estimates of current emissions, is similar at 320±40 Tg. While there are no direct observational constraints on this quantity, estimates based on ozonesonde measurements suggest a

tropospheric burden of about  $335 \pm 10$  Tg [Wild, 2007]. The primary sources of  $O_3$  in the troposphere are chemical production ( $5100 \pm 600$  Tg/yr) and influx from the stratosphere ( $550 \pm 170$  Tg/yr), and removal is governed by chemical destruction ( $4650 \pm 730$  Tg/yr) and deposition ( $1000 \pm 200$  Tg/yr) [Stevenson *et al.*, 2006]. Reviews of these budget terms show significant differences among different model studies, but note much closer agreement than found in earlier studies published in the 1990s, principally reflecting greater consensus on global precursor emissions [Wild, 2007; Wu *et al.*, 2007].

Stevenson *et al.* [2006] evaluated the ACCENT/PHOTOCOMP models against global ozonesonde measurements and found that model results and observations generally fell within one standard deviation of each other throughout the depth of the troposphere. However, there were notable discrepancies at some locations, with multi-model mean  $O_3$  overestimated north of  $30^\circ N$  by about 10 ppbv ( $\sim 25\%$ ) in winter, for example. Jonson *et al.* [2010] confirmed that the multi-model ensemble from the HTAP intercomparison captures the seasonal climatology and further evaluated these models with twice daily ozonesondes from the year 2001 (see Figure 4.2). The model ensemble mean bias compared to observations is smallest in winter and autumn and larger during the more photochemically active spring and summer months [Jonson *et al.*, 2010]. Individual models differ greatly in their ability to reproduce the day-to-day variability measured by ozonesondes, generally faring better at measurement locations closer to major source regions than in remote locations [Jonson *et al.*, 2010]. The plumes sometimes observed at more remote locations are generally not well resolved by the coarse resolution global models.

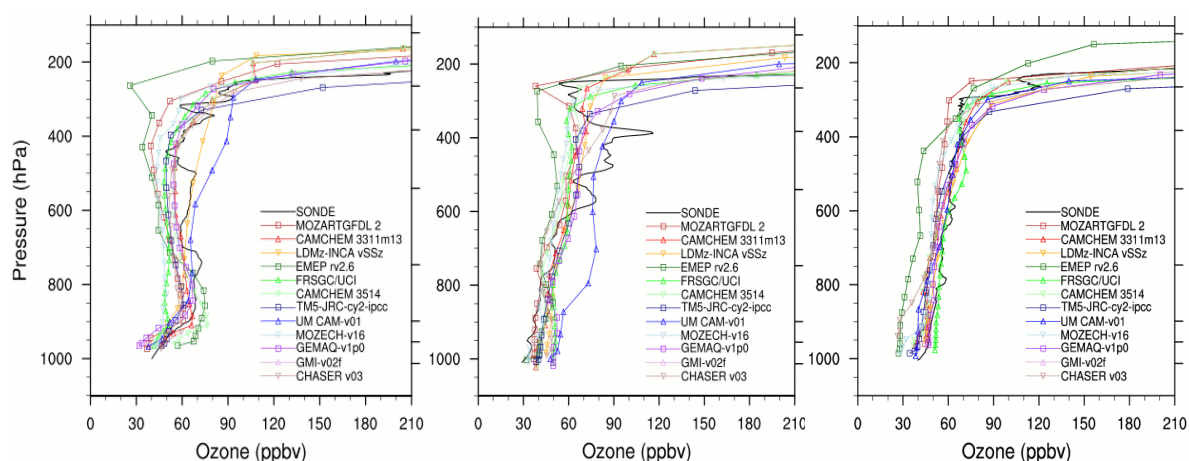


**Figure 4.2.** Comparison of observed  $O_3$  profiles from Goose Bay, Canada (13 June 2001, left) Uccle, Belgium (1 June 2001, centre) and Yakutsk, Siberia (8 April 2001, right) with modelled profiles from the HTAP intercomparison. [Adapted from Figure 13 in Jonson, J. E., *et al.* (2010), A multi-model analysis of vertical ozone profiles, *Atmospheric Chemistry and Physics*, 10: 5759-5783.]

#### 4.2.2. Surface ozone

While individual CTMs are routinely compared with observations for specific scientific studies, comprehensive evaluations against observations in some regions of interest for HTAP remain limited. In the HTAP intercomparison, the model ensemble mean captures observed monthly mean surface  $O_3$  throughout the year over Europe and the western U.S. but overestimates it substantially during summer and early fall over the eastern U.S. where sites are influenced by major pollutant sources and over Japan where simulations are sensitive to the timing and extent of the summer monsoon [Figure 4.3, Fiore *et al.*, 2009]. These results are consistent with observational comparisons during the ACCENT/PHOTOCOMP study, which showed that, despite large inter-model differences, the model ensemble annual mean generally fell within 5-10 ppbv of observed values, except for South Asia where the models exhibited a systematic positive bias of 15-20 ppbv compared to the limited measurements available [Dentener *et al.*, 2006; Ellingsen *et al.*, 2008]. The seasonality in surface  $O_3$  was reproduced relatively well [Ellingsen *et al.*, 2008].



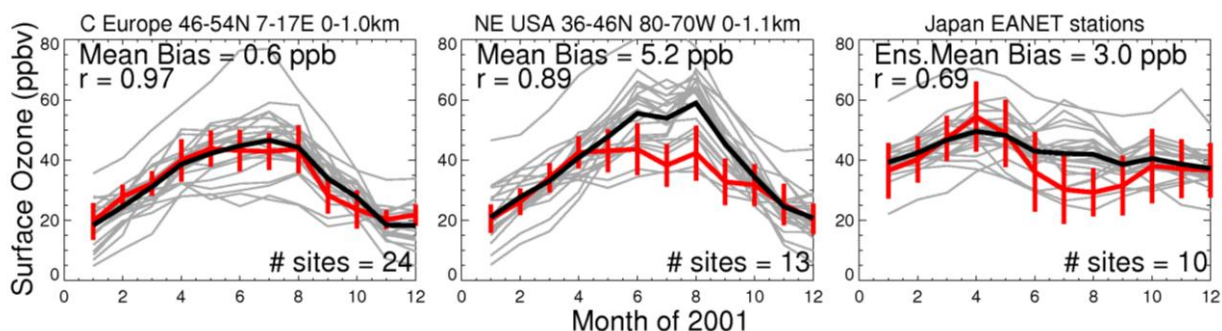


**Figure 4.3.** Comparison of monthly mean surface  $O_3$  from models contributing to the HTAP intercomparison (grey lines; multi-model ensemble mean in black) compared with observed  $O_3$  (red; vertical lines denote  $\pm 1\sigma$  variability in the monthly mean over the different stations) from measurement networks over the northeastern U.S. (CASTNet), central Europe (EMEP) and Japan (EANET). Models are sampled at the nearest grid points to each station. [Adapted from Figure 2 of Fiore, A. M., et al. (2009), Multimodel estimates of intercontinental source-receptor relationships for ozone pollution, *Journal of Geophysical Research*, 114(D4): D04301.]

Reidmiller et al. [2009] conducted an extensive evaluation of the HTAP CTMs with the policy-relevant maximum daily 8-h average ozone (MDA8  $O_3$ ) metric from the Clean Air Status and Trends Network (CASTNet) observations in the U.S. They found that the multi-model mean represents the observations well (mean  $r^2=0.57$ , ensemble bias= $+4.1$  ppbv for all U.S. regions and all seasons), though individual model results vary widely. The models generally reproduce the observed day-to-day variability well [e.g., Figures 5 and A5 in Reidmiller et al., 2009], with the strongest correlations between simulated and observed MDA8  $O_3$  in the northeastern U.S. during spring and fall ( $r^2=0.68$ ) and weakest in the midwestern U.S. in summer ( $r^2=0.46$ ), but biases of  $+10$ - $20$  ppbv occur in summer over all eastern U.S. regions (as in Figure 4.3 for the monthly mean values). The seasonal and daily variability is fairly well reproduced, but there is a systematic negative bias at high altitude sites in the mountainous western U.S. which are more influenced by free tropospheric air that contains larger contributions from foreign emissions (i.e., those outside the region) see Figure 4.4. More information for particular regions of the U.S. and for different seasons is provided in Reidmiller et al. [2009].

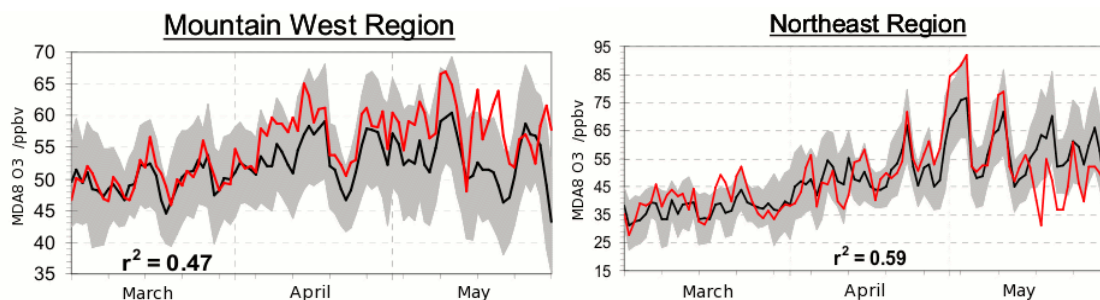


**Figure 4.4.** Comparison of maximum daily 8-hour averaged surface  $O_3$  (MDA8  $O_3$ ) over different parts of the U.S. in spring 2001 from models contributing to the HTAP intercomparison with observations from the CASTNet network. The model mean is shown in black (grey shading indicates  $\pm 1\sigma$ ) and observations are shown in red. [Adapted from Figure 5 in Reidmiller, D. R., et al. (2009), The influence of foreign vs. North American emissions on surface ozone in the US, *Atmospheric Chemistry and Physics*, 9: 5027-5042.]

**FINDING (ozone):** Current global models reproduce the observed regional and seasonal variability in surface ozone at most locations, demonstrating our ability to represent the key large-scale processes controlling the formation, transport and removal of ozone and its precursors. However, significant discrepancies exist on shorter spatial and temporal scales indicating weaknesses in our representation of local- and urban-scale processes in current models.

### 4.2.3. Trends in surface ozone

Over recent decades, significant trends in tropospheric O<sub>3</sub> have been detected from many observational platforms (aircraft, balloons, high-altitude stations, and satellites) over different regions and time periods. Taken together, these observations paint a complex picture with differences in the magnitude and sign of trends across parts of the northern hemisphere [NRC, 2010, and references therein; Royal Society, 2008b; TFHTAP, 2007]. For surface O<sub>3</sub>, measured trends are more consistent qualitatively, with general increases ranging from 0.1–0.5 ppbv yr<sup>-1</sup> in the western U.S. and Western Europe, though some observational records suggest little change or a recent stabilization [see summaries of literature by NRC, 2010, Tropospheric ozone trends workshop, 2009; Royal Society, 2008b; TFHTAP, 2007; Vingarzan, 2004]. Differences in observational sampling frequency and time periods combined with large interannual fluctuations in meteorology and emissions complicates both interpretation of trends from measurements and reproduction of the magnitude of long-term O<sub>3</sub> changes using models.

Because the HTAP model experiments were focused on a single year, no explicit evaluation of trends was included in the HTAP intercomparison. However, past studies with models that participated in the intercomparison have been evaluated against observed trends, with mixed results. Under a major European modelling initiative, RETRO, 40-year simulations (from 1960 to 2000) were conducted with three global CTMs and evaluated with long-term O<sub>3</sub> measurements [Schultz *et al.*, 2007]. All models indicate an increase in O<sub>3</sub> of 5–15 ppbv over Europe, North America and East Asia south of 55°N over this period and capture much of the observed interannual variability [Schultz *et al.*, 2007]. However, increases observed at central European mountain stations are not reproduced, suggesting weaknesses in our understanding of source changes, including emissions and the influx of O<sub>3</sub> from the stratosphere. More recent studies with two chemistry-climate models using new assessments of historical emission changes show a positive trend in surface O<sub>3</sub> at many locations, but this is generally somewhat lower than has been observed [Lamarque *et al.*, 2010], as shown in Figure 4.5. Regional modelling studies over East Asia have shown a similar underestimate of observed surface O<sub>3</sub> trends [Tanimoto *et al.*, 2009]. Future effort is needed to reconcile modelled and observed O<sub>3</sub> trends based on improved understanding of processes and emission changes before these trends can be reliably attributed to particular sources, or before we can definitively determine whether this inability to capture the observed trend reflects fundamental problems with current models.

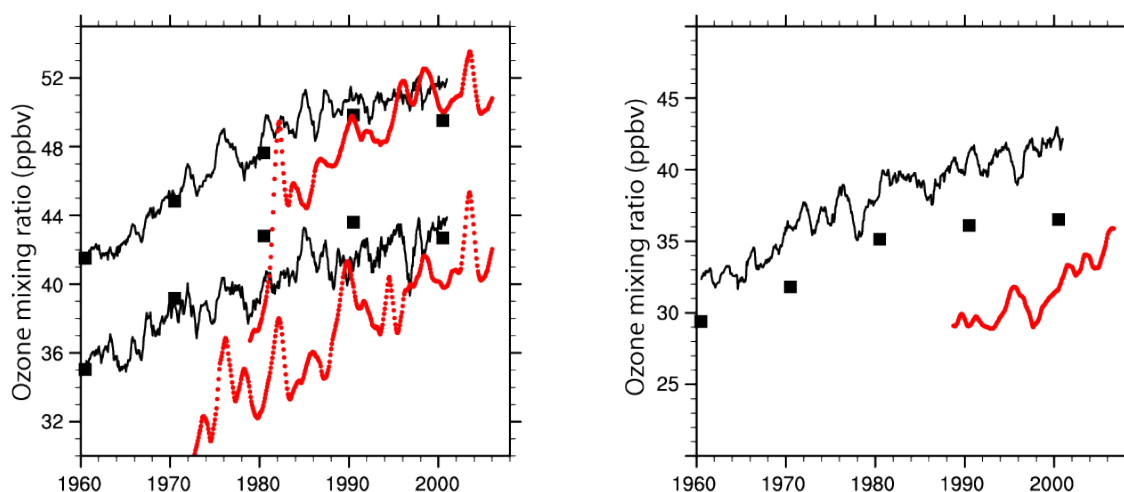


**Figure 4.5.** Comparison of surface O<sub>3</sub> trends (12-month running mean) from CAM-Chem (black line) and GISS-PUCCINI (black squares) against observations (red) at Zugspitze and Hohenpeissenberg, Germany (left) and US Pacific Coast sites (right). [Adapted from Figure 5 in Lamarque, J. F., et al. (2010), Historical (1850–2000) gridded anthropogenic and biomass burning emissions of reactive gases and aerosols: Methodology and application, *Atmospheric Chemistry and Physics*, 10: 7017–7039.]

**FINDING (trends ozone):** Recent model studies have shown increases in surface ozone between 1960 and 2000, but the magnitude and regional variation in this trend does not compare well with observations. Observed increases at remote locations are generally underestimated in model simulations, indicating that precursor emissions and/or atmospheric processes are not represented well in current models.

**RECOMMENDATION (ozone trends):** Research is needed to characterise and explain the observed trends in surface ozone. Multi-year model simulations that account for changing emissions and meteorology are necessary to (1) explain and attribute changes, (2) put observed regional trends in a global context, and (3) critically test model ability to reproduce long-term composition changes. Proposals under the IGAC/SPARC AC&C activity to ‘hindcast’ observed composition changes over past decades should be encouraged and supported.

#### 4.2.4. Source attribution

Model studies of pre-industrial conditions demonstrate that anthropogenic emissions have had a large impact on tropospheric O<sub>3</sub>, contributing about 100 Tg (9 DU) to the global burden [Gauss *et al.*, 2006; Prather *et al.*, 2001], about 30% of the current burden of 335±10 Tg [Wild, 2007]. Around 40% of this change is due to increases in CH<sub>4</sub> and the rest to changes in emissions of NO<sub>x</sub>, CO, and NMVOCs [Shindell *et al.*, 2005]. The contribution of anthropogenic emissions to surface O<sub>3</sub> is thought to be significantly larger, with O<sub>3</sub> concentrations roughly doubling between 1850 and the present day [e.g., Berntsen *et al.*, 2000; Lelieveld and Dentener, 2000]. Recent studies with a number of models suggest that anthropogenic emissions by year 2000 have caused global surface O<sub>3</sub> to rise from a preindustrial level of about 17±3 ppbv to about 28±5 ppbv [Royal Society, 2008b]. However, there is large uncertainty in our ability to simulate the preindustrial atmosphere as the few surface O<sub>3</sub> measurements available from the 19<sup>th</sup> century reveal substantially lower concentrations than current models can reproduce [Mickley *et al.*, 2001]. This suggests that models may be underestimating the anthropogenic contribution to surface O<sub>3</sub>. In light of this, we have high confidence that current surface O<sub>3</sub> is significantly higher than preindustrial levels [NRC, 2010].

The HTAP intercomparison suggests that annual average surface O<sub>3</sub> levels over the four HTAP regions are currently about 37±4 ppbv. Of this, 20-25% originates from the stratosphere, and a similar proportion is formed from natural precursor sources: lightning, soils, vegetation and fire, along with oxidation of natural CH<sub>4</sub> [Lelieveld and Dentener, 2000; Sudo and Akimoto, 2007]. The anthropogenic contribution thus typically exceeds 50% over these regions. About half of this contribution originates from sources over the region itself (8-10 ppbv) and about half is transported from sources outside the region. However, this simple attribution masks strong regional, seasonal and daily variability in both O<sub>3</sub> abundance and in the contribution of different sources. We also note that while the contributions shown in Figure 4.6 are indicative of average northern mid-latitude conditions, they do not represent ‘background’ conditions at any particular location.

**FINDING (attribution of ozone):** We have high confidence that emissions from human activities contribute substantially to baseline ozone. Annual average surface O<sub>3</sub> levels over the four HTAP regions are estimated to be 37±4 ppbv, of which over 50% may be attributed to anthropogenic sources. About half of this anthropogenic component originates from sources over the region itself (8-10 ppbv) and the other half is transported from sources outside the region. Another 20-25% of surface O<sub>3</sub> originates from the stratosphere, and a similar proportion is formed from natural precursor sources: lightning, soils, vegetation and fire, and from oxidation of natural hydrocarbons.

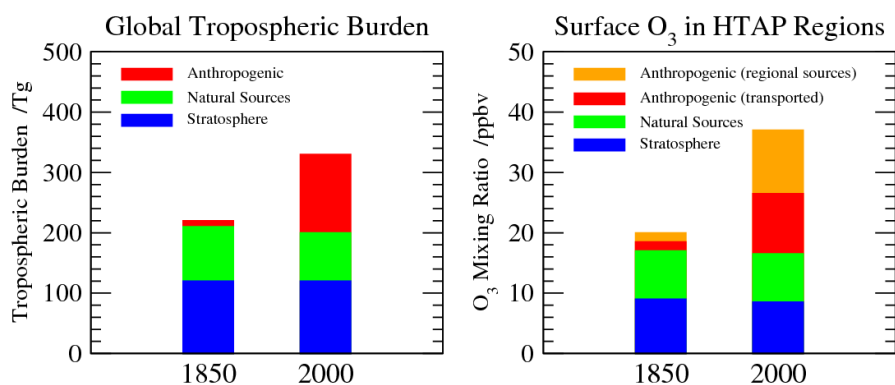


**Figure 4.6.** Source attribution for tropospheric O<sub>3</sub> over the globe (left) and for annual mean surface O<sub>3</sub> over the four HTAP regions (right) estimated by the report authors from source contributions in earlier published studies [Berntsen *et al.*, 2000; Gauss *et al.*, 2006; Lelieveld and Dentener, 2000; Sudo and Akimoto, 2007].

**FINDING (attribution of ozone):** We have confidence that human activities contribute to the observed positive trend in surface ozone, and that the anthropogenic component to hemispheric mean ozone levels has grown significantly since ~1850. However, there remain large uncertainties in our estimates of the source attribution for these changes.

**RECOMMENDATION (attribution of ozone):** Dedicated model studies focussing on source attribution of ozone are needed to reduce the uncertainties in current estimates, and to better characterize the strong regional, seasonal and daily variability in both ozone abundance and in the contribution of different sources. Improved, observation-based constraints are needed to provide a critical test for these model estimates.

#### 4.2.5. Source-receptor relationships for surface ozone

A number of published studies have estimated the influence of foreign sources on surface O<sub>3</sub> in different parts of the northern hemisphere [TFHTAP, 2007]. These studies have applied a wide variety of techniques (described in Section 4.1.2) and these differences in focus and approach contribute to the wide range of estimates, which for some S/R pairs disagree in sign and span an order of magnitude. In addition, prior efforts adopted varied regional definitions, metrics and periods of study, making it difficult to draw meaningful, quantitative estimates from a literature survey. By adopting a single approach across all models the HTAP intercomparison limits the factors contributing to differences in individual model estimates to treatment of emissions, chemistry, transport and resolution.

#### *Estimates of intercontinental transport from the HTAP intercomparison for surface O<sub>3</sub>*

The annual and spatial mean surface O<sub>3</sub> decreases in each of the receptor regions resulting from 20% reductions of anthropogenic O<sub>3</sub> precursor emissions for each source region are given in Table 4.2, along with the range of HTAP model predictions expressed in terms of the standard deviation between the different models. As expected the largest changes occur in the source regions. For example, a 20% change in the anthropogenic emissions in North America (NA) leads to a mean change in surface O<sub>3</sub> of ~1 ppbv, and these source region responses vary from a high of 1.26 ppbv in South Asia to 0.82 ppbv in Europe. The results also show that substantial changes in surface O<sub>3</sub> occur far away from the source regions. For example, the annual mean surface O<sub>3</sub> mixing ratio in Europe changes by 0.37 ppbv when current emissions in North America are changed by 20%.

To quantify the importance of changes in emissions outside the receptor area on surface O<sub>3</sub> within the receptor region, we define the relative annual intercontinental response metric. This represents the ratio of the response in a particular region due to the combined influence of sources in the three other regions to the response from all source regions. This metric varies from 0% (receptor response entirely due to receptor region emissions) to 100% (receptor response entirely due to emissions elsewhere), with 50% representing the point at which the response from emissions outside the region is equal to the response from receptor region emissions. The relative annual

intercontinental response for annual average surface O<sub>3</sub> over each region is shown in Table 4.2, and varies from 43% for Europe, to 32% for NA and SA. This indicates that in all four regions, emission changes in the three other source regions are 50-75% as important as emission changes over the receptor region itself.

**Table 4.2.** Annual and spatial mean surface O<sub>3</sub> response (ppbv) to 20% decreases in anthropogenic precursor emissions (NO<sub>x</sub>, CO, NMVOC, plus aerosols and their precursors). Values are mean (median) ± one standard deviation across the 15 models that conducted the regional perturbation simulations (SR6). Bold font denotes responses to foreign emission perturbations that are at least 10% of the response to domestic emission perturbations. Also shown is the relative annual intercontinental response for each receptor region defined as the ratio of the total response in mean surface O<sub>3</sub> due to changes in the other three source regions compared to that due to changes in all regions.

Source Region	Receptor Region			
	NA	EU	EA	SA
<i>Annual mean decrease</i>				
NA	1.04(1.03)±0.23	<b>0.37(0.37)±0.10</b>	<b>0.22(0.24)±0.05</b>	<b>0.17(0.19)±0.04</b>
EU	<b>0.19(0.18)±0.06</b>	0.82(0.68)±0.29	<b>0.24(0.24)±0.08</b>	<b>0.24(0.25)±0.05</b>
EA	<b>0.22(0.23)±0.06</b>	<b>0.17(0.17)±0.05</b>	0.91(0.86)±0.23	<b>0.17(0.17)±0.05</b>
SA	0.07(0.07)±0.03	0.07(0.07)±0.03	<b>0.14(0.13)±0.03</b>	1.26(1.18)±0.26
<i>Relative annual intercontinental response</i>				
	32%	43%	40%	32%

The spatial distribution of the changes in mean surface O<sub>3</sub> levels due to 20% changes in anthropogenic precursors for each of the source regions in springtime are shown in Figure 4.7. As noted above, the largest changes in O<sub>3</sub> occur over the source regions, but the influence is shown to extend throughout the northern hemisphere. These results indicate that a 20% decrease in North American anthropogenic emissions decreases mean surface O<sub>3</sub> across the northern hemisphere by 0.1-0.5 ppbv. The decrease in European emissions has a marginally smaller impact, reducing mean surface O<sub>3</sub> over North America by less than 0.35 ppbv and by 0.1-0.5 ppbv over Asia. The impact from a 20% decrease in East Asian anthropogenic emissions is slightly smaller, generally less than 0.3 ppbv except over western North America. The response to emission reductions over South Asia is more localized, with a decrease of less than 0.1 ppbv across much of the northern mid-latitudes, reflecting greater export into the tropical free troposphere. Over the Arctic, the largest impacts on surface O<sub>3</sub> are from European emissions (~0.4 ppbv) and the smallest are from South Asian emissions (<0.1 ppbv). The differences between the contributing models (not shown here) are appreciable, with one standard deviation of 20-50% of the mean value over both source and receptor regions. This variation, a measure of uncertainty in the estimates, is largest at northern mid-latitudes for European emissions, for which the standard deviation reaches ~0.2 ppbv, roughly the same order as the multi-model mean decrease. On an annual basis, the standard deviation is generally less than half of the multi-model mean decrease in surface O<sub>3</sub>.



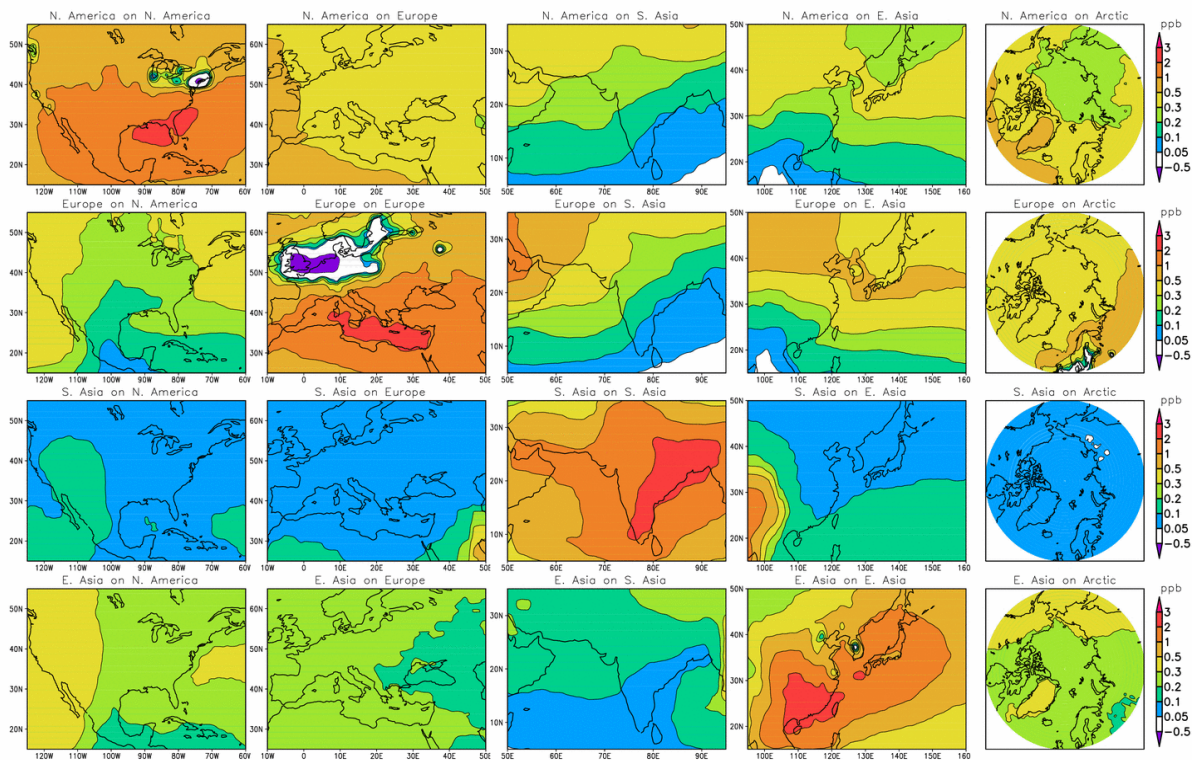


**Figure 4.7.** Model ensemble mean surface  $O_3$  decrease in springtime (in ppbv) for the combined 20% emission reduction over each source region showing the spatial variation over each region and over the Arctic. Each row shows the responses from a particular source region.

The range of estimates across the models participating in the HTAP intercomparison is generally smaller than that obtained from a survey of the literature, see Table 4.3. For a direct comparison with previous studies which have taken differing approaches to estimating intercontinental contributions, the  $O_3$  responses in the HTAP studies derived from 20% emission changes are scaled by a factor of 5 to represent 100% emission changes. The uncertainties associated with this extrapolation are discussed later in Section 4.2.11. The largest intercontinental influence occurs for North American emissions on European surface  $O_3$ , where the response to foreign emissions is between 1.0 and 2.55 ppbv. The largest S/R relationships are for NA→EU; EU→SA; EU→EA; and NA→EA. These numbers are significant when compared with the changes in surface  $O_3$  due to changes in emissions from domestic sources. The largest values in Table 4.3 from prior studies (e.g., over NA in summer and over EU and EA for annual mean values) were estimated from simulations in which anthropogenic emissions were set to zero, or in which  $O_3$  production throughout the tropospheric column over a source region was considered to represent the effect of emissions from the source region. None of the models in the HTAP intercomparison suggest estimates near the upper end of this range.

**Table 4.3.** Annual and seasonal mean estimates for the contribution to surface O<sub>3</sub> (in ppbv) over the receptor region from anthropogenic O<sub>3</sub> precursor emissions in foreign source regions, arranged from largest (first row) to smallest (last row). The top entry in each cell is the full range from the 15 models that participated in the SR6 set of HTAP simulations. The response to the 20% emission perturbation was multiplied by five to estimate the full contribution; the limitations of this approach are discussed in the text. Also shown (italics) is the full range from the published literature included in Table 5.2 in HTAP [2007] and Figure 11 in Fiore et al. [2009], supplemented with estimates from more recent studies [Lin et al., 2010b; West et al., 2009b; Zhang et al., 2009]

Source/Receptor	Annual	DJF	MAM	JJA	SON
NA → EU	1.00-2.55 <i>2.-15.</i>	0.70-2.35 <i>0.4</i>	1.05-3.10 <i>0.2</i>	1.05-2.65 <i>-0.3-5.</i>	1.00-2.45 <i>-0.9</i>
EU → SA	0.70-1.60	0.55-2.00	0.75-1.95	0.75-1.80	0.65-1.45
EU → EA	0.60-1.85 <i>0.-5.4</i>	0.35-2.95	0.75-2.80 <i>3.</i>	0.40-1.15 <i>3.</i>	0.65-1.70
NA → EA	0.60-1.55 <i>0.2-4.5</i>	0.65-2.05	0.50-1.60	0.30-1.35	0.60-1.70
EA → NA	0.50-1.55 <i>1.</i>	0.50-1.80	0.65-2.05 <i>4.</i>	0.30-1.15 <i>1.-3.</i>	0.45-1.20
NA → SA	0.50-1.15	0.40-1.55	0.60-1.45	0.35-0.85	0.45-1.00
SA → EA	0.50-1.10	0.50-1.30	0.55-1.25	0.30-0.90	0.45-1.05
EU → NA	0.40-1.55 <i>0.2-0.9</i>	0.30-1.90	0.55-1.95	0.30-2.05	0.45-1.15
EA → SA	0.40-1.45	0.40-2.30	0.30-1.05	0.30-0.95	0.25-1.85
EA → EU	0.35-1.30 <i>0.8-7.</i>	0.35-1.45	0.40-1.70	0.30-1.05	0.35-1.05
SA → EU	0.20-0.75	0.20-1.00	0.20-0.85	0.15-0.55	0.05-0.70
SA → NA	0.20-0.65	0.20-0.90	0.25-0.85	0.10-0.45	0.15-0.60

### Seasonal responses

The annual mean surface O<sub>3</sub> responses presented in Table 4.2 mask a large seasonal variability in the response to emission perturbations, as is evident from Table 4.3. Surface O<sub>3</sub> responses to 20% emission changes in individual models are shown as a function of month in Figure 4.8. There is significant variability in the calculated responses in both source and receptor regions which varies by season and location. However, there is good agreement between models on the strong seasonal variations. For example, the response of European surface O<sub>3</sub> to North American emissions, which averages 0.37 ppbv over the year, varies between 0.47 ppbv in spring, when the effects of intercontinental transport are generally largest in the Northern Hemisphere, and 0.29 ppbv in summer when O<sub>3</sub> production from domestic emissions is greatest. The smallest responses are from South Asian emissions over North America, which average 0.07 ppbv over the year but range from 0.10 ppbv in February to 0.03 ppbv in August. At northern mid-latitudes the intercontinental influence is largest in boreal spring, with a secondary peak in fall in some locations, and is smallest during summer when southerly flow is more prevalent over these regions. For the South Asian region there is less variation and the seasonality is reversed, reflecting the transition between dry and monsoon

seasons. The combined response of surface  $O_3$  over South Asia to foreign emissions varies from 0.4 to 0.9 ppbv, approximately 50% of the response due to domestic emissions reductions, and the seasonality of domestic and intercontinental influences is similar, in contrast to the other regions considered here. Over the Arctic, the largest surface  $O_3$  response from all source regions occurs between April and June, with a secondary maximum in October and November, and this strong seasonality is most greatly influenced by European sources. These results indicate that while the intercontinental influence over many regions is important, decreasing domestic emissions is more effective at decreasing the highest  $O_3$  levels (e.g., as occur in July in EA, EU, and NA) [Fiore *et al.*, 2009; Reidmiller *et al.*, 2009].

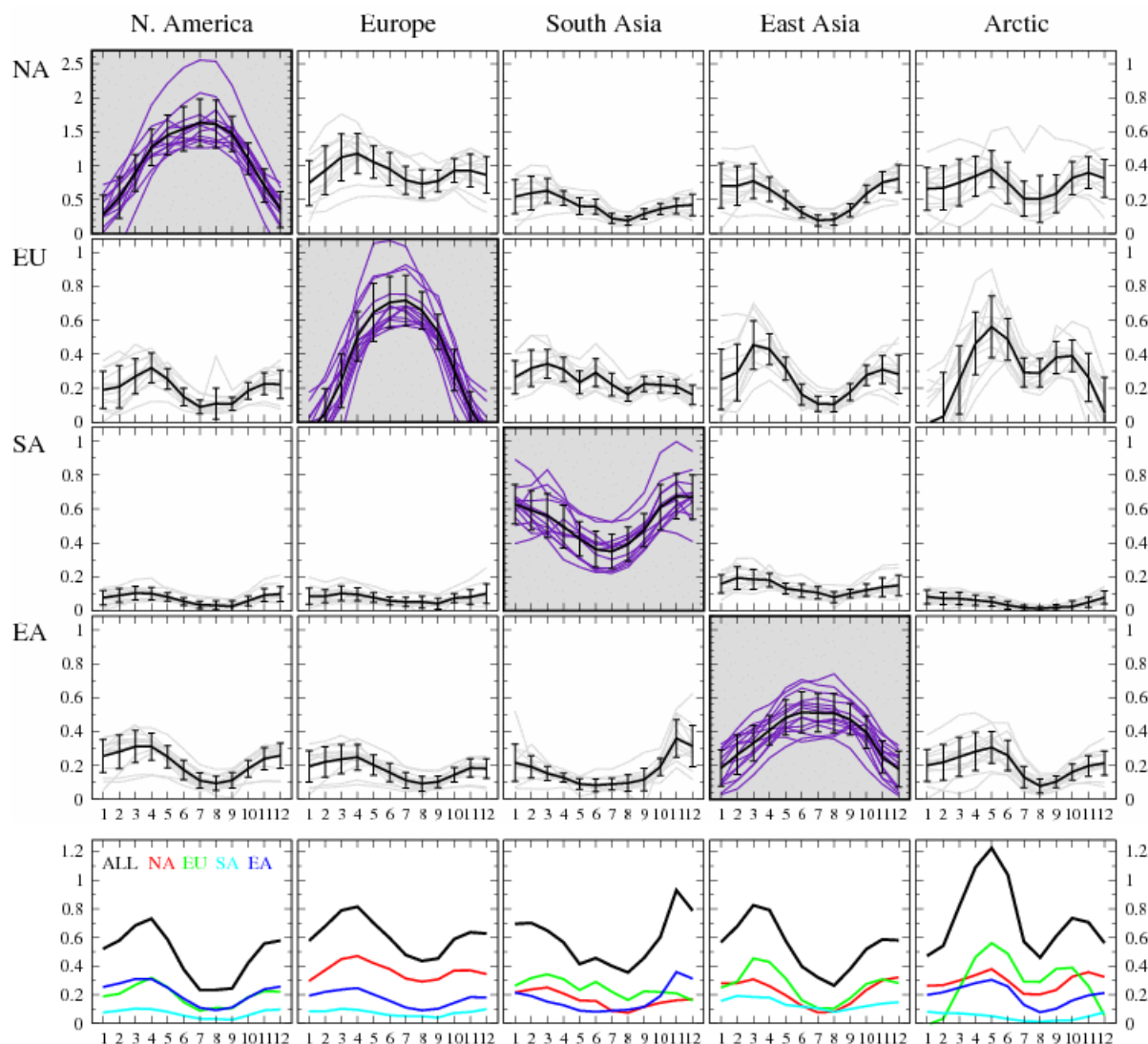


**Figure 4.8.** Monthly mean surface  $O_3$  decreases (in ppbv) over receptor regions for the combined 20% emission reductions (HTAP SR6 simulations) showing (1) the seasonality of the responses (black line: ensemble mean  $\pm 1\sigma$ ), and (2) the variability between models (grey lines). Each row shows the responses from a particular source region. For clarity, the vertical scale for the source regions (shaded panels, 0-2.5 ppbv) is different from that for the receptor regions (0-1 ppbv). The bottom row summarises the ensemble mean response over each receptor region from other source regions; the black line is the sum of the  $O_3$  decreases to emission changes in the three other regions (four for the Arctic).

### *The role of methane ( $CH_4$ )*

Emissions of chemically-active species may have a long-term effect on receptor regions through indirect effects on chemical composition that are often overlooked.  $O_3$  precursors alter the



abundance of atmospheric OH radicals and thus affect the abundance and distribution of atmospheric CH<sub>4</sub>; these changes lead to changes in O<sub>3</sub> abundance on a longer time scale reflecting the response time of CH<sub>4</sub>, ~12 years [Prather, 1996; Wild and Prather, 2000]. This effect can be particularly significant for NO<sub>x</sub> emissions which have a relatively large effect on OH, and lead to long-term reductions in O<sub>3</sub>, which partly counterbalance the short-term increase [Derwent *et al.*, 2001; Wild *et al.*, 2001]. Most studies of intercontinental transport have focused on periods of no more than a year or two, and therefore neglect these long-term responses; however, more thorough analysis requires that these transient effects are also included. Where the response time of CH<sub>4</sub> has been characterized in a model, these long-term O<sub>3</sub> responses can be estimated.

To address the importance of these effects, additional HTAP model studies were undertaken in which the globally-fixed CH<sub>4</sub> abundance (1760 ppbv in the base simulations) was decreased by 20%. From these simulations, we estimate the response to 20% decreases in regional anthropogenic CH<sub>4</sub> emissions as described in HTAP [2007] and Fiore *et al.* [2009], and compare the results to the response from 20% reductions in NO<sub>x</sub>, NMVOC, and CO, the O<sub>3</sub> precursors that have traditionally been regulated, in Figure 4.9. While domestic emission controls on NO<sub>x</sub>, NMVOC and CO combined are clearly most effective for lowering domestic O<sub>3</sub>, the O<sub>3</sub> response to anthropogenic emissions of CH<sub>4</sub> from distant source regions is nearly as large as that to emissions of the traditional O<sub>3</sub> precursors in these regions. This highlights the importance of controlling CH<sub>4</sub> emissions for improving air quality as well as for reducing total greenhouse gas emissions that influence climate. Fiore *et al.* [2008] explored the contribution of CH<sub>4</sub> emissions to air quality and climate, and estimated that anthropogenic sources of CH<sub>4</sub> accounted for about 50 Tg of the annual mean tropospheric O<sub>3</sub> burden and contributed about 5 ppbv to global mean surface O<sub>3</sub>, based on results from earlier model studies.

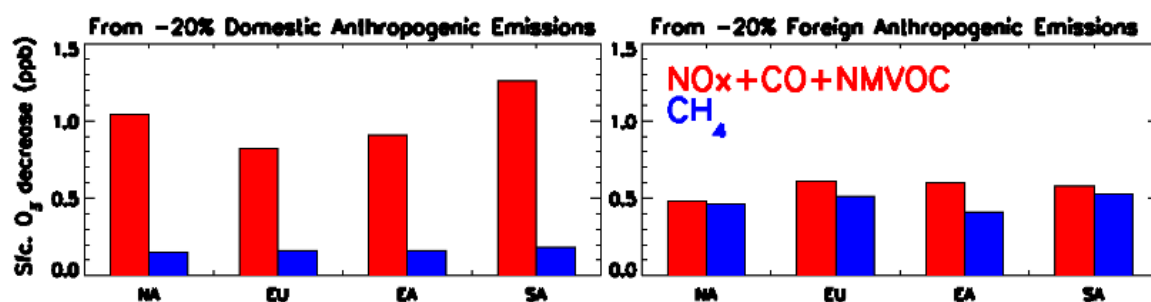


**Figure 4.9.** Model ensemble surface O<sub>3</sub> decrease (ppbv), annually and spatially averaged over the HTAP regions from 20% decreases in anthropogenic emissions of NO<sub>x</sub>, CO and NMVOC (red) versus 20% decreases in anthropogenic CH<sub>4</sub> (blue). Influence of each source region on surface O<sub>3</sub> within the same region (termed “domestic”, left panel), and the sum of the O<sub>3</sub> responses to emission changes within the three other source regions (termed “foreign”, right panel). [Adapted from Figure 2 of Fiore, A. M., *et al.* [2010], Interactions between climate and air quality, (Section 6.1) in *Air Pollution Modelling and its Application XX*, edited by D. G. Steyn and S. T. Rao, with kind permission of Springer Science and Business Media B.V.10.]

The long-term response of O<sub>3</sub> through the effects of precursor emissions on OH and thus CH<sub>4</sub> was found to be negligible (less than 3% for all months and all regions) for the HTAP simulations in which anthropogenic O<sub>3</sub> precursor emissions were reduced simultaneously (SR6). However, this long term response has a larger influence when O<sub>3</sub> precursor emissions were altered individually. For example, the long-term response reduced the overall response to foreign NO<sub>x</sub> emission changes by 15-20% when only NO<sub>x</sub> emissions were perturbed, and increased the overall response to foreign NMVOC emission changes by 10% and to foreign CO emission changes by 30-40% [Fiore *et al.*, 2009]. Considering these findings and other studies quantifying the long-term impact of O<sub>3</sub> precursor emissions on surface O<sub>3</sub> [West *et al.*, 2007; West *et al.*, 2009b], we conclude that the long-term feedback may be important when individual O<sub>3</sub> precursor emissions are perturbed by different amounts. In Table 4.2 and Figures 4.7 and 4.8 we focus on the SR6 set of simulations in which NO<sub>x</sub>, NMVOC and CO were reduced together by 20% and the long-term feedback through CH<sub>4</sub> is negligible.

**FINDING (S/R relationships ozone):** The impact of 20% changes in anthropogenic emissions in one region on annual regional-mean surface ozone in the other regions lies between 0.07 and 0.37 ppbv, based on the ensemble mean from the HTAP simulations. However, these values mask large temporal and geographic variability, and responses can vary by more than a factor of two from month to month and from location to location within a region.

**FINDING (S/R relationships ozone):** The relative annual intercontinental response for annual mean surface O<sub>3</sub> is found to vary from 43% for Europe, to 40% for EA, to 32% for NA and SA in the HTAP simulations. These results indicate that in all four regions, emissions changes in the other three source regions are about half as important as the same domestic emissions change.

**FINDING (CH<sub>4</sub>):** Anthropogenic sources of CH<sub>4</sub> are estimated to contribute about 50 Tg to the annual mean tropospheric O<sub>3</sub> burden and about 5 ppbv to global mean surface O<sub>3</sub>. Controlling CH<sub>4</sub> is of major importance in limiting increases in baseline surface ozone, and has additional benefit for climate.

**RECOMMENDATION:** The temporal and geographic variability in S/R relationships needs to be better characterized so that the influence of intercontinental transport can be more reliably quantified in critical locations (e.g., population centres, sensitive ecosystems) over the annual cycle.

#### 4.2.6. Policy-relevant metrics

The ensemble mean changes in surface O<sub>3</sub> for the four S/R regions and the Arctic are shown in Figure 4.7. This reveals that there is appreciable spatial variability in the O<sub>3</sub> response within the regions. While the continental-scale spatial averages discussed thus far are useful for gauging the relative influence of different foreign emission regions and seasonal variability in hemispheric transport, an understanding of sub-continental variability in foreign contributions to surface O<sub>3</sub> is desirable for managing local air quality.

##### *Maximum daily 8-hour average ozone (MDA8 O<sub>3</sub>)*

Reidmiller et al. [2009] illustrated the regional variability for MDA8 O<sub>3</sub> levels (the metric used to assess compliance with the U.S. national O<sub>3</sub> air quality standard) in nine U.S. regions during spring, reproduced below in Figure 4.10. The surface O<sub>3</sub> response to 20% decreases in foreign anthropogenic emissions of O<sub>3</sub> precursors varies across the nine regions, though a consistent pattern occurs in that the EA influence is slightly larger than that from EU, both of which are much greater than the SA influence (an exception is in the Northeast where the EU influence is slightly larger than that from EA) [Reidmiller et al., 2009]. The foreign influence throughout the distribution of total surface O<sub>3</sub> is also shown in Figure 4.10; in the western U.S., the O<sub>3</sub> response to a 20% decrease in EA emissions is ~0.45 ppbv throughout the O<sub>3</sub> distribution, whereas in the eastern states, the response is largest (at ~0.25 ppbv) for the 35-45 ppbv range of simulated total surface O<sub>3</sub>, and approximately equivalent to the response to EU emissions (0.2-0.4 ppbv in the 35-65 ppbv range). In contrast, the response to domestic emissions is largest for the highest simulated total O<sub>3</sub> concentrations [5-6 ppbv for total O<sub>3</sub> above 75 ppbv, Figure 12 of Reidmiller et al., 2009].

##### *Contribution to non attainment*

While much of this report addresses monthly or annual mean S/R relationships, it is important to stress that the determination of a regional violation of the MDA8 O<sub>3</sub> NAAQS typically depends only on a small number of days with ground-level concentrations above the threshold value. Thus, the relevance of intercontinental transport for attainment of standards depends only on the contribution of foreign sources to the most polluted days. The results discussed above for springtime in North America show that the contributions from distant sources to surface O<sub>3</sub> levels are nearly as significant for elevated O<sub>3</sub> levels (>65 ppbv), as lower values. However spring is not the highest O<sub>3</sub> season in North America. As shown in Figure 4.11, the maximum contribution of imported O<sub>3</sub> occurs on moderate O<sub>3</sub> days, when surface values fall between 50-70 ppbv and the anthropogenic contribution from Asia and Europe reaches 14 ppbv [Fiore et al., 2002]. Similar results have been found using a regional model at higher (36 km) resolution, with Asian and European contributions over the U.S.

reaching 24 ppbv [Lam and Fu, 2009]. The highest ozone levels typically occur under stagnant meteorological conditions which trap local precursor emissions and suppress the influence of distant sources [Fiore et al., 2002]. This would suggest that reducing domestic emissions is the most effective method of reducing the highest O<sub>3</sub> levels. Nevertheless, intercontinental transport can sometimes make an appreciable contribution under these conditions through entrainment of free tropospheric air into the boundary layer during the morning increase in mixing depth [Huang et al., 2010; Parrish et al., 2010]. As the threshold level for known O<sub>3</sub> health impacts (and associated air quality regulation) decreases, the importance of intercontinental ozone transport increases. Whereas Figure 4.11 and Fiore et al. [2002] reflect continent-wide, summertime distributions, similar patterns emerge at regional and seasonal scales [e.g., Reidmiller et al., 2009].

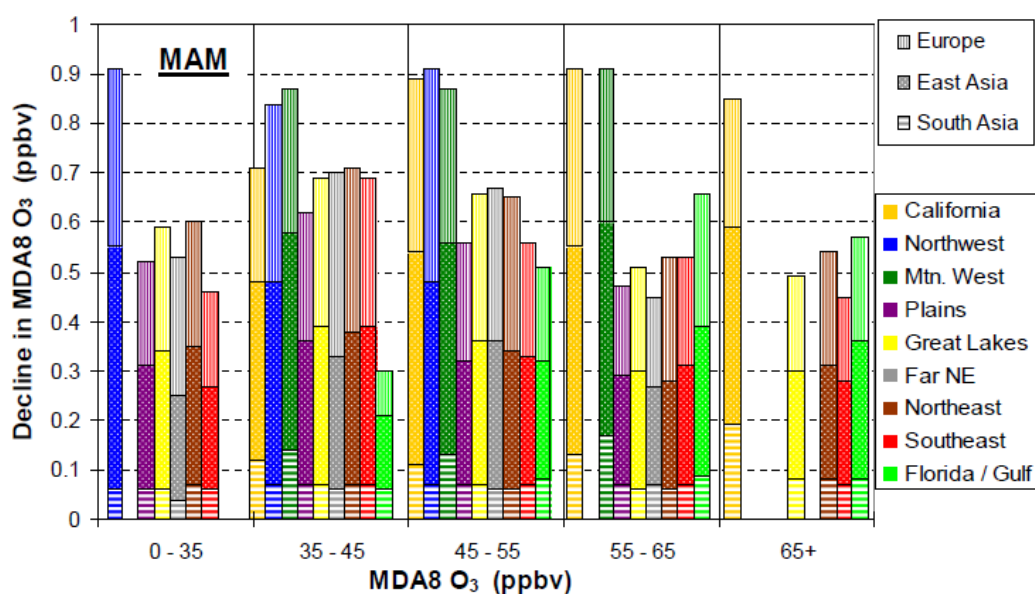


**Figure 4.10.** The multi-model mean springtime response of daily maximum 8-hour surface O<sub>3</sub> over 9 regions of the U.S. to 20% anthropogenic emission reductions in all precursors from European, East Asian and South Asian sources binned over different ranges of the O<sub>3</sub> distribution. [Reprinted from Figure 9 in Reidmiller, D. R., et al. (2009), The influence of foreign vs. North American emissions on surface ozone in the US, *Atmospheric Chemistry and Physics*, 9: 5027-5042.]

### Urban versus rural responses

Evaluation of the effect of intercontinental transport on attainment of air quality standards is complicated by the strong dependency of O<sub>3</sub> chemistry on the ratio of NO<sub>x</sub> to VOCs, suggesting that imported O<sub>3</sub> and precursors will have qualitatively different impacts on urban and rural areas. To demonstrate the influence of intercontinental transport on urban O<sub>3</sub>, the O<sub>3</sub> response in eighteen cities was analyzed from six models that provided hourly output, comparing both hourly and maximum 8-hour values (MDA8 O<sub>3</sub>). Annual MDA8 O<sub>3</sub> values are shown in Figure 4.12, where the total contribution from the other three source regions is presented. Also shown are the impacts due to changes in domestic emissions. For the majority of these cities, the impact of a 20% decrease in domestic anthropogenic emissions results in an ensemble mean decrease in MDA8 O<sub>3</sub> of 0.1 to 2 ppbv, but with the an upper quartile positive response, reflecting the non-linearity of O<sub>3</sub> chemistry in high emission regions. In contrast the net effect of a 20% decrease in the other source regions is to decrease MDA8 O<sub>3</sub> values at the receptor cities by ~0.25 to 1.25 ppbv. These values are of the same order of magnitude or larger than the influences of the domestic sources.

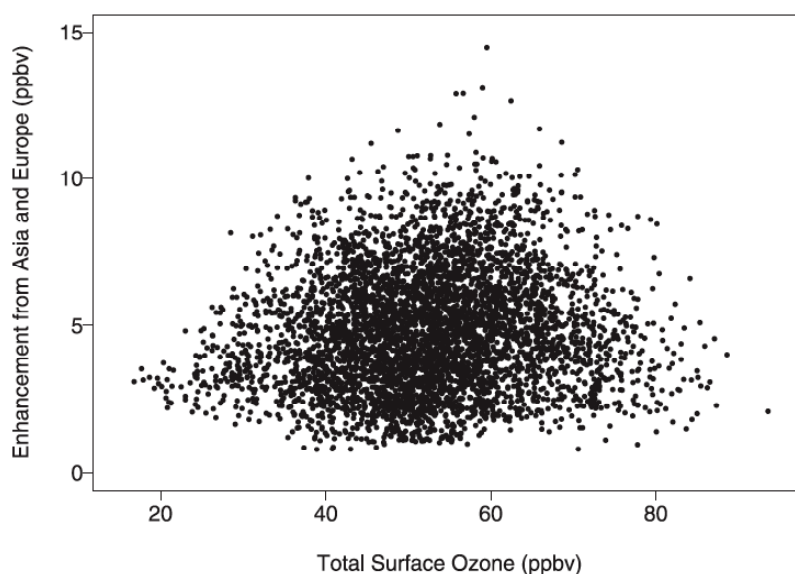


**Figure 4.11.** Enhancement to afternoon (1300-1700 LT) background O<sub>3</sub> in surface air over the U.S. in summer due to anthropogenic precursor emissions from both Asia and Europe, plotted as a function of total O<sub>3</sub> abundance in the model surface layer. [Reprinted from Figure 15 in Fiore, A. M., et al. (2002), Background ozone over the United States in summer: origin, trend, and contribution to pollution episodes, *Journal of Geophysical Research*, 107(D15): 4275-4299.]

**FINDING (exceedances):** The maximum influence of intercontinental transport on ground-level ozone generally occurs on mid-range pollution days (i.e., near the middle of the ozone probability distribution, typically 50-70 ppbv). Highest ozone levels frequently occur under stagnant meteorological conditions due to trapping of local precursor emissions; while the influence of distant sources is generally suppressed via this mechanism, the contribution of transported O<sub>3</sub> can still be appreciable under some conditions. These results indicate that while the intercontinental influence to various geographic regions is important, reducing domestic emissions is more effective at reducing the highest O<sub>3</sub> levels.

#### 4.2.7. Interannual variability

Interannual differences in S/R relationships for surface O<sub>3</sub> evaluated over the large continental-scale regions used here are found to be relatively small, particularly for the mid-latitude NA, EU and EA regions, and are far less than the differences across individual models. However, the importance of interannual meteorological variability becomes much greater when comparing smaller receptor regions, as the effects of shifts in transport patterns typically occur over smaller spatial scales than the continental-scale regions considered here [Calori et al., 2001], and the sensitivity of pollutant transport to smaller scale processes for boundary layer ventilation (e.g., convective and monsoonal processes versus synoptic frontal lifting events) increases. In addition, interannual variability in natural emissions (lightning, wildfires, biogenic hydrocarbons) may alter S/R relationships for anthropogenic emissions by influencing O<sub>3</sub> production over the source regions and chemical evolution during transport.

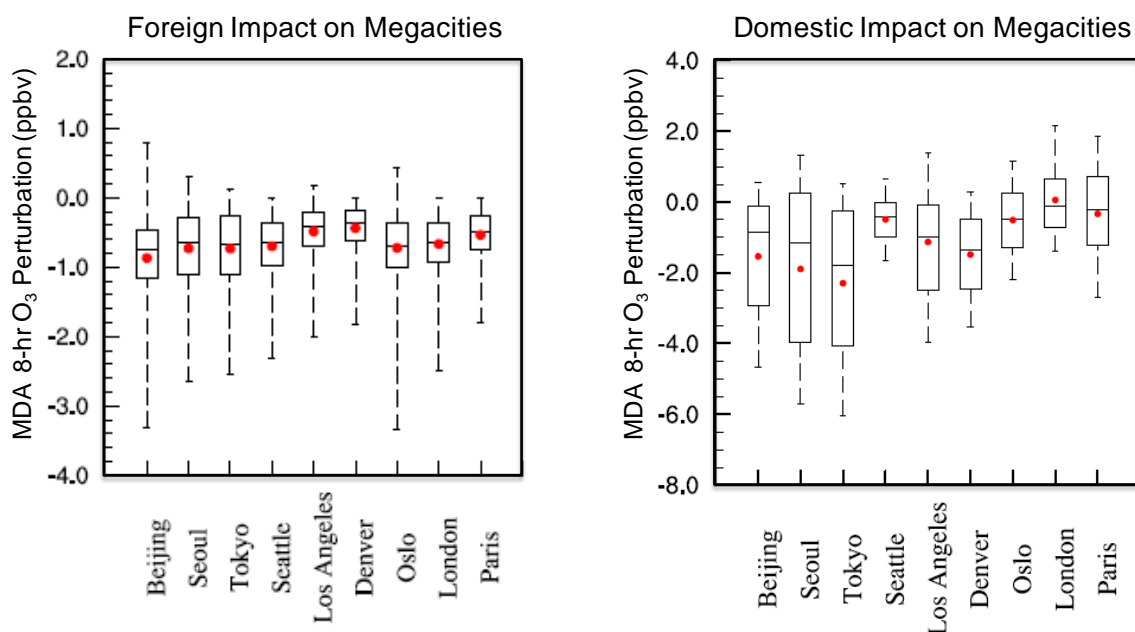


**Figure 4.12.** Change in surface maximum 8-hour O<sub>3</sub> (MDA8 O<sub>3</sub>) in model grid cells containing major cities from HTAP intercomparison simulations with all anthropogenic emissions reduced by 20% (SR6 runs). Boxes show the median and quartiles of the daily MDA8 O<sub>3</sub> change, whiskers show maximum and minimum, and red dots show the mean. The response due to the combined effect of precursor emission changes in the other three regions is shown in the left panel (e.g., the effect of NA, EU and SA on Beijing), and the response due to domestic emission changes is shown in the right panel (e.g., the effect of EA on Beijing).

**FINDING (interannual variability ozone): Interannual differences in S/R relationships for surface O<sub>3</sub> due to year-to-year meteorological variations are small when evaluated over continental-scale regions. However, these differences may be greater when considering smaller receptor regions or when variations in natural emissions are accounted for.**

#### 4.2.8. Influence of intercontinental transport through the depth of the troposphere

The vertical extent of the source region impacts on O<sub>3</sub> are presented in Figure 4.13, which shows the seasonal response of the model-mean tropospheric profile of the O<sub>3</sub> change for each S/R pair [Jonson *et al.*, 2010]. In most regions, O<sub>3</sub> changes in the source region are largest near the surface in summer, while the impacts from intercontinental transport are largest in the mid-troposphere, where they are typically twice as large as near the surface (cf. Figure 4.8). The altitude of the peak in intercontinental contribution on a monthly-mean basis ranges from about 600 hPa (4 km) from European sources to about 200 hPa (~8-10 km) for East and South Asian sources, as in previous studies [Stohl *et al.*, 2002; Wild and Akimoto, 2001], reflecting differences in the efficiency of lifting processes, particularly deep convection, over the source regions. There is a notable difference in the seasonality of intercontinental contributions with altitude over the HTAP receptor regions. For example, in summer they tend to be largest in the upper troposphere, but smallest at the surface, reflecting efficient convection, a shorter O<sub>3</sub> lifetime and greater prevalence of southerly flow (in contrast to predominantly westerly flow in other seasons). These profiles emphasize the importance of transport in the free troposphere and indicate that subsiding air masses influence intercontinental contributions for surface O<sub>3</sub>. These results also indicate that the S/R relationships for near-surface air pollution may differ from metrics relevant for climate change that are weighted towards upper tropospheric O<sub>3</sub> where radiative forcing is strongest.

### HTAP SR: O<sub>3</sub> [ppbv]

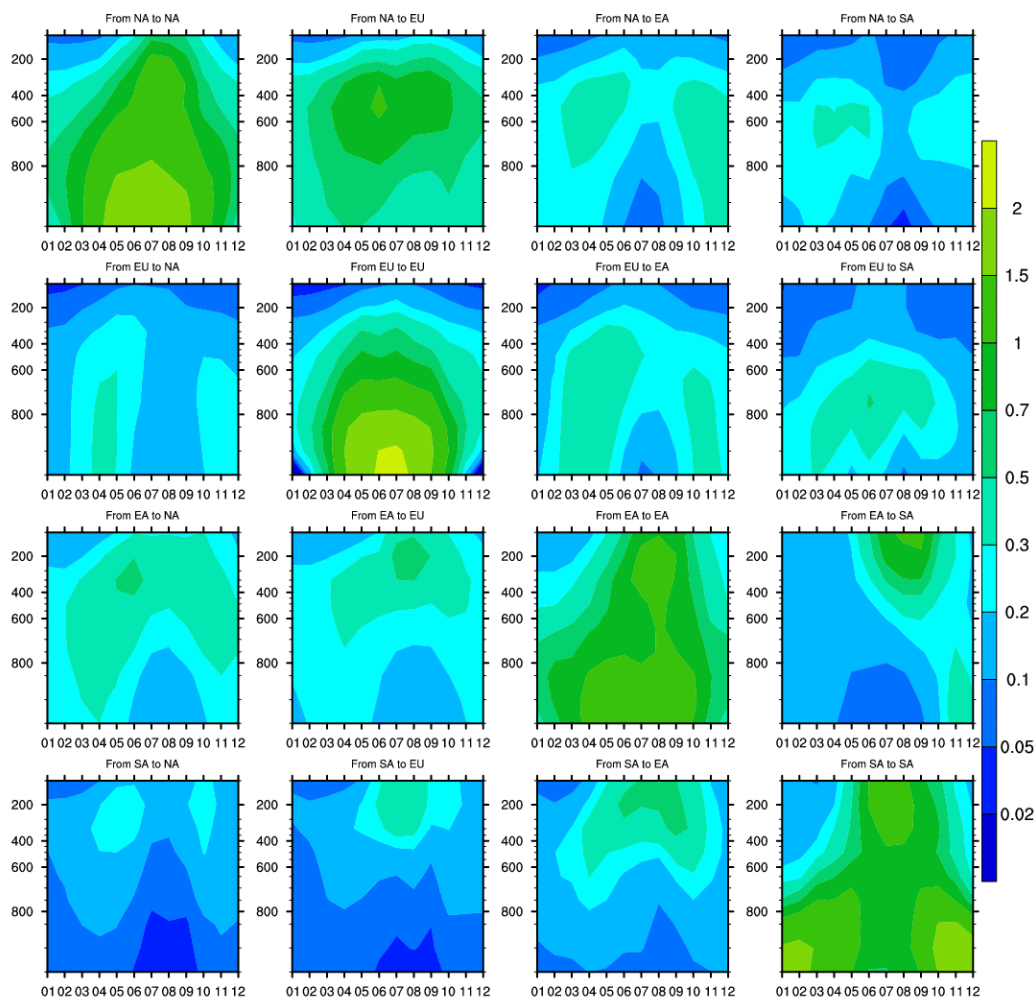


**Figure 4.13.** Altitude profile of S/R relationships for O<sub>3</sub> (in ppbv) based on 20% emissions reductions used in the HTAP intercomparison, showing the seasonal and altitudinal evolution of these relationships. The vertical coordinate is pressure (in hPa) ranging from 1000 to 100 hPa (0-16 km). [Reprinted from Figure 2 in Jonson, J. E., et al. (2010), A multi-model analysis of vertical ozone profiles, *Atmospheric Chemistry and Physics*, 10: 5759-5783.]

Changes in tropospheric O<sub>3</sub> columns resulting from reducing anthropogenic NO<sub>x</sub> emissions by 20% in each region are shown in Figure 4.14, and are compared with the effect of 20% reduced emissions from all other regions. Over EU, the tropospheric O<sub>3</sub> column response to emission changes in NA is as large as the response to domestic emissions. The response of O<sub>3</sub> columns to foreign (NA+EA+SA) emission changes is nearly twice as large as the response to domestic emissions, and the relative annual intercontinental response is 62%. The North American O<sub>3</sub> column is less strongly impacted by emission changes in other regions, and the relative intercontinental response is only 39%. In EA, the influence of EU emissions is as great as over the EU region itself, and the foreign contribution to EA O<sub>3</sub> columns is 40% larger than the domestic one, giving a relative intercontinental response of 60%. Over SA, the domestic impact on the O<sub>3</sub> column is larger than the foreign impact, and the three northern mid-latitude regions NA, EU, and EA make roughly equal contributions. Note that over all receptor regions the O<sub>3</sub> column responses are larger than the corresponding surface O<sub>3</sub> responses, and this is reflected in higher relative intercontinental responses. There is also closer agreement between models on the O<sub>3</sub> column response than there is on the surface O<sub>3</sub> response, reflected in the smaller 1 $\sigma$  variability.



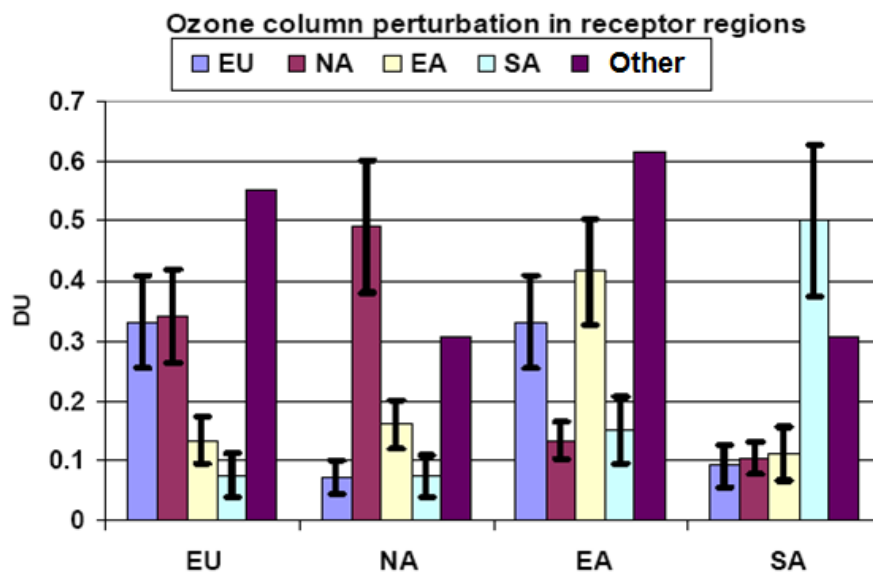


**Figure 4.14.** Reductions in annual mean  $O_3$  columns (DU=Dobson Unit,  $2.69 \times 10^{16} O_3$  molecules  $cm^{-2}$  integrated from surface to 150 hPa) over each receptor region resulting from a 20% decrease in  $NO_x$  emissions from each source region, and from all 'foreign' source regions (labelled 'Other'). The bars depict the 14-model mean, and the whiskers span  $\pm 1$  standard deviation over the models.

**FINDING (ozone column):** Substantial  $O_3$  transport takes place above the boundary layer in the free troposphere, where it can be brought to lower altitudes over distant receptors during subsidence, and mix with local emissions. The relative annual intercontinental responses are larger for  $O_3$  column than for surface  $O_3$ , and exceed 50% over EU and EA.

#### 4.2.9. Import/Export budgets from different regions

The hemispheric transport of  $O_3$  to this point has been analyzed in terms of changes in  $O_3$  abundance, but it is important to analyze further the meteorological and chemical processes influencing S/R relationships. For example, it is useful to assess the export of pollution from the source regions. Ozone can be produced in the source region and exported, or can be produced elsewhere in the troposphere following export of its precursors. Transport of longer-lived oxidized nitrogen species ( $NO_y$ ) which survive for more than a few days, particularly peroxyacetyl nitrate (PAN), provides a pathway for export of  $NO_x$  to the free troposphere, where the efficiency of subsequent  $O_3$  production is much larger than in polluted source regions. Sanderson et al. [2008] quantified the export efficiency for  $NO_y$  from 15 models contributing results to the HTAP intercomparison, see Figure 4.15. Based on 20%  $NO_x$  emission changes, they found that most of the  $NO_y$  is deposited within the source region, and that between 12% and 24% of the  $NO_x$  emitted is exported from the HTAP emission regions as  $NO_y$  on an annual basis, with the greatest export from Europe and the least from East Asia. Export is most efficient in winter or spring, reflecting a balance between the longer  $NO_y$  lifetime and the meteorological timescales for transport. Additional studies have extended this analysis by quantifying the relative importance for  $O_3$  transport of precursor export vs.  $O_3$  export. For emissions of short-lived precursors (e.g.,  $NO_x$ ), direct export of  $O_3$  produced over the source region dominates the intercontinental influence whereas for longer-lived precursors (e.g., CO) the import of precursors into receptor regions contributes to additional  $O_3$  production within the receptor region [Collins et al., 2010b; West et al., 2009a]. The source regions are always net exporters of both  $O_3$  and precursors.



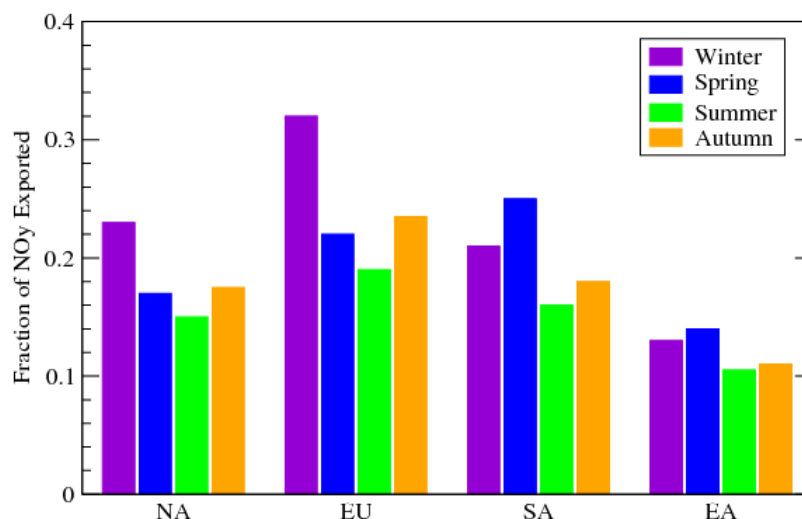


**Figure 4.15.** Export fractions for  $\text{NO}_y$  from each HTAP source region for each season for 15 models from the HTAP intercomparison analysed by Sanderson et al. [Reprinted from Figure 2 in Sanderson, M. G., et al. (2008), A multi-model study of the hemispheric transport and deposition of oxidised nitrogen, *Geophysical Research Letters*, 35(L17815).]

Models can also provide insight into the specific meteorological conditions leading to export. For example, Fang et al. [2009] determined that 65% of CO exported through the northern and eastern boundaries of the U.S. occurs during synoptic-scale transport in mid-latitude cyclones, with the remaining 35% attributed to other meteorological conditions, such as westward extensions of the Bermuda high or deep convection. Chen et al. [2009a] found that the CO export flux from India and Southeast Asia decreases by a factor of 3-4 from spring to summer, while fluxes from China are only 30% lower in summer than in spring due to deep convection transporting CO to higher altitudes.

#### 4.2.10. Contribution to observed ozone trends

Using the annual mean  $\text{O}_3$  responses from the HTAP intercomparison and estimates of historical changes in regional and global  $\text{O}_3$  precursor emissions we can estimate the contribution of anthropogenic emission changes to observed surface  $\text{O}_3$  trends. Figure 4.16 shows the regional changes in surface  $\text{O}_3$  estimated by linearly scaling the results from the six models that contributed to all HTAP simulations and using gridded anthropogenic emission changes for  $\text{NO}_x$ , CO and NMVOC between 1960 and 2000 from Lamarque et al. [2010]. Following these historical changes in emissions we see relatively small changes in surface  $\text{O}_3$  over North America and Europe, ranging from 0.2 ppbv/year increases between 1960 and 1980 to small decreases over the past decade, but stronger, more uniform increases over South and East Asia of up to 0.25 ppbv/yr. These are slightly larger than the 0.1 ppbv/year increases estimated by Fiore et al. [2009]. However, these surface  $\text{O}_3$  increases remain significantly smaller than the 0.1-0.5 ppbv/year range derived from observations at remote sites at northern mid-latitudes (see Chapter 2) and are similar to, or somewhat smaller than, those seen in previous model studies (see Section 4.2.3). This may suggest that there is a significant component in the observed trend controlled by natural sources and sinks, e.g., increases in stratosphere-troposphere exchange. It may also indicate that remote observation sites are not representative of the regional scales considered here. Focusing on the western U.S., Reidmiller et al. [2009] used the HTAP results to estimate that a 10% per year increase in East Asian precursor emissions would lead to an increase in MDA8  $\text{O}_3$  of  $\sim 0.2$  ppbv/year (0.1-0.32 ppbv/year across the full model range), close to the 0.34 ppbv/year increase in mean daytime  $\text{O}_3$  reported by Jaffe and Ray [2007] for that region.

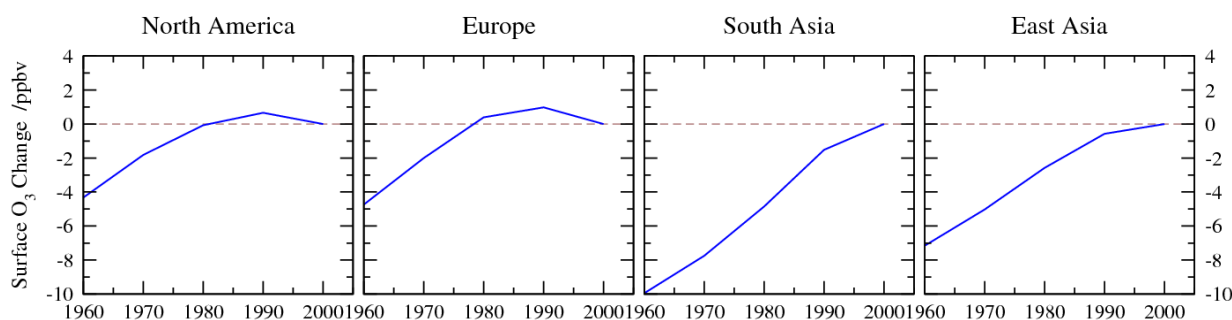


**Figure 4.16.** Changes in annual mean surface  $O_3$  over the HTAP receptor regions between 1960 and 2000 based on linearization of the results from six models that contributed to all SR simulations in the HTAP intercomparison. Changes are referenced to surface  $O_3$  in 2000.

#### 4.2.11. Robustness of HTAP S/R Results

##### *Consistency between attribution and S/R analysis*

The HTAP S/R relationships discussed above can be compared with recent results from source attribution analysis by [Nagashima *et al.*, 2010]. They looked at source attribution for the six-year period 2000-2005 using a global model with a focus on East Asia regional receptors. Their results are summarized below in Figure 4.17. These results further underscore the spatial variability within the East Asia receptor, and can be compared to the HTAP S/R results. For example this attribution study found that EU and NA contributed from 2 to 8 ppbv to ground level  $O_3$  in EA in MAM, and 1-3.4 ppbv in JJA. SA contributed from 0.3-8.2 and 0.3-7 ppbv in MAM and JJA, respectively, to surface  $O_3$  in EA. When extrapolated to a 100% source contribution, the HTAP results suggest that EU and NA contribute from 1-5 ppbv and 1-2.5 ppbv to surface  $O_3$  in EA in MAM and JJA, respectively; while SA contributes 0.5-1.5 and 0.3-1 ppbv to EA in MAM and JJA, respectively. The HTAP results are consistently lower, partly reflecting the fact that the source attribution looked at all global sources and not just the anthropogenic component from the HTAP regions. The interannual variability in the attribution for the annual mean country wide mean totals was found to be less than 6%, but for specific months and sub-regions was at large as 30%. In general, these results are broadly consistent with those presented in Section 4.2.5, although the seasonal variability is slightly larger here due to the smaller source regions considered.

##### *Adjoint analysis*

Adjoint analysis calculates sensitivities to specific processes backwards in time in an Eulerian model and identifies those source regions that have a direct influence on the receptor locations. An example of adjoint application to quantify regional versus intercontinental influence on surface  $O_3$  is shown in Figure 4.18 for Mt. Bachelor Observatory in Oregon, USA (2.7 km altitude) during May 2006. Mount Bachelor is most sensitive to  $O_3$  produced within the North American region within the previous few days, but large contributions are also found for  $O_3$  produced over the North Pacific and Asian regions within the previous week to month, and for  $O_3$  produced elsewhere in the world. All regions contribute to raising the hemispheric baseline level, as evidenced by the long tail on the sensitivities extending out to 60 days and beyond.

##### *Scalability of S/R relationships with respect to size of emission perturbation*

The S/R relationships quantified in this section represent the  $O_3$  responses to 20% emission changes, and provide a good estimate of sensitivity to current emissions. However, they do not allow a simple estimation of the total contribution of one source region on another due to the nonlinear response of  $O_3$  production to the changing abundance of  $NO_x$ . For given levels of  $CH_4$ ,  $CO$ , and  $VOC$ , the  $O_3$  production efficiency of  $NO_x$  falls as the abundance of  $NO_x$  increases [e.g., Liu *et al.*, 1987]. At high  $NO$  emission rates typical of polluted urban regions, localised net  $O_3$  destruction may occur, and this has a particularly large effect at higher latitudes in winter where insolation is weak, days are short, and temperatures are relatively low (e.g., over Europe in January, see Figure 4.7). The consequence of these effects is that the  $O_3$  response to a 20% precursor emission change may be

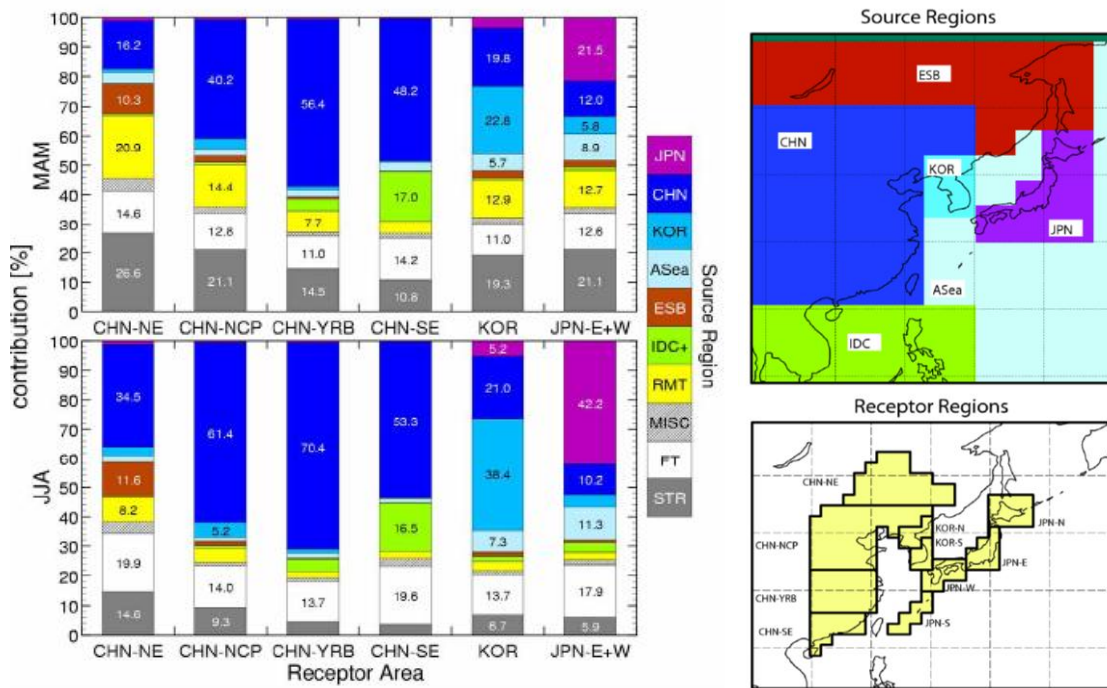


**Figure 4.17.** Seasonal mean percentage contribution from source regions to receptor regions in East Asia for spring (top) and summer (bottom) averaged over 6 years. Source regions are shown on the right and include Japan (JPN), China (CHN), Korea (KOR), adjacent marine regions (ASa), E. Siberia (ESB), SE Asia (IDC+), other N. Hemispheric mid-latitude regions (RMT), the free troposphere (FT) and stratosphere (STR). Receptor regions include NE China (CHN-NE), the North China Plain (CHN-NCP), Yangtze River basin (CHN-YRB), SE China (CHN-SE), Korea and mainland Japan (JPN-E+W). [Adapted from Figures 1, 4, and 5 in Nagashima, T., et al. (2010), The relative importance of various source regions on East Asian surface ozone, *Atmospheric Chemistry and Physics*, 10: 11305-11322.]

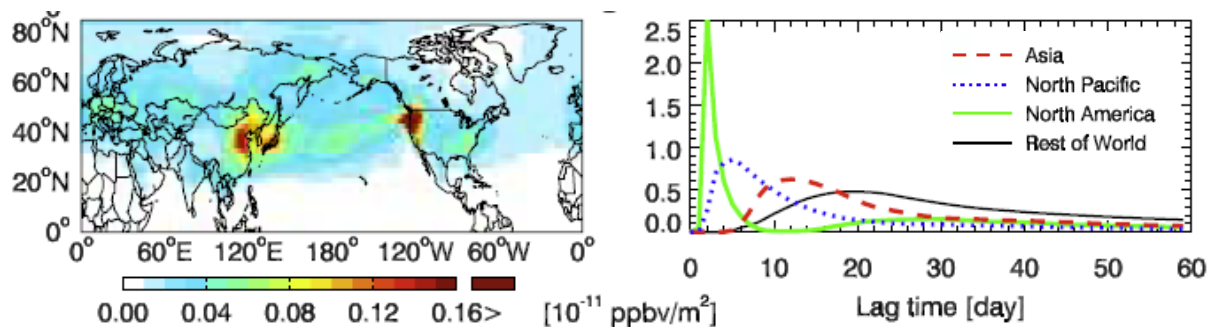


**Figure 4.18.** Sensitivity of surface O<sub>3</sub> abundance at Mt. Bachelor in the western U.S. to O<sub>3</sub> production in different regions of the world as inferred from the GEOS-Chem adjoint model for the period April 17 – May 15, 2006 [Zhang et al., 2009]. Left: sensitivities integrated in time over the depth of the tropospheric column. Right: time-dependent sensitivities (going back in time) to O<sub>3</sub> production (in ppbv/day) over Asia, the North Pacific, North America, and the Rest of World. These results demonstrate that production over any one region (e.g., North America) includes long-range transport from distant precursor sources as well as local emissions. [Adapted from Figure 2a in Zhang, L., et al. (2009), Intercontinental source attribution of ozone pollution at western U.S. sites using an adjoint method, *Geophysical Research Letters*, 36(L11810).]

significantly less than one fifth of the contribution from that source [e.g., Wu *et al.*, 2009]. These effects are illustrated in Figure 4.19, which shows how S/R relationships change with the magnitude of emissions for NO<sub>x</sub> emission changes over Europe in one model. The effects depend on the representation of the different chemical environments over the source region, and are thus highly model-dependent, but are clearest for the European NO<sub>x</sub> scenario; other source regions at lower latitudes experience greater insolation, and altering emissions of other precursors (e.g., CO, VOC) at the same time reduces the magnitude of these effects.

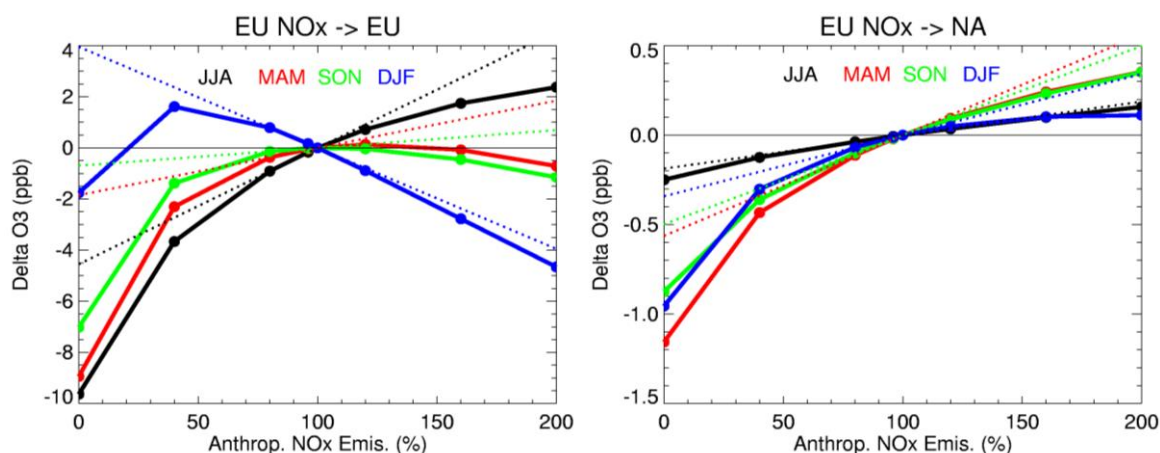


**Figure 4.19.** Sensitivity of the calculated S/R relationship to the magnitude of NO<sub>x</sub> emission changes over Europe relative to current conditions. Over the source region (left) O<sub>3</sub> production continues to increase with increased NO<sub>x</sub> emissions in summer (black), but decreases through titration processes in winter (blue). Extrapolation of a 20% reduction in each season (dotted lines) leads to an incorrect estimate of the contribution of the source as derived from complete removal of NO<sub>x</sub> emissions, and both these estimates differ from a true source attribution. The O<sub>3</sub> change over North America (right) shows that the effects are far smaller over distant receptor regions, but highlights that extrapolation from 20% changes may underestimate the source contribution by about a factor of two. [Adapted from Figure 9 in Fiore, A. M., et al. (2009), Multimodel estimates of intercontinental source-receptor relationships for ozone pollution, *Journal of Geophysical Research*, 114(D04301).]

**FINDING (S/R and source attribution ozone): Substantial non-linearity in O<sub>3</sub> chemistry prevents HTAP results for S/R relationships being linearly scaled to provide an estimate of full source contributions. Source attributions generated this way underestimate the contribution of distant sources.**

### 4.3. Quantifying intercontinental transport of aerosol

#### 4.3.1. Aerosol budgets and transport

Long-range transport of aerosol particles (particulate matter) is clearly documented by satellite and surface observations of dust outbreaks and plumes from large fires. Occasionally, such aerosol clouds can be followed for many days around the globe by means of repeated satellite observations [Damoah *et al.*, 2004]. Dust has been shown to cross regularly the Pacific Ocean, the Atlantic Ocean and the Mediterranean Sea [Darmenova *et al.*, 2005; Husar *et al.*, 2001; Kaufman *et al.*, 2005; Moulin *et al.*, 1998; Wilkening *et al.*, 2000].

It is commonly believed that aerosols are removed from the atmosphere within hours to several days, but observational evidence indicates that there are many exceptions to this averaged timescale, as shown in a number of examples in chapter 2. In contrast to episodic hemispheric scale transport, the role of more continuous transport not readily detectable on satellite images is poorly understood. However, this may be an important mechanism for anthropogenic aerosol transport and may lead to a rise in the estimated hemispheric background PM concentration levels. For example, a

recent study estimates annual transport of PM pollution from Asia to North America of 4 Tg/year; this is about 25% of the non-dust aerosol that leaves Asia [Yu *et al.*, 2008]. In comparison, 240 Tg/year of dust is thought to be transported from the Sahara with 50 Tg/year deposited in the Amazon basin and another 50 Tg/year deposited in the Caribbean [Kaufman *et al.*, 2005]. Although much of this transport is episodic, it reoccurs all year long. In the trans-Pacific case, most of the transport occurs in Spring (~1.7 Tg) due to dry weather and considerable dust lifting contributing to PM transport, with an additional ~0.9 Tg in Winter, ~0.7 Tg in Summer and ~0.9 Tg in Autumn.

A number of studies have explored S/R relationships for aerosol burdens and surface concentrations on continental scales. Trans-Pacific transport of Asian pollution has been found to account for 30% of background sulphate in both the western and eastern U.S., suggesting that meeting the U.S. EPA's visibility objectives will require a combination of domestic and international emission controls [Park *et al.*, 2004]. Foreign dust and sulphate have been found to account for about 50% and 30% of background PM<sub>2.5</sub> concentrations over North America, respectively [Liu *et al.*, 2009]. However, another study indicates that trans-Pacific transport of Asian pollution contributes less than 10% of the surface ammonium sulphate concentrations over North America, but that dust originating from Asia can make a significant contribution to surface fine particulate concentrations [Chin *et al.*, 2007]. Studies with the GISS model suggest that the export of aerosols from source regions is large: 70-80% by mass of most anthropogenic aerosol species is exported from Europe, Asia and North America [Koch *et al.*, 2007]. South and East Asia contribute about 15% of global sulphate and 30% of global black carbon (BC) pollution loads; Europe and North America each contribute about 5% of global BC and sulphate pollution loads. These results seem to be in contrast to those from the European Union project PHOENICS [Krol, 2005]; however, those show the importance of natural dust and sea salt entering Europe, and substantial export of anthropogenic BC, particulate organic matter (POM), SO<sub>4</sub> and NO<sub>3</sub>. Results from the PHOENICS study indicate that European anthropogenic emissions contribute 40-80% to European aerosol column loadings, depending on aerosol component, and 1-5 % to aerosol load outside Europe. Sources from East and South Asia together have been found to contribute more than 50 % to global radiative absorption by BC [Reddy and Boucher, 2007]. The trans-Pacific transport of BC and PM<sub>2.5</sub> into North America has been studied using aircraft and surface observations from the Cloud Indirect Forcing Experiment (CIFEX) [Roberts *et al.*, 2006] and the IMPROVE network, and a CTM [Hadley *et al.*, 2007]. This study found that the trans-Pacific flux of BC across the western boundary of North America in April 2004 was ~75% of North American BC emissions. Furthermore ~80% of the BC mass transport over the Pacific Ocean occurs above 2 km. BC of Asian origin was estimated to contribute ~20% of the observed BC at IMPROVE measurement sites at 1 km elevation, and over 50% at sites at 2 km elevation and higher.

### ***HTAP Model Simulations of Hemispheric Transport***

In the HTAP intercomparison, thirteen models contributed aerosol (PM) diagnostics, of which five models contributed to the earlier AeroCom intercomparison [Textor *et al.*, 2006]. Model results presented below are from the HTAP SR6 experiment in which a 20% reduction in all anthropogenic emissions of aerosol precursors and aerosol primary emissions was introduced for each of the four source regions. The results of these simulations were compared to the SR1 reference experiment with unperturbed emissions to establish S/R responses for each region and to trace the fate of the different chemical species. Table 4.4 and Figures 4.20-4.23 show the results of these experiments. Shown in Table 4.4 are the relative annual intercontinental responses for surface concentrations, deposition, and column loadings for the four HTAP regions. In general, the smallest intercontinental responses are for surface concentrations and the largest for column loadings. The responses also vary by region. For example, the contribution from other source regions relative to the contribution from all sources to surface concentrations of PM (estimated as the sum of SO<sub>4</sub> and POM) varies from 5% for EU to 20% for SA. The large responses for the SA region can be attributed to the definition of the HTAP regions, as the SA region is close to and immediately downwind of the EU region.

**Table 4.4.** Multi-model derived relative annual intercontinental responses (RAIRs) for surface concentration, deposition and column load of anthropogenic black carbon (BC), particulate organic matter (POM), sulphate (SO<sub>4</sub>) and all sulphur species (SO<sub>2</sub>+SO<sub>4</sub>). Note that PM concentration is estimated as the sum of SO<sub>4</sub> and POM. The RAIR for a region is defined as the ratio of the effect of other source regions to the effect of all source regions. The variability between the contributing models is given in brackets as one standard deviation.

Receptor region:	EU	NA	SA	EA	No. of models
<b><i>Surface Concentration Response</i></b>					
PM	5% (4%)	7% (6%)	20% (11%)	9% (8%)	9
<b><i>Deposition Import Response</i></b>					
SO <sub>4</sub>	9% (7%)	8% (5%)	24% (10%)	12% (8%)	11
Sulphur (SO <sub>2</sub> +SO <sub>4</sub> )	3% (2%)	3% (3%)	16% (7%)	5% (3%)	11
BC	1% (1%)	4% (2%)	12% (19%)	3% (1%)	8
POM	1% (1%)	3% (2%)	11% (19%)	4% (1%)	8
<b><i>Column Load Response</i></b>					
SO <sub>4</sub>	25% (19%)	25% (19%)	37% (16%)	24% (17%)	11
BC	17% (12%)	24% (19%)	16% (3%)	15% (5%)	7
POM	21% (17%)	23% (19%)	12% (5%)	19% (6%)	7

The relative intercontinental response also varies by species. For example, the response for sulphate is three times larger than for total sulphur (SO<sub>2</sub>+SO<sub>4</sub>). The spatial dispersion of total sulphur deposition is dominated by sulphur dioxide deposition, which occurs close to the sources. The fraction of total emitted anthropogenic sulphur from a given region that reaches the receptor regions is thus small. The deposition response for total anthropogenic sulphur varies between 3 and 16%. In contrast, the sulphate aerosol produced from SO<sub>2</sub> emissions has a longer lifetime. Thus, the impact from other regions on sulphate deposition and sulphate aerosol column load is considerable, as shown in Figure 4.20. The relative intercontinental response for SO<sub>4</sub> column load varies between 24 and 37%. This demonstrates the importance of aerosol transport above the PBL. Over the Arctic, the influence of Asian anthropogenic emissions is comparable to or exceeds that from European emissions for the atmospheric column. This is because material emitted in Asia is lifted into the free troposphere more efficiently, while that emitted in Europe tends to stay in the boundary layer.

Analysis with a smaller number of models also shows that emissions of POM and BC have a larger impact than sulphate on the source region itself. Import contributes between 15 and 24% of the anthropogenic BC column load and between 12 and 23% of the POM column. The diverse treatment of secondary organic aerosol may cause such differences between models.

The HTAP intercomparison allows for the first time an investigation of the differences among models of the specific aerosol life cycles experienced by aerosol originating from different regions. Figure 4.21 illustrates the diversity in sulphur lifetimes in the models. The impact of one region on another depends on the transport pathways, their length, and the intensity of the removal processes that the aerosol experiences along the way. In general models with longer lifetimes predict larger import sensitivities. The differences in lifetime between regions are consistently described by the individual models. Aerosol from North America and East Asia appear to be slightly more efficiently removed than those from Europe and South Asia. As in AeroCom, the model diversity in sulphur lifetimes in absolute terms for a given region is considerable (a factor of four), and reflects differences in process-level model formulations.

Analysis of the surface aerosol concentrations reveals that the annual average anthropogenic PM<sub>2.5</sub> for the HTAP regions is increased by 4-18% through transport from the other regions (see Table 4.5). There is consistency among the models in the relative importance of the import contribution to a



region, but appreciable diversity among model predictions in terms of the absolute contributions (see Figure 4.22). As discussed above, the SA region is found to receive the highest PM load from abroad. However, the limited number of models with similar complexity, especially with regard to organic aerosols, makes the results rather uncertain (see also the high standard deviations in Table 4.5).

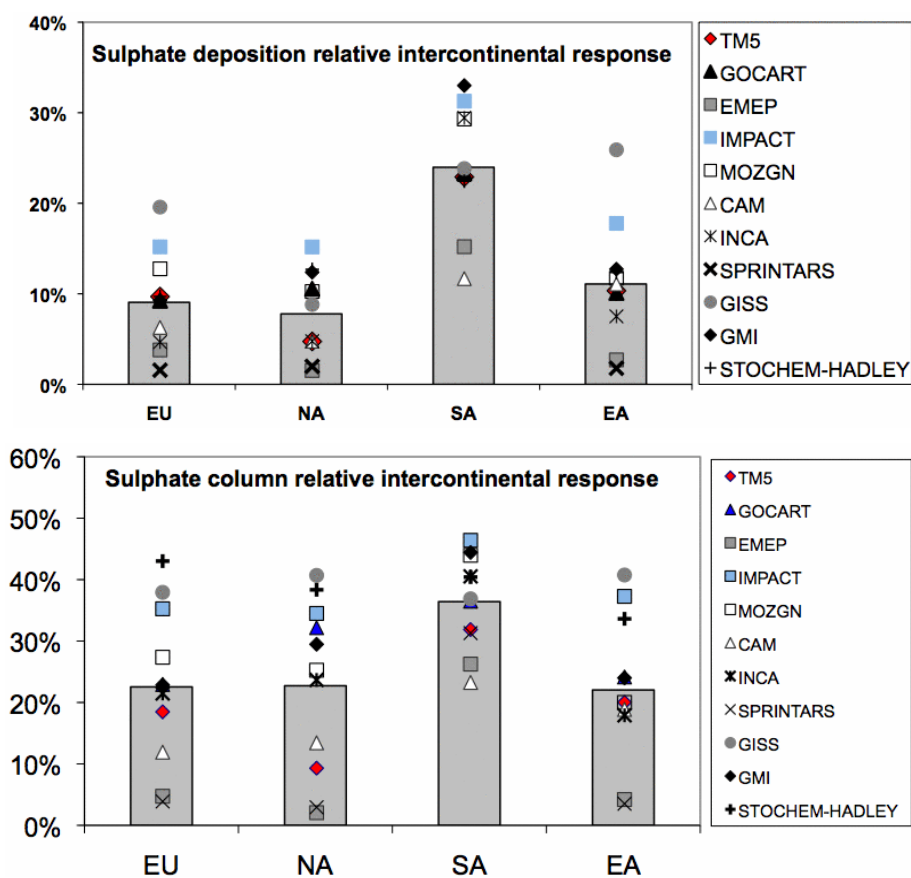


**Figure 4.20.** Relative annual intercontinental response (RAIR) of total sulphate deposition (upper panel) and sulphate aerosol column burden (lower panel) over each receptor region. The RAIR is the ratio of the imported deposition/column sulphate to the deposition/column load from all four HTAP source regions. Individual model results are shown with symbols.

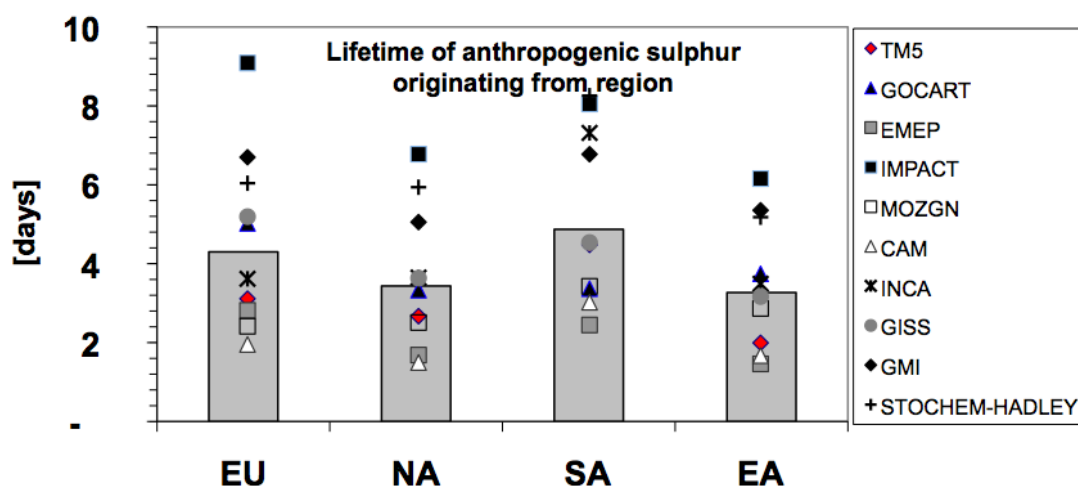


**Figure 4.21.** Lifetime of sulphate originating from different regions showing the mean lifetime (bars) and lifetime in different models (symbols). The lifetime is calculated from the anthropogenic sulphur burden response and total deposition response due to perturbation of emissions in each region.



**Table 4.5.** Multi-model (9 models) response of a) annual mean surface PM ( $\text{ng m}^{-3}$ ) estimated as the sum of  $\text{SO}_4$  and POM; b) column load of sulphate and c) POM in receptor regions (columns) to 20% reductions of anthropogenic gas and aerosol emissions in the source regions (rows). Contributions of a region on itself (termed ‘domestic’) are shown in bold. Inter-model standard deviations are shown in parentheses.

Source region	Receptor Region			
	EU	NA	SA	EA
<i>Annual Mean Response of surface PM [<math>\text{ng/m}^3</math>]</i>				
EU	<b>-711 (313)</b>	-8 (5)	-76 (20)	-22 (16)
NA	-18 (9)	<b>-352 (116)</b>	-9 (7)	-6 (3)
SA	-4 (6)	-1 (2)	<b>-627 (225)</b>	-19 (6)
EA	-7 (5)	-10 (7)	-27 (18)	<b>-738 (338)</b>
Total Import	4%	6%	18%	6%
<i>Annual Mean Response of column load sulphate [<math>\mu\text{g/m}^2</math>]</i>				
EU	<b>-964 (271)</b>	-53 (46)	-266 (92)	-129 (94)
NA	-173 (137)	<b>-587 (195)</b>	-48 (47)	-48 (49)
SA	-47 (40)	-35 (36)	<b>-696 (213)</b>	-103 (61)
EA	-102 (93)	-122 (104)	-100 (78)	<b>-950 (303)</b>
Total Import	33%	36%	59%	30%
<i>Annual Mean Response of column load POM [<math>\mu\text{g/m}^2</math>]</i>				
EU	<b>-180 (211)</b>	-4 (4)	-25 (24)	-12 (16)
NA	-16 (19)	<b>-95 (86)</b>	-4 (3)	-4 (4)
SA	-13 (9)	-9 (8)	<b>-410 (283)</b>	-47 (26)
EA	-13 (18)	-16 (21)	-25 (20)	<b>-293 (258)</b>
Total Import	23%	30%	13%	21%

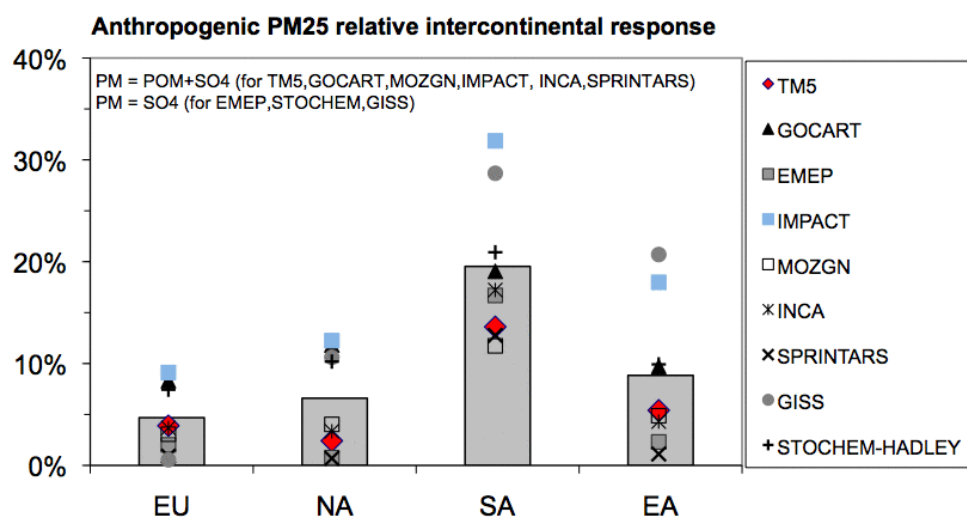


**Figure 4.22.** Relative annual intercontinental response of surface PM concentration over the HTAP regions (bars). Results from individual models are shown with symbols.

**FINDING (aerosol): Models calculate a wide range of surface aerosol concentrations and relative annual intercontinental responses to emission perturbations, reflecting large uncertainties in emissions, atmospheric processes and analysis methods.**

***Sulphur budget derived from HTAP perturbation experiments***

The HTAP model simulations SR1 and SR6 allow preparation of a budget of emitted SO<sub>2</sub> with respect to deposition and transformation to aerosol sulphate. Figure 4.23 summarizes this budget across models to illustrate the split in removal processes between the source regions and the rest of the world. A large part of the emissions (75%) stays within the large HTAP regions. Wet deposition accounts for 55% of the removal and becomes dominant outside of the source regions. The dry removal of SO<sub>2</sub> within the source regions can be identified as an important process determining the overall export.

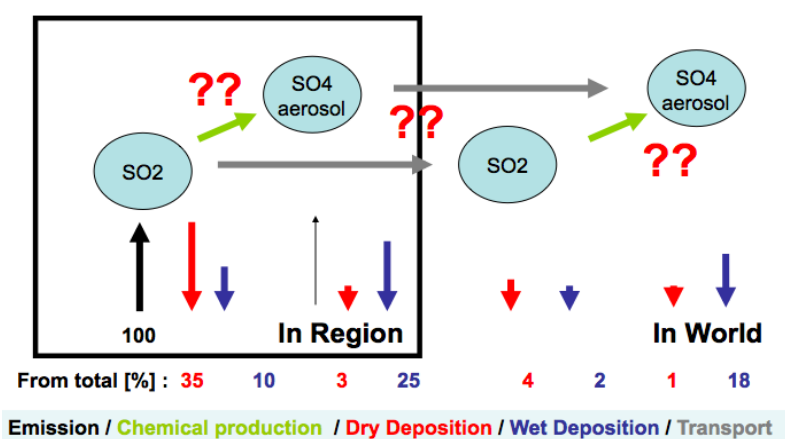


**Figure 4.23.** Model mean sulphur budget averaged over all four HTAP regions. Numbers represent the fraction of total sulphur emission deposited as SO<sub>2</sub>/SO<sub>4</sub> via dry (red numbers) and wet (blue) deposition within source regions (under black box) and in the rest of the world. The regional SO<sub>4</sub> formation rate, and hence the partitioning of SO<sub>2</sub> and SO<sub>4</sub> in exported sulphur, were not diagnosed in the HTAP experiments (indicated by question marks).

This can be also seen in Figure 4.24 where the SO<sub>2</sub> dry deposition from all individual HTAP SR6 model runs is shown against the overall export fraction from the source regions. The more SO<sub>2</sub> is removed close to the sources by dry deposition, the smaller the fraction that is available for export from the region as SO<sub>2</sub> or SO<sub>4</sub>. A large spread is seen indicating that this process is likely to be responsible for a large part of the variability in export of sulphur. High dry deposition rates to the surface can be the result of both high concentrations at the surface and efficient dry removal. High surface concentrations can result from inefficient vertical mixing and inefficient wet removal and further analysis is needed to diagnose the role of these competing processes in the fate of the emitted SO<sub>2</sub>.

**4.3.2. AEROCOM-HTAP aerosol-specific experiments**

Dust and wild fire emissions can contribute substantially to inter-hemispheric transport of particulate matter and may affect and perturb regional air quality control efforts. Secondly, import sensitivities for secondary sulphate may change with the amount of reduction of anthropogenic emissions of precursors and oxidants. These problems have been selected for additional HTAP aerosol experiments.

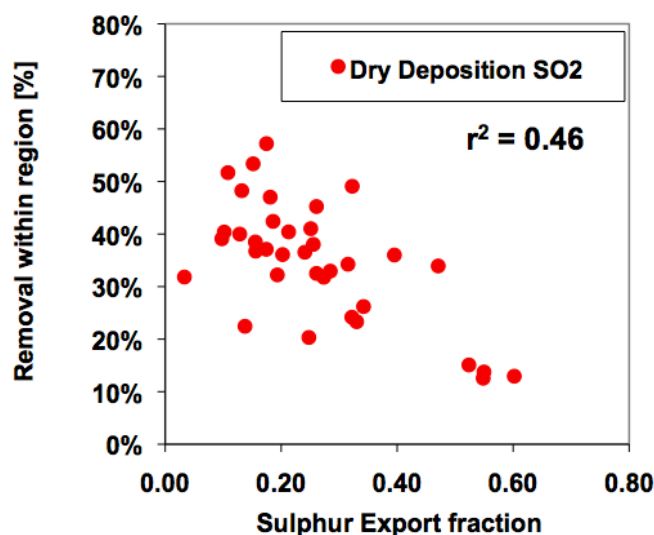


**Figure 4.24.** Sulphur export fraction out of source regions as computed by HTAP models, shown from all four HTAP regions as a function of dry removal within source regions.

We now focus on the S/R relationships and source attribution of aerosols. In addition to the HTAP SR6 experiments focusing on anthropogenic aerosol, three additional experiments were performed to assess the impact of dust and biomass burning aerosols on regional air quality. A subset of 6 models contributed to these experiments (GISS-PUCCINI-modelE, GMI, GOCART, LLNL-IMPACT, SPRINTARS, and ULAQ). Anthropogenic emissions of aerosols and precursor gases were reduced to zero in SR6z, one region at a time (cf. 20% reduction in SR6); dust emissions were turned off from North Africa (AF), Middle East (ME), and Asia (AS) one region at a time in SR6d; and biomass burning emissions in North American boreal (NW), Eurasian boreal (NE), low-latitude regions of North America (SW) and Africa-Asia (SE) were turned off in SR6b. The regional domains are shown in Figure 4.25. In all studies, the NA, EU, EA, and SA source regions are also considered as receptor regions, and the Arctic (AR, north of 66.6°N) is examined as an additional receptor region. Emissions of sulphur and BC from four anthropogenic source regions, POM from four biomass burning regions, and dust from three major desert regions are shown in Figure 4.26, together with emissions from the rest of the world. Note that both anthropogenic and biomass burning aerosols consist of multiple components, such as sulphate, BC, and POM.

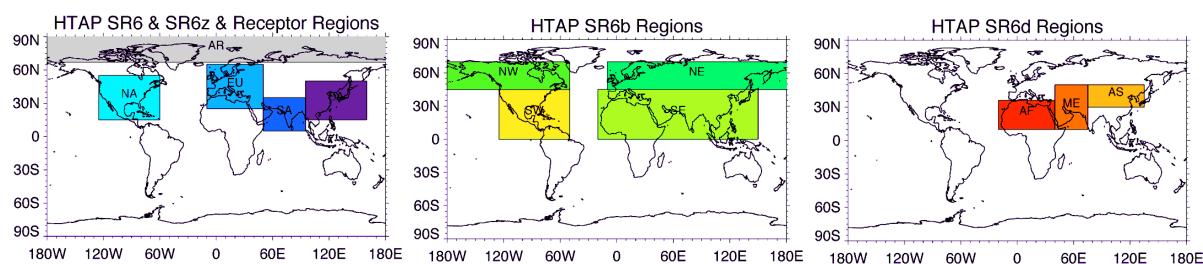


**Figure 4.25.** Regional domains for anthropogenic and biomass burning sources in SR6 and SR6z (left), for biomass burning sources in SR6b (centre), and for dust source regions in SR6d (right). The left-hand panel also shows the Arctic receptor region used here.

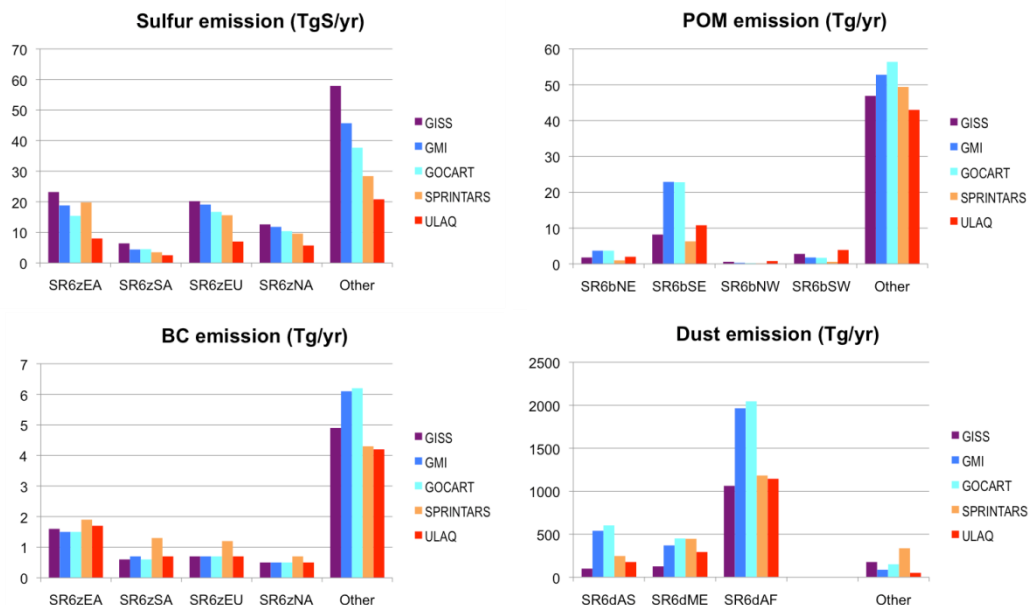


**Figure 4.26.** Emissions of anthropogenic sulphur (mostly SO<sub>2</sub>) and BC in anthropogenic source regions, POM in biomass burning regions, and dust in desert regions. Emissions from other global regions are shown as “other”.

#### 4.3.3. Seasonal variation of surface aerosol concentrations

Figure 4.27 shows the simulated seasonal cycle of sulphate, BC, POM, and dust at the key receptor regions. There are similarities between models, for example, a summer minimum of BC over the EA and SA, a dust peak in spring time over all regions and a summer maximum of POM in the Arctic in most models. However, there are substantial differences between models, in both seasonal cycle and aerosol concentrations. If we use the term “diversity” to describe the model differences, which is the ratio of standard deviation and the model mean [Textor *et al.*, 2006], then we see that over EA, SA, EU, and NA the diversity of sulphate, BC, and POM is generally 10-70% but higher for dust (40-100%). The largest diversity is seen over the Arctic which can be as high as 100-150% for all species during winter/spring, reflecting large differences in model transport and deposition processes. However, Figure 4.27 also indicates that the large diversity is often driven by a single model; for this reason, we use the model median, instead of model mean, to characterize the model results.

#### 4.3.4. Source attribution

Despite substantial differences in surface concentrations among the models, they are in much closer agreement in terms of source attribution in most cases. Over the polluted regions of EA, SA, EU, and NA, regional anthropogenic emissions are the most prominent source of sulphate, BC, and POM, except for surface POM over North America where combined biomass burning and other sources (e.g., biogenic source of the secondary organic aerosol) can contribute as much as, or even more than, anthropogenic emissions. Sulphate coming from dust regions in the GISS model is due to heterogeneous sulphate chemical production on dust surfaces [Bauer and Koch, 2005]; such reactions are not considered in the other models. Surface dust in EA, SA, and EU is mainly from deserts in Asia, Middle East, and Africa, respectively; but over NA, three of the models indicate that the African dust is the dominant source of surface dust concentration while another two attribute about half of the surface dust to long-range transport from Asian deserts.

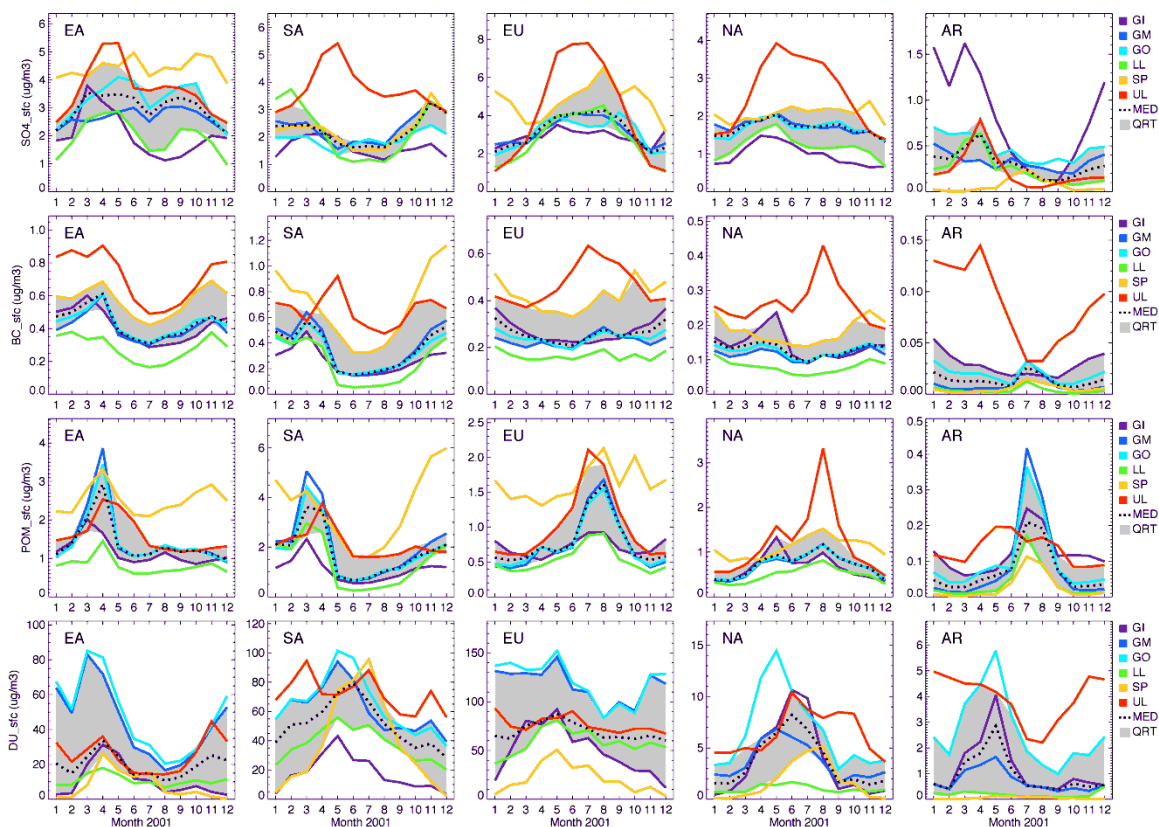


**Figure 4.27.** Seasonal variations of surface concentrations of sulphate (top row), BC (second row), POM (third row) and dust (bottom row) for the five receptor regions from six models (in colour). The model median is shown as a dotted black line and the upper and lower quartiles are bounded with the grey shading (GI: GISS-PUCCINI-modeIE, GM: GMI, GO: GOCART, LL: LLNL-IMPACT, SP: SPRINTARS, UL: ULAQ, MED: median, QRT: quartile).

The median values of the source attribution in the 5 receptor regions are listed in Table 4.6.

To summarize:

- The contribution of pollution sources to regional POM is considerably less than sulphate and BC, ranging from 29% over NA to 65% over EU. Biomass burning and biogenic sources become important for POM surface concentrations.
- For surface dust, 90% in EA, 75% in SA, and 85% in EU are from the deserts over Asia, Middle East, and Africa, respectively. In NA, the contribution from African dust is about 3 times more than that from Asia.
- Biomass burning in the NE domain (Eurasia boreal) plays a major role in determining the amount of surface BC and POM (41% and 48%, respectively). Nearly half of the dust at the Arctic surface is from Asia (47%), with 39% from Africa and 18% from the Middle East.

**FINDING (attribution aerosols):** Multi-model experiments show that, over the four HTAP source regions, the surface concentrations of sulphate and BC are mostly (60-90%) from pollution sources within the region. However, contributions from outside the source region are increasingly large at higher altitudes. Over the surface in the Arctic, European pollution is the most significant source of sulphate while Eurasian biomass burning is the major contributor to BC and POM. More than 80% of surface dust is from Asia and Africa.

**Table 4.6.** Surface concentrations in  $\mu\text{g}/\text{m}^3$  in five receptor regions based on the median values of annual averages in 2001 from six global models. Contributions from source regions are given in percent below. The range is shown in parenthesis. Blue shading denotes SR6 experiments, green SR6b, brown SR6d, and pink is the difference from a global undisturbed simulation (including natural sources and anthropogenic/ biomass burning sources outside of designated regions). Dominant source regions are highlighted in bold.

	Receptor Region				
	EA	SA	EU	NA	AR
<b>Sulphate:</b>					
Surface Conc.	2.94 (1.96-4.42)	2.24 (1.61-3.51)	3.10 (2.76-4.78)	1.69 (0.98-2.72)	0.36 (0.10-0.81)
% from EA	<b>76.3 (72.5-87.0)</b>	6.1 (1.9-9.6)	0.8 (0.0-1.6)	4.4 (0.0-5.3)	5.9 (4.3-11.8)
% from SA	1.8 (1.5-3.2)	<b>58.2 (50.3-71.9)</b>	1.3 (0.0-6.8)	0.5 (0.0-0.7)	0.7 (0.2-2.9)
% from EU	5.0 (0.3-9.8)	16.2 (12.1-22.1)	<b>78.2 (66.5-91.0)</b>	2.6 (0.8-4.6)	<b>41.0 (29.8-42.5)</b>
% from NA	0.7 (0.1-2.5)	1.1 (0.3-3.5)	2.2 (1.1-4.6)	<b>79.5 (69.0-83.9)</b>	5.2 (3.6-10.6)
% from NE	0.1 (0.0-0.5)	0.01 (0.0-0.4)	0.1 (0.0-0.2)	0.0 (0.0-0.2)	1.3 (0.0-2.1)
% from NW	0.0 (0.0-0.007)	0.0 (0.0-0.5)	0.0 (0.0-0.006)	0.1 (0.0-0.2)	0.1 (0.0-1.9)
% from SE	0.3 (0.0-0.5)	0.8 (0.0-1.2)	0.07 (0.0-0.17)	0.0 (0.0-3.4)	0.2 (0.0-2.1)
% from SW	0.0 (0.0-0.003)	0.0 (0.0-0.3)	0.0 (0.0-0.2)	0.4 (0.0-1.4)	0.04 (0.0-2.2)
% from Other	12.1 (0.0-18.9)	13.1 (6.8-19.1)	12.3 (0.0-17.1)	15.7 (10.1-19.0)	36.3 (6.0-51.7)
<b>Black Carbon, BC:</b>					
Surface Conc.	0.42 (0.28-0.71)	0.35 (0.25-0.69)	0.26 (0.17-0.49)	0.13 (0.08-0.30)	0.03 (0.008-0.101)
% from EA	<b>84.6 (81.1-95.0)</b>	4.8 (3.7-19.5)	1.0 (0.09-4.2)	2.7 (0.6-4.9)	8.8 (2.9-28.7)
% from SA	2.9 (1.7-5.8)	<b>71.3 (57.2-90.6)</b>	1.2 (0.5-11.1)	0.7 (0.09-2.8)	0.8 (0.2-11.3)
% from EU	1.0 (0.5-3.9)	4.3 (3.2-10.6)	<b>88.7 (76.7 -96.6)</b>	1.4 (0.2-6.1)	<b>34.3 (21.7-41.2)</b>
% from NA	0.2 (0.02-0.5)	0.5 (0.04-0.8)	1.1 (0.2-2.1)	<b>79.1 (54.5-98.2)</b>	4.7 (1.9-10.1)
% from NE	1.8 (0.7-2.7)	0.4 (0.07-0.6)	2.4 (1.1-5.9)	0.5 (0.2-1.1)	<b>35.1 (7.4-62.0)</b>
% from NW	0.007 (0.001-0.05)	0.02 (0.001-0.4)	0.07 (0.009-0.2)	2.7 (0.8-6.4)	1.1 (0.4-5.5)
% from SE	8.2 (3.2-9.2)	17.4 (3.4-19.3)	3.0 (1.0-6.5)	1.0 (0.07-5.1)	1.0 (0.2-8.4)
% from SW	0.02 (0.0-0.04)	0.1 (0.004-0.6)	0.1 (0.0-1.1)	9.0 (2.9-22.5)	0.2 (0.02-3.2)
% from Other	0.6 (0.0-3.3)	0.3 (0.0-4.7)	0.9 (0.0-3.4)	0.3 (0.0-3.5)	10.7 (6.7-26.4)
<b>Particulate Organic Matter, POM:</b>					
Surface Conc.	1.46 (0.81-2.52)	1.93 (1.10-3.56)	0.75 (0.53-1.64)	0.70 (0.49-1.43)	0.20 (0.06-0.23)
% from EA	<b>52.2 (47.8-77.2)</b>	2.8 (1.9-5.4)	0.4 (0.02-1.0)	0.6 (0.2-1.7)	1.9 (0.7-5.9)
% from SA	3.1 (1.6-6.8)	<b>48.6 (44.1-78.1)</b>	0.8 (0.5-5.2)	0.3 (0.05-0.6)	0.4 (0.07-3.0)
% from EU	0.4 (0.2-0.9)	1.8 (0.6-2.7)	<b>56.2 (41.9-80.6)</b>	0.3 (0.06-0.7)	7.6 (3.6-15.1)
% from NA	0.07 (0.02-0.1)	0.1 (0.03-0.5)	0.5 (0.2-0.8)	28.0 (19.1-56.6)	1.1 (0.4-2.4)
% from NE	8.1 (1.1-9.7)	0.6 (0.1-0.9)	8.1 (2.1-20.1)	0.7 (0.2-1.9)	<b>40.9 (17.9-67.5)</b>
% from NW	0.03 (0.003-0.04)	0.02 (0.002-0.5)	0.2 (0.03-0.3)	5.2 (0.8-14.7)	1.0 (0.6-11.6)
% from SE	20.9 (5.9-28.3)	26.8 (4.6-35.1)	9.2 (1.7-13.1)	1.0 (0.09-2.7)	0.8 (0.2-5.5)
% from SW	0.05 (0.004-0.25)	0.2 (0.007-0.4)	0.3 (0.0-1.3)	16.9 (3.2-45.9)	0.3 (0.02-4.4)
% from Other	12.3 (2.7-17.1)	14.9 (0.0-23.8)	22.4 (14.6-25.3)	<b>38.9 (18.5-44.8)</b>	38.2 (26.4-49.5)
<b>Dust:</b>					
Surface Conc.	17.4 (7.9-48.3)	46.6 (17.7-64.5)	87.9 (21.2-129.6)	3.7 (1.0-7.0)	1.0 (0.06-4.5)
% from AS	<b>88.9 (80.5-94.7)</b>	5.9 (2.7-15.8)	0.4 (0.0-1.4)	10.6 (4.5-37.5)	<b>43.7 (29.5-52.4)</b>
% from ME	3.9 (2.0-6.8)	<b>74.6 (66.8-89.5)</b>	14.3 (9.0-16.7)	4.7 (2.5-8.5)	17.8 (11.8-31.8)
% from AF	5.5 (1.8-13.4)	13.9 (7.8-30.7)	<b>86.6 (78.3-90.1)</b>	<b>51.6 (21.8-82.2)</b>	39.5 (31.0-46.4)
% from Other	1.3 (0.0-26.3)	0.7 (0.0-13.7)	0.5 (0.0-10.2)	22.8 (16.3-68.4)	0.4 (0.0-10.8)

#### 4.3.5 Linearity of source-receptor relationships

Linearity is another important characteristic of the S/R relationship. In most CTMs, which neglect the influence of air pollutants on climate, tracer transport shows almost linear behaviour, and any non-linearities in S/R relationships are generally caused by chemical processes. For primary aerosols (e.g., BC, primary organic carbon and mineral dust) the S/R relationship is usually linear, but for secondary aerosols (e.g., sulphate, nitrate), the S/R relationship depends on the relative abundance of aerosol precursors (e.g.,  $\text{SO}_2$  for sulphate aerosol) and the oxidants responsible for conversion to aerosol (e.g., OH). Over polluted regions where concentrations of precursor gases are usually higher



than those of oxidants, a non-linear relationship between precursor emission and aerosol formation is expected, and thus the S/R relationship is non-linear.

Analysis of the SR6 (20% reduction) and SR6z (100% reduction) experiments indicates that surface concentration changes generally respond linearly to emission changes for BC and POM, but that the sulphate response to “domestic” SO<sub>2</sub> emissions over polluted EA, EU and NA source regions is not linear. Surface sulphate concentrations are reduced by 12-14% in response to 20% domestic anthropogenic SO<sub>2</sub> emission reductions. If extrapolated linearly, a 100% emission reduction would lead to a 60-70% reduction in surface concentrations, but the SR6z results show a rather larger reduction of 80-82%. This is because sulphate is a secondary pollutant formed from SO<sub>2</sub>, and the oxidation of SO<sub>2</sub> is often limited in more polluted air by the availability of oxidants such as OH and H<sub>2</sub>O<sub>2</sub>. This “oxidant limitation” over polluted regions causes the non-linear response of sulphate concentration to SO<sub>2</sub> emission reductions [e.g., *Barth and Church, 1999; Chin et al., 1996; Chin et al., 2000; Koch et al., 1999*]. A study by Liu et al. [2008] found that this non-linear S/R relationship between SO<sub>2</sub> emissions and sulphate concentrations only occurs over the source region (due to lower concentration of oxidants, e.g., H<sub>2</sub>O<sub>2</sub>, OH, than SO<sub>2</sub> in polluted regions) but that the relationship becomes linear during trans-oceanic transport.

Non-linearities in S/R relationships as a function of emission reduction may exist for other aerosol components such as nitrate and secondary organic aerosol. Lin et al. [2008b] found that the non-linearity of the NO<sub>y</sub> family response to NO<sub>x</sub> perturbations leads to a relative increase of nitric acid (HNO<sub>3</sub>) in the source region and a decrease in nitrate aerosol in downwind regions in response to reducing emissions by 100% vs. by 25%. Thus, setting source region emissions to zero in S/R perturbation simulations may lead to underestimation of the long-range transport of nitrate aerosols which are relatively long-lived compared to HNO<sub>3</sub>. Leibensperger et al. [2010] examined changes in PM<sub>2.5</sub> caused by zeroing anthropogenic CO and NO<sub>x</sub> emissions in the U.S. and China, and found that NO<sub>x</sub> and CO emissions in the U.S. each increased surface PM in Europe and East Asia by up to 0.25 µg/m<sup>3</sup>. East Asian NO<sub>x</sub> and CO emissions had nearly as great an effect on PM abundances in Europe and up to 0.1 µg/m<sup>3</sup> in the U.S. These impacts are not due to direct transport of nitrate, which is negligibly small, but to increases in oxidants. NO<sub>x</sub> emissions in the U.S. increase tropospheric O<sub>3</sub> by 3.5%, OH by 3.8% and H<sub>2</sub>O<sub>2</sub> by 0.3% in the Northern Hemisphere. These increases promote formation of sulphate and nitrate, and were found to be largest in population centres with high domestic SO<sub>2</sub>, NO<sub>x</sub>, and ammonia emissions. These enhancements are comparable to or greater than the intercontinental effect of SO<sub>2</sub> emissions. These results underscore the multifaceted nature of the consequences of a rising hemispheric background of pollution levels in the northern hemisphere on local pollution levels.

Surface concentrations over the Arctic respond nearly linearly to any anthropogenic emission change in the HTAP source regions. Overall, they are most sensitive to the change of emissions over EU. Shutting down all anthropogenic emissions in the tagged anthropogenic source regions would reduce the surface sulphate by 55% and BC by 45%, but only reduce the POM by 10%. This is because on an annual average basis most POM in the Arctic is from boreal biomass burning sources rather than from mid-latitude anthropogenic sources, although the relative importance of these sources is highly dependent on season.

**FINDING (nonlinear S/R relationships aerosol):** Surface aerosol concentrations generally respond linearly to changing emissions from both local and upwind source regions. There is a small non-linearity in secondary aerosols such as sulphate due to “oxidant limitation”, where oxidant availability limits conversion of precursor gases to aerosol particles.

**FINDING (S/R for secondary aerosols):** An increase in regional and hemispheric background of photo-oxidant levels can change S/R relationships involving secondary aerosol components significantly and may increase domestic formation of secondary aerosol. The relative annual intercontinental responses for PM may depend as much on emissions of NO<sub>x</sub> and CO as on hemispheric transport of PM.



#### 4.3.6 Model sulphur trend evaluation

The change in SO<sub>2</sub> emissions and its impact on long-range transport of aerosols can be tested with transport models. Manktelow et al. [2007] have shown that oxidant limitation can cause different life times for sulphur from different regions, changing over time. They find that because emissions have moved southward to latitudes where in-cloud oxidation is less oxidant limited, the 12% reduction in global SO<sub>2</sub> emissions between 1985 and 2000 caused only a 3% decrease in global sulphate. Emission inventories such as the IPCC AR5 emissions [Lamarque et al., 2010] or a similar dataset based on work of David Streets in a compilation by Thomas Diehl have been used for the AeroCom hindcast simulations. These emissions have been used in three hindcast simulations performed by the GOCART, SPRINTARS and INCA models. Figure 4.28 shows the observed and simulated trend in sulphate deposition in the last three decades. It appears that the observed trend is biased towards those regions with more historic measurements because the regional availability of measurements has changed with time. Deposition seems to have declined more rapidly than simulated by the models based on the emission inventories.

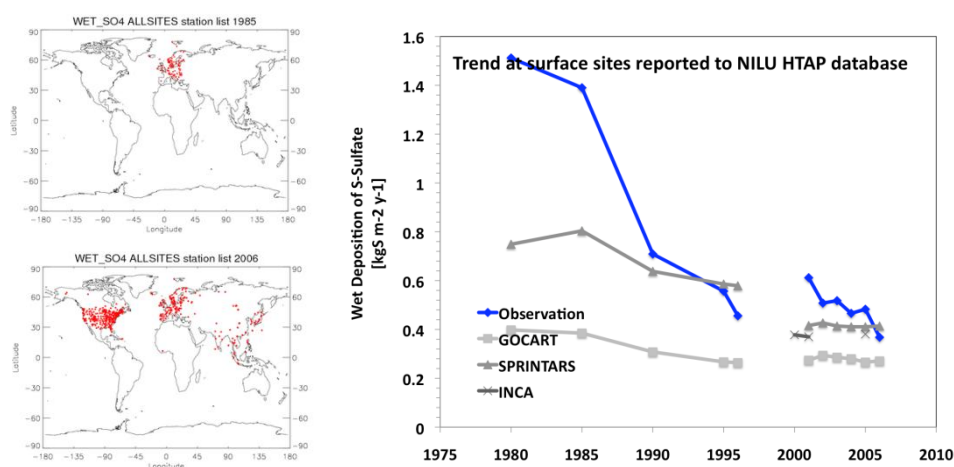


**Figure 4.28.** Sulphate wet deposition retrieved from the HTAP NILU database against three hindcast simulations. Small panels show the location of measurement sites in 1985 and 2006.

**FINDING (trends aerosols):** Current estimates show a general increase of anthropogenic emissions of aerosols and precursor gases over Asia and other developing countries, but a decrease over North America and Europe since 1980.

#### 4.3.7. Interannual variability and impacts of resolution on S/R relationships

To assess the effects of the meteorological factors on the S/R relationship, one of the HTAP models, GEM-AQ/EC, was run with fixed global anthropogenic aerosol emissions including sulphate, BC, and organic carbon over 10 years (1995-2004). The S/R relationship and its dependence on varying meteorology is quantified in Figure 4.29 by the vertically integrated import and export fluxes (Tg day<sup>-1</sup>) for a region and their standard deviation. The zonal transports across the EA, NA and SA regions exhibit an interannual variability from 22% to 26%, and the meridional transports experience larger interannual variability from 36% to 700%, although they are much weaker than the zonal transports. The variation of 700% at the northern border (65°N) of the EU region is caused by the interactions of the trough/ridge of the westerly wave and the Arctic circulation. The interannual variability in atmospheric circulations, cloud and precipitation largely reflects the influence of the El Niño–Southern Oscillation phenomenon (ENSO) [Gong et al., 2006].

**FINDING (interannual variability/resolution on PM<sub>2.5</sub>):** A limited model study shows that meteorological variability, which affects the transport routes and strength, can have a significant impact on S/R relationships. Meridional transport is smaller but more variable than circumpolar hemispheric transport. Model resolution was shown to have little impact on PM<sub>2.5</sub> export.

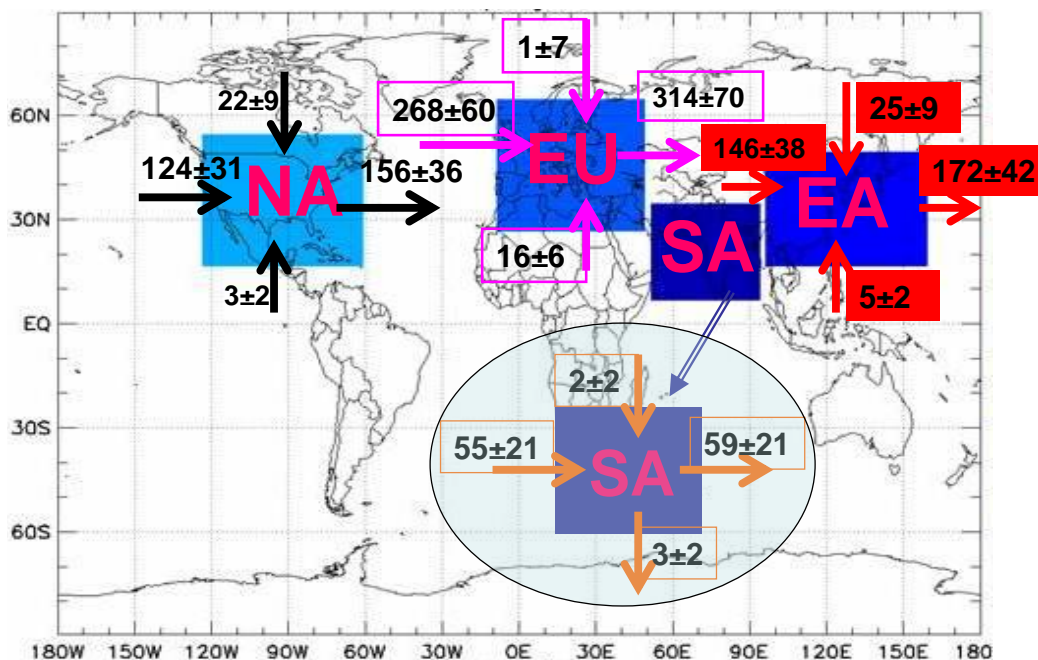


**Figure 4.29.** Averaged annual import and export fluxes ( $\text{Tg day}^{-1}$ ) from/into HTAP regions for total PM (composed of anthropogenic sulphate, BC and OC, excluding natural aerosols such as dust, wild fires and sea salt) and their standard deviations from 10 year simulations. The numbers represent the fluxes and deviations crossing each boundary of the HTAP-defined regions from surface to the model top.

#### 4.4. Hemispheric Transport Influences on deposition

##### 4.4.1. Deposition of sulphur and reactive nitrogen, $N_r$

Deposition of nitrogen and sulphur above certain levels are thought to damage some ecosystems. The concept of “critical loads” can be used to characterize the vulnerability of specific ecosystems [Bouwman *et al.*, 2002]. Determination of critical loads is complicated, particularly for nitrogen, and uncertainties are large. Reactive nitrogen consists of oxides of nitrogen and ammonia in gaseous and condensed forms (referred to here as  $N_r = \text{NO}_y + \text{NH}_x$ ) and plays a central role in the gas-phase and aerosol chemistry of the atmosphere. Wet and dry deposition of  $N_r$  contributes to both acidification and eutrophication, as it is a key nutrient of marine, freshwater and terrestrial ecosystems. Critical loads for  $N_r$  depend on the type of vegetation, and, in general, low temperatures, dry soil conditions, long frost periods and low base saturation lead to higher sensitivities. Critical loads for sulphur depend on the buffering capacity of soils [Bouwman *et al.*, 2002, and references therein]. The ensemble mean annual deposition patterns for sulphur and  $N_r$  from the HTAP intercomparison are shown in Figures 4.30 and 4.31. The largest deposition of sulphur is calculated for North America, Europe, and East Asia. The largest deposition of  $N_r$  is seen in parts of North America, Europe and East and South Asia; assuming a crude critical load of  $1000 \text{ ng m}^{-2} \text{ yr}^{-1}$  we find that this is exceeded in the eastern parts of North America, and in large parts of Europe and East and South Asia. Also shown are the changes in the pattern of deposition for 20% reductions in anthropogenic emissions in the individual HTAP source regions. The intercontinental contributions are small, and it is clear that for both sulphur and  $N_r$  regional deposition is dominated by domestic emissions. However, even such small contributions may cause impacts to particularly vulnerable ecosystems as discussed in Section 5.2.2.3.

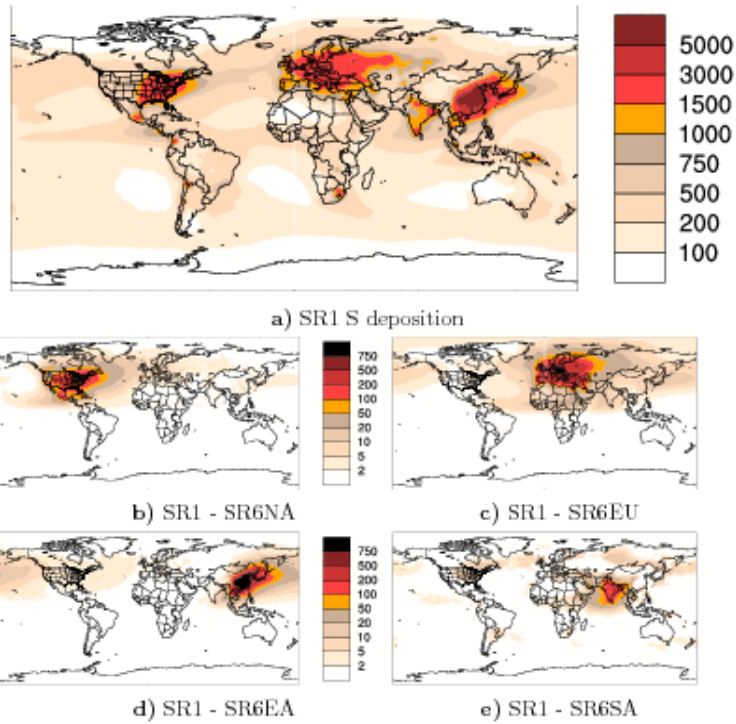


**Figure 4.30.** Total ensemble-mean deposition (wet and dry,  $\text{ng m}^{-2} \text{yr}^{-1}$ ) of oxidized sulphur (upper panels) and the effects of 20% emission reductions in the four HTAP regions (lower panels).

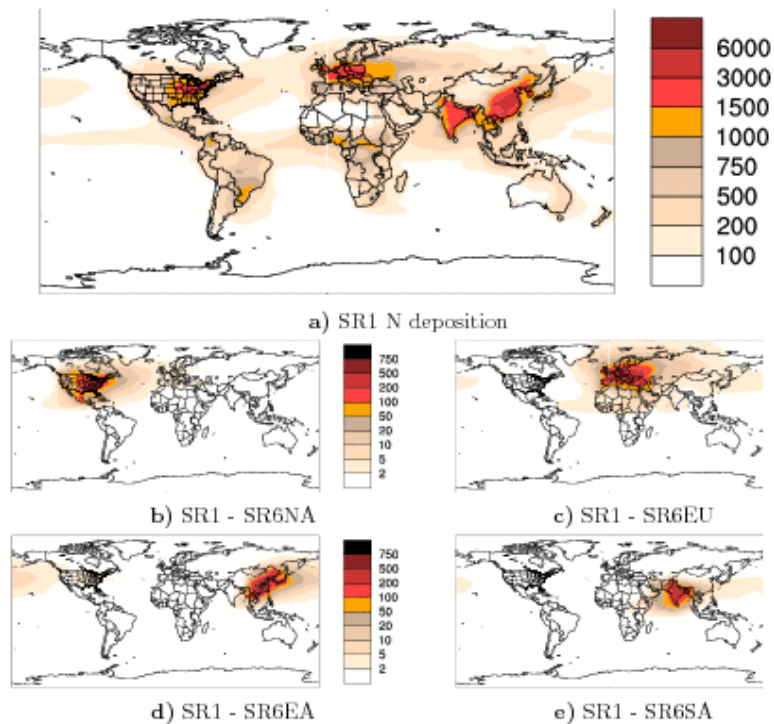


**Figure 4.31.** Total ensemble-mean deposition of  $\text{N}_r$  (wet and dry,  $\text{ng m}^{-2} \text{yr}^{-1}$ ) from the HTAP intercomparison (upper panel), and the effects of 20% emission reductions in the four HTAP regions (lower panels).

#### 4.4.2. S/R relationships

In Table 4.7 we present the influence of a 20% decrease in anthropogenic NO<sub>x</sub> emissions from each HTAP source region to the overall change in deposition in each receptor region. For the EU receptor region, 96% of the change in deposition is due to emissions changes in the EU region, while 4% of the change in deposition arises from changes in emissions over the other HTAP regions. It should be noted that in this model analysis no changes in emissions outside the HTAP regions were considered. The fractional deposition changes from transported N<sub>r</sub> shown here are small, reflecting the relatively short atmospheric lifetime of most of the constituent N species, and deposition of anthropogenic N<sub>r</sub> is clearly dominated by emissions from the same region.

**Table 4.7.** Fractional contribution to total N<sub>r</sub> deposition changes over each receptor region resulting from 20% anthropogenic NO<sub>x</sub> emission perturbations in each of the four source regions.

Source Region	Receptor Region			
	EU	NA	SA	EA
EU	<b>0.961</b>	0.009	0.076	0.033
NA	0.028	<b>0.974</b>	0.020	0.013
SA	0.005	0.003	<b>0.881</b>	0.025
EA	0.006	0.014	0.033	<b>0.929</b>

#### 4.4.3. The Arctic

Figure 4.32 shows the sensitivity of Arctic near-surface concentrations of CO, sulphate, BC and O<sub>3</sub> (from NO<sub>x</sub> perturbations) to regional source perturbations. For CO, sulphate and BC, the largest calculated contributions are from Europe in winter. For O<sub>3</sub>, the contributions from Europe, North America and East Asia are of similar magnitude in spring, summer and autumn. In winter the European contributions are negative for most models, caused by the direct reaction of NO<sub>x</sub> with O<sub>3</sub> in the relatively dark European winter months. Even though the variability between the models is very large, in particular for BC and sulphate, Shindell et al. [2008] found that the differences in sensitivities to emission perturbations in various regions are robust across most models, particularly the large Arctic sensitivity to European emissions. The ensemble annual mean accumulated deposition of BC from 13 HTAP models is shown in Figure 4.33. BC in snow is assumed to remain in the snow during the melting in spring; this makes the snow appear darker and subsequently enhances melting of the snow-pack, thus further decreasing the surface albedo. The inter-model variations in deposition of BC are large, and comparable to the variations in BC concentration shown in Figure 4.33.

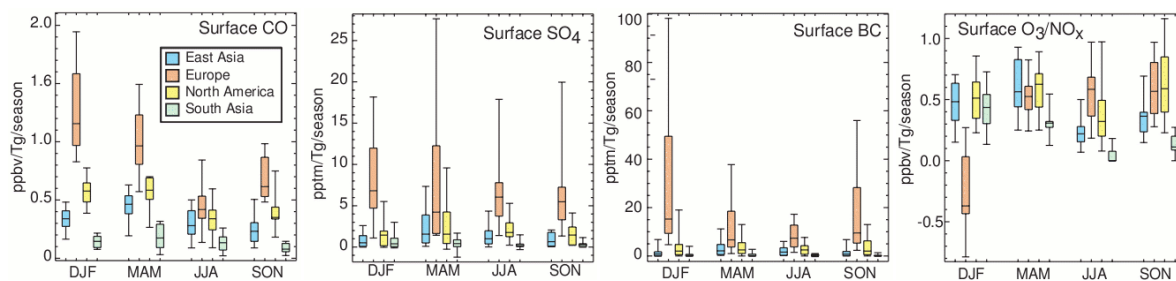


**Figure 4.32.** Sensitivity of surface CO, SO<sub>4</sub>, BC and O<sub>3</sub> over the Arctic to emissions from the principal HTAP source regions. The sensitivity is defined as the response to a 20% emission change normalized by the size of the emission change of the species (CO, BC) or its precursor (S in SO<sub>2</sub> for SO<sub>4</sub>; N in NO<sub>x</sub> for O<sub>3</sub>). Boxes show the central 50% of results, while bars show the full range of model sensitivities. [Reprinted from Figure 2 in Shindell, D. T., et al. (2008), A multimodel assessment of pollution transport to the Arctic, *Atmospheric Chemistry and Physics*, 8(17): 5353-5372.]

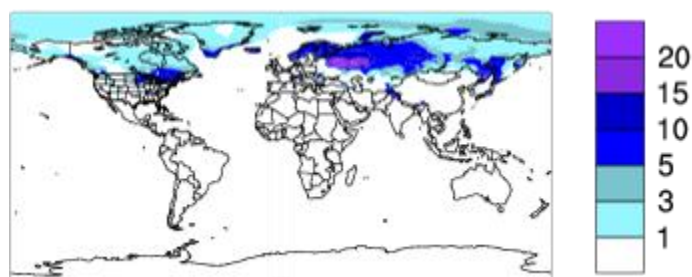


**Figure 4.33.** Accumulated deposition of BC on snow ( $\text{mg m}^{-2} \text{yr}^{-1}$ ) from an ensemble of 13 models contributing to the HTAP intercomparison.

#### 4.4.4. Attribution to source categories

There is growing interest in extending the source attribution analysis to include specific source sectors, as emission reduction measures are strongly sector-based. For example Henze et al. [2009] applied an adjoint technique to analyze the source contributions to the inorganic portion of  $\text{PM}_{2.5}$  in the continental U.S. Figure 4.34 shows the spatial distribution of the emissions contributing to surface  $\text{PM}_{2.5}$  in the U.S., while Table 4.8 shows the integrated impacts of specific source types. The largest contributions to inorganic  $\text{PM}_{2.5}$  in NA from distant sources are from sulphur sources associated with industry and shipping sectors (see ROW contributions in Table 4.8).

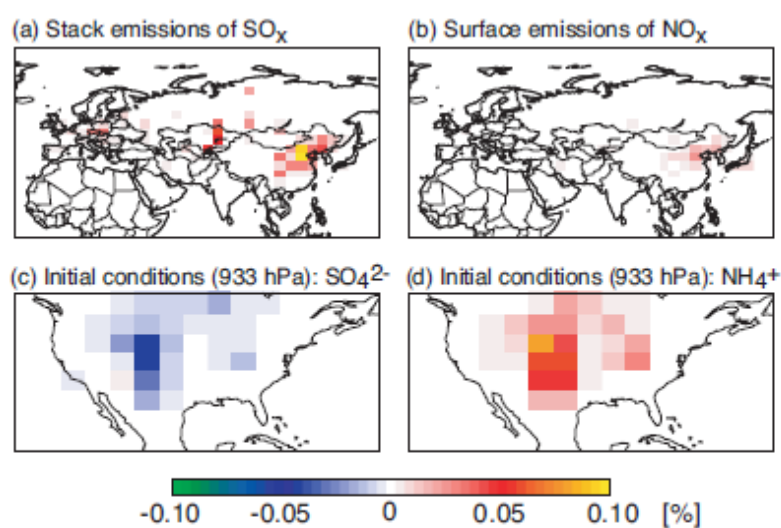


**Figure 4.34.** Normalized sensitivities of the surface  $\text{PM}_{2.5}$  concentrations in April with respect to (a) stack  $\text{SO}_x$  emissions, (b)  $\text{NO}_x$  surface emissions, (c)  $\text{SO}_4^{2-}$  initial conditions, and (d)  $\text{NH}_4^+$  initial conditions. Note the scale is from -0.1% to +0.1%. [Reprinted from Figure 4 in Henze, D. K., et al. (2009), Inverse modelling and mapping US air quality influences of inorganic  $\text{PM}_{2.5}$  precursor emissions using the adjoint of GEOS-Chem, *Atmospheric Chemistry and Physics*, 9: 5877-5903.]



**Table 4.8.** The influence of specific emissions sectors on daily average inorganic PM<sub>2.5</sub> concentrations over the U.S./N. America for the domain shown in Figure 4.34. The total integrated percent influence is presented (Total) along with a breakdown of this total into contributions from spatial regions (ROW is Rest of World. [Reprinted from Table 4 in Henze, D. K., et al. (2009), Inverse modeling and mapping US air quality influences of inorganic PM<sub>2.5</sub> precursor emissions using the adjoint of GEOS-Chem, *Atmospheric Chemistry and Physics*, 9: 5877-5903.]

Emission Sector	Total	Percent from each region			
		US	Canada	Mexico	RoW
SO <sub>x</sub> surface	11.1	57.8	8.2	23.9	10.1
SO <sub>x</sub> stack	30.1	75.1	16.7	3.4	4.7
SO <sub>x</sub> shipping	2.0	67.9	6.9	6.4	19.9
SO <sub>x</sub> biomass burning	0.2	16.2	1.1	77.3	5.4
SO <sub>x</sub> biofuel	0.03	2.9	25.4	36.1	35.6
NH <sub>3</sub> anthropogenic	19.6	90.0	6.0	2.3	1.7
NH <sub>3</sub> natural	9.2	89.4	8.4	0.1	1.3
NH <sub>3</sub> biomass burning	0.6	60.1	2.3	33.3	3.1
NH <sub>3</sub> biofuel	3.5	95.4	3.9	0.4	0.2
NO <sub>x</sub> surface	6.7	84.4	5.3	8.3	2.0
NO <sub>x</sub> stack	2.7	97.7	1.1	0.4	0.8
NO <sub>x</sub> lightning	0.1	68.3	1.1	24.3	6.2
NO <sub>x</sub> soil	0.7	65.3	4.1	28.8	1.7

The role of the transportation sector on tropospheric ozone has recently been studied by Koffi et al., [2010] using a global CTM and perturbing the aircraft, shipping and road traffic components of the transport sector emissions by 5%. The results for O<sub>3</sub> tropospheric column and surface mixing ratios are shown in Figure 4.35. The values shown are scaled to 100% by taking the 5% response and multiplying by a factor of 20. The transport sector is shown to contribute 2 to 8 ppbv O<sub>3</sub> over most of the northern hemisphere, with significant spatial variations. The percent contribution of these enhancements due to shipping, road and aircraft are also presented. The surface concentrations are dominated by road traffic over land and shipping over the seas. Road traffic dominates the column amounts in the northern hemisphere, but aircraft also make a significant contribution (30%).

**FINDING (influence on deposition):** In many regions, deposition of oxidised sulphur and nitrogen is large, and exceedance of critical loads occurs widely over many ecosystems. The intercontinental contribution to these exceedances is small except in the Arctic.

**FINDING (sector analysis):** There is growing interest in extending the source attribution analysis to include specific source sectors, as emission reduction measures are strongly sector-based. Current modelling approaches can utilize additional information in the emissions inventory to provide such estimates. The transport sector is shown to contribute 2 to 8 ppbv of O<sub>3</sub> over most of the northern hemisphere, with significant spatial variations. The surface concentrations are dominated by road traffic over land and shipping over the seas. Road traffic dominates the column amounts in the northern hemisphere, but aircraft also make a significant contribution (30%).

**RECOMMENDATION:** Adopt a multi-pollutant perspective to assess the combined impacts, including deposition, air quality, and climate. Particular attention should be paid to the effects of long range transport to the Arctic where ecosystems are likely to be more vulnerable and local sources are small. Furthermore, the analysis should be extended to include sector-based contributions.

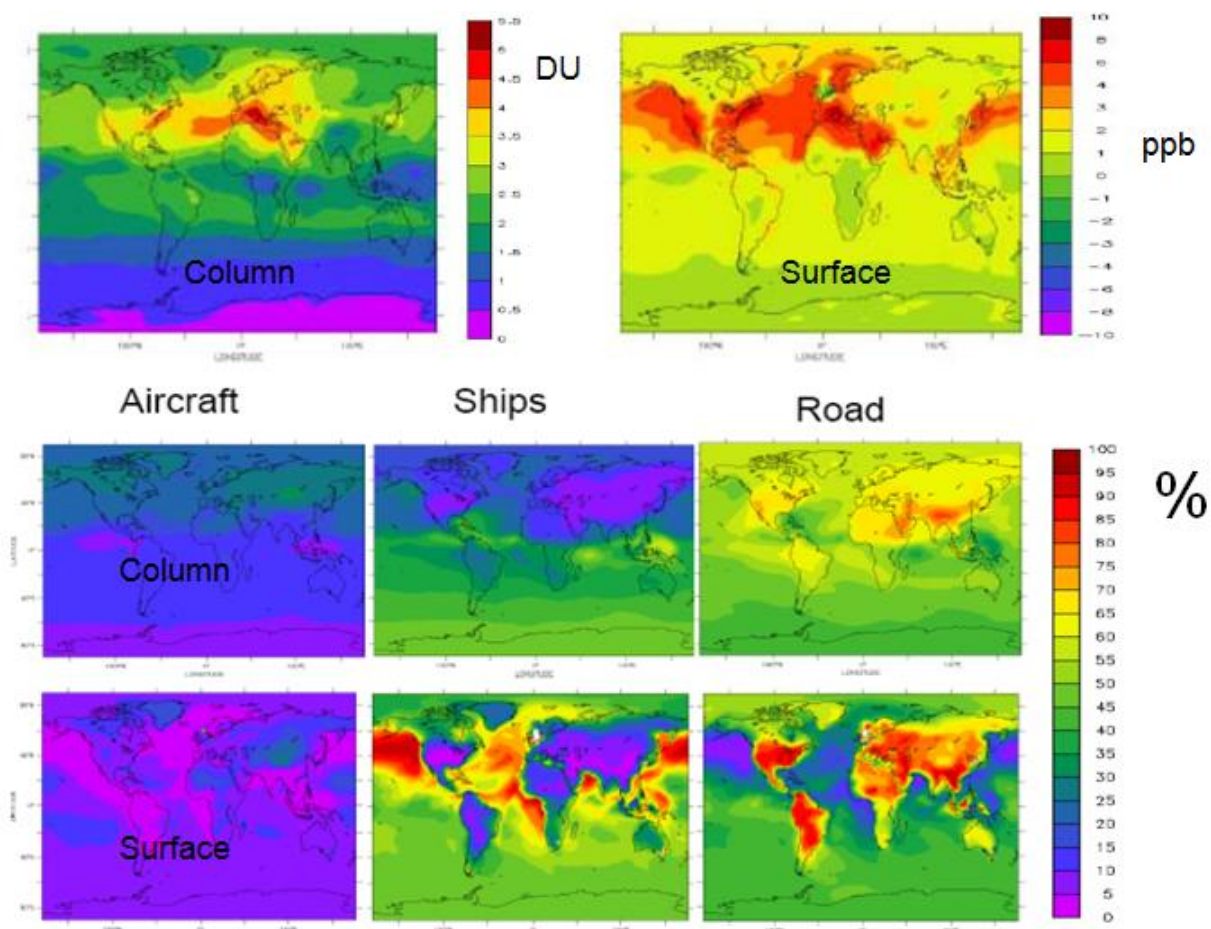


**Figure 4.35.** Attribution of aircraft, shipping and traffic sectors on column and surface ozone by Koffi et al. [Adapted from Figures 1, 2, and 3 in Koffi, B., et al. (2010), Present and future impact of aircraft, road traffic and shipping emissions on global tropospheric ozone, *Atmospheric Chemistry and Physics*, 10: 11681–11705.]

#### 4.5. Uncertainty in model estimates of intercontinental transport

The results presented in this chapter show that there can be appreciable differences in the predictions obtained with different models and between predictions and observations. Uncertainties in modelled magnitudes and distributions of O<sub>3</sub> and PM result from uncertainties in the major inputs and processes (emissions, transport, gas phase and heterogeneous chemical transformation, and wet and dry removal) represented in the models and from numerical aspects (e.g., horizontal and vertical grid resolution). Below we discuss these uncertainties in more detail.

##### 4.5.1. Uncertainty in model transport processes

Differences in intercontinental transport in models may arise from differences in the algorithms for tracer transport, particularly parameterization of boundary layer mixing processes, convection and subsidence, all of which occur at smaller physical scales than those resolved in current global models. Comparison of results between different models often also reflects differences in the source of the meteorological fields used. Studies with single models have highlighted the magnitude of differences arising from use of different meteorological fields [e.g., Wu *et al.*, 2007]. Other studies have focused on the importance of the parameterization of particular processes (e.g., boundary layer mixing [Lin and McElroy, 2010], deep convection [Tost *et al.*, 2010], and horizontal transport [Prather *et al.*, 2008]). In addition, Auvray *et al.* [2007] find differences in the sign of net chemical tendencies (i.e., photochemical production and loss rates) in the middle troposphere in the North Atlantic and North Pacific, which they attribute to differences in model transport schemes and water vapour transport as well as lightning. To date the contribution of uncertainties in these process



treatments to differences in long range transport have not been adequately assessed. An experiment within the HTAP intercomparison was designed to help quantify these uncertainties by focusing on standardised tracer process studies using a range of CO- and VOC-like tracers with specified emissions and specified atmospheric lifetimes. The use of identical emissions and globally-uniform decay rates allows differences in model results to be attributed to differences in the driving meteorology and in the parameterization of transport processes.

Results from this HTAP experiment are illustrated in Figure 4.36, which shows the ratio of the abundance of the artificial CO tracer from North American sources in the lowest 3 km to the abundance in the lowest 500 m over the source region. This provides an indication of the efficiency of mixing in different models, with a ratio of one indicating well-mixed conditions and ratios below unity representing greater concentrations of CO close to the surface. The seasonal variation is very similar in the models, with greater mixing in the summer that reflect greater boundary layer depths and increased convective activity. However, significant differences exist between the models, with annual mean ratios varying between 0.51 and 0.73 over this region, reflecting large differences in the timescales for transport of pollutants away from surface sources. The figure also shows the ratio for CO from South Asian sources over North America, reflecting the efficiency of mixing pollutants from distant sources down to the surface. While all models show relatively well-mixed conditions in summer, there are large differences at other times of year, particularly in spring when the magnitude of South Asian influence is largest. The factor of two differences in spring highlights the uncertainty in simulating vertical mixing and the processes dictating subsidence from the free troposphere to the surface. These differences reflect the uncertainties in sub-grid scale parameterized processes, particularly deep convection, atmospheric boundary layer mixing, atmospheric boundary layer venting, and wet deposition [Lawrence and Rasch, 2005; Murazaki and Hess, 2006], which are not particularly well represented in current global models.

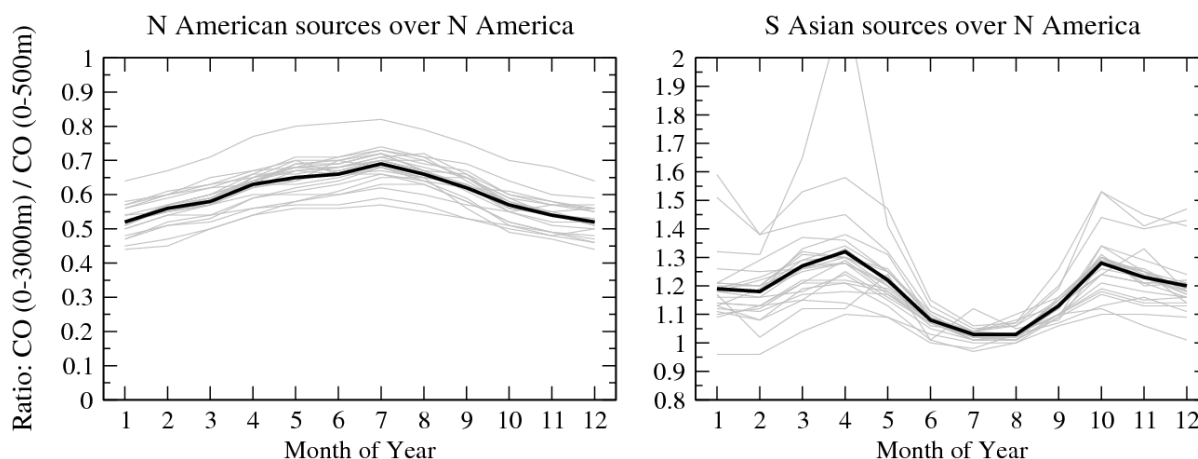


**Figure 4.36.** Ratio of CO abundance in the lowest 3 km of the atmosphere to the abundance in the lowest 500 m for North American sources over North America (left), and for South Asian sources over North America (right). Models with ratios closer to unity have more vigorous boundary layer mixing and venting. Results are from the constrained tracer process (TP) studies in the HTAP intercomparison.

An important fraction of continental pollutant export occurs in distinct episodes associated with particular meteorological conditions, e.g., low-level outflow associated with frontal systems or lifting associated with convection or warm conveyor belts. Pollutant outflow under these conditions often occurs in discrete plumes close to, or below, the scales resolved in regional and global models, and thus representing plume movement, dispersion and chemical evolution is particularly challenging. As discussed in Chapter 2 there is a large amount of information on long range pollution transport provided through measurement campaigns. Measurement campaigns provide clear evidence of plume outflow in well-defined structures that maintain their identity for a week or more (see Chapter 2). However, coarse resolution Eulerian models typically lose the signature of outflow plumes too quickly due to numerical diffusion, thus diminish the impacts of vigorous episodic transport events [Fang *et al.*, 2009; Heald *et al.*, 2003; Pfister *et al.*, 2006; Wild *et al.*, 2004b]. Rastigejev *et al.*, [2010]

showed that numerical methods currently used are unable to preserve plume features and that to do so would require a significant increase in grid resolution. Novel methods such as adaptive grids or embedded Lagrangian plumes are also needed. Important questions remain about the sensitivity of pollution transport and chemical evolution to model resolution [Chen *et al.*, 2009a; Lin *et al.*, 2008c; Lin *et al.*, 2009; Lin *et al.*, 2010b; Liu *et al.*, 2010], and how estimated S/R relationships vary within a region [e.g., Lin *et al.*, 2008b; Lin *et al.*, 2010b; Reidmiller *et al.*, 2009]. These topics are discussed in the following sections.

#### 4.5.2. The influence of model resolution

##### **Impact of resolution on export**

Currently it is too computationally expensive to run high-resolution models at the global scale. Instead, higher resolution over areas of interest is achieved by running regional scale models coupled to lower-resolution global models. For example, a recent study compared two high-resolution regional scale atmospheric chemistry models (WRF-Chem and CMAQ;  $0.3 \times 0.3^\circ$ ) with a global scale model (MOZART,  $1.9 \times 1.9^\circ$ ) [Lin *et al.*, 2010b]. Figure 4.37 illustrates a case study of pollution venting during a vigorous cold surge event over East Asia. The high-resolution WRF-Chem model predicts strong CO updrafts and deep convection extending into the upper troposphere over a region between  $100\text{--}110^\circ\text{E}$  longitudes, coinciding with the leading edge of the convergence zone. The outflow of CO (and other pollutants including ethane,  $\text{O}_3$ , and PAN) to the upper troposphere and the layered structure simulated in the high-resolution model is consistent with aircraft observations of pollution lofting during the TRACE-P campaign. The global MOZART model largely confined the pollution plume below 4 km, as did the global GEOS-Chem model [Liu *et al.*, 2003]. Vertical profiles of CO at three stations along the East Asian coast show that neither of the global models captured the strong upper-troposphere outflow observed by the aircraft and simulated in the high-resolution models during this frontal event. Differences in the eastward export flux of CO are shown in Figure 4.38 and are about 30% lower for MOZART than for WRF-Chem.

Other studies have shown a similar resolution-dependence for the key processes controlling large-scale continental export, including the localization of intense advection and convection [Chen *et al.*, 2009a] and the influence of orographic forcing over complex terrains [Chen *et al.*, 2009b; Henne *et al.*, 2004; Henne *et al.*, 2005]. Inadequate treatment of these transport processes can lead to insufficient lofting of pollution to higher altitudes. Surface pollutants that are lofted to higher altitudes undergo more efficient transport in stronger winds, and the mixing of these plumes into the surrounding tropospheric air can lead to increased levels of background  $\text{O}_3$  over downwind continents [Fiore *et al.*, 2002].

Model resolution also impacts chemical and removal processes. For example, export of  $\text{O}_3$  from the planetary boundary layer (PBL) has been explored over eastern China during 2008 with the CMAQ modelling system at 36- and 12-km horizontal grid resolution [Liu *et al.*, 2010; Zhang, 2010]. Monthly-mean export of  $\text{O}_3$  ranges from  $-0.23$  to  $1.17$  Gmole/day at 36-km resolution to  $-0.35$  to  $1.03$  Gmole/day at 12-km resolution, and the annual mean export flux is about 25% lower at 12-km resolution,  $0.34$  compared with  $0.47$  Gmole/day. The major processes governing  $\text{O}_3$  (advection, deposition, and chemistry) make similar contributions to the regional  $\text{O}_3$  budget, but there are substantial differences at particular locations at the two horizontal grid resolutions. For example, in the PBL over Beijing gas-phase chemistry and vertical transport contribute to the production and accumulation of  $\text{O}_3$  on most days at 36-km resolution and horizontal transport carries this  $\text{O}_3$  away. At 12-km resolution, gas-phase chemistry is a major sink for  $\text{O}_3$  through titration by high levels of emitted  $\text{NO}_x$  that are not reproduced at coarser resolution, and transport processes thus bring  $\text{O}_3$  into the PBL at this location. These differences over polluted regions account for the overestimate of  $\text{O}_3$  export at coarser grid resolutions and highlight the importance of resolving key emission regions. In contrast, the processes controlling the  $\text{O}_3$  budget in the free troposphere are very similar at the two resolutions.

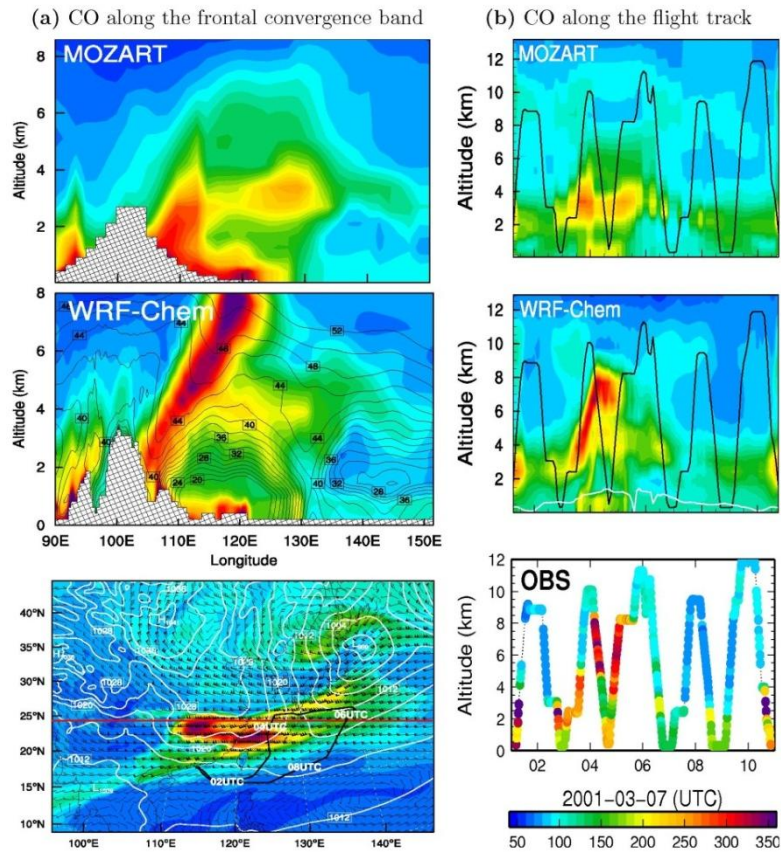


**Figure 4.37.** Comparison of CO vertical distributions in the high-resolution (WRF-Chem) and global-scale (MOZART) models with aircraft observations of a pollution lofting event over East Asia. (a) CO vertical cross-section along the frontal convergence band near 25°N (the red line in the lower left panel). The lower left plot shows the simulated CO mixing ratios (colours) and horizontal flux (vectors) at the 5 km level superimposed with sea level pressure (white contours) of CO along the flight track of NASA DC-8 during the TRACE-P campaign. [Adapted from Figures 3, 4, and 5 in Lin, M., et al. (2010), Quantifying pollution inflow and outflow over East Asia in spring with regional and global models, *Atmospheric Chemistry and Physics*, 10(9): 4221-4239.]

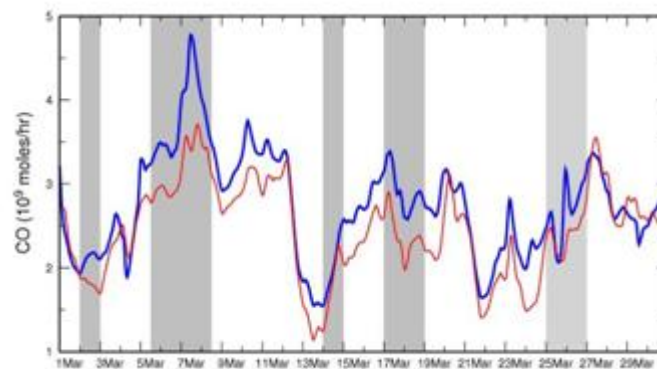


**Figure 4.38.** Calculated eastward flux of CO through a wall at 25-40°N along 140°E at altitudes between 4-8.5 km calculated with WRF-Chem (blue) and MOZART (red) models. [Reprinted from Figure 2 in Lin, M., et al. (2010b), Quantifying pollution inflow and outflow over East Asia in spring with regional and global models, *Atmospheric Chemistry and Physics*, 10(9): 4221-4239.]

### Effect of model resolution on import of ozone

Model resolution determines the ability to resolve local features that influence import processes and chemical transformation. In particular, topography affects the mixing of free tropospheric pollutants into the atmospheric boundary layer, and sharp gradients in the chemical environment (especially in urban regions) affect the strength of surface  $O_3$  responses to emission changes. Sensitivity studies perturbing chemical boundary conditions in regional models enable a critical assessment of global model estimates of S/R relationships described in Section 4.2.5 [Lin *et al.*, 2010b]. The impact of model resolution on the calculated  $O_3$  response over the East Asian domain due to a 20% perturbation in European emissions is shown in Figure 4.39. Both global and regional models show large spatial variability in the response of  $O_3$  to changes in EU emissions, with the global model showing higher peak values and a larger area of impact.

Model resolution also affects the response of pollutants at specific receptors of interest, e.g., megacities. This is illustrated by looking at the response of surface  $O_3$  in grid cells representing major metropolitan areas. The responses differ from the region-wide average depending on season (Figure 4.40); the domain wide responses for NA and EA are shown, along with responses for grid cells containing individual cities. In an analysis of March 2001, Lin *et al.* [2010a] also found that  $O_3$  in megacities in Asia cities such as Seoul and Tokyo showed the smallest response to 20% enhancements in European emissions due to titration by the elevated  $NO_x$  levels. These results indicate that model resolution is an important source of uncertainty in the analysis of human health impacts in urban areas (section 5.1.2), as urban areas are not adequately resolved in global models. Studies to quantify the impacts of emissions at fine spatial scales such as mega-cities [Lawrence *et al.*, 2006] are few, but are increasingly important given the rapid projected growth of world cities. Because aerosol chemistry is more linear than that for  $O_3$ , this limitation in calculating intercontinental contributions to urban PM is less of a problem.

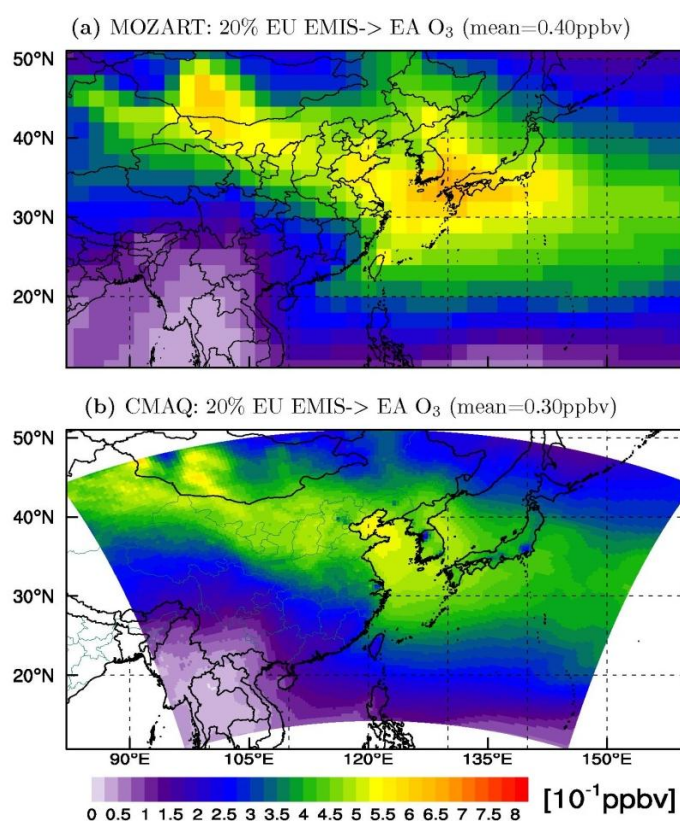


**Figure 4.39.** Impacts of model resolution on the calculated  $O_3$  response over East Asia in March 2001 to a 20% reduction in anthropogenic emissions of  $O_3$  precursors in Europe. The global model (MOZART) has a horizontal resolution of  $2^\circ \times 2^\circ$  compared to the regional model (CMAQ) resolution of  $\sim 0.3^\circ \times 0.3^\circ$  [Reprinted from Figure 7 in Lin, M., *et al.* (2010b), Quantifying pollution inflow and outflow over East Asia in spring with regional and global models, *Atmospheric Chemistry and Physics*, 10(9): 4221-4239.]

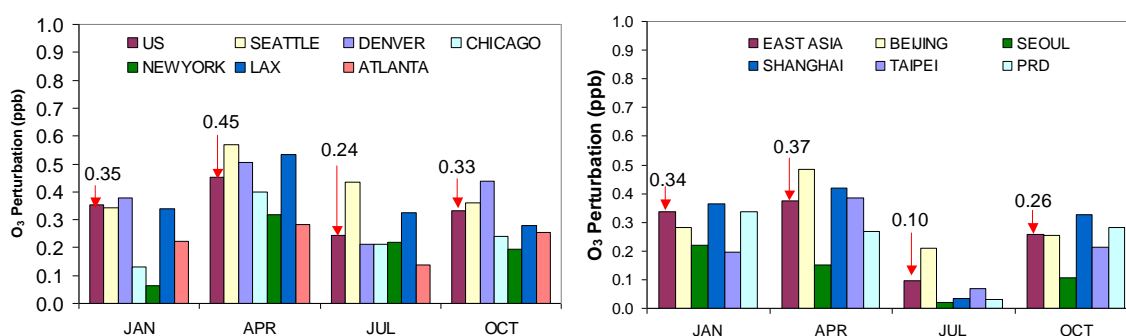


**Figure 4.40.** Seasonal variations in the effect of 20% emission changes in E. Asia on monthly mean surface O<sub>3</sub> in major cities in the U.S. (left) and the effect of N. America emission changes on cities in East Asia (right) from studies with the CMAQ model at 36-km resolution.

**FINDING (processes ozone):** Regional model studies suggest that sub-grid-scale processes (convection, frontal lifting, heterogeneous PBL mixing, etc.) have a major effect on pollution export.

**RECOMMENDATION (resolution):** Support the application of high-resolution global and regional models to investigate the effect of smaller-scale processes on continental import and export budgets.

**RECOMMENDATION (evaluation):** Develop new standardised approaches for model evaluation against observations to focus on improving representation of poorly-characterized processes in models (e.g., vertical transport, PBL mixing, wet and dry deposition, aerosol and cloud processes).

#### 4.5.3 Uncertainty in model chemical mechanisms and natural emissions

The parameterization of key processes is also a source of uncertainty. For example, the chemical mechanisms used in models play a critical role in determining how O<sub>3</sub> changes due to perturbations in emissions. The nonlinearities in the response of O<sub>3</sub> to NO<sub>x</sub> emissions have been discussed earlier. It is important to recognize the significant uncertainties in modelled chemical schemes including the treatment of N<sub>2</sub>O<sub>5</sub> hydrolysis, PAN formation and loss, the chemistry of isoprene nitrates, HO<sub>x</sub> and NO<sub>x</sub> recycling, and NO<sub>3</sub> nighttime chemistry [e.g., *Emmerson and Evans, 2009; Hofzumahaus et al., 2009; Paulot et al., 2009*]. In particular, PAN decomposition enhances O<sub>3</sub> far from source regions, as observed in subsiding Asian and North American plumes [*Fischer et al., 2009; Heald et al., 2003; Hudman et al., 2004; Moxim et al., 1996; Real et al., 2007; Zhang et al., 2008a*]. PAN formation differs by up to a factor of 2-5 across global and regional models [e.g., *Adhikary et al., 2009; Lin et al., 2009; Lin et al., 2010b*]. Using sensitivity studies altering NO<sub>y</sub> boundary conditions in a regional model, Lin et al. [2010b] estimated that the O<sub>3</sub> enhancement over East Asia driven by PAN decomposition contributes 20% of the spatially averaged total O<sub>3</sub> response to European emissions perturbations in March, and occasionally contributes as much as 50% of the total O<sub>3</sub> response in subsiding plumes at mountain observatories (at about 2 km altitude). They also found that the calculated response to decomposing PAN is strongly affected by the O<sub>3</sub> formation regimes, which vary with the model chemical mechanisms and NO<sub>x</sub>/VOC emissions. Because of the non-linear nature of photochemical oxidation, results from emission perturbation studies need to be interpreted carefully.

These nonlinearities and uncertainties in chemical processes are exacerbated by the uncertainties in “natural” emissions (biogenic NMVOC, biogenic NO<sub>x</sub> and lightning NO<sub>x</sub> in particular). For example, if models underestimate the lightning NO<sub>x</sub> source, they will tend to overestimate background ozone production and the fractional contribution of PAN to NO<sub>x</sub> export. Therefore, a model underestimate of lightning NO<sub>x</sub> may lead to an overestimate of the downwind O<sub>3</sub> production due to anthropogenic NO<sub>x</sub> export [*Fang et al., 2010*].



**FINDING (urban/rural differences in ozone S/R):** Many urban areas have strong gradients in emissions and topography, and this can lead to imported O<sub>3</sub> and precursors having qualitatively different impacts on urban areas and their surroundings due to the strong dependency of O<sub>3</sub> chemistry on the ratio of NO<sub>x</sub> to VOCs. The modelled relative annual intercontinental response over large cities is very sensitive to model resolution.

**RECOMMENDATION (scale):** Efforts are required to address scale biases, particularly when quantifying exceedance of threshold values used for assessing agricultural and health impacts. There is a need to develop tools to bridge scales, e.g., resolving the effects of urban regions in regional and global models.

**RECOMMENDATION (chemistry):** There is a need for additional laboratory studies of chemical processes and for further evaluation of chemical schemes against field observations using box models to allow more critical testing of key reaction uncertainties in current models. Key areas of uncertainty include heterogeneous reactions, night time chemistry, chemistry of biogenic hydrocarbons, PAN decomposition and recycling of HO<sub>x</sub> and NO<sub>x</sub>.

#### *4.5.4. Summary of principal sources of model uncertainty and research needs*

A summary of various uncertainties associated with the calculation of S/R relationships and source attribution (S/A) discussed in this chapter are presented in Figure 4.41. Shown are qualitative estimates of the uncertainty in our understanding of specific components/aspects of the model (e.g., gas phase chemistry, continental outflow, emissions) and the likelihood that this uncertainty impacts the final estimates of S/R and source attribution. Differences between the estimates of O<sub>3</sub> and PM are also noted. The top right quadrant of the figure indicates those aspects that are important, but are better quantified because we have less uncertainty in the underlying quantities. The top-left quadrant indicates major elements contributing to the uncertainty in current model estimates of S/R and S/A. In general, the estimates of S/R relationships at continental scales are more robust than estimates of S/A in an absolute sense, but they are very similar in a relative ranking of the sources of uncertainty. Therefore, the uncertainties for S/R and S/A are shown in the same figure. Uncertainties in emissions are particularly important in source attribution studies, as absolute amounts of the pollutant are estimated. Biomass burning (O<sub>3</sub> precursors and particles), natural (including dust, sea salt, biogenic hydrocarbons and lightning NO<sub>x</sub>) and primary aerosol emissions from anthropogenic sources have large uncertainty and these have a very important impact on the source attribution. Included in this figure are estimates associated with key model processes related to chemistry and removal. Gas phase chemistry plays a critical role in O<sub>3</sub> and secondary PM. While important gaps remain in our knowledge of gas phase chemistry remain, it is better understood than heterogeneous chemistry processes, which play an important role in the prediction of secondary PM and the aging of BC. The uncertainty in removal processes plays a significant role in the large differences in the estimated lifetime of aerosols in global models. Also shown are uncertainties associated with large scale export and import. Continental outflow includes vertical mixing, convection, and frontal systems, while inflow includes large scale subsidence and the interaction of aged air masses with fresh local emissions. The large uncertainty in the inflow reflects, in part, the fact that fewer studies have focused on this aspect of long range transport. The interannual variability and the impacts of climate change in S/R and S/A are uncertain for a similar reason. The estimates get more uncertain as the receptor size and time interval of averaging decreases. Resolving S/R and S/A at sub-continental scales increases the requirements on the meteorological inputs and model resolution.

Reducing the uncertainty in model-based S/R relationships and S/A requires improving the models and their inputs. The upper left quadrant of Figure 4.41 gives guidance into where research is needed to improve (reduce uncertainty) estimates of intercontinental transport of pollutants. These include improvements in emission estimates, better understanding of key processes such as wet removal, better quantification of interannual variability, climate change impacts and continental inflow, and improvements in model resolution. Research needs aimed at improving our understanding of key processes and improving emission estimates have been discussed in Chapters 2 and 3.

## Intercontinental Source Attribution (SA) and Source-Receptor (S/R) relationships

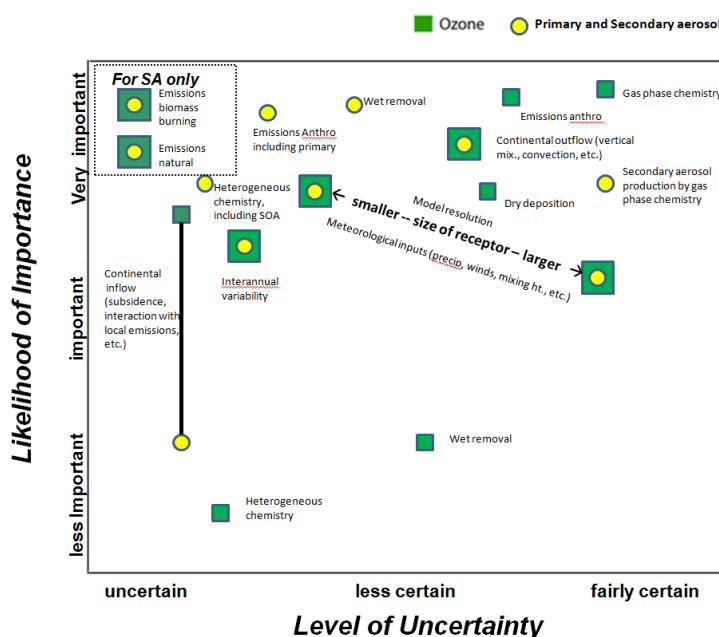


**Figure 4.41.** Uncertainties associated with modelling intercontinental transport and its impacts on source/receptor relationships and source attribution as summarised in this chapter.

From a model development perspective there is a clear need to increase model resolution, through dynamic downscaling using regional CTMs, or through much higher resolution global CTMs, both to advance our understanding of atmospheric processes and to inform decision-making on air quality management. Due to the compensating effects on surface  $O_3$  responses over downwind continents, future high-resolution hemispheric model analysis should provide further insights into how the export and import processes interact, and will help to narrow the uncertainty of intercontinental S/R relationships. Treatment of boundary inflow can be problematic in coordinating global and regional models, and additional research is needed on larger scale regional simulations (e.g. trans-Pacific; trans-Atlantic), higher resolution global simulations [e.g. *Adhikary et al.*, 2009; *Lin et al.*, 2010b], evaluating the role of physical parameterizations versus resolution, and developing two-way nesting approaches. In light of the strengths and limitations of each modelling framework, there is also a need for further analysis of regional processes affecting global transport and further development of models to improve skill in key processes (in particular orographic forcing, intense plume rise, deep convection and associated cloud and chemical processing). Additional analysis in areas with more extensive measurements of atmospheric constituents in the boundary layer and in the free troposphere would also increase our understanding of hemispheric transport affecting surface air quality. Further analysis of some of these key processes is currently being addressed in the Atmospheric Chemistry and Climate (AC&C) project. This model intercomparison activity builds upon the HTAP studies and includes many of the same researchers and models. Specific studies are designed to address the large uncertainties in modelled distributions of trace species in the upper troposphere, including those associated with convection and scavenging processes.

Reducing many of the key uncertainties requires a closer integration between the modelling, emissions and observing elements identified in this Chapter and in Chapters 2 and 3 and 4. As discussed in the NRC report [2010], enhancing our capabilities requires a strategy that improves the individual components needed to perform S/A and more closely integrates these components. A key modelling-specific research element of this strategy is the need for closer integration of satellite observations with the emissions and modelling components through data assimilation and inverse modelling to obtain better emission estimates in terms of spatial distribution and absolute magnitude. This was introduced earlier in Chapter 3, section 5. Models provide a powerful tool to interpret satellite observations, especially when analyzed in concert with in situ measurements, to achieve a process-level understanding. In this regard, a limitation of the model simulations used in this report to



assess long-range transport is that they have not been fully evaluated with all the various satellite observations. Comparison of model simulations with different types of observational geometries provides valuable information on the advection pathways, the frequency of the transport events, and the altitude of the transported plumes. A combined analysis would, for example, clearly help to better evaluate diffusion issues in the models. Future assessments should address this deficiency.

Additional development and application of computationally efficient data assimilation algorithms are essential for integrating multiple observations in a common model background. Research into the closer integration of observations and models has increased over the last few years [Carmichael *et al.*, 2008]. A growing number of models are engaged in advanced chemical data assimilation (e.g., 4dVar, ensemble Kalman Filter) and some are moving towards operational status (e.g., the European Union Global and regional Earth-system (Atmosphere) Monitoring using Satellite and in-situ data (GEMS and MACC projects <http://gems.ecmwf.int/>). Adjoint and other inverse methods are valuable for quantifying model sensitivities to multiple parameters, such as to long-range transport dynamics or emission sources. Further efforts are needed to evaluate and refine the impact of these assimilation approaches on source attribution applications. These approaches also need to be engaged in the design of new observing systems, including the information content associated with specific parameters and sampling location, and including new satellite platforms such as geostationary satellites. To accomplish these goals the model and emission inventory components need to be refined and aligned with the observational strategies.

**FINDING (processes): The HTAP intercomparison and related studies have highlighted the areas of greatest uncertainty in global air pollution modelling: deposition and scavenging, vertical transport/mixing, hydrocarbon oxidation chemistry and secondary organic aerosol and new particle formation. There are also uncertainties associated with model resolution, in particular vertical transport processes and the ability to resolve plumes and layered structures.**

**FINDING (research): Assessing the suitability of current CTMs for simulating hemispheric transport is limited by the fact that the S/R relationships and source attributions of interest are model constructs, and currently there are no simple means of evaluation though proxies available in long-term trends, and daily, seasonal and interannual variability.**

**FINDING (research): A limitation of the model simulations used to assess long-range transport is that they have not been fully evaluated with observations from all available measurement platforms, including satellite.**

**FINDING (research): Improving our capability to quantify the contributions from specific source regions and sectors over the geographic regions of concern requires a strategy that: 1) improves the individual components needed to perform source attributions; and 2) more closely integrates these components.**

**FINDING (research): Adjoint models and data assimilation techniques are valuable for quantifying model sensitivities to multiple parameters, such as to long-range transport dynamics or emission sources, and complement emission perturbation experiments within forward model simulations. Further efforts are needed to evaluate and refine the impact of these assimilation approaches on source attribution applications.**

**RECOMMENDATION (research): Support further process-oriented studies aimed at improving CTMs, e.g., the Atmospheric Chemistry and Climate (AC&C) project. This model intercomparison activity builds upon the HTAP studies and focuses on addressing the large uncertainties in modelled distributions of trace species by targeting treatment of key processes (e.g., convection) in the light of available observational data.**

**RECOMMENDATION (research): In light of the strengths and limitations of each modelling framework, there is a need for further analysis of regional processes affecting global transport. Additional analysis is needed in areas with more extensive measurements of atmospheric constituents in the boundary layer and in the free troposphere.**

**RECOMMENDATION (approaches):** Apply newly-available modelling tools (e.g., multiple-nested models from global to urban scales, assimilation and bias-correction approaches) along with remote-sensing data to improve assessment and representation of intercontinental transport processes.

**RECOMMENDATION (research):** Future assessments should include a comprehensive comparison with satellite observations. Comparison of model simulations with different types of observational geometries (e.g., nadir-integrated information along with good horizontal resolution, limb-viewing sampling of the UTLS with improved vertical resolution and active lidar measurements) would provide valuable information on advection pathways, the frequency of transport events, and the altitude of transported plumes. A combined analysis would clearly help to better evaluate diffusion issues in the models, for example.

**RECOMMENDATION (research):** An integrated science source attribution program should be established in order to assess the contribution of distant sources to air quality and to evaluate the effectiveness of national control strategies to meet environmental targets. A key component of this program should be focused on increased efforts to facilitate a closer integration of in situ observations, satellite, and models. This activity will reduce uncertainties in CTMs as a result of more critical evaluation of the predictions, better calibration/evaluation of observation-based and model-based source attributions, and improved measurement strategies. This effort will also lead to better emission estimates in terms of spatial distribution and absolute magnitude, and thus reduce key uncertainties in present estimates of S/R and S/A.

## 4.6. Future changes in S/R relationships

### 4.6.1. Changes with future emissions

#### *Changes in ozone*

Future changes in tropospheric O<sub>3</sub> have been explored under a variety of possible emission scenarios [Dentener *et al.*, 2006; Gauss *et al.*, 2003; Prather *et al.*, 2003; Stevenson *et al.*, 2006]. Multi-model studies using SRES emission scenarios show near-surface O<sub>3</sub> increases of 2-7 ppbv in the northern hemisphere between 2000 and 2030, with increases exceeding 20 ppbv by 2100 in the most extreme SRES-A2 scenario [Prather *et al.*, 2003]. Recent studies suggest changes in global surface O<sub>3</sub> by 2030 of 4.3±2.2 ppbv under this scenario, but indicate smaller changes of 1.5±1.2 ppbv if current air quality legislation is implemented immediately, and even reductions in surface O<sub>3</sub> of 2.3±1.1 ppbv by 2030 if all currently feasible emission reduction technologies are applied [Dentener *et al.*, 2006]. Six of these models examined O<sub>3</sub> changes out to 2050 under the ‘current legislation’ scenario, finding surface O<sub>3</sub> reductions of about 5 ppbv across northern hemisphere mid-latitudes [Royal Society, 2008b]. However, there were also notable seasonal changes, with increases in polluted regions in wintertime partly offsetting the summertime reductions.

Changes in the global distribution of trace gas emissions following economic development are likely to lead to changes in the relative importance of intercontinental transport from different source regions. Valuable insight into the resulting O<sub>3</sub> responses can be gained by linearising the results of the original HTAP intercomparison studies. The full set of 18 SR runs provide O<sub>3</sub> changes following emission changes for each precursor (NO<sub>x</sub>, CO, VOCs) over each source region, and also the effect of CH<sub>4</sub> concentration changes. With additional simulations employing 20% global emission reductions, all anthropogenic global sources of O<sub>3</sub> precursors are covered. Any future global emission scenarios can then be decomposed into a linear combination of regional precursor emission perturbations. While emissions changes are relatively small, the surface O<sub>3</sub> responses are close to linear [Fiore *et al.*, 2009; Wu *et al.*, 2009]. To quantify these changes, we consider emissions between 2000 and 2050 following the Representative Concentration Pathways (RCP) constructed for IPCC-AR5. The resulting O<sub>3</sub> changes for each region are shown in Figure 4.42 for each of the four emission pathways as an ensemble mean for the six models that simulated responses for global emission reductions. These scenarios suggest changes in surface O<sub>3</sub> by 2030 over North America and Europe ranging from changes of about 1 ppbv in the ‘business-as-usual’ RCP 8.5 scenario to reductions of about 5 ppbv in the ‘cleaner’ RCP 2.6 scenario. South Asia sees the greatest increases, ranging up to more than 5 ppbv for RCP 8.5, while East Asia shows increases of about 2 ppbv for RCP 8.5 and reductions of about 4 ppbv for RCP 2.6.

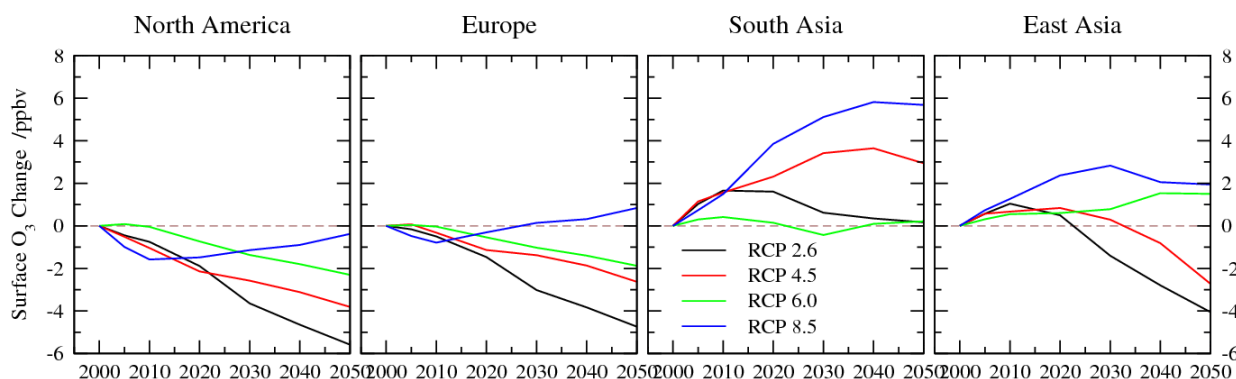


**Figure 4.42.** Mean surface O<sub>3</sub> changes over the four HTAP receptor regions following the four RCP scenarios from 2000 to 2050, based on linearization of the six models that contributed results to all SR simulations in the HTAP intercomparison.

To verify the validity of this linearization, additional ‘future emission’ (FE) simulations were defined for the HTAP intercomparison focusing on the most extreme RCP 8.5 scenario in 2030, when precursor emissions are at a maximum. The resultant annual mean surface O<sub>3</sub> changes between 2000 and 2030 for each region are shown in Figure 4.43 for several models, along with the corresponding linear estimates. In general, the agreement between the models on the magnitude of the expected changes is good, and the linear estimates are close to the results of the full simulations and within the uncertainty range shown by the different models.

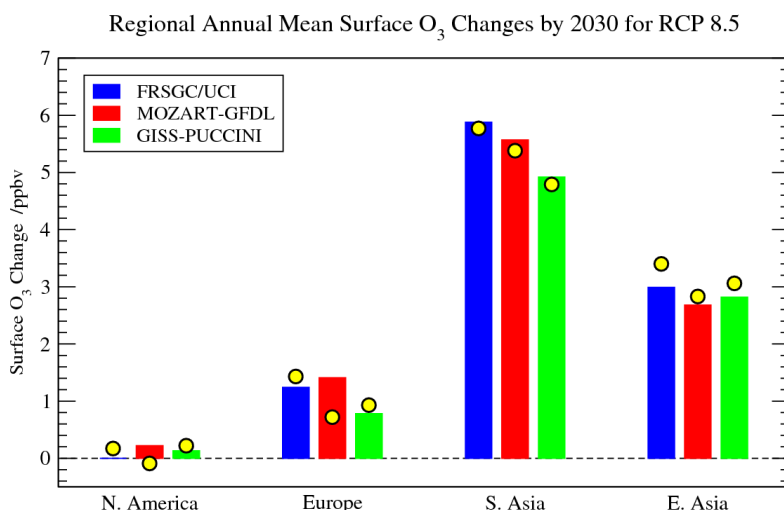


**Figure 4.43.** Regional annual mean surface O<sub>3</sub> changes between 2000 and 2030 following the most polluted RCP 8.5 emission scenario for three models contributing to the HTAP Future Emission runs. Yellow points mark the linearised estimate for the corresponding model.

The changes in S/R relationships are shown in Figure 4.44 for the RCP 8.5 and RCP 2.6 scenarios, which constitute realistic bounds on feasible emissions pathways in the near future. For the RCP 8.5 scenario, it is clear that surface O<sub>3</sub> changes over most regions are strongly affected by the large increases in global CH<sub>4</sub> concentrations, particularly by 2050 and beyond. Over South and East Asia, regional emission changes dominate until 2030-2050, when CH<sub>4</sub> changes overtake them. For the RCP 2.6 scenario, O<sub>3</sub> changes are principally governed by regional precursor emission changes, with roughly equal reductions in CH<sub>4</sub> and in O<sub>3</sub> from sources outside the region. It is interesting to note that the imported contribution increases for the North American region in these scenarios (by about 20% for RCP 8.5 by 2030), reflecting increases in emissions occurring over Asia in the next two decades, but decreases for the other regions (by 10-15% by 2030) driven by North American reductions. In contrast, the regional (domestic) contribution falls by almost 50% over North America in the RCP 8.5 scenario and by 25% over Europe, but increases by 45% over East Asia and by 80% over South Asia.

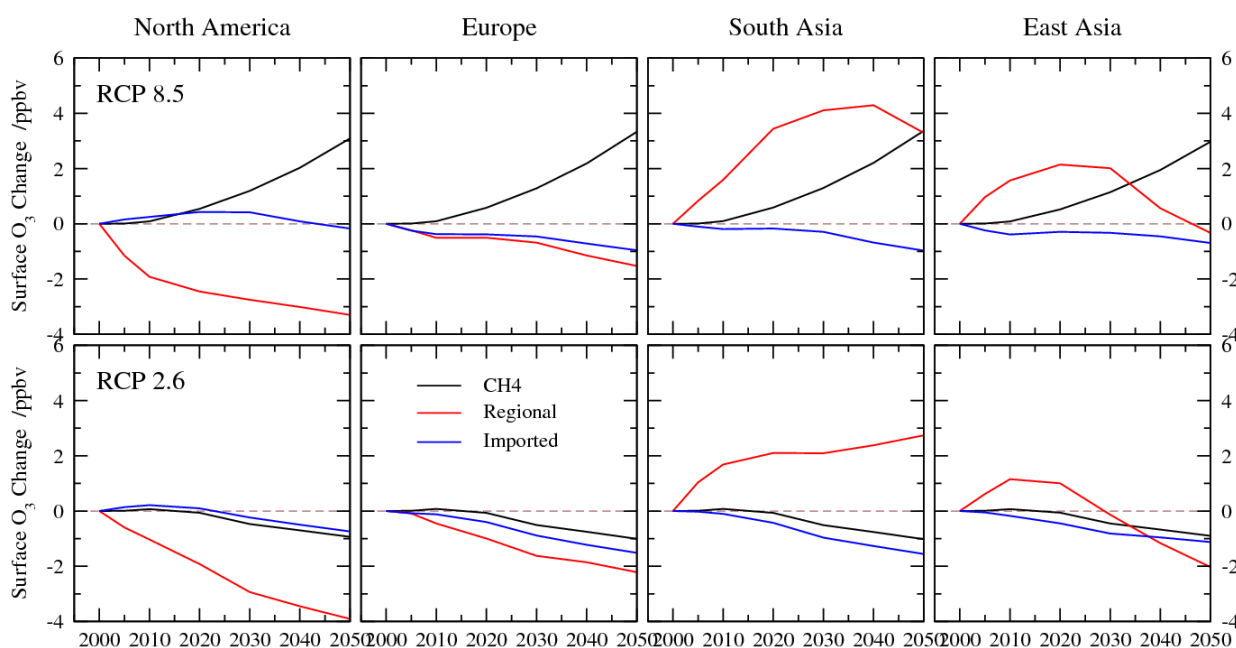


**Figure 4.44.** Contribution to annual mean surface O<sub>3</sub> changes for RCP 8.5 (top row) and RCP 2.6 (bottom row) scenarios from changes in CH<sub>4</sub> concentration, emission changes over the receptor region ('Regional') and emission changes from outside the receptor region ('Imported'). Ensemble mean values for the six models contributing results to Figure 4.42.

The changes in the relative annual intercontinental response metric are shown in Table 4.9. In the RCP 8.5 scenario, the relative annual intercontinental response for EU remains relatively constant, as domestic emission reductions are matched by the combination of reductions over NA and increases elsewhere. For SA the response decreases strongly as domestic sources increase and other sources decrease. However, the relative annual intercontinental response for NA increases by 60%, as the 50% domestic emission reduction builds on a 20% increase in O<sub>3</sub> from upwind sources, and the metric exceeds 50% indicating that the response to emission changes outside the region exceeds that of the same fractional change to domestic emissions.

**Table 4.9.** Relative annual intercontinental response under different future emission scenarios. This is defined as the ratio of the O<sub>3</sub> response in one region due to the combined influence of sources in the other three regions to the response from all sources, see Section 4.2.5. Mean results from 12 models.

Scenario	NA	EU	SA	EA
Current: 2000	32%	41%	32%	39%
RCP 8.5: 2030	52%	44%	20%	29%
RCP 2.6: 2050	49%	43%	14%	40%

**FINDING (future emissions):** Regional emission changes in coming decades are not sufficiently large to cause substantial non-linear responses, so changes in S/R relationships can be estimated from current conditions. The importance of foreign emission changes compared to domestic changes is likely to increase substantially, and for North America is expected to double before 2050 under all four RCP emission scenarios as domestic emissions fall and emissions from South and East Asia continue to grow. The sensitivity to changes in geographical distribution of emissions within a particular region has not been adequately assessed yet.

**FINDING (CH<sub>4</sub>):** CH<sub>4</sub> is of major importance as a contributor to surface ozone. Roughly 40% of the annual mean O<sub>3</sub> increase since the preindustrial is believed to be due to anthropogenic CH<sub>4</sub> and future changes in atmospheric CH<sub>4</sub> concentrations have a large influence on surface O<sub>3</sub> changes following the RCP scenarios.

**RECOMMENDATION (future emissions):** Further studies are needed to develop estimates of future changes in the geographic distribution of emissions, and to evaluate the impact of these changes on the S/R relationships.

#### 4.6.2. Changes with future climate

##### *Changes in chemistry and transport processes*

Changes in climate at the global and regional level will modify the chemical environment and pollutant lifetimes and hence the concentrations of pollutants arriving at downwind continents. Changes in climate may also affect meteorological transport processes, and hence alter the export and import of pollution, as outlined in Section 1.5.2. Globally averaged changes in tropospheric O<sub>3</sub> simulated for 1979-99 show a relationship to changes in surface temperature [Hess and Mahowald, 2009], but the tropospheric O<sub>3</sub> response to temperature changes is relatively small compared to several other chemical species, reflecting the many compensating influences of climate change on O<sub>3</sub> (Section 1.5.2; Jacob and Winner [2009]). Surface temperature and surface insolation changes have been reported as the main drivers of future simulated changes in maximum daily 8-hour average surface O<sub>3</sub> across the USA [Weaver *et al.*, 2009].

Enhanced isoprene emissions in a future warmed climate have been simulated in a number of studies [Andersson and Engardt, 2010; Hedegaard *et al.*, 2008; Lin *et al.*, 2008a; Sanderson *et al.*, 2003; Wu *et al.*, 2008; Zeng *et al.*, 2008] that employ interactive isoprene emissions based on Guenther *et al.* [1995]. Ozone production increases with higher isoprene emissions in high NO<sub>x</sub> regions increasing O<sub>3</sub> export, but in low NO<sub>x</sub> environments O<sub>3</sub> production decreases [Wu *et al.*, 2008; Zeng *et al.*, 2008]. However, there is major uncertainty in the extent of CO<sub>2</sub> inhibition of isoprene emissions in a future higher CO<sub>2</sub> climate [Arneth *et al.*, 2007; Heald and Spracklen, 2009; Young *et al.*, 2009] and in isoprene oxidation chemistry and its impacts on O<sub>3</sub> and organic aerosol [e.g., Carlton *et al.*, 2009; Heald *et al.*, 2008; Paulot *et al.*, 2009; Zhang *et al.*, 2008b]. Another key uncertainty is how dry deposition decreases in a warmer climate [Andersson and Engardt, 2010] and in particular in regions where warming is likely to be accompanied by drying- such as in the sub-tropics [Held and Soden, 2006]. Warmer temperatures may increase emissions of NO<sub>x</sub> from soils [Wu *et al.*, 2008]. Increases in temperature will decrease the lifetime of PAN and contribute to reduced export of NO<sub>x</sub> in this form and thus alter the long-range transport of O<sub>3</sub>.

Increased water vapour in a future warmer atmosphere will lead to increased O<sub>3</sub> destruction and shorter O<sub>3</sub> lifetimes, and this is a prominent and robust feature of previous model studies [Stevenson *et al.*, 2006]. This may cause a reduction in the contribution of Asian emissions to background O<sub>3</sub> over the United States [Lin *et al.*, 2008a; Murazaki and Hess, 2006]. However, in highly polluted regions, increased water vapour has competing effects on O<sub>3</sub> production [Jacob and Winner, 2009]. A number of model studies show that increased water vapour in high emission regions often leads to increased local production of O<sub>3</sub>, and hence greater local O<sub>3</sub> export [Hauglustaine *et al.*, 2005; Murazaki and Hess, 2006]. Higher water vapour concentrations may also lead to higher concentrations of H<sub>2</sub>O<sub>2</sub>, the main oxidant of SO<sub>2</sub>, and thus increase sulphate concentrations [Jacob and Winner, 2009].

Changes in cloud amount and precipitation will affect O<sub>3</sub> production from lightning, photolysis rates, and deposition and removal rates for PM. Increases in wet removal in wetter regions will reduce PM lifetimes reducing transport distances [U.S. EPA, 2009]. Changes in export from source regions together with changes in transport patterns will determine future S/R relationships. Although it may be difficult to separate the competing effects of higher water vapour and temperature in determining changes in O<sub>3</sub> concentrations, reductions in the lifetimes of both PAN and O<sub>3</sub> suggest reduced intercontinental transport from source regions. These changes will also impact the production of secondary aerosols and are likely to increase them. The net effect of changes in chemistry and removal rates on the hemispheric transport of aerosols requires further study.

Changes in climate may affect meteorological transport processes through changes in synoptic and convective transport and changes in circulation. One robust feature of greenhouse-forced multi-model climate simulations is a strengthening of the Brewer-Dobson circulation [Butchart *et al.*, 2006] leading to enhanced stratosphere-troposphere exchange [Stevenson *et al.*, 2006]. Ozone of stratospheric origin entering the upper troposphere may then undergo long-range transport to receptor regions. The impact of enhanced stratosphere-troposphere exchange on the tropospheric O<sub>3</sub> budget and source attribution remains poorly understood.

A number of GCM simulations indicate a poleward shift in the mid-latitude cyclone storm tracks [Bengtsson *et al.*, 2006; Yin, 2005], an increase in cyclonic circulation patterns over the Arctic [Cassano *et al.*, 2005], and a decrease in the frequency of northern mid-latitude cyclones in winter [Geng and Sugi, 2006; Lambert and Fyfe, 2006; Meehl *et al.*, 2007; Yin, 2005]. These effects result from a shift and reduction of baroclinicity forced by weakened meridional temperature gradients [Geng and Sugi, 2006; Yin, 2005]. However, GCM-derived results may be sensitive to the height of the model upper boundary in the stratosphere. Future decreases in the frequency of synoptic activity would decrease large-scale venting of the boundary layer in polluted northern mid-latitude regions [Jacob and Winner, 2009]. Late 20<sup>th</sup> century and future decreases in synoptic frequency have been associated with increased summertime ozone pollution episodes [Forkel and Knoche, 2006; Leibensperger *et al.*, 2008; Mickley *et al.*, 2004; Murazaki and Hess, 2006; Wu *et al.*, 2008] as well as increases in PM [Liao *et al.*, 2006]. These changes in transport generally favour reduced export of pollutants from regions such as North America. An expansion of the Hadley cell associated with poleward shifts in the mid-latitude storm tracks has been observed in recent decades and this is reproduced in climate models which attribute it to anthropogenic forcing [Seidel *et al.*, 2008]. A future weakening of the Hadley circulation has also been simulated [Lu *et al.* 2007], favouring reduced export from tropical/sub tropical source regions. However, there is considerable uncertainty in how atmospheric transport patterns will change in the future. Climate models underestimate the observed changes in the Hadley Cell expansion [Johanson and Fu, 2009]. In addition, studies of future changes in the behaviour of blocking anticyclones, which disrupt the passage of mid-latitude cyclones in summer in Europe, suggest a decrease in blocking frequency but an increase in the length of individual blocking events [Royal Society, 2008a].

Changes in convective transport in a future climate are also uncertain. From theoretical considerations and GCM simulations, Held and Soden [2006] show that atmospheric warming results in a decrease in tropical deep convective mass fluxes, and an enhancement in patterns of evaporation and precipitation (i.e., dry locations such as the sub-tropics get dryer and wet locations moister). Convective mass fluxes determine how much pollution reaches the free troposphere (Section 1.2.3). However, increases in updraft speeds over land in a warmer climate have been suggested, and convective plumes may then reach higher altitudes Del Genio *et al.*, [2007]. Deeper convection is likely to result in increased lightning and hence increased O<sub>3</sub> production [Wu *et al.*, 2008].

Finally, considering climate variability (Section 1.5.1), a trend towards a positive phase of the North Atlantic Oscillation (NAO) is a feature of many greenhouse-forced 21st-century GCM simulations [Miller *et al.*, 2006]. This largely agrees with a poleward preferential location of mid-latitude storm tracks. However, model projections vary widely in the magnitude of their response [Miller *et al.*, 2006; Osborn, 2004]. A future trend towards more El Niño-like conditions has been reported in several studies, but there is no overall consensus [Collins *et al.*, 2010a].

### **Changes in S/R relationships**

For the four HTAP regions we have simulated S/R relationships for O<sub>3</sub> for the 2090s using three chemistry transport models driven by GCMs (GISS-PUCCINI-ModelEaer, STOC-HadAM3, UM-CAM). These simulations were designed to isolate the effects of climate change on S/R relationships and therefore anthropogenic emissions and methane concentrations were held fixed at 2001 values as in earlier HTAP experiments (Section 4.1.3; Fiore *et al.*, [2009]). The models use interactive lightning NO<sub>x</sub> emissions that are sensitive to changes in cloud parameters in a future climate. The STOC-HadAM3 model also employed an interactive isoprene emission scheme [Guenther *et al.*, 1995]. The atmospheric GCMs were in turn driven by sea-surface temperatures from coupled ocean-atmosphere model

integrations that were forced by greenhouse-gas emissions from the SRES A2 scenario [IPCC, 2000]. Two base case 5-year integrations were carried out using meteorology for the 2000s and 2090s decades and fixed emissions, similar to the SR1 simulations in experiment set 1 (Section 4.2.5).

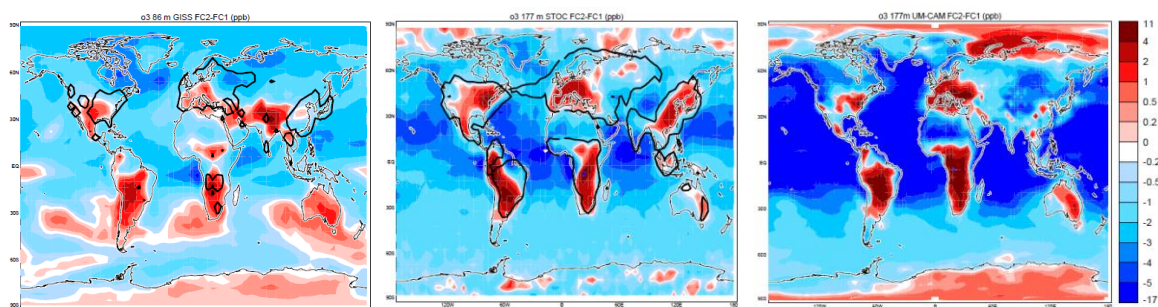


**Figure 4.45.** Difference in annual-average surface O<sub>3</sub> concentrations (ppbv) between the 2090s and 2000s decade for a) GISS-PUCCINI-ModelE, b) STOC-HadAM3 and c) UM-CAM. The differences are due to climate and climate-sensitive natural emissions changes alone (lightning for both models; isoprene for STOC-HadAM3). The 500 ppt contour of NO<sub>x</sub> concentrations for the 2000s decade is shown in black.

The surface O<sub>3</sub> response to the 2090s warmed climate shows characteristic features described in previous studies [e.g., *Stevenson et al.*, 2006]: reduced surface O<sub>3</sub> concentrations in unpolluted regions and generally enhanced surface O<sub>3</sub> concentrations in highly polluted regions (Figure 4.45) as described above. Higher water vapour concentrations lead to reduced surface O<sub>3</sub> in unpolluted regions. In polluted regions (delineated by the 500 ppt NO<sub>x</sub> contours for the 2000s) the response is mixed, although increased surface O<sub>3</sub> occurs over most major source emission regions. In addition, enhanced isoprene emissions in high NO<sub>x</sub> emission regions may augment O<sub>3</sub> levels further, and may be the dominant mechanism for O<sub>3</sub> increases in the 2090s compared to the 2000s in several regions in panel (b) of Figure 4.45 (in particular in tropical continental regions S. America and S.E USA). This illustrates changes in background and regional O<sub>3</sub> concentrations which will affect S/R relationships. Figure 4.45 suggests that additional emissions controls would be needed to achieve a targeted level of O<sub>3</sub> abatement since O<sub>3</sub> concentrations are 2-6 ppbv higher over the major source regions in the 2090s as compared to the 2000s, due to climate change alone. The term “climate penalty” has previously been used to describe this result for the daily maximum 8-hour O<sub>3</sub> metric [*Wu et al.*, 2008].

The effect of the 20% emissions reduction in NA over the receptor continents is depicted in Figure 4.46 under 2000s and 2090s climate conditions. The 5-year mean O<sub>3</sub> reductions for the 2000s for the three models lie within the multi-model range of results from 15 models for 2001 (MM01) [*Fiore et al.*, 2009]. For each model the effect of the 20% emissions reduction in the 2090s future climate is very similar to that in the 2000s climate, showing that the emissions reduction has a greater effect than the change in climate. The surface O<sub>3</sub> response is slightly enhanced in the NA source region (by ~0.1 ppbv) and slightly reduced in the EU (~0.05 ppbv) and EA (~0.03 ppbv) receptor regions in the 2090s compared to the 2000s decade. There is little seasonal or interannual variation (not shown) in the surface O<sub>3</sub> response between the two climate periods. Emission perturbation simulations (SR6) for the three other source regions yield similar results, with a slightly greater surface O<sub>3</sub> response to a 20% emission reduction in the source region and a slightly reduced response in downwind continents in a warmer moister future climate.



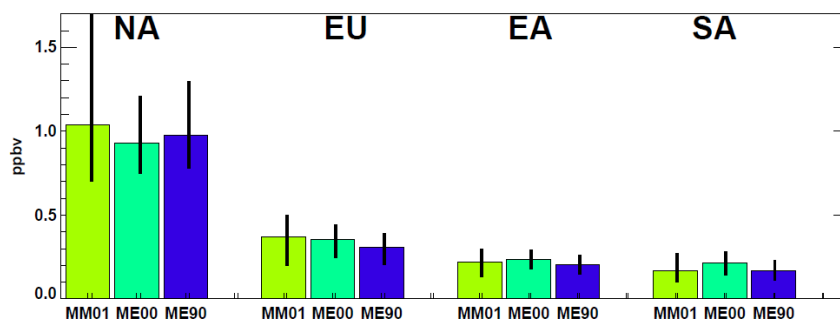


**Figure 4.46.** Impact of 20% reductions of the O<sub>3</sub> precursor emissions (NO<sub>x</sub>, NMVOCs, and CO) in the NA source region on annual-mean surface O<sub>3</sub> over the receptor regions for the 2000s (00) and 2090s (90) decades. MM01= Multi-model mean and ranges with 2001 climate [Fiore *et al.*, 2009]. ME00 = 3 model-mean for 2000s climate; ME90= 3 model-mean for 2090s; For ME00 and ME90 results are 5-year mean averages.

We attribute this effect to shorter lifetimes for both PAN and O<sub>3</sub> in the future. The former leads to more local NO<sub>x</sub> remaining in the source region and less transport as PAN downwind to receptor regions in a future warmer climate. The latter reduces the transport of O<sub>3</sub> but generates OH locally leading to faster oxidation and production of O<sub>3</sub> in the source region. In these simulations there is little evidence of meteorological transport effects such as shifts in storm tracks or reduced ventilation of the continental boundary layer. We conclude that the dominant effects of future climate on S/R relationships for O<sub>3</sub> are via temperature and water vapour effects on the chemical environment and on the lifetime of O<sub>3</sub> and its precursors .

**FINDING (future climate):** Future changes in climate are expected to increase the effect of precursor emissions on surface O<sub>3</sub> concentrations over source regions and to reduce the effect over downwind receptor regions. However, the magnitude of these effects is relatively small, and is driven by changes in the lifetime of O<sub>3</sub> and NO<sub>y</sub> and not by changes in transport patterns. The effect of natural emission changes (e.g. soil and wildfire emissions) and wider climate-related feedbacks have not been evaluated fully yet.

**RECOMMENDATION:** Further studies are needed to determine the impacts of future changes in climate on PM (including SOA components) and on S/R relationships and source attribution of PM.

## References

- Adhikary, B., et al. (2009), Trans-Pacific transport and evolution of aerosols and trace gases from Asia during the INTEX-B field campaign, *Atmospheric Chemistry and Physics Discussions*, 9: 16381-16439.
- Andersson, C., and M. Engardt (2010), European ozone in a future climate: Importance of changes in dry deposition and isoprene emissions, *Journal of Geophysical Research*, 115(D02303).
- Arneth, A., et al. (2007), CO<sub>2</sub> inhibition of global terrestrial isoprene emissions: potential implications for atmospheric chemistry, *Geophysical Research Letters*, 34(L18813).
- Auvray, M., and I. Bey (2005), Long-range transport to Europe: Seasonal variations and implications for the European ozone budget, *Journal of Geophysical Research*, 110(D11303).
- Auvray, M., et al. (2007), A model investigation of tropospheric ozone chemical tendencies in long-range transported pollution plumes, *Journal of Geophysical Research*, 112(D05304).
- Barth, M., and A. Church (1999), Regional and global distribution and lifetimes of sulfate aerosols from Mexico City and southeast China, *Journal of Geophysical Research*, 104(D23): 30231-30239.
- Bauer, S. E., and D. Koch (2005), Impact of heterogeneous sulfate formation at mineral dust surfaces on aerosol loads and radiative forcing in the Goddard Institute for Space Studies general circulation model *Journal of Geophysical Research*, 110(D17202).
- Bengtsson, L., et al. (2006), Storm Tracks and Climate Change, *Journal of Climate*, 19(15): 26.

- Berntsen, T., et al. (1996), Impacts of increased anthropogenic emissions in Asia on tropospheric ozone and climate: A global 3-D model study, *Tellus B*, 48(1): 13-32.
- Berntsen, T. K., et al. (2000), Time evolution of tropospheric ozone and its radiative forcing, *Journal of Geophysical Research*, 105: 8915-8930.
- Bey, I., et al. (2001), Asian chemical outflow to the Pacific in Spring: Origins, pathways, and budgets, *Journal of Geophysical Research - Atmospheres*, 106(D19): 23097-23113.
- Bian, H., et al. (2007), Sensitivity of global CO simulations to uncertainties in biomass burning sources, *Journal of Geophysical Research*, 112(D23): D23308.
- Bouwman, A. F., et al. (2002), Global analysis of acidification and eutrophication of terrestrial ecosystems, *Water Air and Soil Pollution*, 141(1-4): 349-382.
- Butchart, N., et al. (2006), Simulations of anthropogenic change in the strength of the Brewer-Dobson circulation, *Climate Dynamics*, 27(7-8): 727-741.
- Calori, G., et al. (2001), Interannual variability in sulfur deposition in Asia, *Journal of Global Environmental Engineering*, 7: 1-16.
- Carlton, A. G., et al. (2009), A review of Secondary Organic Aerosol (SOA) formation from isoprene, *Atmospheric Chemistry and Physics*, 9: 4987-5005.
- Carmichael, G. R., et al. (2008), Predicting air quality: Improvements through advanced methods to integrate models and measurements, *Journal of Computational Physics*, 227(7): 3540-3571.
- Cassano, J. J., et al. (2005), Changes in synoptic weather patterns in the polar regions in the 20th and 21st centuries, Part 1: Arctic, *International Journal of Climatology*, 26: 1181-1199.
- Chen, D., et al. (2009a), Regional CO pollution in China simulated by the high-resolution nested-grid GEOS-Chem model, *Atmospheric Chemistry and Physics*, 9: 3825-3839.
- Chen, Y., et al. (2009b), Aircraft study of mountain chimney effect of Beijing, China, *Journal of Geophysical Research*, 114(D08306).
- Chin, M., et al. (1996), A global three-dimensional model of tropospheric sulfate, *Geophysical Research Letters*, 101(D13): 18667-18690.
- Chin, M., et al. (2000), Atmospheric sulfur cycle simulated in the global model GOCART: Model description and global properties, *Journal of Geophysical Research*, 105(D20): 24671-24688.
- Chin, M., et al. (2007), Intercontinental transport of pollution and dust aerosols: implications for regional air quality, *Atmospheric Chemistry and Physics*, 7(21): 5501-5517.
- Collins, M., et al. (2010a), The impact of global warming on the tropical Pacific Ocean and El Nino, *Nature Geoscience*, 3: 391-397.
- Collins, W. J., et al. (2010b), How vegetation impacts affect climate metrics for ozone precursors, *Journal of Geophysical Research*, 115(D23308).
- Damoah, R., et al. (2004), Around the world in 17 days - hemispheric-scale transport of forest fire smoke from Russia in May 2003, *Atmospheric Chemistry and Physics*, 4: 1311-1321.
- Darmenova, K., et al. (2005), Characterization of east Asian dust outbreaks in the spring of 2001 using ground-based and satellite data, *Journal of Geophysical Research*, 110(D02204).
- Del Genio, A. D., et al. (2007), Will moist convection be stronger in a warmer climate?, *Geophysical Research Letters*, 34(L16703).
- Dentener, F., et al. (2006), The global atmospheric environment for the next generation, *Environmental Science & Technology*, 40(11): 3586-3594.
- Derwent, R. G., et al. (2001), Transient behaviour of tropospheric O<sub>3</sub> precursors in a global 3-D CTM and their indirect greenhouse effects, *Climatic Change*, 49: 463-487.
- Ellingsen, K., et al. (2008), Global ozone and air quality: a multi-model assessment of risks to human health and crops, *Atmospheric Chemistry and Physics Discussions*, 8: 2163-2223.

- Emmerson, K. M., and M. J. Evans (2009), Comparison of tropospheric gas-phase chemistry schemes for use within global models, *Atmospheric Chemistry and Physics*, 9: 1831-1845.
- Fang, Y., et al. (2009), Estimating the contribution of strong daily export events to total pollutant export from the United States in summer, *Journal of Geophysical Research*, 114(D23302).
- Fang, Y., et al. (2010), Sensitivity of the NO<sub>y</sub> budget over the United States to anthropogenic and lightning NO<sub>x</sub> in summer, *Journal of Geophysical Research*, 115(D18312).
- Fiore, A. M., et al. (2002), Background ozone over the United States in summer: origin, trend, and contribution to pollution episodes, *Journal of Geophysical Research*, 107(D15): 4275-4299.
- Fiore, A. M., et al. (2008), Characterizing the tropospheric ozone response to methane emission controls and the benefits to climate and air quality, *Journal of Geophysical Research*, 113(D08307).
- Fiore, A. M., et al. (2009), Multimodel estimates of intercontinental source-receptor relationships for ozone pollution, *Journal of Geophysical Research*, 114(D04301).
- Fiore, A. M., et al. (2010), Interactions between climate and air quality, in *Air Pollution Modelling and its Application XX*, edited by D. G. Steyn and S. T. Rao, Springer Science and Business Media B. V.
- Fischer, E. V., et al. (2009), Meteorological Controls on Observed Peroxyacetyl Nitrate (PAN) at Mount Bachelor during the spring of 2008, *Journal of Geophysical Research*, 115(D03302).
- Forkel, R., and R. Knoche (2006), Regional climate change and its impact on photooxidant concentrations in southern Germany: Simulations with a coupled regional climate-chemistry model, *Journal of Geophysical Research*, 111(D12302).
- Galmarini, S., et al. (2004), Ensemble dispersion forecasting--Part II: application and evaluation, *Atmospheric Environment*, 38(28): 4619-4632.
- Gauss, M., et al. (2003), Radiative forcing in the 21st century due to ozone changes in the troposphere and the lower stratosphere, *Journal of Geophysical Research*, 108(D9): 4292-4312.
- Gauss, M., et al. (2006), Radiative forcing since preindustrial times due to ozone change in the troposphere and the lower stratosphere, *Atmospheric Chemistry and Physics*, 6(3): 575-599.
- Geng, Q., and M. Sugi (2006), Possible change of extratropical cyclone activity due to enhanced greenhouse gases and sulfate aerosols - study with a high-resolution AGCM, *Journal of Climate*, 16: 2262-2274.
- Gong, S. L., et al. (2006), A simulated climatology of Asian dust aerosol and its trans-Pacific transport. Part II: Interannual variability and climate connections, *Journal of Climate*, 19: 104-122.
- Guenther, A., et al. (1995), A global model of natural volatile organic compound emissions, *Journal of Geophysical Research*, 100(D5): 8873-8892.
- Hadley, O., et al. (2007), Trans-Pacific transport of black carbon and fine aerosol ( $d < 2.5 \mu\text{m}$ ) into North America, *Journal of Geophysical Research*, 112(D05309).
- Hakami, A., et al. (2006), Adjoint sensitivity analysis of ozone nonattainment over the continental United States, *Environmental Science & Technology*, 40(12): 3855-3864.
- Hauglustaine, D. A., et al. (2005), Future tropospheric ozone simulated with a climate-chemistry-biosphere model, *Geophysical Research Letters*, 32: L24807.
- Heald, C. L., et al. (2003), Asian outflow and trans-Pacific transport of carbon monoxide and ozone pollution: An integrated satellite, aircraft, and model perspective, *Journal of Geophysical Research*, 108(D244804).
- Heald, C. L., et al. (2008), Predicted change in global secondary organic aerosol concentrations in response to future climate, emissions, and land use change, *Journal of Geophysical Research*, 113(D05211).
- Heald, C. L., and D. V. Spracklen (2009), Atmospheric budget of primary biological aerosol particles from fungal spores, *Geophysical Research Letters*, 36(L09806).
- Hedegaard, G. B., et al. (2008), Impacts of climate change on air pollution levels in the Northern Hemisphere with special focus on Europe and the Arctic, *Atmospheric Chemistry and Physics*, 4: 497-509.

- Held, I. M., and B. J. Soden (2006), Robust responses of the hydrological cycle to global warming, *Journal of Climate*, 19(21): 5686-5699.
- Henne, S., et al. (2004), Quantification of topographic venting of boundary layer air to the free troposphere, *Atmospheric Chemistry and Physics*, 4(2): 497-509.
- Henne, S., et al. (2005), Influence of mountain venting in the Alps on the ozone chemistry of the lower free troposphere and the European pollution export *Journal of Geophysical Research*, 110(D22307).
- Henze, D. K., et al. (2009), Inverse modeling and mapping US air quality influences of inorganic PM<sub>2.5</sub> precursor emissions using the adjoint of GEOS-Chem, *Atmospheric Chemistry and Physics*, 9: 5877-5903.
- Hess, P., and N. Mahowald (2009), Interannual variability in hindcasts of atmospheric chemistry: the role of meteorology, *Atmospheric Chemistry and Physics*, 9: 5261-5280.
- Hofzumahaus, A., et al. (2009), Amplified Trace Gas Removal in the Troposphere, *Science*, 324(5935): 1702-1704.
- Horowitz, L. W., et al. (1998), Export of reactive nitrogen from North America during summertime: sensitivity to hydrocarbon chemistry, *Journal of Geophysical Research*, 103D(11): 13451-13476.
- Huang, M., et al. (2010), Impacts of transported ozone on California air quality during the ARCTAS-CARB period - a multiscale modeling study, *Atmospheric Chemistry and Physics*, 10: 6947-6968.
- Hudman, R. C., et al. (2004), Ozone production in transpacific Asian pollution plumes and implications for ozone air quality in California, *Journal of Geophysical Research*, 109(D23S10).
- Husar, R. B., et al. (2001), Asian dust events of April 1998, *Journal of Geophysical Research*, 106(D16): 18317-18330.
- IPCC (2000), Emissions Scenarios, edited by N. Nakicenovic and R. Swart, 570 pp., Cambridge University Press, Cambridge.
- Jacob, D. J., et al. (1999), Effect of rising Asian emissions on surface ozone in the United States, *Geophysical Research Letters*, 26(14): 2175-2178.
- Jacob, D. J., and D. A. Winner (2009), Effect of climate change on air quality, *Atmospheric Environment*, 43(1): 51-63.
- Jaffe, D., and J. Ray (2007), Increase in surface ozone at rural sites in the western US, *Atmospheric Environment*, 41(26): 5452-5463.
- Johanson, C. M., and Q. Fu (2009), Hadley Cell Widening: Model simulations versus observations, *Journal of Climate*, 22: 2713-2725.
- Jonson, J. E., et al. (2010), A multi-model analysis of vertical ozone profiles, *Atmospheric Chemistry and Physics*, 10: 5759-5783.
- Kaufman, Y. J., et al. (2005), Dust transport and deposition observed from the Terra-Moderate Resolution Imaging Spectroradiometer (MODIS) spacecraft over the Atlantic Ocean, *Journal of Geophysical Research*, 110(D10S12).
- Klug, W., et al. (1992), *Evaluation of long range atmospheric transport models using environmental radioactivity data from Chernobyl accident*, Elsevier Science Publishers, Essex.
- Koch, D., et al. (1999), Tropospheric sulfur simulation and sulfate direct radiative forcing in the Godard Institute for Space Studies general circulation model, *Journal of Geophysical Research*, 104(D2): 23799-23822.
- Koch, D., et al. (2007), Global impacts of aerosols from particular source regions and sectors, *Journal of Geophysical Research*, 112(D02205).
- Koffi, B., et al. (2010), Present and future impact of aircraft, road traffic and shipping emissions on global tropospheric ozone, *Atmospheric Chemistry and Physics*, 10: 11681-11705.
- Krol, M. (2005), Results in *PHOENICS Synthesis and Integration Report*, University of Crete, Heraklion, Greece.

- Lam, Y. F., and J. S. Fu (2009), A novel downscaling technique for the linkage of global and regional air quality modeling, *Atmospheric Chemistry and Physics*, 9: 9169-9185.
- Lamarque, J. F., et al. (2010), Historical (1850-2000) gridded anthropogenic and biomass burning emissions of reactive gases and aerosols: Methodology and application, *Atmospheric Chemistry and Physics*, 10: 7017-7039.
- Lambert, S. J., and J. C. Fyfe (2006), Changes in winter cyclone frequencies and strengths simulated in enhanced greenhouse warming experiments: results from the models participating in the IPCC 4., *Climate Dynamics*, 26(7-8): 713-728.
- Law, R. M., et al. (2008), TransCom model simulations of hourly atmospheric CO<sub>2</sub>: Experimental overview and diurnal cycle results for 2002, *Global Biogeochemical Cycles*, 22(GB3009).
- Lawrence, M. G., and P. J. Rasch (2005), Tracer transport in deep convective updrafts: Plume ensemble versus bulk formulations, *Journal of the Atmospheric Sciences*, 62(8): 2880-2894.
- Lawrence, M. G., et al. (2006), Regional pollution potentials of megacities and other major population centers, *Atmospheric Chemistry and Physics*, 6: 13323-13366.
- Legras, B., et al. (2003), Vertical diffusivity in the lower stratosphere from Lagrangian back-trajectory reconstructions of ozone profiles, *Journal of Geophysical Research*, 108(D18): 4562-4570.
- Leibensperger, E., et al. (2010), Intercontinental influence of NO<sub>x</sub> and CO emissions on particulate matter air quality, *Geophysical Research Letters*, in review.
- Leibensperger, E. M., et al. (2008), Sensitivity of U.S. air quality to midlatitude cyclone frequency and implications of 1980-2006 climate change, *Atmospheric Chemistry and Physics*, 8(23): 7075-7086.
- Lelieveld, J., and F. J. Dentener (2000), What Controls tropospheric ozone?, *Journal of Geophysical Research*, 105(D3): 3531-3551.
- Li, Q., et al. (2002), Transatlantic transport of pollution and its effects on surface ozone in Europe and North America, *Journal of Geophysical Research*, 107(D134166).
- Li, Y. F., et al. (2008), North America - China joint project on reduction of lindane usage in China and its impact globally and on North America, Montreal.
- Liao, H., et al. (2006), Role of climate change in global predictions of future tropospheric ozone and aerosols, *Journal of Geophysical Research*, 111(D12304).
- Lin, J.-T., et al. (2008a), Effects of intercontinental transport on surface ozone over the United States: Present and future assessment with a global model, *Geophysical Research Letters*, 35(L02805).
- Lin, J. T., and M. B. McElroy (2010), Impacts of boundary layer mixing on pollutant vertical profiles in the lower troposphere: Implications to satellite remote sensing, *Atmospheric Environment*, 44: 1726-1739.
- Lin, J. T., et al. (2010a), Constraint of anthropogenic NO<sub>x</sub> emissions in China from different sectors: A new methodology using multiple satellite retrievals, *Atmospheric Chemistry and Physics*, 10: 63-78.
- Lin, M., et al. (2008b), Long-range transport of acidifying substances in Asia - Part II: Source-receptor relationships, *Atmospheric Environment*, 42(24): 5956-5967.
- Lin, M., et al. (2008c), Long-range transport of acidifying substances in East Asia - Part I: Model evaluation and sensitivity studies, *Atmospheric Environment*, 42(24): 5939-5955.
- Lin, M., et al. (2009), Multi-scale model analysis of boundary layer ozone over East Asia, *Atmospheric Chemistry and Physics*, 9: 3277-3301.
- Lin, M., et al. (2010b), Quantifying pollution inflow and outflow over East Asia in spring with regional and global models, *Atmospheric Chemistry and Physics*, 10(9): 4221-4239.
- Liu, H., et al. (2003), Transport pathways for Asian combustion outflow over the Pacific: Interannual and seasonal variations, *Journal of Geophysical Research*, 108(D20): 8786-8811.
- Liu, J., et al. (2008), Source-receptor relationships between East Asian sulfur dioxide emissions and Northern Hemisphere sulfate concentrations, *Atmospheric Chemistry and Physics*, 8: 3721-3733.

- Liu, J., et al. (2009), Evaluating inter-continental transport of fine aerosols: (2) Global Health Impacts, *Atmospheric Environment*, 43(28): 4339-4347.
- Liu, S. C., et al. (1987), Ozone production in the rural troposphere and the implications for regional and global ozone distributions, *Journal of Geophysical Research*, 92(D4): 4191-4207.
- Liu, X.-H., et al. (2010), Understanding of regional air pollution over China using CMAQ: Part II. Process analysis and ozone sensitivity to precursor emissions, *Atmospheric Environment*, 44(30): 3719-3727.
- Manktelow, P. T., et al. (2007), Regional and global trends in sulfate aerosol since the 1980s, *Geophysical Research Letters*, 34(L14803).
- Meehl, G. A., et al. (2007), Global climate projections, in *Climate Change 2007: The Physical Science Basis*, edited by S. D. Solomon, et al., 747-845 pp., Cambridge University Press, Cambridge, United Kingdom and New York, NY.
- Mickley, L. J., et al. (2001), Uncertainty in preindustrial abundance of tropospheric ozone: Implications for radiative forcing calculations, *Journal of Geophysical Research*, 106(D4): 3389-3399.
- Mickley, L. J., et al. (2004), Climate response to the increase in tropospheric ozone since preindustrial times: A comparison between ozone and equivalent CO<sub>2</sub> forcings, *Journal of Geophysical Research*, 109(D05106).
- Miller, R. L., et al. (2006), Forced annular variations in the 20th century intergovernmental panel on climate change Fourth Assessment Report models, *Journal of Geophysical Research*, 111(D18101).
- Moulin, C., et al. (1998), Satellite climatology of Africa dust transport in the Mediterranean atmosphere, *Journal of Geophysical Research*, 103(D11): 13137-13144.
- Moxim, W. J., et al. (1996), Simulated global tropospheric PAN: Its transport and impact on NO<sub>x</sub>, *Journal of Geophysical Research*, 101(D7): 12621-12638.
- Murazaki, K., and P. Hess (2006), How does climate change contribute to surface ozone change over the United States?, *Journal of Geophysical Research*, 111(D05301).
- Nagashima, T., et al. (2010), The relative importance of various source regions on East Asian surface ozone, *Atmospheric Chemistry and Physics*, 10: 11305-11322.
- NRC (2010), Global sources of local pollution: an Assessment of long-range transport of key air pollutants to and from the United States, 234 pp, National Research Council, The National Academies, Washington, DC.
- Osborn, T. J. (2004), Simulating the winter North Atlantic Oscillation: The roles of internal variability and greenhouse forcing, *Climate Dynamics*, 22: 605-623.
- Park, R. J., et al. (2004), Natural and transboundary pollution influences on sulfate-nitrate ammonium aerosols in the United States: Implications for policy, *Journal of Geophysical Research*, 109(D15204).
- Parrish, D. D., et al. (2010), Impact of transported background ozone inflow on summertime air quality in a California ozone exceedance area, *Atmospheric Chemistry and Physics*, 10: 10093-10109.
- Paulot, F., et al. (2009), Isoprene photooxidation: new insights into the production of acids and organic nitrates, *Atmospheric Chemistry and Physics*, 9: 1479-1501.
- Pfister, G. G., et al. (2006), Ozone production from the 2004 North American boreal fires, *Journal of Geophysical Research*, 111(D24S07).
- Prather, M., et al. (2001), Atmospheric chemistry and greenhouse gases, in *Climate change 2001: The scientific basis: Contribution of Working Group I to the Third Assessment Report of the Intergovernmental Panel on Climate Change*, edited by J. T. Houghton, et al., 49 pp., Cambridge University Press, New York.
- Prather, M., et al. (2003), Fresh air in the 21st century?, *Geophysical Research Letters*, 30(2): 1100-1103.
- Prather, M. J. (1996), Timescales in atmospheric chemistry: Theory, GWPs for CH<sub>4</sub> and CO<sub>2</sub>, and runaway growth, *Geophysical Research Letters*, 23(19): 2597-2600.

- Prather, M. J., et al. (2008), Quantifying errors in trace species transport modeling, *Proceedings of the National Academy of Science, USA*, 105(50): 19617-19621.
- Rastigejev, Y., et al. (2010), Resolving intercontinental pollution plumes in global models of atmospheric transport, *Journal of Geophysical Research*, 115(D02302).
- Real, E., et al. (2007), Processes influencing ozone levels in Alaskan forest fire plumes during long-range transport over the North Atlantic, *Journal of Geophysical Research*, 112: D10S41.
- Reddy, M. S., and O. Boucher (2007), Climate impact of black carbon emitted from energy consumption in the world's regions, *Geophysical Research Letters*, 34: L11802.
- Reidmiller, D. R., et al. (2009), The influence of foreign vs. North American emissions on surface ozone in the US, *Atmospheric Chemistry and Physics*, 9: 5027-5042.
- Roberts, G., et al. (2006), North American and Asian aerosols over the eastern Pacific Ocean and their role in regulating cloud condensation nuclei, *Journal of Geophysical Research*, 111(D13205).
- Royal Society (2008a), Sustainable biofuels: prospects and challenges, 90 pp, The Royal Society, London.
- Royal Society (2008b), Ground-level ozone in the 21st century: future trends, impacts and policy implications, 148 pp, The Royal Society, London.
- Sanderson, M. G., et al. (2003), Effect of climate change on isoprene emissions and surface ozone levels, *Geophysical Research Letters*, 30(18): 1936-1939.
- Sanderson, M. G., et al. (2008), A multi-model study of the hemispheric transport and deposition of oxidised nitrogen, *Geophysical Research Letters*, 35(L17815).
- Schultz, M. G., et al. (2007), A global data set of anthropogenic CO, NO<sub>x</sub>, and NMVOC emissions for 1960-2000, ICG-2, Research Center Jülich [http://retro.enes.org/data\\_emissions.shtml](http://retro.enes.org/data_emissions.shtml)
- Seibert, P., and A. Frank (2004), Source-receptor matrix calculation with a Lagrangian particle dispersion model in backward mode, *Atmospheric Chemistry and Physics*, 4: 51-63.
- Shindell, D. T., et al. (2005), An emissions-based view of climate forcing by methane and tropospheric ozone, *Geophysical Research Letters*, 32(L04803).
- Shindell, D. T., et al. (2008), A multimodel assessment of pollution transport to the Arctic, *Atmospheric Chemistry and Physics*, 8(17): 5353-5372.
- Stevenson, D. S., et al. (2006), Multimodel ensemble simulations of present-day and near-future tropospheric ozone, *Journal of Geophysical Research*, 111(D08301).
- Stohl, A., et al. (1998), Validation of the Lagrangian particle dispersion model FLEXPART against large scale tracer experiments, *Atmospheric Environment*, 32: 4245-4264.
- Stohl, A., et al. (2002), On the pathways and timescales of intercontinental air pollution transport, *Journal of Geophysical Research*, 107(D23): 4684-4700.
- Sudo, K., and H. Akimoto (2007), Global source attribution of tropospheric ozone: Long-range transport from various source regions, *Journal of Geophysical Research*, 112(D12302).
- Tanimoto, H., et al. (2009), Asian anthropogenic emissions and decadal trends in springtime tropospheric ozone over Japan: 1998-2007, *Geophysical Research Letters*, 36(L23802).
- Textor, C., et al. (2006), Analysis and quantification of the diversities of aerosol life cycles within AeroCom, *Atmospheric Chemistry and Physics*, 6: 1777-1813.
- TFHTAP (2007), Hemispheric transport of air pollution 2007, 146 pp, UN - Economic Commission for Europe, Geneva. *Air Pollution Studies No. 16*
- Tost, H., et al. (2010), Uncertainties in atmospheric chemistry modelling due to convection parameterisation and subsequent scavenging, *Atmospheric Chemistry and Physics*, 10: 1931-1951.
- U.S. EPA (2009), Risk assessment to support the review of the PM primary national ambient air quality standards (External review draft), Office of Air Quality Planning and Standards, United States Environmental Protection Agency, Research Triangle Park, NC. *EPA/450/P-09-006*



- Vautard, R., et al. (2006), Is regional air quality model diversity representative of uncertainty for ozone simulation?, *Geophysical Research Letters*, 33(L24828).
- Vingarzan, R. (2004), A review of surface ozone background levels and trends, *Atmospheric Environment*, 38(21): 3431-3442.
- Wang, Y., et al. (1998), Global simulation of tropospheric O<sub>3</sub>-NO<sub>x</sub>-hydrocarbon chemistry: 2. Model evaluation and global ozone budget., *Journal of Geophysical Research*, 103(D9): 10727-10756.
- Wang, Y., et al. (2004), Asian emissions of CO and NO<sub>x</sub>: Constraints from aircraft and Chinese station data, *Journal of Geophysical Research*, 109(D24304).
- Weaver, C. P., et al. (2009), A Preliminary Synthesis of Modeled Climate Change Impacts on U.S. Regional Ozone Concentrations, *Bulletin of the American Meteorological Society*, 90(12): 1843-1863.
- West, J. J., et al. (2007), Ozone air quality and radiative forcing consequences of changes in ozone precursor emissions, *Geophysical Research Letters*, 34(L06806).
- West, J. J., et al. (2009a), Effect of regional precursor emission controls on long-range ozone transport - Part 1: Short-term changes in ozone air quality, *Atmospheric Chemistry and Physics*, 9: 6077-6093.
- West, J. J., et al. (2009b), Effect of regional precursor emission controls on long-range ozone transport - Part 2: Steady-state changes in ozone air quality and impacts on human mortality, *Atmospheric Chemistry and Physics*, 9(16): 6095-6107.
- Wild, O., and M. J. Prather (2000), Excitation of the primary tropospheric chemical mode in a global 3-D model, *Journal of Geophysical Research*, 105(D20): 24647-24660.
- Wild, O., and H. Akimoto (2001), Intercontinental transport of ozone and its precursors in a three dimensional globe CTM, *Journal of Geophysical Research* 106(D21): 27729-27744.
- Wild, O., et al. (2001), Indirect long-term global radiative cooling from NO<sub>x</sub> emissions, *Geophysical Research Letters*, 28(9): 1719-1722.
- Wild, O., et al. (2004a), Trans-Eurasian transport of ozone and its precursors, *Journal of Geophysical Research*, 109(D11302).
- Wild, O., et al. (2004b), Chemical transport model ozone simulations for spring 2001 over the western Pacific: Regional ozone production and its global impacts, *Journal of Geophysical Research*, 109(D15S02).
- Wild, O. (2007), Modelling the global tropospheric ozone budget: Exploring the variability in current models, *Atmospheric Chemistry and Physics*, 7: 2643-2660.
- Wilkening, K. E., et al. (2000), Atmospheric science: Trans-Pacific air pollution, *Science*, 290(5489): 65-67.
- Wu, R., et al. (2009), Findings from quality assurance activities in the Integrated Atmospheric Deposition Network, *Journal of Environmental Monitoring*, 11: 277-296.
- Wu, S., et al. (2007), Why are there large differences between models in global budgets of tropospheric ozone?., *Journal of Geophysical Research*, 112(D05302).
- Wu, S., et al. (2008), Effects of 2000-2050 global change on ozone air quality in the United States, *Journal of Geophysical Research* 113(D06302).
- Yin, J. H. (2005), A consistent poleward shift of the storm tracks in simulations of the 21st century climate., *Geophysical Research Letters*, 32(L18701).
- Young, P. J., et al. (2009), The CO<sub>2</sub> inhibition of terrestrial isoprene emission significantly affects future ozone projections, *Atmospheric Chemistry and Physics*, 9: 2793-2803.
- Yu, H., et al. (2008), A satellite-based assessment of transpacific transport of pollution aerosol, *Journal of Geophysical Research*, 113(D14S12).
- Zeng, X., et al. (2008), Development and validation of congener-specific photodegradation model for polybrominated diphenyl ethers, *Environmental Toxicology and Chemistry*, 27(12): 2427-2435.

- Zhang, L., et al. (2008a), Transpacific transport of ozone pollution and the effect of recent Asian emission increases on air quality in North America: An integrated analysis using satellite, aircraft, ozonesonde, and surface observations, *Atmospheric Chemistry and Physics*, 8(20): 6117-6136.
- Zhang, L., et al. (2009), Intercontinental source attribution of ozone pollution at western U.S. sites using an adjoint method, *Geophysical Research Letters*, 36(L11810).
- Zhang, Y., et al. (2008b), Impacts of regional climate change on biogenic emissions and air quality, *Journal of Geophysical Research*, 113(D18310).
- Zhang, Y. (2010), Combat Air Pollution in a Changing Climate: Sciences, Modeling Tools, and Strategies, paper presented at 3rd International Conference on Environmental Technology and Knowledge Transfer (3rd ICET), Hefei, Anhui Province, China, May 13-14, 2010.

## Chapter 5

### Impacts on Health, Ecosystems, and Climate

**Lead authors:** J. Jason West, Lisa Emberson

**Contributing authors:** Elisabeth Ainsworth, Susan C. Anenberg, Steve Arnold, Mike Ashmore, Richard Atkinson, Nicolas Bellouin, Aaron Cohen, Bill Collins, Pierre Delmelle, Ruth Doherty, Nasreen Farah, Jürg Fuhrer, Kevin Hicks, Tracey Holloway, Kazuhiko Kobayashi, Junfeng Liu, Denise Mauzerall, Lina Mercado, Gina Mills, Michael Sanderson, Drew Shindell, Stephen Sitch, David Stevenson, Juha-Pekka Tuovinen, Rita van Dingenen, Jun Wang, Hongbin Yu, Christian Zdanowicz

Given the LRT of ozone ( $O_3$ ) and particulate matter (PM) discussed in previous chapters, this chapter reviews the literature on the impacts of that LRT on human health, ecosystems, and climate. Concerns over human health and ecosystems have been the major drivers for air pollution regulations. In addition,  $O_3$  and PM are important for climate, so actions to reduce emissions relevant for  $O_3$  and PM will also influence climate. Other impacts of the LRT of  $O_3$  and PM that are not addressed in this chapter include the degradation of visibility (mainly due to PM) and damage to materials [U.S. EPA, 2006; 2009b].

Figures 5.1 and 5.2 show selected Air Quality Standards (AQS) and guidelines for  $O_3$  and PM from around the world, relative to baseline levels. These standards and guidelines have been motivated to protect health, ecosystems, and visibility, although some are explicitly only motivated for health purposes. Nonetheless, research has not identified clear “threshold” concentrations of  $O_3$  or PM below which there are no adverse health effects [Krzyzanowski and Cohen, 2008; WHO, 2006] and therefore current standards do not necessarily fully protect human health. For ozone, present-day baseline concentrations approach the lowest of the air quality standards, and as shown in chapters A2 and A4, measured baseline levels for  $O_3$  have sometimes exceeded these standards.

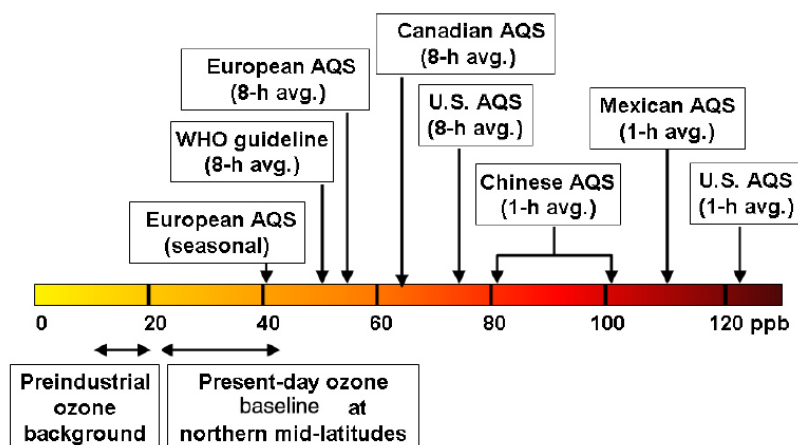


**Figure 5.1.** Ozone air quality standards in ppb for different nations, as well as international guidelines and estimates of the preindustrial background (i.e., with no anthropogenic emissions) and present-day baseline (i.e., not affected by local pollution). Note that the different standards use different averaging times and the determination of violations also differ among nations. [Reprinted with permission from Figure 2.1 in *Global Sources of Local Pollution: an Assessment of Long-Range Transport of Key Air Pollutants to and from the United States* (2010), by the National Academy of Sciences, Courtesy of the National Academies Press, Washington, D.C.]

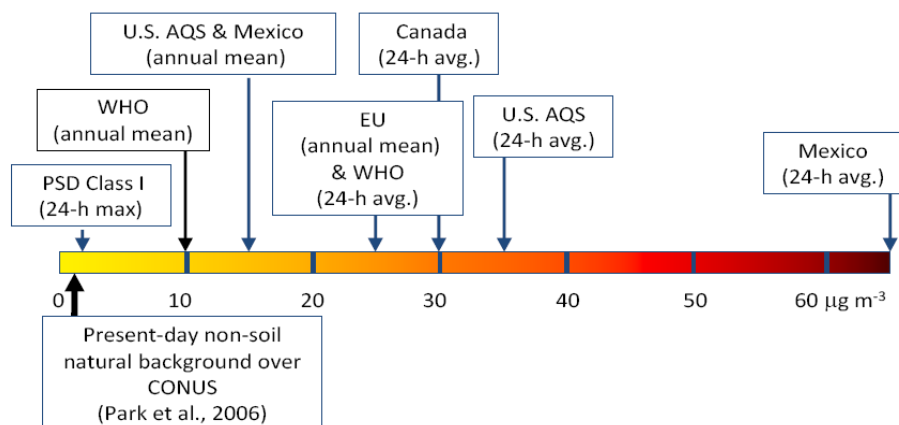


**Figure 5.2.** Current 24-hr. and annual mean  $PM_{2.5}$  standards for selected countries, and U.S. allowable 24-hr emissions increment for Class I areas under the Prevention of Significant Deterioration rule (CONUS is the continental United States). [Reprinted with permission from Figure 3.4 in *Global Sources of Local Pollution: an Assessment of Long-Range Transport of Key Air Pollutants to and from the United States* (2010), by the National Academy of Sciences, Courtesy of the National Academies Press, Washington, D.C.]

## 5.1 Impacts of Long-range Transport on Human Health

### 5.1.1. Evidence for effects of ozone and PM on human health

Over the past 20 years, evidence showing the health effects of air pollution has grown exponentially. It is now widely accepted that exposure to outdoor air pollution, a complex mixture of particles and gases, contributes to a broad range of acute and chronic health effects, ranging from minor physiological disturbances to death from respiratory and cardiovascular disease [ATS, 2000; Bascom et al., 1996a; b; Brook et al., 2010; Royal Society, 2008]. Evidence for these health effects comes in several forms. Epidemiologic studies that find statistical relationships between air pollutant concentrations and health outcomes, looking at effects over large populations, provide the strongest quantitative basis for understanding health impacts of air pollution. These studies also offer the strongest evidence that pollutants have widespread effects in a population, and the large body of epidemiologic studies has provided the foundation for establishing ambient air quality standards and policy guidelines, nationally and internationally. Based on this evidence, WHO estimated that urban outdoor  $PM_{2.5}$  caused 800,000 deaths (1.2% of all deaths) and 6.4 million years of lost healthy life globally in the year 2000. Thus, outdoor air quality ranks as the third most important environmental risk factor for mortality in the WHO Global Burden of Disease study, behind unsafe water, sanitation and hygiene, and indoor air pollution from household use of solid fuels [Cohen et al., 2004; Ezzati et al., 2004].

In addition to epidemiologic studies, other types of studies provide strong supporting evidence linking air pollutants and human health: direct human exposures under controlled conditions; laboratory exposures of rodents and other animals; and *in vitro* studies of exposure of cells and tissues to air pollutants [WHO, 2006]. In this section, we summarize the epidemiologic research on the health effects of PM and  $O_3$ , two components of air pollution mixtures with well-established adverse health effects.

Epidemiologic research plays a key role in air pollution health effects science and in policy, providing estimates of the health effects of both short- and long-term exposure to air pollution in many parts of the world. The epidemiology of air pollution takes advantage of the fact that concentrations of outdoor air pollution, and thus human exposure, vary in both time and space. Short-term temporal variation in concentrations of air pollution over days or weeks has been used to estimate effects on daily mortality and morbidity in time-series studies. They provide estimates of the proportional increase in the number of deaths brought forward in time by recent exposure. Spatial variation in long-term average concentrations of air pollution has provided the basis for cohort studies of long-term exposure. Cohort studies include not only those whose deaths were brought forward by

recent exposure to air pollution, but also those who died from chronic disease caused by long-term exposure [Künzli *et al.*, 2000]; thus, they provide a more complete estimate of the effects and, for this reason, are used to estimate public health impacts in terms of annual attributable deaths and changes in duration of survival [Brunekreef *et al.*, 2007; Pope III *et al.*, 2009]. Estimates of effect are often expressed in relative terms, either as a relative risk or as a percent increase in incidence of mortality in a study population under different exposure conditions, with the precision of the relative risk expressed as a confidence interval.

Epidemiologic studies of the health effects of outdoor air pollution are generally based on measurements of air pollution at fixed monitoring sites that have been established to ensure compliance with air quality standards. Most human populations are exposed to a complex mixture of air pollutants in a variety of indoor and outdoor environments, but studies have found that there are strong correlations between personal exposure to pollutants from outdoor sources and the concentrations measured at fixed monitoring sites [Janssen and Mehta in WHO, 2006]. Air pollutant concentrations have been measured routinely in North America and Western Europe since the 1970s; currently, these networks are extensive. Networks are more limited but expanding in Latin America and South and East Asia, but are virtually non-existent in Africa, Central Asia and the Middle East. Consequently, epidemiologic evidence for the health effects of air pollutants is most extensive in North America and Western Europe [HEI, 2004; 2010]. In epidemiologic studies the monitored levels are used either alone or as part of more complex geo-spatial models to estimate the individual exposure of study participants [Jerrett *et al.*, 2005]. Neither approach, however, is entirely accurate, and measurement error in exposure remains a concern in all epidemiologic research. Generally, such errors will be smaller for pollutants which tend to be uniformly distributed over large urban areas, and which penetrate efficiently indoors, such as fine PM produced by combustion. If the errors in the estimates of exposure are uncorrelated with the risk of the health outcome, then the estimates of relative risk attributable to air pollution will, in most cases, be too low, but the precision of relative risk estimates will be reduced [Navidi and Lurmann, 1995; Szpiro *et al.*, 2008; Zeger *et al.*, 2000].

Epidemiologic studies of the adverse health effects of outdoor air pollution are almost always observational studies. Therefore, the validity of their results requires that they account for other factors related to human health that may be correlated in space or time with exposure to air pollution and whose effects could potentially be confused with those of air pollution. Such factors, termed confounders, include season, meteorology, influenza, tobacco smoking, indoor burning of solid fuels, and access to medical care. In addition, because outdoor air pollution comprises a mixture of pollutants whose concentrations are often highly correlated, estimates of the effects of single pollutants must be interpreted with caution. Epidemiologists address these issues in either the design or the statistical analysis of study data, for example by restricting study populations to those who are unexposed to potential confounders (e.g., non-smokers) or through multivariable regression techniques [Rothman *et al.*, 2008].

**FINDING: There is broad consensus that exposure to ambient PM and ozone causes adverse health effects that range from minor sensory irritation to death.**

#### ***Health effects of particulate air pollution (PM)***

Particulate air pollution is a complex mixture whose chemical and physical characteristics vary over space and time due to different emission sources and atmospheric conditions. Small particles emitted directly into the ambient environment or formed in the atmosphere as a result of combustion or mechanical processes may be inhaled into the respiratory tract (inhalable PM or PM<sub>10</sub>). Smaller particles (respirable PM or PM<sub>2.5</sub>) may be deposited in the deep lung, potentially causing effects on the cardiovascular and other organ systems. There are a variety of potential mechanisms through which inhalable and respirable PM could cause adverse effects on the respiratory and cardiovascular systems, including via effects on neurologic, immunologic and inflammatory responses. Inflammation induced by oxidative stress has recently emerged as a possible common underlying mechanism for a variety of adverse effects of PM [WHO, 2006]. Definitive knowledge of which specific characteristics of PM<sub>10</sub> or PM<sub>2.5</sub> are responsible for effects is currently lacking, though current epidemiologic and toxicologic findings suggest that certain physical characteristics (e.g., particle size, number and surface area) and

chemical characteristics (e.g., transition metal content) may play a role [U.S. EPA, 2009b; WHO, 2006]. Because current evidence does not support species-specific PM risk characterization, air quality guidelines from WHO and national regulatory standards specify limits for undifferentiated mass concentrations of PM<sub>10</sub> or PM<sub>2.5</sub> (Figure 5.2). There is limited information on the extent to which the LRT of PM alters its toxicologic properties. One recent laboratory study reported that the toxicity of diesel emissions in mice was enhanced by exposure to sunlight and the addition of VOCs. Although aging of diesel PM appears to increase toxicity, it is currently unknown which of the reaction products are responsible, as O<sub>3</sub> also increased [Zielinska *et al.*, 2010].

Hundreds of studies of short-term exposure to air pollution and adverse health effects have been conducted in many regions of the world [WHO, 2006]. PM, measured as Total Suspended Particles (TSP), PM<sub>10</sub>, PM<sub>2.5</sub>, and Black Smoke, has been associated with increases in daily mortality rates from all natural causes, and specifically from respiratory and cardiovascular causes, hospital admissions for respiratory diseases (from all causes, chronic obstructive pulmonary disease, asthma, or pneumonia), and hospital admissions for cardiovascular diseases (from acute myocardial infarction or congestive cardiac failure [Pope III and Dockery, 2006]). Exposure to particulate air pollution has also been associated with adverse reproductive outcomes, including low birth weight and pre-term birth [Glinianaia *et al.*, 2004], and acute lower respiratory tract infections in young children [Romieu *et al.*, 2002].

Meta-analytic summaries of the results of individual studies, and coordinated multi-city studies, which apply a common analytic approach to data from multiple cities, now provide the most robust and precise estimates of the effects of short-term exposure to PM<sub>10</sub> on daily mortality (Figure 5.3). The evidence is consistent among different regions of the world with small relative increases in daily mortality rates, on the order of 0.05 and 0.1 percent increase in daily mortality per 1 µg m<sup>-3</sup> PM<sub>10</sub>. There are fewer reports for PM<sub>2.5</sub> associations. However, the available evidence from meta-analysis and multi city studies around the world are generally consistent, suggesting associations of around 0.1% per 1 µg m<sup>-3</sup> PM<sub>2.5</sub> (Table 5.1). A recent systematic review and meta-analysis by Smith *et al* [2009] assessed current evidence for health effects associated with short-term exposure to both sulphate and black carbon (indicated by black smoke) and concluded that short-term exposure time-series studies of black smoke and sulphate PM was associated with increased daily mortality (Table 5.1). For PM associations, larger relative effects tend to be seen in older people and for mortality from cardiovascular and respiratory causes.

PM transported between continents has also been associated with increases in daily mortality. A recent study in Barcelona observed increased daily mortality from all-natural causes associated with both the coarse (PM<sub>10</sub> minus PM<sub>2.5</sub>) and fine (PM<sub>2.5</sub>) PM components during Saharan dust episodes in 2003-2004 [Perez *et al.*, 2008]. Larger relative effects were reported for exposure to both fine and coarse PM on Saharan dust days versus non-Saharan dust days, but the effects were particularly increased for the coarse fraction. This was not explained by differences in chemical composition, and the authors hypothesized that unmeasured biological agents (“irritants and allergens”) might be responsible [e.g., Griffin *et al.*, 2001].

The literature on exposure to particulate air pollution and mortality in adults from chronic disease has been recently and extensively reviewed [e.g., U.K. COMEAP, 2009; U.S. EPA, 2009b; WHO, 2006]. These reviews, and other efforts specifically designed to elicit the views of the expert community on the strength of the existing scientific evidence [Cooke *et al.*, 2007; Roman *et al.*, 2008; U.K. COMEAP, 2009] support the conclusion that exposure to particulate air pollution is causally related to mortality from chronic cardiovascular and respiratory disease and lung cancer.

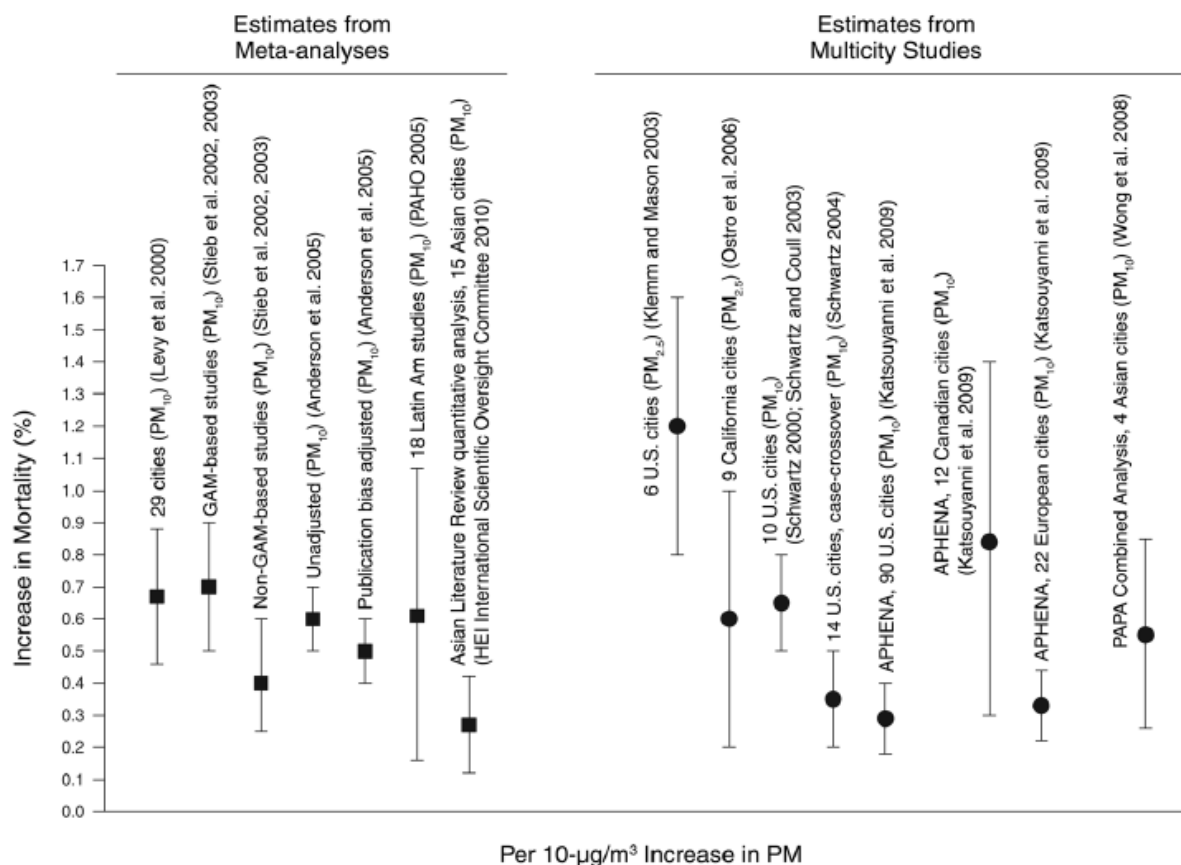


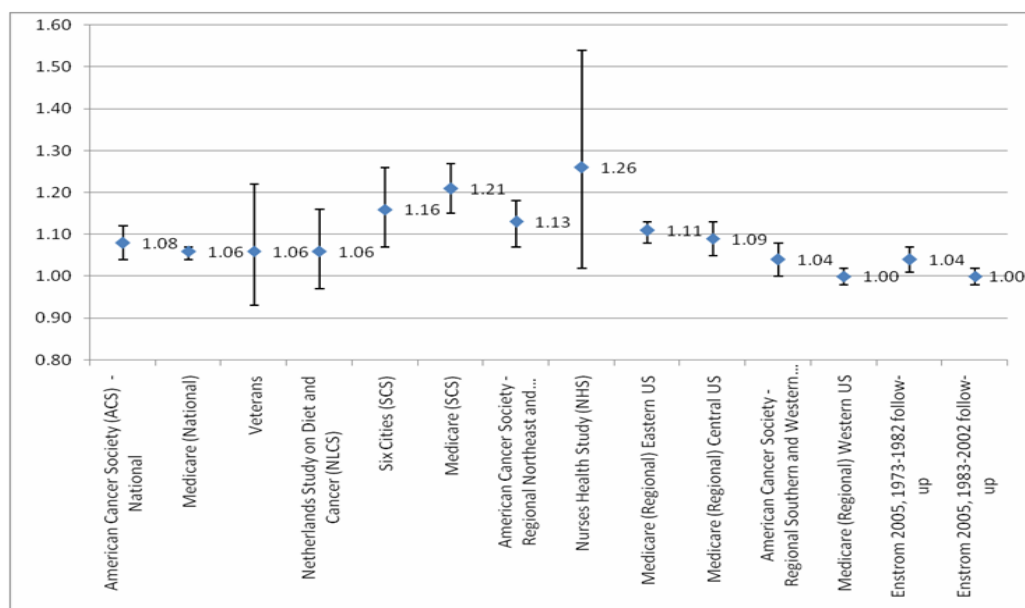
**Figure 5.3.** Estimates of the effect on all natural mortality per 10 µg m<sup>-3</sup> increase in PM reported in several recent meta-analyses and multicity studies. (APHENA = Air Pollution and Health: A European and North American Approach; GAM = generalized additive model; PAPA = Public Health and Air Pollution in Asia program). [Based in part on Katsouyanni, K., et al. (2009), *Air Pollution and Health: A Combined European and North American Approach (APHENA)*, Research Report 142, Health Effects Institute, Boston, MA.]

Although time-series studies of the effects of short-term exposure are numerous and have been conducted in most regions of the world, only nine cohort studies in the US and Europe have estimated the relationship between long-term exposure to PM<sub>2.5</sub> and mortality (Figure 5.4). No cohort studies of long-term exposure to PM<sub>2.5</sub> and mortality outside of North America and Europe have been published to-date, although, as noted above, evidence from time-series studies in other regions, such as Asia, find results that are similar to those reported in North America and European studies, as do Asian studies of chronic effects of long-term exposure on respiratory symptoms, asthma, lung cancer and adverse birth outcomes [HEI, 2010].

The largest cohort study, and the one that has been used most extensively for quantitative risk assessment, is the American Cancer Society study that relates PM<sub>2.5</sub> with risks of mortality for adults in 50 US cities. Since the original American Cancer Society study, subsequent studies have extended and reanalyzed the results [Krewski et al., 2009; Pope III et al., 1995; 2002]. Krewski et al. [2009] find results that are similar to, though generally higher than earlier analyses, reporting an increased relative risk of all cause mortality of 0.3% (95% CI of 0.1-0.5%) per 1 µg m<sup>-3</sup> PM<sub>2.5</sub>, and increases in relative risk for ischemic heart disease (1.5%, 95% CI of 1.1-2%) (Table 5.1). Smith et al. [2009] recently reviewed the evidence regarding the relative toxicity of short-lived greenhouse pollutants, black carbon and sulphate components of PM<sub>2.5</sub>, and ozone. This review included new analyses of the American Cancer Society cohort and concluded that although it was difficult to draw firm conclusions regarding the relative toxicity of the three pollutants, sulphate particles “seem[ed] to have the most robust effects in multi-pollutant models” (Table 5.1).



A



B

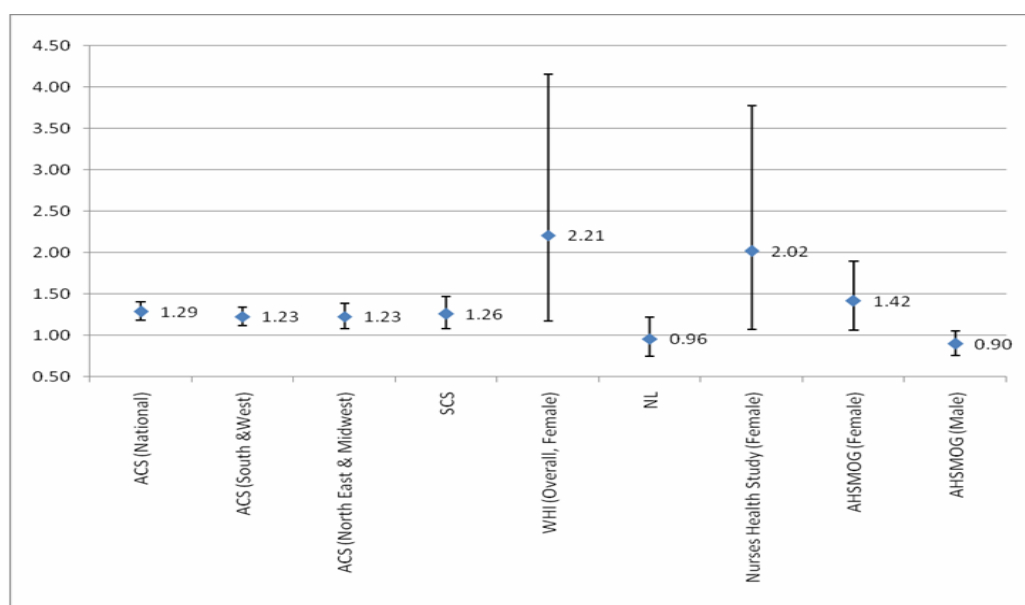


**Figure 5.4.** Relative risk (95% CIs) of mortality from (A) all-natural causes and (B) ischemic heart disease per  $10 \mu\text{g m}^{-3}$   $\text{PM}_{2.5}$  from current U.S. and European cohort studies. Based on on-going work of the Global Burden of Disease, Outdoor Air Pollution Expert Group, <http://www.globalburden.org/>.

Long-term reductions in ambient levels of PM have been associated with reduced mortality rates and improved life-expectancy in the US [Laden *et al.*, 2006; Pope III *et al.*, 2009]. More rapid changes in air pollutant concentrations, including the closing of industrial facilities [Pope III *et al.*, 1992], reductions in residential coal burning [Clancy *et al.*, 2002], and restrictions on the sulphur content of fuel [Hedley *et al.*, 2002] have also been associated with reduced mortality from cardiovascular and respiratory disease.

**Table 5.1.** Results from selected cohort and time series studies of PM and human mortality

<i>Study</i>	<i>Outcome</i>	<i>Risk estimate</i> <sup>1</sup>	<i>95% Confidence Interval</i>
<b>PM<sub>2.5</sub></b>			
<i>Cohort studies</i>			
American Cancer Society; Krewski et al. [2009]	All causes	0.3	(0.1 to 0.5)
American Cancer Society; Krewski et al. [2009]	Ischaemic Heart Disease	1.5	(1.1 to 2.0)
<i>Time series studies</i>			
Single-city estimates (n=42); Smith et al. [2009]	All causes	0.10	(0.08 to 0.13)
Multi-city studies			
10 Canadian cities; Brook et al. [2007]	All causes	0.11	(0.01 to 0.21)
25 US Communities; Franklin et al. [2008]	All causes	0.07	(0.04 to 0.11)
5 Australian cities; Simpson et al. [2005]	All causes	0.90	(-0.70 to 2.53)
9 French cities; Blanchard et al. [2008]	All causes	0.16	(0.08 to 0.24)
<b>Sulfate particles</b>			
<i>Time series studies</i>			
Single city estimates (10 studies); Smith et al. [2009]	All causes	0.21	(0.11 to 0.30)
<i>Cohort studies</i>			
American Cancer Society; Smith et al. [2009]	All causes	1.07	(0.73 to 1.40)
American Cancer Society; Smith et al. [2009]	Cardiopulmonary	1.51	1.01 to 2.01)
<b>Carbon</b>			
<i>Time series studies (Black Smoke)</i>			
Single city estimates (25 studies) Smith et al. [2009]	All causes	0.05	(0.03 to 0.07)
<i>Cohort studies (Elemental Carbon)</i>			
American Cancer Society; Smith et al. [2009]	All causes	2.11	(-2.44 to 6.89)
American Cancer Society; Smith et al. [2009]	Cardiopulmonary	2.09	(-4.53 to 9.18)

<sup>1</sup> Percent per increment of 1  $\mu\text{g m}^{-3}$  in pollutant

As noted above, short-term exposure to coarse PM has been associated with increased daily mortality. However, there is currently little evidence for a relationship between *long-term* exposure to coarse PM and annual average mortality. Two large cohort studies of women reported no evidence of an effect [Miller et al., 2007; Puett et al., 2008]. A smaller cohort study reported increased mortality in women (but not men), but the results were inconsistent across a range of statistical models [Chen et al., 2005]. The effects of long-term exposure to PM on mortality from chronic cardiovascular and respiratory disease have only been studied over the range of ambient concentrations that exist in the US and Western Europe: approximately 5–30  $\mu\text{g m}^{-3}$ . Over that range the concentration-response relationship appears to be both linear and monotonic [Krewski et al., 2009]. Because no cohort studies of mortality have been conducted in Asia or other regions with higher annual average PM concentrations, the concentration-response function at those higher levels is currently unknown. This contributes considerable uncertainty to global quantitative risk assessments of air pollution [Anenberg et al., 2010; Cohen et al., 2004], including the assessments of impacts of LRT in Section 5.1.2. Additional sources of uncertainty in such risk assessments include uncertainties in the baseline rates of mortality and levels of exposure to PM in many low- and middle- income countries (see Section 5.1.4).

**FINDING: Short-term exposure to PM is associated with increased daily mortality and morbidity in hundreds of studies worldwide; long-term exposure to PM<sub>2.5</sub> is associated with**

**increased mortality from chronic cardiovascular and respiratory disease in multiple studies. Adverse effects appear to extend linearly to levels below current air quality standards with no evidence of a threshold. Although ambient air pollution is a complex mixture, most assessments of the public health impacts of ambient air pollution have focused on PM, because of the strength and consistency of the evidence for PM. Current impact estimates are subject to considerable uncertainty due to lack of information on the concentration-response function for PM and mortality in the most highly polluted regions.**

### *Health effects of ozone*

The adverse effects of both short- and long-term exposure to O<sub>3</sub> are well-documented and have been recently reviewed [U.S. EPA, 2006; WHO, 2006]. Experimental evidence from studies in humans and animals indicates that short-term exposure causes the exacerbation of existing lung diseases, and toxicologic and epidemiologic studies indicate that long-term exposure can produce irreversible changes in the lung structure and function.

Ground-level O<sub>3</sub> is formed by the chemical reaction between NO<sub>x</sub> and VOCs in the presence of sunlight; so ambient concentrations and human exposure, are typically higher in warm seasons. Experimental studies in animals designed to simulate these conditions appear to indicate cumulative impacts of seasonal exposure, and long-term exposure to high seasonal levels of O<sub>3</sub> have been associated with reduced lung function growth in children [Gauderman *et al.*, 2000; 2002; Rojas-Martinez *et al.*, 2007].

Daily time series studies of O<sub>3</sub> and mortality have shown consistent adverse health effects. These include many single-city studies which have then been analyzed in meta-analyses [Anderson *et al.*, 2004; Bell *et al.*, 2005; Ito *et al.*, 2005; Levy *et al.*, 2005; Thurston and Ito, 2001] and large multi-city studies [Bell *et al.*, 2004; Gryparis *et al.*, 2004; Katsouyanni *et al.*, 2009] (Table 5.2). These results also illustrate the variability in the size and precision of effect estimates observed in different studies. The recent APHENA study, a multi-city study of over 100 cities in North America and Europe [Katsouyanni *et al.*, 2009], estimated that all-cause mortality increased by 0.52% for a 10 ppb increase in O<sub>3</sub> across the two continents, with considerably larger values and imprecision for Canadian studies. Adverse health effects of O<sub>3</sub> on mortality have also been observed at concentrations below current air quality guidelines. If a threshold exists, a concentration below which ozone has no measurable effects, then it is likely at concentrations below the current air quality standards [Bell and Dominici, 2006; Gryparis *et al.*, 2004; Katsouyanni *et al.*, 2009; U.S. EPA, 2006].

There is currently limited evidence that long-term exposure to O<sub>3</sub> causes increased mortality from chronic cardiovascular or respiratory disease. Recently, however, Jerrett *et al.* [2009] reported an association between long-term exposure to O<sub>3</sub> and respiratory mortality in the American Cancer Society cohort (Table 5.2). A 10 ppb increase in O<sub>3</sub> is associated with a 4% (95% confidence interval, 1.3-6.7%) increase in relative risk of mortality from non-malignant respiratory disease. This study, however, did not detect an increase in cardiovascular mortality that could be attributed to O<sub>3</sub> independent of the influence of PM<sub>2.5</sub>. An earlier study had reported increased respiratory mortality associated with long-term exposure to O<sub>3</sub> with more pronounced increases in men than women [Abbey *et al.*, 1999]. Given well-documented acute and chronic effects of exposure to O<sub>3</sub> on the respiratory system, these associations seem plausible.

**FINDING: Short-term exposure to ozone is associated with increased daily mortality and morbidity in many studies worldwide. However, the current evidence linking long-term exposure to ozone with mortality from cardiovascular and respiratory disease is limited. Adverse effects appear to extend linearly to levels below current air quality standards with no evidence of a threshold.**

**Table 5.2.** Results from selected cohort and time series studies of ozone and human mortality

<i>Study</i>	<i>Outcome</i>	<i>Risk estimate<sup>1</sup></i>	<i>95% Confidence Interval</i>
<i>Cohort studies</i>			
American Cancer Society; Jerrett et al. [2009]	All causes	0.1	(-0.4 to 0.7)
	Cardiovascular	1.1	(0.3 to 2.3)
	Respiratory	2.9	(1.0 to 4.8)
<i>Time series studies<sup>2</sup></i>			
<b>Multi-city studies</b>			
95 US urban communities; Bell [2004]	All causes	0.52	(0.27 to 0.77)
23 European cities; Gryparis et al. [2004]	All causes	0.06	(-0.36 to 0.42)
APHENA (Canada, US, Europe); Katsouyanni et al. [2009]	All causes	0.52	(0.30 to 0.74)
<b>Meta-analysis (24-hr)</b>			
Thurston & Ito [2001]	All causes	0.89	(0.56 to 1.22)
Stieb et al [2003]	All causes	1.12	(0.32 to 1.92)
Levy et al [2001]	All causes	0.98	(0.59 to 1.58)
Anderson et al [2004]	All causes	1.11	(0.55 to 1.67)
Bell et al [2005]	All causes	0.87	(0.55 to 1.18)

1 Percent per increment of 10 ppb in ozone

2 Results are for daily mean ozone concentration except Gryparis et al. [2004] where the daily 8-hr maximum is used

### ***Evidence for interaction between PM and ozone***

Although air pollution is always present as a complex mixture of particles and gases, the overwhelming majority of studies have estimated the effects of single pollutants, sometimes controlling analytically for the effects of other pollutants. Few studies have explored whether the effects of specific components of the mixture enhance or suppress the effects of others, and as a result, there is relatively little information about whether the health effects of exposure to PM or O<sub>3</sub> are dependent on the co-existing levels of the other pollutants in space or time. The APHENA study [Katsouyanni et al., 2009], which analyzed data from over 120 major cities in Europe and North America, observed that in the US cities with higher levels of O<sub>3</sub>, the effects of short-term exposure to PM<sub>10</sub> on daily mortality among the elderly (>=75 yr.) were smaller. However, a study in Shanghai reported that the percent increase in daily mortality associated with PM<sub>10</sub> was increased at higher levels of O<sub>3</sub> and that the effect of O<sub>3</sub> was increased at higher levels of PM<sub>10</sub> [Chen et al., 2005]. Katsouyanni et al. [2009] also reported that the effects on daily mortality of short-term exposure to PM<sub>10</sub> were greater at higher levels of NO<sub>2</sub> (an ozone precursor) and when the NO<sub>2</sub>/PM<sub>10</sub> ratio was higher, a pattern more pronounced in Europe than the US.

#### ***5.1.2. Quantified influences of long-range transport on human health***

Although the influence of particular emission sources on atmospheric concentration is generally greatest near those sources, LRT influences pollutants far downwind. As pollutants move to downwind regions and continents, much larger populations may be exposed to this change in concentration. The total risks for human health in downwind continents may be comparable to the risks within the source continent, even if the effects on the concentrations that people breathe are much smaller [e.g., Anenberg et al., 2009].

Several studies have specifically modelled the LRT of O<sub>3</sub> and PM, and have estimated the effects of this LRT on premature mortality. These several studies have all used similar methods, and uncertainties in these methods should be addressed in future research. First, all studies used global

CTMs to represent LRT. While these coarse resolution CTMs (typically 200 km in horizontal resolution) are necessary to represent LRT, their use for health impact analysis may cause uncertainties in concentrations and exposures near urban regions, where there are strong gradients in population density and pollutant concentrations and urban chemistry may modify the effects of LRT (Chapter A4). Second, all studies apply concentration-response relationships from epidemiological studies in industrialized nations to the rest of the world. While some studies in developing nations suggest that the same relationships may hold, the body of evidence is weaker. These uncertainties can be reduced when considering cause-specific mortalities and when using appropriate baseline mortality rates based on observed disease incidence in different world regions. Therefore, while epidemiological studies provide strong evidence for quantifying health impacts, and while it is common to use regional CTMs to drive health impact analyses within North America or Europe, the use of global CTMs for global health impact analyses should be a focus of future research to improve methods [NRC, 2010]. Recommendations to resolve these uncertainties are in Section 5.1.4.

**FINDING: LRT of ozone and PM can have widespread effects on human health in other continents, as the combined populations of affected regions are likely greater than that of the source region.**

#### *Impacts of the long-range transport of ozone on premature mortality*

Modelled contributions of LRT to O<sub>3</sub> concentrations have been shown to be significant causes of premature mortality. Anenberg et al. [2009] modelled the effects of intercontinental O<sub>3</sub> from the HTAP SR6 model simulations, in which anthropogenic emissions of NO<sub>x</sub>, non-methane volatile organic compounds (NMVOCs), and carbon monoxide (CO) were reduced by 20% from each of the four HTAP source regions (see Chapter A4). Avoided premature cardiopulmonary mortalities were calculated for the multi-model mean change in O<sub>3</sub>, as shown in Table 5.3 and Figure 5.5. Changes in emissions from any of the four regions have widespread effects throughout the Northern Hemisphere, influencing mortality in population centres on other continents.

When the influences of all four source regions are combined, foreign emissions contribute roughly 30%, 30%, 20% and >50% to the avoided mortalities in the receptor regions NA, EA, SA, and EU (Table 5.3). In particular, EU is shown to be influenced strongly by emissions from NA. The reductions in emissions in NA and EU are estimated to cause more avoided mortalities outside of these source regions than within, due to the large populations affected in downwind regions. In addition, many CTMs show small decreases in local O<sub>3</sub> within parts of the NA and EU source regions, due to nonlinear chemical processes, which contributes to the small numbers of avoided mortalities in these regions relative to the whole hemisphere.

Anenberg et al. [2009] also found that for some source-receptor pairs, the uncertainty in the avoided premature mortalities associated with the modelled O<sub>3</sub> responses is greater than the uncertainty caused by the health impact function parameters (Figure 5.6), although neither the range of CTM responses nor the confidence intervals on relative risk fully reflect the total uncertainty. In particular, the several models analyzed showed a large discrepancy in the response of O<sub>3</sub> to changes in precursor emissions within the source region. The uncertainties in source-receptor responses were large enough to change the conclusions above about the relative numbers of avoided mortalities within versus outside of the source regions.

**FINDING: For ozone, one study based on the HTAP multi-model comparison found that ozone resulting from emissions from foreign regions is estimated to contribute 20% to >50% of ozone mortalities, subject to large uncertainty.**

The finding that O<sub>3</sub> precursor reductions in NA and EU cause more avoided mortalities outside of the source regions than within is supported by Duncan et al. [2008] and West et al. [2009]. Duncan et al. [2008] modelled the full contribution of European emissions on nearby regions by removing anthropogenic emissions from Europe. They found that Europe has a large impact on surface O<sub>3</sub> concentrations in Northern Africa, the Middle East, and the Former Soviet Union, and smaller influences elsewhere in the Northern Hemisphere. While O<sub>3</sub> caused by European emissions

causes ~18,000 annual premature mortalities within Europe, Duncan et al. [2008] find a total of ~51,000 mortalities in the Northern Hemisphere.

**Table 5.3.** Annual avoided premature cardiopulmonary mortalities (hundreds) following 20% NO<sub>x</sub>, NMVOC, and CO emission reductions in each region, for the HTAP SR6 multi-model mean (relative to SR1), assuming no concentration threshold (italics) and assuming a concentration threshold of 35 ppb (normal font). Confidence intervals (95%) reflect uncertainty in the CRF only. [Reprinted with permission from Table 2 in Anenberg, S., et al. (2009), Intercontinental impacts of ozone pollution on human mortality, *Environmental Science and Technology*, 43(17): 6482-6487. Copyright 2009 American Chemical Society.]

Source Region	Receptor Region				
	NA	EA	SA	EU	NH
NA	<i>9 (4 - 13)</i>	<i>7 (3 - 10)</i>	<i>6 (3 - 9)</i>	<i>11 (5 - 17)</i>	<i>36 (18 - 55)</i>
	9 (4 - 14)	4 (2 - 6)	5 (3 - 8)	6 (3 - 9)	27 (13 - 41)
EA	<i>2 (1 - 3)</i>	<i>43 (21 - 66)</i>	<i>6 (3 - 9)</i>	<i>5 (3 - 8)</i>	<i>59 (29 - 91)</i>
	1 (1 - 2)	40 (19 - 61)	5 (2 - 8)	3 (1 - 4)	49 (24 - 76)
SA	<i>1 (0 - 1)</i>	<i>4 (2 - 6)</i>	<i>76 (37 - 117)</i>	<i>2 (1 - 3)</i>	<i>85 (41 - 130)</i>
	0 (0 - 1)	3 (1 - 4)	66 (32 - 101)	1 (0 - 2)	71 (34 - 108)
EU	<i>2 (1 - 3)</i>	<i>8 (4 - 12)</i>	<i>6 (3 - 10)</i>	<i>17 (8 - 26)</i>	<i>38 (18 - 58)</i>
	1 (0 - 1)	6 (3 - 8)	6 (3 - 9)	25 (12 - 38)	40 (19 - 61)

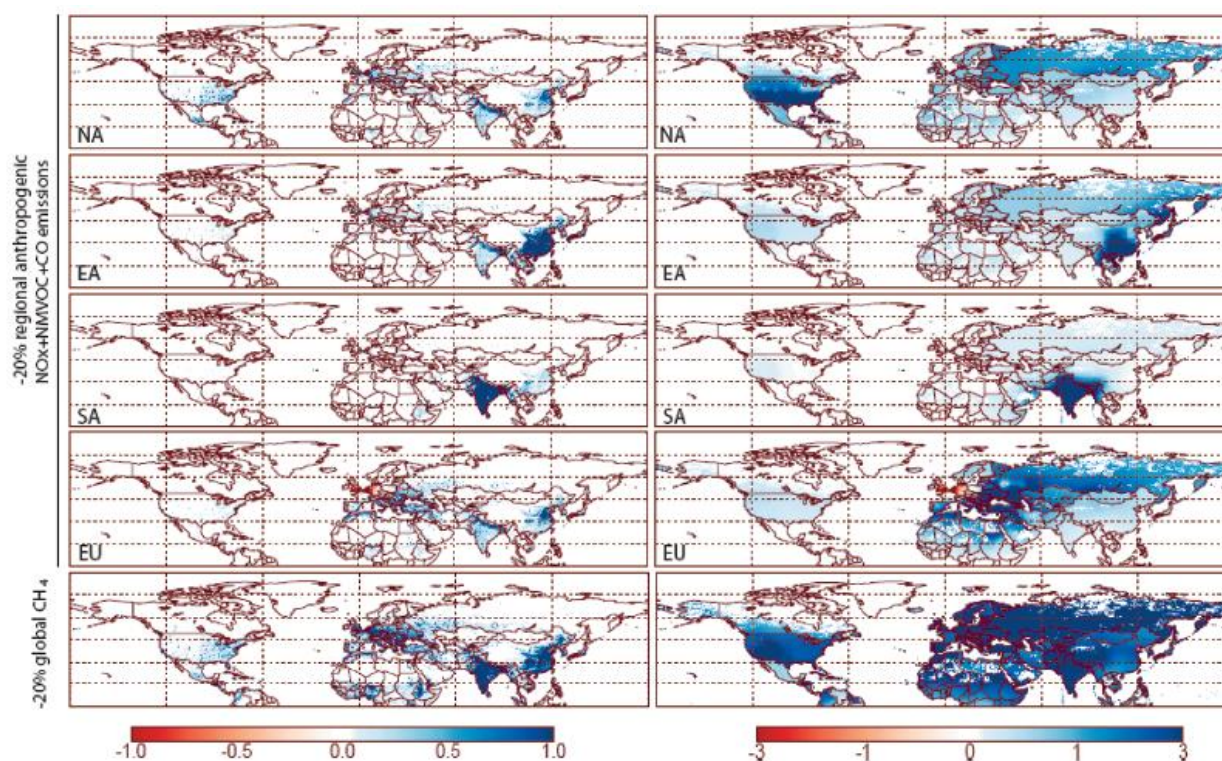


**Figure 5.5.** Annual avoided premature cardiopulmonary mortalities per 1,000 km<sup>2</sup> (left) and per million people (right) resulting from 20% NO<sub>x</sub>, NMVOC, and CO emission reduction in the region shown and a 20% global methane mixing ratio reduction, assuming no low-concentration threshold. [Reprinted with permission from Figure 1 in Anenberg, S., et al. (2009), Intercontinental impacts of ozone pollution on human mortality, *Environmental Science and Technology*, 43(17): 6482-6487. Copyright 2009 American Chemical Society.]



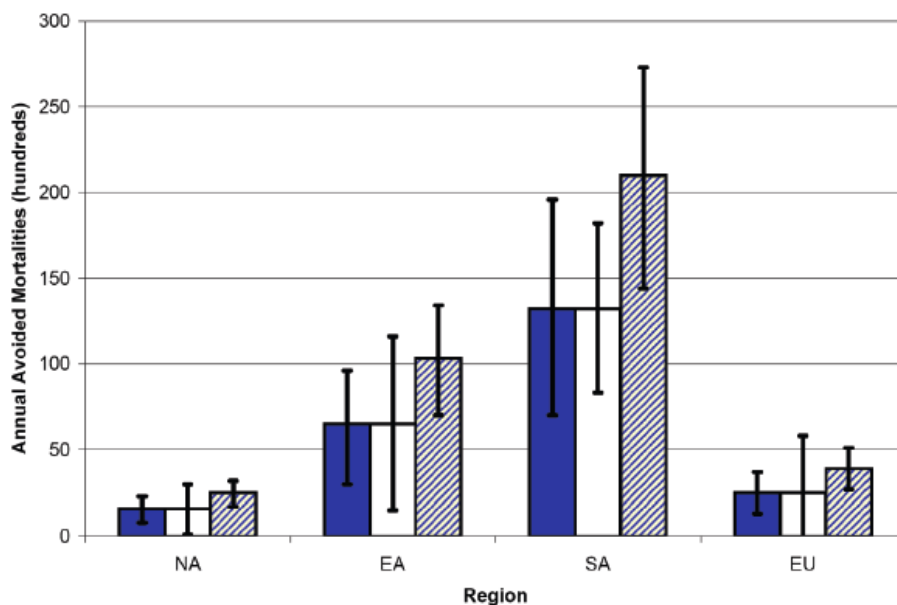


**Figure 5.6.** Annual avoided premature nonaccidental mortalities (hundreds) in each region from 20% NO<sub>x</sub>, NMVOC, and CO emission reductions in the same region using the concentration-response function (CRF) and confidence interval (95%) from Bell et al. [2004] (solid bars), using the CRF from Bell et al. [2004] and confidence intervals (68%) from  $\pm 1$  standard deviation of the model ensemble O<sub>3</sub> perturbation in each grid cell [Fiore et al., 2009] (white bars), and using the mean and confidence intervals (95%) of the CRFs from three meta-analyses of O<sub>3</sub> mortality [Bell et al., 2005; Ito et al., 2005; Levy et al., 2005] (striped bars). [Reprinted with permission from Figure 2 in Anenberg, S., et al. (2009), Intercontinental impacts of ozone pollution on human mortality, *Environmental Science and Technology*, 43(17): 6482-6487. Copyright 2009 American Chemical Society.]

West et al. [2009] analyzed 10% reductions in anthropogenic NO<sub>x</sub> emissions from each of nine world regions, and 10% combined reductions of O<sub>3</sub> precursors from three world regions. Reductions in emissions from North America and Europe each caused more avoided mortalities outside of these source regions than within, for the NO<sub>x</sub> reductions, combined O<sub>3</sub> precursor reductions, and for short-term and steady-state results. The same was also true for NO<sub>x</sub> reductions from the Former Soviet Union. In analyzing the changes in long-term O<sub>3</sub> via methane, NO<sub>x</sub> reductions in one hemisphere were estimated to increase O<sub>3</sub> and premature mortalities in the opposite hemisphere, as NO<sub>x</sub> reductions increase the lifetime of methane (see Chapter A4). In fact, the NO<sub>x</sub> reduction in Australia was found to cause a net increase in mortality, as the long-term increase in O<sub>3</sub> in the Northern Hemisphere was shown to dominate (Figure 5.7).

Reductions in global methane emissions and impacts on O<sub>3</sub> and health have also been estimated by West et al. [2006] and Anenberg et al. [2009]. For the HTAP SR2 simulations, a 20% decrease in the global methane mixing ratio was shown to result in 16,000 avoided premature cardiopulmonary mortalities annually in the Northern Hemisphere, with the greatest numbers in highly populated regions [Anenberg et al., 2009]. These results agree roughly with those of West et al. [2006], after accounting for differences in study design, who found that a 20% decrease in global anthropogenic methane emissions (in 2010) would result in ~30,000 avoided premature mortalities in 2030 globally, and ~370,000 accumulated over the period 2010-2030. These benefits of avoided mortalities exceed the marginal costs of methane reduction using known technologies, depending on the valuation of mortalities, and can justify the 20% methane reduction without considering non-health benefits of reduced O<sub>3</sub> and decreased climate change (see Section 5.3) [West et al., 2006].



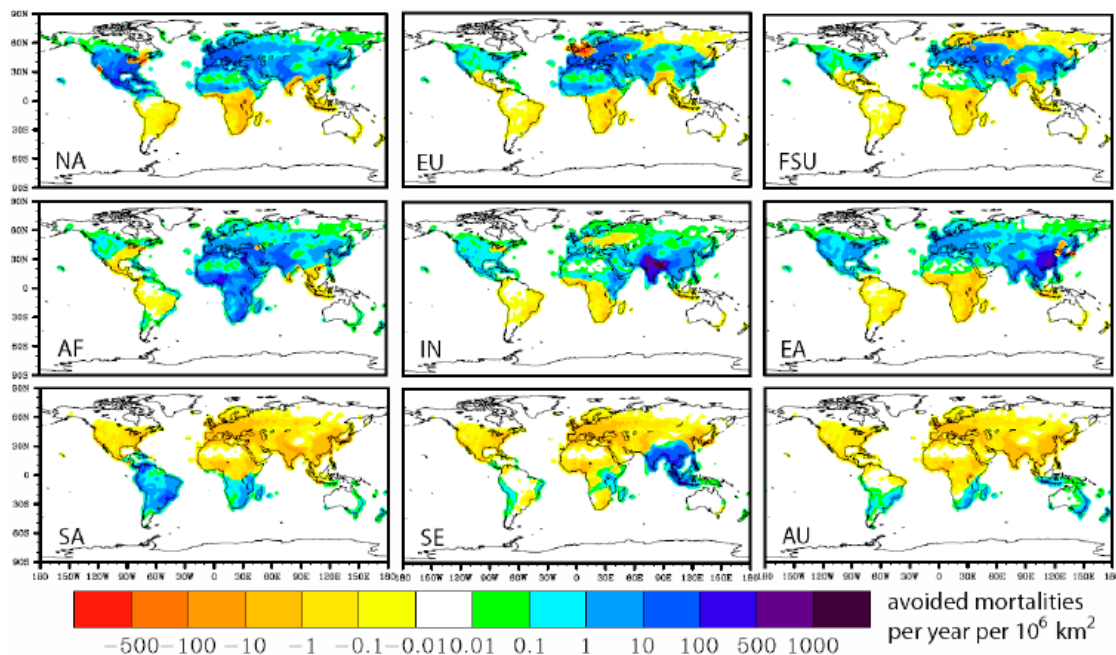


**Figure 5.7.** Annual avoided premature mortalities from 10% anthropogenic NO<sub>x</sub> reductions in each of nine world regions, at steady state and using a low-concentration threshold of 25 ppb. [Reprinted from Figure 3 in West, J. J., et al. (2009), Effect of regional precursor emission controls on long-range ozone transport - Part 2: Steady-state changes in ozone air quality and impacts on human mortality, *Atmospheric Chemistry and Physics*, 9(16): 6095-6107.]

All of the studies of O<sub>3</sub> mortality described here use the same daily time series study [Bell *et al.*, 2004] to give the concentration-response function, and comparable but not identical population and baseline mortality rates, but make different assumptions about a low-concentration threshold, below which changes in O<sub>3</sub> are assumed to have no effect on premature mortality, and may report results for total (non-accidental) mortality or for cardiovascular and respiratory mortality. More recent findings suggest that O<sub>3</sub> may influence chronic mortality to a greater extent than is represented by the daily time series studies [Jerrett *et al.*, 2009]; were these studies to be reproduced with new concentration-response functions, the total avoided mortalities would likely be greater, but the relative importance of source-receptor pairs would not be likely to change.

**FINDING: Three studies have estimated that reductions in ozone precursor emissions may avoid more premature mortalities outside of some source regions than within, mainly because of larger populations outside of those source regions.**

***Impacts of the long-range transport of PM on premature mortality***

LRT of PM can adversely impact public health in downwind regions. In Chapter A4, source-receptor relationships for aerosols were presented, based on the HTAP SR6 multi-model experiments. A new analysis conducted for this report examined the impacts of these source-receptor relationships on premature mortality. Mortalities were calculated using the median annual average surface PM<sub>2.5</sub> (taken as the sum of black carbon (BC), polycyclic/particulate organic matter (POM), and sulphate (SO<sub>4</sub>)) response from the multi-model SR6 simulations of regional 20% primary PM and PM precursor emissions reductions, and using the long-term concentration-response factor from Krewski *et al.* [2009] for adults age 30+. The same concentration-response factor is assumed to apply to all chemical components of PM<sub>2.5</sub>. Methods for estimating mortalities and baseline mortality rates are comparable to those used previously for ozone [Anenberg *et al.*, 2009].

The results show that every region is influenced most by its own emissions (Table 5.4). In contrast to O<sub>3</sub>, the large majority of mortalities in each receptor region is due to emissions from within that region, with only 3-5% resulting from emissions in the three other regions. This finding for

mortality is consistent with the findings in Chapter A4 that the import sensitivities for PM are less than that for O<sub>3</sub>.

**Table 5.4.** Annual avoided premature cardiopulmonary and lung cancer mortalities (in hundreds) due to 20% reductions in primary PM<sub>2.5</sub> and PM precursor emissions in each region, assuming no concentration threshold and assuming a low-concentration threshold of 5.8 µg m<sup>-3</sup> (*italics*). Confidence intervals (95%) reflect uncertainty in the CRF only.

Source Region	Receptor Region				
	NA	EA	SA	EU	World
NA	103 (76-130)	4 (3-5)	2 (1-2)	10 (7-12)	121 (90-152)
	<i>71 (52-89)</i>	<i>4 (3-5)</i>	<i>2 (1-2)</i>	<i>8 (6-10)</i>	<i>84 (62-105)</i>
EA	2 (1-2)	941 (715-1161)	5 (4-6)	4 (3-4)	958 (727-1182)
	<i>1 (1-1)</i>	<i>926 (703-1142)</i>	<i>5 (4-6)</i>	<i>3 (2-4)</i>	<i>935 (710-1154)</i>
SA	0 (0-0)	8 (6-10)	442 (342-541)	1 (1-1)	455 (351-556)
	<i>0 (0-0)</i>	<i>8 (6-10)</i>	<i>428 (330-523)</i>	<i>1 (1-1)</i>	<i>437 (337-534)</i>
EU	2 (1-2)	16 (12-20)	14 (11-17)	364 (256-451)	413 (313-511)
	<i>1 (1-1)</i>	<i>16 (12-20)</i>	<i>11 (9-14)</i>	<i>293 (221-362)</i>	<i>321 (243-398)</i>

While PM has lower import sensitivities than O<sub>3</sub>, its concentration-response factor for human mortality is also stronger. Consequently, the total mortalities avoided by 20% emission reductions are much greater for PM, with most of those benefits realized within the source regions. We find that the inter-continental influences on mortality are comparable for PM and O<sub>3</sub>; inter-continental O<sub>3</sub> mortalities in Table 5.3 are greater for O<sub>3</sub> for most source-receptor pairs, but are greater for PM for pairs not separated by an ocean – EU on EA, EU on SA, and SA on EA. Because of the large uncertainties in atmospheric modelling (including the fact that we do not account for all components of PM) and in applying concentration-response functions globally, and because of new findings suggesting chronic mortality effects of O<sub>3</sub> [Jerrett *et al.*, 2009], we conclude that the influences of LRT on human mortality are comparable for O<sub>3</sub> and PM.

Among the source regions, the 20% reduction in EU has the largest impact on the other three regions (~3,200 premature mortalities annually), while the reduction in EA causes the greatest overall decrease in mortality (~96,000) due to the large population density and high PM concentrations. Of the total avoided mortalities from the emissions in EA and SA, only 2% and 3% result outside of those source regions, while 15% and 12% occur outside of NA and EU due mainly to smaller populations within those source regions. In total, transport of PM from the four HTAP regions is estimated to result in ~9,600 avoided mortalities annually (for the 20% reductions).

Since the PM<sub>2.5</sub> concentration-response factor from Krewski *et al.* [2009] was based on concentrations ranging from 5.8-30 µg m<sup>-3</sup>, effects of PM<sub>2.5</sub> on mortality outside of that range are unknown. Applying a high-concentration threshold of 30 µg m<sup>-3</sup>, above which additional PM<sub>2.5</sub> is assumed to have no additional impact on health, has no impact on these results, since modelled annual average concentrations for all scenarios are below the threshold. However, applying a low-concentration threshold of 5.8 µg m<sup>-3</sup> causes the estimated avoided mortalities to decrease. The low-concentration is much more important for the receptor regions NA and EU (32% and 20% reductions) than for EA and SA, since PM concentrations are generally lower and therefore more frequently below the threshold. Here, the definition of PM<sub>2.5</sub> includes only BC, POM, and SO<sub>4</sub>, and inclusion of

dust, nitrates, and other PM<sub>2.5</sub> components would likely raise concentrations in many cases to above the low-concentration threshold, reducing the impact of the threshold on estimated mortalities.

Related studies by Liu et al. [2009a; 2009b] tracked the intercontinental transport of PM<sub>2.5</sub> by tagging aerosols (including sulphate, black carbon, organic carbon, and mineral dust) originating from 10 continental regions in year 2000, and quantified the global impact of this transport on premature mortality. They found that the simulated annual mean population-weighted concentrations of total PM<sub>2.5</sub> were highest in East Asia (EA, 30 µg m<sup>-3</sup>) and lowest in Australia (3.6 µg·m<sup>-3</sup>). The global annual premature mortalities (for adults over age 30) due to inter-continental transport of PM<sub>2.5</sub> were nearly 380,000 in 2000 (95% confidence interval of 68,000-910,000). Figure 5.8a shows that approximately half of these deaths occurred in the Indian subcontinent (IN), mostly due to dust aerosols transported from Africa and the Middle East (ME). Dust is the dominant component of PM<sub>2.5</sub> transported between continents and approximately 290,000 deaths globally were associated with exposure to foreign (i.e., originating outside a receptor region) dust PM<sub>2.5</sub>. Intercontinental transport of non-dust aerosols accounted for nearly 90,000 deaths in 2000. As shown in Figure 5.8b, more than half of the premature mortalities associated with foreign non-dust aerosols are due to aerosols originating from Europe, ME and EA; and nearly 60% of the 90,000 deaths occur in EA, IN, and Southeast Asia. These estimates are substantially greater than those in Table 5.4 (after multiplying by five because of the 20% reduction) mainly because of the inclusion of natural dust emissions.

Influence potentials (IPs), which quantify the human exposure that occurs in a receptor region as a result of a unit of emissions from a source region, were developed in Liu and Mauzerall [2007]. Inter-continental IPs are usually less than domestic IPs by 1–3 orders of magnitude. They found high influence potentials connecting Eurasian regions with Africa (Figure 5.9), and found that NA is impacted less by foreign PM<sub>2.5</sub> than are receptors in Eurasia. However, in 2000 nearly 6,600 premature deaths in North America (NA) were associated with exposure to foreign PM<sub>2.5</sub> (5,500 from dust PM<sub>2.5</sub>) [Liu et al., 2009b].

The conclusion that PM causes most mortalities domestically was supported by Saikawa et al. [2009], who analyzed the effect of China's emissions of SO<sub>2</sub>, SO<sub>4</sub>, organic carbon (OC) and BC on PM concentrations and mortality in 2000 and for three emission scenarios in 2030. In 2000, aerosols from Chinese emissions were estimated to have caused approximately 470,000 premature deaths in China and an additional 30,000 deaths globally. In 2030, aggressive emission controls were found to reduce premature deaths in China by half (relative to 2000) and to 10,000 elsewhere, while under a high emissions scenario premature deaths increased 50% in China and to 40,000 elsewhere [Saikawa et al., 2009].

Finally, Corbett et al. [2007] used similar methods to model the contribution of ship emissions to global PM<sub>2.5</sub> concentrations and related premature mortalities. They estimated that ~60,000 cardiovascular and lung cancer mortalities can be attributed to ship emissions annually, with most of these mortalities near the coastlines of Europe, East Asia, and South Asia.

**FINDING: Intercontinental transport of PM is estimated to cause human mortalities that are comparable to those estimated for ozone, due to the stronger relationships between PM and mortality, and despite the smaller fraction of PM being transported between continents. A large majority (>80%) of the health benefits of reductions in PM are expected to be realized within the source continent.**

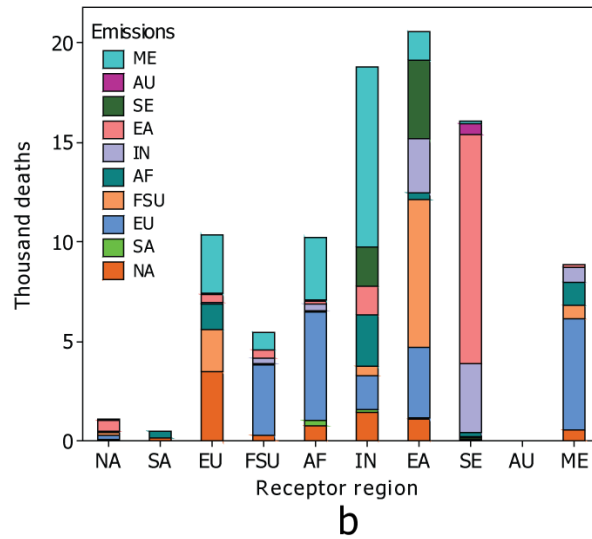
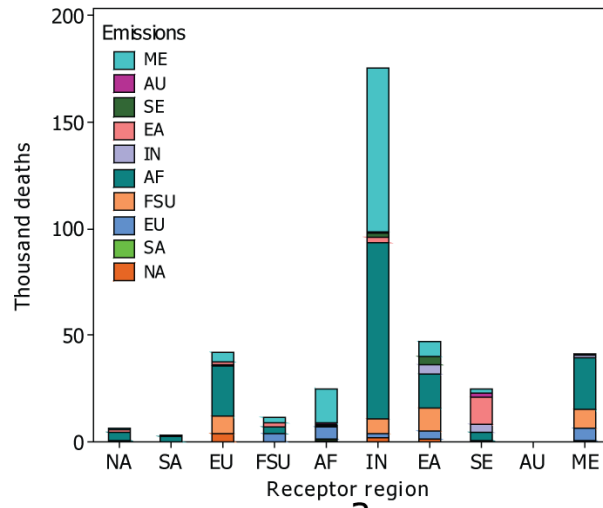


**Figure 5.8.** Annual adult (age 30 and over) premature mortalities in each receptor region associated with inter-continental transport of (a) fine aerosols (PM<sub>2.5</sub>) (b) non-dust aerosols from the nine other source regions. [Reprinted from Figure 2 in Liu, J., et al. (2009a), Evaluating inter-continental transport of fine aerosols: (2) Global Health Impacts, *Atmospheric Environment*, 43(28): 4339-4347.]

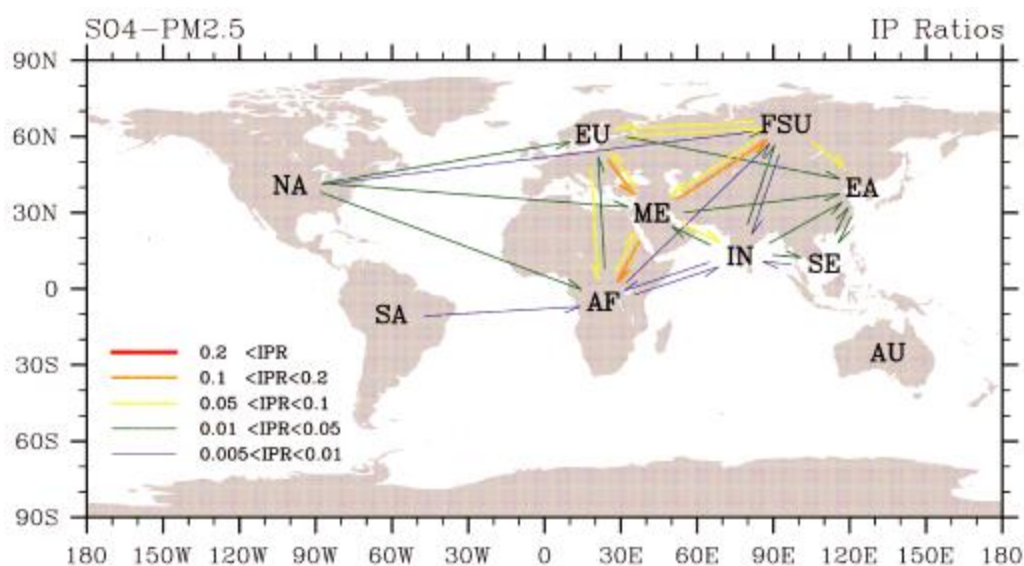


**Figure 5.9.** Influence potential ratios (IPR) of inter-continental transport of fine ( $PM_{2.5}$ ) sulphate aerosols. Arrows indicate the influence direction from a source to a receptor region. Colours indicate the magnitudes of IPR ranging from red (strong influence) to blue (weak influence). Arrows with IPR less than 0.005 are not shown. [Reprinted from Figure 5 in Liu, J., and D. L. Mauzerall (2007), Evaluating the potential influence of inter-continental transport of sulphate aerosols on air quality, *Environmental Research Letters*, 2(4): 045029.]

### 5.1.3. Future changes in human health impacts due to LRT

In Chapter A3, the future emissions of air pollutants from different regions of the world are presented for the “Representative Concentration Pathway” (RCP) scenarios. These scenarios show that emissions of ozone precursors, and PM and its precursors are generally expected to decline in NA and EU to 2050, but depending on the pollutant and emissions scenario, will increase in SA and EA before declining. CTM simulations with future emission scenarios (Chapter A4) suggest that for ozone the importance of foreign emission changes compared to domestic changes is likely to increase substantially for NA and EU, as domestic emissions fall and emissions from EA and SA continue to grow. The ozone-related health impacts due to LRT of EA and SA emissions are therefore likely to be enhanced in the future. Since, for most future RCP emission scenarios, ozone concentrations in NA and EU decline in 2050 (Figure 4.45; section 4.6.1), ozone-related human health impacts due to LRT from these two source regions would be expected to lessen. While PM in these scenarios is not modelled in Chapter A4, the emissions scenarios project similar relationships, suggesting that the relative importance of foreign emissions for PM concentrations in NA and EU may also grow.

The impact of climate change is such that when applying the same emission reductions of ozone precursors to the same baseline emissions for a present-day (2000s) and for a future (2090s) climate, the impact on ozone concentrations is slightly greater in the future as compared to present-day (Section 4.6.2). In terms of health impacts it is likely that the downwind ozone-related effects will be reduced due to climate change. The impact of climate change on future LRT of PM has not been modelled.

While ozone LRT may decrease in the future as emissions decline and because of climate change, populations are also likely to increase, particularly in less industrialized nations, leading to greater exposure to LRT and pollutants in general, and the total incidence of mortality caused by LRT may increase [e.g., *West et al.*, 2007b]. Future estimates of health effects should account for changing populations and health characteristics. Improved health care globally may increase life expectancy, possibly making populations more susceptible to cardiopulmonary disease and therefore to health effects associated with air pollutants.

### 5.1.4. Major uncertainties and research needs

Quantitative estimates of the health impacts of air pollutants have large uncertainties, and assessments of the health effects associated with LRT compound several uncertainties. As discussed

earlier, the existing studies of LRT influences on mortality apply concentration-response functions from the US and Europe globally, assume that all components of PM are equally toxic, and ignore possible interactions between pollutants for human health. There are also important uncertainties related to the use of coarse resolution global models, which are not designed to represent urban concentrations well [Chapter A4, *Lin et al.*, 2010]. The overall uncertainties are likely greater than represented in the individual studies in Section 5.1.2, because the uncertainty in concentration-response functions from a single epidemiological study does not reflect the full scientific uncertainty, and because of the combination of factors discussed here. The approaches used in Section 5.1.2 reflect the current state of knowledge and analytical tools, and there are clear opportunities to reduce these uncertainties through future research.

**RECOMMENDATION: Estimates of health impacts of air pollutants and long-range transport are uncertain and can be improved through research on: concentration-response relationships in less industrialized nations and over a range of concentrations, including short-term and long-term effects and possible low- or high-concentration thresholds; improving the resolution of global atmospheric models and improving nested models that encompass the global, regional, and urban scales, to better represent concentration gradients in and near urban areas; the possible differential toxicity of different PM components and particle sizes; possible changes in PM and pollutant mixtures as they are transported and age, and the effects of such changes on toxicity; and possible interactive effects of PM, ozone, and other pollutants on human health.**

## 5.2. Impact of Long-range Transport on Ecosystems

The doubling of tropospheric ozone ( $O_3$ ) in the Northern Hemisphere since the Industrial Revolution [Chapter 1, 2] [*Vingarzan*, 2004] has had significant, negative impacts on crop production, forest productivity and has been shown to cause changes in the species composition of semi-natural systems [*Ashmore*, 2005]. Rapid industrialization in the Northern Hemisphere has also resulted in increases in emissions of pollutants such as  $SO_2$ ,  $NO_x$  and BC that enhance atmospheric PM and can impact ecosystems through acidification, eutrophication and perturbations to the quality of photosynthetically active radiation. Here we make a first attempt to investigate the implications of intercontinental long-range transport (ICT) of these pollutants for ecosystems. The focus of this section is on terrestrial ecosystems, however impacts on oceans are also briefly covered.

### 5.2.1. Evidence for effects of ozone and PM on ecosystems

The regional distribution of experimental evidence for impacts on ecosystems is predominantly driven by the historical identification of impacts related to the regional occurrence of elevated pollutant concentrations and associated deposition. Hence, most evidence has been collected from North America and Europe over the past 30 years. The relatively recent advent of rapid industrialization and associated pollutant emissions in Asia [*Ohara et al.*, 2007] has led to a disconnect between the level of experimental evidence available and the scale of the pollutant problem by world region.

#### *Impacts on ecosystems caused by $O_3$*

The majority of the existing experimental evidence comes from bio-monitoring and Open Top Chamber studies that have been conducted first in North America [under the NCLAN Programme, *Heck et al.*, 1988] and later in Europe under the European Open Top Chamber [EOTC, see review by *Jager et al.*, 1992] and UNECE ICP Vegetation Programmes [*Hayes et al.*, 2007; *Mills et al.*, 2000]; these have mainly focussed on arable crops. Over the last decade similar studies are now increasingly being conducted in Asia [*Emberson et al.*, 2009]. The Free Air Concentration Enrichment approach has recently been used as an experimental method to assess impacts on crops (soybean in the US; [*Morgan et al.*, 2006]; rice in China: [*Shi et al.*, 2009]) forest trees (Aspen, Maple and birch) in Wisconsin, US: [*Karnosky et al.*, 2003]; mature beech stands in Bavaria, Germany: [*Matyssek et al.*, 2010]) and grasslands (alpine semi-natural grassland in the Swiss Alps [*Volk et al.*, 2006]). These methods have advantages of being closer to field conditions but are limited in their ability to define impacts at or below ambient pollutant concentrations and in defining dose-response relationships which are necessary for regional scale risk assessments.

In addition to experimental studies, epidemiologic methods have also been used, initially driven by a need to overcome difficulties in extrapolating experimental studies conducted on young forest tree species in Open Top Chambers to understand effects on mature trees growing under forest stand conditions [Bussotti and Ferretti, 2009]. Such studies have consistently demonstrated that O<sub>3</sub> can negatively influence a variety of forest responses from crown condition to radial growth [Braun S et al., 2010]. More recently, similar spatially relevant studies have been extended to crop loss assessments [Fishman et al., 2010; Kaliakatsou et al., 2010]. These studies have found that the influence of O<sub>3</sub> can be detected in regional level production statistics and field trial data although damage estimates have been found to differ from those obtained from risk assessments performed using empirically derived dose-response relationships [Kaliakatsou et al., 2010]. This may be due to these methods being most effective in those regions characterized by higher average O<sub>3</sub> concentrations [Fishman et al., 2010] where the O<sub>3</sub> signal is strong enough to overcome the influence of confounding variables affecting yield.

Rising background concentrations experienced over the last few decades can particularly enhance spring and autumn O<sub>3</sub> levels [see Fiore et al., 2008], in effect lengthening the period of elevated O<sub>3</sub> concentrations from the existing summer peak O<sub>3</sub> exposures; the influence of these new seasonal profiles on ecosystems needs to be understood, this can only be achieved with new experimental investigations. To date, such new investigations have used diurnal fumigation patterns that emphasise chronic rather than peak O<sub>3</sub> exposures and investigation of species with growth periods that extend into those times of the year when ICT is a more substantial fraction of the total pollution load i.e. the spring and autumn periods [RoTAP, 2010].

### **Range of response parameters**

Key impacts for agriculture include visible injury to leafy crop species [Emberson et al., 2003; Mills et al., 2010, in press]; declines in arable yields [Mills et al., 2007] and effects on crop quality (e.g. nitrogen content of grains, tubers etc. and nutritive quality of forage crops) [Pleijel et al., 1999]. Importantly, impacts have been found to vary substantially according to crop species and cultivars [Betzelberger et al., 2010]. Prevailing climatic and meteorological conditions and agricultural management practices (e.g. irrigation) will also affect response to O<sub>3</sub> [Fuhrer and Booker, 2003].

For forest trees, O<sub>3</sub> has been shown to impact visible foliar injury, accelerate leaf senescence, reduce photosynthesis, alter carbon allocation, and reduce growth and productivity [Karnosky et al., 2007; Skarby et al., 1998]; again, these effects vary by forest tree species and genotype [Karnosky and Steiner, 1981]. O<sub>3</sub> also appears to weaken tree resilience to a range of biotic (e.g. pest and pathogen attack) and abiotic (e.g. drought, frost hardiness) stresses. The extent to which results obtained from tree seedlings/saplings can be extrapolated to mature trees under real forest condition has been severely challenged [Kolb and Matyssek, 2001] and resulted in a study conducted at Kranzberg Forest, Germany on naturally growing and late-successional, adult forest trees [Matyssek and Sandermann, 2003; Matyssek et al., 2010]. This study found reductions in annual whole-stem volume increments for beech which, when scaled to stand level, supported modelling predictions that claim elevated O<sub>3</sub> to cause substantial reduction of C sink strength in trees [Sitch et al., 2007].

Semi-natural grasslands are genetically highly diverse multi-species communities ranging from low to high productivity depending on site conditions and management. Component species differ strongly in their sensitivity to O<sub>3</sub> [Bungener et al., 1999; Hayes et al., 2007; Timonen et al., 2004] and thus community response to O<sub>3</sub> is likely to be species-driven [Jones et al., 2007]. However, changes in productivity and species composition in established temperate [Volk et al., 2006], calcareous [Thwaites et al., 2006] or alpine grassland [Bassin et al., 2007] are difficult to detect against a background of considerable natural spatial and temporal variability. Subtle changes in C-assimilation and water economy in selected component species, as inferred from shifts in stable C and O isotopic signatures [Bassin et al., 2008; Jaggi and Fuhrer, 2007], reduced leaf longevity [Bassin et al., 2007], and altered biomass partitioning suggest that in the longer run, productivity may decline and species dominance may change in response to ICT. This is in contrast to observations in Mediterranean therophytic grasslands, where short-term effects on reproductive traits of annuals have



been observed [Gimeno *et al.*, 2004]. Experimental studies in the US and Europe have also highlighted O<sub>3</sub> impacts on nutritive quality of forage crops [Krupa *et al.*, 2004].

**FINDING: There is evidence that O<sub>3</sub> can cause a variety of damage responses to crops, forests and grasslands. The strength of this evidence varies with receptor type and location, with more evidence on crops than forest trees, more on trees than grasslands, and equal evidence in North America and Europe, but less in Asia.**

#### **Experimental derivation of dose-response indices**

The experimental campaigns conducted in North America [NCLAN: Heck *et al.*, 1988] and Europe [EOTC: Jager *et al.*, 1992] were instrumental in providing experimental data describing yield and growth responses for a range of crop species (and a far more limited number of forest and grassland species) that could be used to define O<sub>3</sub> metrics and dose-response relationships (see Box 5.1). It is important to note that in Europe, the selection of the AOT (accumulated ozone concentration over a threshold over a growing season) cut-off concentration of 40 ppb was actually driven by consideration of the level of background O<sub>3</sub> concentrations; AOT30 was as statistically robust in terms of defining crop damage but was considered to have implications for control strategies outside of Europe and hence the 40 ppb cut-off concentration was retained [Karenlampi and Skarby, 1996]. Since the background O<sub>3</sub> level can vary considerably across different regions, and most importantly with altitude, a single cut-off value may not be suitable for risk assessments in every geographical region with important implications for use of such threshold indices for assessment of ICT.

In the development of these indices it was recognised that high O<sub>3</sub> concentrations tended to co-occur with environmental conditions that restrict uptake (e.g. hot, dry sunny conditions). In Europe this has led to the development of the O<sub>3</sub> flux metric, PODy (Phytotoxic O<sub>3</sub> dose above a stomatal flux threshold y; formerly known as the accumulated stomatal O<sub>3</sub> flux, AFstY) [LRTAP Convention, 2010]. Re-analysis of existing Open Top Chamber experimental data for European wheat and potato [Pleijel *et al.*, 2007] and for a number of forest trees [Karlsson *et al.*, 2007] showed PODy to more accurately predict yield or biomass loss as compare to the AOT40 index. Although the flux metrics still have a threshold, which is assumed to act as a surrogate for the internal detoxification capacity of the plant [Pleijel *et al.*, 2007], the ambient O<sub>3</sub> concentrations that can contribute to accumulated flux will be substantially lower than the 40 ppb cut-off concentration used in the AOT40 index under optimum environmental conditions for plant gas exchange. Hence, the flux metric is likely to be better suited to assess the implications of rising background O<sub>3</sub> concentrations. It should also be noted that the increasing levels of background O<sub>3</sub> concentration translate into proportionally higher risk estimates, since both AOT40 and PODy involve a threshold value. This is due to a fundamental property of any similar threshold index and effectively means that with an increasing threshold these metrics become increasingly sensitive to the exceedance of the threshold value [Tuovinen *et al.*, 2007]. The sensitivity also depends on the characteristics of the frequency distribution of the data. Owing to the relatively wider distribution of stomatal fluxes, the PODy index for crops has been shown to be less sensitive to such perturbations than the corresponding AOT index [Tuovinen *et al.*, 2007].

**Box 5.1 Explanation of different ozone metrics used to derive dose-response relationships.**

Table 5.5 describes the formulation of different metrics that have been developed to assess O<sub>3</sub> damage to crops, forests and grasslands in both North America and Europe. The profile of the dose-response relationship relating the characterization of O<sub>3</sub> exposure to the response is also described along with the international organisations that have adopted the metrics. These metrics have evolved from average mean growing season indices (e.g. M7 and M12 (here referred to jointly as Mx indices) to indices that give greater weight to higher or peak O<sub>3</sub> concentrations deemed more biologically relevant to the induction of damage (e.g. AOT40 in Europe, SUM06 and W126 in North America) and most recently to flux based metrics (PODy). The profile of the dose-response relationship should also be considered; for example the curvilinearity of the M7/M12 indices essentially results in lower average O<sub>3</sub> concentrations contributing less to damage thereby having a similar effect in terms of weighting the relative importance of higher end O<sub>3</sub> concentrations albeit as growing season values rather than hourly averages; the importance of this effect varies according to the species-specific relationship. It should also be noted that dose-response relationships have yet to be derived for Asian conditions.

**Table 5.5.** O<sub>3</sub> metrics used to derive dose-response relationships for ecosystem protection in air quality management.

Metric	Definition	Formulation	Dose-response relationship	Application
M7 or M12	Daylight (7 or 12 hours) growing season average	M7 = mean 7 hour daylight [O3] M12 = mean 12 hour daylight [O3]	Weibull	-
AOT40	Accumulated concentration over a threshold of 40 ppb over a growing season	$AOT40 = \sum_{i=1}^n [O3 - 40]_i \text{ for } [O3] \geq 40 \text{ ppb}$ during daylight hours [AOT40 units: ppb.hrs]	Linear	UNECE, EU
W126	Weighted accumulation over a growing season	$W126 = \sum_{i=1}^n [O3]_i * W_i$ where $w_i = (1 / (1 + 4403 * \exp(-0.126 * [O3])))$ over 24 hours [W126 units: ppb.hrs]	Curvilinear	USEPA (under consideration)
SUM06	The sum of all hourly ozone concentrations greater than 0.06 ppm, accumulated over a growing season	$SUM06 = \sum_{i=1}^n [O3]_i \text{ for } [O3] > 60 \text{ ppb}$ over 24 hours [SUM06 units: ppb.hrs]	Curvilinear	USEPA (under consideration)
PODy	Phytotoxic ozone dose expressed as the accumulated stomatal ozone flux over a threshold of y nmol m <sup>-2</sup> s <sup>-1</sup> over a growing season	$POD_y = \sum_{i=1}^n [FO3 - y]_i \text{ for } [FO3] \geq y \text{ nmol m}^{-2} \text{ s}^{-1}$ [PODy units: mmol m <sup>-2</sup> ]	Linear	UNECE

N.B. [O3] is the hourly mean O<sub>3</sub> concentration, i is the index, w<sub>i</sub> is a weighting scheme that relates ambient O<sub>3</sub> concentrations to flux into the plant, FO3 is calculated stomatal flux into the plant, y is a threshold above which stomatal O<sub>3</sub> flux causes damage and n is the number of hours over which O<sub>3</sub> concentrations are summed.

A recent study [Mills *et al.*, 2010] collating evidence from across Europe for ~30 species of agricultural and horticultural crops and almost 150 (semi)natural vegetation species (trees were excluded) between 1990 to 2006 showed that risk maps based on stomatal O<sub>3</sub> flux were better predictors of the areas where O<sub>3</sub> damage occurred than those based on AOT40. Under Mediterranean conditions, such improved performance of flux based risk assessments have been attributed to dry summer conditions that dramatically limit the accumulated stomatal flux through the occurrence of drought-limited gas exchange, despite the occurrence of higher O<sub>3</sub> concentrations that result in enhanced seasonal AOT40 values [Gerosa *et al.*, 2008]. Similar results were found by [Matyssek *et al.*, 2007] for mature beech trees growing under drought conditions in Bavaria, Germany.

Regional scale impact assessment studies that have used different metrics and appropriate dose-response relationships have illustrated considerable differences in resulting yield loss predictions. For example, a global study by van Dingenen *et al.* [2009] showed differences in crop yield losses of up to 74% using M7 and AOT40 indices. The cause of such inconsistencies are unclear and could be related to variability in the experiments used to derive dose-response indices (e.g. cultivar sensitivity, experimental O<sub>3</sub> concentration profiles) or application of the risk assessment methods (e.g. uncertainties in modelling O<sub>3</sub> concentrations, local O<sub>3</sub> concentration profiles, local conditions affecting the connection between O<sub>3</sub> concentration and absorbed O<sub>3</sub> dose).

### **Mechanisms of adverse effects of O<sub>3</sub> relevant for ICT**

Phenology will play an important role in determining the importance of ICT damage to ecosystems. The timing and duration of growth periods will determine species exposure to ICT. For example, early or late season crops such as oil seed rape and maize may be more at risk, similarly forests and grasslands which have appreciably longer growth periods will be more likely to experience ICT. Within life-cycle and annual growing season variability in sensitivity may also be important. For example, Wieser *et al.* [2003] found that age dependent changes in leaf morphology were related to changes in the defence capacity against oxidative stress, with concentrations of antioxidants increasing with tree age; therefore, early season ICT O<sub>3</sub> exposures may occur when anti-oxidative defence capacities are still establishing. In more remote regions with early springtime peaks in O<sub>3</sub>, together with conditions favouring high stomatal conductance, the situation may be worse as the advancement of plant development may lead to more frequent co-occurrence of sensitive stages and early-season O<sub>3</sub> stress [Karlsson *et al.*, 2007].

Species distribution will also affect vulnerability to ICT. For example, many forests and grassland communities extend to high altitudes where the planetary boundary is more likely to be coupled to the lower layers of the free troposphere and hence more prone to ICT influence. Forests also host understory species, which often have ephemeral growth periods in the spring before closure of the forest canopy restricts growth.

**FINDING: Concentration-based indices to assess the importance of O<sub>3</sub> damage, especially those which use thresholds (e.g. AOT40) may not be appropriate for assessment of damage resulting from ICT. O<sub>3</sub> flux metrics (e.g. PODy) that incorporate the effects of differences in phenology and environmental conditions in estimates of O<sub>3</sub> damage are more suitable for assessments of the potential impact of ICT.**

### ***Impacts on ecosystems caused by PM***

PM can affect ecosystems in a number of ways depending on its characteristics, atmospheric concentration and deposition mechanisms; here we identify acidification, eutrophication and changes in radiation quality as the most important of these in terms of ICT.

Sulphur and nitrogen (N) deposition can cause soil and water acidification through long-term deposition of nitrate, ammonium and sulphate, which combine to add to the acidifying load that soils and aquatic ecosystems receive [Fowler *et al.*, 1991]. Such acidification potential can be counteracted by atmospheric deposition of base cations (calcium, potassium and magnesium) that contribute to the buffering capacity of sensitive soils and can negate the effects of acidic deposition [e.g., Johnson *et*

al., 1994]. Acidification has been linked to adverse effects on forest growth and vitality, to loss of sensitive fish populations and to changes in soil and aquatic invertebrate communities.

In ecosystems for which N is the limiting nutrient, moderate rates of N deposition can also result in stimulation of plant growth; increasing forest and grassland productivity. Likewise, moderate rates of sulphur deposition can enhance growth in sulphur deficient soils [McGrath and Zhao, 1995]. However, excess rates of N deposition can cause the loss of characteristic plant species of N limited systems and reductions in species diversity in terrestrial systems, it can also cause oxygen deficiency in fresh surface waters that are N, rather than P limited, with an associated loss of biodiversity and habitat degradation.

Since the process by which PM impacts ecosystems through eutrophication and acidification is reasonably well understood and is linked only to the total annual deposition load (i.e. will not be affected by within year variation in deposition loads resulting from ICT), we discuss these mechanisms of PM impacts only in relation to current knowledge based on ICT modelling studies in section 2.3.1.

While little is known about the broad scale impact on marine ecosystems, there are several recent papers [Duce et al., 2008; Krishnamurthy et al., 2009] that have investigated the impact of the deposition of anthropogenic N species on the biological productivity of the open ocean, and the impacts are not insignificant. For example, Duce et al. [2008] suggest that currently the quantity of atmospheric anthropogenic fixed N entering the open ocean (i.e. ocean fertilization) could account for up to a third of the ocean's external (non-recycled) N supply and up to ~3% of the annual new marine biological production, ~0.3 petagram of carbon per year. The resulting drawdown of CO<sub>2</sub> from the atmosphere would represent ~10% of the ocean's entire drawdown of atmospheric anthropogenic CO<sub>2</sub> each year, leading to a decrease in radiative forcing. However, the atmospheric deposition of anthropogenic N could also lead to increased production of nitrous oxide in seawater, and its subsequent emission to the atmosphere could offset some of the radiative forcing effects from atmospheric CO<sub>2</sub> reduction.

Atmospheric PM (including dust, sulphates, nitrates, secondary organics, OC, BC, and directly emitted PM) can also alter radiation quality by scattering and reflecting incoming solar radiation leading to an increase in the diffuse component. Up to a certain point the resulting increase in the diffuse component can enhance plant growth as this type of radiation is used more efficiently in photosynthesis with implications for the terrestrial carbon sink [Mercado et al., 2009]. The response to PM changes in radiation quality vary by vegetation type [Niyogi et al., 2004] and has been explained as an effect of canopy architecture and influence on light distribution through the canopy. Niyogi et al. [2004] found forest and croplands to be more sensitive to changes in diffuse radiation than grasslands [Niyogi et al., 2004]. Unfortunately, only very few experimental studies have been conducted investigating PM influence on radiation quality.

**FINDING: There is evidence that PM can affect crop, forest and grassland production through the processes of acidification, eutrophication and alteration of radiation quality. Acidification and eutrophication are associated with the loss of characteristic species and a reduction of species diversity in sensitive terrestrial and aquatic ecosystems. Limited evidence also suggests that biological productivity of the ocean is affected through fertilization by N deposition with implications for atmospheric CO<sub>2</sub> and radiative forcing. Alteration of radiation quality can enhance crop and forest photosynthesis, up to a threshold value of PM above which photosynthesis can decrease.**

#### **Critical thresholds for adverse effects of PM**

The long-term nature of effects of acidification and eutrophication (which have cumulative impacts over decades) coupled with limited experimental data, mean that dose-response relationships cannot be identified to assess the impacts of ICT of PM. Instead, critical thresholds for adverse effects are used to assess impacts.

The effects based approach, developed by the UNECE CLRTAP for use in Europe [LRTAP Convention, 2010] employs the concept of critical loads, the maximum deposition below which significant harmful effects on specified sensitive elements of the ecosystem will not occur. These critical loads refer to long-term effects of acidification and eutrophication. For acidification and nutrient mass balance, steady-state biogeochemical models are used to determine the deposition rate that results in the exceedance of a pre-defined chemical threshold value in environmental media (e.g. soil, surface waters) for effects in different ecosystems [Spranger *et al.*, 2008]. The calculation of these critical loads depends on local soil and water characteristics, climate and land use. For eutrophication, empirical critical N loads have also been established based on field experiments and gradient studies; these focus on impacts on biodiversity in natural and semi-natural systems [Bobbink *et al.*, 2003]. A recent synthesis of results of European N addition experiments in grasslands, (sub)Arctic and alpine vegetation, and temperate forests showed clear relationships between exceedance of empirical N critical loads and either plant species richness or similarity to reference plant species composition [Bobbink, 2008] thus supporting the use of this method to identify the harmful effects of eutrophication across Europe [Bobbink *et al.*, 2010].

Empirical critical loads are primarily defined for temperate and arctic-alpine ecosystems of Europe, although values have also been identified from field experiments in North America. A recent overview of the evidence of effects of N deposition on terrestrial plant diversity [Bobbink *et al.*, 2010] identifies that the critical load for many sensitive ecosystems lies in the range 10-15 kilograms per hectare per year ( $\text{kg ha}^{-1} \text{y}^{-1}$ ), but may fall to 5-10  $\text{kg ha}^{-1} \text{y}^{-1}$  for particular sensitive ecosystems or groups of organisms. Bobbink *et al.* [2010] identify Mediterranean ecosystems of southern Europe and California, and sensitive ecosystems in southern and eastern Asia as systems where there may already be impacts of N deposition but critical loads have not been defined.

Discussion of metrics to quantify effects of PM enhancing diffuse radiation on ecosystems photosynthesis has been limited to interpretation of modelling studies that attempt to calculate the diffuse fraction value (threshold) at which photosynthesis starts decreasing. A study by Knohl *et al.* [2008] for a broad leaf forest site in Germany estimates that above a diffuse fraction of 0.4, forest photosynthesis will decrease. A similar value for the same location was found in the modelling performed by Mercado *et al.* [2009]. A modelling study by Alton [2008] claimed that diffuse radiation under cloudy skies makes plants photosynthesise less; however, these global fields of diffuse radiation were not extensively validated leading to uncertainties in the results and interpretation of this work. As such, a suitable metric may be one that is able to capture the effect of diffuse radiation fraction on photosynthesis with a threshold defined as that diffuse radiation fraction at which photosynthesis starts decreasing. However, this is difficult to estimate using experimental or modelling studies in isolation. Once models are better calibrated and evaluated using data for single sites, it might be possible, on consideration of the sensitivities of the model, to estimate such thresholds.

**FINDING: In contrast to O<sub>3</sub>, PM dose-response relationships are not available to estimate the effects of intercontinental transported PM. Critical thresholds to prevent long-term adverse effects can be identified or modelled, but much of the empirical evidence from which these thresholds have been identified comes from Europe and North America limiting applicability to other parts of the world.**

### 5.2.2. Quantified influences of ICT pollution on ecosystems

#### **Role of ecosystems in determining long-range transport**

Ecosystems play an important role in determining the global mass balance of atmospheric gases and aerosols by providing an effective sink for the removal of substantial fractions of atmospheric O<sub>3</sub> and PM by dry deposition. For O<sub>3</sub>, this surface removal has been found to exceed the net stratospheric input term [Stevenson *et al.*, 2006]; these same deposition processes induce a potentially harmful load to ecosystems. This load depends not only on the atmospheric abundance of pollutants but also on the efficiency of dry deposition. Therefore an improved mechanistic understanding of the atmosphere-biosphere exchange processes would contribute to our understanding of both ICT and ecological impacts of pollutants. For O<sub>3</sub>, in particular, it is necessary to differentiate

between the stomatal and non-stomatal deposition pathways, as it is the former that provide the primary potential for plant injury [Emberson *et al.*, 2001]. Modelling studies [Solberg *et al.*, 2008] have shown that reduced stomatal uptake, and consequently slower depletion by dry deposition, significantly enhances ground-level O<sub>3</sub> concentrations; such conditions tend to occur during hot and dry periods in which stomates close to limit plant water loss. Given these criteria it is likely that climate change will play a significant role in determining future dry deposition removal processes by ecosystems with implications for atmospheric concentrations and human health [see section 5.2.4.4 and Klingberg *et al.*, 2011]

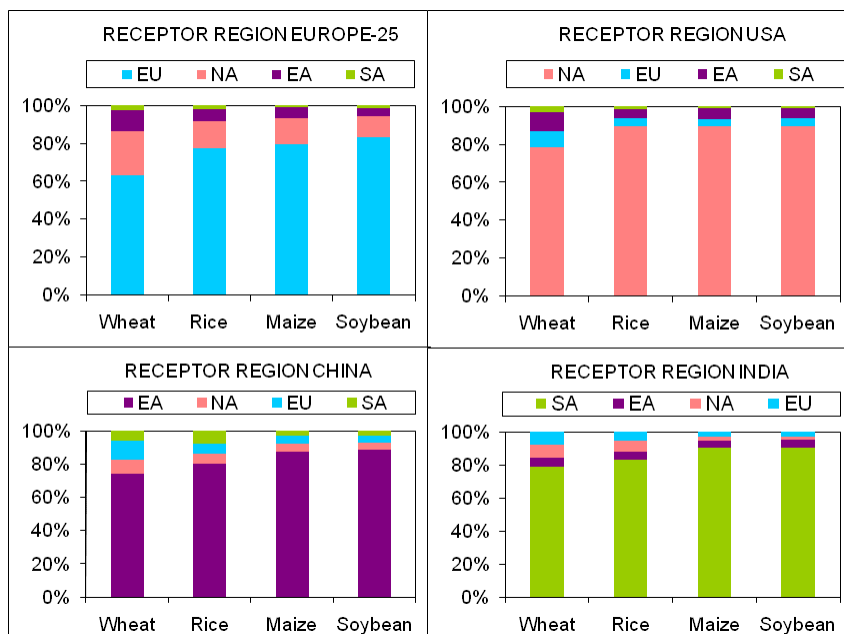
**FINDING: Deposition of pollutants to vegetated land surfaces plays an important role in determining atmospheric pollution mass balance and hence ICT. These same deposition processes also represent the pathways by which ecosystems are impacted by air pollution. As such, an integrated approach to improve our understanding of these deposition processes may benefit our understanding of ICT as well as impacts.**

#### *Impacts of long-range transport of ozone on crop yield*

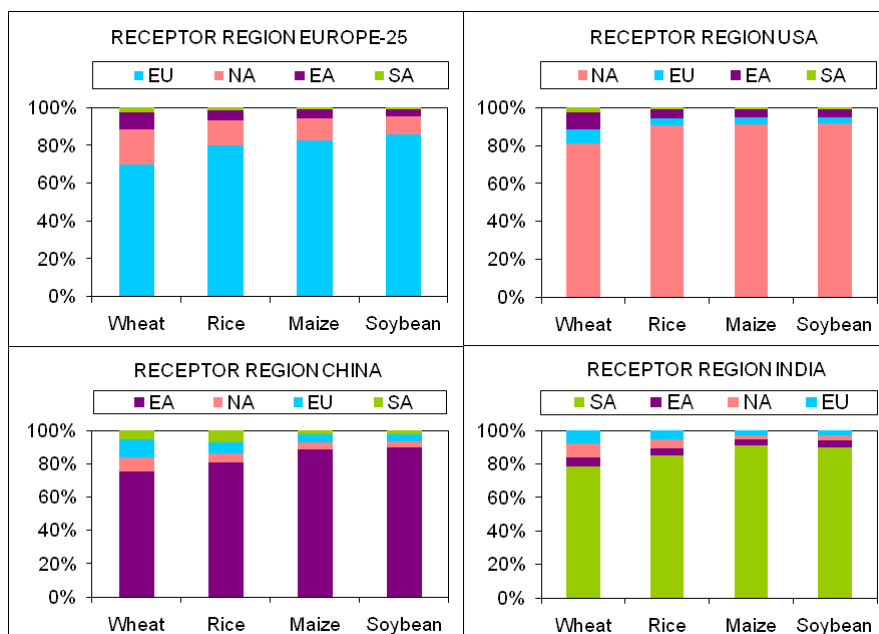
The impact of ICT of tropospheric O<sub>3</sub> on ecosystems has not previously been investigated in published studies. Specifically for this report, crop losses were estimated from the HTAP model ensemble of O<sub>3</sub> concentration based metrics (flux based metrics could not be used since this methodology has not yet been parameterized for application at the global scale). Using hourly O<sub>3</sub> concentration output of a subset of models, AOT40 and Mx metrics for four staple crops (wheat, rice, maize and soybean) were estimated for crop specific growing seasons according to climatically determined growth periods [as described in Van Dingenen *et al.*, 2009]. For each individual model, the difference in AOT40 and Mx between the base run and each of the four perturbation simulations (20% emission reductions in each of the four regions) was calculated on the model's own grid resolution and then interpolated to a 1°x1° grid to provide the ensemble average. The resulting ensemble AOT40 and Mx 1°x1° fields were then analyzed as in Van Dingenen *et al.* [2009], leading to gridded fields of crop relative yield loss, which were then aggregated to regional averages. The regional averages were used to calculate Relative Annual Intercontinental Response (RAIR) values in terms of relative crop yield loss. As in Chapter 4, the RAIR values are calculated for each region as the sum of the changes due to emission changes in the three other regions divided by the sum of the changes due to emission changes in all four regions combined.

Figure 5.10 shows the Relative Annual Intercontinental Response (RAIR) of each HTAP region to changes in ozone crop damage (expressed as relative yield loss) in each of four receptor regions for simulation set SR6 (20% emission reductions of NO<sub>x</sub>, VOC, CO, SO<sub>2</sub>, and PM). These results clearly show that emissions from one region can cause yield losses in another region. The contribution of ICT from the three other source regions to yield losses in each receptor region varies between ~5 and 35% of the estimated losses. However, this range is very dependent upon the response function used and should be considered with caution, especially given the disadvantages in using the AOT40 index for estimating the influence of ICT. The largest influence of ICT is found from North American emissions impacting on European crop yields. The difference in the influence of ICT on damage to each crop for a given region depends upon differences in the contribution of domestic emissions to O<sub>3</sub> concentration, crop growing season and geographical location and the crop-specific response function. It should also be noted that emission reductions outside the indicated HTAP areas have not been included and could further impact background O<sub>3</sub>; Also, the indicators have not been corrected for the crop canopy height. As such, limiting analyses of these results to relative rather than absolute contributions to crop damage makes the results more robust (as also appears from the very similar outcome for both indicators) since inter-model differences of absolute yield losses are rather large, and more difficult to interpret.

a). The contribution of source regions to relative yield losses estimated using growing season Mx concentration response functions specific to each of four staple crops.



b). The contribution of source regions to relative yield losses estimated using AOT40 concentration response functions specific to each of four staple crops.



HTAP region key: EU = Europe, NA = North America, EA = East Asia, SA = South Asia

**Figure 5.10.** The relative contribution of each HTAP region to crop damage (expressed as relative yield loss) in each of 4 regions for run SR6 (20% decrease of O<sub>3</sub> and PM precursor emissions) using Mx and AOT40 indices.

In a separate, and as yet unpublished study, the TOMCAT global chemical transport model [Arnold et al., 2005 ; Chipperfield, 2006] has been used to investigate the impact of hemispheric-scale transport of O<sub>3</sub> and its precursors on crops using the AOT40 O<sub>3</sub> index to assess crops yield loss. In this study three perturbation simulations were carried out where NO<sub>x</sub> emissions over three major



global regions were cut by 90%. Similar to the HTAP study described above, these results also suggested that of all global regions, it was emissions from North America impacting on European yields that gave the largest transboundary effect. The use of 90% NO<sub>x</sub> reductions in this study is likely to provide a stronger indication of the actual contributions from the different emission sources. This is due to the threshold nature of the AOT40 index, which means that contributions to AOT40 exposure can only be defined against a given scenario of local and non-local O<sub>3</sub> precursor emissions. The contribution of a non-local NO<sub>x</sub> source to AOT40 is dependent on the extent to which that source enhances surface O<sub>3</sub> concentrations above 40ppb, which will change depending on the strength of local and other non-local sources. In this sense, the AOT40 contributions from ICT diagnosed over each region are particular to the current configuration of local emissions in each region, whereas non-local contributions to the mean O<sub>3</sub> (represented by the M<sub>x</sub> indices) over each region are largely independent of local emissions. This further emphasizes the weakness in the use of threshold indices such as AOT40 in attributing plant O<sub>3</sub> damage to different emission sources.

A further key limitation of the model based risk assessment studies discussed above is associated with uncertainties in the simulated O<sub>3</sub> concentrations. While there are dense networks of near-surface O<sub>3</sub> measurements in North America, Europe and Japan [EEA, 2009; EMEP, 2010; Oltmans *et al.*, 2006; U.S. EPA, 2009a], the availability of measurement data for model validation is more limited for Africa, Latin America and China [Ellingsen *et al.*, 2008], and often non-existent in rural parts of these regions due to the focus on monitoring to assess risks to human health. It has also been found that models tend to be less accurate in their predictions of higher O<sub>3</sub> concentrations; this coupled with the increased mathematical sensitivity of the threshold-based risk indices makes the quantification of such indices more uncertain than that of mean concentrations [Tuovinen *et al.*, 2007].

**FINDING: There is considerable uncertainty as to how much of the damage to ecosystems caused by O<sub>3</sub> is attributable to hemispheric ICT. Provisional results from HTAP model-based risk assessments using AOT40 and M<sub>x</sub> indices indicate that emissions from one continent have the potential to influence crop productivity on other continents by affecting O<sub>3</sub> concentrations, with the largest influence of ICT found from North American emissions impacting on European crop yields. Based on the HTAP multi-model experiments, ICT may be responsible for about 5 to 35% of the estimated crop yield losses depending on the location, crop, and response function used, subject to large uncertainties.**

#### ***Impacts and potential vulnerability of ecosystems to long-range transport of PM***

The observations of forest decline and lake acidification in Europe and North America during the 1970s and 1980s [Fowler *et al.*, 1999] prompted research which clearly identified the adverse effects of deposition of S, and to a lesser extent, N. Emission control programmes have helped to improve the situation in these regions, and attention is now focused on the rate and nature of recovery of soils and waters from long-term acidification [e.g. Ormerod and Durance, 2009]. The region of greatest concern is now Asia, where acidification problems are expected to increase in the future [Fowler *et al.*, 1999]. There are now indications that acidification may have already occurred in parts of China related to air pollution [Hicks *et al.*, 2008]. Modelling by Hicks *et al.* [2008] has described the variability in susceptibility to acid rain across south and east Asia, and suggests that soil acidification effects are unlikely to be widespread due to insensitivity of soils and high concentrations of alkaline dust in the atmosphere, and the timescale for significant acidification is likely to be long. Areas at risk of acidification over the next 50 years are mainly restricted to southern East and Southeast Asia (Figure 5.12) but the characteristics and severity of these problems vary with biotic and abiotic factors [e.g. Hicks *et al.*, 2008].

HTAP model ensemble results presented in Sanderson *et al.* [2006] examined acidification risk of soils in the present day and 2090s using a single chemistry-transport model coupled to a global climate model, and examined the impact of climate change. The areas most at risk from acidification were projected to be the eastern parts of the U.S., central Europe, and particularly south and east Asia for both time periods. Future deposition fluxes of N and sulphur compounds were mostly controlled by changes in emissions. Climate change and atmospheric composition (which will affect the oxidising capacity of the atmosphere) had only a small impact on pollutant transport and deposition.

In terms of observed effects in the region, it is also important to note that the forest decline that has occurred in some areas of China may be due to direct effects of gaseous SO<sub>2</sub>, and to extremely acidic mist or rain events, which are due to local emissions, rather than the long-term effects of soil acidification caused by regional and ICT sulphur and N deposition. Hence, although parts of east and south east Asia can be identified as the third largest acid rain prone region in the world, more information on rates of change and the regional sensitivity to acidification, and the importance of pollutant emissions from local sources, are needed before accurate assessment of the impact of ICT can be undertaken.

In relation to eutrophication, recent global modelling studies suggest that N deposition related to NO<sub>x</sub> and NH<sub>3</sub> emissions are now as high in some parts of south, south-east and southern east Asia as they are in Europe and North America (Figure 5.11). There is growing scientific consensus that impacts will also be considerable in sensitive ecosystems of Asia, although local evidence is only just starting to emerge. For example, in China, manipulation experiments suggest that N deposition has the potential to influence the species richness of the under-storey of temperate and tropical forests [Bobbink *et al.*, 2010]. The WWF terrestrial Global 200 eco-regions were ranked by conservation status identifying those that were critical, endangered, or vulnerable as a result of direct human impacts [Olson and Dinerstein, 2002]. Figure 5.12 shows that many of the WWF G200 eco-regions of global conservation significance in Asia already had deposition rates in 2000 that are well above the critical load for sensitive ecosystems that have been established in Europe, while the threshold range for sensitive ecosystems of 10-15 kg ha<sup>-1</sup> y<sup>-1</sup> is reached in eco-regions in several other parts of the world.

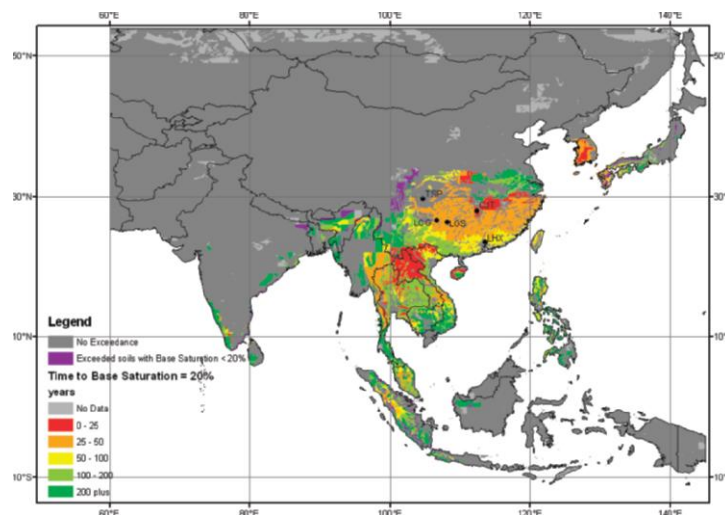


**Figure 5.11.** Time development of soil acidification damage according to a modelling study for Asia using best available data for soil and deposition parameters and deposition estimates obtained using a rather pessimistic emission scenario (IPCC SRES A2) for 2030. The model calculates the time it takes for the neutralizing capacity of the soil (expressed as base saturation) to be reduced to a level where acidification effects are observed (i.e., approx. 20% base saturation). [Reprinted from Figure 3 of Hicks, W. K., et al. (2008), Soil sensitivity to acidification in Asia: Status and prospects, *Ambio*, 37, 295-303. Copyright: the Royal Swedish Academy of Sciences.]

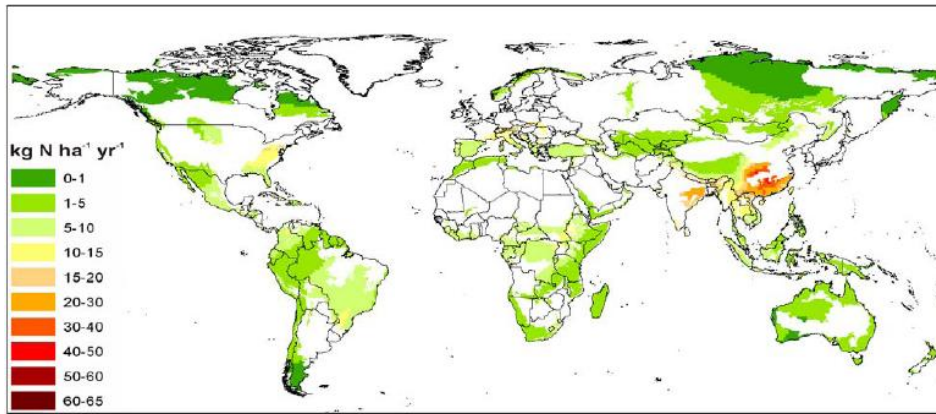


**Figure 5.12.** The WWF G200 regions [Olson and Dinerstein, 2002], showing total N deposition rates for the year 2000. N deposition to areas outside the G200 regions is not shown. [Reprinted from Figure 5(a) of Bobbink, R., et al. (2010), Global assessment of nitrogen deposition effects on terrestrial plant diversity: a synthesis, *Ecological Applications*, 20: 30-59.]

The importance of ICT to these exceedances of critical loads in regions with globally significant eco-regions cannot be quantified with large certainty. Reduced N ( $\text{NH}_x$ ) is important in determining local eutrophication but due to its lower average atmospheric lifetime (e.g. the mean residence time of  $\text{NH}_x$  is 5 hours, compared to 30 hours for  $\text{NO}_y$ ); mean travel distances of  $\text{NH}_x$  are only 150 kilometres (km) compared with 1,000 km for  $\text{NO}_y$  [NEG-TAP, 2001]. Hence  $\text{NH}_x$  is not often considered in the context of ICT although ammonium sulphate has a longer lifetime than ammonia (approximately 5 days) and can be transported larger distances. A recent study by Sanderson et al. [2008] attempted to quantify the ICT of oxidised N ( $\text{NO}_y$ ) from one source region to another in the Northern Hemisphere. They used results from 15 chemistry-transport models to quantify the transport of  $\text{NO}_y$  across four major source regions in the Northern Hemisphere. They found that 8-15% of  $\text{NO}_x$  emitted from each region is transported over 1,000 km and that between 3-10% of the  $\text{NO}_x$  emitted from each region is deposited as  $\text{NO}_y$  in the other three regions. However, a fixed reduction in emissions in one source region had little influence in other regions, with the percentage change in deposition in any receptor region being typically only 1-2% of the change in emissions in the source region; the one exception was east Asia, for which there was a 6.4% reduction from emission reductions in South Asia. We note here however, that these numbers mask large geographical variability, and that in sub-regions closer to the source the impacts can be larger.

On this basis, it is unlikely that ICT makes substantial contributions to large scale adverse effects of N deposition in other regions. However, it is important to emphasise that the situation may be different for specific remote and sensitive regions. For example, Arctic systems are very sensitive to eutrophication and may have a critical load close to  $5 \text{ kg ha}^{-1} \text{ y}^{-1}$  [Bobbink et al., 2010]. These areas have very little influence from local sources, but Wolfe et al. [2006] have suggested that N deposition from distant sources can contribute to changes in the biogeochemistry and ecology of two remote lakes on Baffin Island in the eastern Canadian Arctic. In addition, deposition of transported PM to snow and ice surfaces in the Arctic has been linked to accelerated melting [Shindell, 2007] with implications for ecosystems. More analysis of the significance of ICT in specific remote and sensitive parts of each region would be valuable since these are the locations where it may be most significant.

**FINDING: There is considerable uncertainty over the importance of the contribution of ICT of PM to regional acidification and eutrophication. However, on a regional basis, the contribution of ICT of  $\text{NO}_x$  to adverse effects on sensitive ecosystems is likely to be small. Focus is needed on specific remote and sensitive ecosystems where the contribution of ICT may be more significant.**

### 5.2.3. The potential vulnerability of ecosystems to long-range transport of $\text{O}_3$

This section investigates the vulnerability of ecosystems to ICT, through identification of ecosystems of particular global importance in terms of agriculture, forest cover and biodiversity. This type of analysis equates with findings from the health section (see section 5.1.2) that identified the

added importance of foreign sourced emissions to pollution in regions of high population density. Here we replace high population density with ecosystem importance to identify equivalent regions where ICT may be of particular relevance.

### **Agriculture and Food security**

O<sub>3</sub> crop yield response functions have been used with global chemistry transport models to estimate current and future relative yield losses due to O<sub>3</sub> [e.g., *Tong et al.*, 2007; *Van Dingenen et al.*, 2009; *Wang and Mauzerall*, 2004]. Although each of these modelling studies uses different O<sub>3</sub> models and crop production and distribution data they all make use of the range of dose-response response functions described in Box 5.1, and hence provide a reasonably standardized indication of production and economic losses associated with O<sub>3</sub> exposures. Currently, global yield losses are predicted to range between 3% and 5% for maize, 7% and 12% for wheat, 6% and 16% for soybean, and 3% and 4% for rice, which represents an annual economic loss of \$14-\$26 billion [see Figure 5.2.3 for wheat production losses due to O<sub>3</sub>, *Van Dingenen et al.*, 2009]. Agricultural regions in North America, Europe and Asia are identified as particularly vulnerable to O<sub>3</sub> damage. About 40% of this damage was found to occur in parts of China and India. The substantial impacts found in the Asian region may be particularly relevant given the importance of agriculture within these country economies; e.g. losses were estimated to offset a significant portion (between 20 to 80%) of the increase in GDP in the year 2000 in such economies.

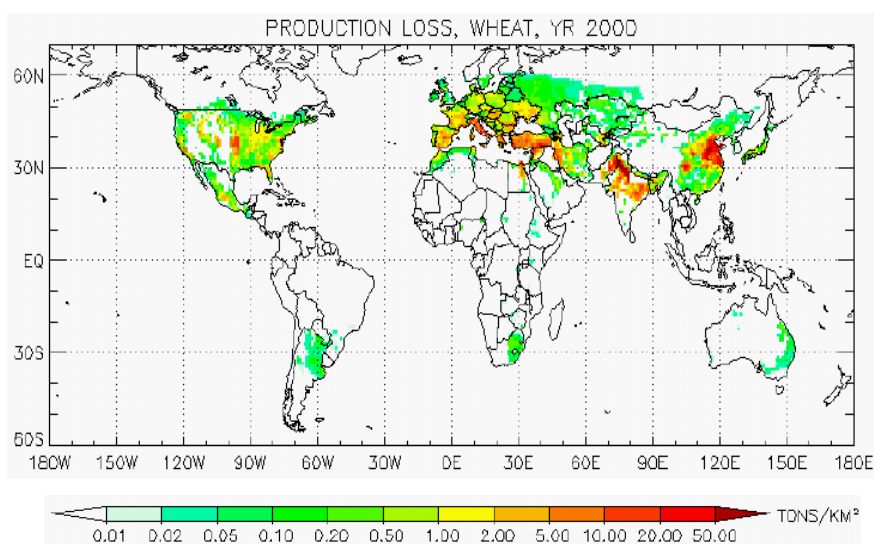


**Figure 5.13.** Average wheat crop production losses due to O<sub>3</sub> estimated for the year 2000 using European and North American concentration based exposure-response relationships. [Adapted from Figure 10 of Van Dingenen, R., et al. (2009), *The global impact of ozone on agricultural crop yields under current and future air quality legislation*, *Atmospheric Environment*, 43(3): 604-618, with permission from Elsevier.]

Importantly, these modelling studies have relied on North American or European dose-response relationships to assess the yield losses caused by O<sub>3</sub>; a recent synthesis of data [*Emberson et al.*, 2009] strongly suggests that key Asian crops and cultivars may well be more sensitive to O<sub>3</sub> concentrations when growing under Asian conditions suggesting that the production and subsequent economic loss estimates for this region may be underestimated.

Globally, there are a number of agricultural production areas that are vulnerable to increasing O<sub>3</sub> pollution. The “Cornbelt” in the United States produces 40% of the world’s corn and soybean crops, and this region is already potentially losing 10% of its soybean production to O<sub>3</sub> [*Tong et al.*, 2007]. In the U.S. as a whole, agronomic crop loss to O<sub>3</sub> is estimated to range from 5 – 15%, with an approximate cost of \$3-\$5 billion annually [*Fiscus et al.*, 2005; *U.S. EPA*, 2006]. In Europe, similar studies have identified substantial economic losses due to O<sub>3</sub>, for example, *Holland et al.* [2007] estimated losses for 23 crops in 47 countries in Europe of €4.4 to 9.3 billion/year, around a best estimate of €6.7 billion/year for year 2000 emissions. Despite the overwhelming evidence that current

O<sub>3</sub> concentrations are causing yield losses, new O<sub>3</sub> tolerant crop cultivars are not being developed for a future higher-O<sub>3</sub> world [Ainsworth *et al.*, 2008; Booker *et al.*, 2009]. Recent successes in identifying quality trait loci associated with O<sub>3</sub> tolerance in rice indicate the breeding for O<sub>3</sub> tolerance in food crops is possible [Frei *et al.*, 2008; Frei *et al.*, 2010], yet currently, there is little if any industrial effort in this direction.

In the case of PM, eutrophying and acidifying deposition is not likely to pose a particular threat to agriculture; in the first instance, agricultural systems are often N limited and require applications of N fertilizer to enhance productivity. The adverse effects caused by acidifying substances can be negated through the application of lime in heavily managed systems although such management comes with an associated economic cost and hence may be a less favourable option in developing countries. The role that atmospheric PM may play on agricultural productivity has not been specifically assessed.

### ***Forest health, grasslands and biodiversity***

In contrast to agriculture, little work has been done to assess the impacts of ground level O<sub>3</sub> on important global forest biomes. Work that has been conducted has been confined to studies in Europe and North America. A Scandinavian study estimated timber yield losses due to O<sub>3</sub> at 2.2% in Sweden over the period 1993-2003 [Karlsson *et al.*, 2005]. The resulting economic loss was estimated to be a 2.6% decline, which is equivalent to €56 million based on 2004 prices for timber and pulpwood. Additionally, Muller and Mendelsohn [2009] estimated annual timber yield losses equivalent to \$80 million in the U.S.

Little is therefore known of the response to O<sub>3</sub> by forest ecosystems that cover vast swathes of the Northern Hemisphere, even though heavily forested areas coincide with regionally high O<sub>3</sub> concentrations in east and southeast Asia, northern Asia, and boreal North America. Recent studies in Scandinavia have identified certain aspects of O<sub>3</sub> exposure of the more northerly, boreal forest ecosystems that could particularly enhance vulnerability to ICT. These include the earlier onset of the growing season as climate changes, the extensive periods of 24 hour daylight that allow more or less continuous gas exchange leading to a large cumulative O<sub>3</sub> dose, and lack of recovery from oxidative stress during darkness [Karlsson *et al.*, 2007]. In terms of tropical forests, Fowler *et al.* [1999] estimated that O<sub>3</sub> concentrations in excess of 60 ppb were experienced by an area of 3 million km<sup>2</sup> in 1990 (almost 20 % of total tropical forest cover) with the increase particularly great in southeast Asia. In spite of this rapid increase in exposure, our knowledge of O<sub>3</sub> impacts on forest ecosystems of tropical biomes is extremely limited [Emberson *et al.*, 2003].

A similar situation exists for grasslands. Projections of O<sub>3</sub> effects on semi-natural grasslands in different regions with widely varying climatic conditions are difficult because of the diversity of this ecosystem type, substantial intra-specific differences in O<sub>3</sub> sensitivity among populations [Bassin *et al.*, 2004; Yoshida *et al.*, 2001], and a lack of experimental data for most systems. In temperate latitudes, such as northwestern Europe, grasslands are dominated by perennial C3 species, whereas in warmer climates annual species form a greater component. These latter systems may be more sensitive to O<sub>3</sub> due to their dependence on reproductive output, which was found to respond most sensitively to elevated O<sub>3</sub> [Gimeno *et al.*, 2004]. Highly diverse communities with an important conservation value in regions with a warmer climate may be more vulnerable than perennial grasslands in temperate and montane habitats. This may concern regions where C3 species predominate and where typically high O<sub>3</sub> levels are observed, such as the Mediterranean basin in Europe or in coastal parts of southern California. Grasslands dominated by C4 grasses in warmer regions such as India, southeast Asia, southern China and in much of the Southern Hemisphere may be less sensitive to O<sub>3</sub> as the C4 photosynthetic pathway (which is capable of providing a near constant and optimum supply of CO<sub>2</sub> for photosynthesis with relatively low stomatal conductance) will confer some protection against O<sub>3</sub>. Similarly, therophytic grasslands in arid and semi-arid regions such as northern China may be less affected with only a few percent simulated reductions in net primary production due to O<sub>3</sub> alone [Ren *et al.*, 2007].

**FINDING: There is evidence of impacts of O<sub>3</sub> on vulnerable and important agricultural, forest and grassland ecosystems across the Northern Hemisphere; over such ecosystems the enhancement of locally derived O<sub>3</sub> concentrations by ICT may be particularly important.**

#### 5.2.4. Interactions with climate change

##### *Effect of atmospheric composition on plant physiology*

Vegetation plays an important role in determining surface O<sub>3</sub> levels, via dry deposition of O<sub>3</sub> to the interior of leaves through stomata. As atmospheric CO<sub>2</sub> levels rise, the stomata will not need to open as widely to allow sufficient CO<sub>2</sub> to enter for photosynthesis. This may reduce O<sub>3</sub> uptake, decreasing the sensitivity of the plants to O<sub>3</sub> [Sitch *et al.*, 2007]. Such reductions in stomatal conductance of plants would result in both lower uptake rates and increased O<sub>3</sub> concentrations in the boundary layer. Sanderson *et al.* [2007] found that surface O<sub>3</sub> levels over parts of Europe, Asia and the Americas were 4-8 ppb larger under doubled CO<sub>2</sub> conditions during April, May and June (the approximate growing season for crops in northern Europe). Similarly, Klingberg *et al.* [2011] found that despite substantially increased modelled future O<sub>3</sub> concentrations in central and southern Europe, the flux-based risk for O<sub>3</sub> damage to vegetation is predicted to remain unchanged or decrease at most sites, mainly as a result of projected reductions in stomatal conductance under rising CO<sub>2</sub> concentrations although soil moisture and temperature were also found to play an important role in determining stomatal O<sub>3</sub> flux. However, the relationship between stomatal conductance and CO<sub>2</sub> concentration may prove to be more complex and depend on O<sub>3</sub>-CO<sub>2</sub> interactions [Uddling *et al.*, 2010]. In addition, recent research has found that effective regulation of stomatal conductance under drought conditions was disrupted by increasing background O<sub>3</sub> concentration [Mills *et al.*, 2010; Wilkinson and Davies, 2009; 2010]. For a further discussion of potential climate change effects on O<sub>3</sub> fluxes, see Fowler *et al.* [2009] and Fuhrer [2009].

##### *Impact of future atmospheric conditions on ecosystems*

Models simulate that global mean precipitation increases with global warming [Meehl *et al.*, 2007]. However, there are substantial spatial and seasonal variations. Increases in the amount of precipitation are *very likely* in high latitudes, while decreases are *likely* in most subtropical land regions (section 1.5.2), continuing observed patterns in recent trends in observations. Precipitation is projected to decrease in many areas already suffering from water shortages [e.g., the Mediterranean and parts of Africa, IPCC, 2007a], which together with rising temperatures, will increase stress among plants. Reduced stomatal conductance that may occur in response to elevated CO<sub>2</sub> may enhance water use efficiency of plants, which may help to partly alleviate the effects of reduced rainfall. The projected increase in temperatures in many parts of the world mean that yields from crops may also be reduced [Lobell and Field, 2007]. Increased water stress in a warmer climate may be expected to decrease sensitivity to O<sub>3</sub> via reduced uptake; however O<sub>3</sub> induced damage to stomatal functioning (Mills *et al.*, 2010, Wilkinson and Davies, 2009, 2010) might confound this effect. The exact impacts of pollutants on vegetation in the future will be complicated by the differential response of plants to climate change and rising CO<sub>2</sub> levels, whereby the latter will increase growth and might offset some of the projected yield losses from crops by the former.

A mechanistic model of plant-O<sub>3</sub> interactions was implemented into the Hadley Centre land surface model and run with O<sub>3</sub> scenarios from the STOCHEM chemistry transport model driven with SRES A2 emission scenario [Sanderson *et al.*, 2003; Sitch *et al.*, 2007]. Results suggest a large negative impact of near-surface O<sub>3</sub> on plant productivity. These model results have been used to identify eco-regions where a significant effect on global primary productivity might be expected to occur [Royal Society, 2008]. The results in Figure 5.14 are based on the 'low sensitivity' simulation of Sitch *et al.* [2007] which is overlain with the G200 regions and used to assess threats of O<sub>3</sub> deposition to biodiversity. This identifies eco-regions of south and east Asia, central Africa and Latin America as being at risk from elevated O<sub>3</sub> levels during this century, in addition to areas of North America and Europe where the effects of O<sub>3</sub> are better documented. However, there is almost no information available on whether the plant communities in these other regions of the world are as sensitive to O<sub>3</sub>



as those that have been used to define critical levels, and hence the real significance of these areas of potential risk to biodiversity is completely unknown.

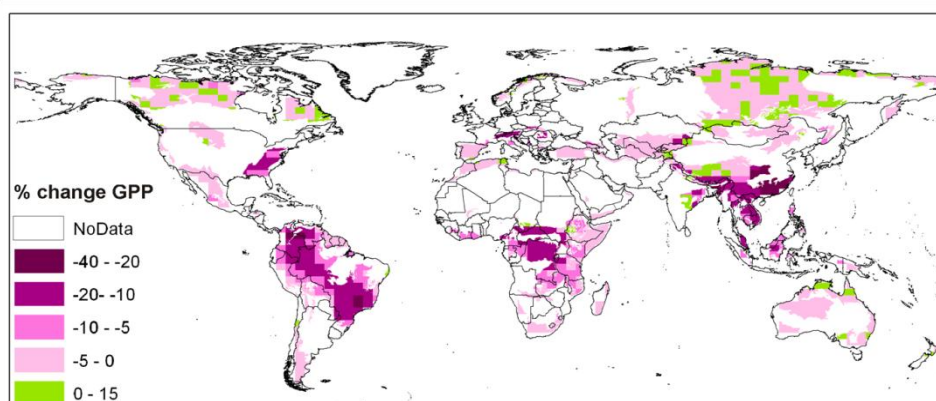


**Figure 5.14.** Global assessment of the key biodiversity areas at high risk from O<sub>3</sub> impacts; the figure shows the projected percent decrease in gross primary productivity due to O<sub>3</sub> within the Global 200 priority conservation areas. [Reprinted from Figure 8.8 in *Ground-level ozone in the 21st century: future trends, impacts and policy implications* (2008), RS Policy document 15/08, The Royal Society, London, United Kingdom.]

### ***Impact of air pollution on climate change***

The direct radiative impact of pollutants and their ICT is covered in detail in section 5.3. Here we cover indirect climate impacts of pollutants mediated through their effects on ecosystems.

A recent study by *Sitch et al.* [2007] found a significant suppression of the global land carbon sink due to O<sub>3</sub> induced damage to vegetation leading to reduced net primary productivity; with estimates of the reduction in land carbon sequestration being up to 260 PgC by 2100 based on SRES A2 emission scenarios. This reduced carbon sequestration leads to a higher atmospheric CO<sub>2</sub> concentration which was estimated to constitute an indirect radiative forcing that could exceed warming due to the direct radiative effect of tropospheric O<sub>3</sub> increases. However, elevated CO<sub>2</sub> concentrations may provide a degree of protection against O<sub>3</sub> damage, though there is uncertainty as to the magnitude and temporal longevity of this protection as well as which species groups would be affected (see Section 5.2.4.1).

The O<sub>3</sub> changes from the HTAP O<sub>3</sub> precursor experiments from the STOCHEM-HadGEM model have been applied to the offline dynamic vegetation model of *Sitch et al.* [2007] to quantify their impact on the carbon cycle [Collins *et al.*, 2010, see Figure 5.2.6]. The impacts of O<sub>3</sub> on vegetation and hence the land carbon storage are closely tied to the O<sub>3</sub> footprints of the precursor changes themselves. For NO<sub>x</sub> emission changes, the impact of ICT on vegetation is small, with the possible exception of south Asian emissions impacting on east Asian vegetation. For emissions of longer-lived species such as CO, the resulting O<sub>3</sub> causing vegetation damage has a small component from ICT, but the dominant impact comes from emissions within the source region. On a 20 year timescale, O<sub>3</sub> precursor emissions cause a larger temperature change through indirectly increasing CO<sub>2</sub> than from the changes in O<sub>3</sub> or methane themselves.



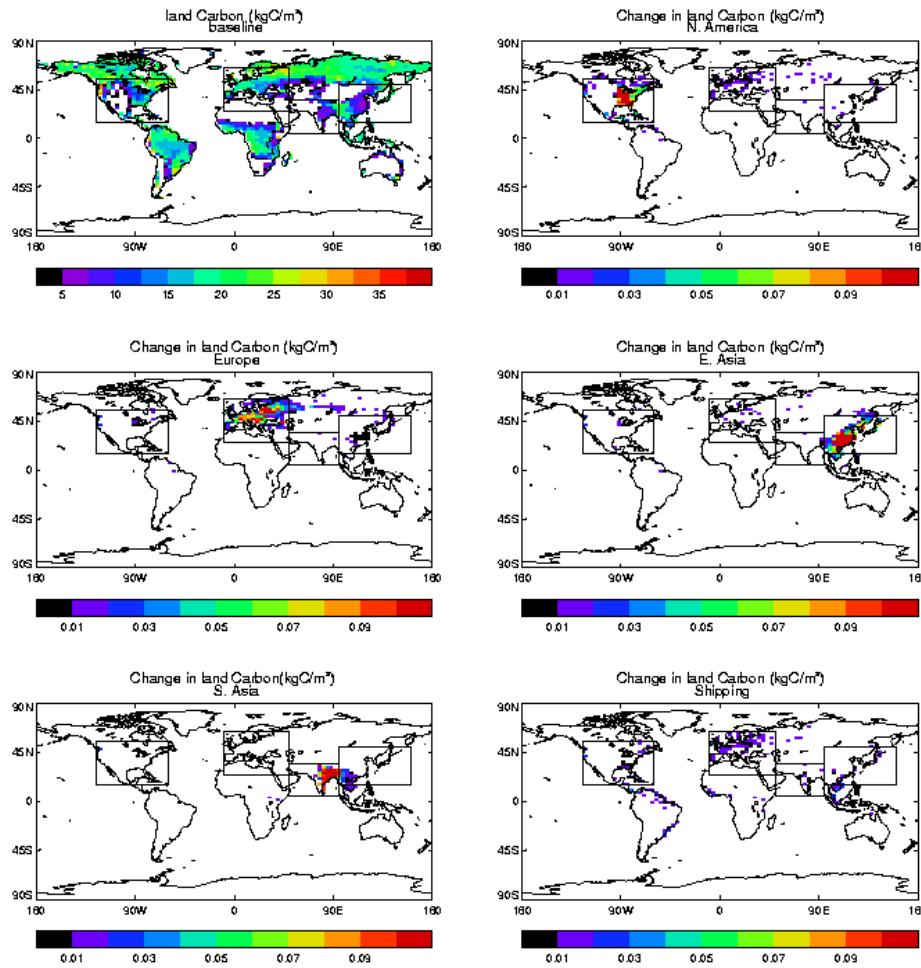


**Figure 5.15.** Change in land carbon at the end of the year following the HTAP 20% NO<sub>x</sub> emission reductions. Boxes show the extent of the HTAP regions.

Global models that are now able to separate direct and diffuse radiation to assess the contribution of sunlit and shaded leaves to canopy photosynthesis [Mercado *et al.*, 2009] have recently been incorporated into fully coupled land-ocean atmosphere simulations and are hence capable of accounting for effects of short time-scale variability of PM loading. A first attempt to quantify the effects of PM and clouds on the regional and global C sinks [Mercado *et al.*, 2009] has estimated changes in diffuse fraction of -5 % to 30% during the global dimming period (1950-1980) which correspond to a contribution to the regional C sink of up to 30 gC m<sup>-2</sup> yr<sup>-1</sup> across Europe, eastern U.S., east Asia and some tropical regions in Asia (Figure 5.16). Conversely, during the brightening period (1980-2000), a reduction in diffuse fraction over Europe, eastern USA, western Australia, and some regions of Russia and China, led to a lower regional contribution to the land C sink from diffuse radiation. Globally, over the 1960-2000 period, diffuse radiation effects associated with changes in PM and clouds in the atmosphere enhanced the land C sink by about 25%. This more than offsets the negative effect of reduced surface radiation on the land carbon sink, giving a net effect of changes in radiation on the land carbon sink of 10% [Mercado *et al.*, 2009].

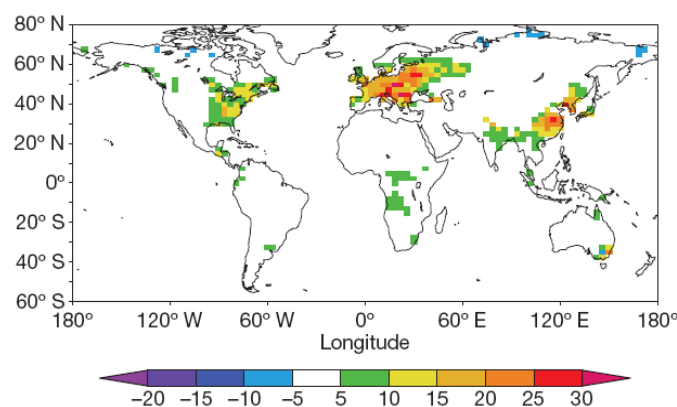


**Figure 5.16.** Simulated change (colour scale, grams carbon per square metre per year) in diffuse fraction contribution to land carbon accumulation between 1950 and 1980. [Reprinted from Figure 3(d) in Mercado, L. M., et al. (2009), Impact of changes in diffuse radiation on the global land carbon sink, *Nature*, 458: 1014-1017.]

### 5.2.5. Interactions with other pollutants

Damage to plants by a single pollutant can be altered by the presence of other pollutants, frequently with synergistic effects (e.g. between  $\text{NO}_2$  and  $\text{SO}_2$ ), but calculating response functions for each pollutant in the presence of others is difficult [Bell, 1985; Bender and Weigel, 1993].

There are also indirect feedback effects on climate of N and  $\text{O}_3$  deposition to ecosystems. In particular, the enhanced atmospheric levels of N species and ground-level  $\text{O}_3$  in Asia mean that this region will play an important role in determining the magnitude of these potential feedbacks with important implications for the climate system.

N deposition can lead to increased emissions of the potent GHG nitrous oxide ( $\text{N}_2\text{O}$ ) from soils. It can also increase soil emissions of nitric oxide (NO), one of the important chemical precursors for  $\text{O}_3$  formation. N deposition can also enhance the growth-rates of N-limited forests [Hungate et al., 2009] resulting in enhanced uptake/sequestration of C in terrestrial ecosystems where N is the limiting nutrient; under enhanced  $\text{CO}_2$  conditions, N limitation may become more common. However, where N deposition exceeds critical loads, adverse effects on growth and carbon sequestration can occur.

There is some evidence that a long-term trend of increased productivity in European forests is associated with environmental factors, including N deposition, as well as increased  $\text{CO}_2$ , and climate change [Nabuurs et al., 2003], and is not simply due to improved management. These factors ameliorate the resilience of trees against  $\text{O}_3$ , but, on the other hand,  $\text{O}_3$  itself is considered a factor potentially capable of reducing the “benefits” of  $\text{CO}_2$  and N fertilization [King et al., 2005; Magnani et al., 2007]. Semi-natural grasslands are often limited by nutrients such as N or phosphorous. Alleviating such constraints for instance by the addition of N could decrease the sensitivity of the plant community to  $\text{O}_3$  through increasing biochemical detoxification capacity, or increase the sensitivity through increased stomatal conductance. However, to date evidence of these effects is limited and contradictory. Research into the N cycle is relatively less well developed than for the carbon cycle. Incorporation of the N cycle into earth system models is urgently needed to make further progress in assessing the interactions between air quality pollutants and climate.

**FINDING: There are important interactions between  $\text{O}_3$  and N deposition, and between both pollutants and climate and  $\text{CO}_2$  concentrations, which have implications for future crop and forest production and global GHG budgets. However, these interactive effects are currently not well quantified.**

**RECOMMENDATIONS:** Conduct experimental studies using O<sub>3</sub> profiles that simulate enhanced background O<sub>3</sub> concentrations to develop an improved understanding of the processes by which seasonality in O<sub>3</sub> exposure influence damage to ecosystems, perhaps with a focus on crops, forests and grasslands that have growth periods extending into those seasonal periods when the relative ICT contribution to pollution is greatest. Conduct a pan-Asian Open Top Chamber/Free Air Concentration Enrichment field campaign to establish dose-response relationships specific for Asian species (crops, forests and grasslands) growing under Asian climatic and management conditions. Assess the suitability of the flux-based O<sub>3</sub> index to identify ICT effects on ecosystems. Develop flux networks so that monitoring of O<sub>3</sub> fluxes in addition to other biogeochemical species (such as N, C and water vapour) is performed as standard. Conduct global modelling experiments that use flux-based indices to estimate the influence of ICT on ecosystem damage. Improve critical loads for tropical and Asian ecosystems. Improve understanding of how ICT may influence recovery or time-development of damage of ecosystems to acidification and eutrophication. Improve understanding of the aerosol-loading limit up to which ecosystems respond positively to an increase in diffuse fraction, the global and regional effect of diffuse radiation changes on the hydrological cycle, the implications for aerosol-based geo-engineering schemes and, the effect of diffuse radiation on croplands. Improve understanding of the interactions between acidification, eutrophication, ground level O<sub>3</sub>, atmospheric aerosol loading and climate change. Research could be led by modelling efforts which identify knowledge gaps and hence drive experimental design to further scientific understanding. Improved modelling of ICT feedbacks to global climate taking into account the effects of ICT pollutants on GHG absorption by vegetation.

### **5.3 Impact of Long-range Transport on Climate**

Ozone (O<sub>3</sub>) and particulate matter (PM) have mainly been addressed by policy because of their impacts on air quality, but these air pollutants also have important influences on the Earth's climate. This section emphasizes the effects of anthropogenic O<sub>3</sub> and PM on regional and global climate, at present and in the future, and the effects of actions to reduce emissions to address these pollutants. In doing so, we mainly consider effects on radiative climate forcing, as well as on climate parameters. We do not estimate the ultimate impacts of climate change, including those to human health, ecosystems, agriculture and food supply, and coastal infrastructure. These impacts of climate change are detailed elsewhere [IPCC, 2007b].

The previous sections on the health and ecosystem impacts associated with LRT emphasize the effects of emissions from a source region on impacts in a receptor region, determined by pollutant concentrations or deposition. For climate, however, the effect of emissions from a source region on the climate of a receptor region is not determined entirely by pollutant concentrations over the receptor, and the source-receptor relationships in Chapter A4. Rather, the effects of emissions on regional forcings and atmospheric circulation become important, as do the effects on global average forcings and climate. Nonetheless, since O<sub>3</sub> and PM are short-lived climate forcing agents, the effect of a unit change in emissions on global and regional climate will vary with the location of those emissions.

We begin by analyzing the radiative forcing associated with the emissions relevant for O<sub>3</sub> and PM, and the effects of changes in emissions from different world regions. We then consider the importance of regional forcings for their ultimate influences on regional and global climate, and highlight the Arctic as a unique region that is clearly influenced by LRT. We conclude by considering future changes in the forcings of O<sub>3</sub> and PM and provide recommendations for future research.

### 5.3.1. Effects of ozone and particulate matter on global average radiative forcing

#### **Radiative forcing and its relation to global climate change**

Climate change can be driven by changes in atmospheric composition (e.g., carbon dioxide, methane, O<sub>3</sub>, and PM), surface albedo (e.g., through changes in land use), and solar irradiance. Radiative forcing (RF) has been designated and extensively used to measure and compare, to a first order, the global climate impacts of different climate change drivers. RF is defined as the difference in net (down-welling minus upwelling) irradiance (solar plus thermal infrared radiation, in Watts per meter squared, Wm<sup>-2</sup>) between an initial and a perturbed state of forcing agents, usually at the tropopause or the top of the atmosphere (TOA), with surface and tropospheric temperatures and state held fixed [Forster *et al.*, 2007]. To assess anthropogenic RF, the initial state is usually set in 1750, the approximate start of the industrial era, and the perturbed state in a recent year. By definition, a negative (positive) RF implies that the change in a climate driver exerts a cooling (warming) influence on the Earth-atmosphere system. Figure 5.17 summarizes the Intergovernmental Panel on Climate Change (IPCC) Fourth Assessment Report (AR4) estimates of major components of global average RF between 1750 and 2005 [Forster *et al.*, 2007]. While Figure 5.17 shows global mean annual average RF, the RF of particular forcing agents varies strongly with location and season.

For a sustained forcing, RF can be linearly related to the global mean equilibrium surface temperature response ( $\Delta T_s$ ),

$$\Delta T_s = \lambda \text{ RF}$$

where  $\lambda$  is the climate sensitivity. For forcing agents like long-lived greenhouse gases (LLGHGs), approximately the same value of  $\lambda$  applies. However, for O<sub>3</sub> or aerosols,  $\lambda$  can be substantially different from that of LLGHGs, and more uncertain, and the estimated ratio of  $\lambda$  for a given forcing to that of CO<sub>2</sub> is defined as “climate efficacy” (Figure 5.17). Although RF does not reflect the overall climate response, providing only a limited measure of climate change, it is the most simple and commonly accepted indicator for quantitatively assessing the drivers of climate change [NRC, 2005].

#### **Mechanisms and magnitudes of anthropogenic radiative forcing**

##### **Ozone**

Anthropogenic emissions of O<sub>3</sub> precursors – NO<sub>x</sub>, CO, NMVOCs, and methane – react chemically in the troposphere to produce O<sub>3</sub>. Since O<sub>3</sub> is a radiatively active gas, absorbing in both the short-wave and long-wave, changes in O<sub>3</sub> precursors that increase O<sub>3</sub> will lead to a positive RF from O<sub>3</sub>. However, these chemical reactions also affect methane and aerosol concentrations, leading to forcings that may affect the net RF [Shindell *et al.*, 2009], as discussed in section 5.3.2.1.

The AR4 estimate for the forcing from tropospheric O<sub>3</sub> changes from 1750 to 2000, due to anthropogenic emissions of precursors, is 0.25-0.65 Wm<sup>-2</sup> (5-95%) with a best estimate of 0.35 Wm<sup>-2</sup>. These estimates of O<sub>3</sub> forcing are largely based on chemistry model results, since few measurements are available of pre-industrial O<sub>3</sub>. Gauss *et al.* [2006] showed that uncertainty in the O<sub>3</sub> forcing is largely driven by the variation in the O<sub>3</sub> changes simulated by the chemistry models, reflecting differing sensitivities of model chemistry schemes to changes in emissions of O<sub>3</sub> precursors.

O<sub>3</sub> also has an indirect warming effect on climate by inhibiting the natural uptake of CO<sub>2</sub> [Sitch *et al.*, 2007], as discussed in section 5.2.2.5. This may have led to a doubling of the climate forcing attributable to O<sub>3</sub> since pre-industrial times. The estimates are very uncertain as studies of O<sub>3</sub> impacts have focused on crop species, with fewer studies of natural forests (especially in the tropics).

Radiative forcing of climate between 1750 and 2005

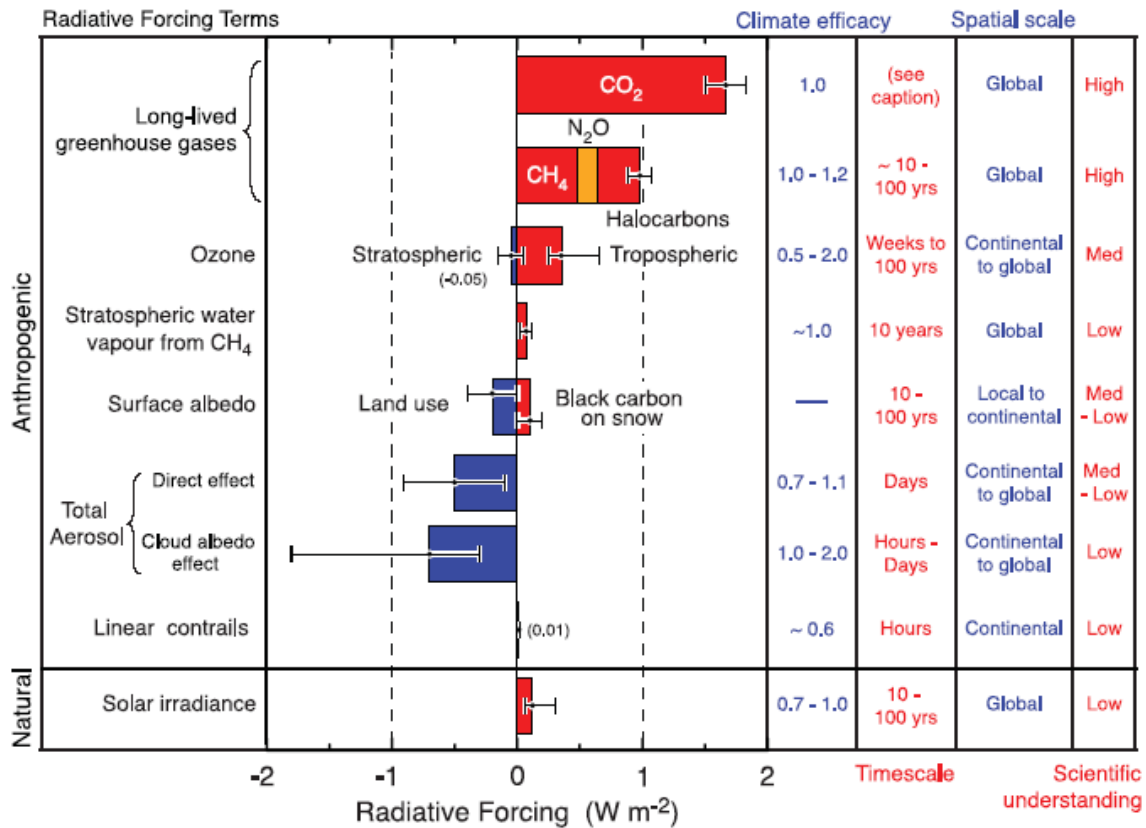


**Figure 5.17** IPCC AR4 summary of averages and ranges of global mean radiative forcing (RF) in units of Watts per square meter (Wm<sup>-2</sup>) between 1750 and 2005 for major forcing agents, including carbon dioxide (CO<sub>2</sub>), methane (CH<sub>4</sub>), nitrous oxide (N<sub>2</sub>O), ozone, land use, aerosols, and solar irradiance. Typical climate efficacy, timescale, geographical extent of forcing, and the assessed level of scientific understanding are also given. No CO<sub>2</sub> time scale is given, as its removal from the atmosphere involves a range of processes that can span long time scales, and thus cannot be expressed accurately with a narrow range of lifetime values. [Adapted from Forster, P. et al. (2007), Changes in atmospheric constituents and radiative forcing, *Climate Change 2007: The Physical Scientific Basis*, Cambridge University Press, Cambridge, United Kingdom and New York, NY, USA.]

**PM**

Aerosols perturb the Earth’s energy budget *directly* by scattering and absorbing radiation and *indirectly* by acting as cloud condensation nuclei and in doing so changing cloud properties. Box 5.2 describes a suite of mechanisms by which aerosols interact with radiation and affect climate. The IPCC estimates that anthropogenic aerosol direct RF is -0.5 [±0.4] Wm<sup>-2</sup> and indirect RF through the cloud albedo effect on liquid water clouds is -0.7 [-1.8, -0.3] Wm<sup>-2</sup>. Globally-averaged, the sum of aerosol direct and indirect RF of -1.2 Wm<sup>-2</sup> [-2.4 to -0.6 Wm<sup>-2</sup>] (cooling) is significant compared to the positive (warming) forcing of 2.63 [±0.26] Wm<sup>-2</sup> by anthropogenic LLGHGs [Forster et al., 2007]. However, the uncertainty in aerosol RF is much greater than that of LLGHGs, and is among the most important uncertainties in understanding anthropogenic climate change [Andreae et al., 2005]. These uncertainties result from the strong spatial heterogeneity in concentrations, uncertainties in emissions, chemical processing and lifetimes, and uncertainties in the effects of aerosols on cloud processes. Different aerosol components may provide warming or cooling based on the properties of the aerosol, atmosphere, and underlying surface. BC is estimated to cause a total globally-averaged positive forcing of 0.34 (0.09 to 0.59) Wm<sup>-2</sup> (Figure 5.17). This includes a forcing from deposition on snow estimated as +0.1 [±0.1] Wm<sup>-2</sup>, or +0.05 Wm<sup>-2</sup> [0.007, 0.13 Wm<sup>-2</sup>] in a recent study [Flanner et al., 2007].

## Box 5.2. Mechanisms of Aerosol Radiative Forcing

Aerosols interact strongly with solar and terrestrial radiation in several ways, as illustrated in Figure 5.18. They scatter and absorb radiation, thereby perturbing the radiative balance of the Earth-atmosphere system [McCormick and Ludwig, 1967]; these are described as “aerosol direct effects”. Aerosol direct effects in the solar spectrum generally dominate over that in the thermal infrared, except for large particles such as mineral dust. Purely scattering aerosols (including sulphates, nitrates, and sea salt) exert a negative RF by reflecting solar radiation back to the space, while partly absorbing aerosols (including dust and organics) may exert a negative RF over dark oceans and vegetated land but a positive RF over bright surfaces such as deserts, snow, ice, and clouds. Black carbon is a strongly absorbing aerosol, expected to give a positive global average RF. As particles age, their chemical composition can change to more of a mixture, affecting their optical properties, lifetimes, and uptake of water.

Aerosols also interact indirectly with radiation through acting as cloud condensation nuclei and/or ice nuclei. Increases in aerosol particle concentrations may increase the ambient concentration of cloud condensation and ice nuclei, causing smaller but more numerous cloud droplets for fixed cloud water content [Twomey, 1977]. This makes clouds reflect more solar radiation, causing a negative RF (the “indirect effect” or “cloud albedo effect”).

Other effects of aerosols are also important for climate change. Both aerosol scattering and absorption decrease the solar radiation reaching the surface, causing the negative RF at the surface to be stronger than at the TOA. Aerosol absorption can also increase atmospheric radiative heating. The simultaneous surface cooling and atmospheric heating alter convection and cloud formation, thus changing cloud extent and optical properties as well as circulation and precipitation patterns [Hansen et al., 1997]. The changes in cloud microphysics due to increases in aerosols may also alter the likelihood and intensity with which a cloud eventually precipitates [e.g., Albrecht, 1989; Gunn and Phillips, 1957], but these effects, particularly on mixed-phase or ice clouds, are not well understood. It has proven difficult to establish climatically meaningful relationships between aerosols, clouds, and precipitation [Stevens and Feingold, 2009].

Finally, the deposition of absorbing aerosols such as black carbon and dust in snow can reduce the albedo of snow, mainly in the visible, because of enhanced absorption by multiple scattering in the snowpack. This causes a positive RF and promotes melting of snow and ice [Warren and Wiscombe, 1980].

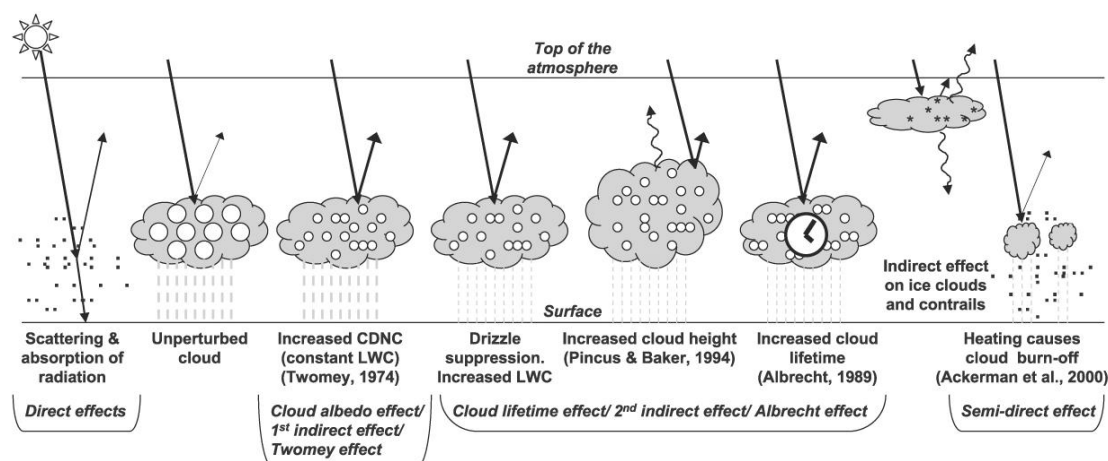


**Figure 5.18.** Schematic diagram showing the major radiative forcing mechanisms related to aerosols. The small black dots represent aerosol particles; the larger open circles cloud droplets. Straight lines represent the incident and reflected solar radiation, and wavy lines represent terrestrial radiation. The filled white circles indicate cloud droplet number concentration (CDNC). The unperturbed cloud contains larger cloud drops as only natural aerosols are available as cloud condensation nuclei, while the perturbed cloud contains a greater number of smaller cloud drops as both natural and anthropogenic aerosols are available as cloud condensation nuclei (CCN). The vertical grey dashes represent rainfall, and LWC refers to the liquid water content. [Adapted from Forster, P., et al. (2007), *Changes in atmospheric constituents and radiative forcing, Climate Change 2007: The Physical Scientific Basis*, Cambridge University Press, Cambridge, United Kingdom and New York, NY, USA.]

These aerosol forcing assessments, based largely on model calculations, are also constrained as much as possible by observations. For example, the IPCC estimate of aerosol RF based on forward calculations has recently been corroborated by an inverse calculation of  $-1.1 \text{ Wm}^{-2}$  [ $-1.9$  to  $-0.3 \text{ Wm}^{-2}$ ] [Murphy *et al.*, 2009]. Similarly, updated estimates of the aerosol direct RF, based on satellite observations, include  $-0.65 \text{ Wm}^{-2}$  [Bellouin *et al.*, 2008] and  $-0.9 [\pm 0.4] \text{ Wm}^{-2}$  [Quaas *et al.*, 2008], which is stronger than the IPCC AR4 estimate and model-based estimates generally, and Myhre [2009] estimates a weaker direct RF of  $-0.3 [\pm 0.2] \text{ Wm}^{-2}$ .

**FINDING: Increases in ozone and PM since preindustrial times have caused significant climate forcing. Ozone is a greenhouse gas that causes warming; in addition, damage to plants by ozone inhibits the natural uptake of CO<sub>2</sub>. PM is a mixture containing components that mainly cool, including sulphate and organic aerosols, and black carbon that warms. PM also influences climate by changing clouds.**

#### *Short-lived vs. Long-lived Forcings and Relations to Air Pollution*

Because O<sub>3</sub> and PM affect climate, actions to reduce air pollutant concentrations also affect climate. Reductions in O<sub>3</sub> would both improve air quality and slow global climate change. However, as discussed in section 5.3.2, reductions in emissions of O<sub>3</sub> precursors also influence methane, and can influence aerosols and the global carbon cycle. Therefore, the net effects of changes in emissions of each O<sub>3</sub> precursor need to be evaluated for both air quality and net radiative climate forcing. Among the components of PM, BC aerosols are identified as the only form that causes warming on a global scale, and reductions in BC emissions would likely improve PM air quality and slow climate change. Other components of PM have a net cooling influence, and so reducing these emissions likely exacerbate warming. However, analysts and governments have been reluctant to treat emissions of PM and their precursors as a benefit to climate, for two main reasons: (i.) their significant effects on air quality, health, and ecosystems, and (ii.) the possible effects of their regionally-specific forcings on climate (Section 5.3.3).

**FINDING: Any change in emissions that influences ozone and/or PM will generate a climate forcing.**

O<sub>3</sub> and PM differ from the major greenhouse gases in that perturbations to them produce relatively short-lived forcings (Figure 5.17). Whereas CO<sub>2</sub> and N<sub>2</sub>O perturbations persist in the atmosphere for over a century, and those of methane decay on decadal timescales, the lifetime of O<sub>3</sub> is on the order of weeks, while those of PM and its precursors are on the order of days. Despite their short life, emissions of PM and its precursors significantly counteract the RF due to the accumulation of years of emissions of the LLGHGs. As emissions continue in the future, the LLGHGs will continue to accumulate in the atmosphere, while the short-lived forcings will not. Over the long term, LLGHGs will very likely dominate. However, because of the short lifetimes of O<sub>3</sub>, BC, and also methane, actions to reduce these emissions would be very effective at slowing the short-term rate of global warming over the coming decades [Hansen *et al.*, 2000], leading some to define Short-Lived Climate Forcers (SLCFs) as a problem separate from, but related to the warming of LLGHGs [Jackson, 2009; U.S. CCSP, 2008]. Despite the clear benefits of reducing these emissions, BC and O<sub>3</sub> precursors (with the exception of methane) have not been included in international actions to address climate change. Similarly, reductions in PM components other than BC will exacerbate short-term warming, and may cause the rate of climate change to be greatest before the 2030s [Raes and Seinfeld, 2009].

**FINDING: Emissions relevant for ozone and PM have short atmospheric lifetimes, compared to the long-lived greenhouse gases, and will strongly influence the rate of climate change in the coming decades. There are opportunities to improve air quality while slowing climate change, but many actions to reduce PM would exacerbate warming.**

For LLGHGs, it is common to compare the climate forcings of different changes in emissions by using the Global Warming Potential (GWP), which integrates forcing over a selected time horizon, typically 20 or 100 years. Because O<sub>3</sub> and PM have lifetimes much shorter than that of LLGHGs, the choice of time horizon has a large influence on the estimated GWP.



Because short-lived species are distributed inhomogeneously, the resulting forcing will depend on where the species are emitted and where they or their products are transported. Section 5.3.2 addresses the spatial extent of RF caused by emissions from a source region, as well as the nonlinear dependencies of forcing on precursor emissions. The impacts of spatially inhomogeneous forcings on regional and global climate are then addressed in Section 5.3.3.

### 5.3.2. Radiative Forcing of Ozone and PM: Regional Extent and Effects of Varying Precursor Emissions

Because O<sub>3</sub> and PM have short lifetimes, their forcings are largely exerted on regional to intercontinental scales. In this section, we address the spatial extents of forcings from regional emissions and the importance of LRT for climate. In addition, for both O<sub>3</sub> and PM, the effects of changes in emissions depend strongly on chemistry, gas-aerosol interactions, and other factors. Consequently, we explore the importance of these many influences in determining the RF of changes in emissions of different precursors from different world regions.

#### Ozone

RF generated by increases in tropospheric O<sub>3</sub> since pre-industrial times [e.g., *Berntsen and Isaksen, 1997; Gauss et al., 2006; Shindell et al., 2003*], and also projected for the future [e.g., *Gauss et al., 2003; Stevenson et al., 2006*], has a distinct regional structure. This is the result of spatial variations in several contributing factors: (i) horizontal and vertical distributions of changes in O<sub>3</sub>; (ii) various physical aspects of the climate system that determine the passage of radiation through the atmosphere (e.g., surface and cloud albedos, for short wave radiation; and surface and vertical profiles of temperature and clouds, for long wave radiation); and (iii) how (i) and (ii) overlap. While local changes in O<sub>3</sub> at the surface are very important for air quality, changes in O<sub>3</sub> over a larger area, and in the middle to upper troposphere (where O<sub>3</sub> exerts a larger RF per unit change in concentration) become particularly important for climate. While O<sub>3</sub> at a given location has a complex dependency on precursor emissions from local and distant sources (Chapter A4), the above factors make this picture even more complicated for RF.

Some studies have calculated RFs due to emissions from specific regions [e.g., *Derwent et al., 2008; Naik et al., 2005; Naik et al., 2007; Stevenson and Derwent, 2009*]. Figure 5.19 shows O<sub>3</sub> RFs resulting from 10% NO<sub>x</sub> emissions reductions from specific regions, including only RFs from the initial, short-term increase in O<sub>3</sub>, and not the long-term impacts on O<sub>3</sub> associated with changes in CH<sub>4</sub>. The O<sub>3</sub> RF is partly determined by the extent of transport of O<sub>3</sub> and its precursors away from source regions. The extent of transport depends upon the wind field and the lifetimes of the species, both of which may vary seasonally and inter-annually, and may also change as climate changes. Naik et al. [2005] found that the short-term O<sub>3</sub> RF from NO<sub>x</sub> emissions varies with season of emission, with typically the largest O<sub>3</sub> RF occurring in the summer. The strong influences of emissions from North America (NA), Europe (EU) and East Asia (EA) result from the large emissions in these regions. Figure 5.20 shows that when RF is normalized by NO<sub>x</sub> emissions, SE Asia (SE), S America (SA) and India (IN) produce the largest O<sub>3</sub> RF per unit NO<sub>x</sub> emission, illustrating greater sensitivity in the tropics than mid- and high-latitudes. In a similar study of aircraft NO<sub>x</sub> emissions, Stevenson and Derwent [2009] found that regions with low background NO<sub>x</sub> generated the most O<sub>3</sub> RF per unit NO<sub>x</sub> emission, whereas latitude was a less important influence.

Changes in emissions of O<sub>3</sub> precursors (NO<sub>x</sub>, CH<sub>4</sub>, CO and VOCs) have additional impacts on RF, as they alter hydroxyl radical (OH) concentrations, affecting the removal rate and, therefore, the concentration of CH<sub>4</sub>. NO<sub>x</sub> emissions tend to increase OH (which reduces CH<sub>4</sub>, Figure 5.20); whereas CH<sub>4</sub>, CO and VOC emissions tend to consume OH (which increases CH<sub>4</sub>). In addition, oxidation of these C-containing species produces CO<sub>2</sub>. The effects of decreasing emissions of NO<sub>x</sub> have been shown to cause a positive net RF, as the RF of the CH<sub>4</sub> increase is greater than that of the ozone decrease [e.g., *Wild et al., 2001*], and this has been shown to be the case for NO<sub>x</sub> emissions from all world regions (Fig. 5.3.4). Further forcings arise because CH<sub>4</sub> oxidation is a significant source of tropospheric O<sub>3</sub>, in addition to stratospheric H<sub>2</sub>O, and NO<sub>x</sub> produces nitrate aerosol. Any change in oxidants will also affect formation rates of secondary aerosols.

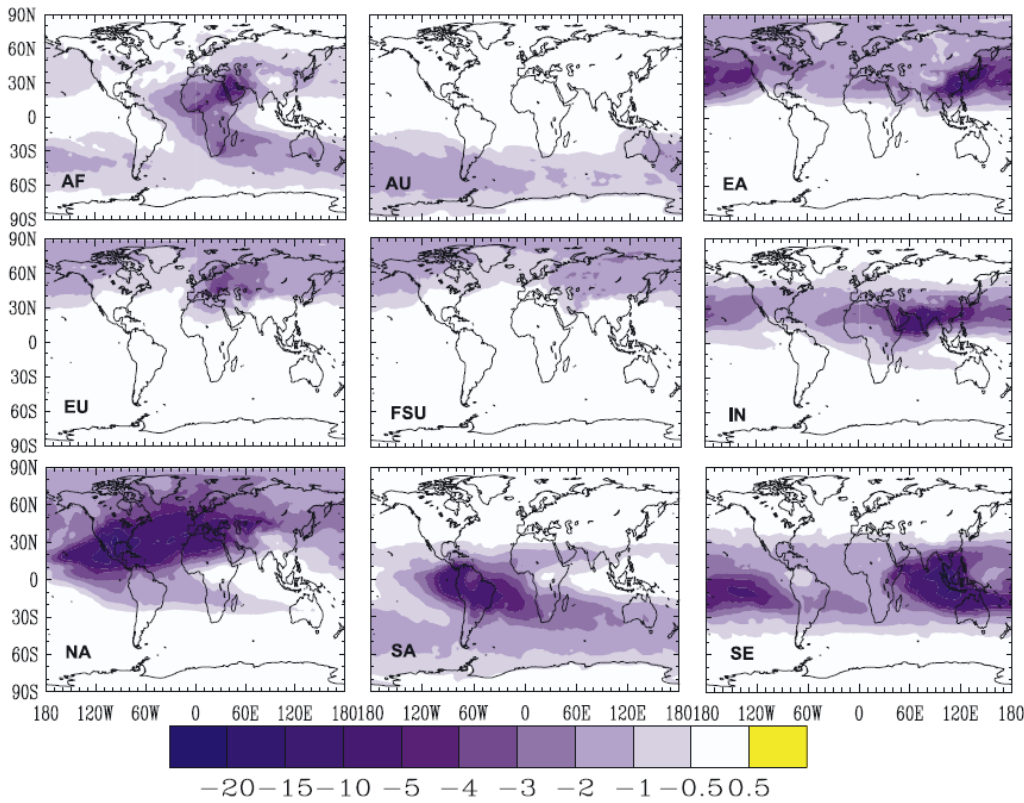


**Figure 5.19.** Annual total-sky instantaneous RF ( $\text{mWm}^{-2}$ ) due to short-term changes in  $\text{O}_3$  from a 10% reduction in surface anthropogenic  $\text{NO}_x$  emissions from each of nine world regions. [Reprinted from Figure 7 in Naik, V., et al. (2005), Net radiative forcing due to changes in regional emissions of tropospheric ozone precursors, *Journal of Geophysical Research*, 110 (D24306).]

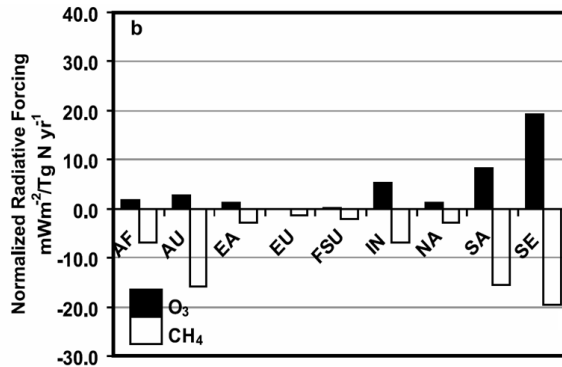


**Figure 5.20.** The change in annual average RF per unit change in  $\text{NO}_x$  emissions for 10% regional  $\text{NO}_x$  reductions in Figure 5.19 [adapted from Figure 9b in Naik, V., et al. (2005), Net radiative forcing due to changes in regional emissions of tropospheric ozone precursors, *Journal of Geophysical Research*, 110 (D24306)]. The  $\text{O}_3$  RFs include an estimate of the long-term contribution due to changes in methane. Associated estimates of methane RF are also shown; these have the opposite sign as the  $\text{O}_3$  RFs, and are larger in magnitude.

By modelling the effects of emissions of each precursor, the IPCC AR4 Assessment [Forster et al., 2007] attributed the global mean annual average RF (in  $\text{Wm}^{-2}$ ) to anthropogenic changes in emissions: 0.86 from  $\text{CH}_4$ , 0.27 from CO and VOCs, and  $-0.21$  from  $\text{NO}_x$ . These emissions-based estimates of forcing differ from the abundance-based estimates in Figure 5.17, and include the effects of

methane on CO<sub>2</sub>, O<sub>3</sub>, and stratospheric water vapour, the effects of NO<sub>x</sub> on O<sub>3</sub>, methane and nitrate aerosols, and the effects of CO and VOCs on CO<sub>2</sub>, methane and O<sub>3</sub>. A recent study [Shindell *et al.*, 2009] found somewhat different RF values (Wm<sup>-2</sup>) for these O<sub>3</sub> precursor species (Figure 5.21): 0.99 from CH<sub>4</sub>, 0.25 from CO+VOCs (0.19 from CO and 0.06 from VOCs), and -0.29 from NO<sub>x</sub>. Differences relative to AR4 resulted largely from the inclusion of additional gas-aerosol interactions, so that these calculations included the effect of all emissions on sulphate and nitrate aerosols. For changes in methane emissions, the temperature change 20 years after a methane emission pulse is ~57 times that of CO<sub>2</sub> on a kg/kg basis. This factor of 57 can be broken down into 41 from the direct effect, 10 via tropospheric ozone production and 6 via stratospheric water vapour [Boucher *et al.*, 2009].

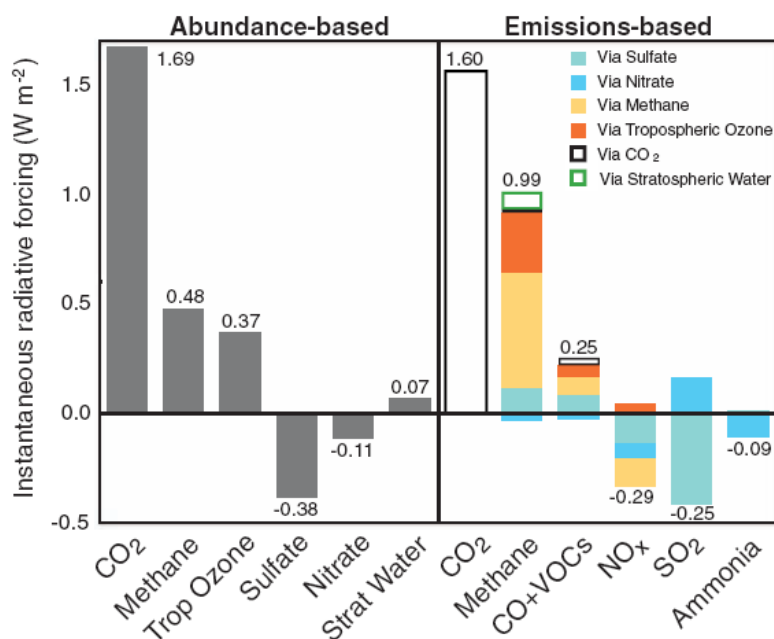


**Figure 5.21.** Radiative forcing from 1750 to 2000. Numerical values within the figure give the net forcing (instantaneous at the tropopause). Uncertainties in the abundance-based values are 0.16 for CO<sub>2</sub>, 0.05 for methane, +0.15 to -0.10 for ozone, 0.20 for sulphate, 0.10 for nitrate, and 0.05 for stratospheric water. For emissions-based values, uncertainties are estimated as 0.14 for methane, 0.04 for CO+VOCs, 0.09 for NO<sub>x</sub>, 0.23 for sulphate, and 0.10 for ammonia. The aerosol indirect effect is not included. [From Figure 1 from Shindell, D., *et al.* (2009), Improved attribution of climate forcing to emissions, *Science*, 326(5953): 716-718. Reprinted with permission from AAAS.]

The estimates of anthropogenic RF in Figure 5.21 also have bearing on the RF from changes in emissions. At a global scale, reductions in emissions of O<sub>3</sub> precursors have been studied for their effects on both surface O<sub>3</sub> air quality and radiative climate forcing. Among O<sub>3</sub> precursors, global reductions in methane emissions have been shown to best reduce RF per unit improvement in O<sub>3</sub> air quality metrics, mainly because of the reduction in methane itself, followed by CO and NMVOCs, while NO<sub>x</sub> emissions are expected to lead to a net positive RF [West *et al.*, 2007a]. These conclusions are supported by Fig 5.3.5, where effects on aerosol species are included. Note, however, that the above calculations do not include the effect of O<sub>3</sub> on carbon uptake (section 5.2.2.5).

Except for methane, the effects of O<sub>3</sub> precursor emissions on global mean RF differ with the location of those emissions, depending upon factors such as the local chemical regime, lifetime, and photolysis rates of key species. Several modelling studies have attempted to quantify the RF of the geographic distribution, altitude and season of O<sub>3</sub> precursor emissions [e.g., Berntsen *et al.*, 2005; Derwent *et al.*, 2008; Fuglestedt *et al.*, 1999; 2010; Naik *et al.*, 2005]. In Figure 5.20, reductions in surface NO<sub>x</sub> emissions from all world regions cause a positive RF, for sustained emissions changes at steady state, although the sensitivity of O<sub>3</sub> and CH<sub>4</sub> per unit change in emissions varies considerably

among regions. Most studies suggest high altitude aircraft NO<sub>x</sub> emissions produce a net warming [e.g., Köhler *et al.*, 2008; Lee *et al.*, 2009; Wild *et al.*, 2001], whilst others suggest a net cooling [Stevenson *et al.*, 2004; Stevenson and Derwent, 2009]. Background levels of NO<sub>x</sub> were the primary determinant of the net climate forcing from aircraft NO<sub>x</sub>, with larger net forcings produced by emissions into cleaner regions; latitude of emission was a lesser influence [Stevenson *et al.*, 2004; Stevenson and Derwent, 2009]. Analyses of the dependence of RF on the location of CO and VOC emissions have not been as detailed as for NO<sub>x</sub>, nor have seasonal dependencies been quantified, and the available studies of regional emissions do not include the effects on aerosols [Shindell *et al.*, 2009], nor the effect of O<sub>3</sub> on plants and the carbon cycle [Sitch *et al.*, 2007].

The time dependence of the climate impact has been studied by Collins *et al.* [2010], who analysed year-long pulse emission reductions from the HTAP regions, accounting for changes in both O<sub>3</sub> and methane. In Figure 5.22, the HTAP NO<sub>x</sub> reductions initially cool climate since less O<sub>3</sub> is produced; however this effect decays and is replaced by a warming due to less destruction of methane. For VOC and CO emissions the O<sub>3</sub> and methane changes both cool climate. The initial dip (more pronounced for the VOC emissions) is due to the impact on O<sub>3</sub>, the longer tail due to the impact on methane. As for Naik *et al.* [2005] and Berntsen *et al.* [2005], the O<sub>3</sub> is most sensitive to NO<sub>x</sub> emissions in a cleaner atmosphere (S. Asia) although it is least sensitive to the VOC emissions here. The methane destruction is most sensitive to tropical emissions (S. Asia). For CO, the only noticeable regional dependence is for European emissions, which being at the highest latitude have the least impact on methane. This study does not include the impact of O<sub>3</sub> on plants and the carbon cycle, and assumes a constant forcing per unit column burden and constant climate sensitivity regardless of location. Berntsen *et al.* [1997] and Shindell and Faluvegi [2009] suggest these quantities have a latitudinal dependence.

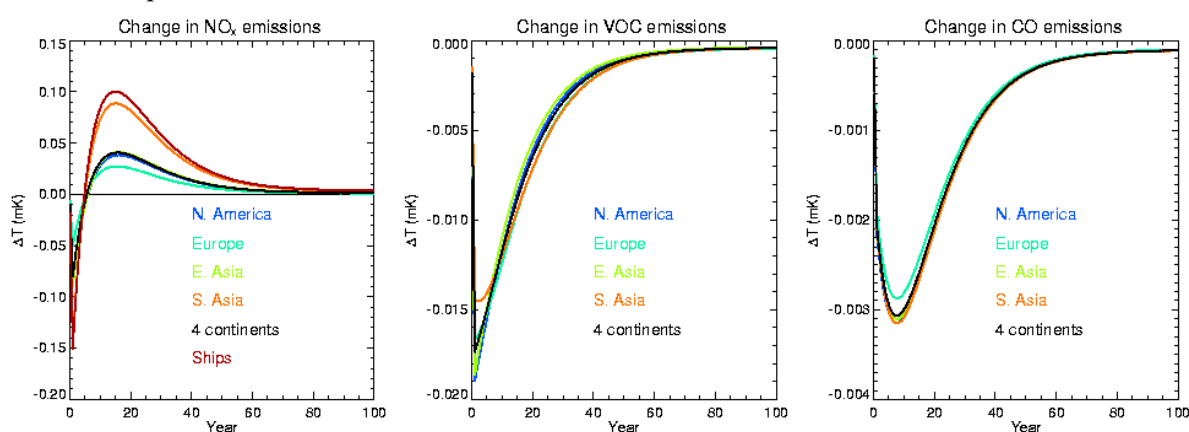


**Figure 5.22.** Change in global surface temperature for the years following a 1 Tg emission reduction in the first year. The normalisation is per Tg N, C and CO for NO<sub>x</sub>, VOC and CO. [Adapted from Figure 7 in Collins, W. J., *et al.* (2010), How vegetation impacts affect climate metrics for ozone precursors, *Journal of Geophysical Research*, 115 (D23308).]

**FINDING: Among ozone precursors, widespread reductions in emissions of CH<sub>4</sub>, CO, and NMVOCs better decrease net climate forcing than reducing NO<sub>x</sub>, which may increase forcing.**

**FINDING: Except for methane, the effects of ozone precursor emissions on global mean RF differ with the location of those emissions.**

### PM

Like O<sub>3</sub>, the distribution and magnitude of the aerosol direct and indirect RFs are mainly determined by the spatial patterns of PM concentrations, but also depend on the absorption and scattering properties of those aerosols, their possible roles as cloud condensation nuclei, and environmental factors such as surface albedo and the presence of clouds [Forster *et al.*, 2007]. Industrialised regions of North America, Europe and Asia, and biomass-burning regions of Africa and South America are associated with large, negative aerosol direct forcing. Positive aerosol direct

forcing occurs where absorbing aerosols overlie bright surfaces, such as in the stratocumulus regions and over ice surfaces of the polar regions.

The spatial extents of aerosol direct RF from regional emissions and the role of aerosol LRT are revealed by a preliminary analysis comparing the HTAP PM SR6 perturbation runs (20% reductions in regional anthropogenic emissions), relative to SR1. We calculate direct RF from the archived aerosol optical depth fields for each component (i.e., sulphate, BC, or POM) from SR6 and SR1, in combination with RF efficiencies (forcing per unit optical depth) from the GOCART model [Yu *et al.*, 2006]. The seven models used in this preliminary analysis are: CAMCHEM (version 3311m13 and version 3514), ECHAM5-HAMMOZ, GISS-PUCCINI modelE, GMI, GOCART, and SPRINTARS. Figure 5.23 shows that emissions from North America, Europe, and East Asia exert significant RF on intercontinental and hemispheric scales. Emissions from South Asia have relatively small impacts mainly over the tropical Pacific. For all four regions, the extent of direct RF is much smaller in winter than in other seasons (not shown).

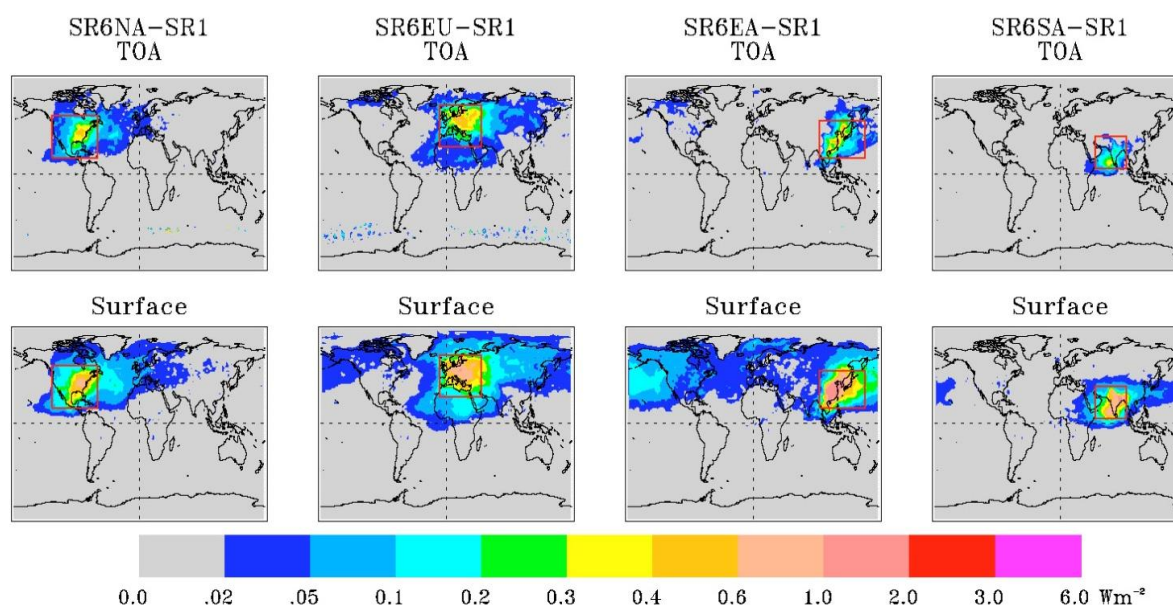


**Figure 5.23.** The annual average all-sky aerosol direct RF ( $\text{Wm}^{-2}$ ) at the top of atmosphere (TOA) (top panel) and at the surface (bottom panel) resulting from 20% reductions of anthropogenic emissions over North America (NA), Europe (EU), East Asia (EA), and South Asia (SA), respectively. A positive RF represents that the aerosol direct RF is weakened by the reduction of emissions. Each of the four source regions is overlaid on corresponding SR6xx-SR1 maps.

As in Chapter A4, we calculate the relative annual intercontinental response (RAIR) as the direct RF response in a receptor region to the combined influence of 20% emission reduction in the three foreign emission regions, divided by the response to 20% emission reduction in all four regions. RAIR in a region represents the percentage contribution of LRT of foreign emissions relative to a sum of foreign and domestic emissions. RAIRs for aerosol optical depth (AOD) (Table 5.6) and direct RF (Table 5.7) depend on both region and species. For all regions and species, import from LRT is significant, with RAIR ranging from 9 to 30%. South Asia is most influenced by import of sulphate aerosol, and North America is most influenced by import of BC, followed by POM. For sulphate, POM, and BC combined, South Asia RF is most strongly influenced by foreign sources, and North America and Europe is the least. These rankings also reflect the strength of local emissions, relative to world emissions. Interestingly, RAIR values for optical depth and direct forcing of sulphate are much smaller than that for aerosol column loading [see Table 4.4 in Chapter A4]. This probably stems from transported sulphate aerosols experiencing lower relative humidity at high altitude (resulting in lower

optical depth) than local aerosols, which generally remain at lower altitudes. Finally, model variability is very large, highlighting the significant uncertainties in modelling aerosol processes.

**Table 5.6.** Multi-model derived relative annual intercontinental response (RAIR) (mean  $\pm$  std. dev) for aerosol optical depth for four HTAP regions, in SR6 simulations relative to SR1, by chemical component. Standard deviations measure the model variability in simulating aerosol transport. BC stands for black carbon aerosol, and POM for particulate organic matter aerosol.

Receptor	NA	EU	EA	SA
BC	27% $\pm$ 16%	19% $\pm$ 12%	15% $\pm$ 3%	17% $\pm$ 6%
POM	21% $\pm$ 14%	19% $\pm$ 11%	19% $\pm$ 4%	12% $\pm$ 6%
Sulphate	14% $\pm$ 8%	12% $\pm$ 6%	16% $\pm$ 6%	30% $\pm$ 8%
BC+POM+Sulphate	16% $\pm$ 8%	14% $\pm$ 5%	16% $\pm$ 5%	25% $\pm$ 7%

**Table 5.7.** As Table 5.6, but for RAIR for TOA all-sky aerosol direct RF.

Receptor	NA	EU	EA	SA
BC	29% $\pm$ 17%	22% $\pm$ 13%	16% $\pm$ 4%	21% $\pm$ 6%
POM	21% $\pm$ 15%	19% $\pm$ 12%	21% $\pm$ 6%	11% $\pm$ 6%
Sulfate	13% $\pm$ 8%	12% $\pm$ 6%	16% $\pm$ 6%	29% $\pm$ 8%
BC+POM+Sulphate	9% $\pm$ 10%	10% $\pm$ 8%	17% $\pm$ 10%	26% $\pm$ 9%

These general findings on the extent of RF from regional emissions are supported by other studies. Reddy and Boucher [2007] and Shindell et al. [2008c] found that BC emitted in Asia contributes 20% of the BC burden in North America. Bond [2004] found that BC exerts a regional scale radiative forcing much larger than its local influence on air quality. On a regional scale again, Lau et al. [2006] suggest that locally large BC and mineral dust concentrations in India, combined with the specific orographic features of the Indian subcontinent, profoundly affect the Asian monsoon and Himalayan climate. Wang and Christopher [2006] found that the transport of Central American smoke aerosols to the southern U.S. in spring can decrease the monthly-averaged air temperature in Texas near the surface by 0.2°C, but enhance the upper boundary layer air temperature by ~0.1°C.

**FINDING: In the four HTAP regions, the contribution of foreign regions to aerosol RF may be roughly 10-30% of the total.**

The global mean anthropogenic RF has been attributed by the IPCC AR4 to emissions of particular species (in  $\text{Wm}^{-2}$ ): 0.44 for BC, and -0.19 for OC. In general, RF is expected to respond roughly linearly to changes in emissions for primary PM species, but may be nonlinear for secondary aerosols. In Figure 5.21, estimates of RF attributable to anthropogenic sulphur dioxide and ammonia include the interaction between the resulting sulphate and nitrate aerosols, finding forcings of -0.25 for  $\text{SO}_2$  and -0.09 for ammonia, and the -0.29 for  $\text{NO}_x$  includes both gas-phase and aerosol changes. Future research will need to evaluate anthropogenic contributions to global secondary organic aerosols, both through emissions of VOCs and through changes in atmospheric oxidants.

Just as aerosols exert a RF regionally, the effects of changes in emissions of PM and its precursors on global mean RF also varies with region. Table 5.8 lists changes of global annual average TOA direct



RF in response to the 20% reduction of anthropogenic emissions in four HTAP source regions. The global mean annual average TOA direct RF from baseline (SR1) simulations of 6 models is  $-0.74 \pm 0.27$ ,  $-0.26 \pm 0.09$ , and  $+0.36 \pm 0.12 \text{ Wm}^{-2}$  for sulphate, POM, and BC, respectively, where both anthropogenic and natural sources are included. Uncertainties are likely to be systematically underestimated due to the use of a single model to calculate RF from all models' simulated aerosol changes. The combined impact of 20% emission reductions in the four regions is to weaken the RF by 9%, 4%, and 9% for sulphate, POM, and BC, respectively. Relative contributions from individual regions vary. For sulphate, the change of global average RF due to the reduction of emissions in South Asia is substantially smaller than that due to the emission reductions from the other regions. For POM and BC, the reduction of emissions in East Asia makes the largest contribution to the change of global average RF. Table 5.9 shows the global annual average TOA all-sky aerosol direct RF efficiency per unit emissions from the source regions. The forcing efficiency for BC is an order of magnitude higher than that for sulphate and POM. While some models show large regional dependence of the forcing efficiency for some components, the multi-model average forcing efficiency is not strongly dependent on region. Note that these results do not include aerosol indirect effects, nor warming resulting from BC deposition on snow and ice.

**Table 5.8.** Global annual average TOA all-sky aerosol direct RF (unit:  $\text{mWm}^{-2}$ ) in response to the 20% reduction of anthropogenic emissions in 4 source regions, for the mean  $\pm$  std. dev for SR1 and SR6 simulations of six HTAP models.

Source Region	Sulfate	POM	BC	Sulphate+POM+BC
NA	16.1 $\pm$ 5.6	1.6 $\pm$ 1.0	-4.5 $\pm$ 1.9	13.2 $\pm$ 5.2
EU	26.7 $\pm$ 9.5	1.9 $\pm$ 1.2	-7.4 $\pm$ 2.3	21.2 $\pm$ 9.5
EA	19.6 $\pm$ 7.2	3.2 $\pm$ 1.8	-14.5 $\pm$ 8.0	8.4 $\pm$ 10.2
SA	6.1 $\pm$ 1.9	2.5 $\pm$ 1.3	-5.5 $\pm$ 2.4	3.1 $\pm$ 3.2
NA+EU+EA+SA	68.4 $\pm$ 22.9	9.1 $\pm$ 5.0	-31.9 $\pm$ 13.7	45.9 $\pm$ 24.6

For BC, the relative impact on global mean RF for emissions from different areas has been calculated [Fuglestedt *et al.*, 2010; Reddy and Boucher, 2007; Rypdal *et al.*, 2009]. Reddy and Boucher [2007] found that BC transport to the Arctic is dominated by European emissions. The RF per unit emissions of BC can thus be significantly larger for emissions from Europe than for other regions, because of the higher forcing efficiency of BC over bright surfaces such as in the Arctic, while other results find greater RF for emissions from open burning in Northern Asia [Bond *et al.*, 2010]. The diversity in BC transport and deposition among numerical simulations is large, especially in Northern Eurasia and the Arctic [Koch *et al.*, 2009]. Source-receptor relationships are therefore likely to be model dependent. Nonetheless, analysis of these relationships in 17 HTAP models showed that even for transport to the Arctic, the models are quite consistent in the relative importance of transport from different regions, despite the diversity of absolute transport amounts [Shindell *et al.*, 2008c]. Rypdal *et al.* [2009] and Fuglestedt *et al.* [2010] generally showed higher forcing per unit emission for BC emissions from South Asia and to a lesser extent South America, somewhat higher values for emissions from Africa in many models, and typically lesser values for emissions from East Asia, Europe and North America. Variations are roughly a factor of 2 from high to low regions. For sulphate, the response to emission changes in North America is roughly twice the magnitude of the response to emissions from South and East Asia [Shindell *et al.*, 2008a], indicating that regional variations appear to again be substantial. Note that for BC in particular, due to its impact on snow and ice, localized impacts may be highly sensitive to both the location and also the season of emissions. Similarly, sulphur dioxide and short-lived O<sub>3</sub> precursors may have different impacts during different times of year when emitted near polar regions.



**Table 5.9** Global annual average TOA all-sky aerosol direct RF efficiency per unit change in emissions from 4 source regions (unit:  $\text{mWm}^{-2}$  per  $\text{Tg yr}^{-1}$ ) as derived from analysis of SR1 and SR6 runs of six HTAP models. The forcing efficiency for sulphate is calculated with respect to  $\text{SO}_2$  emissions, although some models with fully coupled chemistry include changes of sulphate resulting from the reductions of other emissions.

Source Region	Sulphate	POM	BC
NA	$-3.6 \pm 1.2$	$-4.4 \pm 1.2$	$42.0 \pm 14.7$
EU	$-3.7 \pm 1.3$	$-4.5 \pm 1.5$	$47.8 \pm 16.0$
EA	$-2.5 \pm 1.1$	$-3.4 \pm 1.1$	$43.4 \pm 23.0$
SA	$-3.2 \pm 0.7$	$-3.7 \pm 1.0$	$37.6 \pm 17.5$
NA+EU+EA+SA	$-3.2 \pm 1.1$	$-3.8 \pm 1.1$	$43.1 \pm 19.0$

The RF of any forcing can be compared using the GWP (global warming potential), which is defined as the RF from a unit mass pulse emission integrated over a number of years (typically 20 or 100) compared to that of  $\text{CO}_2$ . Thus the climate impact of any emission control measure for these species can be calculated. For shorter-lived species such as methane (lifetime  $\sim 9$  years), or aerosols and  $\text{O}_3$  precursors (lifetimes  $\sim 1$  week), GWPs can be calculated, but are less easy to interpret. For instance, the  $\text{GWP}_{100}$  for BC aerosols has been estimated to be 680 [Bond and Sun, 2005], or 374 to 677 depending on emission region [Reddy and Boucher, 2007] (Figure 5.24). However the timescales that BC and  $\text{CO}_2$  act on are so different that the  $\text{GWP}_{100}$  is less meaningful. The RF from 1 kg BC in the week after its emission is 6 orders of magnitude larger than that of  $\text{CO}_2$  but within weeks drops to near zero, while  $\text{CO}_2$  continues to exert a forcing for well over 100 years. Shine et al. [2007] introduced the concept of a global temperature potential as a more policy relevant metric. Boucher and Reddy [2007] applied this to BC and calculated a  $\text{GTP}_{100}$  of  $\sim 100$ , which is up to a factor of 7 lower than the  $\text{GWP}_{100}$ , since after 100 years much of the climate impact of BC has disappeared. Other methods have similarly been proposed to quantify the relative climate influence of short-lived forcers [e.g., Bond et al., 2010].

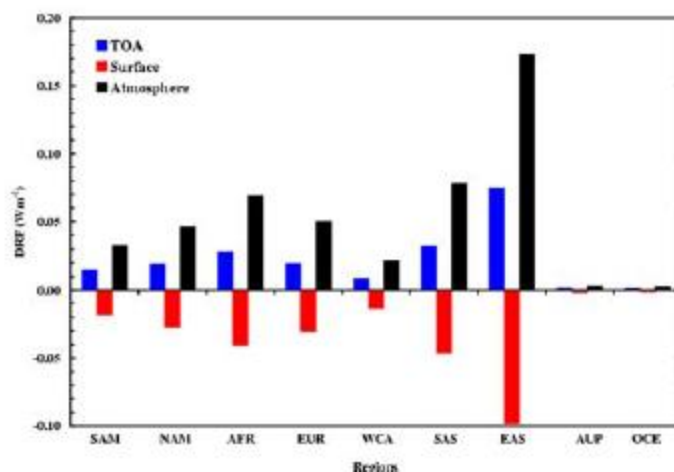


**Figure 5.24.** Global annual mean all-sky SW DRF at top-of-atmosphere (left bar), at surface (middle bar), and in the atmosphere (right bar) by BC emissions from different regions. [Reprinted from Figure 3 in Reddy, M. S., and O. Boucher (2007), Climate impact of black carbon emitted from energy consumption in the world's regions, *Geophysical Research Letters*, 34 (L11802).]

**FINDING: Reductions in PM would improve air quality and reduce premature mortality, but reductions in cooling aerosols, including sulphate, nitrate, and organic carbon would generally exacerbate global warming. Reductions in BC are likely to benefit both air quality and climate.**

**FINDING: The RF resulting from emissions of PM and its precursors is exerted regionally, and the effect on global annual mean RF varies with the location of the emissions.**

### 5.3.3. Relevance of Regional Forcings for Regional and Global Climate

The regional RFs associated with O<sub>3</sub> and PM likely influence climate over a larger area than the forcing itself, as they influence atmospheric heating and dynamics. However, current understanding of regional climate sensitivities to regional forcings is incomplete. Both detection and attribution studies and climate models have examined the geographic patterns of surface temperature response to inhomogeneous RF. Most of these studies, however, have investigated the response to changes occurring over much of the globe (e.g. preindustrial to present-day changes in aerosols). Such studies indicate that at small scales (hundreds to thousands of km) climate responses are typically not closely correlated with the location of RF and instead the spatial pattern of response at these scales appears to broadly match the patterns of response to more homogeneous forcings such as the well-mixed long-lived greenhouse gases (LLGHGs) [Boer and Yu, 2003; Hansen et al., 2005; Levy et al., 2008; Mitchell et al., 1995; Shindell et al., 2008b; Taylor and Penner, 1994]. These studies also show that at larger scales, the location of RF does influence the response. For example the change in NH temperature exceeds the SH response when the NH RF is greater.

More insight comes from several recent studies. One showed clearly that climate in the Arctic and over the high-latitude Southern Ocean was far more sensitive to non-local influences than climate in most other areas [Boer and Yu, 2003]. Chou et al. [2005] indicated that climate response to localized forcing could extend well beyond the forcing location. Another study looked at the effect of regional forcings on global and regional temperatures in a systematic way [Shindell and Faluvegi, 2009]. It found that global mean temperatures follow the global mean RF fairly closely, with an enhancement of ~45% for extratropical forcings relative to tropical ones for idealized CO<sub>2</sub> changes [similar to results in Hansen et al., 1997]. This reflects the influence of strong climate feedbacks in higher latitude regions, particularly snow and ice albedo feedbacks. For CO<sub>2</sub>, global sensitivity to NH extratropical forcing was ~75% larger than to SH forcing, due to the greater area covered by land and strong positive snow and ice albedo feedbacks. For sulphate, values were similar to those for CO<sub>2</sub> at mid-latitudes, but for high-latitudes the response appears to depend upon aerosol indirect effects: when they were included, the global mean sensitivity was again ~50% greater than for tropical forcing, but when they were not, the sensitivity decreased to only one-quarter of the sensitivity to tropical forcing. This is because the reflective properties of sulphate (the direct effect) have less impact over the bright snow and ice surfaces found at high latitudes.

Shindell and Faluvegi [2009] further demonstrated that tropical mean temperatures follow the global mean forcing fairly closely regardless of where the forcing is imposed, though the response is enhanced (~40%) for local forcings. For other regions, however, the response to non-local forcings is not necessarily simply proportional to either the global mean forcing or the mean forcing within the remote area. The response in extratropical regions decreases as the forcing becomes more remote. These results suggest that the tropics, with its enormous thermal mass, acts as an effective buffer between the two extratropical regions. Hence the uneven distribution of forcing over the Earth's surface has little effect on the global or tropical climate response, but can profoundly affect the extratropical responses. This is especially true in the Arctic (Section 5.3.4), consistent with the earlier results [Boer and Yu, 2003]. A new study quantifying the spatial scales over which RF influences climate found that over land areas from 30S-60N, the response extended ~3500 km (30 degrees) in the meridional direction, and at least 12,000 km in the zonal direction, with consistent results across several climate models [Shindell et al., 2010].

For other aspects of climate change, such as precipitation, fewer results are available. Those studies that do exist, however, suggest that at the largest spatial scales, the asymmetric distribution of aerosols between the two hemispheres may affect the location of the intertropical convergence zone

and its associated rainfall [Chou *et al.*, 2005; Chung and Seinfeld, 2005; Ming and Ramaswamy, 2009; Rotstayn and Lohmann, 2002]. Several detailed studies of the Asian monsoon suggest that regional forcing by absorbing aerosols may substantially alter precipitation patterns [e.g., Chung and Seinfeld, 2005; Meehl *et al.*, 2006; Ramanathan and Carmichael, 2008; Wang *et al.*, 2009].

**FINDING: Ozone and PM exert radiative forcings that are not globally uniform, but extend from the location of (precursor) emissions over regional and intercontinental scales. These heterogeneous forcings affect global climate change, and can influence patterns of regional climate change including temperature and precipitation. In general, high latitudes are more sensitive to RF, as a result of snow/ice feedbacks.**

#### 5.3.4 Impacts of Long-Range Transport on Climate in the Arctic

The Arctic is experiencing rapid climate change, as global warming is amplified in this region due to the large albedo feedbacks associated with changes in snow and ice cover. O<sub>3</sub> and PM have particular RF effects in the Arctic due to the high surface albedo and low atmospheric moisture content, which increases aerosol lifetimes. In addition to the forcings from O<sub>3</sub> and PM directly in the Arctic region, changes in circulation driven by forcings outside of the Arctic are important to Arctic climate. Because emissions of air pollutants within the Arctic itself are low, it is clear that emissions from outside of the Arctic dominate Arctic climate changes, including LRT to the Arctic. Air pollution and climate change in the Arctic are significant concerns for possible increased human activities, including shipping, in the region [e.g., Granier *et al.*, 2006].

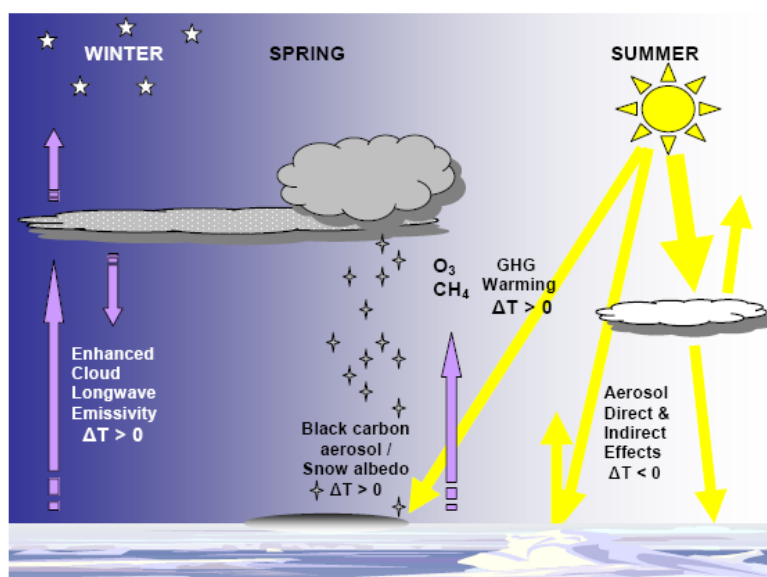


**Figure 5.25.** Forcing mechanisms in the Arctic environment resulting from the poleward transport of mid-latitude gas and particulate phase pollutants. The season of maximum forcing at the surface ( $F_s$ ) is indicated for each forcing agent.  $\Delta T$  indicates the surface temperature response. [Reprinted from Figure 1 in Quinn, P. K., et al. (2008), Short-lived pollutants in the Arctic: Their climate impact and possible mitigation strategies, *Atmospheric Chemistry and Physics*, 8(6): 1723-1735.]

A summary of the radiative effects of various pollutants on the Arctic is given by Quinn *et al.* [2008], and shown schematically in Figure 5.25. An estimate of the anthropogenic temperature change in the Arctic (Figure 5.26) shows that reflective aerosols, BC, and ozone have influences that are comparable to the warming from CO<sub>2</sub>. BC aerosol from fossil fuel or fire plumes has strong shortwave absorbance and can therefore warm the Arctic troposphere and stratosphere as well as reduce the net irradiance at the surface, especially above a high-albedo surface such as snow. The magnitude of this forcing, however, is highly variable in space and is not well-constrained [Baumgardner *et al.*, 2004]. The indirect RF associated with deposition of BC in Arctic snow (darkening) is receiving increased attention as ice-core and direct observational evidence suggest that soot levels, which had declined

through the late 20th century, may now be rising again [Eleftheriadis *et al.*, 2009; McConnell *et al.*, 2007; Sharma *et al.*, 2006]. Very small quantities of BC can significantly reduce the albedo of snow, thereby increasing snow aging and melt rates and further enhancing surface radiative warming through a positive feedback. It is thought that this mechanism may be contributing to accelerated glacier melting and sea ice cover reduction since the late 1990s [e.g., Kim *et al.*, 2005; Qian *et al.*, 2009]. As a result, the climate forcing efficacy due to BC in snow is estimated to be substantially larger than that of CO<sub>2</sub> [Hansen and Nazarenko, 2004]. Flanner *et al.* [2007] estimated that the anthropogenic contribution to the overall RF associated with BC deposition in the Arctic is in excess of 80%, and the resulting warming in the Arctic in the 20th century may have been as large as ~0.1-0.2 °C [Flanner *et al.*, 2007; Hansen and Nazarenko, 2004; Koch *et al.*, 2009].

High concentrations of pollution-derived sulphate aerosols may also impact Arctic climate by modifying the size distribution of ice nuclei in low-level clouds during the cold season, resulting in a reduced infrared radiation flux reaching the surface [Girard *et al.*, 2005]. Kristjansson *et al.* [2005] point out that the response of the Arctic climate system to direct and indirect effects of aerosols may also manifest itself in circulation anomalies induced by changes in sea-level pressure, but recent climatological observations have yet to validate these predictions. Model simulations and recent observations at Barrow, Alaska, indicate that the interaction of haze and thin water clouds in spring or summer can lead to a local surface temperature warming of +1° to 1.6°C, due an increase in longwave emissivity from these clouds [Garrett and Zhao, 2006; Girard *et al.*, 2005]. The combined effect of Arctic Haze (a combination of reflective and absorbing aerosols) and biomass burning aerosols is an estimated surface cooling of -0.93°C [Isaksen, 2009; Quinn *et al.*, 2008].

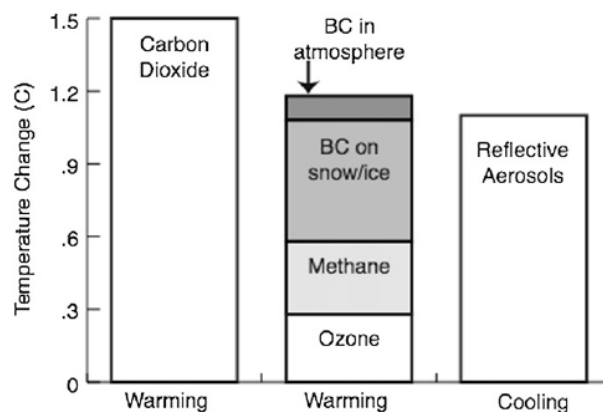


**Figure 5.26.** Estimates of the contribution of particular species to preindustrial to present-day Arctic (60° to 90° N) surface temperature trends. Values are based on the assessment of modelling and observations of Quinn *et al.*, and do not include aerosol indirect effects. Reflective aerosols include sulphate and organic carbon. [Reprinted from Figure 41 of Isaksen, I. S. A., *et al.* (2009), *Atmospheric composition change: Climate-chemistry interactions*, *Atmospheric Environment*, 43(33): 5138-5192, with permission from Elsevier.]

The strong influence of meridional heat transport into the Arctic also leads to substantial climate sensitivity to forcing outside the Arctic [Boer and Yu, 2003; Shindell and Faluvegi, 2009]. Additionally, both O<sub>3</sub> and BC aerosols absorb solar radiation and thus heat the atmosphere, altering meridional circulation in ways that forcing from greenhouse gases or sulphate does not. Thus, for forcing in the Arctic, the climate response per unit tropopause or surface RF can be quite different for short-lived species than the global mean response. Surface temperatures in the Arctic are strongly influenced by both local forcing and forcing at Northern Hemisphere mid-latitudes (Chapter A4). As the latter is typically much greater, it can often play a more important role in driving Arctic climate changes for regionally inhomogeneous forcing [Shindell and Faluvegi, 2009].

Shindell and Faluvegi [2009] estimate that between 1976 and 2007, aerosols may have contributed ~1.09 °C to the observed Arctic surface temperature increase of 1.48 °C. In contrast, tropospheric O<sub>3</sub> increases since preindustrial times are estimated to be responsible for about 0.3°C

annual average and about 0.4-0.5°C during winter and spring to the 20th-century Arctic warming [Shindell *et al.*, 2006].

**FINDING: The Arctic is experiencing rapid climate change. Arctic climate is affected by ozone and PM that are the result of long-range transport from other regions, as well as by ozone and PM outside of the Arctic. Deposition of black carbon in snow is an important contributor to warming in the Arctic.**

### 5.3.5 Future Changes in Forcings

The future forcing from short-lived pollutants is very scenario dependent since (unlike for CO<sub>2</sub>) control measures have a very rapid impact on atmospheric concentrations. Stevenson *et al.* [2006] analysed three possible future scenarios for O<sub>3</sub> precursors and found that the forcing from O<sub>3</sub> between 2000 and 2030 varied from -45 to 63 to 155 mWm<sup>-2</sup>. The three scenarios were IIASA MFR (maximum feasible reduction), IIASA CLE (current legislation) and SRES A2 (unrestricted growth). The methane forcing over the same period varied from 0 to 116 to 141 mWm<sup>-2</sup> for these three scenarios. Note the methane forcings were from an earlier transient run [Dentener *et al.*, 2005] and included the impacts of the non-methane O<sub>3</sub> precursors on the methane lifetime. The forcings compare with values for CO<sub>2</sub> - ranging from around 800 (SRES B2) to 1,050 (SRES A2) mWm<sup>-2</sup> over the 2000-2030 period [Stevenson *et al.*, 2006]. Although the absolute numbers are higher for CO<sub>2</sub>, the range in the combined forcing of methane and ozone was 341mWm<sup>-2</sup> from cleanest to dirtiest. This compares to a range of 250mWm<sup>-2</sup> for the two CO<sub>2</sub> scenarios. This suggests that controls on short-lived pollutants could be at least as effective for climate mitigation in the short term as controls on CO<sub>2</sub>. Controls on particulate matter were not considered by Stevenson *et al.* [2006], but are also expected to have a large short term climate impact.

A new set of scenarios (RCPs) have been produced and reflect options to mitigate long term climate change [Moss *et al.*]. First results from these scenarios are presented in chapter A4.

The impact of climate change on the Stevenson *et al.* [2006] forcings was to mitigate the RF of methane by 26 mWm<sup>-2</sup>, since methane is removed more efficiently in a warmer climate. The impact of climate change on the O<sub>3</sub> forcing was much more uncertain. Those models that simulated an increase in stratosphere-troposphere exchange [Collins *et al.*, 2003; Sudo *et al.*, 2003; Zeng and Pyle, 2003] with climate predicted a larger O<sub>3</sub> forcing in future. Those that did not predicted a lower O<sub>3</sub> forcing due to more efficient removal of O<sub>3</sub> [Johnson *et al.*, 2001]. These studies did not explicitly look at the impact of climate change on the response to emissions, but from the signs of the changes reported (more rapid removal of methane and O<sub>3</sub>, greater stratosphere-troposphere exchange), we might expect the forcing attributable to emissions changes to decrease in the future.

Future climate is likely to increase overall precipitation and hence increase aerosol removal rates in many regions. However it will also increase the rate of oxidation of SO<sub>2</sub> to sulphate. Decreases in snow cover will make aerosol forcings less positive (more negative). Changes in clouds due to the combination of climate change and changes in PM may be very important.

### 5.3.6. Future Research Needs

Estimates of the RFs due to O<sub>3</sub> and PM are among the most important uncertainties in our current understanding of climate change. For both O<sub>3</sub> and PM, there is a need to understand the RF for present day concentrations relative to concentrations in the preindustrial period, for which there are limited observations. In addition, the possible effects of PM on cloud formation and lifetime pose particularly strong uncertainties. Substantial reduction in the aerosol RF uncertainty estimates requires continued, focused efforts on acquiring better observations, improving model representations of atmospheric processes, and developing a synergistic strategy [U.S. CCSP, 2009].

**RECOMMENDATION: The radiative forcings due to ozone and PM are highly uncertain, and are among the most important uncertainties in our understanding of climate change. Observations of aerosol absorption, vertical distributions, and cloud properties (the indirect effect) are particularly needed to reduce these uncertainties.**

**RECOMMENDATION: The forcings resulting from changes in emissions of aerosols, their precursors, and ozone precursors (except methane) depend strongly on location, timing, and the background composition, and these dependencies merit further research.**

There are also several research needs which are not particular to improving understanding of the climate effects of O<sub>3</sub> and PM, but would be shared with the health and ecosystems communities, and observational capabilities should be improved and designed with these different endpoints in mind.

**RECOMMENDATION: Deficiencies in current observations of air pollutants limit the ability to understand effects on health, ecosystems and climate in large regions of the world. Improvements to observations through ground-based and satellite measurements, and in emissions and models, can be important for improving understanding of the health, ecosystem and climate effects of air pollutants. Improvements to these systems should be made with health, ecosystem and climate effects in mind.**

**RECOMMENDATION: Assessment of impacts of intercontinental transport of air pollutants on human health, ecosystem, and climate relies on global models with coarse resolution. There is a pressing need to establish modelling systems that link the local, regional, intercontinental, and global scales.**

## References

- Abbey, D. E., et al. (1999), Long-Term Inhalable Particles and Other Air Pollutants Related to Mortality in Nonsmokers *American Journal of Respiratory and Critical Care Medicine*, 159(2): 373-382.
- Ainsworth, E. A., et al. (2008), Targets for crop biotechnology in a future high-CO<sub>2</sub> and high-O<sub>3</sub> world, *Plant Physiology*, 147: 13-19.
- Albrecht, B. (1989), Aerosols, cloud microphysics, and fractional cloudiness, *Science*, 245: 1227-1230.
- Alton, P. B. (2008), Reduced carbon sequestration in terrestrial ecosystems under overcast skies compared to clear skies, *Agricultural and Forest Meteorology*, 148(10): 1641-1653.
- Anderson, H. R., et al. (2004), Meta-analysis of time-series and panel studies of Particulate Matter (PM) and Ozone (O<sub>3</sub>): report of a WHO task group., 80 pp, World Health Organization, Copenhagen, Denmark.
- Andreae, M. O., et al. (2005), Strong present-day aerosol cooling implies a hot future, *Nature*, 435: 1187-1190.
- Anenberg, S., et al. (2009), Intercontinental impacts of ozone pollution on human mortality, *Environmental Science & Technology*, 43(17): 6482-6487.
- Anenberg, S. C., et al. (2010), An Estimate of the Global Burden of Anthropogenic Ozone and Fine Particulate Matter on Premature Human Mortality Using Atmospheric Modeling, *Environmental Health Perspectives*, 118(9): 1189-1195.
- Ashmore, M. R. (2005), Assessing the future global impacts of O<sub>3</sub> on vegetation, *Plant, Cell and Environment*, 28: 949-963.
- ATS (2000), What Constitutes an Adverse Health Effect of Air Pollution?, *American Journal of Respiratory and Critical Care Medicine*, 161(2): 665-673.
- Bascom, R., et al. (1996a), Health effects of outdoor air pollution. Part 1. Committee of the Environmental and Occupational Health Assembly of the American Thoracic Society, *American Journal of Respiratory and Critical Care Medicine*, 153(1): 3-50.
- Bascom, R., et al. (1996b), Health effects of outdoor air pollution. Part 2. Committee of the Environmental and Occupational Health Assembly of the American Thoracic Society, 153(1): 477-498.
- Bassin, S., et al. (2004), Modeling seasonal ozone fluxes to grassland and wheat with ODEM: model improvement, testing, and application, *Atmospheric Environment*, 38(15): 2349-2359.
- Bassin, S., et al. (2007), Nitrogen deposition but not ozone affects productivity and community composition of sub-alpine grassland after three years of treatment, *New Phytologist*, 175(3): 523-534.
- Bassin, S., et al. (2008), Effects of combined ozone and nitrogen deposition on the in situ properties of 11 key plant species of a subalpine pasture, *Oecologia*, 158(4): 747-756.

- Baumgardner, D., et al. (2004), Warming of the Arctic lower stratosphere by light absorbing particles, *Geophysical Research Letters*, 31(L06117).
- Bell, J. N. B. (1985), SO<sub>2</sub> effects on productivity of grass species, in *Effects of SO<sub>2</sub> on Plant Productivity*, edited by Mooney and A. H. Goldstein, 209-266 pp., Stanford University Press.
- Bell, M., and F. Dominici (2006), Analysis of threshold effects for short-term exposure to ozone and increased risk of mortality, *Epidemiology*, 17: S223-S223.
- Bell, M. L., et al. (2004), Ozone and short-term mortality in 95 US urban communities, 1987-2000, *Journal of American Medical Association* 292(19): 2372-2378.
- Bell, M. L., et al. (2005), A meta-analysis of time-series studies of ozone and mortality with comparison to the National Morbidity, Mortality, and Air Pollution Study, *Epidemiology*, 4: 436-445.
- Bellouin, N., et al. (2008), Updated estimate of aerosol direct radiative forcing from satellite observations and comparison against the Hadley Centre climate model, *Journal of Geophysical Research*, 113(D10205).
- Bender, J., and H. J. Weigel (1993), Crop responses to mixtures of air pollutants, in *Air Pollution and Crop Responses in Europe*, edited by H. J. Jager, et al., 445-453 pp., CEC, Brussels.
- Berntsen, T. K., and I. S. A. Isaksen (1997), A global three-dimensional chemical transport model for the troposphere: Model description and CO and ozone results, *Journal of Geophysical Research*, 102(D17): 21239-21280.
- Berntsen, T. K., et al. (2005), Response of climate to regional emissions of ozone precursors: Sensitivities and warming potentials, *Tellus Series B - Chemical and Physical Meteorology*, 57: 283-304.
- Betzlberger, A. M., et al. (2010), Effects of chronic elevated ozone concentration on antioxidant capacity, photosynthesis and seed yield of 10 soybean cultivars, *Plant Cell & Environment*, 33(9): 1569-1581.
- Blanchard, M. (2008), Analyse des liens à court terme entre pollution atmosphérique urbaine et mortalité dans neuf villes françaises, 44 pp, Institut de veille sanitaire - Programme de surveillance air et santé, Saint-Maurice, France.
- Bobbink, R., et al. (2003), Empirical nitrogen critical loads for natural and semi-natural ecosystems: 2002 update, in *Empirical critical loads for nitrogen, Expert Workshop, Berne 11-13 November 2002. Proceedings*, edited by D. Achermann and R. Bobbink, 43-170 pp., Swiss Agency for Environment, Forest, and Landscape (SAEFL), Federal Office for the Environment (FOEN), Berne.
- Bobbink, R. (2008), The Derivation of Dose-response Relationships 4 between N Load, N Exceedance and Plant Species Richness for EUNIS Habitat Classes, in *Critical Load, Dynamic Modelling and Impact Assessment in Europe*, edited by J. Hettelingh, et al., 63-72 pp., Netherlands Environmental Assessment Agency.
- Bobbink, R., et al. (2010), Global assessment of nitrogen deposition effects on terrestrial plant diversity: a synthesis, *Ecological applications*, 20: 30-59.
- Boer, G. J., and B. Yu (2003), Climate sensitivity and response, *Climate Dynamics*, 20: 415-429.
- Bond, T. C. (2004), Can warming particles enter global climate discussions?, *Environmental Research Letters*, 2(4).
- Bond, T. C., and H. Sun (2005), Can Reducing Black Carbon Emissions Counteract Global Warming?, *Environmental Science & Technology*, 39(16): 5921-5926.
- Bond, T. C., et al. (2010), Quantifying immediate radiative forcing by black carbon and organic matter with the Specific Forcing Pulse, *Atmospheric Chemistry and Physics Discussion*, 10(6): 15713-15753.
- Booker, F., et al. (2009), The ozone component of global change: Potential effects on agricultural and horticultural plant yield, product quality and interactions with invasive species, *Journal of Integrative Plant Biology*, 51: 337-351.
- Boucher, O., et al. (2009), The indirect global warming potential and global temperature change potential due to methane oxidation, *Environmental Research Letters*, 4(4): 044007.
- Braun S, et al. (2010), Use of sap flow measurements to validate stomatal functions for mature beech (*Fagus sylvatica*) in view of ozone uptake calculations., *Environmental Pollution*, 158(9): 2954-2963.
- Brook, J. R., et al. (2007), Further interpretation of the acute effect of nitrogen dioxide observed in Canadian time-series studies, *Journal of Exposure Analysis and Environmental Epidemiology*, 17(S2): S36-S44.



- Brook, R. D., et al. (2010), Particulate Matter Air Pollution and Cardiovascular Disease. An Update to the Scientific Statement From the American Heart Association *Circulation - Journal of the American Heart Association*, 121(21): 2331-2378.
- Brunekreef, B., et al. (2007), The Brave New World of Lives Sacrificed and Saved, Deaths Attributed and Avoided, *Epidemiology*, 18(6): 785-788
- Bungener, P., et al. (1999), Growth response of grassland species to ozone in relation to soil moisture condition and plant strategy, *New Phytologist*, 142: 283-293.
- Bussotti, F., and M. Ferretti (2009), Visible injury, crown condition, and growth responses of selected Italian forests in relation to ozone exposure, *Environmental Pollution*, 157(5): 1427-1437.
- Chen, L. H., et al. (2005), The Association between Fatal Coronary Heart Disease and Ambient Particulate Air Pollution: Are Females at Greater Risk, *Environmental Health Perspectives*, 113(12): 1723-1729.
- Chou, C., et al. (2005), Local and Remote Impacts of Aerosol Climate Forcing on Tropical Precipitation\*, *Journal of Climate*, 18(22): 4621-4636.
- Chung, S. H., and J. H. Seinfeld (2005), Climate response of direct radiative forcing of anthropogenic black carbon, *Journal of Geophysical Research*, 110(D11102).
- Clancy, L., et al. (2002), Effect of air-pollution control on death rates in Dublin, Ireland: an intervention study, *Lancet*, 360: 1210-1214.
- Cohen, A. J., et al. (2004), Urban air pollution. In Comparative quantification of health risks: Global and regional burden of disease due to selected major risk factors, 81 pp, World Health Organization, Geneva.
- Collins, W. J., et al. (2003), Effect of stratosphere-troposphere exchange on the future tropospheric ozone trend, *Journal of Geophysical Research*, 108(D12): 8528-8537.
- Collins, W. J., et al. (2010), How vegetation impacts affect climate metrics for ozone precursors, *Journal of Geophysical Research*, 115(D23308).
- Cooke, R. M., et al. (2007), A Probabilistic Characterization of the Relationship between Fine Particulate Matter and Mortality: Elicitation of European Experts, *Environmental Science & Technology*, 41(18): 6598-6605.
- Corbett, J. J., et al. (2007), Mortality from ship emissions: a global assessment, *Environmental Science & Technology*, 41(24): 8512-8518.
- Dentener, F., et al. (2005), The impact of air pollutant and methane emission controls on tropospheric ozone and radiative forcing: CTM calculations for the period 1990-2030, *Atmospheric Chemistry and Physics*, 7(5): 1731-1755.
- Derwent, R. G., et al. (2008), How is surface ozone in Europe linked to Asian and North American NO<sub>x</sub> emissions?, *Atmospheric Environment*, 42(32): 7412-7422.
- Duce, R. A., et al. (2008), Impacts of Atmospheric Anthropogenic Nitrogen on the Open Ocean, *Science*, 320(5878): 893-897.
- Duncan, B. N., et al. (2008), The influence of European pollution on the air quality in the Near East and northern Africa, *Atmospheric Chemistry and Physics*, 8: 2267-2283.
- EEA (2009), Assessment of ground-level ozone in EEA member countries, with a focus on long-term trends, 56 pp, European Environment Agency, Copenhagen, Denmark. *EEA Technical report No 7/2009*
- Eleftheriadis, K., et al. (2009), Aerosol black carbon in the European Arctic: Measurements at Zeppelin station, Ny-Alesund, Svalbard from 1998-2007, *Geophysical Research Letters*, 36(L02809).
- Ellingsen, K., et al. (2008), Global ozone and air quality: a multi-model assessment of risks to human health and crops, *Atmospheric Chemistry and Physics Discussions*, 8: 2163-2223.
- Emberson, L. D., et al. (2001), Modelling and mapping ozone deposition in Europe, *Water Air and Soil Pollution*, 130: 577-582.
- Emberson, L. D., et al. (2003), Air Pollution Impacts on Crops and Forests-A Global Assessment, edited, Imperial College Press, London.
- Emberson, L. D., et al. (2009), Dose-response relationships derived in North America underestimate the effects of ozone (O<sub>3</sub>) on crop yields in Asia, *Atmospheric Environment*, 43: 1945-1953.

- EMEP (2010), Convention on Long-Range Transboundary Air Pollution, Chemical Co-ordinating Centre of EMEP (CCC), <http://tarantula.nilu.no/projects/ccc/index.html>
- Ezzati, M., et al. (2004), Mortality and burden of disease attributable to individual risk factors, in *Comparative quantification of health risks: Global and regional burden of disease due to selected major risk factors*, edited by M. Ezzati, et al., 2141-2165 pp., World Health Organization, Geneva.
- Fiore, A. M., et al. (2008), Characterizing the tropospheric ozone response to methane emission controls and the benefits to climate and air quality, *Journal of Geophysical Research*, 113(D08307).
- Fiore, A. M., et al. (2009), Multimodel estimates of intercontinental source-receptor relationships for ozone pollution, *Journal of Geophysical Research*, 114(D04301).
- Fiscus, E. L., et al. (2005), Crop responses to ozone: uptake, modes of action, carbon assimilation and partitioning, *Plant Cell Environment*, 28: 997-1011.
- Fishman, J., et al. (2010), An investigation of widespread ozone damage to the soybean crop in the upper Midwest determined from ground-based and satellite measurements, *Atmospheric Environment*, 44(18): 2248-2256.
- Flanner, M. G., et al. (2007), Present-day climate forcing and response from black carbon in snow, *Journal of Geophysical Research*, 112(D11202).
- Forster, P., et al. (2007), Changes in atmospheric constituents and radiative forcing. Climate Change 2007: The Physical Scientific Basis 6pp, Cambridge University Press, Cambridge, United Kingdom and New York, NY, USA.
- Fowler, D., et al. (1991), Inputs of trace gases, particles and cloud droplets to terrestrial surfaces, *Proceedings of the Royal Society of Edinburgh - Section B*, 97: 35-39.
- Fowler, D., et al. (1999), The global exposure of forests to air pollutants, *Water Air and Soil Pollution*, 116: 5-32.
- Fowler, D., et al. (2009), Atmospheric composition change: ecosystems-atmosphere interactions, *Atmospheric Environment*, 43: 5193-5267.
- Franklin, M., et al. (2008), The Role of Particle Composition on the Association Between PM<sub>2.5</sub> and Mortality, *Epidemiology*, 19(5): 680-689
- Frei, M., et al. (2008), Genotypic variation in tolerance to elevated ozone in rice: dissection of distinct genetic factors linked to tolerance mechanisms, *Journal of Experimental Botany*, 59: 3741-3752.
- Frei, M., et al. (2010), Mechanisms of ozone tolerance in rice: characterization of two QTLs affecting leaf bronzing by gene expression profiling and biochemical analysis, *Journal of Experimental Botany*, 61(5): 1405-1417.
- Fuglestedt, J. S., et al. (1999), Climatic forcing of nitrogen oxides through changes in tropospheric ozone and methane; global 3D model studies, *Atmospheric Environment*, 33(6): 961-977.
- Fuglestedt, J. S., et al. (2010), Transport impacts on atmosphere and climate: Metrics, *Atmospheric Environment*, 44(37): 4648-4677.
- Fuhrer, J., and F. Booker (2003), Ecological issues related to ozone: agricultural issues, *Environment International*, 29: 141-154.
- Fuhrer, J. (2009), Ozone risk for crops and pastures in present and future climates, *Naturwissenschaften*, 96: 173-194.
- Garrett, T. J., and C. Zhao (2006), Increased Arctic cloud longwave emissivity associated with pollution from mid-latitudes, *Nature*, 440: 787-789.
- Gauderman, J. W., et al. (2000), Association between Air Pollution and Lung Function Growth in Southern California Children, *American Journal of Respiratory and Critical Care Medicine*, 162(4): 1383-1390.
- Gauderman, W. J., et al. (2002), Association between Air Pollution and Lung Function Growth in Southern California Children: Results from a Second Cohort, *American Journal of Respiratory and Critical Care Medicine*, 166(1): 76-84.
- Gauss, M., et al. (2003), Radiative forcing in the 21st century due to ozone changes in the troposphere and the lower stratosphere, *Journal of Geophysical Research*, 108(D9): 4292-4312.

- Gauss, M., et al. (2006), Radiative forcing since preindustrial times due to ozone change in the troposphere and the lower stratosphere, *Atmospheric Chemistry and Physics*, 6(3): 575-599.
- Gerosa, G., et al. (2008), Comparison of seasonal variations of ozone exposure and fluxes in a Mediterranean Holm oak forest between the exceptionally dry 2003 and the following year, *Environmental Pollution*, 157: 1737-1744.
- Gimeno, B. S., et al. (2004), Assessment of the effects of ozone exposure and plant competition on the reproductive ability of three therophytic clover species from Iberian pastures, *Atmospheric Environment*, 38: 2295-2303.
- Girard, E., et al. (2005), Effects of sulphuric acid aerosols on wintertime low-level atmospheric ice crystals, humidity and temperature at Alert, Nunavut, *Atmospheric Research*, 73: 131-148.
- Glinianaia, S. V., et al. (2004), Particulate Air Pollution and Fetal Health: A Systematic Review of the Epidemiologic Evidence, *Epidemiology*, 15(1): 36-45
- Granier, C., et al. (2006), Ozone pollution from future ship traffic in the Arctic northern passages, *Geophysical Research Letters*, 33(L13807).
- Griffin, D. W., et al. (2001), Dust in the wind: Long range transport of dust in the atmosphere and its implications for global public and ecosystem health, *Global Change & Human Health*, 2(1): 20-33.
- Gryparis, A., et al. (2004), Acute effects of ozone on mortality from the "air pollution and health: a European approach" project, *American Journal of Respiratory & Critical Care Medicine*, 170(10): 1080-1087.
- Gunn, R., and B. B. Phillips (1957), An experimental investigation of the effect of air pollution on the initiation of rain, *Journal of Meteorology*, 14: 272-280.
- Hansen, J., et al. (1997), Radiative forcing and climate response, *Journal of Geophysical Research*, 102(D6): 6831-6864.
- Hansen, J., et al. (2000), Global warming in the twenty-first century: An alternative scenario, *Proceedings of the National Academy of Sciences of the U.S.A.*, 97(18): 9875-9880.
- Hansen, J., and L. Nazarenko (2004), Soot climate forcing via snow and ice albedos, *Proceedings of the National Academy of Sciences of the U.S.A.*, 101(2): 423-428.
- Hansen, J., et al. (2005), Efficacy of climate forcings, *Journal of Geophysical Research*, 110(D18104).
- Hayes, F., et al. (2007), Meta-analysis of the relative sensitivity of semi-natural vegetation species to ozone, *Environmental Pollution*, 146(3): 754-762.
- Heck, W. W., et al. (1988), *Assessment of Crop Loss from Air Pollutants*, 552 pp., Elsevier Applied Science, London.
- Hedley, A. J., et al. (2002), Cardiorespiratory and all-cause mortality after restrictions on sulphur content of fuel in Hong Kong: an intervention study, *Lancet*, 360: 1646-1652.
- HEI (2004), International Scientific Oversight Committee: Health effects of outdoor air pollution in developing countries of Asia: a literature review, 117 pp, Health Effects Institute, Boston. *Special Report 15*
- HEI (2010), Public Health and Air Pollution in Asia (PAPA): Coordinated Studies of Short-Term Exposure to Air Pollution and Daily Mortality in Four Cities, Health Effects Institute, Boston, MA. *Research Report 154*
- Hicks, W. K., et al. (2008), Soil sensitivity to acidification in Asia: Status and prospects, *Ambio*, 37: 295-303.
- Holland, M., et al. (2007), Development of a framework for probabilistic assessment of the economic losses caused by ozone damage to crops in Europe, Centre for Ecology and Hydrology, Bangor.
- Hungate, B. A., et al. (2009), Nitrogen and climate change, *Science*, 203: 1512-1513.
- IPCC (2007a), Summary for Policymakers, in *Climate Change 2007: The Physical Science Basis. Contribution of Working Group I to the Fourth Assessment Report of the Intergovernmental Panel on Climate Change*, edited by S. D. Solomon, et al., 18 pp., Cambridge University Press, Cambridge, United Kingdom and New York, NY.
- IPCC (2007b), Contribution of Working Group II to the Fourth Assessment. Report of the Intergovernmental Panel on Climate Change, edited by M. L. Parry, et al., Cambridge University Press, Cambridge, UK.
- Isaksen, I. S. A., et al. (2009), Atmospheric composition change: Climate-chemistry interactions, *Atmospheric Environment*, 43(33): 5138-5192.

- Ito, K., et al. (2005), Associations between ozone and daily mortality: analysis and meta-analysis, *Epidemiology*, 16(4): 446-457.
- Jackson, S. C. (2009), Parallel pursuit of near-term and long-term climate mitigation, *Science*, 326: 526-527.
- Jager, H. J., et al. (1992), Effects of air pollution on agricultural crops in Europe - Results of the European open-top chamber project, Commission of the European Communities, Brussels. *Air Pollution Research Report 46*
- Jaggi, M., and J. Fuhrer (2007), Oxygen and carbon isotopic signatures reveal a long-term effect of free-air ozone enrichment on leaf conductance in semi-natural grassland, *Atmospheric Environment*, 41: 8811-8817.
- Jerrett, M., et al. (2005), A review and evaluation of intraurban air pollution exposure models, *Journal of Exposure Analysis and Environmental Epidemiology*, 15(2): 185-204.
- Jerrett, M., et al. (2009), Long-term ozone exposure and mortality, *New England Journal of Medicine*, 360(11): 1085-1095.
- Johnson, A. H., et al. (1994), Acid rain and soils of the Adirondacks: III. Rates of soil acidification in a montane spruce-fir forest at Whiteface Mountain, New York, *Canadian Journal of Forest Research*, 24: 663-669.
- Johnson, C. E., et al. (2001), Role of climate feedback on methane and ozone studied with a coupled Ocean-Atmosphere-Chemistry model, *Geophysical Research Letters*, 28(9): 1723-1726.
- Jones, M. L. M., et al. (2007), Predicting ozone sensitivity to ozone, using Ellenberg indicator values, *Environmental Pollution*, 146: 744-753.
- Kaliakatsou, E., et al. (2010), The impact of tropospheric ozone pollution on trial plot winter wheat yields in Great Britain - An econometric approach, *Environmental Pollution*, 158(5): 1948-1954.
- Karenlampi, L., and L. Skarby (Eds.) (1996), *Critical levels for ozone in Europe: Testing and finalizing the concepts*, University of Kuopio, Department of Ecology and Environmental Science, Kuopio, Finland
- Karlsson, P. E., et al. (2005), Economic assessment of the negative impacts of ozone on crop yields and forest production. A case study of the Estate Ostads Sateri in Southwestern Sweden., *AMBIO: A Journal of the Human Environment*, 34(1): 32-40.
- Karlsson, P. E., et al. (2007), Risk assessments for forest trees: The performance of the ozone flux versus the AOT concepts, *Environmental Pollution*, 146: 608-616.
- Karnosky, D. F., and K. C. Steiner (1981), Provenance variation in response of *Fraxinus americana* and *Fraxinus pennsylvanica* to sulfur dioxide and ozone, *Phytopathology*, 71: 804-807.
- Karnosky, D. F., et al. (2003), Tropospheric O<sub>3</sub> moderates responses of temperate hardwood forests to elevated CO<sub>2</sub>: a synthesis of molecular to ecosystem results from the Aspen FACE project, *Functional Ecology*, 17(3): 289-304.
- Karnosky, D. F., et al. (2007), Perspectives regarding 50 years of research on effects of tropospheric ozone air pollution on US forests, *Environmental Pollution*, 147: 489-506.
- Katsouyanni, K., et al. (2009), Air Pollution and Health: A Combined European and North American Approach (APHENA), 120 pp, Health Effects Institute, Boston, MA. *Research Report 142*.  
[http://journals.lww.com/epidem/Fulltext/2006/11001/Air\\_Pollution\\_and\\_Health\\_\\_A\\_Combined\\_European\\_and\\_5.aspx](http://journals.lww.com/epidem/Fulltext/2006/11001/Air_Pollution_and_Health__A_Combined_European_and_5.aspx)
- Kim, Y., et al. (2005), Possible effect of boreal wildfire soot on Arctic sea ice and Alaska glaciers, *Atmospheric Environment*, 39(19): 3513-3520.
- King, J. S., et al. (2005), Tropospheric O<sub>3</sub> compromises net primary production in young stands of trembling aspen, paper birch and sugar maple in response to elevated atmospheric CO<sub>2</sub>, *New Phytologist*, 168(3): 623-636.
- Klingberg, J., et al. (2011), Ozone risk for vegetation in the future climate of Europe based on stomatal ozone uptake calculations, *Tellus A*, 63(1): 174-187.
- Knohl, A., and D. D. Baldocchi (2008), Effects of diffuse radiation on canopy gas exchange processes in a forest ecosystem, *Journal of Geophysical Research*, 113(G02023).
- Koch, D., et al. (2009), Evaluation of black carbon estimations in global aerosol models, *Atmospheric Chemistry and Physics*, 9: 9001-9026.

- Köhler, M. O., et al. (2008), Impact of perturbations to nitrogen oxide emissions from global aviation, *Journal of Geophysical Research*, 113: D11305.
- Kolb, T. E., and R. Matyssek (2001), Limitations and perspectives about scaling ozone impact in trees, *Environmental Pollution*, 115: 373-393.
- Krewski, D., et al. (2009), Extended follow-up and spatial analysis of the American Cancer Society study linking particulate air pollution and mortality, Health Effects Institute, Cambridge, MA. *HEI Report 140*. <http://pubs.healtheffects.org/view.php?id=315>
- Krishnamurthy, A., et al. (2009), Impacts of increasing anthropogenic soluble iron and nitrogen deposition on ocean biogeochemistry, *Global Biogeochemical Cycles*, 23(GB3016).
- Kristjansson, J. E., et al. (2005), Response of the climate system to aerosol direct and indirect forcing: Role of cloud feedbacks, *Journal of Geophysical Research*, 113(D24206).
- Krupa, S. V., et al. (2004), Effects of ozone on plant nutritive quality characteristics for ruminant animals, *The Botanica*, 54: 1-12.
- Krzyzanowski, M., and A. Cohen (2008), Update of WHO air quality guidelines, *Air Quality, Atmosphere & Health*, 1(1): 7-13.
- Künzli, N., et al. (2000), Public-health impact of outdoor and traffic-related air pollution: A European assessment, *Lancet*, 356(9232): 795-801.
- Laden, F., et al. (2006), Reduction in fine particulate air pollution and mortality: Extended follow-up of the Harvard Six-Cities Study, *American Journal of Respiratory and Critical Care Medicine*, 173: 667-672.
- Lau, K. M., et al. (2006), Aerosol induced anomalies in the Asian summer monsoon - the role of the Tibetan Plateau, *Climate Dynamics*, 26(7-8): 855-864.
- Lee, C., et al. (2009), Retrieval of vertical columns of sulfur dioxide from SCIAMACHY and OMI: Air mass factor algorithm development and validation, *Journal of Geophysical Research*, 114(D22303).
- Levy, H., II, et al. (2008), Strong sensitivity of late 21st century climate to projected changes in short-lived air pollutants, *Journal of Geophysical Research*, 113(D06102).
- Levy, J. I., et al. (2001), Assessing the Public Health Benefits of Reduced Ozone Concentrations, *Environmental Health Perspectives*, 109(12).
- Levy, J. I., et al. (2005), Ozone exposure and mortality: an empiric Bayes metaregression analysis, *Epidemiology*, 16(4): 458-468.
- Lin, M., et al. (2010), Quantifying pollution inflow and outflow over East Asia in spring with regional and global models, *Atmospheric Chemistry and Physics*, 10(9): 4221-4239.
- Liu, J., and D. L. Mauzerall (2007), Potential influence of inter-continental transport of sulfate aerosols on air quality, *Environmental Research Letters*, 2(4): 045029.
- Liu, J., et al. (2009a), Evaluating inter-continental transport of fine aerosols: (2) Global Health Impacts, *Atmospheric Environment*, 43(28): 4339-4347.
- Liu, J., et al. (2009b), Evaluating inter-continental transport of fine aerosols: (1) Methodology, global aerosol distribution and optical depth, *Atmospheric Environment*, 43(28): 4327-4338.
- Lobell, D. B., and C. B. Field (2007), Global scale climate - crop yield relationships and the impacts of recent warming, *Environmental Research Letters*, 2(1): 014002.
- LRTAP Convention (2010), Mapping critical levels for vegetation. Manual on methodologies and criteria for modelling and mapping critical loads & levels and air pollution effects, risks, and trends, 254 pp, United Nations Economic Commission for Europe Convention on Long-Range Transboundary Air Pollution, Geneva.
- Magnani, F., et al. (2007), The human footprint in the carbon cycle of temperate and boreal forests, *Nature*, 447: 848-851.
- Matyssek, R., and H. Sandermann (2003), Impact of ozone on trees: an ecophysiological perspective, in *Progress in Botany 64*, edited by K. Esser, et al., 349-404 pp., Springer-Verlag, Heidelberg, Germany.
- Matyssek, R., et al. (2007), Promoting the O<sub>3</sub> flux concept for European forest trees, *Environmental Pollution*, 146: 587-607.

- Matyssek, R., et al. (2010), Advances in understanding ozone impact on forest trees: Messages from novel phytotron and free-air fumigation studies, *Environmental Pollution*, 158(6): 1990-2006.
- McConnell, J., et al. (2007), 20th-century industrial black carbon emissions altered Arctic climate forcing, *Science*, 317: 1381-1384.
- McCormick, R., and J. Ludwig (1967), Climate modification by atmospheric aerosols, *Science*, 156(3780): 1358-1359.
- McGrath, and Zhao (1995), A risk assessment of sulphur deficiency in cereals using soil and atmospheric data, *Soil Use and Management*, 11: 100-114.
- Meehl, G. A., et al. (2006), Effects of black carbon aerosols on the Indian monsoon, *Journal of Climate*, 21: 2869-2882.
- Meehl, G. A., et al. (2007), Global climate projections, in *Climate Change 2007: The Physical Science Basis*, edited by S. D. Solomon, et al., 747-845 pp., Cambridge University Press, Cambridge, United Kingdom and New York, NY.
- Mercado, L. M., et al. (2009), Impact of changes in diffuse radiation on the global land carbon sink, *Nature*, 458: 1014-1017.
- Miller, K. A., et al. (2007), Long-Term Exposure to Air Pollution and Incidence of Cardiovascular Events in Women, *New England Journal of Medicine*, 356(5): 447-458.
- Mills, G., et al. (2000), Development of a multi-factor model for predicting the effects of ambient ozone on the biomass of white clover, *Environmental Pollution*, 109: 533-542.
- Mills, G., et al. (2007), A synthesis of AOT40-based response functions and critical levels of ozone for agricultural and horticultural crops, *Atmospheric Environment*, 41: 2630-2643.
- Mills, G., et al. (2010), Evidence of widespread effects of ozone on crops and (semi-)natural vegetation in Europe (1990-2006) in relation to AOT40 and flux-based risk maps, *Global Change Biology*, in press.
- Ming, Y., and V. Ramaswamy (2009), Nonlinear climate and hydrological responses to aerosol effects, *Journal of Climate*, 22: 1329-1339.
- Mitchell, J. F. B., et al. (1995), On surface temperature, greenhouse gases, and aerosols: Models and observations, *Journal of Climate*, 8: 2364-2386.
- Morgan, P. B., et al. (2006), Season-long elevation of ozone concentration to projected 2050 levels under fully open-air conditions substantially decreases the growth and production of soybean, *New Phytologist*, 170(2): 333-343.
- Moss, R. H., et al. (2010), The next generation of scenarios for climate change research and assessment, *Nature*, 463(7282): 747-756.
- Muller, N., and R. Mendelsohn (2009), Efficient pollution regulation: Getting the prices right, *American Economic Review*, 99: 1714-1739.
- Murphy, D. M., et al. (2009), An observationally based energy balance for the Earth since 1950, *Journal of Geophysical Research*, 114(D17017).
- Myhre, G. (2009), Consistency between satellite-derived and modeled estimates of the direct aerosol effect, *Science*, 325: 187-190.
- Nabuurs, G. J., et al. (2003), Temporal evolution of the European forest sector carbon sink from 1950 to 1999, *Global Change Biology*, 9: 152-160.
- Naik, V., et al. (2005), Net radiative forcing due to changes in regional emissions of tropospheric ozone precursors, *Journal of Geophysical Research*, 110: D24306.
- Naik, V., et al. (2007), On the sensitivity of radiative forcing from biomass burning aerosols and ozone to emission location, *Geophysical Research Letters*, 34(L03818).
- Navidi, W., and F. Lurmann (1995), Measurement error in air pollution exposure assessment, *Journal of Exposure Analysis and Environmental Epidemiology*, 5(2): 111-124.

- NEG-TAP (2001), Transboundary air pollution: Acidification, eutrophication and ground-level ozone in the UK, National Expert Group on Transboundary Air Pollution, Cooperative Programme for Monitoring and Evaluation of the Long-range Transmission of Air Pollutants in Europe, United Kingdom. *Defra Contract EPG 1/3/153*. [http://www.uk-pollutantdeposition.ceh.ac.uk/sites/uk-pollutantdeposition.ceh.ac.uk/files/NEG-TAP\\_10Dec2001.pdf](http://www.uk-pollutantdeposition.ceh.ac.uk/sites/uk-pollutantdeposition.ceh.ac.uk/files/NEG-TAP_10Dec2001.pdf)
- Niyogi, D., et al. (2004), Direct observations of the effects of aerosol loading on net ecosystem CO<sub>2</sub> exchanges over different landscapes, *Geophysical Research Letters*, 31(L20506).
- NRC (2005), Radiative forcing of climate change: expanding the concept and addressing uncertainties, 224 pp, National Research Council, National Academy of Sciences, Washington, DC. <http://www.nap.edu/openbook/0309095069.html>
- NRC (2010), Global sources of local pollution: an Assessment of long-range transport of key air pollutants to and from the United States, 234 pp, National Research Council, The National Academies, Washington, DC.
- Ohara, T., et al. (2007), An Asian emission inventory of anthropogenic emission sources for the period 1980-2020, *Atmospheric Chemistry and Physics*, 7(16): 4419-4444.
- Olson, D. M., and E. Dinerstein (2002), The Global 200: Priority Ecoregions for Global Conservation, *Annals of the Missouri Botanical Garden*, 89(2): 199-224.
- Oltmans, S. J., et al. (2006), Long-term changes in tropospheric ozone, *Atmospheric Environment*, 40(17): 3156-3173.
- Ormerod, S. J., and I. Duran (2009), Restoration and recovery from acidification in upland Welsh streams over 25 years, *Journal of Applied Ecology*, 46(1): 164-174.
- Park, R. J., et al. (2006), Regional visibility statistics in the United States: Natural and transboundary pollution influences, and implications for the Regional Haze Rule, *Atmospheric Environment*, 40(28): 5405-5423.
- Perez, L., et al. (2008), Coarse Particles From Saharan Dust and Daily Mortality, *Epidemiology*, 19(6): 800-807
- Pleijel, H., et al. (1999), Grain protein accumulation in relation to grain yield of spring wheat (*Triticum aestivum* L.) grown in open-top chambers with different concentrations of ozone, carbon dioxide and water availability, *Agriculture, Ecosystems & Environment*, 72(3): 265-270.
- Pleijel, H., et al. (2007), Ozone risk assessment for agricultural crops in Europe: Further development of stomatal flux and flux-response relationships for European wheat and potato, *Atmospheric Environment*, 41: 3022-3040.
- Pope III, C. A., et al. (1992), Daily mortality and PM<sub>10</sub> pollution in Utah Valley, *Archives of Environmental Health*, 47: 211-217.
- Pope III, C. A., et al. (1995), Particulate air pollution as a predictor of mortality in a prospective study of U.S. adults, *American Journal of Respiratory and Critical Care Medicine*, 151(3): 669-674.
- Pope III, C. A., et al. (2002), Lung cancer, cardiopulmonary mortality, and long-term exposure to fine particulate air pollution, *Journal of the American Medical Association*, 287(9): 1132-1141.
- Pope III, C. A., and D. W. Dockery (2006), Health effects of fine particulate air pollution: Lines that connect, *Journal of the Air and Waste Management Association*, 56: 709-742.
- Pope III, C. A., et al. (2009), Fine-particulate air pollution and life expectancy in the United States, *New England Journal of Medicine*, 360(4): 376-386.
- Puett, R. C., et al. (2008), Chronic Particulate Exposure, Mortality, and Coronary Heart Disease in the Nurses' Health Study, *American Journal of Epidemiology*, 168(10): 1161-1168.
- Qian, Y., et al. (2009), Effects of soot-induced snow albedo change on snowpack and hydrological cycle in western United States based on Weather Research and Forecasting chemistry and regional climate simulations, *Journal of Geophysical Research*, 114(D03108).
- Quaas, J., et al. (2008), Satellite-based estimate of the direct and indirect aerosol climate forcing, *Journal of Geophysical Research*, 113(D05204).
- Quinn, P. K., et al. (2008), Short-lived pollutants in the Arctic: Their climate impact and possible mitigation strategies, *Atmospheric Chemistry and Physics*, 8(6): 1723-1735.



- Raes, and Seinfeld (2009), Climate change and air pollution abatement: A bumpy road, *Atmospheric Environment*, 43: 5132-5133.
- Ramanathan, V., and G. R. Carmichael (2008), Global and regional climate changes due to black carbon, *Nature Geoscience*, 1: 221-227.
- Reddy, M. S., and O. Boucher (2007), Climate impact of black carbon emitted from energy consumption in the world's regions, *Geophysical Research Letters*, 34: L11802.
- Ren, W., et al. (2007), Influence of ozone pollution and climate variability on net primary productivity and carbon storage in China's grassland ecosystems from 1961-2000, *Environmental Pollution*, 149: 327-335.
- Rojas-Martinez, R., et al. (2007), Lung Function Growth in Children with Long-Term Exposure to Air Pollutants in Mexico City, *American Journal of Respiratory and Critical Care Medicine*, 176(4): 377-384.
- Roman, H. A., et al. (2008), Expert Judgment Assessment of the Mortality Impact of Changes in Ambient Fine Particulate Matter in the U.S, *Environmental Science & Technology*, 42(7): 2268-2274.
- Romieu, I., et al. (2002), Outdoor Air Pollution and Acute Respiratory Infections Among Children in Developing Countries, *Journal of Occupational and Environmental Medicine*, 44(7): 640-649.
- RoTAP (2010), Review of Transboundary Air Pollution, 335 pp, Center for Ecology & Hydrology, UK Department for Environment, Food & Rural Affairs, Penicuik.
- Rothman, K. J., et al. (2008), *Modern Epidemiology, 3rd Edition*, 733 pp., Lippincott Williams & Wilkins, Philadelphia, PA.
- Rotstayn, L. D., and U. Lohmann (2002), Tropical rainfall trends and the indirect aerosol effect, *Journal of Climate*, 15(15): 2103-2116.
- Royal Society (2008), Ground-level ozone in the 21st century: future trends, impacts and policy implications, 148 pp, The Royal Society, London, United Kingdom. *RS Policy Document 15/08*.
- Rypdal, K., et al. (2009), Costs and global impacts of black carbon abatement strategies, *Tellus B*, 61(4): 625-641.
- Saikawa, E., et al. (2009), Present and potential future contributions of sulfate, black and organic carbon aerosols from China to global air quality, premature mortality and radiative forcing, *Atmospheric Environment*, 43: 2814-2822.
- Sanderson, M. G., et al. (2003), Effect of climate change on isoprene emissions and surface ozone levels, *Geophysical Research Letters*, 30(18): 1936-1939.
- Sanderson, M. G., et al. (2006), Present and future acid deposition to ecosystems: The effect of climate change, *Atmospheric Environment*, 40(7): 1275-1283.
- Sanderson, M. G., et al. (2007), Stomatal conductance changes due to increasing carbon dioxide levels: Projected impact on surface ozone levels, *Tellus Series B-Chemical and Physical Meteorology*, 59: 404-411.
- Sanderson, M. G., et al. (2008), A multi-model study of the hemispheric transport and deposition of oxidised nitrogen, *Geophysical Research Letters*, 35(L17815).
- Sharma, S., et al. (2006), Variations and sources of the equivalent black carbon in the high Arctic revealed by long-term observations at Alert and Barrow: 1989-2003, *Journal of Geophysical Research*, 111(D14208).
- Shi, G., et al. (2009), Impact of elevated ozone concentration on yield of four Chinese rice cultivars under fully open-air field conditions, *Agriculture, Ecosystems & Environment*, 131(3-4): 178-184.
- Shindell, D., et al. (2006), Role of tropospheric ozone increases in 20th-century climate change, *Journal of Geophysical Research*, 111(D08302).
- Shindell, D. (2007), Local and remote contributions to Arctic warming, *Geophysical Research Letters*, 34(L14704).
- Shindell, D., et al. (2008a), Climate forcing and air quality change due to regional emissions reductions by economic sector, *Atmospheric Chemistry and Physics*, 8: 7101-7113.

- Shindell, D., et al. (2008b), Multi-model projections of climate change from short-lived emissions due to human activities, *Journal of Geophysical Research*, 113(D11109).
- Shindell, D., and G. Faluvegi (2009), Climate response to regional radiative forcing during the twentieth century, *Nature Geoscience*, 2: 294-300.
- Shindell, D., et al. (2009), Improved attribution of climate forcing to emissions, *Science*, 326(5953): 716-718.
- Shindell, D., et al. (2010), Spatial scales of climate response to inhomogeneous radiative forcing, *Journal of Geophysical Research*, 115: D19110.
- Shindell, D. T., et al. (2003), Preindustrial-to-present-day radiative forcing by tropospheric ozone from improved simulations with the GISS chemistry-climate GCM, *Atmospheric Chemistry and Physics*, 3: 1675-1702.
- Shindell, D. T., et al. (2008c), A multimodel assessment of pollution transport to the Arctic, *Atmospheric Chemistry and Physics*, 8(17): 5353-5372.
- Shine, K. P., et al. (2007), Comparing the climate effect of emissions of short- and long-lived climate agents, *Philosophical Transactions of the Royal Society A: Mathematical, Physical and Engineering Sciences*, 365(1856): 1903-1914.
- Simpson, R., et al. (2005), The short-term effects of air pollution on daily mortality in four Australian cities, *Australian and New Zealand Journal of Public Health*, 29(3): 205-212.
- Sitch, S., et al. (2007), Indirect radiative forcing of climate change through ozone effect on land-carbon sink, *Nature* 448: 791-794.
- Skarby, L., et al. (1998), Impacts of ozone on forests: A European perspective, *New Phytologist*, 139: 109-122.
- Smith, K. R., et al. (2009), Public health benefits of strategies to reduce greenhouse-gas emissions: health implications of short-lived greenhouse pollutants, *The Lancet*, 374(9707): 2091-2103.
- Solberg, S., et al. (2008), European surface ozone in the extreme summer 2003, *Journal of Geophysical Research*, 113(D07307).
- Spranger, T., et al. (2008), Modelling and mapping long-term risks due to reactive nitrogen effects - an overview of LRTAP convention activities, *Environmental Pollution*, 154: 482-487.
- Steib, D., et al. (2003), Meta-analysis of time-series studies of air pollution and mortality: update in relation to the use of generalized additive models, *Journal of Waste Management Association*, 53(3): 258-261.
- Stevens, B., and G. Feingold (2009), Untangling aerosol effects on clouds and precipitation in a buffered system, *Nature*, 461: 607-613.
- Stevenson, D. S., et al. (2004), Radiative forcing from aircraft NO<sub>x</sub> emissions: Mechanisms and seasonal dependence, *Journal of Geophysical Research*, 109(D17307).
- Stevenson, D. S., et al. (2006), Multimodel ensemble simulations of present-day and near-future tropospheric ozone, *Journal of Geophysical Research*, 111(D08301).
- Stevenson, D. S., and R. G. Derwent (2009), Does the location of aircraft nitrogen oxide emissions affect their climate impact?, *Geophysical Research Letters*, 36(17): L17810.
- Sudo, K., et al. (2003), Future changes in stratosphere troposphere exchange and their impacts on future tropospheric ozone simulations, *Geophysical Research Letters*, 30(24).
- Szpiro, A. A., et al. (2008), Accounting for Errors from Predicting Exposures in Environmental Epidemiology and Environmental Statistics, *University of Washington Biostatistics Working Paper Series, Working Paper 330*.
- Taylor, K. E., and J. E. Penner (1994), Response of the climate system to atmospheric aerosols and greenhouse gases, *Nature*, 369: 734-737.
- Thurston, G. D., and K. Ito (2001), Epidemiological studies of acute ozone exposures and mortality, *Journal of Exposure Analysis and Environmental Epidemiology*, 11: 286-294.
- Thwaites, R. H., et al. (2006), The effects of tropospheric ozone on species dynamics of calcareous grassland, *Environmental Pollution*, 144: 500-509.
- Timonen, U., et al. (2004), Ozone sensitivity of wild field layer plant species of Northern Europe: A review, *Plant Ecology*, 172: 27-39.

- Tong, D., et al. (2007), The use of air quality forecasts to assess impacts of air pollution on crops: Methodology and case study, *Atmospheric Environment*, 41: 8772-8784.
- Tuovinen, J.-P., et al. (2007), Robustness of modelled ozone exposures and doses, *Environmental Pollution*, 146: 578-586.
- Twomey, S. (1977), The influence of pollution on the shortwave albedo of clouds, *Journal of Atmospheric Science*, 34: 1149-1152.
- U.K. COMEAP (2009), Long-term exposure to air pollution: effect on mortality, Committee on the Medical Effects of Air Pollutants (COMEAP), UK Health Protection Agency, London, UK.
- U.S. CCSP (2008), Climate Projections Based on Emissions Scenarios for Long-Lived and Short-Lived Radiatively Active Gases and Aerosols 100 pp, Climate Change Science Program Working Groups, Washington DC. *Synthesis and Assessment Product 3.2*
- U.S. CCSP (2009), Atmospheric Aerosol Properties and Climate Impacts, A Report by the U.S. Climate Change Science Program and the Subcommittee on Global Change Research, National Aeronautics and Space Administration, Washington, DC.
- U.S. EPA (2006), Air quality criteria for ozone and related photochemical oxidants (final), National Center for Environmental Assessment, U.S. Environmental Protection Agency, Research Triangle Park, NC. *EPA/R-05/004aF-cF*. <http://purl.access.gpo.gov/GPO/LPS86552>
- U.S. EPA (2009a), Photochemical Assessment Monitoring Stations (PAMS), United States Environmental Protection Agency, <http://www.epa.gov/oar/oaqps/pams>
- U.S. EPA (2009b), Integrated Science Assessment for Particulate Matter, U.S. Environmental Protection Agency, Washington, DC. *EPA 600/R-05/004aF*
- Uddling, J., et al. (2010), Stomatal uptake of O<sub>3</sub> in Aspen and Aspen-birch forests under free-air CO<sub>2</sub> and O<sub>3</sub> enrichment, *Environmental Pollution*, 158(6): 2023-2031.
- Van Dingenen, R., et al. (2009), The global impact of ozone on agricultural crop yields under current and future air quality legislation, *Atmospheric Environment*, 43(3): 604-618.
- Vingarzan, R. (2004), A review of surface ozone background levels and trends, *Atmospheric Environment*, 38(21): 3431-3442.
- Volk, M., et al. (2006), Grassland yield declined by a quarter in 5 years of free-air ozone fumigation, *Global Change Biology*, 12: 74-83.
- Wang, C., et al. (2009), Impact of anthropogenic aerosols on Indian summer monsoon, *Geophysical Research Letters*, 36(L21704).
- Wang, J., and S. A. Christopher (2006), Mesoscale modeling of Central American smoke transport to the United States 2: Smoke regional radiative impacts on surface energy budget and boundary layer evolution, *Journal of Geophysical Research*, 111(D14S92).
- Wang, X., and D. L. Mauzerall (2004), Characterising distributions of surface ozone and its impacts on grain production in China, Japan and South Korea, *Atmospheric Environment*, 38(26): 4383-4402.
- Warren, S. G., and W. J. Wiscombe (1980), A model for the spectral albedo of snow II: Snow containing atmospheric aerosols, *Journal of the Atmospheric Sciences*, 37: 2734-2745.
- West, J. J., et al. (2006), Global health benefits of mitigating ozone pollution with methane emission controls, *Proceedings of the National Academy of Sciences of the U.S.A.*, 103(11): 3988-3993.
- West, J. J., et al. (2007a), Ozone air quality and radiative forcing consequences of changes in ozone precursor emissions, *Geophysical Research Letters*, 34(L06806).
- West, J. J., et al. (2007b), Human mortality effects of future concentrations of tropospheric ozone, *Comptes Rendus Geosciences*, 339(11-12): 775-783.
- West, J. J., et al. (2009), Effect of regional precursor emission controls on long-range ozone transport - Part 2: Steady-state changes in ozone air quality and impacts on human mortality, *Atmospheric Chemistry and Physics*, 9(16): 6095-6107.
- WHO (2006), Air quality guidelines: Global update 2005: Particulate matter, ozone, nitrogen dioxide, and sulfur dioxide, 22 pp, World Health Organization, Geneva. *WHO/SDE/PHE/OEH/06.02*. [http://whqlibdoc.who.int/hq/2006/WHO\\_SDE\\_PHE\\_OEH\\_06.02\\_eng.pdf](http://whqlibdoc.who.int/hq/2006/WHO_SDE_PHE_OEH_06.02_eng.pdf)

- Wieser, G., et al. (2003), The influence of microclimate and tree age on the defense capacity of European beech (*Fagus sylvatica* L.) against oxidative stress, *Annual Forest Science*, 60: 131-135.
- Wild, O., et al. (2001), Indirect long-term global radiative cooling from NO<sub>x</sub> emissions, *Geophysical Research Letters*, 28(9): 1719-1722.
- Wilkinson, S., and W. J. Davies (2009), Ozone suppresses soil drying- and abscisic acid (ABA)-induced stomatal closure via an ethylene-dependent mechanism, *Plant, Cell & Environment*, 32(8): 949-959.
- Wilkinson, S., and W. J. Davies (2010), Drought, ozone, ABA and ethylene: new insights from cell to plant to community, *Plant, Cell & Environment*, 33(4): 510-525.
- Wolfe, A. P., et al. (2006), Are current rates of atmospheric nitrogen deposition influencing lakes in the eastern Canadian Arctic?, *Arctic, Antarctic, and Alpine Research*, 38: 465-476.
- Yoshida, L. C., et al. (2001), Differences in above- and below-ground responses to ozone between two populations of a perennial grass, *Plant and Soil*, 233: 203-211.
- Yu, H., et al. (2006), A review of measurement-based assessments of the aerosol direct radiative effect and forcing, *Atmospheric Chemistry and Physics*, 6: 613-666.
- Zeger, S. L., et al. (2000), Exposure Measurement Error in Time-Series Studies of Air Pollution: Concepts and Consequences, *Environmental Health Perspectives*, 108(5): 419-426.
- Zeng, G., and J. A. Pyle (2003), Changes in tropospheric ozone between 2000 and 2100 modeled in a chemistry-climate model, *Geophysical Research Letters*, 30(7): 1392-1395.
- Zielinska, B., et al. (2010), Atmospheric Transformation of Diesel Emissions, Health Effects Institute, Boston, MA. *Research Report 147*



## Chapter 6 Summary

**Lead Authors: Terry Keating and Frank Dentener**

**Contributing Authors: Oliver Wild**

### 6.1. Observational Evidence for Intercontinental Transport

Observations from the ground, aircraft, and satellites provide a wealth of evidence that ozone ( $O_3$ ) and particulate matter (PM) concentrations throughout the Northern Hemisphere are influenced by intercontinental and hemispheric transport of pollutants. Transport in the Northern Hemisphere mid-latitudes is dominated by the westerly winds that transport emissions from East Asia across the North Pacific Ocean to North America, from North America across the North Atlantic Ocean to Europe, and from Europe into the Arctic and central Asia. The signature of long-range pollutant transport in measurements made downwind of sources depends on the lifetime of the particular pollutant. Discrete plumes of enhanced concentrations characterize pollutants with short lifetimes and no photochemical sources, while continuous distributions of concentrations represent transport of pollutants with longer lifetimes. In the latter case, the entire troposphere can be envisioned as completely filled with plumes of continuously varying concentrations in the process of intermixing and dispersing.

For PM, important evidence of transport is provided by satellite imagery of visible plumes of smoke and dust from wildfires and deserts that extend for thousands of kilometres. Over the last few years satellites have begun to provide quantitative information on intercontinental aerosol transport, including estimates of the amount of pollution transported, the altitude of transport and, in some cases, aerosol properties. Ground-based lidar networks and mountain top measurement sites in Europe, North America and Asia provide large continuous data sets that characterize the frequency of occurrence of aerosol transport events, the meteorological conditions responsible for them, and important information on aerosol particle properties. Evidence of intercontinental transport is also provided in the form of long-term trends in surface-site observations from remote islands, which in some cases compare well with the trends in emissions in upwind areas. Some in situ measurements have illuminated the importance of secondary aerosol formation from transported precursors. Long-range transport of aerosols can have significant air quality and environmental implications, especially in the outflow of the Asian and African continents and in the Arctic regions. Observations of the trace element composition and stable isotope ratios of aerosols have been useful in assessing the importance of natural and anthropogenic sources and studying processing of aerosols in transit.

For  $O_3$ , the evidence is provided in plumes of elevated  $O_3$  observed in the free troposphere or at high elevation sites and, more importantly, in an increasing trend in baseline  $O_3$  concentrations measured consistently at a number of remote sites across the Northern Hemisphere. Measurements suggest that during the latter half of the 20th century, concentrations of  $O_3$  at northern mid-latitudes increased by a factor of two or more. It is likely that much of this increase is due to increases in anthropogenic emissions of  $O_3$  precursors. Within the limits of the measurement records, the increase has been comparable throughout all longitudes, and has occurred in all seasons. More recently, more rapid increases have been observed downwind of eastern Asia in the free troposphere, whereas the increases within the boundary layer of central Europe and North America have slowed down. Measurements at some locations on the western coasts of Europe and North America clearly show that trans-oceanic air flows can carry  $O_3$  concentrations that approach or exceed air quality standards and objectives, and that air can mix to the surface and contribute substantially to air quality standard violations. This is particularly noticeable in areas with low emission. The impact on surface air quality depends upon vertical mixing of air into the boundary layer, which is enhanced by complex topography.

Although the observational record is sufficient to demonstrate that intercontinental transport occurs, to understand the contribution of the intercontinental transport of these pollutants to air pollution impacts and the significance of these flows for air quality management now and in the

future, the observational evidence must be combined with quantitative models that describe the processes of emission, transport, transformation, and removal that drive the observed concentrations and deposition.

## 6.2. Modelling Analyses of Intercontinental Transport

Current global models of O<sub>3</sub> and PM reproduce much of the observed regional and seasonal variability in surface concentrations and deposition relatively well and have been used to predict the path of pollutants during individual intercontinental transport events. This ability gives us some confidence that we can quantitatively represent the key processes controlling the formation, transport and removal of O<sub>3</sub>, PM, and their precursors. However, on finer spatial and temporal scales, significant discrepancies exist among estimates from different models and between model estimates and observations, indicating weaknesses in our representation of many processes at the resolution of current models. Furthermore, current global models are not able to reproduce entirely historical measurements and observed trends, raising concern about our ability to predict changes in the future.

Even with these limitations, current models provide useful insights regarding what emissions sources contribute to observed concentrations and how observed concentrations will change with emissions changes. Using various source attribution techniques, current models can estimate the contribution that different precursors, emissions source categories, or source regions make to observed concentrations or deposition. Source-receptor sensitivity analyses can be used to estimate how each of these fractions will change with changes in emissions or other factors.

The Task Force on Hemispheric Transport of Air Pollution (TF HTAP) coordinated several sets of multi-model experiments to better understand the ability of current models to describe intercontinental transport. As part of this effort, a set of emission perturbation experiments were conducted to compare model estimates of how emission changes in one region of the world impact air quality in other regions of the world. Multiple models were used to examine the global impacts of 20% emission reductions of relevant anthropogenic pollutants in four regions, approximately covering the major populated areas of North America, Europe, South Asia, and East Asia. These names are used hereinafter to refer to these rectangular regions, which encompass more than 75% of the anthropogenic emission sources in the Northern Hemisphere and, in some cases, include significant areas of ocean. Specific analyses were also made to quantify the impact in the Arctic of emission changes in these four source regions. These simulations provide information about source-receptor sensitivities as well as some information about source attribution.

### 6.2.1. Source Attribution

Attributing tropospheric O<sub>3</sub> back to the emission sources that contribute to its formation is complicated by the fact that O<sub>3</sub> is not emitted, but is formed in the atmosphere through a non-linear system of photochemical reactions of emitted precursors, including nitrogen oxides (NO<sub>x</sub>), volatile organic compounds (VOC), carbon monoxide (CO), and methane (CH<sub>4</sub>). Conceptually, observed surface O<sub>3</sub> concentrations may be thought of as composed of four fractions:

- O<sub>3</sub> that is formed in the stratosphere
- O<sub>3</sub> that is formed in the troposphere from
  - natural precursor emissions, including lightning, soil, fire, and vegetation emissions
  - anthropogenic precursor emissions that have been transported on intercontinental scales
  - anthropogenic precursor emissions from local or regional sources

The O<sub>3</sub> precursors from different sources interact in the atmosphere such that O<sub>3</sub> may be produced from natural or anthropogenic, local or transported, or a combination of natural and anthropogenic or local and transported emissions.

Each of the fractions that comprise observed O<sub>3</sub> differs in terms of (1) sensitivity to changes in precursor emissions, (2) the extent to which they can be controlled by a national or sub-national



jurisdiction, and (3) the magnitude of the contribution. The relative contribution of each fraction varies widely by location and season and has evolved over time. We have confidence that human activities contribute to the observed positive trend in surface O<sub>3</sub>, and that the anthropogenic component to mean O<sub>3</sub> levels in the Northern Hemisphere has grown significantly since about 1850. However, there remain large uncertainties in our estimates of the source attribution for these changes.

Based on modelling performed for the HTAP multi-model experiments, the annual average ground-level O<sub>3</sub> mixing ratio averaged across the four study regions (North America, Europe, South Asia, and East Asia) and the ensemble of participating models is about 37 parts per billion by volume (ppbv) (± 4 ppbv standard deviation). This annual average, region-wide O<sub>3</sub> concentration masks large seasonal and geographic variability, and large differences across models. However, it provides a useful point of reference for considering the magnitude of intercontinental transport. Based on estimates in the literature, 20%-25% of this annual average ground-level concentration originates from the stratosphere, and a similar fraction is formed from natural precursor sources. The remainder is due to anthropogenic sources of precursors from within the region itself and transported from outside the region. The relative contribution of anthropogenic and natural, regional and extra-regional sources varies by location, season, and year.

Models indicate that in the northern mid-latitudes, intercontinental transport of air pollution typically peaks in boreal spring and fall, and is smallest during the summer months when O<sub>3</sub> levels are highest, due to the peak in production from local and regional emissions. Over the South Asia region, both the local and regional and the intercontinental influences are largest in late fall through winter and early spring. Intercontinental contributions to surface O<sub>3</sub> in the Arctic are largest in April through June, with a secondary maximum in October and November.

The maximum influence of intercontinental transport on ground-level O<sub>3</sub> generally occurs on mid-range pollution days (i.e., near the middle of the O<sub>3</sub> probability distribution, typically 50-70 ppbv), suggesting that import is less significant on days with the highest O<sub>3</sub> levels. These high O<sub>3</sub> conditions are typically due to trapping of local precursor emissions under stagnant meteorological conditions which also suppress the influence of distant sources. These results indicate that decreasing local or regional emissions is more effective at decreasing the highest O<sub>3</sub> levels, but that O<sub>3</sub> associated with stratospheric origins, natural emissions sources, and intercontinental transport comprise a significant fraction of tropospheric O<sub>3</sub> that is not within the control of local and regional political jurisdictions.

As with O<sub>3</sub>, PM concentrations or deposition can also be apportioned into several fractions based on emission sources. These PM fractions are associated with emissions from:

- volcanic eruptions, vegetation, and wind-blown dust (the last of which can be exacerbated by anthropogenic factors)
- open biomass (vegetation) burning, some of which is natural and some of which may be anthropogenic
- anthropogenic emissions that have been transported on intercontinental scales
- local and regional anthropogenic sources

The relative magnitudes of these fractions and their sensitivity to emission changes differs by location, season, year, and chemical component. Primary particles such as dust and black carbon, which are directly emitted into the atmosphere, respond linearly to changes in their emission sources. Secondary particles such as sulphate and organic aerosols, have a slight non-linear response due to their dependence on oxidation and other reactions. The fractions also differ to the extent to which they can be controlled by a local or regional jurisdiction.

There is a wide range of surface aerosol concentrations predicted by current models, reflecting large uncertainties in emissions and atmospheric processes as represented in the models. The HTAP multi-model experiments suggest that, in the four regions studied, ground-level concentrations of wind-blown soil dust from deserts in Africa, Asia, and the Middle East can be a

factor of 1.5 to almost 20 higher than that from anthropogenic and open biomass burning sources on a region-wide, annual average basis. Of the ground-level PM concentration originating from anthropogenic and open biomass burning sources, intercontinental transport of anthropogenic emissions accounts for between 5% and 35% and transport from open biomass burning contributes between 4% and 14% on a region-wide, annual-average basis in each region.

In terms of the chemical components of PM, the HTAP multi-model experiments provided information for four components: sulphate, black carbon, particulate organic matter (POM), and mineral (or soil) dust. For North America, Europe, South Asia, and East Asia, anthropogenic sources of emissions within each region account for 60-90% of the sulphate and black carbon concentrations. For POM, the contribution of anthropogenic sources within the region is less than for sulphate and black carbon, with biomass burning and biogenic emissions also contributing to the estimated concentrations.

In the Arctic, European pollution is the largest contributor to surface sulphate, followed by volcanic emissions. Biomass burning in the boreal forests of Eurasia plays a major role in determining the surface concentrations of black carbon and POM in the Arctic. Nearly half of the mineral dust at the Arctic surface is from Asia, with smaller amounts from Africa and the Middle East.

The fraction of PM associated with intercontinental transport increases with altitude, indicating the importance of transport above the boundary layer. As a result, the contribution of intercontinental transport to total column loading tends to be 15 to 25% higher than the contribution to surface concentrations or deposition.

As is the case with O<sub>3</sub>, annual average, region-wide statistics mask significant variability between seasons and within a given region. The seasonal cycles of aerosol concentration and intercontinental transport vary by chemical component and by region. However, there are substantial differences between the seasonal cycles in surface concentration predicted by models participating in the HTAP multi-model experiments. The model differences are larger for dust than they are for sulphate, black carbon, and POM, and are larger for the Arctic than for the mid-latitude regions.

In many regions, deposition of oxidised sulphur and nitrogen is large, and exceedance of critical loads occurs widely over many ecosystems. The intercontinental contribution to these exceedances is small. However, particular attention should be paid to the effects of long-range transport to polar regions where ecosystems are likely to be more vulnerable.

### 6.2.2. Source-Receptor Sensitivity

As part of the HTAP multi-model experiments, a set of emission perturbation experiments were conducted to compare model estimates of how emission changes in one region of the world impact air quality in other regions of the world. These experiments have provided the first set of comparable estimates of intercontinental source-receptor relationships from multiple models.

In the emission perturbation experiments, multiple models were used to examine the global impacts of 20% emission reductions of relevant anthropogenic pollutants in the four study regions.

For O<sub>3</sub>, the impact of 20% changes in anthropogenic emissions of NO<sub>x</sub>, VOC, CO, sulphur dioxide (SO<sub>2</sub>), and direct PM in one region on surface O<sub>3</sub> in the other regions varies from 0.07 to 0.37 ppbv on an annual average, region-wide basis, as estimated by the mean of the model ensemble. These values are significant in comparison to the response of surface O<sub>3</sub> to 20% decreases of emissions within the region itself, which vary from 0.8 to 1.3 ppbv. These annual average, region-wide values mask large temporal and geographic variability. For example, the values can vary by up to a factor of two from season to season and from grid cell to grid cell within a region.

The largest source-receptor relationship, in an absolute sense, is the impact of North American emissions on European surface O<sub>3</sub> levels. This is followed by the impact of European emissions on South Asian and East Asian surface O<sub>3</sub>. The annual average impact of East Asian emissions on North American surface O<sub>3</sub> is similar to the impact of North American emissions on East Asian surface O<sub>3</sub>, but with peaks in different seasons. European emissions have the largest influence on Arctic surface O<sub>3</sub> followed by North American emissions.

To quantify the relative importance of emissions changes outside each of these regions, as compared to emissions changes inside each of these regions, we defined the Relative Annual Intercontinental Response (RAIR) metric. RAIR is defined as the sum of the changes in the annual average, regionally-averaged concentration within a region due to a 20% decrease in emissions in the three other regions, divided by the sum of the changes in concentration within a region due to a 20% decrease in emissions in all four regions. The value of the metric ranges from 0%, indicating no intercontinental influence, up to 100%, indicating that air quality in a region is completely dominated by intercontinental sources. Thus, the RAIR is a measure of how much benefit a region may receive from emission reductions in other regions when emission reductions are coordinated on an intercontinental scale.

The RAIRs for O<sub>3</sub> estimated by the HTAP multi-model experiments range from 43% for Europe, to 40% for East Asia, to 32% for South Asia and North America. These values suggest that, in all four of the source-receptor regions, at least 30% of the total concentration changes within each of the regions is related to emission changes in the other three regions. Substantial O<sub>3</sub> transport takes place above the boundary layer in the free troposphere, where it can be brought to lower altitudes over distant receptors during subsidence, and mix with local emissions. The RAIRs are larger for column O<sub>3</sub> than for ground-level O<sub>3</sub>, and the column RAIRs exceed 50% in Europe and East Asia.

Imported O<sub>3</sub> and precursors may have qualitatively different impacts on urban areas than rural areas due to the strong dependency of O<sub>3</sub> chemistry on the ratio of NO<sub>x</sub> to VOCs. Results from the global models used in the HTAP multi-model experiments suggest that the response of annual average O<sub>3</sub> concentrations in large cities to changes in intercontinental transport may be as large or larger than the response to changes in regional emissions. Global models are not well suited to estimate responses at urban scales, as the resolution of current models is too coarse to resolve the strong chemical contrasts associated with urban regions. New studies using regional air quality models show that the higher resolution models are better able to resolve local topography, finer variations in land cover and use, and O<sub>3</sub>-VOC-NO<sub>x</sub> chemical non-linearities, which all have effects on the strength of surface O<sub>3</sub> responses to emission changes. For example in East Asia, results using a regional model predicted a smaller mean response in O<sub>3</sub> from European sources, but with much larger spatial variability.

The HTAP multi-model experiments also examined the sensitivity of O<sub>3</sub> to changes in CH<sub>4</sub> by decreasing the globally fixed CH<sub>4</sub> concentration by 20%. From those simulations, we estimated the response to 20% decreases in regional anthropogenic CH<sub>4</sub> emissions. While local and regional emission controls are clearly most effective for lowering local and regional O<sub>3</sub>, the O<sub>3</sub> response to anthropogenic emissions of CH<sub>4</sub> from distant source regions is nearly as large as that to emissions of the traditional O<sub>3</sub> precursors in these regions. The O<sub>3</sub> response to changes in CH<sub>4</sub> emissions requires several decades to be fully realized, given the relatively long atmospheric lifetime of CH<sub>4</sub>. Thus, controlling CH<sub>4</sub> is an important component of a strategy to limit increases in baseline surface O<sub>3</sub>, and as an important greenhouse gas, has additional benefits for climate change mitigation.

For PM, the HTAP multi-model experiments estimate RAIRs for PM surface concentrations of 20% for South Asia, 9% for East Asia, 7% for North America, and 5% for Europe. The RAIRs for surface deposition of sulphate, reactive nitrogen, black carbon and POM are similar to those for surface concentrations. The RAIRs for aerosol column loadings are generally larger (24%-37% for sulphate, 15%-24% for black carbon, and 12% to 23% for POM), reflecting the importance of transport above the boundary layer and implying more significant contributions to visibility and radiative forcing impacts.

Ground-level PM concentrations or deposition in the Arctic are most sensitive to emission changes in Europe. However, total column loadings of particulate matter over the Arctic are equally sensitive to changes in emissions from Europe or Asia, due to the fact that Asian emissions have a stronger tendency to be lifted and transported aloft than do European emissions.

Ground-level PM concentrations generally respond linearly to changing emissions from both local and upwind source regions. However, sulphate and some fraction of particulate organic matter are not directly emitted, but are formed in the atmosphere through oxidation, and can be affected by

non-linear systems of chemical reactions. For example, present-day North American emissions of  $\text{NO}_x$  and  $\text{CO}$ , together, are estimated to increase surface PM in Europe and East Asia by up to  $0.5 \mu\text{g}/\text{m}^3$ . These impacts are not due to direct transport of secondary PM produced in the source region and then transported to other continents, which is negligibly small. These increases are due to increases in oxidants, leading to enhanced production rates of secondary aerosols during long-range transport and in the receptor region. These results underscore the multifaceted nature of the consequences of a rising background of pollution levels in the Northern Hemisphere on local pollution levels.

### 6.3. The Impacts of Intercontinental Transport

$\text{O}_3$  and PM pollution are serious public health and environmental problems in many parts of the world. Ample experimental and epidemiological evidence indicates that exposure to ambient PM and  $\text{O}_3$  concentrations cause adverse health effects that range from minor sensory irritation to premature death.  $\text{O}_3$  also causes damage to a variety of different ecosystems including crops, forests and grasslands, which are also damaged by PM through the processes of acidification. These ecosystem impacts have important implications for productivity, biodiversity, and food security.  $\text{O}_3$  and PM pollution also significantly contribute to climate change on regional and global scales. The intercontinental transport of  $\text{O}_3$  and PM contributes to each of these adverse impacts.

As explained above, the highest concentrations of  $\text{O}_3$  and PM are typically associated with stagnant conditions, when the contribution from intercontinental transport is low and the contribution of local and regional sources are most important. However, intercontinental transport has increased baseline  $\text{O}_3$  concentrations to the point where they exceed thresholds for protection of vegetation in many locations and exceed thresholds for the protection of human health occasionally in some locations. Intercontinental transport events associated with forest fires or dust storms produce exceedances of short-term PM public health standards (e.g., the impact of Saharan dust events on PM levels in Southern Europe). On a longer-term basis, current levels of intercontinental transport of PM interfere with the ability to meet natural visibility targets in western North America. If public health-based air quality standards continue to be tightened based on new health effects research, the contribution of intercontinental transport to exceedances of such standards will continue to increase.

Relatively few studies have tried to quantify the human health impacts of intercontinental transport of  $\text{O}_3$  and PM specifically. Those studies that have been conducted have focused on the impact on the relationship between annual average concentrations and premature mortality. These studies suggest that intercontinental transport can contribute significantly to health impacts of air pollution within a given receptor region. For  $\text{O}_3$ , one study based on the HTAP multi-model experiments estimated that intercontinental transport of  $\text{O}_3$  contributes from 20% to more than 50% of  $\text{O}_3$ -related premature adult mortalities in a given receptor region, subject to large uncertainty. For PM, contributions to PM from emissions within any given region are expected to be much more important for human health than emissions from intercontinental transport. Based on the HTAP multi-model experiments, intercontinental transport of PM may be responsible for 3% to 5% of the PM-related mortalities in a region.

The sum of the health impacts of transported pollution in downwind foreign regions can be larger than the health impacts of emissions in the source region itself. Although the impact on ambient concentrations in downwind foreign regions may be much less than in the source region itself, the total population exposed in those downwind regions is much greater. For  $\text{O}_3$ , three studies have suggested that emission reductions in North America and Europe will avoid more mortalities outside these source regions than within the regions themselves. For PM, one study based on the HTAP multi-model experiments has suggested that 15% and 12% of the total PM-related mortalities associated with emissions from North America and Europe, respectively, are estimated to be realized outside of these source regions.

Several previous studies have found that global and intercontinental transport of sulphur and nitrogen contribute to the acidification and eutrophication of natural ecosystems with consequences for productivity and biodiversity. For  $\text{O}_3$ , recent experimental studies on field crops, adult forest

stands and different grassland ecosystems have found significant impacts associated with ecologically realistic free-air O<sub>3</sub> fumigations that mimic the observed increases in background O<sub>3</sub> concentrations.

Global crop yield losses of four staple crops due to exposure to O<sub>3</sub> are estimated to be between 3% and 16%, depending on the crop, and are valued at \$14 billion - \$26 billion per year. Based on the HTAP multi-model experiments, intercontinental transport may be responsible for about 5% to 35% of the estimated crop yield losses depending on the location, crop, and response function used. However, there is significant uncertainty in these estimates, part of which is due to the limited representativeness of available exposure-response functions based on threshold indices (e.g. AOT40 and SUM06).

On a global basis, O<sub>3</sub> and PM are significant contributors to climate forcing. Intercontinental transport influences the distributions of O<sub>3</sub> and PM, and therefore the shape and magnitude of their forcings. O<sub>3</sub> is a greenhouse gas that causes warming directly, and damage to plants by O<sub>3</sub> inhibits the natural uptake of CO<sub>2</sub>. PM is a mixture containing components that mainly cool, including sulphate and organic aerosols, and black carbon that warms, while aerosols also influence climate by changing clouds. Anthropogenic emissions of black carbon, CH<sub>4</sub>, carbon monoxide, and non-methane volatile organic compounds (which are O<sub>3</sub> precursors) are estimated to have caused a climate forcing since 1750 roughly as large as that from anthropogenic CO<sub>2</sub>. Because these compounds (and O<sub>3</sub>) have short lifetimes compared to the long-lived greenhouse gases, reducing these emissions will both improve air quality and slow the rate of climate change in the near term.

The climate forcings resulting from changes in emissions of PM, its precursors, and O<sub>3</sub> precursors (except CH<sub>4</sub>) depend strongly on location, timing, and the background composition. The radiative forcings and climate effects exerted by O<sub>3</sub> and PM are not globally uniform, but extend from the location of precursor emissions over regional and intercontinental scales. Based on the HTAP multi-model experiments, the Relative Annual Intercontinental Response (RAIR) of aerosol optical depth and direct radiative forcing was calculated for each of the four continental regions and each PM component. For all regions and PM components, emission changes outside the region had a significant effect relative to emission changes within the region, with RAIR of radiative forcing ranging from 9% to 30%. The change in radiative forcing over South Asia is most influenced by the import of sulphate aerosol, and North America is most influenced by the import of black carbon. For the change in radiative forcing due to sulphate, black carbon, and POM combined, South Asia is the region most strongly influenced by foreign sources, and North America and Europe are the least. The variability between models is very large, highlighting the significant uncertainties in modelling aerosol processes and transport.

This inhomogeneous forcing affects climate change at the global scale and at the regional scale, influencing atmospheric heating and dynamics and ultimately patterns of temperature and precipitation. The largest climatic impacts do not necessarily occur where the radiative forcing occurs and may occur downwind of the source region.

The Arctic is experiencing rapid climate change. Arctic climate is affected by O<sub>3</sub> and aerosols that are transported into the Arctic from other regions, as well as by the climate forcing of O<sub>3</sub> and aerosols outside of the Arctic. Deposition of black carbon on snow and ice is understood to be an important positive (warming) forcing in the Arctic.

Among O<sub>3</sub> precursors, widespread decreases in emissions of CH<sub>4</sub>, CO, and VOCs will likely reduce climate warming. Decreasing NO<sub>x</sub> may increase climate warming over decadal time scales because less NO<sub>x</sub> leads to less hydroxyl radical, increasing the lifetime of CH<sub>4</sub>. The increase in radiative forcing from the increased lifetime of CH<sub>4</sub> is greater than the decrease in radiative forcing from decreased O<sub>3</sub> formation. Reductions in PM would improve air quality, but for cooling aerosols, including sulphate, nitrate and organic carbon, this would generally exacerbate global warming. Reductions in black carbon would typically benefit both air quality and climate.

## 6.4. Future Scenarios

The significance of intercontinental transport for the achievement of environmental policy objectives may change in the future due to changes in the magnitude and spatial distribution of emissions. These changes may be caused by the continuing implementation of pollution control measures, regional differences in the pace of economic development, the growth in shipping and aviation emissions, and the implementation of climate change mitigation measures. In addition, changes in transport patterns, chemical evolution, depositional losses in transit, and emissions sources due to climate change may change the magnitude of intercontinental transport.

The current levels of intercontinental transport and hemispheric baseline concentrations of O<sub>3</sub> and PM are a result of emissions that, on a global basis, increased rapidly between 1950 and 1990. Since 1990, global emissions leading to O<sub>3</sub> and PM concentrations have experienced little change or have begun to decrease. In Europe and North America, which have been the dominant sources of anthropogenic emissions until recent decades, emissions of most precursors are constant or declining, due to the implementation of air pollution control policies. In East Asia and South Asia, emissions of precursors have risen dramatically in recent years, due to economic growth and development in these regions.

The implications of changes in anthropogenic emissions were explored in the HTAP multi-model experiments by considering a set of global emission scenarios developed to inform the Intergovernmental Panel on Climate Change's fifth assessment report, known as the Representative Concentration Pathways (RCPs). Three of the four scenarios assume some climate change mitigation policy will be adopted, and all four assume that the implementation of air pollution control policies will increase as development and income increase. As a result, all four of the scenarios suggest that between now and 2050, global emissions of most O<sub>3</sub> and PM precursors will decline, up to 76% for SO<sub>2</sub> emissions. However, the regional distribution of emissions in the Northern Hemisphere is expected to shift, with steeper and earlier declines in Europe and North America and shallower declines or actual increases in South and East Asia. Under the lowest emissions scenario, NO<sub>x</sub> emissions between 2000 and 2050 decline by 78%, 63%, and 48% in North America, Europe, and East Asia, respectively, but increase in South Asia by 42%. Under the highest emissions scenario, NO<sub>x</sub> emissions peak in 2030 with decreases of 43% and 16% in North America and Europe, respectively, and increases of 65% and 91% in East Asia and South Asia, respectively.

As part of the HTAP multi-model experiments, the impact of this redistribution of future emissions and expected changes in future global CH<sub>4</sub> concentrations, as specified by the RCP scenarios, was explored using linear approximations of the intercontinental source-receptor sensitivities determined under current conditions. To illustrate the range of future levels of air pollution, we assessed the RAIRs for 2050 under the lowest emissions scenario and for 2030, when global emissions peak, under the highest emissions scenario. For North America ground-level O<sub>3</sub> concentrations, the RAIR is estimated to increase to around 50% under both the high and low emissions scenarios, suggesting that, in the future, changes in emissions of O<sub>3</sub> precursors outside the region may be as important as changes within the region. For Europe, the RAIR for ground-level O<sub>3</sub> increases relatively little under the highest and lowest scenarios, due to simultaneously declining air pollution emissions in North America. For East Asia, the RAIR decreases under a high emission scenario, under which emissions within the region increase, and increases under a low emission scenario, under which emissions in the region decline. For South Asia, the RAIR for ground-level O<sub>3</sub> declines under both the low and high scenarios. Note that the sensitivity to changes in geographical distribution of emissions within a particular region has not been adequately assessed yet.

Using the linear approximation, the influence of changing CH<sub>4</sub> concentrations can be separated from the influence of changing intercontinental transport and local and regional emissions over the historical emission trends and future emission scenarios. Roughly 40% of the O<sub>3</sub> increase since the preindustrial period is believed to be due to anthropogenic CH<sub>4</sub>. By 2050, the RCP scenarios suggest a wide range of possible changes in CH<sub>4</sub> concentrations, ranging from an increase greater than 50% to a decrease greater than 15%. Under the highest scenario, expected increases in CH<sub>4</sub>

concentrations have a large influence on ground-level O<sub>3</sub> changes, in some cases offsetting significant decreases in O<sub>3</sub> formation associated with local and regional emissions.

The HTAP multi-model experiments also examined the potential impacts of changes in meteorology and transport patterns expected as a result of climate change. Future changes in climate are expected to increase the effect of O<sub>3</sub> precursor emissions over source regions and reduce the effect over downwind receptor regions. However, the magnitude of these effects is relatively small, and is driven by changes in atmospheric chemistry and not by changes in transport patterns. The effect of natural emission changes and wider climate-related feedbacks have not been evaluated fully yet.

## **6.5. Implications for International Policy**

Taken together, O<sub>3</sub> associated with natural sources and anthropogenic intercontinental transport comprise a large fraction of observed O<sub>3</sub>. By themselves, these sources create O<sub>3</sub> concentrations that are damaging to human health and ecosystems, contribute significantly to near-term climate change, exceed ambient standards for the protection of ecosystems in many areas, and, in some cases, exceed ambient standards for the protection of public health. Likewise, PM associated with natural sources and anthropogenic intercontinental transport can often exceed short-term ambient standards for the protection of public health and contribute to acidification, eutrophication, near-term climate change, and visibility degradation. The sources of these pollutants are not within the control of national or sub-national political jurisdictions. Thus, without further international cooperation to mitigate intercontinental flows of air pollution, many nations are not able currently to meet their own goals and objectives for protecting public health and environmental quality.

Mitigation of intercontinental transport is not a substitute for emission reductions at the local and regional scale. In most cases, concentrations within a source region are more sensitive to emission changes within that region. However, as emissions at the local and regional scale are reduced, the relative importance of intercontinental transport increases. Furthermore, as emissions increase in some parts of the world and decrease in others, the absolute importance of intercontinental transport increases. The import of pollution from outside a region increases the control costs needed to meet fixed ambient air quality objectives, offsetting progress made by emission reductions within the source region. Modelling performed under the HTAP multi-model experiments has demonstrated that comparable mitigation efforts carried out in key regions across the Northern Hemisphere can have significant benefits within source regions, as well as downwind across the entire Northern Hemisphere. Thus, international cooperation to reduce intercontinental transport of pollution is an effective and necessary complement to local and regional emission controls.

The anthropogenic emission sources that contribute most to intercontinental transport are often the same, regardless of whether considering O<sub>3</sub> or PM. Typically, these sources are associated with combustion of fossil fuels in the electricity, transportation, industrial, and residential sectors, or with anthropogenic biomass burning. These are also important sources of long-lived greenhouse gases. Different mitigation strategies will have different implications for the mix of emissions that result and the associated impacts on public health, agriculture, natural ecosystems, and climate change on the local, regional, intercontinental, and global scales. Examining these issues together, there is a potential to find solutions that maximize multiple benefits on multiple spatial scales.

## **6.6. Further research and analysis needs**

The variability in current model estimates of transport magnitudes and the inability to explain some of the observed trends suggests that more research is needed to satisfactorily assess the significance of intercontinental transport. In particular, further efforts are needed to improve: the accuracy and spatial and temporal resolution of emissions estimates; the spatial, temporal, vertical, and chemical resolution of the current observing system; and the description of some chemical and physical processes in current models.

Improving our assessment of intercontinental and hemispheric transport will require an integrated approach where the best available knowledge from observations, emissions, and models is combined. A robust observational system, using multiple observational platforms and methods, is



needed to provide data for the evaluation and improvement of chemical transport models and emissions inventories. Further analytical efforts are needed to decrease the range of current model estimates for source-receptor relationships and improve our confidence in the assessment of intercontinental source-receptor relationships.

### *Key Challenges*

Some of the key challenges that we face are outlined below. Addressing each of these challenges requires linking information across the areas of observation, emissions, and modelling to:

- Improve the modelling of transport processes using existing and new field campaign data. Focused evaluation of models using field campaign data is needed to improve descriptions of small-scale boundary layer venting, atmospheric subsidence of transported polluted air masses into the boundary layer, wet scavenging, and transport processes.
- Advance understanding of the role that deposition of pollutants to vegetated land and ocean surfaces plays in determining atmospheric pollution mass balance and hence intercontinental transport. These same deposition processes also represent the pathways by which terrestrial and marine ecosystems are impacted by air pollution. As such, an integrated approach to improve our understanding of these deposition processes may benefit our understanding of intercontinental transport as well as impacts.
- Improve global emissions inventories, using existing information at the national and sub-national scales, inverse modelling, and other methods to compare emissions estimates to ground-based, aircraft, and satellite observations.
- Identify and explain observed long-term trends by filling gaps in the observing system, developing reliable emission trends, and improving model descriptions. The current observational system has limited coverage and resolution in most regions of the world and provides limited information about the vertical distribution of pollutants. Better observational information is essential for improving the ability to detect and explain long-term changes.
- Develop a robust understanding of current source-receptor relationships using multiple modelling techniques and analyses of observations. The initial results of the HTAP multi-model experiments provide some useful information about the significance of intercontinental transport, but further detailed analyses are needed.
- Estimate future source-receptor relationships under changing emissions and climate. Such scenarios should consider future years from 2020 to 2050 and 2100 and be coordinated with efforts under the Intergovernmental Panel on Climate Change.
- Improve organizational relationships and information management infrastructures to facilitate necessary research and analysis. Efforts should further the implementation of the strategy for Integrated Global Atmospheric Chemistry Observations, building upon the World Meteorological Organization's Global Atmospheric Watch program and contributing to the Global Earth Observation System of Systems.

## Appendix A

### Editors, Authors, & Reviewers

Contributor	Organization / Affiliation	Country
Elizabeth Ainsworth	Agricultural Research Service, USDA	USA
Hajime Akimoto	Asia Center for Air Pollution Research	Japan
Susan C. Anenberg	University of North Carolina, Chapel Hill & Environmental Protection Agency	USA
Ahmareen Arif	Air University	Pakistan
Steve Arnold	University of Leeds	United Kingdom
Mike Ashmore	Stockholm Environment Institute, York	United Kingdom
Richard Atkinson	St. George's University of London	United Kingdom
Marianne Bailey	Environmental Protection Agency	USA
Paul Bartlett	St. Peter's College & CUNY	USA
William Battye	EC/R Inc.	USA
Nicolas Bellouin	Met Office Hadley Centre	United Kingdom
Terry Bidleman	Environment Canada	Canada
Knut Breivik	Norwegian Institute for Air Research	Norway
O. Russell Bullock	Environmental Protection Agency	USA
Greg Carmichael	University of Iowa	USA
Elton Chan	Environment Canada	Canada
Gao Chen	National Aeronautics & Space Administration	USA
Mian Chin	National Aeronautics & Space Administration	USA
Sergio Cinnirella	CNR Institute of Atmospheric Pollution Research	Italy
Aaron Cohen	Health Effects Institute	USA
William Collins	Met Office Hadley Centre, Exeter	United Kingdom
Owen Cooper	National Oceanographic & Atmospheric Administration	USA
Elizabeth Corbitt	Harvard University	USA
Daniel Cossa	IFremer Centre de Méditerranée	France
Ashu Dastoor	Environment Canada	Canada
John Dawson	Environmental Protection Agency	USA
Pierre Delmelle	University of York	United Kingdom
Hugo Denier van der Gon	TNO Built Environment and Geosciences	Netherlands
Frank Dentener	Joint Research Centre – European Commission	European Community
Richard Derwent	rdscientific, Newbury	United Kingdom
Ruth Doherty	University of Edinburgh	United Kingdom
Pat Dolwick	Environmental Protection Agency	USA
Aurélien Dommergue	Université Joseph Fourier-Grenoble	France
Robert A. Duce	Texas A&M University	USA
Sergey Dutchak	EMEP/MSC-E	Russia
Kristie L. Ebi	IPCC WGII-TSU, Carnegie Institution for Science	USA
Ralf Ebinghaus	Helmholtz-Zentrum Geesthacht - Institute for Coastal Research	Germany
David Edwards	National Center for Atmospheric Research	USA
Lisa Emberson	Stockholm Environment Institute, York	United Kingdom
David Evers	Biodiversity Research Institute	USA
Nasreen Farah	Hydrocarbon Development Institute of Pakistan	Pakistan
Xinbin Feng	Chinese Academy of Science	China

<b>Contributor</b>	<b>Organization / Affiliation</b>	<b>Country</b>
Arlene Fiore	National Oceanographic & Atmospheric Administration	USA
Gerd Folberth	Met Office Hadley Centre	United Kingdom
Hans Friedli	National Center for Atmospheric Research	USA
Joshua Fu	University of Tennessee	USA
Jürg Fuhrer	Agroscope Research Station ART	Switzerland
Savitri Garivait	JGSEE - King Mongkut's University of Technology Thonburi	Thailand
Sunling Gong	Environment Canada	Canada
Claire Granier	Service d'Aéronomie, Centre National de la Recherche Scientifique (CNRS)	France
Doug Grano	EC/R Inc.	USA
Ramon Guardans	Ministry of the Environment and Rural and Marine Affairs	Spain
Alex Guenther	National Center for Atmospheric Research	USA
Alexey Gusev	EMEP/MSC-E	Russia
Mae Gustin	University of Nevada, Reno	USA
Kimberly Hageman	University of Otago	New Zealand
Simon Hales	University of Otago, Wellington	New Zealand
Crispin Halsall	Lancaster University	United Kingdom
Tom Harner	Environment Canada	Canada
Ian M.Hedgecock	CNR Institute of Atmospheric Pollution Research	Italy
Peter Hess	Cornell University	USA
Kevin Hicks	Stockholm Environment Institute & University of York	United Kingdom
Anne Hollander	Radboud University Nijmegen	Netherlands
Tracey Holloway	University of Wisconsin - Madison	USA
Christopher Holmes	Harvard University	USA
Ivan Holoubek	Masaryk University	Czech Republic
Hayley Hung	Environment Canada	Canada
Iliia Ilyin	EMEP/MSC-E	Russia
Lyatt Jaeglé	University of Washington	USA
Dan Jaffe	University of Washington - Bothell	USA
Liisa Jantunen	Environment Canada	Canada
S. Gerard Jennings	National University of Ireland, Galway	Ireland
Jan Eiof Jonson	Norwegian Meteorological Institute	Norway
Gerlinde Jung	University of Bremen	Germany
Roland Kallenborn	Norwegian Institute for Air Research	Norway
Maria Kanakidou	University of Crete	Greece
Terry Keating	Environmental Protection Agency	USA
Gerald J. Keeler	University of Michigan	USA
Zbigniew Klimont	International Institute for Applied Systems Analysis	Austria
Kazuhiko Kobayashi	The University of Tokyo	Japan
Dorothy Koch	Department of Energy	USA
Hans Herbert Kock	Helmholtz-Zentrum Geesthacht - Institute for Coastal Research	Germany
Charles E. Kolb	Aerodyne Research, Inc.	USA
David Krabbenhoft	United States Geological Survey	USA
Paolo Laj	Laboratoire de Glaciologie, Centre National de la Recherche Scientifique (CNRS)	France

<b>Contributor</b>	<b>Organization / Affiliation</b>	<b>Country</b>
Yun-Fat Lam	University of Tennessee	USA
Jean-Francois Lamarque	National Center for Atmospheric Research	USA
Gerhard Lammel	Max Planck Institute for Chemistry	Germany
Kathy Law	Service d'Aéronomie, CNRS	France
Leonard Levin	Electric Power Research Institute	USA
Yi-Fan Li	Environment Canada	Canada
Che-Jen Lin	Lamar University	USA
Meiyun Lin	Princeton University & National Oceanographic & Atmospheric Administration	USA
Junfeng Liu	Princeton University & National Oceanographic & Atmospheric Administration	USA
Zifeng Lu	Argonne National Laboratory	USA
Jianmin Ma	Environment Canada	Canada
Robie Macdonald	Fisheries and Oceans Canada	Canada
Matthew MacLeod	Swiss Federal Institute of Technology	Switzerland
Greet Maenhout	Joint Research Centre - European Commission	European Community
Randall Martin	Dalhousie University	Canada
Robert Mason	University of Connecticut	USA
Denise Mauzerall	Princeton University	USA
David McCabe	Clean Air Task Force	USA
Lina Mercado	Centre for Ecology & Hydrology	United Kingdom
John Methven	University of Reading	United Kingdom
Torsten Meyer	University of Toronto	Canada
Gina Mills	Centre for Ecology & Hydrology	United Kingdom
Manju Mohan	Indian Institute of Technology (IIT), Delhi	India
Paul Monks	University of Leicester	United Kingdom
Arun B. Mukherjee	University of Helsinki	Finland
Toshimasa Ohara	National Institute for Environmental Studies	Japan
Koyo Ogasawara	IDEA Consultants, Inc	Japan
Elisabeth G.Pacyna	Norwegian Institute for Air Research	Norway
Jozef Pacyna	Norwegian Institute for Air Research	Norway
Li Pan	Lamar University	USA
Damian Panasiuk	Norwegian Institute for Air Research (NILU- Polska)	Poland
David Parrish	National Oceanographic & Atmospheric Administration	USA
Stuart Penkett	University of East Anglia	United Kingdom
Nicola Pirrone	CNR Institute of Atmospheric Pollution Research	Italy
Håkan Pleijel	University of Gothenburg	Sweden
Pruek Pongprueksa	Lamar University	USA
Joe Prospero	University of Miami	USA
Patricia Quinn	National Oceanographic & Atmospheric Administration	USA
David Reidmiller	University of Washington - Bothell	USA
Lorraine Remer	National Aeronautics & Space Administration	USA
Glenn Rice	Harvard University	USA
Sergiu Robu	Academy of Sciences of Moldova	Moldova
Andrew Ryzhkov	Environment Canada	Canada
Michael Sanderson	Met Office Hadley Centre	United Kingdom
Rich Scheffe	Environmental Protection Agency	USA
David Schmeltz	Environmental Protection Agency	USA

<b>Contributor</b>	<b>Organization / Affiliation</b>	<b>Country</b>
Michael Schulz	Norwegian Meteorological Institute	Norway
Christian Seigneur	Centre d'Enseignement et de Recherche en Environnement Atmosphérique	France
Noelle Eckley Selin	Massachusetts Institute of Technology	USA
Victor Shatalov	EMEP/MSC-E	Russia
Drew Shindell	National Aeronautics & Space Administration	USA
Staci Simonich	Oregon State University	USA
Stephen Sitch	University of Leeds	United Kingdom
Henrik Skov	National Environmental Research Institute	Denmark
Steven Smith	Pacific Northwest National Laboratory	USA
Francesca Sprovieri	CNR Institute of Atmospheric Pollution Research	Italy
Johannes Staehelin	Institute for Atmospheric and Climate Science	Switzerland
David S. Stevenson	University of Edinburgh, School of Geosciences	United Kingdom
Andreas Stohl	Norwegian Institute for Air Research (NILU)	Norway
David Stone	Environment Canada (retired)	Canada
David Streets	Argonne National Laboratory	USA
Yushan Su	Environment Canada	Canada
Elsie Sunderland	Harvard University	USA
Kyrre Sundseth	Norwegian Institute for Air Research	Norway
Noriyuki Suzuki	National Institute for Environmental Studies	Japan
Andy Sweetman	Lancaster University	United Kingdom
Shoaib-Raza Syed	University of Strasbourg	France
Akinori Takami	National Institute for Environmental Studies	Japan
Hiroshi Tanimoto	National Institute for Environmental Studies	Japan
Shu Tao	Peking University	China
Jochen Theloke	University of Stuttgart	Germany
Valerie Thouret	Laboratoire d'Aérodologie, CNRS	France
Oleg Travnikov	EMEP/MSC-E	Russia
Thomas Trickl	Karlsruher Institut für Technologie	Germany
Juha-Pekka Tuovinen	Finnish Meteorological Institute	Finland
Solene Turquety	Laboratoire de Météorologie Dynamique, CNRS	France
Harry Vallack	University of York	United Kingdom
John van Aardenne	European Environment Agency	European Community
Rita van Dingenen	Joint Research Centre – European Commission	European Community
Jun Wang	University of Nebraska, Lincoln	USA
Yuxuan Wang	Tsinghua University	China
Peter Weiss	Umweltbundesamt	Austria
J. Jason West	University of North Carolina, Chapel Hill	USA
Jeffrey L. West	Environmental Protection Agency	USA
Oliver Wild	Lancaster University	United Kingdom
Wilfried Winiwarter	International Institute of Applied Systems Analysis	Austria
Hongbin Yu	University of Maryland & National Aeronautics & Space Administration	USA
Christian Zdanowicz	Natural Resources Canada	Canada
Yang Zhang	North Carolina State University	USA
Jerry Ziemke	National Aeronautics & Space Administration	USA
André Zuber	European Commission	European Community